

**Maynooth
University**

National University
of Ireland Maynooth

Optimal control and model reduction for wave energy systems:

A moment-based approach

Nicolás Faedo

A thesis submitted in partial fulfillment
of the requirements for the degree of
Doctor of Philosophy

Maynooth University
Faculty of Science and Engineering
Department of Electronic Engineering
Centre for Ocean Energy Research

August 2020

Supervisor

Prof. John V. Ringwood

Head of Department

Prof. Ronan Farrel

VIVA Committee

Examiners:

Dr. Jørgen Hals Todalshaug
CorPower Ocean & Norwegian University of Science and Technology.

Dr. Oliver Mason
Hamilton Institute, Department of Mathematics and Statistics, Maynooth University.

Independent Chair:

Dr. David Malone
Hamilton Institute, Department of Mathematics and Statistics, Maynooth University.

Written in 2020 by Nicolás Faedo.

Colophon

This thesis was typeset with **KOMA-Script** and **L^AT_EX** using the **kaobook** class, with some minor modifications. The **L^AT_EX** editor utilised was GNU Emacs v. 26.1, in combination with AUCTeX v. 12.2, running on Ubuntu 18.04.4 LTS.

Electronic version

First version – Generated in May 2020.

Second version – Generated in August 2020 (*current*).

Para mis viejos.

“No heredamos la tierra de nuestros antepasados. La legamos a nuestros hijos.”
– A. de Saint-Exupéry.

La ciencia es la expresión de una necesidad inherente al ser humano y, en todo caso, está ligada a la función superior de su naturaleza inteligente: **la capacidad de crear**.*

– Dr. René Gerónimo **Favaloro**.

Buenos Aires, Argentina.

(1923 - 2000)



This photograph was taken at a symposium held in Cleveland, on 12-13 November 1992 to celebrate the 25th anniversary of Dr. Favaloro's pioneering coronary artery bypass graft. Photo courtesy of the authors of [1] and the Cleveland Clinic Foundation.

* *Loosely translated as:* "Science is the expression of an intrinsic necessity of every human being which, in any case, is linked to the supreme function of its intelligent nature: **the ability to create.**"

Abstract

Following the sharp increase in the price of traditional fossil fuels, in combination with issues of security of supply, and pressure to honor greenhouse gas emission limits, *much* attention has turned to renewable energy sources in recent years. Ocean wave energy is a massive and untapped resource, which can make a valuable contribution towards a sustainable, global, energy mix. Despite the fact that ocean waves constitute a vast resource, wave energy converters (WECs) have yet to make significant progress towards commercialisation. One stepping stone to achieve this objective is the availability of appropriate *control technology*, such that energy conversion is performed as economically as possible, minimising the delivered energy cost, while also maintaining the structural integrity of the device, minimising wear on WEC components, and operating across a wide range of sea conditions.

Suitable *energy-maximising* control technology depends upon the availability of two *fundamental* 'pieces': A *control-oriented* dynamical model, describing the motion of the WEC, and a model-based *optimal control framework*, able to efficiently compute the corresponding energy-maximising control law, subject to a set of constraints, defined according to the physical limitations of the device.

Following the requirements for successful WEC control, and both using and extending key tools arising from the framework of model reduction by *moment-matching*, this thesis presents two main contributions. Firstly, this monograph proposes a comprehensive *moment-based model reduction framework*, tailored for WEC systems, addressing *linear* and *nonlinear* model reduction cases, providing a systematic method to compute control-oriented models from complex target structures. These approximating models inherit steady-state response characteristics of the target system, via the proposed moment-matching reduction framework.

Secondly, by recognising that, besides being a powerful model reduction tool, the parameterisation of the steady-state response of a system in terms of moment-based theory can be explicitly used to transcribe the energy-maximising control problem to a finite-dimensional nonlinear program, a comprehensive *moment-based optimal control framework*, tailored for WEC systems, is proposed. This framework considers both *linear* and *nonlinear* optimal control cases, while also including robust solutions with respect to both system, and input uncertainty, providing an efficient method to compute the energy-maximising control law for WECs, under different modelling assumptions.

Throughout this thesis both model reduction, and optimal control frameworks, are presented for a *general class* of WEC devices, and their performance is analysed via multiple case studies, considering different devices, under different sea state conditions.

Declaration of authorship

I, Nicolás Faedo, declare that this thesis entitled "*Optimal control and model reduction for wave energy systems: A moment-based approach*", and the work presented in it, are my own. I confirm that:

- ▶ This work was done wholly or mainly while in candidature for a research degree at this University.
- ▶ Where any part of this thesis has previously been submitted for a degree or any other qualification at this University or any other institution, this has been clearly stated.
- ▶ Where I have consulted the published work of others, this is always clearly attributed.
- ▶ Where I have quoted from the work of others, the source is always given. With the exception of such quotations, this thesis is entirely my own work.
- ▶ I have acknowledged all main sources of help.
- ▶ Where the thesis is based on work done by myself jointly with others, I have made clear exactly what was done by others and what I have contributed myself.



Nicolás Faedo
August 13, 2020

Acknowledgments

First and foremost, my deepest gratitude goes to Prof. John Ringwood, who, in a now seemingly distant 2017, not only gave me the fantastic opportunity of immersing myself in the world of *wave energy*, but has been an outstanding supervisor, making my Ph.D. a very enjoyable experience. The materialisation of this thesis is undoubtedly a result of his guidance, feedback and support. I owe my gratitude to Prof. Alessandro Astolfi and Dr. Giordano Scarciotti for the time spent at the Control and Power Research Group, Imperial College London, and their invaluable input on moment-based theory.

My warmest thank goes to present and former members of the COER group, both for the many discussions, and for making the (countless!) hours at the lab *truly* enjoyable: Alexis Mérigaud, Alix Untrau, Julie Brault, Louis Papillion, Francesco Paparella, Simone Giorgi, Ricky Novo, Leo Pio Pistillo, LiGuo Wang, Bingyong Guo, Jake Cunningham, Ahsan Said, Hasana Bagnall-Hare, Edwin Calla-Durandal, and Fernando Jaramillo. I would also like to thank Ann Dempsey, Joanne Bredin, John Maloco and Denis Buckley (from EE) for their constant administrative and technical support.

A special thanks go to Yerai “el Vasco” Peña-Sanchez, Markel “el Abuelo” Peñalba-Retes, Giuseppe “el Tano” Giorgi, and Christian “el Alemán” Windt, for their invaluable input and collaborations, but, mostly, for their amazing friendship. You all made my stay in Ireland truly unique. A big thanks to my long-time friends and ‘copatriots’ Demi García-Violini and Fran “Pancho” Dores, who not only greatly influenced the research presented in this monograph, but also made me feel closer to home.

The last bit of this acknowledgment goes to my friends, family, and life partner, for their unconditional support throughout these years. I’m taking the liberty of writing these last lines in my native language (Spanish).

Gracias a mis amigos de fierro, que literalmente me hicieron sentir como si nunca hubiese dejado Argentina: el dúo Bussi, Uli y David “el Panda”, mi pseudo-hermano Fede “Pollo” Piaggio, Ivan “el Puma” Guasch-Vives, Nico “el Gordardo” Márquez y Juampi Pollini.

Gracias a mi familia, a la que le debo absolutamente todo (y más también). A mis hermanos, Nahuel y Ailén, que estuvieron ahí para hacerme sonreír siempre, y a mis viejos, Elisa y Sergio, a quienes no me va a alcanzar la vida para agradecerles todo el apoyo y sacrificio.

Por último, el agradecimiento más grande es para mi compañera de vida, Nati, sin quién todo esto no hubiese sido ni remotamente posible. Gracias por bancarme en absolutamente TODAS, las buenas, las malas y las peores. Sin tu apoyo incondicional, hoy no estaría escribiendo esta página.

Institutional

I owe my gratitude to Science Foundation Ireland for supporting this research work, under Grant No. 13/IA/1886. I'm also grateful with the Royal Society for their support, under the International Exchange Cost Share programme IEC\R1\180018.

Detailed Contents

Abstract	ix
Declaration of authorship	x
Acknowledgments	xi
Detailed Contents	xiii
List of Acronyms	xviii
1 Introduction	1
1.1 Motivation	3
1.1.1 Towards control-oriented models: Model reduction	4
1.1.2 Addressing and solving the energy-maximising OCP	5
1.2 Main objectives, contributions, and organisation of the thesis	7
1.2.1 Part I: Preliminaries	8
1.2.2 Part II: Moment-based model reduction	9
1.2.3 Part III: Moment-based optimal control	10
1.2.4 Part IV: Conclusions and future work	12
1.2.5 Connection between parts: a thesis 'path'	12
1.2.6 List of publications	13
1.3 Notation & conventions	16
Part I: Preliminaries	19
2 Hydrodynamic WEC modelling and model reduction	20
2.1 Ocean waves: Linear theory	21
2.1.1 Regular waves	22
2.1.2 Irregular waves	23
2.2 Conservation of mass and momentum: the Navier-Stokes equations	25
2.3 Towards control-oriented models	27
2.3.1 Linear potential flow theory	27
2.3.2 Hydrodynamic effects in linear potential flow theory	30
2.4 Cummins' equation and state-space modelling	34
2.5 Nonlinear extensions to Cummins' formulation	38
2.5.1 Nonlinear restoring effects	39
2.5.2 Nonlinear viscous drag effects	39
2.6 Model reduction: state-of-the-art	40
2.6.1 Linear strategies	40
2.6.2 Nonlinear strategies	44
2.7 Conclusions	44

3	Energy-maximising control of WECs	46
3.1	The impedance-matching principle	47
3.2	Optimal control problem formulation	51
3.2.1	Estimation and forecasting of wave excitation	53
3.3	Impedance-matching-based controllers: state-of-the-art	54
3.3.1	Latching control	56
3.3.2	Causal stochastic control	57
3.3.3	Advantages and disadvantages	58
3.4	Optimisation-based controllers: state-of-the-art	59
3.4.1	Numerical solution methods for optimal control	60
3.4.2	Direct optimal control in wave energy	64
3.4.3	Advantages and disadvantages	74
3.5	Conclusions	75
4	Moment-based theory	78
4.1	The notion of moments	78
4.1.1	Linear systems	78
4.1.2	Nonlinear systems	82
4.2	Model reduction by moment-matching	83
4.2.1	Linear systems	83
4.2.2	Nonlinear systems	86
	Part II: Moment-based model reduction	89
5	Reduced models for linear SISO WECs	90
5.1	Moment-based WEC formulation for model reduction	91
5.2	Reduced models achieving moment-matching	97
5.2.1	Input-output dynamics	97
5.2.2	Radiation dynamics	100
5.3	Case study: a toroidal geometry	101
5.3.1	Input-output model reduction	102
5.3.2	Radiation model reduction	105
5.4	On the properties of radiation models	107
5.4.1	Enforcing passivity	109
5.4.2	Enforcing zeros at $s = 0$	113
5.5	Conclusions	114
6	Reduced models for linear MIMO WECs	115
6.1	Model reduction by moment-matching for linear MIMO systems	117
6.2	Moment-based WEC formulation for MIMO model reduction	120
6.3	Reduced models achieving moment-matching	124
6.3.1	Input-output dynamics	125
6.3.2	Radiation dynamics	127
6.4	Input-output case study: an array of CorPower-like devices	127

6.5	Synergy between moments and unknown-input estimation	134
6.6	Radiation case study: a multi-DoF CorPower-like device	140
6.6.1	On the properties of radiation models	142
6.7	Conclusions	144
7	Reduced models for nonlinear WECs	146
7.1	Nonlinear moment-based WEC formulation for model reduction	148
7.2	On the approximation of π	152
7.2.1	A Galerkin-like approach	155
7.3	Practical aspects and considerations	156
7.3.1	Projection of the residual mapping	156
7.3.2	Extension to multiple trajectories	157
7.3.3	Modifications to the mapping Ω^k	158
7.3.4	On the eigenvalues of the reduced model	159
7.4	Extension to MIMO WEC systems	160
7.5	WEC systems under regular wave excitation	162
7.5.1	Deterministic regular excitation	164
7.5.2	Stochastic regular excitation	166
7.6	WEC systems under irregular wave excitation	168
7.6.1	On the definition of the signal generator	168
7.6.2	On the definition of the set of training trajectories	169
7.6.3	Numerical study	170
7.7	Conclusions	175
	Part III: Moment-based optimal control	177
8	Energy-maximising control for linear SISO WECs	178
8.1	Optimal control problem	180
8.2	Moment-based WEC formulation for optimal control	182
8.3	Energy-maximising moment-based control formulation	185
8.3.1	Handling of state and input constraints	189
8.4	Case study: a CorPower-like device	191
8.5	Receding-horizon optimal control problem	194
8.6	Receding-horizon energy-maximising moment-based control formulation	196
8.6.1	Input representation	196
8.6.2	Receding-horizon controller	199
8.7	Case study revisited: inclusion of estimation and forecasting	200
8.7.1	Sensitivity analysis: Estimation	202
8.7.2	Sensitivity analysis: Forecasting	205
8.8	Conclusions	206
9	Energy-maximising control for linear MIMO WECs	208
9.1	Optimal control problem	210
9.2	Moment-based WEC array formulation for optimal control	211

9.3	Energy-maximising moment-based WEC array control formulation	214
9.3.1	Handling of state and input constraints	216
9.4	Case study: an array of CorPower-like devices	218
9.5	Conclusions	223
10	Robust energy-maximising control for WECs	225
10.1	Moment-based control under <i>system</i> uncertainty	228
10.1.1	Robust formulation under system uncertainty	232
10.1.2	Handling of state and input constraints	234
10.2	Moment-based control under <i>input</i> uncertainty	236
10.2.1	Robust formulation under input uncertainty	239
10.2.2	Handling of state and input constraints	241
10.3	A note on considering system and input uncertainty simultaneously	242
10.4	Case study: WEC under system uncertainty	243
10.4.1	On the definition of the uncertainty polytope \mathcal{P}	243
10.4.2	Performance assessment under regular waves	245
10.4.3	Performance assessment under irregular waves	248
10.4.4	Data-driven characterisation of system uncertainty	251
10.5	Case study: WEC under input uncertainty	254
10.5.1	On the definition of the uncertainty polytope \mathcal{P}	255
10.5.2	Performance assessment	256
10.6	Conclusions	258
11	Nonlinear energy-maximising control for WECs	260
11.1	Optimal control problem	262
11.2	Nonlinear moment-based WEC formulation for optimal control	263
11.2.1	On the approximation of π for optimal control	266
11.3	Nonlinear moment-based energy-maximising OCP	271
11.3.1	Handling of state and input constraints	275
11.4	Case study: A CorPower-like device	277
11.4.1	Characterisation of nonlinear hydrodynamic effects	277
11.4.2	Results and discussion	279
11.5	Conclusions	282
	Part IV: Conclusions and future work	283
12	Conclusions and future directions	284
12.1	Main conclusions	284
12.2	Future directions	287
12.2.1	Model reduction	287
12.2.2	Optimal control	288

List of Acronyms

A

AR Auto-Regressive model.

B

BEM Boundary Element Method.

BIBO Bounded-Input Bounded-Output.

C

CARIMA Controlled Auto-Regressive Moving Average.

CFD Computational Fluid Dynamics.

D

DMC Dynamic Matrix Control.

DoF Degree-of-Freedom.

E

EKF Extended Kalman Filter.

F

FFT Fast Fourier Transform.

FOH First-Order-Hold.

G

GA Genetic Algorithm.

GPC Generalised Predictive Control.

H

HRCF Half-Range Chebyshev Fourier.

I

IPM Interior Point Method.

J

JONSWAP Joint North Sea Wave Project.

K

KF Kalman Filter.

L

LCoE Levelised Cost of Energy.

LQG Linear Gaussian Quadratic.

LTI Linear Time-Invariant.

LTV Linear Time-Variant.

M

MIMO Multiple-Input, Multiple-Output.

MPC Model Predictive Control.

MPHC Model Predictive Heuristic Control.

MWR Mean Weighted Residual.

N

NMAPE Normalised Mean Absolute Percentage Error.

NP Nonlinear Program.

NRMSE Normalised Root Mean Square Error.

O

OCP Optimal Control Problem.

OPT Ocean Power Technologies.

P

PMP Pontryagin's Maximum(Minimum) Principle.

PSM Pseudospectral Method.

PTO Power Take-Off.

Q

QP Quadratic Program.

S

SDF Spectral Density Function.

SISO Single-Input, Single-Output.

SOH Second-Order-Hold.

SPM Spectral Method.

SQP Sequential Quadratic Programming.

SVD Singular Value Decomposition.

SWL Still Water Level.

U

USD United States Dollar.

W

WCP Worst-Case Performance.

WEC Wave Energy Converter.

Z

ZOH Zero-Order-Hold.

Figures

1.1	Investment in renewable energy technologies per year	1
1.2	Average annual wave energy transport	2
1.3	Block diagram of the energy-maximising OCP for WECs	4
1.4	Block diagram illustrating the interconnection between parts of this thesis	13
2.1	Definition of coordinate system and domain boundaries for long-crested waves.	22
2.2	Linear and overturning (or breaking) waves	22
2.3	Different characterisations of ocean waves in terms of a JONSWAP SDF	24
2.4	Illustrative representation of Remark 2.1.3.	25
2.5	Free-surface elevation for regular and irregular waves.	25
2.6	Graphical representation of linear potential flow theory	28
2.7	Body-fixed (local) coordinate system.	30
2.8	Hydrodynamic characterisation of a sphere	34
2.9	Hydrodynamic input-output structure adopted in this thesis.	35
3.1	Impedance-matching principle	48
3.2	Device motion under impedance-matching control	50
3.3	Optimal force-to-velocity frequency-response under impedance-matching conditions.	51
3.4	Estimation and forecasting of wave excitation effects	53
3.5	Approximate impedance-matching controller architecture	55
3.6	Power absorption for the impedance-matching-based strategies [103] and [107]	56
3.7	Schematic diagram of latching and declutching strategies	57
3.8	Latching control operating principle	57
3.9	Illustration of the MPC principle for reference tracking	62
3.10	Diagrammatic illustration of spectral and pseudospectral methods for optimal control	64
3.11	Distribution of linear and nonlinear WEC models considered in the literature	67
3.12	Example of an uncertain model in the frequency-domain	68
3.13	Half-range Chebyshev-Fourier polynomials	70
3.14	Distribution of objective function nature among MPC WEC studies	71
3.15	Distribution of objective function nature among SPM/PSM WEC studies	72
4.1	Diagrammatic illustration of linear moment-based theory	81
4.2	Diagrammatic illustration of nonlinear moment-based theory	83
4.3	Linear model reduction by moment-matching example case	85
4.4	Nonlinear model reduction by moment-matching example case	88
5.1	Radiation system as a feedback term	92
5.2	Moment-based analysis of the WEC system	93
5.3	Schematic of the toroidal device considered in this section	101
5.4	Frequency-domain characteristics of the toroidal device	101
5.5	SDF corresponding with the JONSWAP spectrum considered	102

5.6	Frequency-domain performance of the reduced models (toroidal device).	103
5.7	Time-domain performance of the reduced models (toroidal device).	105
5.8	Frequency-domain performance of the radiation reduced models (toroidal device)	106
5.9	Pole-zero map for the different radiation reduced models (toroidal device)	108
5.10	Nyquist plot for the different radiation reduced models (toroidal device)	109
5.11	Frequency-domain characteristics of radiation reduced models with preservation of passivity (toroidal device)	112
5.12	Nyquist plot for radiation reduced models with preservation of passivity (toroidal device)	112
6.1	Regular-polytope-type WEC array layout	128
6.2	Schematic of the CorPower-like device	128
6.4	JONSWAP spectra utilised to generate the wave inputs	129
6.3	Hydrodynamic characteristics of the WEC farm	129
6.5	Singular values plot for the target WEC array	130
6.6	Sigma-values plot for the (input-output) reduced models by moment-matching (WEC array)	131
6.7	Bode plot for the (input-output) reduced models by moment-matching (WEC array)	132
6.8	Time-domain response of the moment-matching-based model (WEC array)	134
6.9	Target and estimated wave excitation forces for each device in the WEC array	138
6.10	Bode plots for the approximating reduced models by moment-matching for the estimation problem (WEC array)	139
6.11	Hydrodynamic characterisation of a multi-DoF device	140
6.12	Singular values plot for the radiation system of a multi-DoF device	141
6.13	Bode plots for the radiation reduced models by moment-matching (multi-DoF WEC)	141
6.14	Sigma-plot for the radiation reduced models by moment-matching (multi-DoF WEC)	142
6.15	Pole-zero map for the radiation MIMO reduced model by moment-matching (multi-DoF WEC)	143
6.16	Nyquist plots for the radiation MIMO reduced model by moment-matching (multi-DoF WEC)	143
7.1	Illustration of the set of coefficients a_{qp} for the mapping Ω^k	159
7.2	WEC considered for the case of nonlinear model reduction under regular wave excitation	162
7.3	Output of a nonlinear reduced order model with $k = 3$	165
7.4	Absolute value of the difference between target and approximating output	165
7.5	Output of the nonlinear reduced order model for the inputs corresponding with the (regular) training trajectories	167
7.6	NMAPE for 1000 realisations of regular wave inputs	168
7.7	WEC layout considered for the case of nonlinear model reduction under irregular wave excitation	170
7.8	JONSWAP spectrum utilised to generate the wave input	171
7.9	Sets of amplitudes associated with training trajectories	172

7.10	Output of the nonlinear reduced order model under irregular wave excitation, for the inputs corresponding with each training trajectory	173
7.11	Output of the nonlinear reduced order model for a randomly generated sea-state realisation	173
7.13	NMAPE for 100 realisations of irregular wave inputs	174
7.12	Absolute value of the difference between target and approximating output (irregular excitation)	174
7.14	Normalised run-time for the nonlinear reduced model by moment-matching	175
8.1	Hydrodynamic coefficients for the CorPower-like device (in heave)	191
8.2	Motion and control results for regular wave excitation	192
8.3	JONSWAP spectra used to generate the input waves	193
8.4	Constrained power absorption for the moment-based energy maximising controller	194
8.5	Motion results for irregular wave excitation	194
8.6	Sets and time constants involved in the receding-horizon optimal control formulation	196
8.7	Target excitation input and the (apodised) approximated wave excitation input . .	199
8.8	Constrained energy absorption for the receding-horizon moment-based energy-maximising controller	202
8.9	Illustrative example of sensitivity cases	203
8.10	Performance indicator (2D) for the sensitivity analysis of energy absorption under estimation errors	204
8.11	Performance indicator (3D) for the sensitivity analysis of energy absorption under estimation errors	205
8.12	Sensitivity analysis with respect to forecasting errors	205
8.13	Illustrative example of a forecasted (apodised) excitation force signal	206
9.1	Regular-polytope-type WEC array layout considered for the application case	219
9.2	Hydrodynamic coefficients for the CorPower-like WEC array	219
9.3	Power absorption ratio for different wave period, where the displacement of the device and control input are constrained	220
9.4	Motion results for regular wave excitation	221
9.5	Motion results for irregular wave excitation	223
10.1	Schematic illustration of a nominal WEC system subject to uncertainty	229
10.2	Schematic illustration of a nominal signal generator subject to uncertainty	238
10.3	Uncertainty sets for the case a WEC system with imprecisely known parameters . .	245
10.4	Nominal and robust performance for a single regular wave input under parametric uncertainty	247
10.5	Nominal and robust performance for multiple regular wave inputs under parametric uncertainty	248
10.6	Normalised WCP for nominal and robust performance scenarios	249
10.7	Motion results for both nominal, and robust performance scenarios, under irregular wave excitation	250
10.8	Displacement results for nominal and robust moment-based control techniques, for different uncertain WEC systems	251

10.9 Displacement and energy absorption results for a nonlinear WEC model under robust moment-based control conditions	253
10.10 Uncertainty set for the case a WEC system under uncertain wave excitation . . .	256
10.11 Nominal and robust performance for multiple (regular) wave inputs under excitation force uncertainty	257
10.12 Normalised WCP for nominal and robust performance scenarios, under the presence of input uncertainty	258
11.1 Nonlinear hydrodynamic effects considered	278
11.2 Constrained power absorption for the nonlinear moment-based energy maximising controller	280
11.3 Motion and control results for the nonlinear moment-based controller	281

Tables

2.1 Dynamical properties associated with the radiation impulse response	33
3.1 Reference guide to read Table 3.2	77
3.2 Optimisation-based control strategies reviewed	77
4.1 Parameters of the example case for nonlinear model reduction.	87
5.1 Performance of the input-output reduced models (toroidal device)	104
5.2 Performance of the radiation reduced models (toroidal device)	106
6.1 Simulation results comparison table (WEC array)	133
6.2 Estimation results comparison table (WEC array)	137
6.3 Numerical comparison table for the radiation dynamics case (multi-DoF WEC) . .	142
7.1 MAPE for the moment-based reduction strategy (regular excitation)	166

Contents of this chapter

1.1	Motivation	3
1.1.1	Towards control-oriented models: Model reduction	4
1.1.2	Addressing and solving the energy-maximising OCP	5
1.2	Main objectives, contributions, and organisation of the thesis	7
1.2.1	Part I: Preliminaries	8
1.2.2	Part II: Moment-based model reduction	9
1.2.3	Part III: Moment-based optimal control	10
1.2.4	Part IV: Conclusions and future work	12
1.2.5	Connection between parts: a thesis 'path'	12
1.2.6	List of publications	13
1.3	Notation & conventions	16

The energy demand of the industrialised world has grown exponentially, naturally increasing concerns about future resource provision. As a matter of fact, the majority of the current energy consumption relies on 'traditional' fossil fuels, whose scarcity is making its price rise severely. Following this sharp increase in the price of traditional fossil fuels, in combination with issues of security of supply, and pressure to honor greenhouse gas emission limits¹ (for instance, the Kyoto protocol [3]), *much* attention has turned to renewable energy sources, aiming to fulfill future *increasing* energy needs. To illustrate this fact quantitatively, Figure 1.1 shows global investments in renewable energy technologies from 2004 to 2015 (measured in billion USD per year): In 2004, the world invested 47 billion USD; by 2015, this had increased to 286 billion USD, an increase of more than 600 percent [4].

1: As a matter of fact, the *Energy Roadmap 2050* of the European Union states that EU nations should cut greenhouse gas emissions to 80% below 1990 levels, by 2050 [2].

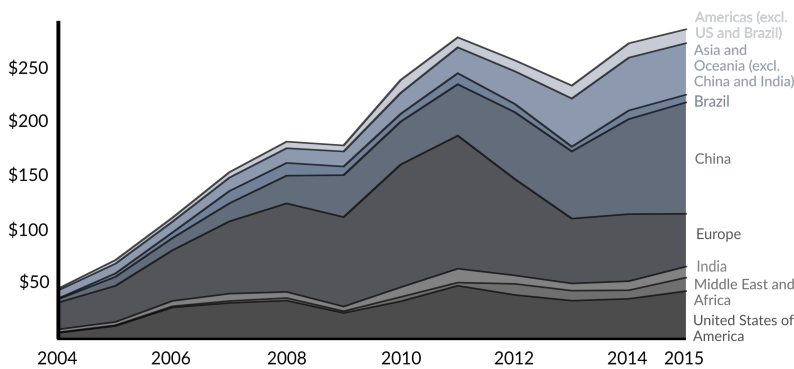


Figure 1.1: Investment in renewable energy technologies per year in billion USD by region, in the period 2004-2015. Adapted from [4].

Amongst the available renewable energy sources, ocean *wave energy*, once economically viable, can make a valuable contribution towards a sustainable, global, energy mix. Ocean waves represent a massive

and untapped source of clean energy: the wave energy resource has been estimated (worldwide) to be around 3.7 [TW] and about 32000 [TWh/yr] in [5] and [6], which would cover $\approx 20\%$ of the current global energy consumption (see Figure 1.2 for a detail on the distribution of the wave energy source worldwide).

Despite being a vast resource, wave energy conversion technology *has not yet reached* commercialisation stage. The main reason for the lack of proliferation of wave energy can be attributed to the fact that harnessing the irregular reciprocating motion of the sea is not as straightforward as, for example, extracting energy from the wind. This is clearly reflected in the striking absence of clear technology convergence, with over a *thousand* different concepts and patents proposed over the years². To date, wave energy converters (WECs) are commonly grouped depending different properties, including, but not limited to, their operation principle. A useful overview of the classification of WECs is offered in, for instance, [8–10].

2: The first patented wave energy converter appeared in 1898 (see [7]).

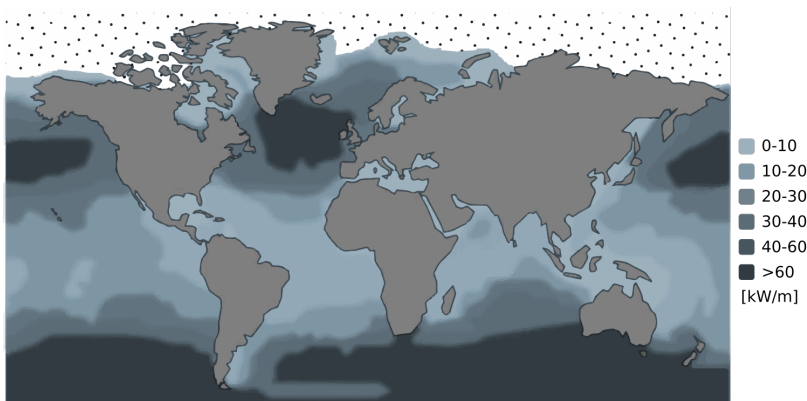


Figure 1.2: Average annual wave energy transport [kW/m]. Image adapted from [11].

Regardless of the type of WEC considered, these all share one common and fundamental objective: Energy conversion *must* be performed as economically as possible, aiming to minimise the delivered energy cost, while also maintaining the structural integrity of the device, minimising wear on WEC components, and operating effectively across a *wide range* of sea conditions.

Dynamic analysis and *control system technology* can impact many aspects of WEC design and operation, including device sizing and configuration, maximising energy extraction from waves, and optimising energy conversion in the power take-off (PTO) system. As a matter of fact, it is already clear (and well-established) that appropriate control technology has the capability to greatly enhance the energy extraction from WECs [12, 13]. This technology, together with the development of so-called WEC arrays (or *farms*), which effectively incorporate several devices in a common sea area, constitute key stepping stones towards successful commercialisation of WEC technology [14].

Though appropriate *energy-maximising* control technology can effectively maximise energy extraction from ocean waves, the control problem itself does not fit into a ‘traditional’ form, *i.e.* tracking/regulation. As a matter of fact, the control problem for WECs naturally lends itself towards *optimal control theory*, where the control objective is, effectively, optimal energy capture, subject to a set of device-dependent physical limitations (translated as *state* and *input* constraints).

That said, energy-maximising control design for WECs, based on an optimal control approach, comes with a number of *fundamental* drawbacks. These directly motivate the research presented throughout this thesis, as detailed in Section 1.1.

1.1 Motivation

As discussed previously in the introduction to this chapter, energy-maximising control of WECs can be cast as an optimal control problem (OCP), where the control objective is to maximise the absorbed energy from incoming ocean waves, while respecting the physical limitations associated with both device, and PTO, characteristics. The definition of this OCP involves a number of fundamental ‘pieces’, depicted in Figure 1.3, which virtually always include:

- (1) A *control-oriented* dynamical model Σ , describing the motion of the WEC, obtained by means of physical principles and the subsequent application of *model reduction* techniques³.
- (2) A *model-based* optimal control framework, which computes the energy-maximising control (PTO) force, subject to a set of (user-defined) constraints, according to the physical limitations of the WEC device.
- (3) A combination of unknown-input estimation and forecasting techniques, to provide instantaneous and future values of the (generally non-measurable) wave excitation force, *i.e.* the force exerted in the device as a consequence of the incoming wave field.

Given that, once a suitable WEC model is determined, item (3) above can be addressed using ‘relatively’ standard unknown-input estimation and forecasting techniques⁴, the motivation behind this thesis is focused on the fundamental challenges involved in obtaining such a control-oriented model Σ , *i.e.* model reduction techniques (item (1) above), and those involved in solving the associated energy-maximising OCP, subject to constraints (item (2) above). These central challenges, associated with both (1) and (2), are discussed in Sections 1.1.1 and 1.1.2, respectively.

3: The model reduction problem can be informally formulated as the problem of finding a simplified description of a dynamical system in specific operating conditions, preserving at the same time specific properties, *e.g.* stability.

4: The reader is referred to [15] for a state-of-the-art review and comparison study for different unknown-input estimation strategies, while [16] discusses optimal forecasting techniques for WECs.

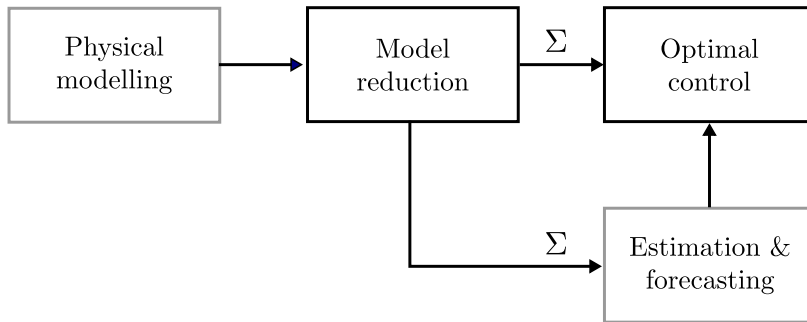


Figure 1.3: Block diagram of the energy-maximising OCP for WECs.

1.1.1 Towards control-oriented models: Model reduction

Regardless of the solution method selected to compute the energy-maximising optimal control law, the definition of the optimal problem itself depends upon the specification of a suitable WEC model Σ . This is also true for the unknown-input estimation stage, which virtually always relies on a model Σ , structured in such a way that modern estimation theory⁵ can be considered.

Not only is the structure of the model relevant for the definition of the OCP, but also its associated *complexity*: given that the energy-maximising control law *must* be computed in *real-time*, there is clearly a limit to the computational complexity of the WEC model employed in the control design procedure, while there is also a limit to the (analytical) complexity⁶ of mathematical models for which a globally optimal control solution can be efficiently found, or even whether it exists (*i.e.* for which the OCP is *well-posed*).

That said, even in the most ‘simplistic’ physical modelling scenario, where linear conditions⁷ are assumed, model reduction techniques are inherently required to provide a control-oriented model: the equation of motion for a WEC under linearity assumptions is non-parametric, intrinsically requiring a model reduction procedure, both to alleviate the computational demand of this non-parametric operator, and to express the dynamical equation in a suitable form for control/estimation procedures (often in terms of a state-space representation). Furthermore, any model reduction technique should compute a control-oriented model which inherits the underlying physical properties of the WEC process, so that the approximating structure is effectively representative. This set of properties include, for instance, internal stability, specific zero dynamics, relative degree, and passivity. This is specifically important for WEC control procedures, which often rely on these dynamical properties to guarantee existence and uniqueness of globally optimal solutions.

If linearity assumptions are adopted, a number of studies can be found in the ‘wider’ marine control/estimation literature, which

5: Most unknown-input estimation techniques arise from the field of fault detection, and virtually always require a mathematical model of the process [17].

6: For linear systems, this is often understood simply in terms of the dimension (order) of the system. For nonlinear systems, this dimensional argument may be inappropriate, as one has to take into consideration also the complexity of the functions involved in the representation of the system.

7: In particular, this refers to so-called *linear potential flow theory* (see Chapter 2 for further detail).

propose model reduction techniques tailored for ocean engineering applications, often considered in the WEC community. These strategies, which are reviewed in Chapter 2, use different approaches, with their own advantages and disadvantages. Nevertheless, to the best of the authors' knowledge, none of these methods is either specifically tailored for the WEC application, nor can they systematically satisfy the underlying physical properties that characterise the behaviour of the WEC, hence directly compromising their application for WEC estimation and control design.

Even though linearity assumptions are often adopted, mostly motivated by their simplicity, the importance of having *nonlinear* control-oriented models has been stressed in recent years: WECs are, by nature, prone to show nonlinear effects, since their principal aim, pursued by the optimal control strategy, is to enhance the amplitude of motion to maximise power extraction. In other words, the assumptions under which the linearisation of WEC models is performed are challenged by the controller itself, particularly in relation to small movements around its equilibrium position⁸. This, in turn, highlights the importance of having *systematic nonlinear model reduction techniques*, which can provide control-oriented nonlinear models, with a level of complexity suitable for the energy-maximising optimal control application. While the availability of nonlinear model reduction techniques would represent an extremely valuable tool, not only for control/estimation procedures, but for a variety of WEC applications (for instance, geometry optimisation, power assessment, among others), there is currently *no literature* addressing this issue within the WEC community.

8: This claim is discussed in depth in Chapter 3.

1.1.2 Addressing and solving the energy-maximising OCP

Once a control-oriented model is computed, according to the specifications of the WEC under analysis, the corresponding energy-maximising OCP must be solved efficiently, *i.e.* such that the computation of the control law can be performed in real-time, while providing globally optimal performance. That said, solving this OCP entails a number of significant challenges, that must be addressed properly, to achieve the control objective as efficiently as required by the WEC application.

First of all, regardless of the characteristics of the control-oriented WEC model Σ , utilised for design and synthesis, solving the energy-maximising OCP virtually always requires suitable numerical routines: Commonly, direct optimal control methods⁹ are considered, where

9: The reader is referred to Section 3.4.1 for a discussion on direct optimal control methods.

both the control objective and system variables are *discretised* appropriately, transcribing the energy-maximising OCP into a nonlinear program (NP). Though the solution of the resulting NP can be (generally) found by means of numerical routines, the computation of the energy-maximising control law must be performed efficiently, in order to have any practical value. This, in turn, strongly depends on having explicit conditions on the existence and uniqueness of globally optimal solutions, so that efficient *convex* optimisation routines can be applied to solve the resulting NP.

Though, to date, some promising results have been presented in the WEC literature, a number of deficiencies can be directly identified in the state-of-the-art of energy-maximising control of WECs¹⁰. In particular, motivated by their analytical simplicity and computational convenience, the vast majority of the available strategies are based on *linear* control-oriented models, even though WECs are, by their nature, prone to show nonlinear effects under controlled conditions. Moreover, even in the linear case, not only do the majority of the available strategies require modification of the energy-maximising objective by introducing ‘additional’ regularisation terms (which inherently bias the true optimal solution), to ensure uniqueness of a globally optimal solution, but most of them obviate any formal proof or recommendation on how to select these regularisation terms to achieve a convex control objective (with some notable exceptions). This is specially true for the case of arrays of devices, where, to the best of the author’s knowledge, *none* of the available strategies reviewed explicitly guarantee existence and uniqueness of globally optimal energy-maximising solutions.

With respect to nonlinearity, considering nonlinear WEC dynamics in the formulation of the OCP complicates the nature of the resulting NP: this optimisation problem has to be commonly solved using ‘generic’ nonlinear programming routines (*i.e.* without a specific ‘structure’), which are generally efficient only if conditions for global optimality are known a-priori. Having knowledge of these conditions facilitates the reduction of the ‘size’ of the search space, consequently enhancing the efficiency of the optimisation routine used. A small number of WEC control strategies, available in the literature, effectively consider nonlinear dynamics in the formulation of the OCP. Nevertheless, to the best of the authors’ knowledge, *none* of these strategies give explicit conditions for global optimality, preventing identification of the class of models that can be used, and limiting the results (and any conclusions) obtained only for the particular application case presented to illustrate the method¹¹.

An additional, yet not properly addressed, issue, when solving the energy-maximising OCP for WECs, is *robustness*. Modelling errors

10: The state-of-the-art of optimal control for WECs is presented in Chapter 3.

11: See Section 3.4.2.4 for further detail.

are ubiquitous in hydrodynamics, especially for the case of linear potential flow theory (see, for instance, [18]). The scarcity of robust strategies among WEC control methods can be attributed to the fact that the design of energy-maximising controllers does not directly fit into a traditional form, unlike the well-known tracking/regulation problem. This intrinsically complicates the application of well-developed robust control strategies, posing an imperative to find novel approaches for the wave energy application.

Though some progress has been reported in robust energy-maximising control for WECs by a handful studies, only *system* uncertainties are considered, and commonly ignore device limitations (*i.e.* the OCP is formulated without state and input constraints). Nonetheless, system uncertainty *is not the only source of error* inherently present in the WEC OCP: Given that the wave excitation force is virtually always approximated by means of a combination of unknown-input estimation and forecasting techniques, *input* uncertainty is also ubiquitous. Though the presence of this type of uncertainty can have a strong impact in the performance of energy-maximising controllers (see, for instance, [19]), the issue of robustness with respect to input uncertainty *has not been addressed* explicitly in the current OCP literature for WECs¹², to the best of the author's knowledge.

12: See Section 3.4.2.1 for further detail.

1.2 Main objectives, contributions, and organisation of the thesis

Motivated by the discussion provided in Section 1.1, this thesis has **two core objectives**, which, at first glance, can be informally summarised in the following two key items:

- ▶ To propose a comprehensive **model reduction framework tailored for WEC systems**, addressing *linear* and *nonlinear* model reduction cases.
- ▶ To propose a comprehensive **optimal control framework tailored for WEC systems**, addressing *linear* and *nonlinear* optimal control cases, and including robust solutions with respect to both system, and input, uncertainty.

To achieve these objectives, this thesis both uses and extends key theoretical results arising from the framework of *model reduction by moment-matching* [20, 21]. Moment-matching methods, also referred to as *interpolation* methods, are largely based on the mathematical notion of *moments*¹³. Moments are intrinsically connected to the input-output characteristics of the dynamical system under analysis, and provide a very specific parameterisation of the steady-state output response (provided it exists) of such a system. That

13: See Chapter 4 for an in depth discussion of moments and their role in moment-matching methods.

said, the model reduction by moment-matching technique consists of the interpolation of the steady-state response of the output of the system to be reduced: a model reduced by moment-matching is such that its steady-state response *matches* the steady-state response of the system to be reduced. Throughout this thesis, the framework induced by the definition of moments is referred to as **moment-based theory**.

A fundamental advantage is that the notion of moments has been defined both for linear and nonlinear systems, by means of a system-theoretic approach. For linear differential systems, the computation of moments depends upon the solution of a Sylvester equation. For nonlinear differential systems, moments arise as the solution of a nonlinear partial differential (invariance) equation, which is closely related to results arising from *centre manifold theory*¹⁴. This thesis recognises that, besides being a powerful model reduction tool, the parameterisation of the steady-state response of a system in terms of moments can be explicitly used to transcribe the energy-maximising control problem to a finite-dimensional nonlinear program. To the best of the author's knowledge, this monograph presents the first application of moments to solve an optimal control problem.

14: See, for instance, [22, Chapter 8].

That said, this thesis is divided in four parts:

- ▶ **Part I:** Preliminaries.
- ▶ **Part II:** Moment-based model reduction.
- ▶ **Part III:** Moment-based optimal control.
- ▶ **Part IV:** Conclusions and future work.

Each of these parts is linked to either a complementary, or core, objective of this thesis, providing a specific set of contributions, as discussed throughout the following sections.

1.2.1 Part I: Preliminaries

Objective 1.1: To introduce control-oriented WEC modelling, and critically identify and analyse the existing gaps in the literature of model reduction for WEC systems.

Contributions: Chapter 2 begins by introducing the fundamentals behind hydrodynamic WEC modelling, starting from the Navier-Stokes equations, progressively moving towards control-oriented models, describing each of the relevant hydrodynamic effects involved in the equation of motion. The intrinsic necessity of model reduction techniques is formally introduced, including the key physical properties that should be retained by any reduction technique. Finally, Chapter 2 includes a critical review of the state-of-the-art of model reduction techniques considered within the wave energy

field, explicitly identifying the existing gaps in model reduction for WEC systems.

Objective 1.2: To introduce energy-maximising control of WECs, and critically identify and analyse the existing gaps in the literature of optimal WEC control systems.

Contributions: Chapter 3 introduces the energy-maximising control problem for WECs, covering, from the fundamentals behind maximum energy absorption under regular (monochromatic) wave excitation, towards optimal control techniques utilised to tackle this control problem. A review of the state-of-the-art of energy-maximising control techniques is provided, explicitly identifying the existing gaps in current optimal control techniques for WEC systems.

Objective 1.3: To introduce and illustrate the fundamental theoretical preliminaries characterising moment-based theory.

Contributions: Chapter 4 recalls some of the key concepts behind moment-based theory, for single-input single-output (SISO) systems. In particular, special emphasis is placed on the formal (mathematical) definition of moments, using a system-theoretic approach. The problem of model reduction by moment-matching is defined and illustrated for both linear and nonlinear systems, by means of intuitive examples.

1.2.2 Part II: Moment-based model reduction

Objective 1.4: To introduce a *linear* model reduction framework tailored for the WEC application, capable of respecting relevant physical properties characterising the WEC process.

Contributions: Chapter 5 proposes an approximation framework for linear SISO WEC systems based on model reduction by moment-matching techniques. To that end, explicit conditions for the existence and uniqueness of a moment-based representation for the non-parametric WEC system are derived. Within this framework, the transfer function of the approximating model obtained by this moment-based approach exactly matches the steady-state behavior of the target WEC system at specific interpolation points (frequencies), which are user-selected. Furthermore, within this system-theoretic interpolation approach, essential physical properties of the device can be retained by the reduced model, such as internal

stability, passivity, and zero dynamics. The use and capabilities of the framework are illustrated by means of a number of case studies, using different WEC systems.

Chapter 6 proposes an approximation framework for linear multiple-input multiple-output (MIMO) WEC systems¹⁵, based on moment-matching model reduction techniques. To achieve such an objective, this chapter proposes a formal extension of the system-theoretic definition of moments, as provided in Chapter 4, for linear MIMO systems. In addition, explicit conditions for the existence and uniqueness of a moment-based representation for the non-parametric equation of motion are given. With this definition, a family of reduced order models, achieving moment-matching, is proposed for MIMO WEC systems. In addition, the existence of an intrinsic connection between the wave excitation force estimation problem and the moment-based reduction method is explicitly shown. The use and capabilities of the framework are illustrated by means of a number of case studies, using different MIMO WEC systems.

15: This includes both WECs in multiple degrees-of-freedom, and WEC arrays.

Objective 1.5: To introduce a *nonlinear* model reduction framework tailored for the WEC application.

Contributions: Chapter 7 presents a moment-matching model reduction framework for nonlinear (SISO and MIMO) WEC systems, capable of preserving the steady-state response characteristics of a target nonlinear model. To that end, the existence and uniqueness of the associated nonlinear moment is discussed, and ensured, for the case of wave energy systems. Given that the definition of nonlinear moments depends upon the solution of a nonlinear partial differential equation, an approximation framework for the computation of the nonlinear moment is proposed, tailored for the WEC application. The use and capabilities of the framework are illustrated by means of case studies, using different WEC systems, under a variety of wave conditions.

1.2.3 Part III: Moment-based optimal control

Objective 1.6: To introduce a *linear* energy-maximising optimal control framework tailored for the WEC application, capable of efficiently computing a globally optimal control law.

Contributions: Chapter 8 proposes an energy-maximising control framework for linear SISO WECs explicitly using moment-based theory. In particular, this chapter shows that, in addition to being a powerful model reduction tool, the parameterisation of the

steady-state response of a system, in terms of moments, can be explicitly used to transcribe the energy-maximising control problem to a finite-dimensional *strictly concave* quadratic program (QP). This systematically guarantees a unique solution for the energy-maximising control objective, subject to both state and input constraints. This facilitates the utilisation of state-of-the-art QP solvers, providing a computationally efficient energy-maximising control framework. The use and capabilities of the framework are illustrated by means of a case study, using a particular WEC system.

Chapter 9 extends the SISO energy-maximising framework presented in Chapter 8, to a MIMO moment-based formulation, capable of maximising energy absorption for WECs in multiple degrees-of-freedom, and WEC arrays. Analogously to the SISO case, this chapter shows that moments can be used to transcribe the MIMO energy-maximising control problem to a finite-dimensional *strictly concave* QP, hence also systematically guaranteeing a unique solution for the energy-maximising control objective, subject to both state and input constraints. The use and capabilities of the framework are illustrated by means of a case study, using a particular WEC array system, composed of 5 devices.

Objective 1.7: To introduce a *robust* energy-maximising optimal control framework, able to articulate both *system* and *input* uncertainty, while being capable of efficiently computing a globally optimal robust control law.

Contributions: Chapter 10 details an energy-maximising moment-based framework which explicitly considers system and input uncertainty in the computation of the optimal control law, while systematically respecting state and input constraints. This is achieved by proposing a suitable moment-based characterisation for the uncertainty set. To this end, the concept of moments is combined with robust optimisation principles, by proposing a worst-case performance approach. Necessary and sufficient conditions on the definition of the uncertainty set are explicitly derived, so that this moment-based robust optimal control framework has always a unique global energy-maximising solution, preserving all the appealing characteristics of the (nominal) control strategy developed in Chapters 8 and 9. The performance of the proposed controller is illustrated and analysed by means of a case study, considering a WEC subject to system and input uncertainty.

Objective 1.8: To introduce a *nonlinear* energy-maximising optimal control framework tailored for the WEC application, capable of efficiently computing a globally optimal robust control law *efficiently*.

Contributions: Chapter 11 proposes an energy-maximising control strategy for WECs subject to nonlinear dynamics. In particular, a method to map the objective function (and system variables) to a finite-dimensional tractable nonlinear program (NP) is proposed. In addition, by showing that the objective function arising from the proposed moment-based strategy belongs to a family of approximately convex/concave mappings, the existence of a global energy-maximising solution is guaranteed, under mild assumptions. Analogously to the case of convex/concave functions, where each local solution is also global, explicit conditions to determine whether a local energy-maximising solution is, effectively, a global maximiser for the proposed moment-based OCP, are given, having strong practical implications when numerically solving the associated NP. Finally, a case study, based on the energy-maximisation problem for a particular WEC system, is presented, subject to different sources of hydrodynamic nonlinearity.

1.2.4 Part IV: Conclusions and future work

Objective 1.9: To provide a critical set of conclusions and outcomes for this thesis, also identifying potential future research directions.

Contributions: Chapter 12 encompasses the main conclusions of this thesis, by critically evaluating the results arising from each different part. Future research directions are offered, both for model reduction, and optimal control cases.

1.2.5 Connection between parts: a thesis ‘path’

Parts I, II and III of this thesis are inherently interconnected, following specific ‘paths’. This is illustrated in the block-diagram presented in Figure 1.4, where the path effectively taken in this thesis is depicted in solid-blue, while a set of ‘alternative’ paths are given, using dashed-lines.

To be precise, Part I provides the fundamentals behind modelling and control for WECs, and recalls key results and tools from moment-based theory. Using (and extending) the results of Part I, Part II proposes a moment-based model reduction framework for WECs, producing tractable models, tailored for the WEC estimation/control application. In this thesis, these models are used for the wave excitation force estimation and forecasting stage, rather than to

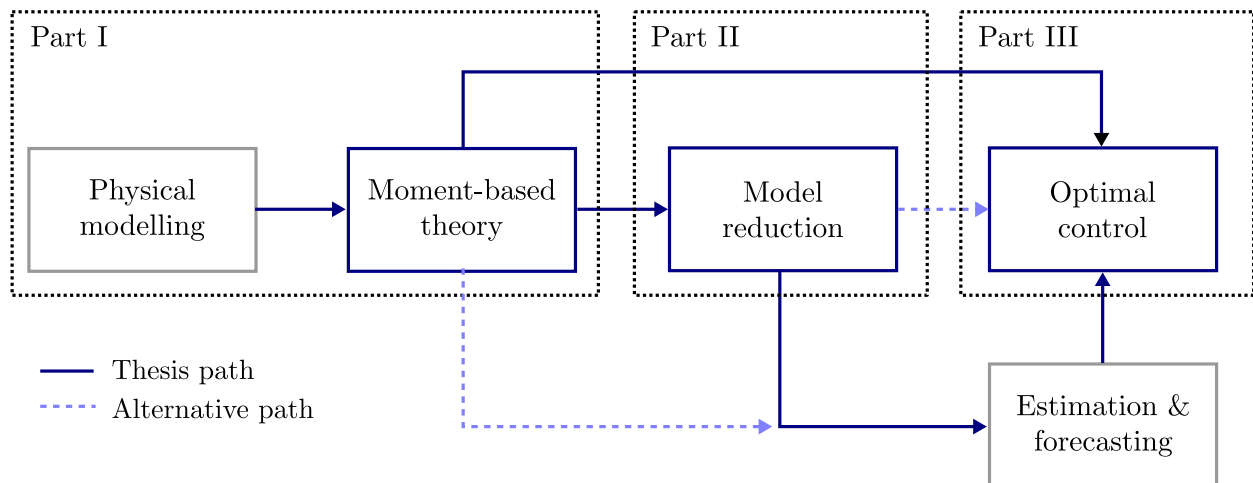


Figure 1.4: Block diagram illustrating the interconnection between parts of this thesis.

formulate the optimal control procedure: as demonstrated in Part III, moment-based theory can be directly used (and extended) to parameterise and solve the energy-maximising OCP for WECs, without explicitly going through the model reduction block first.

Nonetheless, different alternative paths could be taken, depicted in Figure 1.4 using a dashed-line. For instance, one could use the moment-based model reduction framework to produce control-oriented models, which are suitable for a large class of optimal control procedures, according to the user's preference/experience. An additional path (almost naturally) arises from the following argument: if the control problem can be directly solved using moment-based theory, *i.e.* without the need of explicitly going through a model reduction stage, one should be able to solve the estimation problem (which can be effectively seen as the *dual* of the control procedure) by applying similar concepts. Though beyond the scope of this thesis, a step has been taken in this direction, in [23].

1.2.6 List of publications

This section contains a list of peer-reviewed publications (in chronological order), which either constitute key material for the thesis, or are a product of work on the moment-based framework proposed. The following shorthand notation is used to denote the status of the publication: (P) published, (Pr) in press, (A) accepted, (CA) conditionally accepted, (UR) under review, (IP) in preparation. In addition, if a publication is directly linked to thesis contents, *i.e.* it contains key material presented in this thesis, this is clarified by pointing to a specific/s chapter/s.

Journal publications

Status	Publication	Chapter/s
(P)	N. Faedo, S. Olaya and J. V. Ringwood, <i>Optimal Control, MPC and MPC-like algorithms for wave energy systems: An overview</i> , IFAC Journal of Systems and Control, 1, 37–56, 2017.	2, 3
(P)	N. Faedo, Y. Peña-Sanchez and J. V. Ringwood, <i>Finite-order hydrodynamic model determination for wave energy applications using moment-matching</i> , Ocean Engineering, 163, 251–263, 2018.	5
(P)	N. Faedo, G. Scarciotti, A. Astolfi and J. V. Ringwood, <i>Energy-maximising control of wave energy converters using a moment-domain representation</i> , Control Engineering in Practice, 81, 85–96, 2018.	8
(P)	J. V. Ringwood, A. Merigaud, N. Faedo and F. Fusco, <i>An analytical and numerical sensitivity and robustness analysis of wave energy control systems</i> , IEEE Transactions on Control Systems Technology, 28(4), 1337–1348. 2019.	–
(P)	C. Windt, J. Davidson, D. Chandar, N. Faedo and J. V. Ringwood, <i>Evaluation of the overset grid method for control studies of wave energy converters in OpenFOAM-based numerical wave tanks</i> , Journal of Ocean Engineering and Marine Energy, 6, 55–70, 2020.	–
(P)	D. García-Violini, Y. Peña-Sanchez, N. Faedo and J. V. Ringwood, <i>An energy-maximising Linear Time Invariant Controller (LiTe-Con) for wave energy devices</i> , IEEE Transactions on Sustainable Energy (Early access available), 1–9, 2020.	–
(P)	N. Faedo, Y. Peña-Sanchez and J. V. Ringwood, <i>Parametric representation of arrays of wave energy converters for motion simulation and unknown input estimation: a moment-based approach</i> , Applied Ocean Research, 98, 102055, 2020.	6
(P)	N. Faedo, Y. Peña-Sanchez and J. V. Ringwood, <i>Receding-horizon energy-maximising optimal control of wave energy systems based on moments</i> , IEEE Transactions on Sustainable Energy (Early access available), 1–9, 2020.	8
(P)	C. Windt, N. Faedo, D. García-Violini, Y. Peña-Sanchez, J. Davidson, F. Ferri and J. V. Ringwood, <i>Validation of a CFD-based numerical wave tank model of the 1/20th scale Wavestar wave energy converter</i> , Fluids, 5(3), 112–132, 2020.	–
(Pr)	N. Faedo, Y. Peña-Sanchez and J. V. Ringwood, <i>Parameterisation of radiation forces for a multiple degree-of-freedom wave energy converter using moment-matching</i> , International Journal of Ocean and Polar Engineering (IJOPE), 2020.	6
(CA)	N. Faedo, G. Scarciotti, A. Astolfi and J. V. Ringwood, <i>On the approximation of nonlinear moments</i> , IEEE Transactions on Automatic Control, 2020.	7, 11
(UR)	N. Faedo, G. Scarciotti, A. Astolfi and J. V. Ringwood, <i>Energy-maximising moment-based constrained optimal control of ocean wave energy farms</i> , Renewable Energy.	9
(UR)	N. Faedo, G. Scarciotti, A. Astolfi and J. V. Ringwood, <i>Nonlinear energy-maximising control for wave energy systems: A moment-based approach</i> , IEEE Transactions on Control Systems Technology.	11
(UR)	D. García-Violini, Y. Peña-Sanchez, N. Faedo, C. Windt, F. Ferri and J. V. Ringwood. <i>Experimental implementation and validation of a broadband LTI energy-maximising control strategy for the Wavestar device</i> , IEEE Transactions on Control Systems Technology.	–
(UR)	C. Windt, N. Faedo, M. Penalba, F. Dias and J. V. Ringwood. <i>Reactive control of wave energy devices – the modelling paradox</i> , Applied Ocean Research.	–
(UR)	N. Faedo, F. Dores, G. Giorgi and J. V. Ringwood, <i>Nonlinear model reduction for wave energy systems: A moment-matching-based approach</i> , Nonlinear Dynamics.	7

Status	Publication	Chapter/s
(IP)	N. Faedo, G. Scarciootti, A. Astolfi and J. V. Ringwood, <i>Robust energy-maximising control for wave energy systems using a moment-domain representation</i> , IEEE Transactions on Control Systems Technology.	10
(IP)	D. García-Violini, N. Faedo and J. V. Ringwood, <i>Simple controllers for wave energy devices: Compared</i> , Journal of Marine Science and Engineering.	–

Conference publications

Status	Publication	Chapter/s
(P)	N. Faedo, Y. Peña-Sanchez and J. V. Ringwood, <i>Passivity preserving moment-based finite-order hydrodynamic model identification for wave energy applications</i> , Advances in Renewable Energies Offshore: Proceedings of the 3rd International Conference on Renewable Energies Offshore (RENEW), Lisbon, 351–359, 2018.	5
(P)	J. V. Ringwood, A. Merigaud, N. Faedo and F. Fusco, <i>Wave energy control systems: Robustness issues</i> , IFAC conference on Control Applications in Marine Systems, Robotics and Vehicles (CAMS), Opatija, 62–67, 2018.	–
(P)	N. Faedo and J. V. Ringwood, <i>Moment-based constrained optimal control of wave energy converters: A flap-type device</i> , IFAC conference on Control Applications in Marine Systems, Robotics and Vehicles (CAMS), Opatija, 50–55, 2018.	8
(P)	N. Faedo, Y. Peña-Sanchez and J. V. Ringwood, <i>Moment-matching-based identification for wave energy converters: the ISWEC device</i> , IFAC conference on Control Applications in Marine Systems, Robotics and Vehicles (CAMS), Opatija, 189–194, 2018.	5
(P)	Y. Peña-Sanchez, N. Faedo and J. V. Ringwood, <i>Finite-order hydrodynamic model fitting for wave energy applications using moment-matching: A case study</i> , The 28 th International Ocean and Polar Engineering Conference (ISOPE), Sapporo, 641–648, 2018.	5
(P)	J. V. Ringwood, F. Ferri, N. Tom, K. Ruehl, N. Faedo, G. Bacelli, Y. Yu and R. G. Coe, <i>The WECCOMP wave energy control competition – overview</i> , ASME 2019 38 th International Conference on Ocean, Offshore and Arctic Engineering (OMAE), Glasgow, V010T09A035, 2019.	–
(P)	Y. Peña-Sanchez, N. Faedo and J. V. Ringwood, <i>A Critical Comparison Between Parametric Approximation Methods for Radiation Forces in Wave Energy Systems</i> , 29 th International Ocean and Polar Engineering Conference (ISOPE), Honolulu, 174–174, 2019.	–
(P)	N. Faedo, Y. Peña-Sanchez and J. V. Ringwood, <i>Parameterisation of radiation forces for a multiple degree-of-freedom wave energy converter using moment-matching</i> , 29 th International Ocean and Polar Engineering Conference (ISOPE), Honolulu, 166–173, 2019.	6
(P)	Y. Peña-Sanchez, N. Faedo, M. Penalba, G. Giorgi, A. Merigaud, C. Windt, D. García-Violini, L. Wang and J. V. Ringwood, <i>Finite-Order hydrodynamic Approximation by Moment-Matching (FOAMM) toolbox for wave energy applications</i> , European Wave and Tidal Energy Conference (EWTEC), Naples, 1448-1 – 1448-9, 2019.	–
(P)	J. Cunningham, N. Faedo and J. V. Ringwood, <i>Excitation force estimation for wave energy systems using a moment-domain representation</i> , European Wave and Tidal Energy Conference (EWTEC), Naples, 1418-1 – 1418-8, 2019.	–
(P)	N. Faedo, Y. Peña-Sanchez and J. V. Ringwood, <i>Moment-matching-based input-output parametric approximation for a multi-DoF WEC including hydrodynamic nonlinearities</i> , European Wave and Tidal Energy Conference (EWTEC), Naples, 1449-1 – 1449-10, 2019.	–

Status	Publication	Chapter/s
(P)	C. Windt, N. Faedo, M. Penalba and J. V. Ringwood, <i>Assessment of the evaluation framework for energy maximising control systems for the Wavestar wave energy converter</i> , American Control Conference (ACC), Philadelphia, 4791–4796, 2019.	–
(P)	Y. Peña-Sanchez, N. Faedo and J. V. Ringwood, <i>Moment-based parametric identification of arrays of wave energy converters</i> , American Control Conference (ACC), Philadelphia, 4785–4790, 2019.	6
(P)	N. Faedo, G. Scarciotti, A. Astolfi and J. V. Ringwood, <i>Moment-based constrained optimal control of an array of wave energy converters</i> , American Control Conference (ACC), Philadelphia, 4797–4802, 2019.	9
(P)	N. Faedo, G. Scarciotti, A. Astolfi and J. V. Ringwood, <i>Robust moment-based energy-maximising optimal control of wave energy converters</i> , IEEE Control and Decision Conference (CDC), Nice, 4286–4219, 2019.	10
(P)	N. Faedo, D. García-Violini, Y. Peña-Sanchez and J. V. Ringwood, <i>Optimisation- vs. non-optimisation- based energy-maximising control for wave energy converters: A case study</i> , European Control Conference (ECC), Saint Petersburg, 843–848, 2020.	–
(P)	D. García-Violini, Y. Peña-Sanchez, N. Faedo and J. V. Ringwood, <i>LTI energy-maximising control for the Wave Star wave energy converter: Identification, design, and implementation</i> , 21 st IFAC World Congress (IFAC 2020), Berlin, 2020.	–
(A)	A. Astolfi, G. Scarciotti, J. Simard, N. Faedo and J. V. Ringwood, <i>Model Reduction by Moment Matching: Beyond Linearity - A Review of the Last 10 Years</i> , 59 th IEEE Conference in Decision and Control, Jeju Island.	–

1.3 Notation & conventions

Standard notation is considered throughout this thesis, most of which is defined in this section. If additional notation (not included in this section) is introduced, this is defined in the relevant parts of the dissertation.

Sets

\mathbb{R}^+ (\mathbb{R}^-) denotes the set of non-negative (non-positive) real numbers. \mathbb{C}^0 denotes the set of pure-imaginary complex numbers, and $\mathbb{C}_{<0}$ denotes the set of complex numbers with negative real part. The notation \mathbb{N}_q indicates the set of all positive natural numbers up to q , i.e. $\mathbb{N}_q = \{1, 2, \dots, q\}$, while $\mathbb{N}_{\geq q}$ is reserved for the set of natural numbers $\{q, q+1, \dots\} \subset \mathbb{N}$. The span of the set $\mathcal{X} = \{x_i\}_{i=1}^k \subset \mathcal{Z}$, where \mathcal{Z} is a vector space over a field \mathbb{F} , is denoted as $\text{span}\{\mathcal{X}\}$. The closed ball contained in \mathbb{R}^n , with center $z \in \mathbb{R}^n$ and radius $r \in \mathbb{R}^+$, is defined as $\mathcal{B}(z, r) = \{y \in \mathbb{R}^n \mid \|y - z\|_2 \leq r\}$. The convex hull of a set of points $X = \{x_1, \dots, x_n\} \subset \mathcal{X}$, where \mathcal{X} is a finite-dimensional Euclidean space, is denoted as $\text{conv}\{X\}$. Finally, \emptyset denotes the empty set.

Scalars, vectors and matrices

The symbol 0 stands for any zero element, dimensioned according to the context. The symbol \mathbb{I}_n denotes the identity matrix of the space $\mathbb{C}^{n \times n}$. The notation $\mathbf{1}_{n \times m}$ is used to denote a *Hadamard* identity matrix, i.e. a $n \times m$ matrix with all its entries equal to 1. The notations \bar{A} and A^* , with $A \in \mathbb{C}^{n \times n}$, denote the complex conjugate, and the Hermitian transpose of the matrix A , respectively. The spectrum of a matrix $A \in \mathbb{R}^{n \times n}$, i.e. the set of its eigenvalues, is denoted as $\lambda(A)$. The *Frobenius* norm of a matrix is denoted as $\|A\|_F$. The symbol \oplus denotes the direct sum of n (square) matrices, i.e. $\bigoplus_{i=1}^n A_i = \text{diag}(A_1, A_2, \dots, A_n)$. The notation $\Re\{z\}$ and $\Im\{z\}$, with $z \in \mathbb{C}$, stands for the *real-part* and the *imaginary-part* of z , respectively. The *symmetric-part* of a matrix $A \in \mathbb{R}^{n \times n}$ is defined (and denoted) as $\mathcal{H}\{A\} = (A + A^\top)/2$. The *Kronecker product* between two matrices $M_1 \in \mathbb{R}^{n \times m}$ and $M_2 \in \mathbb{R}^{p \times q}$ is denoted by $M_1 \otimes M_2 \in \mathbb{R}^{np \times mq}$. The symbol $e_{ij}^q \in \mathbb{R}^{q \times q}$ denote a matrix with 1 in the ij entry and 0 elsewhere. Likewise, $e_i^q \in \mathbb{R}^q$ denotes a vector with 1 in the i entry and 0 elsewhere. Finally, the symbol $\varepsilon_n \in \mathbb{R}^n$ denotes a vector with odd entries equal to 1 and even entries equal to 0.

Functions

Given two functions, $f : \mathcal{Y} \rightarrow \mathcal{Z}$ and $g : \mathcal{X} \rightarrow \mathcal{Y}$, the composite function $(f \circ g)(x) = f(g(x))$, which maps all $x \in \mathcal{X}$ to $f(g(x)) \in \mathcal{Z}$, is denoted with $f \circ g$. The convolution between two functions f and g , with $\{f, g\} \subset L^2(\mathbb{R})$, over the set \mathbb{R} , i.e. $\int_{\mathbb{R}} f(\tau)g(t - \tau)d\tau$ is denoted as $f * g$, and where $L^2(\mathbb{R}) = \{f : \mathbb{R} \rightarrow \mathbb{R} \mid \int_{\mathbb{R}} |f(\tau)|^2 d\tau < +\infty\}$ is the Hilbert space of square-integrable functions in \mathbb{R} . Let f and g be functions in $L^2(\mathcal{T})$, with $\mathcal{T} \subseteq \mathbb{R}$. Then, the standard inner-product between f and g is defined (and denoted) as $\langle f, g \rangle = \int_{\mathcal{T}} f(t)g(t)dt$. The Laplace transform of a function f (provided it exists), is denoted as $F(s)$, $s \in \mathbb{C}$. With some abuse of notation¹⁶, the same is used for the Fourier transform of f , written as $F(\omega)$, $\omega \in \mathbb{R}$. The *Kronecker delta* function is denoted as δ_j^i . The generalised *Dirac- δ* function, shifted by $t_j \in \mathbb{R}^+$, is denoted as $\delta_{t_j} = \delta(t - t_j)$.

16: The use of the capitalised letter for Laplace or Fourier transforms is always clear from the context.

Additional definitions

This section introduces two important operators, since their definition in the literature can often be ambiguous.

Definition 1.3.1 (Kronecker sum [24]) *The Kronecker sum of two matrices P_1 and P_2 , with $P_1 \in \mathbb{R}^{n \times n}$ and $P_2 \in \mathbb{R}^{k \times k}$, is defined (and denoted) as*

$$P_1 \hat{\oplus} P_2 \triangleq P_1 \otimes \mathbb{I}_k + \mathbb{I}_n \otimes P_2. \quad (1.1)$$

Definition 1.3.2 (Vec operator [24]) *Given a matrix P defined column-wise, i.e. $P = [p_1, p_2, \dots, p_m] \in \mathbb{R}^{n \times m}$, where $p_j \in \mathbb{R}^n$, $j \in \mathbb{N}_m$, the vector valued operator vec is defined as*

$$\text{vec}\{P\} \triangleq \begin{bmatrix} p_1 \\ p_2 \\ \vdots \\ p_m \end{bmatrix} \in \mathbb{R}^{nm}. \quad (1.2)$$

Finally, a useful property of the vec operator is recalled.

Property 1.3.1 [24] *Let $P_3 \in \mathbb{R}^{n \times m}$ and $P_4 \in \mathbb{R}^{m \times q}$. Then*

$$\text{vec}\{P_3 P_4\} = (\mathbb{I}_q \otimes P_3) \text{vec}\{P_4\} = (P_4^T \otimes \mathbb{I}_n) \text{vec}\{P_3\}. \quad (1.3)$$

Part I: Preliminaries

Hydrodynamic WEC modelling and model reduction

2

Contents of this chapter

2.1	Ocean waves: Linear theory	21
2.1.1	Regular waves	22
2.1.2	Irregular waves	23
2.2	Conservation of mass and momentum: the Navier-Stokes equations	25
2.3	Towards control-oriented models	27
2.3.1	Linear potential flow theory	27
2.3.2	Hydrodynamic effects in linear potential flow theory	30
2.4	Cummins' equation and state-space modelling	34
2.5	Nonlinear extensions to Cummins' formulation	38
2.5.1	Nonlinear restoring effects	39
2.5.2	Nonlinear viscous drag effects	39
2.6	Model reduction: state-of-the-art	40
2.6.1	Linear strategies	40
2.6.2	Nonlinear strategies	44
2.7	Conclusions	44

This chapter presents the basics behind WEC hydrodynamic modelling, starting with a description of the mathematical representation of ocean waves, and the intrinsic dynamics associated with fluid-structure interactions. Special emphasis is given to the assumptions required to arrive at the so-called *Cummins' equation* [25], which constitutes the most well-known and widely utilised dynamic description in the literature of WEC control. Though linear with respect to the device internal (motion) variables, the non-parametric nature of this Cummins' operator virtually always requires the utilisation of *model reduction* techniques, which aim to describe Cummins' equation in a state-space representation, *i.e.* a set of first-order differential equations, suitable for modern control and state-estimation design procedures. Nonlinear extensions of Cummins' formulation are also discussed, where 'additional' dynamics are included, aiming to alleviate the underlying linearity assumptions that normally characterise this equation, which can be potentially restricting under certain operating conditions¹.

In particular, Section 2.1 discusses the mathematical representation of ocean waves, while Section 2.2 recalls the basic dynamical principles of fluid-structure interaction. Section 2.3 states the hypotheses adopted to linearly describe the motion of a floating body, discussing each one of the hydrodynamic effects (*i.e.* forces and/or torques) involved in such a representation. Section 2.4 formally introduces Cummins' equation, and discusses different alternatives to compute a state-space representation of this non-parametric operator, by the

1: For instance, when a device is under energy-maximising control conditions, its motion is often exaggerated [12], and nonlinear effects begin to have a significant impact on its dynamic behaviour (see Chapter 3 for further detail).

use of model reduction techniques. The most common nonlinear extensions of Cummins' formulation are discussed in Section 2.5. Finally, Section 2.6 provides a review of the state-of-the-art of model reduction techniques applied to the wave energy conversion field, while Section 2.7 encompasses the main conclusions of this chapter, which motivate Part II of this thesis.

Remark 2.0.1 Note that this chapter is *not* based on a particular book/dissertation on hydrodynamics or fluid mechanics, but rather compiles results from well-known literature, such as, for instance, [26–30], and presents these from a control-oriented perspective, where both notation and conventions commonly adopted in the field of control theory, are used. Additionally, dynamical properties of interest, in accordance with well-known terminology from system dynamics, are highlighted.

2.1 Ocean waves: Linear theory

Attempts to capture the underlying physics of ocean waves, in terms of mathematical models, involve well-known scientists who have contributed to this vast field. Among these personalities, we can find Newton, Lagrange, Laplace, Green, Cauchy, and Poisson (see [28, Chapter 20]). Given the mathematical complexity involved in obtaining an accurate description of waves, numerous theories, with different scopes of application, have been proposed in the literature of ocean engineering. This section focuses on first-order waves, *i.e.* waves exhibiting *linear* behaviour. The theory associated with this type of waves is attributed to the English mathematician George Airy², hence known as *Airy's wave theory*.

Linear wave theory is the most commonly applied description for wind-generated surface gravity waves. It constitutes a fundamental mathematical framework, used in a plethora of ocean engineering applications, varying from seakeeping analysis and probabilistic prediction of short and long term behaviour of marine vessels [28, 29], to wave energy conversion dynamics and power extraction assessment. Though it is limited to waves with small wave height to wavelength ratios, *i.e.* $H_w/L_w \ll 1$, Airy's wave theory provides important insight into the behaviour of ocean waves and, consequently, of floating bodies subject to their effect. To represent these waves in a precise manner, we recall a set of well-known (key) definitions, in the next paragraphs. These can be found in, for instance, [28, Chapter 20], [27, Chapter 1] and [30, Chapter 4],

Let $x \in \mathbb{R}^3$, $x = [x_1, x_2, x_3]^\top$, be a point in space, and let the mapping $\eta : \mathbb{R} \times \mathbb{R} \times \mathbb{R}^+ \rightarrow \mathbb{R}$, $(x_1, x_2, t) \mapsto \eta(x_1, x_2, t)$ be the

²: Besides providing a stepping stone towards the fundamental understanding of ocean waves, Sir Airy (1801–1892) established the prime meridian in Greenwich, which is still in use as the reference for longitude [31].

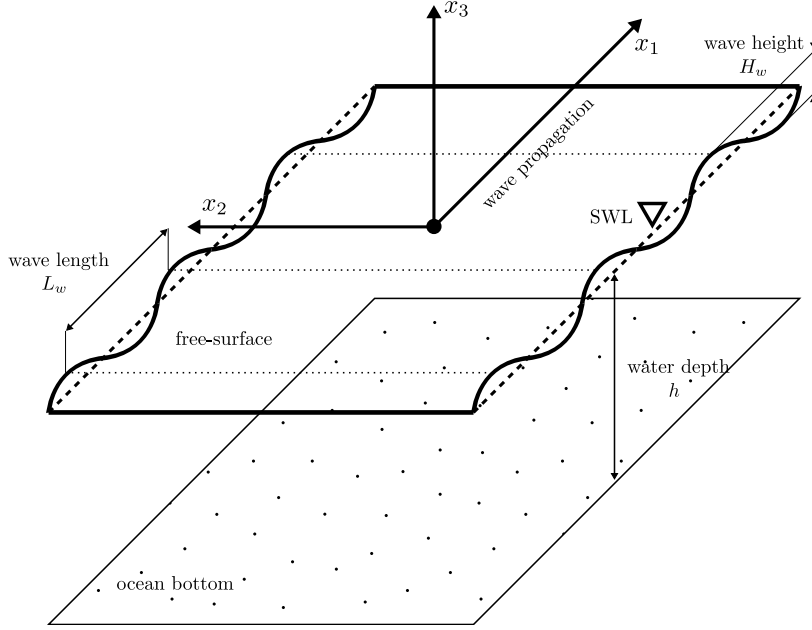


Figure 2.1: Definition of coordinate system and domain boundaries for long-crested waves.

fluid's *free-surface elevation*, *i.e.* the elevation of the free-surface from the still water level (SWL), as in Figure 2.1. Aiming to simplify the description of waves in terms of a two-dimensional mathematical model, it is virtually always assumed that their crests and troughs stretch in the x_2 -direction, with $x_2 \in \mathbb{R}$ (see Figure 2.1). This type of waves are commonly known as *long-crested waves* [30, Chapter 4]. Such an assumption renders η independent of the x_2 -coordinate, *i.e.* from now on we can write $\eta : \mathbb{R} \times \mathbb{R}^+ \rightarrow \mathbb{R}$, $(x_1, t) \mapsto \eta(x_1, t)$. The x_1 -axis points in the direction of wave propagation, and the still water level (SWL), is placed at $x_3 = 0$.

Remark 2.1.1 Within this formulation, the free-surface elevation is *uniquely determined* by the mapping η . More precisely, the function η is assumed to be *analytic*. This automatically excludes overturning or breaking waves from this analysis (see Figure 2.2). The reader is referred to [30, Chapter 6] and [32], for a discussion on mathematical models employed to describe nonlinear waves.

2.1.1 Regular waves

At this point, a clear distinction needs to be made with respect to the nature of the mapping η , *i.e.* the definition of the free-surface elevation. If the wave is composed of a *single* frequency component $\omega \in \mathbb{R}^+$ (or alternatively a fixed period $T_w = 2\pi/\omega$) the free-surface elevation can be compactly described as

$$\eta(x_1, t) = \frac{H_w}{2} \cos(\omega t + \psi_w(x_1, \omega)), \quad (2.1)$$

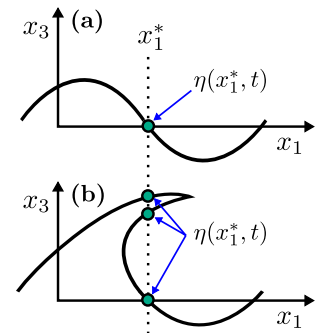


Figure 2.2: Linear (a) and overturning (or breaking) waves (b). Given a fixed location in space, the free-surface elevation in (a) is uniquely determined by the function η . Note that this is clearly not the case in overturning waves (b).

where $\psi_w : \mathbb{R} \rightarrow \mathbb{R}$ defines a phase shift, depending on the x_1 spatial coordinate. In this dissertation, this type of waves is referred to as *regular waves*.

Remark 2.1.2 Note that, for a fixed point in space x^* , and a fixed frequency ω^* , the free-surface elevation described in equation (2.2) depends only on t , *i.e.* we can write

$$\eta(t) = \frac{H_w}{2} \cos(\omega^* t + \psi_w^*), \quad (2.2)$$

where $\psi_w^* = \psi_w(x_1^*, \omega^*)$ is the phase shift associated with the spatial location x_1^* , for $\omega = \omega^*$.

Though the simplistic nature behind regular waves effectively misrepresents a realistic sea-state, this type of waves are useful to derive results of theoretical interest, providing valuable insight into the dynamics of a floating body³.

2.1.2 Irregular waves

Aiming to overcome the misrepresentation inherent to the nature of regular waves, an alternative definition can be made, which relies on a *stochastic* description of waves. To be precise, given a fixed location in space, the time series of the free-surface elevation, *i.e.* $\eta(t)$, corresponds with a spectral density function (SDF) $S_w : \mathbb{R} \rightarrow \mathbb{R}$, $\omega \mapsto S_w(\omega)$, characterising (stochastically) the behaviour of ocean waves at this specific location (provided the Fourier transform of η is well-defined). Examples of widely-used (semi-empirical) SDFs are the JONSWAP spectrum [33], for wind-generated seas with fetch limitations, the Bretschneider spectrum [34] for developing seas, and the Pierson-Moskowitz spectrum [35], for fully-developed seas. From now on, these waves are referred to as *irregular waves* (independently on the particular mapping S_w).

To fully describe these waves, one has to substitute the notions of wave height H_w and wave period T_w , which naturally only hold for regular waves (*i.e.* time-traces fully characterised by a single frequency component), for those of *significant wave height*, \bar{H}_w , and *peak wave period*, \bar{T}_w . The significant wave height is commonly defined as the mean wave height (trough to crest) of the highest third of the waves. The peak wave period is defined as the wave period associated with the most energetic waves, in the total wave (power) spectrum (at a specific point in space). The interested reader is referred to [27] for a thorough discussion on spectral characterisations of ocean waves.

3: As a matter of fact, this monochromatic representation (together with a set of additional assumptions) gives origin to the principle of *impedance-matching*, which is one of the fundamental theoretical foundations for the development of energy-maximising controllers for wave energy devices, as discussed in Chapter 3.

From now on, aiming to achieve consistency in both Parts II and III of this thesis, a JONSWAP SDF characterisation, with different parameter values, is always utilised. In particular, this representation requires three parameters: \bar{H}_w and \bar{T}_w , as defined in the previous paragraph, and the so-called *peak-shape parameter* $\gamma \in \mathbb{R}^+$ (also referred to as *peak-enhancement parameter*)⁴. The corresponding SDF can be written [33] as

$$S_w(\omega) = \frac{\alpha g^2}{\omega^5} \exp \left[-\beta \frac{\bar{\omega}_w^4}{\omega^4} \right] \gamma^{a(\omega)}, \quad (2.3)$$

where g is the acceleration of gravity, $\{\alpha, \beta\} \subset \mathbb{R}^+$ are constant values, $\bar{\omega}_w = 2\pi/\bar{T}_w \in \mathbb{R}^+$ is the *peak-frequency*, and the function $a : \mathbb{R}^+ \rightarrow \mathbb{R}^+$ (i.e. the exponent of the peak-shape parameter γ) depends on the frequency ω . The reader is referred to [33] for further detail on the definition of α, β and a . Figure 2.3 illustrates different spectral density functions S_w , corresponding with JONSWAP spectrums with: varying $\bar{T}_w \in [7, 12]$ [s] **(a)**, $\bar{H}_w \in [0.5, 3]$ [m] **(b)**, and $\gamma \in [1, 3.5]$ **(c)**.

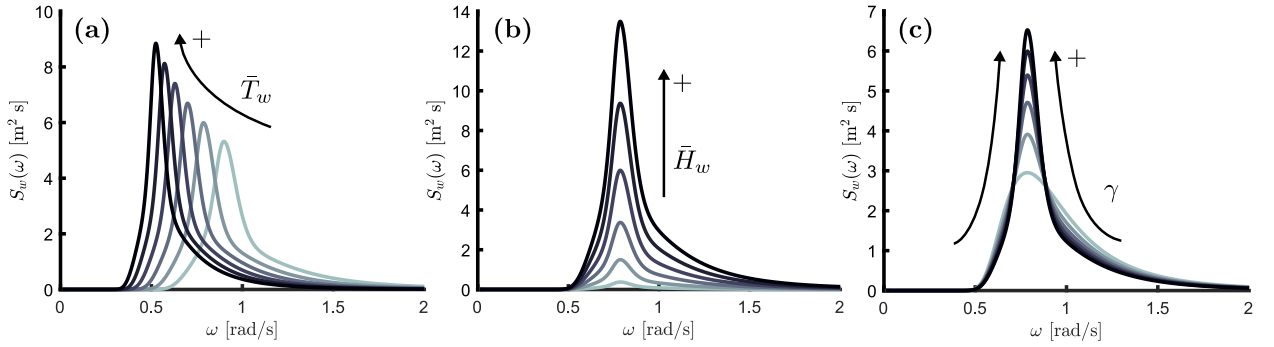


Figure 2.3: Different characterisation of ocean waves in terms of a JONSWAP SDF. Figure **(a)**: $\bar{H}_w = 2$ [m], $\gamma = 3$ and $\bar{T}_w \in [7, 12]$ [s]. Figure **(b)**: $\bar{T}_w = 8$ [s], $\gamma = 3$ and $\bar{H}_w \in [0.5, 3]$ [m]. Figure **(c)**: $\bar{H}_w = 2$ [m], $\bar{T}_w = 8$ [s] and $\gamma \in [1, 3.5]$. The arrows indicate the increasing direction of the corresponding parameter.

Remark 2.1.3 A well-known hypothesis, utilised in the *numerical* generation of ocean waves (which are described by a given SDF S_w), is to assume that, for a fixed point in space x^* , the free-surface elevation can be described as a finite sum of harmonics of a (sufficiently small) fundamental frequency $\omega_0 \in \mathbb{R}^+$. More precisely, we can write

$$\eta(t) = \sum_{p=1}^P \alpha_p \cos(p\omega_0 t) + \beta_p \sin(p\omega_0 t), \quad (2.4)$$

where $P \in \mathbb{N}_{\geq 1}$, and the set of *amplitudes* $\{\alpha_p, \beta_p\}_{p=1}^P \subset \mathbb{R}$ is determined *randomly*⁵, in accordance to the stochastic process described by S_w . This procedure is schematically illustrated in Figure 2.4.

4: After analysing data collected during the Joint North Sea Wave Observation Project JONSWAP, the authors of [33] found that the corresponding wave spectrum was never fully developed, but it rather continues to develop even for long times and distances. This factor γ is added to the Pierson-Moskowitz spectrum, aiming to improve the fit with respect to their measurements.

5: The reader is referred to [36] for further detail on methods to numerically generate a physically representative description of $\eta(t)$.

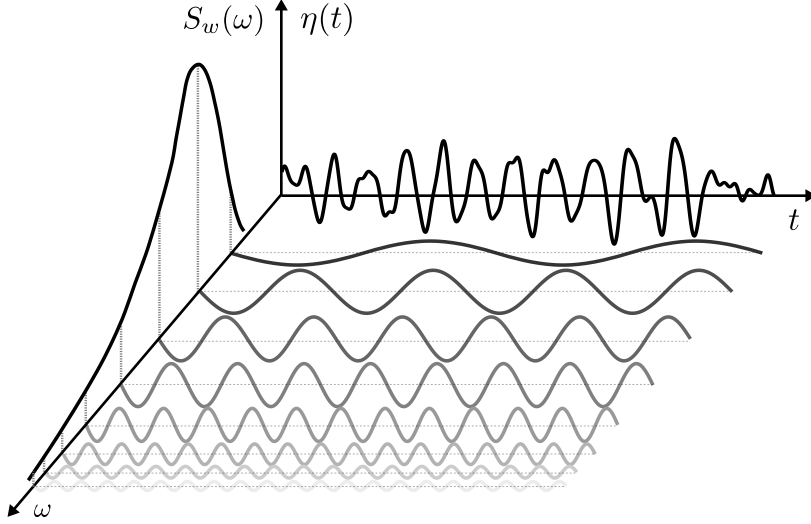


Figure 2.4: Generation of numerical waves as superposition of harmonics, *i.e.* superposition of regular waves.

To finalise this section on ocean waves, and aiming to illustrate the difference between regular and irregular representations, Figure 2.5 shows time-traces of the free-surface elevation for a regular wave (generated as in Remark 2.1.2), with $H_w = 2$ [m] and $T_w = 8$ [s], and an irregular wave, generated from a JONSWAP spectrum (as in Remark 2.1.3), with $\bar{H}_w = 2$ [m], $\bar{T}_w = 8$ [s] and $\gamma = 3$.

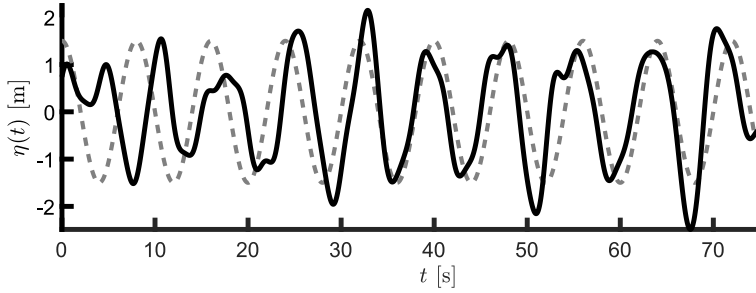


Figure 2.5: Time-traces of the free-surface elevation for a regular wave (dashed-grey) with $H_w = 2$ [m] and $T_w = 8$ [s], and an irregular wave (solid-black) generated from a JONSWAP spectrum, with $\bar{H}_w = 2$ [m], $\bar{T}_w = 8$ [s] and $\gamma = 3$.

2.2 Conservation of mass and momentum: the Navier-Stokes equations

The *Navier-Stokes* equations arise from the conservation of mass and momentum laws, and describe the motion of a fluid (or interaction between fluid and a solid structure) in space, *i.e.* in \mathbb{R}^3 . This set of equations is solved for an unknown velocity mapping $v : \mathbb{R}^3 \times \mathbb{R}^+ \rightarrow \mathbb{R}^3$, $(x, t) \mapsto v(x, t)$ and pressure $p : \mathbb{R}^3 \times \mathbb{R}^+ \rightarrow \mathbb{R}$, $(x, t) \mapsto p(x, t)$, defined for position in space $x \in \mathbb{R}^3$ and $t \in \mathbb{R}^+$. In particular, for an incompressible fluid, these equations [37] are

$$\begin{aligned} \frac{\partial v_i}{\partial t} + \sum_{j=1}^3 v_j \frac{\partial v_i}{\partial x_j} &= \nu \Delta v_i - \frac{\partial p}{\partial x_i} + f_i(x, t), \\ \operatorname{div}\{v\} &= \sum_{i=1}^3 \frac{\partial v_i}{\partial x_i} = 0, \end{aligned} \quad (2.5)$$

with initial condition $v(x, 0) = v_0(x)$, where v_0 is a given \mathcal{C}^∞ divergence-free vector field on \mathbb{R}^3 , $f_i(x, t)$ are the components of the (total) externally applied force (e.g. gravity), $\nu \in \mathbb{R}^+$ is the kinematic viscosity, and the operator $\Delta : \mathbb{R}^3 \rightarrow \mathbb{R}$ denotes the Laplacian in the space variables.

Remark 2.2.1 The first equation in (2.5) is Newton's second law for a fluid element subject to the external force f , and to the forces arising from both pressure and friction. The second equation in (2.5) arises from the conservation of mass principle for an incompressible fluid.

Remark 2.2.2 A set of solution mappings $\{v, p\}$ is said to be physically *reasonable* [37] if $\{v, p\} \subset \mathcal{C}^\infty(\mathbb{R}^3 \times \mathbb{R}^+)$ and $\int_{\mathbb{R}^3} |v(x, t)|^2 < +\infty, \forall t \in \mathbb{R}^+$ (bounded energy).

Though equation (2.5) provides a consistent physical and mathematical description of the motion of a fluid (or fluid-structure interaction), there is no closed-form expression for the solution mappings v and p (perhaps unsurprisingly, given the nature and complexity of such a partial differential equation). As a matter of fact, although these equations were written down in the 19th century, the formal understanding of them remains close to minimal: The problem of existence and smoothness of Navier-Stokes solutions is still an open mathematical problem, gathering much of the attention of the pure mathematics research community⁶.

A significant effort has been put in providing consistent numerical methods which directly attempt to numerically approximate the solutions of Navier-Stokes equation (2.5). As a matter of fact, this gave rise to the field of Computational Fluid Dynamics (CFD), where equations (2.5) are discretised both in space and time, using a variety of techniques [39, 40]. In particular, CFD can be utilised to simulate (at *great* computational expense) the hydrodynamic force acting on an object floating in water, allowing fully nonlinear hydrodynamic calculations, including effects neglected by traditional linear velocity potential theory (as described in Section 2.3), such as viscosity, large wave amplitude, large body motion, and vortex shedding.

Remark 2.2.3 Note that, although CFD can be a highly valuable tool for high-fidelity motion simulation of WECs, the computational expense of these methods, which is in the order of *thousands* of seconds per *second* of simulation [40], automatically prohibits their use in control synthesis and design procedures.

6: Existence and smoothness of (physically *reasonable*) Navier-Stokes solutions on \mathbb{R}^3 is currently one of the seven *Millennium problems* [38] listed by the Clay Mathematics Institute on May 24th, 2000.

2.3 Towards control-oriented models

Having presented both linear ocean wave theory, in Section 2.1, and Navier-Stokes equations, in Section 2.2, this section addresses control (or state-estimation)-oriented modelling of fluid-body interaction, *i.e.* the dynamics of a body subject to ocean waves. Given the theoretical (and practical) complexity behind Navier-Stokes equations (2.5), it is perhaps straightforward to realise that this mathematical description is far from being tractable for any implementable control design/state-estimation purposes (see Remark 2.2.3). In the light of this, some standing assumptions are virtually always adopted in the WEC control literature, aiming to provide a *tractable*⁷ dynamical operator to describe the motion of a body in a fluid, as depicted in Figure 2.6. In particular, these assumptions give rise to the so-called *Cummins' equation* [25], which constitutes a key operator for this thesis.

7: Tractable both in a theoretical (existence of unique solutions) and in a computational sense (real-time capabilities).

This set of assumptions is listed and discussed (to some extent) in the following paragraphs. Note that the aim of this section *is not* to provide a thorough derivation of Cummins' equation, but rather to establish the underlying mathematical and physical assumptions required to arrive at such a representation, aiming to provide a discussion of both its advantages and potential limitations. The interested reader can find a full (step-by-step) formal derivation elsewhere, in a plethora of books and dissertations. This includes, for instance, [26, 28, 41–43].

Remark 2.3.1 Note that an alternative path towards control-oriented models relies on tools from *system identification* [44]: Either CFD codes or real experimentation could be used to construct a set of (sufficiently representative) system outputs, for a specific class of inputs, to later construct control-oriented representations which describe the dynamics of a given WEC, using suitable model structures. This path is not pursued in this thesis, where underlying physical laws are always considered, which (virtually always) render the set of solutions proposed in Parts II and III *independent* of the particular device and input descriptions. The interested reader is referred to [41] for an extensive discussion on linear and nonlinear model structures for WECs, constructed from recorded data.

2.3.1 Linear potential flow theory

Motivated by the discussion provided in the previous paragraph, the following standing assumptions are considered from now on. These give origin to so-called *linear potential flow theory*.

Assumption 2.3.1 The flow is *frictionless* (inviscid), *i.e.* $\nu = 0$ in (2.5), and *irrotational*, *i.e.* flows with no vorticity.

Assumption 2.3.2 The amplitude of the body motion is significantly smaller than the dimension of the body.

Assumption 2.3.3 Linear wave theory (as described in Section 2.1) holds.

Assumption 2.3.1 guarantees that *potential flow theory* holds: The velocity mapping v , defined in (2.5), can always be described in terms of a *potential function* (or potential mapping) $\phi : \mathbb{R}^3 \times \mathbb{R}^+ \rightarrow \mathbb{R}$, $(x, t) \mapsto \phi(x, t)$ such that $v = \nabla\phi$, where $\nabla : \mathbb{R}^3 \rightarrow \mathbb{R}^3$ denotes the gradient operator. Moreover, this potential mapping ϕ obeys the *Laplace* equation, *i.e.* $\Delta\phi = 0$, as a consequence of the conservation of mass principle (see (2.5)). Naturally, under these assumptions, the velocity mapping v is completely characterised in terms of the potential function ϕ .

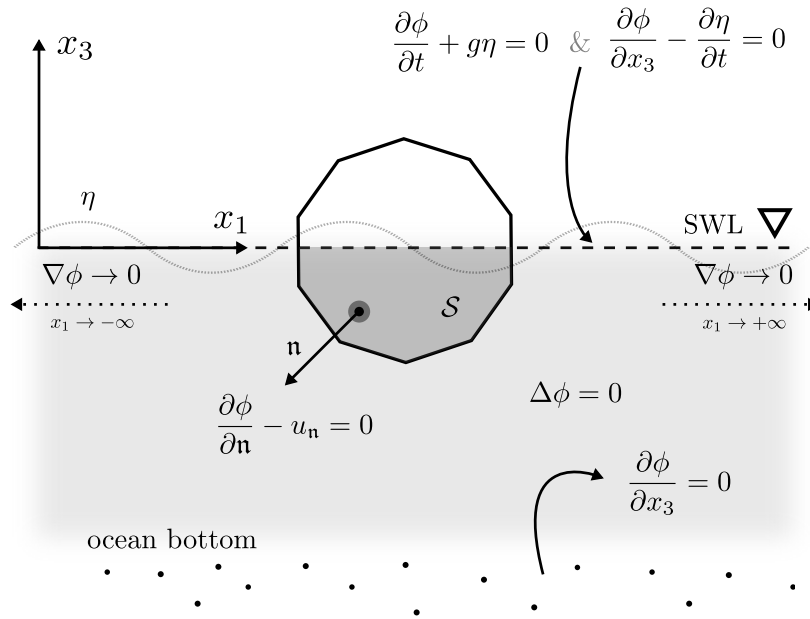


Figure 2.6: Graphical representation of linear potential flow theory.

Solving for ϕ requires the imposition of a set of appropriate boundary conditions on the solution. These are recalled here, for the *linear*⁸ potential flow theory case, *i.e.* under Assumptions 2.3.2 and 2.3.3.

- **Linear dynamic boundary condition:** At the undisturbed free-surface elevation, *i.e.* $x_3 = \eta(x_1, t) = 0$ the fluid pressure has to be equal to atmospheric pressure. Mathematically, the velocity potential has to satisfy

$$\frac{\partial\phi}{\partial t} + g\eta = 0, \quad (2.6)$$

at $x_3 = 0, \forall t \in \mathbb{R}^+$.

8: The nonlinear counterparts of the boundary conditions recalled in this section can be found in, for instance, [28, Chapter 20].

- *Linear kinematic boundary condition*: The fluid particles on the free-surface are assumed to stay in the free-surface for all $t \in \mathbb{R}^+$, i.e. the component of the fluid velocity normal to the surface *must* equal the surface velocity. This linearised condition can be expressed mathematically as

$$\frac{\partial \phi}{\partial x_3} - \frac{\partial \eta}{\partial t} = 0, \quad (2.7)$$

at $x_3 = 0, \forall t \in \mathbb{R}^+$.

- *Impermeability (body)*: The component of the fluid velocity normal to the body surface, $\partial \phi / \partial \mathbf{n}$, has to be equal to the body velocity normal to the body surface, u_n . To be precise, the velocity potential must verify

$$\frac{\partial \phi}{\partial \mathbf{n}} - u_n = 0, \quad (2.8)$$

for every normal vector \mathbf{n} defined on the surface \mathcal{S} .

- *Impermeability and flatness of the ocean bottom*: At a depth $x_3 = -h$, impermeability and flatness of the ocean bottom can be translated to the following boundary condition:

$$\frac{\partial \phi}{\partial x_3} = 0, \quad (2.9)$$

at $x_3 = -h, \forall t \in \mathbb{R}^+$.

- *Decaying amplitude of the wave field*: As the distance from the body increases, the following condition

$$\lim_{x_1 \rightarrow -\infty} \nabla \phi(x_1, t) = \lim_{x_1 \rightarrow +\infty} \nabla \phi(x_1, t) = 0, \quad (2.10)$$

holds $\forall t \in \mathbb{R}^+$.

The set of boundary conditions discussed above is illustrated, for both reference and clarity, in Figure 2.6. In particular, these conditions, together with the Laplace equation $v = \Delta \phi$, form the basis for a family of methods that numerically solve for the potential flow ϕ : the so-called *boundary element methods* (BEMs)⁹.

Remark 2.3.2 Within the ocean engineering community (including the field of wave energy theory and applications), a number of BEM codes have been developed to solve for ϕ , both in the time- and frequency-domains. The most common working codes are WAMIT [46], AQWA [47] (both commercial software), and NEMOH [48] (open-source software), which characterise the potential flow ϕ in the *frequency-domain*.

9: The reader is referred to, for example, [45], for a discussion on the mathematical foundations and range of applicability of BEMs.

Remark 2.3.3 Throughout this thesis, NEMOH is always utilised, motivated by its open-source characteristics.

2.3.2 Hydrodynamic effects in linear potential flow theory

Let the so-called *body-fixed* (local) frame of reference be defined by a coordinate vector $z \in \mathbb{R}^6$ (as in Figure 2.7), where z_1 , z_2 and z_3 represent body translations (*surge*, *sway* and *heave*), and z_4 , z_5 and z_6 body rotations (*roll*, *pitch* and *yaw*). From now on, it is assumed that the origin of this local frame is located at the center of mass of the system. Each one of these modes of motion are traditionally called *degrees-of-freedom* (DoF) of the system (which are six in the case of Figure 2.7).

Remark 2.3.4 Though the dynamic effects described in the following paragraphs are always derived considering 6 DoFs, one can straightforwardly “reduce” the formulation to a lower-dimensional space, to consider a smaller number of modes of motion¹⁰.

Remark 2.3.5 Modelling arrays of bodies, *i.e.* multiple devices interacting in the water, can be done analogously to the multiple-DoF case discussed in this section, in an (almost) straightforward manner [49]. Though arrays are not specifically treated in the following paragraphs, a more detailed discussion on this topic is provided in Chapters 6 and 9 of this thesis, where wave energy arrays are effectively considered, both for moment-based model reduction, and optimal control procedures, respectively.

Let $M \in \mathbb{R}^{6 \times 6}$ be the *generalised* mass-inertia matrix defined as

$$M = (m \otimes \mathbb{I}_3) \oplus I, \quad (2.11)$$

where $m \in \mathbb{R}^+$ is the mass of the floating body, and the matrix $I \in \mathbb{R}^{3 \times 3}$ contains the corresponding moments of inertia associated with the rotational modes of motion of the system. Under the same set of assumptions considered in Section 2.3.1, *i.e.* within the framework of linear potential flow theory (schematically illustrated in Figure 2.6), one can write the equation of motion for a floating body, following Newton's second law, as¹¹

$$M\ddot{z} = f_e(\eta) + f_r(\dot{z}) + f_{re}(z) + f_{ext}(z, \dot{z}, t), \quad (2.12)$$

where $z : \mathbb{R}^+ \rightarrow \mathbb{R}^6$, $t \mapsto z(t)$, denotes the displacement vector of the body as a function of time, $f_e : \mathbb{R} \rightarrow \mathbb{R}^6$ the *wave excitation* effect, $f_r : \mathbb{R}^6 \rightarrow \mathbb{R}^6$ the *radiation* effect, $f_{re} : \mathbb{R}^6 \rightarrow \mathbb{R}^6$ the

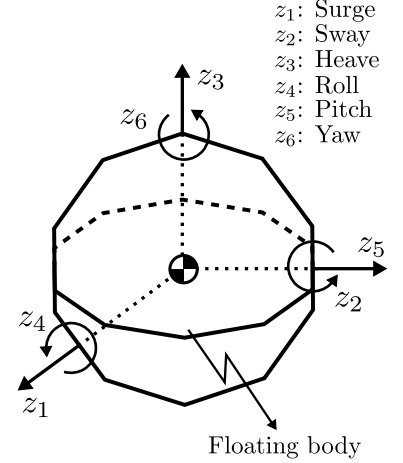


Figure 2.7: Body-fixed (local) coordinate system, in terms of $z \in \mathbb{R}^6$. The symbol \odot denotes the center of mass of the body.

10: This can be especially useful in wave energy control, where the dominant dynamics potentially take place at a single mode of motion, *i.e.* the DoF from where energy is extracted, and the control law is applied.

11: From now on, the dependence on t is dropped when it is clear from the context.

hydrostatic restoring effect, and finally $f_{ext} : \mathbb{R}^6 \times \mathbb{R}^6 \times \mathbb{R}^+ \rightarrow \mathbb{R}^6$ represents the sum of additional external loads, in the more general case (e.g. mooring effects and control input). Over the next paragraphs, the *hydrodynamic* effects listed above, i.e. f_e , f_r and f_{re} , are discussed in detail.

Remark 2.3.6 From now on, and aiming to simplify the notation used throughout this thesis, the term *force* is used to denote hydrodynamic effects taking place in either translational (i.e. forces), or rotational (i.e. torques) DoFs.

2.3.2.1 Wave excitation effects

The *wave excitation*, f_e , is defined as the force acting on the body when it is held fixed in the presence of waves. In the context of linear potential flow theory (i.e. under the set of assumptions of Section 2.3.1), the excitation force is the superposition of the so-called *Froude-Krylov* force¹², and diffraction effects [42], where the Froude-Krylov force is obtained by integrating the pressure, due to the undisturbed incident wave field, over the mean wetted surface of the fixed body. Therefore, the Froude-Krylov effect can be considered as the result of the interaction between waves and a “ghost” body, which feels and reacts to the incident wave field, but does not alter it [42].

Under the effects of Assumption 2.3.2, the diffraction force is not significant compared to the Froude-Krylov effect [42], indicating that the latter effectively constitutes a reasonable approximation of the incident wave excitation [41]. The mapping that characterises f_e , can be formally written, as a function of time, as

$$f_e(t) = \int_{\mathbb{R}} k_e(\tau) \eta(t - \tau) d\tau, \quad (2.13)$$

where the vector $k_e(t) = \sum_{i=1}^6 e_i^6 \otimes k_{e_i}(t) \in \mathbb{R}^6$, with each mapping $k_{e_i} : \mathbb{R} \rightarrow \mathbb{R}$, $k_i \in L^2(\mathbb{R})$, $\forall i \in \mathbb{N}_6$, is the *excitation impulse response function*, and η is the free-surface elevation (according to Airy's wave theory) at the location of the centre of mass of the device.

Remark 2.3.7 A direct interpretation of equation (2.13) yields that the excitation force, f_e , is essentially a filtered version of the free-surface elevation η , i.e. is the output of a linear dynamical system completely characterised by the impulse response function k_e , with η as its input.

12: In this thesis, the excitation force only takes into account the so-called *dynamic* part of the Froude-Krylov force: The excitation f_e is zero in the absence of incident waves. The reader is referred to [42] for a thorough discussion on Froude-Krylov effects.

Remark 2.3.8 The mapping k_e is geometry-dependent, *i.e.* the excitation force experienced by the device naturally depends on the device shape itself.

Though the excitation effect, defined as in (2.13), is conveniently expressed as a linear operator, the impulse response function k_e has one main peculiarity: it is, in general, a non-causal function of t . In other words, future knowledge of the free-surface elevation is required to compute the corresponding wave excitation exerted on the device, for each of the modes of motion (DoFs) involved.

Remark 2.3.9 The non-causal relation $\eta \mapsto f_e$ can be intuitively understood in the case where the impulse response mapping is defined with respect to a point placed at the centre of the body (as in Figure 2.7): The system will effectively experience a force, even before the wave crest has arrived to the body centre [42]¹³.

Remark 2.3.10 The computation of the impulse response mapping k_e can be readily performed using BEM codes, as a function of the potential flow ϕ . If frequency-domain BEMs are utilised (such as WAMIT or NEMOH), the frequency-domain equivalent of k_e is available, *i.e.* $K_e : \mathbb{R} \rightarrow \mathbb{C}^6$, $\omega \mapsto K_e(\omega)$. To show a specific example of this frequency-domain characterisation, Figure 2.8 illustrates real and imaginary parts of $K_e(\omega)$ (centre), for a 1-DoF sphere of radius $r = 2.5$ [m], constrained to move in heave (translational motion z_3).

13: This holds also true if η is considered in a location on the upstream side, or even outside of the body itself. The interested reader is referred to [50] for further detail on the nature of this non-causal behaviour.

2.3.2.2 Radiation effects

The hydrodynamic force applied from the fluid to the body in the absence of incident waves, is called the *radiation force*. Under the framework of linear potential flow theory, the body motion generates a time-changing fluid pressure, which is integrated over a constant surface (\mathcal{S} in Figure 2.6), creating a time-dependent radiation force f_r , given, for $t \in \mathbb{R}^+$, by the expression

$$f_r(t) = -m_\infty \ddot{z}(t) - \int_{\mathbb{R}^+} k_r(\tau) \dot{z}(t - \tau) d\tau, \quad (2.14)$$

where the matrix $k_r(t) = \sum_{i=1}^6 \sum_{j=1}^6 e_{ij}^6 \otimes k_{r_{ij}}(t) \in \mathbb{R}^{6 \times 6}$, with each mapping $k_{r_{ij}} : \mathbb{R}^+ \rightarrow \mathbb{R}$, $k_{r_{ij}} \in L^2(\mathbb{R})$, $\forall \{i, j\} \subset \mathbb{N}_6$, is the (*causal*) *radiation impulse response function*, containing the memory effects associated with the fluid response, and $m_\infty = \lim_{\omega \rightarrow +\infty} A_r(\omega) \in \mathbb{R}^{6 \times 6}$, where $A_r : \mathbb{R} \rightarrow \mathbb{R}^{6 \times 6}$ is the *radiation*

added-mass (also called *radiation reactance*), defined as

$$A_r(\omega) = m_\infty - \frac{1}{\omega} \int_{\mathbb{R}^+} k_r(t) \sin(\omega t) dt. \quad (2.15)$$

Remark 2.3.11 Note that the impulse response function k_r effectively constitutes a hydrodynamic coupling between different modes of motion. In other words, the waves radiated by each DoF affect the overall dynamics of both translational and rotational motions of the device.

The non-parametric term $A_r(\omega)$, together with the so-called *radiation damping* (also called *radiation resistance*) $B_r : \mathbb{R} \rightarrow \mathbb{R}^{6 \times 6}$, given by

$$B_r(\omega) = \int_{\mathbb{R}^+} k_r(t) \cos(\omega t) dt, \quad (2.16)$$

fully characterise the (well-defined) Fourier transform of k_r , *i.e.* we can write $K_r : \mathbb{R} \rightarrow \mathbb{C}^{6 \times 6}$ as

$$K_r(\omega) = B_r(\omega) + j\omega [A_r(\omega) - m_\infty]. \quad (2.17)$$

In particular, radiation damping describes the dissipative effect of the energy transmitted from the oscillating body to the waves (*i.e.* the waves propagate away from the body). The radiation added-mass represents the additional inertial effect due to the acceleration of the water, which moves together with the body. Equations (2.15) and (2.16) are commonly referred to as *Ogilvie's relations* [51], and they stem from the definition of the Fourier transform.

Remark 2.3.12 As in the case of the wave excitation impulse response k_e , the mapping k_r is effectively geometry-dependent. The computation of k_r is also performed, using BEM codes, in the frequency-domain, where the hydrodynamic coefficients $A_r(\omega)$ and $B_r(\omega)$ are fully-characterised by the potential flow ϕ . To show a specific example of this frequency-domain characterisation, Figure 2.8 illustrates $B_r(\omega)$ and $A_r(\omega)$ (right), for a 1-DoF sphere of radius $r = 2.5$ [m], constrained to move in heave (translational motion z_3).

Remark 2.3.13 The radiation impulse response function, k_r , has a set of well-known properties, which have a direct impact on the definition, formulation, and computation of control-oriented models. These are recalled in Table 2.1, and discussed in detail in Section 2.4, together with an assessment of their impact in control-oriented modelling.

Property 1	$\lim_{t \rightarrow +\infty} k_r(t) = 0$
Property 2	$\dot{z} \mapsto k_r * \dot{z}$ is passive
Property 3	$\lim_{\omega \rightarrow 0} K_r(\omega) = 0$
Property 4	$\lim_{\omega \rightarrow +\infty} K_r(\omega) = 0$

Table 2.1: Dynamical properties associated with the radiation impulse response k_r .

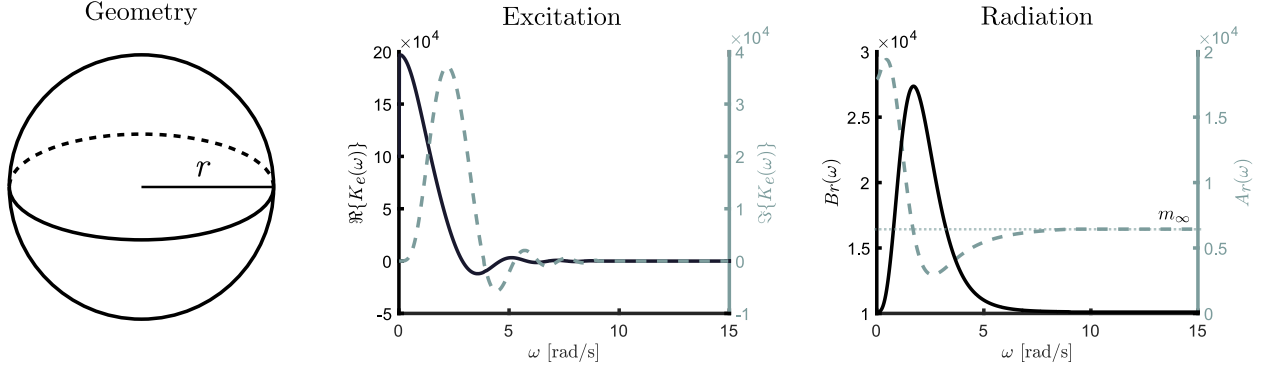


Figure 2.8: Hydrodynamic characterisation of a 1-DoF sphere with $r = 2.5$ [m], constrained to move in heave (translational motion z_3). This figure includes: Body geometry (left), frequency-domain excitation effects (centre) and frequency-domain radiation effects (right). The totality of these frequency-dependent parameters have been computed with the open-source software NEMOH.

2.3.2.3 Restoring effects

The hydrostatic restoring force, f_{re} , arises from the mismatch between the gravitational and buoyancy forces. To be precise, given a motionless floating body, the latter represents the hydrostatic force applied from the water to the body, by integration of the static pressure over the wetted surface \mathcal{S} (see Figure 2.6). For this linear potential theory case, it follows that:

$$f_{re}(t) = -s_h z(t), \quad (2.18)$$

where $s_h \in \mathbb{R}^{6 \times 6}$ is a constant matrix, commonly referred to as the *restoring coefficient matrix*.

2.4 Cummins' equation and state-space modelling

Recall equation (2.12), and each one of the hydrodynamic forces described in Section 2.3.2. The motion of a floating body, *i.e.* a WEC for the case of this thesis, under the assumptions of linear potential theory, can be expressed in terms of a system Σ , described by the set of equations

$$\Sigma : \begin{cases} \ddot{z} = (M + m_\infty)^{-1} (-k_r * \dot{z} - s_h z + k_e * \eta + f_{ext}), \\ y = \dot{z}, \end{cases} \quad (2.19)$$

where the impulse response mappings k_r and k_e are fully characterised using BEM codes. This non-parametric equation is widely known as *Cummins' equation* [25], and belongs to the family of *Volterra* integro-differential equations of the convolution class¹⁴.

¹⁴: The interested reader is referred to [52] for a thorough discussion on this type of operator.

Remark 2.4.1 Note that, without any loss of generality, the output y is set to be the velocity vector associated with the motion of the device \dot{z} , in line with the energy-maximising optimal control problem for WECs, defined in Chapter 3.

Aiming to describe the hydrodynamic effects involved in equation (2.19), let $f_{ext} = 0, \forall t \in \mathbb{R}^+$, for the remainder of this section. In addition, note that the term describing the wave excitation effect in equation (2.19), *i.e.* $f_e = k_e * \eta$, *does not* depend on the internal variables describing the motion of the device (displacement, velocity and acceleration). From a system dynamics perspective, the excitation force can be considered as an external input to the system, as depicted in Figure 2.9, and only depends on the free-surface elevation η . Summarising, from now on, one can write

$$\Sigma : \begin{cases} \ddot{z} = \mathcal{M}(-k_r * \dot{z} - s_h z + f_e), \\ y = \dot{z}, \end{cases} \quad (2.20)$$

where $\mathcal{M} = (M + m_\infty)^{-1}$ is the inverse of the generalised mass matrix of the device. Note that $0 \notin \lambda(\mathcal{M})$ [53] so that the inverse of the mass matrix is always well-defined.

Remark 2.4.2 The numerical generation of wave excitation can be simply performed by applying a filtering action to the generated free-surface elevation η . To be precise, η is generated according to a spectral density function S_w (as in Section 2.1.2), to then compute the corresponding convolution operation with the impulse response function k_e , directly obtaining f_e .

Remark 2.4.3 From now on, we refer to the system Σ , defined in (2.20), as the non-parametric *force-to-motion* representation of the device.

Remark 2.4.4 The internal stability of (2.20) is guaranteed, in the Lyapunov sense, for any physically meaningful parameters and impulse response mapping k_r involved. The proof of this statement can be found in [53], and relies on the passivity property of radiation effects, *i.e.* the passivity of the mapping $\dot{z} \mapsto k_r * \dot{z}$ (see Table 2.1).

Equation (2.20) still contains one non-parametric operator, characterising the radiation forces associated with the fluid memory effects. The mere existence of this non-parametric convolution term represents a drawback for most wave energy applications, including motion simulation, optimal control, and wave excitation force estimation theory perspectives. From a pure simulation point of view, it is well-known that the explicit computation of the convolution operator is computationally inefficient, often worsened both by the

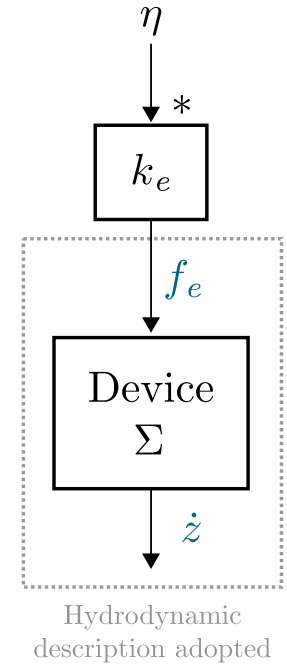


Figure 2.9: Hydrodynamic input-output structure adopted throughout this thesis.

necessity of a small (time) discretisation step to obtain accurate numerical integration¹⁵, and the number of degrees-of-freedom considered. Concerning modern control/state-estimation techniques, their design is virtually always based on the availability of a state-space description (*i.e.* a set of first-order differential equations) of the system under analysis. As a matter of fact, the vast majority of the optimal control/state-estimation techniques considered in wave energy, which are utilised to maximise the energy absorption of WECs, require a state-space representation for the differential operator describing the motion of the device (see Chapter 3).

The most-widely considered solution path, which aims to construct a state-space representation of the input-output system Σ in (2.20), involves the computation of an approximation $\tilde{\Sigma}_r$ of the *radiation* linear-time invariant system Σ_r , fully characterised by the impulse response mapping k_r , *i.e.* a system with input \dot{z} (velocity) and output $y_r = k_r * \dot{z}$.

Remark 2.4.5 Though Σ_r naturally exists, its exact representation is unknown, given the non-parametric nature of the impulse response function k_r , computed with BEM codes. In other words, the relationship between the solution of the linear potential flow boundary value problem (described in Section 2.3.1), and radiation effects, is *always* non-parametric.

The underpinning idea is then to compute an approximating system $\tilde{\Sigma}_r$ in terms of a continuous-time, *finite-dimensional* state-space system, using the information provided by BEM codes, either in the frequency- or the time-domain¹⁶.

Remark 2.4.6 Throughout this thesis, the process of determining a finite-order dynamical model from either time- or frequency-domain data points, is termed *model order reduction* (or simply *model reduction*). This is motivated by the fact that the target non-parametric terms involved, fully arise as a direct biproduct of linear potential flow theory, *i.e.* they specifically respond to a physical law with origins in Navier-Stokes theory, and there is no ‘experimentation’ involved in their determination. In other words, one starts with a defined operator (*i.e.* equation (2.20)), and attempts to ‘reduce it’ by parameterising this model into a tractable form. Nevertheless, note that, if the physical origin of these terms is ignored, this process can be alternatively referred to as *data-driven model reduction*¹⁷ or *system identification*, depending on the context [44] (see also Remark 2.3.1).

15: Even though several algorithms have been proposed to alleviate the computational complexity associated to convolution operations, this still remains as an active area of research and is an open topic [54].

16: This naturally involves the definition of an *error* criterion, which attempts to quantify the difference between the non-parametric system defined by k_r , and the approximating state-space representation $\tilde{\Sigma}_r$. This is discussed further in Section 2.6

17: Where the starting model ‘order’ is effectively the number of frequency/time domain data points available.

To be precise, let $\tilde{\Sigma}_r$ be an approximation of the radiation system of dimension (order) $n_r \in \mathbb{N}_{\geq 1}$, given in state-space form, for $t \in \mathbb{R}^+$, as

$$\tilde{\Sigma}_r : \begin{cases} \dot{\Theta} = F\Theta + G\dot{z}, \\ \tilde{y}_r = Q\Theta + E\dot{z} \approx k_r * \dot{z}, \end{cases} \quad (2.21)$$

where the matrices (F, G, Q, E) are such that $F \in \mathbb{R}^{n_r \times n_r}$, $G \in \mathbb{R}^{n_r \times n}$, $Q \in \mathbb{R}^{n_r \times n_r}$ and $E \in \mathbb{R}^{n_r \times n}$, and n is the number of DoF considered for the device under analysis.

To be physically consistent, any system $\tilde{\Sigma}_r$ approximating the radiation convolution operator, should fulfil the dynamical properties listed in Table 2.1. A discussion on the specific impact of each property in the nature of the state-space formulation (2.21), is provided below (listed in the same order as in Table 2.1). These properties are specifically considered in both Parts II and III of this thesis.

- **Property 1:** Let $\tilde{K}_r : \mathbb{C} \rightarrow \mathbb{C}^{n \times n}$, $s \mapsto \tilde{K}_r(s)$, be the transfer function associated with the approximating system $\tilde{\Sigma}_r$. Then, the set of poles of $\tilde{K}_r(s)$ is always contained in $\mathbb{C}_{<0}$, i.e. system $\tilde{\Sigma}_r$ is bounded-input bounded-output (BIBO) stable.
- **Property 2:** The complex (transfer) function \tilde{K}_r is *positive-real*. For LTI systems, \tilde{K}_r is positive-real if and only if
 - Property 1 holds and
 - The matrix $\tilde{K}_r(\omega) + \tilde{K}_r^*(\omega)$ is positive-definite, $\forall \omega \in \mathbb{R}/0$.
- **Property 3:** $\tilde{K}_r(s)$ has zeros at $s = 0$.
- **Property 4:** $\tilde{\Sigma}_r$ is *strictly proper*, i.e. the feed-through matrix E in (2.21) is identically zero.

Finally, once this suitable approximation is found, obtaining a state-space representation of (2.20) becomes straightforward. Generally speaking, suppose one considers a device moving in n degrees-of-freedom. Equation (2.20) can be approximately represented, for $t \in \mathbb{R}^+$, by a linear time-invariant (LTI) system $\tilde{\Sigma}$ described in state-space as,

$$\tilde{\Sigma} : \begin{cases} \begin{bmatrix} \dot{w} \\ \dot{\Theta} \end{bmatrix} = \begin{bmatrix} A & -BQ \\ GC & F \end{bmatrix} \begin{bmatrix} w \\ \Theta \end{bmatrix} + \begin{bmatrix} B \\ 0 \end{bmatrix} f_e, \\ \tilde{y} = \begin{bmatrix} C & 0 \end{bmatrix} \begin{bmatrix} w \\ \Theta \end{bmatrix} \approx \dot{z}, \end{cases} \quad (2.22)$$

where the state-vector $w = \sum_{i=1}^n e_i^n \otimes [z_i \ \dot{z}_i]^T \in \mathbb{R}^{2n}$ contains displacement and velocities for each DoF involved, and the matrices

$A \in \mathbb{R}^{2n \times 2n}$, $B \in \mathbb{R}^{2n}$ and $C^T \in \mathbb{R}^{2n}$ are defined as

$$\begin{aligned} A &= \sum_{i=1}^n \sum_{j=1}^n e_{ij}^n \otimes \begin{bmatrix} 0 & {}^i_j \delta \\ -\mathcal{M}_{ij} s_{h_i} & 0 \end{bmatrix}, \\ B &= \sum_{i=1}^n \sum_{j=1}^n e_{ij}^n \otimes \begin{bmatrix} 0 \\ \mathcal{M}_{ij} \end{bmatrix}, \\ C &= \mathbb{I}_n \otimes [0 \ 1], \end{aligned} \quad (2.23)$$

where \mathcal{M}_{ij} is the ij -th entry of the inverse generalised mass-inertia matrix $\mathcal{M} = (M + m_\infty)^{-1}$. Note that the radiation state-vector Θ , and the set of matrices (F, G, Q) , are defined as in (2.21).

An alternative route consists of attempting to parameterise system Σ , defined in (2.20), by a reduced model $\tilde{\Sigma}$ directly, *i.e.* from an input-output (force-to-motion) perspective. In this case, the physical notion of each component of the state vector is somewhat lost, though, naturally, the outputs still represent physical variables. Even though this approach is usually not considered in the wave energy control literature (ostensibly because the model becomes more ‘abstract’), it indeed provides some advantages, as discussed in Section 2.6.

2.5 Nonlinear extensions to Cummins’ formulation

Cummins’ equation (2.20), which is a direct product of linear potential flow theory, can lose fidelity when Assumptions 2.3.2 or 2.3.3 do not hold, *i.e.* either the wave amplitude or body displacement increase significantly. The violation of these assumptions introduce nonlinear hydrodynamic effects, and the linear behaviour described by (2.20) can potentially lose fidelity.

Remark 2.5.1 This is specifically relevant for devices under controlled conditions, where the energy-maximising control objective normally requires large displacements and velocities to increase power absorption, as discussed in Chapter 3.

Aiming to alleviate the impact of Assumptions 2.3.2 and 2.3.3, and recognising the essential suitability of the structure provided by Cummins, researchers often ‘extend’ the operational space of equation (2.20), by the incorporation of a number of nonlinear functions, which attempt to narrow the gap between linear potential flow theory and the ‘realistic’ behaviour of the floating body (*i.e.* Navier-Stokes equations (2.5)). The most-utilised nonlinear mappings, within the wave energy control community, are discussed in the following paragraphs¹⁸.

18: Note that other nonlinear hydrodynamic effects have also been considered outside the scope of optimal control applications, including, for example, nonlinear Froude-Krylov effects [42], and nonlinear radiation representations [55].

Remark 2.5.2 Depending on the shape of the WEC, the sea conditions, and the external inputs considered (e.g. control law), not all the nonlinear terms listed in this section may be significant and, hence, necessary in the modelling process. Therefore, it is convenient to use caution in introducing nonlinearities, since a significant increase in both theoretical and computational complexity may be added to the dynamical model, potentially rendering control strategies ill-posed/unsuitable for realistic applications.

Remark 2.5.3 Additional (nonlinear) external forces, such as mooring effects and non-ideal PTO behaviour, can also be added to Cummins' equation, via the mapping f_{ext} defined in (2.19). These are discussed, within the framework of energy-maximising control strategies, in Chapter 3.

2.5.1 Nonlinear restoring effects

The linearity of the restoring term, expressed in equation (2.18), can cease to be a representative expression for the restoring effect, under large (amplitude) body oscillations. To be precise, if the device has a constant cross-sectional area with respect to the displacement of the body, the restoring force is *always* linear, and can be expressed as in (2.18). If this is not the case, and the cross-sectional area changes with the corresponding displacement, the relationship between f_{re} and z is effectively nonlinear, *i.e.* it can be expressed as

$$f_{re}(z) = -s_h z + f_{re}^{nl}(z), \quad (2.24)$$

where f_{re}^{nl} is a static nonlinear mapping, and its definition always depends on the geometry of the body (WEC). Example cases of control studies, that consider this type of nonlinear effect, are [56] and [57].

2.5.2 Nonlinear viscous drag effects

The viscous force, generated by shear stress, is not present in Cummins' equation (2.20). Omitting these effects may lead to unrealistic prediction of the device response, *i.e.* excessive displacement amplitudes and velocities. Commonly, an additional viscous term, f_v , is added to (2.20), in terms of the so-called *Morison-like* equation [58], which describes the force applied to a submerged body by an oscillatory flow. Mathematically, the mapping f_v is given by

$$f_v(\dot{z}) = \frac{1}{2} \rho C_d A_c \dot{z} |\dot{z}|, \quad (2.25)$$

where ρ denotes the fluid density, C_d is the so-called *viscous drag coefficient*, and A_c is the characteristic area of the body. This characterisation of viscous effects has been used within the framework of energy-maximising control studies in, for instance, [59] and [57].

Remark 2.5.4 The determination of the coefficient C_d in (2.25) is far from being trivial: Much inconsistency and uncertainty can be found in the literature, both concerning the value itself, and the identification methods considered to compute such a value. Indeed, drag identification for wave energy applications is particularly challenging, mainly due to the dependence on device dimensions, characteristic flow regimes and large motions. The reader is referred to [42, Chapter 7] and [18] for further discussion on this topic.

2.6 Model reduction: state-of-the-art

After introducing control-oriented modelling, and the intrinsic necessity of suitable model reduction strategies, this section provides a review of the state-of-the-art model reduction techniques considered within the wave energy field¹⁹. To do this in a precise manner, a clear distinction has to be made at this point, in terms of the nature of the non-parametric system involved. In particular, this section is divided in *two* different parts: *Linear* and *nonlinear* model reduction.

The former involves the parameterisation of the linear Cummins' equation (2.20), *i.e.* expressing the input-output dynamics of the device under analysis in a suitable state-space representation. The latter refers to nonlinear model reduction, both in terms of model *order* and model *complexity*: In other words, techniques aiming not only to express Cummins' equation in state-space form, but also to *simplify* the nonlinear operator used to describe the device dynamics.

Remark 2.6.1 Note that Jacobian linearisation is excluded from this latter section, *i.e.* the reduced representation is still assumed to be of a nonlinear nature.

¹⁹: Note that this section *does not* constitute a review in the theory of (general) model reduction, but rather reviews the type of techniques currently employed in WEC control/state-estimation applications. The reader is referred to [60] for a discussion on the state-of-the-art of model reduction techniques, for a generic type of differential operator.

2.6.1 Linear strategies

For the linear model reduction case, *i.e.* expressing equation (2.20) in state-space form, several methods have been proposed in the literature, to approximate the radiation convolution term in terms of

a LTI state-space representation (as described in Section 2.4). This section reviews the most-used strategies within the wave energy field (mostly which are adopted from the marine engineering community). Note that studies that also provide a review on these multiple approximation methods include [61] and [62] (exclusive to the marine and ocean engineering areas), and [63] (wave energy field). These methodologies can be clearly divided into two broad categories: *time-domain* and *frequency-domain* methods. A discussion on both approaches is given in the following.

Remark 2.6.2 Normally, the use of either time- or frequency-domain based methods is strongly linked to the nature of the BEM code utilised to compute the hydrodynamic characteristics of the device (see Remark 2.3.2). In other words, the computation of the hydrodynamic parameters, and the model reduction process, are normally performed in the *same domain*.

2.6.1.1 Time-domain methods

Time-domain methods directly use the impulse response data k_r , which is usually generated either via time-domain BEMs or via inverse Fourier transformation of the frequency-domain data computed by frequency-domain based BEMs²⁰. Key studies in this field, that propose a time-domain formulation to obtain a state-space representation of the radiation convolution term, include [50], [64] and [65].

The pioneering study [50] proposes an approximation method for a vertical cylinder, constrained to oscillate in heave, *i.e.* single DoF device (SISO system). The method is based on a weighted least-squares fitting of the impulse response function k_r , where a set of fixed parameters, describing the state-space matrices (F, G, Q) (see equation (2.21)) in an observer canonical form, is involved in the optimisation process. Neither stability nor passivity of the radiation system are guaranteed by this method, though, naturally, for the application case provided, the computed model is effectively stable (passivity is not discussed).

[64] also uses a least-squares impulse response fitting, but adding some features to the original formulation presented by [50]. In particular, stability is enforced by ‘flipping’ any unstable poles in the complex plane (*i.e.* symmetrising poles with positive real part with respect to the imaginary axis). This practice is, in general, not acceptable within wave energy control applications: Though the radiation damping $B_r(\omega)$ of the ‘flipped’ system (*i.e.* the real part of the frequency-response) stays the same, the added-mass (*i.e.* the

20: This methodology is considered mainly due to the computational effort required to compute the time-domain response directly [63].

imaginary-part) is effectively altered, which results in a significant change in phase response²¹. Passivity is also enforced in [64], using a perturbation approach, *i.e.* introducing minor modifications to the identified system, until a passive system is obtained. Though its simplicity might be appealing at a first glance, this method relies on having minor passivity violations in the first place, which is naturally not guaranteed by the impulse response fitting method, so that it is not clear under which conditions this perturbation approach works.

The authors of [65] propose the use of the method initially introduced by [66]. In particular, this method is based on a singular value decomposition (SVD) of the Hankel matrix²² associated with the (discrete-time) impulse response data $k_r(t_j)$, with $j \in \mathbb{N}_J$, where J is the number of available samples of k_r (*i.e.* the *Markov* parameters of the system). Once the parameters of the discrete-time model have been obtained, the continuous-time equivalent is normally computed using the bilinear transformation [68]. Though the method proposed in [65] can effectively enforce stability, the models computed are, in general, not passive. In addition, the system obtained is biproper (as a consequence of the bilinear transformation), which violates Property 4 in Table 2.1.

This section is finalised by noting that time-domain approximation methods do not have (in general) a direct handle on the frequency-response of the computed models. Given the oscillatory nature of ocean waves (see Section 2.1), frequency-domain analysis constitutes a key tool in the development of dynamical models and energy-maximising control strategies for WECs. Hence, emphasis should be put in producing accurate (and physically representative) frequency-domain characterisations.

2.6.1.2 Frequency-domain methods

Frequency-domain-based model reduction methods are the most well-established strategies in the wave energy field, and attempt to compute a parametric model directly from the frequency-domain data calculated by frequency-domain-based BEMs, *i.e.* $B_r(\omega)$ and $A_r(\omega)$. Generally speaking, two different methodologies are usually adopted: Independent fitting of the hydrodynamic coefficients B_r and A_r , or the frequency-response K_r directly (as in equation (2.17)). Studies applying the former approach are [69] and [70], while the latter has been considered by [71], [72], and [73]. These studies (and approaches) are discussed in the following paragraphs.

21: Having an accurate representation of the phase characteristics of Cummins' equation is *fundamental* for maximum energy extraction, as discussed in Chapter 3.

22: The reader is referred to [67], for further detail on the properties of the Hankel matrix, and its relation to the (extended) controllability and observability matrices of the system under analysis.

Remark 2.6.3 As discussed in Section 2.4, a further approach consists of computing a force-to-motion (input-output) state-space representation of system Σ in (2.20). This has been proposed, in the frequency-domain, by [74], and it is also discussed below.

The authors of [69], which compute a parametric form for each hydrodynamic parameter, *i.e.* added mass A_r and radiation damping B_r , separately, use as model structure a (rational) partial fraction expansion, whose coefficients are obtained based on a least-squares process, *i.e.* in an Euclidian norm sense. No mention of stability nor passivity (or even relative degree) can be found in this study, so that it is not clear when (if ever) the strategy effectively fulfills the radiation properties. The study proposed in [70] relies on the same set of tools as [69], though each coefficient is approximated by a *constant* value (*i.e.* the approximation is independent of ω).

The most well-known (and perhaps more widely considered) approach is that presented in [71], where the model reduction process is defined in the frequency-domain, using raw data representing $K_r(\omega)$, obtained from BEM codes. This method is essentially a least-squares curve fitting process, where the structure of the proposed parametric model is a rational polynomial function, with constant coefficients (these coefficients effectively constitute the optimisation variables involved). Stability cannot be ensured *per se*, so that the authors propose to ‘flip’ any set of unstable poles. Note that this is indeed analogous to the time-domain method [64] discussed in Section 2.6.1.1, and has the exact same issue with the phase of the obtained frequency-response, which can be detrimental for wave energy control applications. Passivity is not ensured by the technique, though the authors suggest that the computed models are, in general, passive.

Both [72] and [73] use a very similar approach to that of [71]. In particular, [72] first defines the model structure in the time-domain, using an observable canonical form, in terms of a set of parameters which define both the characteristic polynomial and the zero-dynamics of the proposed parametric structure. These parameters are computed using a least-squares approach, which is constrained for stability using the well-known Routh-Hurwitz (polynomial) conditions [75]. The issue of passivity is not discussed in this study. Similarly to [71], [73] uses rational functions, the stability is also ensured by a ‘flipping’ process, and passivity is obtained by a perturbation approach (analogously to the time-domain case of [64]), which relies on assuming minor violations of passivity of the parametric structure obtained.

Lastly, and as mentioned earlier in Section 2.4, a further alternative approach, considered in [74], is to compute a state-space representation of the complete force-to-motion dynamics Σ , instead of

finding a parameterisation of the radiation convolution term separately. The methodology is again very similar to that of [71], so that it is not discussed in detail herein. Nevertheless, note that, in this case, the physical notion of each component of the state vector characterising Σ is somewhat lost, though the outputs still represent physical variables. With this overall formulation, the order of the state-space representation obtained is usually lower (for equal fidelity of the overall model) than first computing a parametric form for the convolution term separately, and then embedding it into Cummins' equation (2.20)²³. As a matter of fact, the latter always requires two additional elements in the state-space representation to describe the force-to-motion dynamics, *i.e.* position and velocity, for each DoF considered (the state-vector w defined in equation (2.22)). The difference between both methodologies can be of particular importance, for example, in either model-based state-estimation, or optimal control design for WECs, where an excessive number of model states can render an energy-maximising optimal controller unsuitable for real-time applications.

23: The reason behind this behaviour is discussed in depth in Chapter 5.

2.6.2 Nonlinear strategies

To the best of the author's knowledge, there is currently no literature on systematic²⁴ methods of nonlinear model reduction applied in the wave energy field, even though this would represent an extremely valuable tool for a variety of applications, including, but not limited to, state-estimation and control design for WECs. This is ostensibly related to the fact that linear dynamics (*i.e.* equation (2.20)) are virtually always considered when designing optimal controllers for WECs (see Chapter 3), motivated by both their theoretical simplicity, and their associated computational convenience. In other words, there is currently little appetite to extend these models to include nonlinear effects, despite that the linearity assumption is challenged by the controller itself, as discussed herein in Section 2.4. It is worth mentioning though, that some effort has been done recently in [78], to provide a mathematically consistent *measure* of the impact of each nonlinear effects, and assess which of these significantly affects, for example, power absorption calculations.

24: Studies that produce simpler models by selectively 'ignoring' or 'discarding' nonlinear effects, such as, for instance, [76, 77], are out of the scope of this section, which only deals with techniques that can *systematically* reduce both order and complexity of a given dynamical operator.

2.7 Conclusions

This chapter presents the underlying principles behind control-oriented hydrodynamic modelling of WECs, including the mathematical representation of ocean waves, stating each of the assumptions

required to arrive at the well-known non-parametric Cummins' equation, which describes the dynamics of a floating device. In particular, this equation is an integro-differential equation of the convolution class, where the convolution operations involved characterise the radiation effects.

Model reduction is introduced as the main tool to compute parametric forms of Cummins' formulation, in terms of state-space representations, which are suitable for modern state-estimation and control applications, also avoiding computationally expensive simulations. The underlying physical properties of Cummins' formulation are linked to well-known dynamical properties of systems described in state-space, introducing a set of requirements that should be fulfilled by any approximating structure. In addition, the most-widely considered nonlinear extensions of Cummins' theory are also discussed, aiming to alleviate the inherent limitations of linear potential flow theory.

Finally, a literature review is provided, which addresses the state-of-the-art of both linear and nonlinear model reduction techniques applied in the marine and, particularly, the wave energy field. Though several strategies have been introduced in the linear model reduction case, *i.e.* the parameterisation of equation (2.20) in terms of an approximating state-space model, none of the strategies can systematically fulfil the underlying physical properties that characterise the behaviour of the device. Additionally, given that this set of techniques has been usually developed *outside* the scope of wave energy control literature, none of the parametric structures seem to fit the energy-maximising control problem itself, which requires, for example, a highly accurate frequency-domain representation for particular key input frequencies, such as the resonant frequency of the device (*i.e.* the frequency characterising the \mathcal{H}_∞ -norm of the system). For the case of nonlinear model reduction, despite the importance of having systematic techniques to simplify complex multi-DoF and multi-body (array) nonlinear models, no attempts can be found in the current literature.

Having identified the current issues in model reduction for wave energy applications, Part II of this thesis proposes a *model reduction framework* for wave energy applications, composed of a set of systematic reduction techniques, based on the concept of *moments* and *moment-matching* (discussed in Chapter 4), for both *linear* and *nonlinear* systems. These techniques proposed in Part II, which are effectively able to fulfil the discussed physical properties in the linear case, and deal with complex nonlinear mappings, are designed to be informed by the state-estimation and control process, being especially suitable for the WEC control application.

Energy-maximising control of WECs

3

Contents of this chapter

3.1	The impedance-matching principle	47
3.2	Optimal control problem formulation	51
3.2.1	Estimation and forecasting of wave excitation	53
3.3	Impedance-matching-based controllers: state-of-the-art	54
3.3.1	Latching control	56
3.3.2	Causal stochastic control	57
3.3.3	Advantages and disadvantages	58
3.4	Optimisation-based controllers: state-of-the-art	59
3.4.1	Numerical solution methods for optimal control	60
3.4.2	Direct optimal control in wave energy	64
3.4.3	Advantages and disadvantages	74
3.5	Conclusions	75

Recall, from Section 2.3.2, that the equation of motion for a WEC, under potential flow theory, can be generally written in terms of a system Σ , given by the set of equations

$$\Sigma : \begin{cases} M\ddot{z} = f_r + f_{re} + f_e + f_{ext} - u, \\ y = \dot{z}, \end{cases} \quad (3.1)$$

where z is the displacement vector of the body as a function of time, $y = \dot{z}$ is chosen as the output of Σ , the set of mappings $\{f_r, f_{re}, f_e\}$ denote the radiation, (hydrostatic) restoring, and wave excitation effects, respectively, and where f_{ext} are possible external forces (e.g. mooring effects).

The control input u , supplied by means of a power take-off (PTO) system, plays a key role in the optimisation of the operation of wave energy devices: Ultimately, energy conversion must be performed as economically as possible, to minimise the delivered energy cost, while also maintaining the structural integrity of the device, minimising wear on WEC components, and operating across a wide range of sea conditions. This is virtually always written in terms of an *energy-maximising criterion*, so that the control problem for WECs can be informally posed [12] as:

Design the PTO force (control input) such that:	
<i>Maximises</i>	Energy absorption from incoming waves.
<i>Subject to</i>	WEC dynamics Σ (3.1). Device and actuator physical limitations.

Pioneering studies, tackling this *energy-maximising* optimal control problem, can be traced back to Kjell Budal and Johannes Falnes* [79–81], David Evans† [82, 83], and Stephen Salter‡ [84]. These studies mostly rely on a frequency-domain analysis of the WEC dynamics, heavily inspired by the harmonic nature of waves. During recent years, wave energy control researchers moved towards *optimal control* techniques, where the energy-maximisation design is written in terms of an appropriate optimal control problem (OCP), and well-developed techniques (mainly originated within the theory of calculus of variations [85]) can be considered.

The main objective of this chapter is to introduce the energy-maximising control problem for WECs, covering, from the fundamentals behind maximum energy absorption under regular (monochromatic) wave excitation, towards the set of optimal control techniques utilised to tackle this control problem. In particular, Section 3.1 describes the principle of impedance-matching, for optimal (unconstrained) energy absorption under monochromatic excitation, while Section 3.2 introduces the energy-maximising control problem within an OCP formulation. Section 3.3 provides a review of the state-of-the-art of WEC control techniques based on the impedance-matching principle, denoted here as *impedance-matching-based* controllers, while Section 3.4 provides a review on optimal control techniques applied for the WEC control case, *i.e.* *optimisation-based* controllers. In the case of both impedance-matching- and optimisation-based controllers, the advantages and disadvantages of each family of control strategies are highlighted and discussed. Finally, Section 3.5 encompasses the main conclusions of this chapter, which directly motivate the moment-based control framework proposed in Part III of this thesis.

3.1 The impedance-matching principle

One of the first and fundamental results applied within the wave energy control literature relies on a rather simplistic approach to the energy-maximising problem, where device and actuator constraints are completely neglected. In particular, this principle heavily relies on a *frequency-domain* analysis of the WEC dynamics, and is detailed and discussed in the following paragraphs¹. The reader is also referred to [53] for a treatment of this topic.

Consider the linear Cummins' formulation, defined in equation (2.20). A direct application of the Fourier transform, together with the

1: From now on, for the remainder of this chapter, a single DoF device is considered, unless otherwise stated.

* Budal & Falnes - NTNU (NTH before 1996), Trondheim, Norway.

† University of Bristol, Bristol, United Kingdom.

‡ University of Edinburgh, Edinburgh, United Kingdom.

radiation force frequency-domain equivalent introduced in equation (2.17), yields

$$j\omega(M+m_\infty)\dot{Z}(\omega)+K_r(\omega)\dot{Z}(\omega)+\frac{s_h}{j\omega}\dot{Z}(\omega)=F_e(\omega)-U(\omega), \quad (3.2)$$

where $U : \mathbb{R} \rightarrow \mathbb{C}$ represents the Fourier transform of the controller input $u : \mathbb{R}^+ \rightarrow \mathbb{R}$. From (3.2), it follows directly that

$$\dot{Z}(\omega)=\frac{1}{I(\omega)}[F_e(\omega)-U(\omega)], \quad (3.3)$$

where the mapping $I : \mathbb{R} \rightarrow \mathbb{C}, \omega \mapsto I(\omega)$, defined as

$$I(\omega)=B_r(\omega)+j\omega\left[A_r(\omega)+M-\frac{s_h}{\omega^2}\right], \quad (3.4)$$

denotes the equivalent (intrinsic) *impedance* of the WEC.

Remark 3.1.1 Naturally, Equation (3.3) resembles well-known representations in the field of electronic engineering and circuits theory: the WEC dynamics (3.2) can be equivalently represented by the analogue circuit depicted in Figure 3.1 (a).

Following Remark 3.1.1, the control input $U(\omega)$ can be ‘seen’ as a load, which has to be designed so that maximum power transfer is achieved from the source, *i.e.* the wave excitation input $F_e(\omega)$. From this particular point of view, this problem can be directly addressed using the so-called *impedance-matching* (or *maximum power transfer*) theorem [86]², which is a well-established result within the electronic engineering community. This theorem states that the *load* impedance, I_u , should be designed such that it exactly coincides with the complex-conjugate of the *source* impedance, I . In other words, the control input that maximises power transfer, for the WEC case, is given by

$$U(\omega)=I_u(\omega)\dot{Z}(\omega)=I^*(\omega)\dot{Z}(\omega). \quad (3.5)$$

The result posed in (3.5) is indeed appealing, mainly due to its intrinsic simplicity, and its direct link to fundamental and well-established theory in the field of analogue circuits. Nevertheless, there are several issues associated with the control specifications given in (3.5), which prohibits the ‘smooth’ application of what could potentially be an extremely appealing principle. These are listed and discussed in the following paragraphs.

To begin this discussion, note that the Laplace-transform analogous of equation (3.2), considering zero initial conditions, directly yields,

$$\dot{Z}(s)=G(s)[F_e(s)-U(s)], \quad (3.6)$$

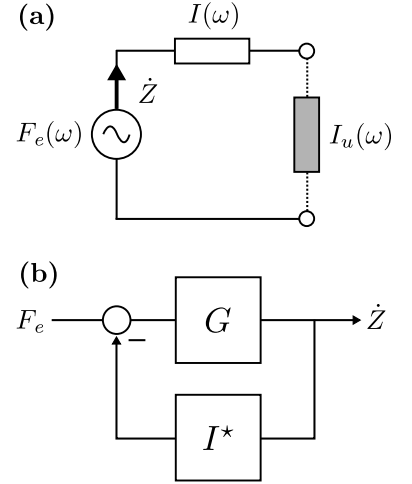


Figure 3.1: Impedance-matching principle. (a) Equivalent circuit for the frequency-domain analysis of Cummins’ equation (3.2). (b) Closed-loop impedance-matching formulation.

²: This result was initially known as *Jacobi’s law*, and it was derived by Moritz von Jacobi. Moritz, the elder brother from one of the most accomplished mathematicians in history, Carl Gustav Jacob Jacobi [87], was a German and Russian engineer, and proposed the impedance-matching principle around 1840, for the (purely) resistive load case.

where the mapping $G : \mathbb{C} \rightarrow \mathbb{C}$, defining the input-output dynamics $f_e - u \mapsto \dot{z}$, is given by

$$G(s) = \frac{K_r^D(s)s}{(M + m_\infty)K_r^D(s)s^2 + K_r^N(s)s + K_r^D(s)s_h}, \quad (3.7)$$

where the Laplace transform of the radiation impulse response, K_r , has been written³, without any loss of generality, as $K_r(s) = K_r^N(s)/K_r^D(s)$. Given the causality property of the radiation force system Σ_r , and the fact that Σ_r is always strictly proper (see Table 2.1), the following relation

$$\deg \{K_r^N(s)\} < \deg \{K_r^D(s)\}, \quad (3.8)$$

where $\deg\{p\}$, $s \mapsto p(s)$, denotes the degree of the polynomial p (defined over the field \mathbb{R}), holds.

Remark 3.1.2 The statement provided in the previous paragraph automatically implies the following properties:

- ▶ $G(s)$ is a strictly proper transfer function.
- ▶ $G(s)$ has relative degree 1.
- ▶ The zeros of $G(s)$ are always contained in \mathbb{C}^- , as a consequence of the BIBO stability of the radiation system Σ_r , i.e. $K_r^D(s)$ is always a Hurwitz polynomial.

Direct observation of equations (3.3) and (3.6) yields that, in the frequency-domain, the relation $I(\omega) = 1/G(\omega)$, holds. In other words, the dynamical system associated with the frequency-response $I(\omega)$ is inherently *non-causal*, as a direct consequence of the fact that the transfer function $G(s)$ is strictly proper (see Remark 3.1.2).

Remark 3.1.3 This poses a major issue with respect to the applicability of result (3.5): the dynamical system associated with the control law (3.5) cannot be practically implemented, due to its intrinsic non-causality.

In addition to this non-causality issue, the following additional implications associated with the matching-principle can be identified:

- ▶ The optimal control law (3.5) implies a different matching-condition for each input-frequency ω .
- ▶ Neither device nor actuator limitations are observed by the matching condition (3.5). As a matter of fact, this control strategy often requires unrealistic displacement, velocity and control input values, to successfully achieve maximum power absorption. This is illustrated in Figure 3.2, where, for example, the displacement of the device, z , is in the range $z \in [-15, 15]$

3: This is a direct consequence of the fact that system Σ_r , characterising radiation effects, is LTI (see Section 2.3.2.2).

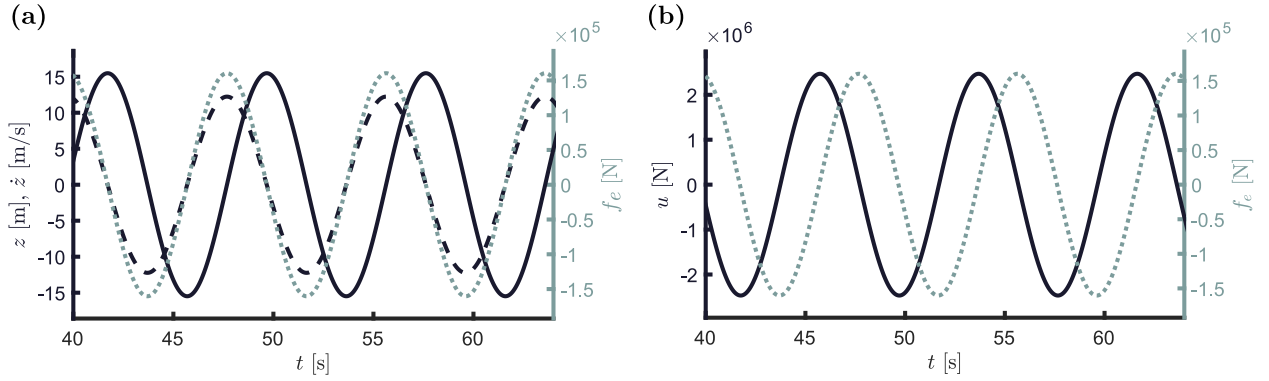


Figure 3.2: Device (sphere $r = 2.5$ [m]) motion under impedance-matching control. The input wave is assumed to be regular, with $H_w = 2$ [m] and $T_w = 8$ [s]. Figure (a), left-axis, shows displacement (solid-black) and velocity (dashed-black). Figure (b), left-axis, illustrates the impedance-matching control input (solid-black). The right-axis in both (a) and (b) shows the excitation input (dotted-grey).

[m], for a sphere of $r = 2.5$ [m], which is (very) far from being practically viable⁴. Note that the input wave (regular), has a height of 2 [m].

- The sensitivity and robustness properties of the control loop associated with the impedance-matching principle (3.5), depicted in Figure 3.1 (b), have been recently questioned in [88]. In particular, [88] shows that any modelling errors can be detrimental in the impedance-matching condition, given that a very specific zero-pole cancellation takes place when u is selected as in (3.5).

4: Note that the device is effectively ‘jumping’ out of the water in Figure 3.2. This is a direct product of the linearising assumptions under which equation (3.1) is derived. In reality, the excitation force f_e is zero once the device clears the water, though this is clearly not accounted for in the dynamical model.

Remark 3.1.4 Note that, the force-to-motion (force-to-velocity in this case) frequency-response mapping, under the impedance-matching condition (3.5), can be readily computed as

$$\dot{Z}(\omega) = \frac{G(\omega)}{1 + G(\omega)I^*(\omega)} F_e(\omega) = \frac{1}{2B_r(\omega)} F_e(\omega), \quad (3.9)$$

where B_r is the radiation damping, as defined in Section 2.3.2.

Remark 3.1.4 facilitates an interesting path to analyse the ‘effect’ of the impedance-matching controller (3.5), on the frequency-domain properties of the system. An optimal condition, for maximum-energy extraction, can be clearly extracted from (3.9):

The velocity of the device, under unconstrained optimal energy absorption, is a scaled version of the excitation input f_e .

In particular, the following conditions simultaneously hold:

- (C.1) The velocity of the device, under optimal energy absorption is *in-phase* with the excitation input f_e .

(C.2) There exists an optimal real-valued scaling function $T : \mathbb{R} \rightarrow \mathbb{R}^+$, which is given by

$$T(\omega) = \frac{1}{2B_r(\omega)}. \quad (3.10)$$

Note that the image of T is effectively contained in \mathbb{R}^+ , as a consequence of the passivity property of the radiation force, *i.e.* $B_r(\omega) > 0, \forall \omega \in \mathbb{R}/0$ (see Section 2.4). Figure 3.3 shows the Bode plot of $T(\omega)$, for a sphere of $r = 2.5$ [m].

Condition **(C.1)**, listed above, can be clearly appreciated in Figure 3.2 **(a)**, where the velocity of the device is locked in phase with the excitation input.

Though impedance-matching, as in (3.5), is far from being applicable (for the reasons discussed above), it effectively describes the underlying dynamics behind maximum energy absorption, in an intuitive approach. As a matter of fact, the two conditions listed above, *i.e.* **(C.1)** and **(C.2)**, gave origin to several *impedance-matching-based* techniques, which attempt to provide implementable approximations of the control law derived in (3.5). These are discussed in detail in Section 3.3.

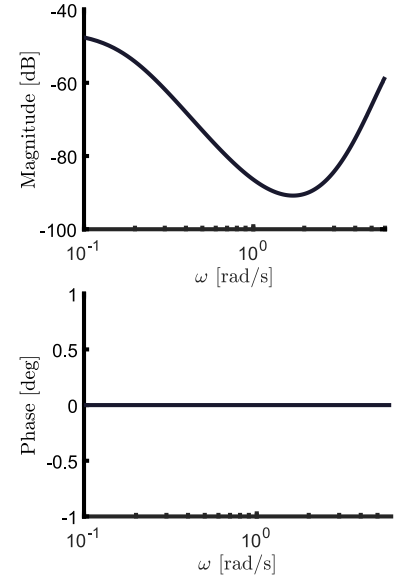


Figure 3.3: Bode plot for the optimal force-to-velocity frequency-response $T(\omega)$, under impedance-matching control conditions.

3.2 Optimal control problem formulation

As discussed in the opening paragraphs of this chapter, WEC optimal control design entails an *energy-maximisation* criterion, where the objective is to maximise the absorbed energy from ocean waves over a finite time interval⁵ $\mathcal{T} = [0, T] \subset \mathbb{R}^+$. To be precise, the useful energy absorbed from incoming waves is converted in the PTO system, and can be directly computed as the time integral of converted (instantaneous) power, *i.e.* this energy-maximising control procedure can be cast as an optimal control problem, with *objective function* $\mathcal{J} : \mathbb{R} \rightarrow \mathbb{R}$ defined as

$$\mathcal{J}(u) = \frac{1}{T} \int_{\mathcal{T}} u(\tau) \dot{z}(\tau) d\tau, \quad (3.11)$$

where $u : \mathcal{T} \rightarrow \mathbb{R}$ denotes the control (PTO) force, to be optimally designed.

In addition, as demonstrated in Section 3.1 for the impedance-matching control solution, the unconstrained energy-maximising optimal control law, *i.e.* maximiser of \mathcal{J} in (3.11), often implies unrealistic device motion and excessively high PTO (control) forces, which consign this optimal unconstrained solution to the academic

⁵: Note that there is no loss of generality in considering 0 as initial time.

realm, far from being practically viable. Aiming to derive an implementable solution, constraints on both the displacement and velocity of the WEC, z and \dot{z} , and the exerted control force u , have to be considered within the optimal control design. This guarantees that the physical limits associated with device and actuator (PTO) dynamics are consistently respected, while effectively maximising, at the same time, absorbed energy from incoming waves. This set of constraints can be compactly written as

$$\mathcal{C} : \begin{cases} |z(t)| \leq Z_{\max}, \\ |\dot{z}(t)| \leq \dot{Z}_{\max}, \\ |u(t)| \leq U_{\max}, \end{cases} \quad (3.12)$$

with $t \in \mathcal{T}$, and where $\{Z_{\max}, \dot{Z}_{\max}, U_{\max}\} \subset \mathbb{R}^+$.

Given the control objective function defined in (3.11), and the set of state and input constraints defined in (3.12), the constrained energy-maximising OCP can be posed as

$$\begin{aligned} u^{\text{opt}} &= \arg \max_{u \in \mathcal{U}} \mathcal{J}(u), \\ \text{subject to:} & \\ & \begin{cases} \text{WEC dynamics } \Sigma, \\ \text{state and input constraints } \mathcal{C}, \end{cases} \end{aligned} \quad (3.13)$$

where \mathcal{U} denotes the set of admissible inputs, and the system Σ describes the dynamic motion of the device, *i.e.* Cummins' equation (2.20), potentially with additional nonlinear effects, as described in Section 2.4.

Remark 3.2.1 The optimal control formulation (3.13), which directly aims to maximise time-averaged power extraction from ocean waves, virtually always requires numerical routines to compute a suitable solution. As a matter of fact, this OCP has been solved using a variety of strategies, mostly inspired by model predictive control (MPC). A review on these techniques is provided in Section 3.4.

An immediate advantage of this optimal-control-based approach is that constraint handling becomes straightforward, *i.e.* one can translate physical limits on device motion and PTO force into state and input constraints in (3.13), *as long as these limitations are represented in terms of a feasible set*⁶. A clear disadvantage is that the real-time capabilities of problem (3.13) depend on a number of factors, primarily the discretisation technique utilised to parameterise the state and input variables, and the hardware available for its implementation. Both advantages and disadvantages of this

⁶: The reader is referred to [89] for a discussion on the feasibility of the set of constraints for the WEC case, as a function of the excitation input.

approach, are discussed in detail in Section 3.4.

Remark 3.2.2 Note that the non-causal behaviour that characterises the impedance-matching principle of Section 3.1, is also present in this OCP formulation: In order to solve the OCP defined in (3.13), full knowledge of the excitation f_e is required for the time-interval \mathcal{T} , *i.e.* solving (3.13) implicitly requires *instantaneous* and *future* values of f_e . This is further discussed in Section 3.2.1.

Remark 3.2.3 Naturally, if the wave excitation force is composed of a single frequency component and the OCP (3.13) is considered to be state-and-input unconstrained, then the control solution computed from (3.13) coincides with that provided by the impedance-matching approach described in Section 3.1.

3.2.1 Estimation and forecasting of wave excitation

The energy-maximising OCP, described in equation (3.13), not only has to be solved efficiently in computational terms, but energy-maximisation can *only* be achieved by having full (*instantaneous* and *future*) knowledge of the wave excitation force, *i.e.* the external input. In other words, f_e has to be known over the time period \mathcal{T} , in which energy absorption is being optimised. This is clearly necessary for the WEC dynamics equality constraint imposed on the OCP (3.13), *i.e.* f_e is required to predict the motion of the device based on the system of differential equations Σ . Unfortunately, for the WEC case, *i.e.* a moving body, f_e is, in general, an immeasurable quantity [90]. Consequently, *unknown-input*⁷ state-estimation strategies are required to provide *instantaneous* values of f_e . A comprehensive review of these strategies, applied to the wave energy field, can be found in [15]. Based on these estimates, a number of forecasting techniques have also been proposed to predict *future* wave excitation force within a certain time interval [16]. Naturally, the uncertainty of such a prediction increases with longer time horizons, offering a relatively precise prediction (in realistic sea state conditions) for no more than 3 ~ 10 [s].

Motivated by both the real-time requirements, and the intrinsic estimation and forecasting needs associated with this OCP, *receding-horizon* approaches to WEC control became popular over the last decade, where a number of solutions emerged, stemming from the basic principles of MPC. These strategies are reviewed here, together with a discussion on the basic principles behind receding-horizon control, in Section 3.4.2.

7: The problem of unknown-input estimation is commonly realised through observers that simultaneously estimate state and exogenous inputs. These techniques are commonly used within the field of *fault-tolerant control*. The reader is referred to, for instance, [17, 91], for further detail on this class of observers.

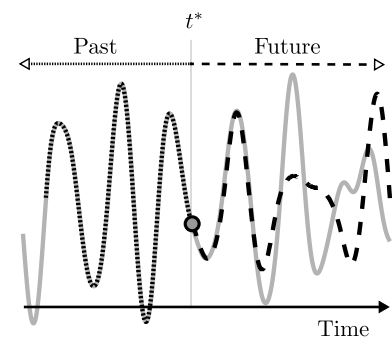


Figure 3.4: Estimation (dotted) and forecasting (dashed) of wave excitation effects. The target f_e is depicted in a solid gray line. The symbol t^* denotes the *current* time instant.

3.3 Impedance-matching-based controllers: state-of-the-art

Though simplistic by nature, the energy-maximising control law derived in (3.5) inspired a set of techniques that aim to approximate such a non-causal and frequency-dependent condition, in terms of an implementable control strategy. Though these controllers are suboptimal by design, their main advantage relies on their simplicity of implementation, which makes this family of strategies appealing for practical applications. In particular, they do not require potentially complex numerical routines to achieve the control objective. This section provides, in the following, a literature review of the state-of-the-art of impedance-matching-based controllers, including so-called *latching* control, in Section 3.3.1, and stochastic strategies, in Section 3.3.2. Finally, advantages and disadvantages of this family of controllers are discussed in Section 3.3.3.

The most commonly used approach, within this set of controllers, is to attempt to compute a *causal* transfer function that effectively approximates the ideal non-realizable impedance-matching condition (3.5) in the frequency interval containing most of the wave energy, according to its stochastic characterisation in terms of a (assumed known) SDF⁸ S_w . Pioneering studies following this approach can be found in [92–95]. In particular, [95] proposes (almost) implementable solutions, where three different causal approximations are considered for a (geometrically simple) WEC, and compared with ideal absorption under an impedance-matching non-causal controller (3.5) (computed in the frequency-domain, with perfect knowledge of the state variables). Note that constraints are not observed in [92, 93, 95]. More contemporary attempts to realise the impedance-matching controller (3.5) subject to motion constraints, include, for instance, [96–102].

One of the most established controllers in the literature, based on the impedance-matching condition (3.5), is that proposed in [103]. The underlying architecture of this controller is depicted in Figure 3.5, and can be clearly divided into two different steps. Using motion measurements, a *detection* block computes estimates of the instantaneous values of amplitude, phase and frequency, A_i , ϕ_i and ω_i , respectively, that characterises the excitation input f_e . These values are utilised to compute an approximation of the excitation force, \hat{f}_e , from which an optimal velocity reference can be obtained directly from equation (3.9). Finally, in a second stage, a tracking control strategy is designed to follow this optimal velocity reference asymptotically⁹.

8: See Section 2.1.2 for the definition of S_w .

9: The tracking controller proposed in [103] is based on the Youla-Küçera parameterisation [104].

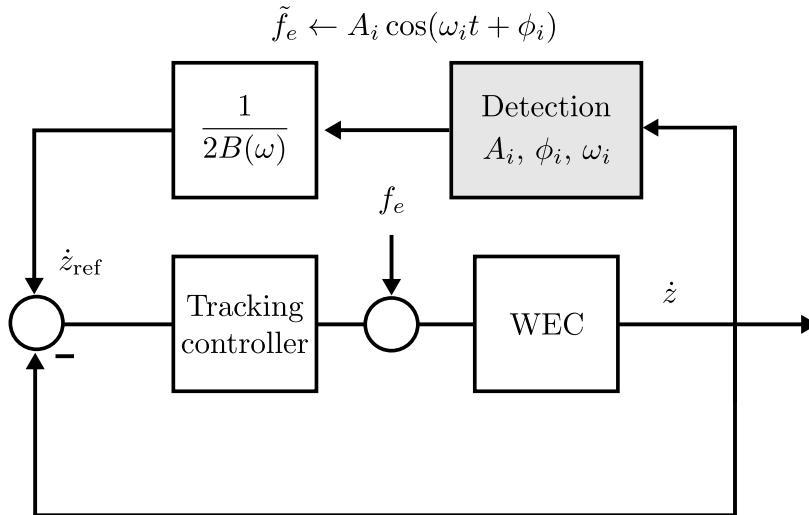


Figure 3.5: Controller architecture proposed in [103], based on the impedance-matching principle.

The detection block, showed in Figure 3.5, is realised through an extended Kalman filter (EKF) in [103]. Suboptimal constraint handling can be imposed for the motion variables either in the tracking control stage, or when computing the velocity reference \dot{z}_{ref} . Note that the success of this suboptimal controller relies on an appropriate detection of A_i , ϕ_i and ω_i . This naturally requires the assumption that the excitation force is characterised by a stochastic narrowbanded process¹⁰.

Attempting to substitute the EKF utilised in [103] (to further simplify the computational complexity of the control loop of Figure 3.5), [105] proposes a detection block based on the Hilbert-Huang transform¹¹. Nevertheless, the performance of the controller is still highly dependent on an instantaneous narrowbanded assumption for the excitation input.

Finally, a noteworthy study, aiming to provide a broadband realisation of the impedance-matching condition, has been recently presented in [107]. This study is based on two main ideas: Firstly, the feedback control law associated with (3.5) is expressed in an equivalent (non-causal) feedforward structure, in the frequency-domain. Secondly, and once the ideal feedforward frequency-response mapping is established, system identification techniques are employed to compute a causal linear time-invariant (LTI) system approximating such a response in a frequency range of interest. The latter is naturally directly linked with the specific SDF characterising the sea-state under analysis. In contrast to [103, 105], the controller developed in [107] dispenses with the narrowbanded assumption, and provides a solution for broadbanded sea-states. The constraint handling mechanism, which is intrinsically suboptimal, can only handle displacement and control force limitations by means of a single (constant) gain. Figure 3.6 shows results extracted from [107, Fig. 8], where unconstrained **(a)** and constrained **(b)** power-absorption results are presented, for

10: This limitation is explicitly declared by the authors in [103].

11: The Hilbert-Huang transform is the result of a combination between empirical mode decomposition and Hilbert spectral analysis. The method was proposed by Norden E. Huang (NASA) *et. al.* in [106].

a spherical heaving WEC (radius 2.5 [m]), for different realisations of a JONSWAP spectrum, with significant wave height $\bar{H}_w = 2$ [m], peak period $\bar{T}_w \in [5, 12]$ [s], and peak enhancement factor of $\gamma = 3.3$. The constraint, considered for the results of Figure 3.6 (b), is a displacement limitation, set to 1.5 [m]. In particular, the solution of [103] (dotted) is compared to that of [107] (dashed), showing improved performance as a consequence of the broadband nature of the controller. The solid line in Figure 3.6 represents the performance of an energy-maximising spectral-based controller [108], which belongs to the family of optimisation-based controllers discussed in Section 3.4, providing a surrogate measure of the theoretical optimum. Note that both impedance-matching-based strategies are always suboptimal with respect to the optimisation-based control law, especially under constrained conditions.

3.3.1 Latching control

Recall, from Section 3.1, that two different optimal conditions can be directly extracted from the impedance-matching strategy, *i.e.* Conditions (C.1) and (C.2). The former refers to a *phase condition* while the latter refers to an optimal motion *amplitude condition*. Naturally, both are required to ensure optimal energy extraction, under the assumptions of impedance-matching control. During the late '70s, several researchers [79, 109, 110], independently developed a (suboptimal) control strategy termed *latching*, which aims to satisfy the phase condition only, *i.e.* Condition (C.1). To be precise, the velocity of the device is kept *in-phase* with the wave excitation input, by locking the wave absorber in a fixed position for an appropriate time interval [12]. This process is schematically represented here in Figure 3.7 (a), while the precise effect of the controller, with respect to device motion, is shown in Figure 3.8.

Referring to Figure 3.8, and starting from $t = t_0$, the device is locked at time t_1 , at the extrema of the displacement (when the velocity is effectively zero), and released at time t_2 , after a latching duration t_L . This process is repeated for all $t \in \mathbb{R}^+$. If the wave is regular, then there exists a closed-form expression for the optimal latching duration t_L , which only depends on the natural period of the device (in the DoF analysed), and the period of the incoming wave [111]. Note that the control input, required to perform such an optimal policy, is inherently discrete, and often requires a fast response from the PTO to effectively lock the device in a specific position throughout the latching duration.

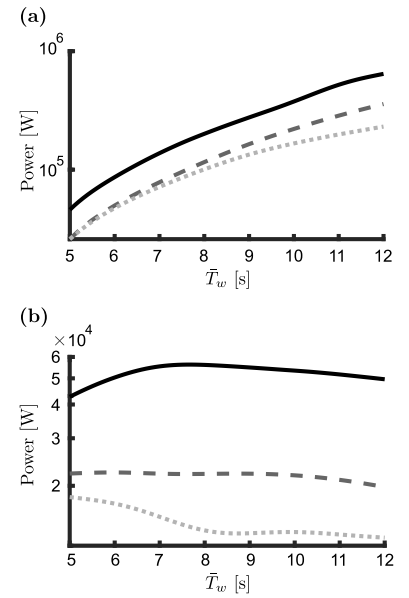


Figure 3.6: (a) Unconstrained and (b) constrained (displacement) power absorption for the impedance-matching-based strategies [103] (dotted) and [107] (dashed), and a spectral-based OCP method [108] (discussed in Section 3.4). Results extracted from [107, Fig. 8].

Remark 3.3.1 As a matter of fact, though originally developed *outside* the framework of optimal control theory, latching control belongs to the family of *bang-bang* controllers [112], and can be directly derived from the OCP (3.13) using Pontryagin's maximum principle (PMP) [85], under certain specific conditions. The reader is referred to [13, Chapter 9], for a thorough discussion on this topic.

Similarly to the impedance-matching control solution discussed in Section 3.1, latching techniques also suffer from non-causality, and their implementation virtually always requires knowledge of the wave excitation input, both for regular and irregular sea-states [113]. In particular, an extra difficulty arises in realistic sea conditions, where the incident wave is effectively composed of an infinite number of frequency components, and the concept of 'phase' between excitation input and device velocity is no longer well-defined, in which case the optimal latching interval is not unique [114], and its determination often relies on numerical routines. A comparison of several latching control strategies in regular (semi-analytical solution) and irregular (numerical solution) seas can be found in [114, 115].

A counterpoint to latching, termed *declutching* (also referred to as *unlatching* [12]), is developed in [116] and [117], where the device is *unloaded* at specific time instants during the cycle (as opposed to the "locking" action of latching). This process is schematically represented here in Figure 3.7 (b). Some recent studies in derivative-free optimisation have been performed for latching [118], declutching [119] and combined latching/declutching [120].

Remark 3.3.2 The issue of choosing between either latching or declutching has been discussed in, for instance, [121], which generally concludes that, for regular seas and linear models, latching is optimal when the device resonant period is shorter than the wave period, while declutching is optimal in the exact opposite situation.

3.3.2 Causal stochastic control

A further approach, considered in the literature, is to analyse the energy-maximising (impedance-matching) condition from a (causal) stochastic approach. In [122] and [123], a linear quadratic Gaussian (LQG) controller is designed for a 3-DoF WEC, subject to state constraints (displacement and velocity). An extension of [123] can be found in [124], where a particular class of nonlinear effects can be accommodated in the final design of the controller. Causal optimal stochastic control is implemented in [125], directly based

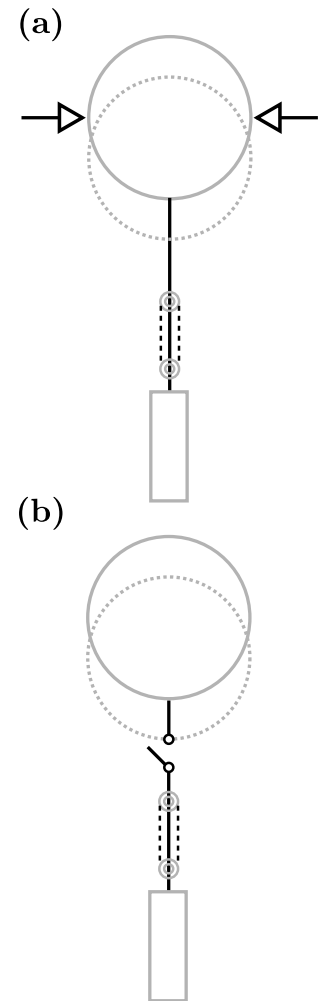


Figure 3.7: Schematic diagram of latching (a) and declutching (b) strategies for a heaving point absorber WEC.

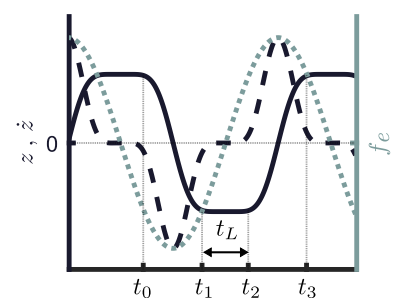


Figure 3.8: Latching control operating principle. The left axis shows displacement (solid) and velocity (dashed), under latching control conditions. The corresponding wave excitation is shown in the right-axis (dotted).

on the spectral characterisation of the sea-state S_w . This approach is designed to be optimal under monochromatic wave excitation, though results under irregular wave force are also presented and discussed.

Remark 3.3.3 Addressing the energy-conversion problem from a stochastic perspective somewhat simplifies the optimality conditions, in the sense that only the SDF S_w , characterising the excitation input, is required to compute an optimal control policy (as opposed to instantaneous and future values of f_e). Nevertheless, this approach, in general, can guarantee motion constraint satisfaction only in an *average* sense, and its performance is sub-optimal with respect to the set of techniques described in Section 3.4, if sufficiently accurate knowledge of f_e is available.

3.3.3 Advantages and disadvantages

In particular, two main advantages for the family of impedance-matching-based control strategies, can be directly identified, from the studies reviewed in this section:

- ▶ *Simplicity of implementation and intuitive appeal*: the vast majority of the strategies reviewed in this section are realised through ‘simple’ systems, mostly characterised by well-known techniques from linear time-invariant theory. This simplicity is naturally appealing at the implementation stage.
- ▶ *No requirement for optimisation routines*¹²: These techniques have mild computational requirements, and their actual implementation of can be performed in real-time with almost any physical hardware platform, including commercial low cost microcontrollers.

12: With the exception of latching control for irregular waves, which requires numerical routines to solve for the optimal latching interval t_L .

These advantages led researchers to consider impedance-matching-based controllers in many WEC applications, including, but not limited to, fatigue analysis [126], design and geometry optimisation [127, 128], and grid integration [129, 130].

Naturally, there exists a clear set of disadvantages in this family of controllers:

- ▶ *Suboptimal energy absorption*: Though ‘simple’ to implement, the performance of these controllers is inherently suboptimal, leading to a significant drop in energy absorption, when compared to the set of optimisation-based strategies, discussed in Section 3.4.
- ▶ *Suboptimal constraint handling*: Constraint handling is virtually always performed by means of simple gains, which do not take into account optimality with respect to power absorption.

In other words, the limitation mechanisms are designed independently from the energy-maximising objective, effectively providing *constrained optimal solutions*, rather than *optimal constrained solutions*. This naturally implies a significant loss of energy absorption under constrained conditions.

- ▶ *Linearity*: Linearity is a standing assumption for their design, which, as discussed in Section 2.4, can be a limiting hypothesis for WECs under controlled conditions, though some effort has been done to accommodate nonlinear effects within this family of controllers (see, for instance, [124]).

3.4 Optimisation-based controllers: state-of-the-art

The inherent suboptimal performance of impedance-matching-based controllers, discussed in Section 3.3, motivated the wave energy control community to approach the energy-maximising optimal control problem from an optimal control perspective. In particular, solving the OCP defined in equation (3.13), became a central topic in the literature of WEC control.

The OCP (3.13) is essentially an optimisation problem defined over an infinite-dimensional function space of admissible inputs \mathcal{U} . Even using well-known techniques from the calculus of variations and optimal control theory, to derive the necessary and sufficient conditions for optimality, the problem of finding the optimal control policy u^{opt} is difficult (if not often impossible) to solve analytically. Thus, naturally, the solution of the OCP (3.13) is approximated using numerical techniques, which can be generally categorised into two families (see, for instance, [131]): *Direct* and *indirect* methods. Indirect methods, often known as “*first optimise then discretise*”, are based on the derivation of the necessary conditions for optimality, and to then numerically finding a solution satisfying such conditions. Direct methods, also called “*first discretise then optimise*”, discretise the variables involved in (3.13), and attempt the maximisation of the resulting nonlinear program (NP) directly.

A discussion on both direct and indirect methods is provided in Section 3.4.1, along with fundamental aspects of the most popular strategies in the wave energy control field. Section 3.4.2 effectively provides a review on the state-of-the-art of optimisation-based strategies, specifically based on direct methods, for the WEC control case, discussing fundamental differences between the control techniques reviewed. Finally, Section 3.4.3 encompasses the main advantages and disadvantages of optimisation-based controllers for WECs.

3.4.1 Numerical solution methods for optimal control

Numerical solutions of optimal control problems can be categorised into two main approaches: *Direct* and *indirect* methods. Indirect methods attempt to numerically solve for a multi-point boundary value problem involving both the state and adjoint variables, by exploiting PMP [132–135]. This approach leads to highly accurate numerical solutions but often requires (deep) knowledge on the necessary and sufficient conditions to set up the optimality system, which have to be derived analytically and are problem-dependent. In addition, a good initial guess for the approximate solution (*i.e.* a trial solution sufficiently close to the target solution) is needed in order to guarantee convergence of the numerical routine [136, 137]. In other words, indirect methods require prior knowledge of the structure of the solution for their successful implementation, which is virtually always far from being trivial.

Motivated by all these drawbacks, virtually all the literature related to energy-maximising control solutions can be enclosed within the family of direct methods, where the state and input variables, involved in (3.13), are discretised using different families of functions (possibly defined on different function spaces), effectively transcribing the original OCP into a nonlinear program. Nevertheless, some notable exceptions, applying indirect methods, can be found in [138], [139] and [140].

In the light of the discussion provided in this section, the main objective is now to review the state-of-the-art of optimisation-based control strategies applied to the energy-maximisation problem for WECs, directly linked to the family of direct methods¹³. Two different direct optimal control approaches have been adopted and gained popularity in the wave energy field, to numerically solve the energy-maximising OCP (3.13): *Model predictive control* (MPC), and *Spectral* and *Pseudospectral* methods, abbreviated as SPM and PSM, respectively. To keep this review as self-contained as possible, the fundamentals behind each of these optimal control methods are discussed in the following paragraphs¹⁴.

3.4.1.1 Model predictive control

The origins of MPC can be traced back to the late 70's, due to Richalet *et al.* [142] and [143], presenting *model predictive heuristic control* (MPHC), and Cutler and Ramaker [144], with *dynamic matrix control* (DMC). The main difference between these two, *i.e.* MPHC and DMC, concerns the class of operators used to describe type of dynamics of the system to control: MPHC uses impulse

13: The interested reader is referred to, for instance, [141], for a general treatment of direct optimal control methods.

14: Note that SPM and PSM share the same theoretical framework, with mild differences, detailed in the following paragraphs.

response models, while DMC characterises the dynamics of the system under analysis in terms of its step response. In 1987, generalised predictive control (GPC) [145] made its first appearance, based on the controlled auto-regressive moving average (CARIMA) input-output model. More contemporary efforts aimed to develop MPC within a state-space framework, *i.e.* within a modern control approach, with pioneering results published in [146]. Significant development has subsequently taken place in the field of MPC, and the reader is referred to, for instance, [147–149], for further detail on state-of-the-art advances in MPC.

In general, the term MPC is used to refer to a wide family of model-based control strategies, which rely on a mathematical model of the system to predict its future evolution, and optimises (minimises or maximises) a given objective function, over a prescribed *sliding* prediction horizon: Only the first control value in the optimal sequence is implemented and, at subsequent sampling times, a new control policy is computed, based on the latest available state estimate. Given its nature as a digital controller, MPC is typically analysed within a discrete framework, even though it is often applied to continuous-time systems, via model discretisation¹⁵.

To summarise, and put this technique in perspective, the unifying features of MPC in discrete-time [148] can be identified as:

- ▶ A *mathematical model* of the process, to predict the output at future time instants (the prediction horizon). Typically, a discrete-time model is used, so that the continuous-time problem must be *discretised* with a chosen technique¹⁶.
- ▶ An *objective function*, defining the control objective within the corresponding optimisation window. Obtaining such an optimal control policy involves either a *constrained* or an *unconstrained* maximisation (or minimisation) procedure, which can be solved with a variety of *optimisation algorithms*, depending on the nature of the objective function, and its transcription as a nonlinear program via discretisation.
- ▶ A *receding strategy* where, at each time instant, the finite horizon is displaced towards the future, and only the first control signal of the optimal sequence calculated is applied at each step.

Remark 3.4.1 Note that the objective function traditionally defined in MPC is directly related to a *tracking* control objective, *i.e.* the objective function penalises the deviation of the state variables from a given reference trajectory, with a given set of transient specifications. This principle behind MPC is illustrated in Figure 3.9.

15: In this context, the connection to direct optimal control becomes automatically evident.

16: Typically a zero-order-hold (ZOH) equivalent is considered.

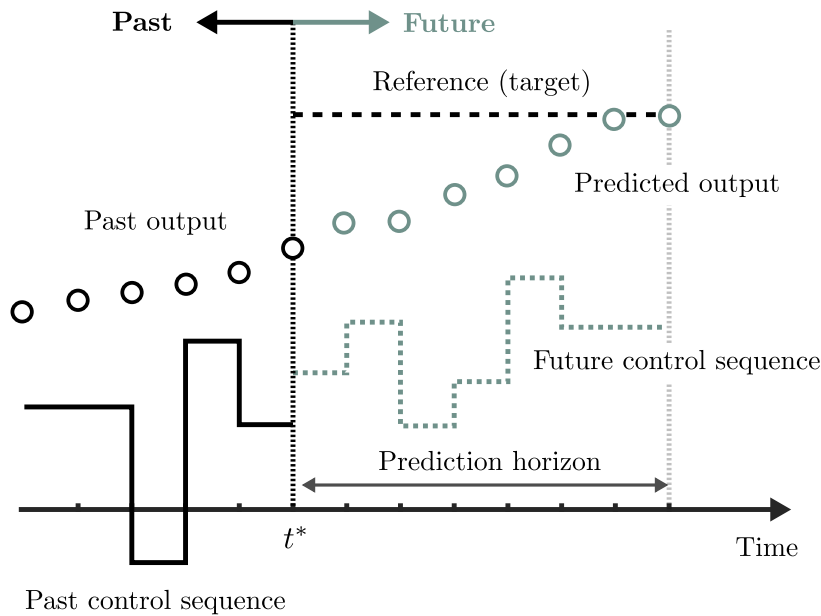


Figure 3.9: Illustration of the MPC principle for reference tracking. The symbol t^* denotes the *current* time instant.

Unlike the traditional MPC objective, described in Remark 3.4.1, the OCP for WECs, defined in (3.13), does not have reference tracking as the control objective: the objective function for the wave energy control problem effectively reflects a maximum energy absorption optimality criterion. In other words, even though a vast literature on MPC is available, many important results, such as those related to uniqueness of control solutions, are *objective function dependent*, which complicate their direct application in the wave energy control field. This motivated a number of ‘modifications’ to the energy-maximising objective function (3.11), such that the control objective ‘resembles’ that defined in traditional MPC. This mainly includes the incorporation of regularisation terms¹⁷, aiming to ensure concavity (or convexity) of the objective function. This is discussed further in Section 3.4.2.

3.4.1.2 Spectral and pseudospectral techniques

Spectral and pseudospectral techniques belong to the family of *mean weighted residual* (MWR) methods [150], which aim to compute approximate solutions of differential equations by ‘expanding’ the system variables onto a set of basis functions, to then minimise a particular (approximation) error function termed the *residual*. Unlike MPC, which is a much more established control solution, the use of SPM and PSM techniques to discretise optimal control problems gained popularity fairly recently, mostly within the aerospace research community, where they originally arose [151–153]. This section (informally) summarises the key features of these strategies¹⁸.

The main idea of optimal control based on SPM and PSM, can

17: These regularisation terms are discretisation dependent, *i.e.* they depend on the set of functions used to parameterise the system variables.

18: A formal treatment of spectral and pseudospectral methods can be found elsewhere in, for instance, [151, 154, 155].

be outlined as follows. Suppose the WEC dynamics are given by the differential equation $\dot{z} = f(z, u)$, with f a known (typically sufficiently smooth) mapping.

- ▶ The state and input variables, z and u , are assumed to belong to a given function space \mathcal{H} . Typically, \mathcal{H} is either a *Hilbert* or a *Sobolev* space¹⁹. Naturally, one uses knowledge of the mapping f to determine the nature of the space \mathcal{H} .
- ▶ Let \mathcal{H}_N be a finite set of N orthogonal functions such that $\mathcal{H}_N \subset \mathcal{H}$. Then, the series expansion of x and u in terms of the N elements of the set \mathcal{H}_N , are denoted as z_N and u_N .
- ▶ A *residual* mapping \mathcal{R} is now constructed, in terms of the corresponding differential operator, and the expansions z_N and u_N , i.e. $\mathcal{R} \leftarrow \dot{z}_N - f(z_N, u_N)$.
- ▶ The residual function is forced to be orthogonal (using the corresponding inner product) to a finite set of functions $\tilde{\mathcal{H}}_N \subset \tilde{\mathcal{H}}$, where $\tilde{\mathcal{H}}$ is a function space, potentially different to that used to expand the state and input variables. The functions in the set $\tilde{\mathcal{H}}_N$ are commonly known as *test functions*²⁰. This projection operation ‘transforms’ the differential equation characterising the residual \mathcal{R} , in a set of algebraic equations $\tilde{\mathcal{R}}$ in the coefficients of the expansions z_N and u_N .
- ▶ The set of algebraic equations $\tilde{\mathcal{R}}$, together with the expansions z_N and u_N , are directly used to parameterise the optimal control problem to be solved (equation (3.13) for the WEC case), which is now a finite-dimensional nonlinear program²¹.

If the test functions are elements of the same set as the basis functions approximating the state and input variables, that is $\tilde{\mathcal{H}}_N = \mathcal{H}_N$, then the method is known as *spectral* (or *Galerkin*) method. If the test functions are a set of translated Dirac-delta functions, i.e. $\tilde{\mathcal{H}}_N = \{\delta(t - t_j)\}_{j=1}^N$ then the method is known as *pseudospectral* (or *collocation*) method, and the time instants t_j are known as *collocation points*. The procedure detailed above is schematically depicted, for SPM (dotted) and PSM (dashed), in Figure 3.10.

In contrast to MPC, SPM/PSM-based controllers can ‘adapt’ the discretisation process, such that it’s tailored for the particular optimal control application. For instance, in the WEC control case, one may be tempted to use trigonometric functions to describe the WEC dynamics, given the harmonic nature of the wave energy process. This is, in fact, exploited in the literature, and a discussion on possible selections for the space \mathcal{H} , adopted in the wave energy field, is given in Section 3.4.2.

19: Informally, Hilbert spaces, named after the German mathematician David Hilbert (1862-1943), are complete infinite-dimensional spaces in which distances and angles can be measured. Sobolev spaces are attributed to the Russian mathematician Sergei Sobolev (1908-1989), and include functions for which all the derivatives up to a certain order, in the distributional sense, belong to L^2 .

20: The name *test function* is inherited from the theory of distributions (see [156]).

21: Depending on the nature of the objective function, an additional projection on the space $\tilde{\mathcal{H}}_N$ may be required. See [152] for further detail.

3.4.2 Direct optimal control in wave energy

This section discusses the state-of-the-art of MPC and SPM/PSM methods in wave energy conversion. Despite the fact that MPC and SPM/PSM methods have ‘technical’ differences, these controllers, applied in the wave energy field, can be characterised using a number of distinguishing features, which ultimately relate to the:

- ▶ Dynamical model considered,
- ▶ discretisation method,
- ▶ objective function and,
- ▶ nature of the resulting nonlinear program.

In the light of this, this section reviews and analyses how each of these key items, listed above, have been tackled in the wave energy optimal control case. Note that a comprehensive list of the studies reviewed in this section can be found in Table 3.2, placed at the end of this chapter²².

Remark 3.4.2 Though not listed above, state and input constraints also play an important role in the definition of the OCP (3.13). Nevertheless, direct methods can inherently handle the set of displacement, velocity and control constraints, defined in equation (3.12), as long as they represent a feasible set (see Section 3.2). In the light of this, state and input constraints are not discussed in the remainder of this section. The interested reader is referred to [12, 13] for further detail on the consideration of additional constraints (to those defined in the set \mathcal{C} in (3.12)), in the wave energy control field.

3.4.2.1 Dynamical models

The vast majority of the studies applying either MPC, or SPM/PSM, in the wave energy field, use a linear hydrodynamic formulation based on Cummins’ equation (see Section 2.4) to describe the motion of the WEC. A number of exceptions can be observed in the literature though, which include either external forces (e.g. mooring effects), or nonlinear hydrodynamic extensions of Cummins’ formulation (as discussed in Section 2.5). These are reviewed in the following.

Linear variations

Variations in Cummins’ linear formulation, can be found both across MPC and SPM/PSM studies. These include the addition of further linear terms, or variations in the parametric approximation of the radiation force (see Section 2.4). In both [138] and [157], a linearised

22: Note that Table 3.1, which can also be found at the end of this chapter, contains a explicit description of each column of Table 3.2.

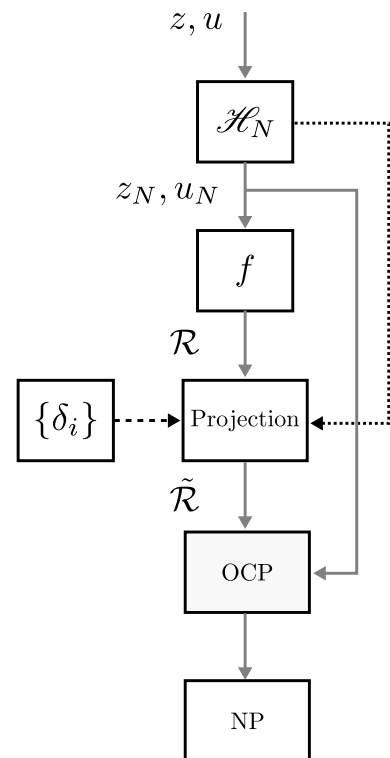


Figure 3.10: Diagrammatic illustration of spectral (dotted) and pseudo-spectral (dashed) methods for optimal control.

viscous force, which directly arises from a Morison-like equation (2.25), is considered in combination with Cummins' formulation²³. In [160], an MPC strategy for a two-body WEC is proposed, with additional linear mooring effects, characterised in terms of a spring with a given (fixed) stiffness. [161] parameterises the PTO force, which is a permanent magnet generator, in terms of a linear time-varying damping term, proportional to the device velocity. An alternative approach can be found in [140], where an energetic model of the buoy is employed, *i.e.* a port-Hamiltonian representation (see, for instance, [162]).

MPC, as applied in the wave energy case, relies on having a state-space representation of the system under analysis, as derived in Section 2.4. Recall that, to arrive to such a representation, model reduction techniques are required to compute a parametric approximation of the radiation effects. While most of the MPC studies reviewed in this section effectively consider suitable model reduction techniques²⁴, some exceptions can be found, that either simply approximate the radiation effect with a constant coefficient, or directly neglect their contribution to the dynamical model. Studies that consider the radiation force as a simple (constant) damping term are [160], [163] and [164]. [138] directly neglects the radiation effects in the model, although that changed in later studies from the same author, namely [165] and [56]. A similar practice can be found in [157, 166], where radiation is also neglected, under the justification that these effects are small (in a Euclidean norm sense) compared to other external forces.

Remark 3.4.3 Note that having an accurate parametric form for the radiation effects naturally results in an increase in computational burden for the MPC strategy, which can lead to requirements that preclude real-time application [131]. This can partially explain the necessity of neglecting such effects in the MPC-based studies reviewed above. This is especially true for those studies that also incorporate nonlinear effects, namely [56, 157, 166], which effectively complicate the nature of the transcribed nonlinear program, and more 'complex' (and less efficient) optimisation routines are often required.

SPM/PSM-based controllers do not, in general, require a state-space representation of the system, to solve the corresponding OCP; rather, the methods can deal with Cummins' equation in its non-parametric form, as a biproduct of the projection²⁵ scheme (see Section 3.4.1.2). In particular, for certain sets of basis functions, the computation involving the numerical integration of the convolution integral can be carried out offline, which reduces the computational load associated with these strategies (see, for instance, [108]). Nonetheless, some SP-

23: This practice is, in general, not recommended, since the determination of a linearised viscous force is not trivial, and has been the subject of several studies, such as, for instance, [158, 159].

24: Note that the most considered techniques for the parameterisation of radiation effects are reviewed, in this thesis, in Section 2.6.

25: In other words, the non-parametric convolution term is approximated in terms of the specific basis functions considered within SPM/PSM.

M/PSM studies, do use an approximating state-space representation for radiation effects. This include both [56], and [167].

Nonlinear effects

The main sources of nonlinear hydrodynamic effects, considered in the WEC control literature reviewed in this section, are effectively those introduced earlier in Section 2.5: Viscous effects, and nonlinear restoring forces. In particular, [57, 59, 168–170], consider nonlinear viscous forces, based on the Morison-like equation (2.25). The controllers proposed in [56], [57] and [168] consider nonlinear restoring forces, accounting for non-uniform cross-sectional areas, for each of their corresponding devices.

Other nonlinearities are also included in the design of optimal control algorithms for WECs, which are outside the hydrodynamic ‘world’: in particular, mooring forces and non-ideal PTO systems are also covered in the reviewed literature, as discussed in the remainder of this paragraph. Acknowledging that the linear mooring model considered in [160] was not appropriate for the analysed device under energy-maximising control conditions, the authors of [157] develop a nonlinear MPC for the same device considered in [160], where now the mooring forces, configured as in [171], are considered to be of a nonlinear nature. [166] also presents a nonlinear mooring term, resulting in a nonlinear MPC formulation, which is based on the same mooring configuration presented in [157]. Finally, a non-ideal nonlinear PTO system has been explicitly considered in [59, 172].

Arrays

As discussed in Chapter 1, the roadmap to successful commercialisation of WECs naturally embodies the development of so-called WEC *arrays* or *farms*, which effectively incorporate several devices in a common sea area, potentially reducing the levelised cost of energy through an economy of scale [14]. Hence, any realistic effort to commercialise a novel WEC technology requires both a single WEC, and a WEC farm, development process.

This naturally motivated researchers in the WEC control community to develop optimal control strategies for WEC arrays, virtually always relying on linear hydrodynamic models. In particular, studies applying MPC to the WEC array case are [165, 169, 173, 174], while SPM/PSM methods for WEC farms can be found in [175–177].

Remark 3.4.4 As it has been reported in the literature, modelling the hydrodynamic interactions between devices in a WEC array (which can be included within the non-parametric radiation force description) can compromise the real-time capabilities of MPC [165, 173]. This motivated researchers to explore decentralised techniques, though these have been shown to be suboptimal in [176], both in terms of energy absorption, and consistent satisfaction of state and input constraints.

Linear vs. nonlinear

As shown in Figure 3.11 (data extracted from Table 3.2), linear dynamics are virtually always considered in the literature reviewed: 82% of the optimisation-based control studies reviewed, independently of the strategy (*i.e* either MPC or SPM/PSM), utilise linear models. This is ostensibly motivated by both their simplicity (in terms of formulation and solution of the corresponding OCP), and their associated computational convenience. In other words, these model-based control strategies *must* compute in real-time, therefore limiting the computational complexity of the hydrodynamic models employed, while there is also a limit to the complexity of mathematical models for which an optimal control solution can be effectively found, either algebraically or numerically.

Nevertheless, despite the list of motives described above, the linearity assumption has been recently questioned (see, for instance, [178, 179] and Section 2.5): WECs are, by nature, prone to show nonlinear effects, since their principal aim, pursued by the optimal control strategy, is to enhance the amplitude of motion to maximise power extraction. In other words, the assumptions under which the linearisation of WEC models is performed are challenged by the controller itself, particularly in relation to small movements around the equilibrium position²⁶. This may, in certain conditions, return poor results, both in terms of accuracy of motion prediction, and power production assessment [178], which are the key variables involved in any energy-maximising OCP. In conclusion, any energy-maximising control framework, aiming to successfully improve the performance of the WEC in terms of energy absorption, *should* be able to incorporate (at least to certain extent) nonlinear effects in the OCP.

Towards robust solutions

Modelling errors are ubiquitous in hydrodynamics, even for the case of linear potential flow theory (see, for instance, [18]). The

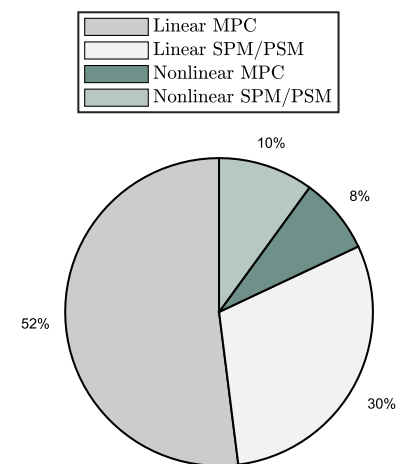


Figure 3.11: Distribution (in percentage) of linear and nonlinear WEC models considered in the literature, for MPC and SPM/PSM methods.

26: Note that this effectively contrasts with traditional set-point tracking control systems, where the control system ensures that the system operation is around the setpoint and actively attempts to reduce the variance around this point.

issue of robustness, in this energy-maximising control problem, has been recently addressed by a few studies belonging to the family of optimisation-based approaches, namely [180, 181] (MPC) and [182, 183] (SPM).

The scarcity of robust strategies among WEC control methods can be attributed to the fact that the design of energy-maximising controllers does not directly fit into a traditional form, unlike the well-known reference tracking problem. This intrinsically complicates the application of well-developed robust control strategies, posing an imperative to find novel approaches for the wave energy application.

To briefly summarise, [180] takes into account possible deviations from the design model by proposing a nominal MPC strategy with an additional correction term in the exerted PTO force, as a function of the (defined) uncertainty. This is intrinsically suboptimal, since the knowledge of the uncertainty is not present in the computation of the energy-maximising optimal control input, but it is rather a correction term to avoid state constraint violation. The authors of [181] propose an uncertainty estimator in the energy-maximising control design procedure, to later solve the optimal control problem using approximate dynamic programming techniques. Finally, the studies performed in [182, 183] re-formulate the resulting WEC optimal control problem using a robust optimisation approach [184], where (structured) modelling uncertainty is explicitly considered in the frequency-domain. This is illustrated in Figure 3.12, where a family of models is considered in [182], in the frequency-domain, for a heaving sphere of radius $r = 2.5$ [m].

Remark 3.4.5 Though some progress has been reported in robust approaches for optimisation-based controllers, only system uncertainties are considered. Robust control synthesis with respect to errors in the estimation and forecasting of the excitation effect, which have a strong impact in the performance of this type of controllers (see, for instance, [19]), *has not been addressed* in the current literature.

3.4.2.2 Model discretisation

As discussed in Section 3.4.1.1, MPC strategies intrinsically require a discrete-time dynamical system, to map the corresponding OCP into a finite-dimensional NP. As detailed throughout Chapter 2, hydrodynamic modelling of WECs is naturally performed in continuous-time, so that suitable discretisation techniques are required for this energy-maximising control application.

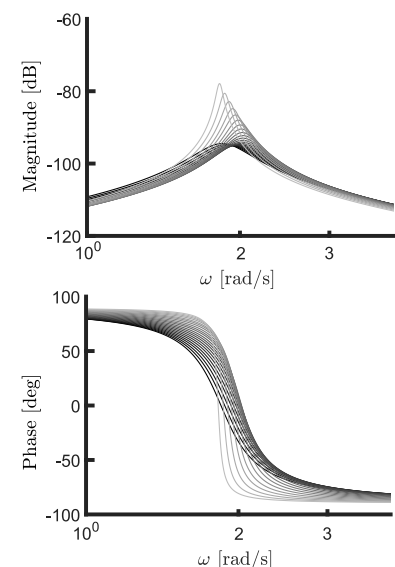


Figure 3.12: Family of models, for a heaving sphere WEC with $r = 2.5$ [m], in the frequency-domain. Figure adapted from [182, Figure 8]. See [182] for more detail on the definition and computation of the uncertainty.

As can be directly appreciated from Table 3.2, the most popular discretisation procedure for MPC, applied to the energy-maximising control problem for WECs, is the standard *zero-order-hold* (ZOH), which is also commonly used in traditional reference tracking predictive control [148]. Some exceptions can be found though, which either use a *first-order-hold* (FOH)²⁷, namely [169, 186–188], or a *second-order-hold* (SOH), considered in [157, 166]. With respect to the use of FOH, in [186], the authors claim that such a discretisation yields improved performance (*i.e.* in terms of absorbed energy) than those obtained with a ZOH. These steps were followed by [169, 187, 188]. For the SOH case, which is considered in [157, 166], the authors claim neither a ZOH nor a FOH are appropriate for the non-linear mooring dynamics considered within their MPC formulation, so that a higher-order-hold (second order in this case) is required. Another variation, for the MPC-based controllers reviewed in this section, can be found in [161, 189, 190], where the WEC dynamics are discretised using *Tustin's method*²⁸. Note that this method effectively preserves stability, though a non-zero feed-through matrix is added to the discrete-time state-space representation obtained.

The case of SPM/PSM methods is substantially different, and there is generally no 'standard' method to select the functions used to approximate the state and input variables, *i.e.* the set \mathcal{H}_N defined in Section 3.4.1.2. In other words, the selection of this set has to be made according to the specifications of the differential equation involved, and the specific OCP to be solved.

Remark 3.4.6 Note that, unlike MPC, spectral and pseudospectral methods are (generally) based on functions defined over the complete control horizon, *i.e.* have *global*, rather than local, support.

Direct appreciation of Table 3.2 shows that Fourier-type of functions, *i.e.* periodic trigonometric polynomials, are the most common choice among the studies reviewed for the WEC control case. This is clearly motivated by the fact that waves, as described in Section 2.1, are essentially assumed to be composed of a linear superposition of trigonometric functions, so that such polynomials 'fit' the particular WEC application. Effectively, given the strong connection between Fourier functions, and the very nature of the dynamical process of WECs, a small number of trigonometric polynomials is usually enough to successfully approximate the corresponding OCP to a reasonable degree of accuracy, which is naturally appealing from a computational perspective²⁹. Though efficient at a first glimpse, these functions come with one specific drawback: they are periodic, which directly complicates the application of this SPM/PSM controllers in a receding-horizon fashion, and limits their potential in

27: The first-order-hold is also commonly known as *triangular hold*, in reference to locally supported 'triangular' (linear) functions [185]

28: Tustin's method is also known as *bilinear transform*, and is a special case of a *Möbius transformation*. The reader is referred to [191] for further detail on this type of mapping.

29: In addition, and differently from most of the studies reviewed both in MPC and SPM/PSM, some results in the theoretical analysis of existence and uniqueness of energy-maximising solutions has been achieved using this set of functions, which is closely related to their representativeness of the process (see Section 3.4.2.3).

a real-time implementation scenario. Nevertheless, this periodicity issue has been solved in [57], where the trigonometric functions are forced to be compactly supported by the use of *windowing* [192] techniques³⁰. This effectively avoids Gibbs phenomenon, which arises as a function of the ‘artificial’ discontinuities introduced from approximating state and input variables over a short time-window, *i.e.* truncation effects.

Other studies, namely [56, 164], use PSM with Legendre polynomials³¹, analogously to the pseudospectral methods developed in the aerospace research community [151]. One more variation can be found in [195–198], where *half-range Chebyshev-Fourier* (HRCF) functions are considered, depicted herein in Figure 3.13. This set of functions, originally termed *half-range Chebyshev* mappings, was introduced recently in 2010 [199], and arise as the solution of the extension of the concept of Fourier series for non-periodic functions. In contrast to the case of trigonometric polynomials, HRCF functions can effectively deal with truncation effects, hence being appropriate for receding-horizon control, while showing real-time capabilities (see [195]). Nevertheless, this set of functions lose the direct theoretical connection to the harmonic nature of the wave energy process, which has an impact in the formulation of the optimisation problem, as discussed in Section 3.4.2.3.

In summary, despite the fact that the most common discretisation approach, for MPC, is the standard ZOH, some variation can be found in the literature, driven by the intrinsic WEC dynamics considered by each study. Naturally, each discretisation technique captures the dynamic of the system differently, having an impact on the performance of the controller, the structure of the resulting nonlinear program, and the computational burden associated with the optimisation procedure (see also Section 3.4.2.3). Nevertheless, note that all the discretisation techniques considered among the MPC formulations in the WEC control case, can be considered as relatively ‘standard’, in the sense that they are well-known within the control community. In contrast, SPM/PSM techniques use a different parameterisation of the state and input variables, which is mostly driven by the specifics of the control problem, potentially diminishing the computational effort required for the receding-horizon control formulation [197]. Nevertheless, the solution method becomes highly dependent on the choice of the set \mathcal{H}_N , which affects both the performance and complexity behind deriving existence and uniqueness results for global optimisers (see Section 3.4.2.3).

30: Windowing, also referred to as *apodisation* (in the mathematics community), is commonly used in the so-called short-term Fourier transform, for the spectral analysis of non stationary signals [193].

31: Legendre functions, attributed to the French mathematician Adrien-Marie Legendre (1752-1833), are polynomials in $\mathcal{C}([-1, 1])$ which are orthogonal under the inner product of L^2 , and solutions of the Legendre differential equation [194].

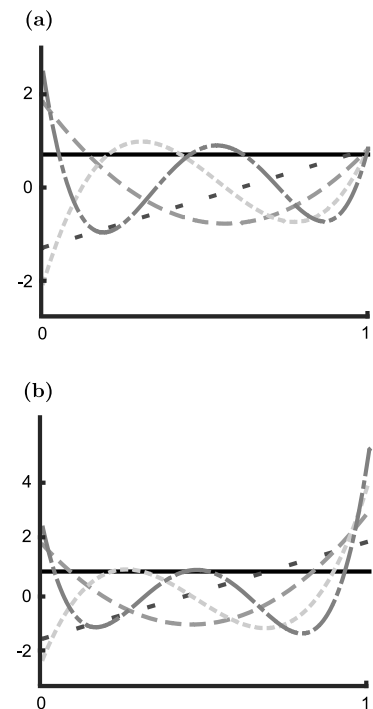


Figure 3.13: Plot of the first five HRCF polynomials of the first (a) and second (b) kind. The reader is referred to [200] for further detail.

3.4.2.3 Objective function

As described in Section 3.2, and in contrast to traditional regulation and tracking control objectives, the optimal control problem for WECs involves the maximisation of absorbed energy from incoming waves, as compactly expressed in equation (3.13), and recalled below, for convenience:

$$u^{\text{opt}} = \arg \max_{u \in \mathcal{U}} \frac{1}{T} \int_{\mathcal{T}} u(\tau) \dot{z}(\tau) d\tau,$$

subject to:

$$\begin{cases} \text{WEC dynamics } \Sigma, \\ \text{state and input constraints } \mathcal{C}. \end{cases}$$

Naturally, the objective function (3.13) (recalled above) differs significantly from the standard MPC formulation: in traditional MPC, the nonlinear program, resulting from the discretisation of the (*linear*) system dynamics, always results in a quadratic program (QP), which has a unique global optimum [148] (*i.e.* it is *concave* or *convex*, depending if the optimisation seeks for a maximum or a minimum, respectively). This motivated the incorporation of ‘additional’ terms in the objective function defined in (3.13), aiming to resemble the concave quadratic objective of traditional MPC. The use of these terms, which are effectively regularisation terms to ensure concavity, has been justified (and applied) in the vast majority of the MPC studies reviewed, in different ways, as discussed in the following paragraphs. In particular, 74% of the MPC studies reviewed considered a control objective which departs from the energy-maximisation criterion, incorporating additional terms to the energy objective function (3.13), denoted herein as \mathcal{J}^* . A complete list can be found in Table 3.2 in column “Objective function - Energy + \mathcal{J}^* ”.

To be precise, the majority of the MPC studies reviewed incorporate a term proportional to the square of the control input, *i.e.* $\mathcal{J}^* \propto u^2$. This includes, for instance, [160, 166, 169, 173, 187, 188, 201–205]. Though some of these studies explicitly declare that these are, effectively, regularisation terms to ensure convergence towards a unique global maximiser, some authors, such as, for instance, [169, 187, 188, 204], either classify these terms as losses for the entire PTO system considered, or suggest that ‘limiting’ control energy should be an additional objective. Note that, within this same MPC WEC application case, [170] debates on the suitability of using $\mathcal{J}^* \propto u^2$ as a loss model for the PTO, and proposes a more comprehensive mathematical representation in terms of a higher-order polynomial in the control input. Some authors also add a term proportional to the square of the device displacement, *i.e.* $\mathcal{J}^* \propto u^2 + z^2$. This includes the references [163, 165, 203, 205]. Finally, [186, 206] consider an

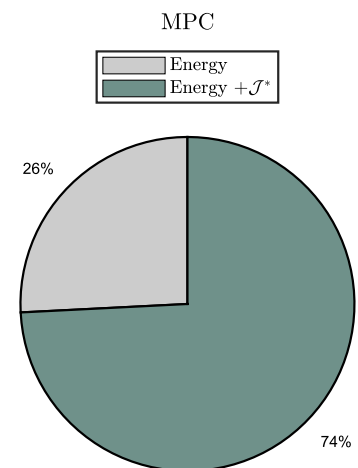


Figure 3.14: Distribution (in percentage) of MPC WEC studies considering either a purely energy-maximising control objective (grey) or a modified objective function (green). Data extracted from Table 3.2.

additional term proportional to the slew rate of the control input, *i.e.* $\mathcal{J}^* \propto \max(du/dt)^2$, while [189, 190] considers PTO efficiency in the objective function, in terms of a signum-like function, adding a discontinuity to the control objective³².

In contrast to MPC-based control strategies, SPM/PSM formulations virtually always consider a purely energy-maximising control strategy, with 90% of the studies agreeing with the target control objective defined in (3.13) (see Figure 3.15). The reasons behind such a success in handling the target energy-maximising objective function is directly related to the specific discretisation utilised, as further discussed in Section 3.4.2.4. Some exceptions can be found in [164, 198], where, similar to MPC, a term proportional to the square of the control input is added. For the case of [198], and as declared by the authors, this term is explicitly added to ensure uniqueness of a global energy-maximising solution for the OCP.

3.4.2.4 Nonlinear programs and globally optimal solutions

Depending on both the nature of the discretisation process, and the mathematical model used to describe the system dynamics, *i.e.* linear or nonlinear, the resulting nonlinear program has a certain complexity, both in theoretical and computational terms, for the same objective function [131]. This naturally implies that the properties of the optimisation process required to compute an optimal solution are substantially different for MPC, compared to SPM/PSM methods (and even between SPM/PSM depending on the set \mathcal{H}_N).

In particular, starting with a *linear* model for the WEC, the nonlinear program arising from MPC, as applied in the wave energy case, is always of a quadratic nature (*i.e.* QP). This allows for a computationally efficient solution *as long as the problem is concave*. If that is the case, then state-of-the-art QP solvers, such as those extensively reported in [207], can be readily utilised. This is exactly what motivates researchers, applying MPC in the wave energy field, to add regularisation terms to the objective function, as it has been reported that, without these terms, unique solutions are, in general, not achievable, for any of the discretisations considered.

Remark 3.4.7 What is somewhat concerning is the fact that the vast majority of the studies adding regularisation terms to obtain a unique solution, *i.e.* modifying the energy-maximising control objective, *do not* formally analyse either existence nor uniqueness of globally optimal solutions, with some noteworthy exceptions, as detailed in Table 3.2 under the column “Is $\exists!$ analysed?”. As a matter of fact, no indication is given in general on how to tune

32: The authors of [189, 190] explicitly declare that their MPC formulation requires a smooth approximation of this discontinuous efficiency term, which is obtained in terms of an hyperbolic tangent function.

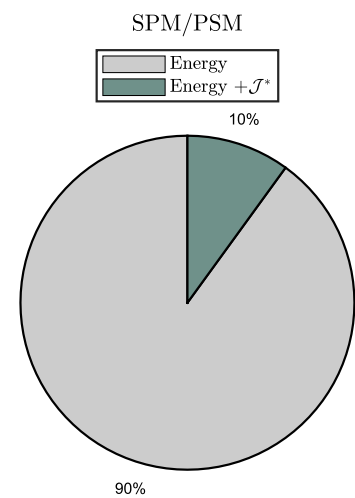


Figure 3.15: Distribution (in percentage) of SPM/PSM WEC studies considering either a purely energy-maximising control objective (grey) or a modified objective function (green). Data extracted from Table 3.2.

the ‘additional’ terms to achieve a global maximiser, hindering the class of dynamical models, *i.e.* WEC devices, that can be considered within the strategy without losing global optimality.

Similarly to MPC, SPM/PSM methods also result in a QP problem for the linear model case, although there is a significant difference with respect to MPC: solutions found with SPM/PSM are, in general, reported to be globally optimal, for the purely energy-maximising control objective. This directly explains why 90% of the reviewed literature does not require modifications of the objective function involved in the OCP (3.13). For the particular case of Fourier functions, the authors of [108] have shown that this particular discretisation always renders a concave QP problem, as a direct consequence of the passivity of the WEC model (see Section 2.4). In other words, global optimality is indeed achieved by a suitable selection of the basis functions, for the single WEC case analysed in [108]. This nice property is effectively lost when using HRCF functions, as detailed in [198], where regularisation terms are required to ensure optimality. Note that, differently from the majority of MPC studies, the authors of [198] do formally provide explicit ‘tuning’ conditions to systematically obtain a concave QP.

Remark 3.4.8 Though [108] provides a proof of uniqueness of global solutions for Fourier basis functions, this only holds for the single WEC case (SISO system), and has not been extended to the array case (MIMO system) in [175–177].

Independently if it’s MPC or SPM/PSM-based control, the QP nature of the problem is clearly lost if a nonlinear model for the WEC is considered. The resulting nonlinear program can be solved using ‘generic’ NP routines, based on, for example, interior-point methods (IPM) [208, 209] and sequential quadratic programming (SQP) [210]. Nevertheless, different computational properties have been reported for MPC and SPM/PSM methods. In particular, as reported in [157, 166, 189], real-time implementation is difficult to achieve for the MPC case, though there is definitely room for improvement if any compiled language (rather than Matlab®) is utilised to code the corresponding control algorithms. On the other hand, efficient nonlinear solutions have been reported for SPM/PSM-based controllers in [57, 168], achieving real-time performance even running on (interpreted) Matlab®.

Remark 3.4.9 Though some of the reviewed studies do consider nonlinear effects, *none* of them give formal and explicit conditions for existence of globally optimal energy-maximising control solutions, as reported in Table 3.2. As a matter of fact, even if a control solution is found, it is not clear under which conditions

this energy-maximising control law is effectively a globally optimal solution. This naturally generates a great deal of uncertainty, specifically in which class of models can be actually used within the available nonlinear formulations, and even if the reported performance corresponds with a global solution at all.

3.4.3 Advantages and disadvantages

As per the case of impedance-matching based controllers, in Section 3.3.3, a set of advantages and disadvantages can be clearly identified for the optimisation-based controllers reviewed in this section. In particular, there are three key advantages of optimisation-based control:

- ▶ *Optimal performance*: Facilitated by a suitable definition of an energy-maximising objective function.
- ▶ *Systematic optimal handling of state and input constraints*: Device safety can be directly addressed by adding a (feasible) set of constraints to the optimisation problem.
- ▶ *Nonlinearity*: Though yet not fully exploited, a general class of nonlinear models can be considered within this optimisation-based approach, overcoming the inherent limitations of models arising from linear potential theory.

These advantages are indeed appealing in terms of performance and design freedom, which is much more limited for the case of impedance-matching-based controllers reviewed in Section 3.3.

Naturally, there is also a set of disadvantages in this family of controllers:

- ▶ *Computational expense*: Depending on the discretisation utilised, optimisation-based controllers may or may not be suitable for a real-time implementation scenario. This is especially true if nonlinearities are considered.
- ▶ *Globally optimal solutions*: It is key to provide conditions where the optimisation can be solved efficiently, which is directly connected with deriving explicit conditions for existence and uniqueness of globally optimal solutions to the energy-maximising nonlinear program, associated with the discretisation selected. This has not been done consistently in the literature, as discussed previously in Section 3.4.2.4.

3.5 Conclusions

This chapter introduces the key concepts behind energy-maximisation control of WECs, starting from the fundamental theory of *impedance-matching*, from which the control law (3.5) can be readily obtained. Though simplistic by nature, the energy-maximising control law derived in equation (3.5) inspired a set of techniques that aim to approximate such a non-causal and frequency-dependent condition. These controllers are suboptimal by design, and their main advantage relies on their simplicity of implementation, which makes this family of strategies appealing for practical implementation. Nevertheless, their performance is severely affected both by the approximation of the condition of equation (3.5), and the suboptimal handling of state and input constraints, which often tends to be ‘rudimentary’.

Aiming to optimally handle maximum energy-absorption under state and input constraints, a large number researchers utilise optimal control theory, where the energy-maximising objective is formulated as an OCP, detailed in (3.13). This OCP is characterised by an objective function, which reflects maximisation of absorbed energy from incoming waves, and a set of state and input constraints, which guarantee safety limitations for the device and actuator components.

The vast majority of the studies available in the literature utilise either MPC or SPM/PSM techniques to discretise the infinite-dimensional OCP (3.13), describing the energy-maximising control problem as a nonlinear program. Though promising results have been presented, a number of issues can be directly identified from the literature review provided in this chapter. In particular, motivated by their simplicity and computational convenience, the current state-of-the-art is mainly based on *linear* strategies, even though WECs are, by nature, prone to show nonlinear effects under controlled conditions (as discussed in Section 3.4.2). Moreover, even in the linear case, not only the majority of the studies require modification of the energy-maximising objective to ensure uniqueness of a globally optimal solution, but most of them obviate any formal proof or recommendation on how to select these regularisation terms (with some notable exceptions).

On the other hand, few studies are effectively considering nonlinear dynamics, with some promising results in the area of SPM/PSM-based controllers, specifically in terms of computational efficiency. Nevertheless, *none* of the reviewed studies, which consider nonlinear effects in the equation of motion, give explicit conditions for global optimality, preventing identification of the class of models that can be used, and limiting the results (and any conclusions) obtained only for the particular application case analysed in each paper.

Some robust approaches can be found in the literature, somewhat aiming to ‘fill the gap’ between linear and nonlinear modelling. Robustness with respect to system uncertainty has been tackled, to some extent, in both MPC and SPM/PSM formulations. Nevertheless, to date, there are no optimisation-based control strategies effectively taking into account errors in the estimation and forecasting of excitation forces process (*i.e.* input uncertainty), which naturally arise in this energy-maximising application.

Motivated by the discussion provided in this section, and the specific issues found in the state-of-the-art of WEC control, Part III of this thesis presents a moment-based framework for energy-maximising optimal control of WECs, addressing linear (SISO and MIMO) control design, robust control with respect to both input and system uncertainties, and, finally, nonlinear optimal control of WECs. Conditions for global optimality of solutions are given *for each* of the scenarios listed above, hence providing computationally efficient solutions that deliver a globally optimal performance, for a generic class of WEC devices.

Table 3.1: Reference guide to read Table 3.2

Column	Brief description
Reference	List of studies reviewed.
Type	Type of control strategy, <i>i.e.</i> MPC/SPM/PSM.
Model	Class of dynamical WEC model considered, <i>i.e.</i> linear or nonlinear.
Objective function	Studies that consider an objective function related to: Energy-maximisation (• in column “Energy”) or energy-maximisation with additional terms (• in column “Energy + \mathcal{J}^* ”).
Is $\exists!$ analysed?	Studies that analyse existence and uniqueness of globally optimal solutions •.
Discretisation	Type of discretisation used. For the case of SPM/PSM-based controllers, this column reflects the basis functions chosen for the set \mathcal{H}_N .

Table 3.2: Optimisation-based control strategies (MPC and SPM/PSM) reviewed in this chapter.

Reference	Type	Model		Objective function		Is $\exists!$ analysed?	Discretisation
		Linear	Nonlinear	Energy	Energy + \mathcal{J}^*		
[138]	MPC	•		•			ZOH
[160]	MPC	•			•	•	ZOH
[157]	MPC		•		•		SOH
[163]	MPC	•			•	•	ZOH
[165]	MPC	•			•		ZOH
[201]	MPC	•			•		ZOH
[211]	MPC	•			•		ZOH
[161]	MPC	•		•			Tustin
[166]	MPC		•		•		SOH
[173]	MPC	•			•		ZOH
[202]	MPC	•			•		ZOH
[189]	MPC	•			•		Tustin
[190]	MPC	•			•		Tustin
[212]	MPC	•		•			ZOH
[187]	MPC	•			•		FOH
[213]	MPC	•		•		•	ZOH
[206]	MPC	•		•			ZOH
[186]	MPC	•			•		FOH
[188]	MPC	•			•		FOH
[214]	MPC	•		•		•	ZOH
[215]	MPC	•		•			ZOH
[169]	MPC		•		•	•	FOH
[203]	MPC	•			•		ZOH
[170]	MPC		•		•		ZOH
[216]	MPC	•		•	•		ZOH
[205]	MPC	•			•	•	ZOH
[217]	MPC	•			•	•	ZOH
[204]	MPC	•			•	•	ZOH
[174]	MPC	•			•	•	ZOH
[180]	MPC	•			•	•	ZOH
[56]	PSM		•	•			Legendre
[218]	SPM	•		•		•	Fourier
[195]	PSM	•		•			HRFC
[164]	PSM	•			•		Legendre
[175]	SPM	•		•			Fourier
[219]	SPM	•		•			Fourier
[176]	SPM	•		•			Fourier
[172]	PSM		•	•			Fourier
[167]	SPM	•		•			Fourier
[108]	SPM	•		•		•	Fourier
[59]	PSM		•	•			Fourier
[177]	SPM	•		•			Fourier
[196]	PSM	•		•			HRFC
[197]	PSM	•		•			HRFC
[220]	PSM	•		•			Fourier
[198]	PSM	•			•	•	HRFC
[168]	SPM		•	•			Fourier
[57]	SPM		•	•			Fourier
[182]	SPM	•		•		•	Fourier
[183]	SPM	•		•		•	Fourier

Contents of this chapter

4.1	The notion of moments	78
4.1.1	Linear systems	78
4.1.2	Nonlinear systems	82
4.2	Model reduction by moment-matching	83
4.2.1	Linear systems	83
4.2.2	Nonlinear systems	86

This chapter briefly recalls some of the key concepts behind *moment-based* theory (also often referred to as *moment-matching* framework throughout this thesis), as developed and discussed in key studies such as, for instance, [20, 21, 221], for single-input single-output systems. In particular, special emphasis is made on the formal (mathematical) definition of *moment*, using a system-theoretic approach. Though originally defined for linear systems only, this system-theoretic approach allows for a natural extension of the concept of moments to nonlinear systems, among other benefits, which are highlighted as this chapter evolves. Note that the concepts, definitions, and theoretical results discussed in this chapter, are fundamental preliminaries for both Part II and III of this manuscript.

In particular, Section 4.1 discusses the mathematical notion of moments for finite-dimensional linear systems, to later recall the corresponding extension to nonlinear dynamical objects, presenting, for each case, the corresponding definition of moment. Using the definitions introduced in Section 4.1, Section 4.2 discusses the model reduction by moment-matching framework, both for linear and nonlinear dynamical systems, including illustrative example cases.

4.1 The notion of moments

4.1.1 Linear systems

Consider a deterministic, finite-dimensional, SISO, continuous-time system, described, for $t \in \mathbb{R}^+$, by the following set of equations¹

$$\begin{aligned} \dot{x} &= Ax + Bu, \\ y &= Cx, \end{aligned} \tag{4.1}$$

¹: From now on, the dependence on t is dropped when clear from the context.

with $x(t) \in \mathbb{R}^n$, $u(t) \in \mathbb{R}$ and $y(t) \in \mathbb{R}$. The (constant) matrices composing (4.1) are such that $A \in \mathbb{R}^{n \times n}$, and $\{B, C^\top\} \subset \mathbb{R}^n$. From now on, it is assumed that system (4.1) is *minimal*, *i.e.* *controllable* and *observable*.

Remark 4.1.1 Equation (4.1) implicitly assumes that the system is strictly proper, *i.e.* there is no (input) direct feed-through matrix in (4.1). This simplification is done in line with the variety of WEC models utilised throughout this manuscript, which, indeed, share this property. Though outside the scope of this thesis, note that analogous results, to those recalled in this chapter, can be easily derived for biproper systems, by introducing minor modifications (see, for example, [21]).

Let $W : \mathbb{C} \rightarrow \mathbb{C}$, $s \mapsto W(s)$, be the transfer function associated with system (4.1). The following fundamental definition of *moments* is recalled from [222].

Definition 4.1.1 [222] *The 0-moment of system (4.1) at $s_i \in \mathbb{C} \setminus \lambda(A)$ is the complex number $\eta_0(s_i) = C (s_i \mathbb{I}_n - A)^{-1} B$. The k -moment of system (4.1) at s_i is the complex number*

$$\eta_k(s_i) = \frac{(-1)^k}{k!} \left[\frac{d^k}{ds^k} W(s) \right]_{s=s_i}, \quad (4.2)$$

with $k \in \mathbb{N}_{\geq 1}$.

Remark 4.1.2 Note that moments, as in Definition 4.1.1, are the coefficients of the Laurent expansion² of the transfer function $W(s)$ about the complex point s_i .

Remark 4.1.3 Though the minimality assumption on system (4.1) does not pose any loss of generality with respect to Definition 4.1.1, it guarantees that the input-output equation (4.2) completely characterises the dynamical behaviour of (4.1).

Motivated by both the lack of a system-theoretic understanding of the concept of moments as defined above and the fact that Definition 4.1.1 is heavily based on the underlying linearity property of system (4.1), *i.e.* it cannot be directly extended to nonlinear systems, a novel characterisation of moments has been presented in [20], aiming to solve these limitations. Before going further with this system-theoretic definition of moments, the following remark is introduced.

Remark 4.1.4 From now on, the theoretical results are limited to the case of 0-moments, for two fundamental reasons, detailed in the following. Firstly, for both the model reduction and optimal

2: Loosely speaking, the Laurent expansion of a function $f : \mathbb{C} \rightarrow \mathbb{C}$ is a generalisation of the well-known Taylor expansion for the case where f is non-holomorphic, *i.e.* f has isolated singularities.

control part of this thesis, it is shown throughout this manuscript that 0-moments are intrinsically connected with the physical process behind wave energy absorption, which is indeed the main concern of this thesis. Secondly, the concept of a moment for nonlinear systems is not necessarily well-posed for higher-order moments, as further discussed in Section 4.1.2.

To be precise in the meaning behind a system-theoretic characterisation of Definition 4.1.1, note that the moments of system (4.1) have been shown to be in a one-to-one relation with the steady-state response (provided it exists) of the output of the interconnection between a *signal generator* (sometimes referred to as *exogenous system* [22]) and system (4.1) itself. A precise description of this signal generator is given in the following.

Consider a signal generator described, for $t \in \mathbb{R}^+$, by the set of differential equations

$$\begin{aligned}\dot{\xi} &= S\xi, \\ u &= L\xi,\end{aligned}\tag{4.3}$$

with $\xi(t) \in \mathbb{R}^\nu$, $S \in \mathbb{R}^{\nu \times \nu}$ and $L^\top \in \mathbb{R}^\nu$. Consider now the interconnected (or *composite*) system

$$\begin{aligned}\dot{\xi} &= S\xi, \\ \dot{x} &= Ax + BL\xi, \\ y &= Cx.\end{aligned}\tag{4.4}$$

Following [20, 21], a relevant set of assumptions is considered, to later formalise the definition of moments using a system-theoretic approach.

Assumption 4.1.1 The triple of matrices $(L, S, \xi(0))$ is minimal.

Remark 4.1.5 The minimality of the triple $(L, S, \xi(0))$ implies *observability* of the pair (S, L) and *excitability* of the pair $(S, \xi(0))$. Excitability refers (with additional technical assumptions, see [223]) to a geometric characterisation of the property that all signals generated by (4.3) are persistently exciting.

Remark 4.1.6 For linear systems excitability is equivalent to *reachability*, i.e. with $\xi(0)$ playing the role of the input matrix, see [223].

Assumption 4.1.1 stems from the fact that the signal generator defined (4.3) does not have any input. As a matter of fact, given that this signal generator characterises inputs to the system under analysis, i.e. system (4.1), it is rather natural to construct (4.3) in

such a way that all the modes of motion described by the dynamic matrix S are excited, and that the inputs generated are effectively observable.

Assumption 4.1.2 The signal generator (4.3) is such that $\lambda(S) \subset \mathbb{C}^0$ with *simple* eigenvalues³.

Assumption 4.1.2 guarantees that the signal generator (4.1) generates *bounded* trajectories. Note that this automatically implies that the output signal $u(t)$, i.e. the input to system (4.1), is also bounded. The following main lemma can now be introduced.

Lemma 4.1.1 [20, 21] *Suppose Assumptions 4.1.1 and 4.1.2 hold, and that system (4.1) is asymptotically stable in the Lyapunov sense, i.e. $\lambda(A) \subset \mathbb{C}_{<0}$. Then, there is a unique matrix $\Pi \in \mathbb{R}^{n \times \nu}$ which solves the Sylvester equation*

$$\Pi S = A\Pi + BL, \quad (4.5)$$

and the steady-state response of the interconnected system (4.1)-(4.3) is $x_{ss}(t) = \Pi\xi(t)$, for any $x(0)$ and $\xi(0)$.

Moreover, under the same set of assumptions, there exists a one-to-one⁴ relation between the moments $\eta_0(s_1), \eta_0(s_2), \dots, \eta_0(s_\nu)$, with $s_i \in \lambda(S), \forall i \in \mathbb{N}_\nu$, and the steady-state output response $y_{ss}(t) = C\Pi\xi(t)$ (as depicted in Figure 4.1). In fact, the moments are uniquely determined by the matrix $C\Pi$.

Definition 4.1.2 *Suppose the assumptions of Lemma 4.1.1 are fulfilled. The matrix $C\Pi$ is the moment of system (4.1) at (S, L) .*

Remark 4.1.7 For this linear moment-based analysis case, the matrix $C\Pi \equiv \underline{Y}$ is equivalently referred to as the *moment-domain equivalent* of the output y of system (4.1).

Clearly, the fundamental result of Lemma 4.1.1 is the relation between moments (which are purely mathematical objects), and the steady-state response of the composite system (4.1)-(4.3), which is completely characterised by the Sylvester invariance equation (4.5). In particular, this connection can be exploited to provide a definition of moments for the nonlinear case, where Definition 4.1.1 is far from being applicable. This is discussed in the following section.

3: Let $A \in \mathbb{R}^{n \times n}$. An eigenvalue $a \in \lambda(A)$ is said to be *simple* if its algebraic multiplicity is equal to 1.

4: *One-to-one* implies that moments are uniquely determined by the steady-state output response y_{ss} and vice-versa.

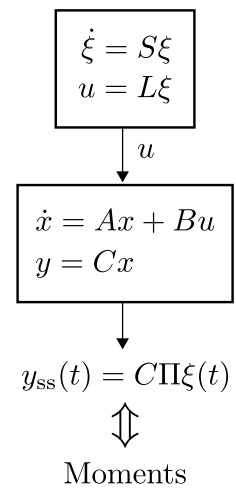


Figure 4.1: Diagrammatic illustration of Lemma 4.1.1.

4.1.2 Nonlinear systems

Consider now a nonlinear, deterministic, finite-dimensional, SISO, continuous-time system, described, for $t \in \mathbb{R}^+$, by the following set of equations

$$\begin{aligned}\dot{x} &= f(x, u), \\ y &= h(x),\end{aligned}\tag{4.6}$$

with $x(t) \in \mathbb{R}^n$, $u(t) \in \mathbb{R}$, $y(t) \in \mathbb{R}$, and f and h sufficiently smooth mappings defined in the neighborhood of the origin of \mathbb{R}^n . Assume system (4.6) is *minimal*, i.e. *observable* and *accessible* (see [21, Chapter 2]), and suppose that $f(0,0) = 0$ and $h(0) = 0$. Similarly to the linear case discussed in Section 4.1.1, consider now the interconnected system

$$\begin{aligned}\dot{\xi} &= S\xi, \\ \dot{x} &= f(x, L\xi), \\ y &= h(x),\end{aligned}\tag{4.7}$$

where S and L are as in (4.3). Following the steady-state notion of moments given in Definition 4.1.2, a nonlinear counterpart of Lemma 4.1.1 can be given in terms of a particular invariance equation, under a similar set of assumptions. This is summarised in the following key result.

Lemma 4.1.2 [20, 21] *Suppose Assumptions 4.1.1 and 4.1.2 hold, and that the zero equilibrium of the system (4.6) is locally exponentially stable in the Lyapunov sense. Then, there exists a unique mapping π , locally⁵ defined in a neighborhood Ξ of $\xi = 0$, with $\pi(0) = 0$, which is the solution of the differential equation*

$$\frac{\partial \pi(\xi)}{\partial \xi} S\xi = f(\pi(\xi), L\xi),\tag{4.8}$$

for all $\xi \in \Xi$, and the steady-state response of the interconnected system (4.6)-(4.3) is $x_{ss}(t) = \pi(\xi(t))$, for any $x(0)$ and $\xi(0)$ sufficiently small.

Definition 4.1.3 *Suppose the assumptions of Lemma 4.1.2 are fulfilled. The mapping $h \circ \pi$ is the moment of system (4.6) at (S, L) .*

Remark 4.1.8 Note that the result of Lemma 4.1.2, and the notion of moments stated in Definition 4.1.3, imply that the moment of system (4.6) at (S, L) computed along a particular trajectory $\xi(t)$ coincides with the (well-defined) steady-state response of the

5: All statements are local, although global versions can be straightforwardly derived.

output of the interconnected system (4.7) (as depicted in Figure 4.2), *i.e.* $y_{ss}(t) = h(\pi(\xi(t)))$.

The result of Lemma 4.1.2 and, specifically, the requirement of Assumption 4.1.2, is closely related to the nonlinear output regulation problem in control theory, and the so-called *centre manifold theory*. The reader is referred to [22, Chapter 8] for a thorough discussion on the topic.

Remark 4.1.9 While, for linear systems, it is possible to define k -moments for every $s_i \in \mathbb{C}$ (see Definition 4.1.1), for nonlinear systems it is virtually impossible to provide general statements as to whether the signal $u(t)$, generated by the signal generator (4.3), is unbounded. This motivates the necessity of Assumption 4.1.2 in Lemma 4.1.2, so that Definition 4.1.3 is well-posed. In other words, both existence and uniqueness of the mapping π , and its connection with the (well-defined) steady-state output response of the corresponding interconnected system, can be guaranteed under the considered set of assumptions.

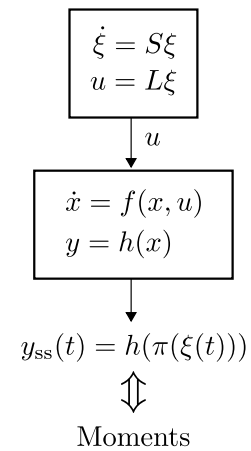


Figure 4.2: Diagrammatic illustration of Lemma 4.1.2.

4.2 Model reduction by moment-matching

Moments, as in Definitions 4.1.2 and 4.1.3, not only provide a very specific parameterisation of the steady-state output response of systems (4.1) and (4.6), respectively, but are also key elements for a powerful state-of-the-art model reduction framework: the family of so-called *moment-matching*-based model reduction techniques.

The reduction technique based on this notion of moments consists of the interpolation of the steady-state response of the output of the system to be reduced⁶: a reduced order model by moment-matching is such that its steady-state response *matches* the steady-state response of either system (4.1) or (4.6), depending on the nature of the target system, *i.e.* linear or nonlinear, respectively. In the following sections, key results associated with this set of tools are recalled, which constitute fundamental preliminaries for Part II of this thesis, both for linear and nonlinear systems.

4.2.1 Linear systems

Based on the steady-state definition of moments discussed in Section 4.1.1, the notion of a reduced order model by moment-matching for linear systems can be now recalled, starting with the following definition.

⁶: Throughout this manuscript, if a given system Σ is reduced by moment-matching to a system $\tilde{\Sigma}$, Σ and $\tilde{\Sigma}$ are referred to as the *target* and *approximating* systems, respectively.

Definition 4.2.1 [20, 21] Consider the signal generator (4.3). The system described by the equations

$$\begin{aligned}\dot{\Theta} &= F\Theta + \Delta u, \\ \theta &= Q\Theta,\end{aligned}\tag{4.9}$$

with $\Theta(t) \in \mathbb{R}^\nu$, $\theta(t) \in \mathbb{R}$, $F \in \mathbb{R}^{\nu \times \nu}$ and $\{\Delta, Q^\top\} \subset \mathbb{R}^\nu$, is a model of system (4.1) at (S, L) , if system (4.9) has the same moments at (S, L) as system (4.1). In addition, system (4.9) is a reduced order model of system (4.1) at (S, L) if $\nu < n$.

Lemma 4.2.1 [20, 21] Consider system (4.1) and the signal generator (4.3). Suppose Assumptions 4.1.1 and 4.1.2 hold, and that system (4.1) is asymptotically stable, i.e. $\lambda(A) \subset \mathbb{C}_{<0}$. Then, system (4.9) is a model of system (4.1) at S if $\lambda(F) \cap \lambda(S) = \emptyset$ and

$$C\Pi = QP,\tag{4.10}$$

where $C\Pi = \underline{Y}$ is the moment-domain equivalent of the output of system (4.1), computed from (4.5), and P is the unique solution of the Sylvester equation

$$PS = FP + \Delta L.\tag{4.11}$$

Remark 4.2.1 The steady-state output of the reduced order model (4.9) exactly matches the steady-state output of the system resulting from the interconnection of system (4.1) and the signal generator (4.3). As a matter of fact, for this linear case, the family of models (4.9) effectively *interpolates* the transfer function $W(s)$ of system (4.1) at the complex points $s_i \in \lambda(S)$, $\forall i \in \mathbb{N}_\nu$ (see Definition 4.1.1).

Note that the computation of the Sylvester equation (4.11) can be avoided, if required. As a matter of fact, as discussed and shown in [20, 21], the family of systems

$$\begin{aligned}\dot{\Theta} &= (S - \Delta L)\Theta + Gu, \\ \theta &= C\Pi\Theta,\end{aligned}\tag{4.12}$$

where Δ is any matrix such that $\lambda(S) \cap \lambda(S - \Delta L) = \emptyset$, belongs to the family (4.9) and contains all the models of dimension ν interpolating the moments of system (4.1) at (S, L) .

The family of models (4.12) is conveniently parameterised in terms of the matrix Δ . This provides an additional degree-of-freedom to enforce specific properties in the reduced order model, such as matching with a prescribed set of eigenvalues Λ , i.e. to guarantee that $\lambda(S - \Delta L) = \Lambda$. In other words, one has full control over

the internal dynamics of the reduced system (4.12)⁷. Naturally, if $\Lambda \subset \mathbb{C}_{<0}$, then the obtained reduced order model is internally stable.

Remark 4.2.2 Note that the spectrum of the matrix $(S - \Delta L)$, i.e. the set $\lambda(S - \Delta L) \subset \mathbb{C}$, defined in the family of systems (4.12), can *always* be assigned *arbitrarily*, as a direct consequence of the observability of the pair (S, L) (which is guaranteed under Assumption 4.1.1).

To illustrate the result of Lemma 4.2.1 and, consequently, the practical use of the family of models described in equation (4.12), the following example case is introduced. Consider a linear system described, for $t \in \mathbb{R}^+$, by the set of equations

$$\begin{aligned} \dot{x} &= \begin{bmatrix} -1 & 1 \\ 0 & -2 \end{bmatrix} x + \begin{bmatrix} 0 \\ 1 \end{bmatrix} u, \\ y &= \begin{bmatrix} 1 & 0 \end{bmatrix} x. \end{aligned} \quad (4.13)$$

Note that system (4.13) is written in Jordan canonical form [224], i.e. it is straightforward to check that both minimality and stability conditions hold. Suppose the system is subject to a constant input u with a given amplitude, which can be realised in terms of a signal generator described by the set of equations

$$\begin{aligned} \dot{\xi} &= 0\xi, \\ u &= l\xi, \end{aligned} \quad (4.14)$$

where $\{l, \xi(0)\} \subset \mathbb{R}$ are such that the triple $(l, 0, \xi(0))$ is minimal. Then, Assumptions 4.1.1 and 4.1.2 hold, and a reduced order model of dimension $\nu = 1$ achieving moment-matching at $(0, l)$ can be constructed directly from (4.12) as

$$\begin{aligned} \dot{\Theta} &= -\Delta l \Theta + \Delta u, \\ \theta &= \begin{bmatrix} 1 & 0 \end{bmatrix} \Pi \Theta, \end{aligned} \quad (4.15)$$

where Π is the solution of the Sylvester equation associated with system (4.13) and the signal generator (4.14) (analogously to equation (4.5)). Note that, as discussed previously in this section, $\Delta \in \mathbb{R}$ can always be chosen such that system (4.13) has a prescribed set of eigenvalues (see Remark 4.2.2).

Figure 4.3 illustrates the output of the target system (4.13) for an input $u = 1$, where the signal generator (4.14) is such that $l = 1$ and $\xi(0) = 1$, and the output of a reduced order model (4.15) with $\Delta = 1$, so that $\lambda(-\Delta l) = -1$, and the slowest (dominant) eigenvalue of system (4.13) is effectively preserved. To be precise,

7: Note that this does not imply one can fully preserve the transient response characteristics of the system. It rather means *some* dynamic characteristics of interest can be preserved, by selecting, for instance, the slow (dominant) eigenvalues of system (4.1) when computing the corresponding reduced order model.

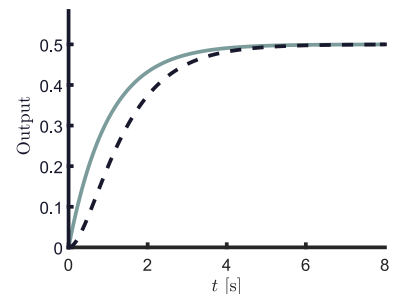


Figure 4.3: Output y of the linear system (4.13) (dashed), and the reduced order model by moment-matching (4.15) θ (solid), for a constant input $u = 1$.

the explicit expression of this reduced order model is given by

$$\begin{aligned}\dot{\Theta} &= -\Theta + u, \\ \theta &= \frac{1}{2}\Theta.\end{aligned}\tag{4.16}$$

The steady-state response matching between target system and reduced model, *i.e.* the moment-matching feature, can be clearly appreciated in Figure 4.3.

4.2.2 Nonlinear systems

Following the moment-based theory of Section 4.1.2, the notion of a reduced order model by moment-matching for nonlinear systems can now be introduced.

Definition 4.2.2 [20, 21] *Consider the signal generator (4.3). The system described by the equations*

$$\begin{aligned}\dot{\Theta} &= \phi(\Theta, u), \\ \theta &= \kappa(\Theta),\end{aligned}\tag{4.17}$$

with $\Theta(t) \in \mathbb{R}^\nu$ and $\theta(t) \in \mathbb{R}$, is a model of system (4.6) at (S, L) , if system (4.17) has the same moments at (S, L) as system (4.6). In addition, system (4.17) is a reduced order model of system (4.6) at (S, L) if $\nu < n$.

Lemma 4.2.2 [20, 21] *Consider system (4.6) and the signal generator (4.3). Suppose Assumptions 4.1.1 and 4.1.2 hold, and that the zero equilibrium of system (4.6) is locally exponentially stable. Then, system (4.17) matches the moments of system (4.6) at (S, L) if the equation*

$$\frac{\partial p}{\partial \xi} S\xi = \phi(p(\xi), L\xi),\tag{4.18}$$

has a unique solution p such that

$$h(\pi(\xi)) = \kappa(p(\xi)),\tag{4.19}$$

where the mapping π is the unique solution of equation (4.8).

Following the result of Lemma 4.2.2, and analogously to the linear case of Section 4.2.1, a family of systems achieving moment-matching at (S, L) [20, 21] can be defined as

$$\begin{aligned}\dot{\Theta} &= (S - \rho(\Theta)L)\Theta + \rho(\Theta)u, \\ \theta &= h(\pi(\Theta)),\end{aligned}\tag{4.20}$$

with $\rho : \mathbb{R}^\nu \rightarrow \mathbb{R}^\nu$ a free mapping. A particularly interesting simplification can be achieved with the selection $\rho(\Theta) = \Delta$, for any constant matrix Δ . This choice produces a family of reduced order models described by a linear differential equation with a nonlinear output map, *i.e.* by a Wiener model.

Remark 4.2.3 Two advantages of the selection of the mapping ρ in the family of models (4.20) as $\rho(\Theta) = \Delta$, can be clearly identified: the matrix Δ can be selected to enforce additional properties to (4.20) such as a set of prescribed eigenvalues, and the determination of the reduced order model achieving moment-matching at (S, L) boils down to the computation of the mapping $h \circ \pi$.

Similarly to the case of Section 4.2.1, an illustrative example is now presented, where explicit use of the family of reduced order models (4.20) is made. Consider a nonlinear system given by the set of equations

$$\begin{aligned} L_1 \dot{x}_1 &= -(1-u)x_2 + E, \\ C_2 \dot{x}_2 &= (1-u)x_1 + x_3 u, \\ L_3 \dot{x}_3 &= -x_2 u - x_4, \\ C_4 \dot{x}_4 &= x_3 - R x_4, \\ y &= x_4, \end{aligned} \tag{4.21}$$

where $x_1(t) \in \mathbb{R}^+$ and $x_3(t) \in \mathbb{R}^-$ describe⁸ currents, $x_2(t) \in \mathbb{R}^+$ and $x_4(t) \in \mathbb{R}^-$ describe voltages, $\{L_1, C_2, L_3, C_4, E, R\} \subset \mathbb{R}^+$ and $u(t) \in (0, 1)$ a continuous (constant) input. Note that this input can be effectively realised using the signal generator described by equations (4.14). The moment of system (4.21) at $(0, l)$ is given [20] by $h(\pi(\xi)) = E(\xi/(\xi - 1))$ and a locally asymptotically stable reduced order model of dimension $\nu = 1$ achieving moment-matching at $(0, l)$ is

$$\begin{aligned} \dot{\theta} &= -\rho(\Theta)l + \rho(\Theta)u, \\ \theta &= E \frac{\Theta}{\Theta - 1}, \end{aligned} \tag{4.22}$$

where $\rho(0) > 0$, which is well-defined if $\xi \neq 1, \forall t \in \mathbb{R}^+$. The parameters of the system are selected as described in Table 4.1 (extracted from [225]). Following Remark 4.2.3, $\rho(\Theta) = \Delta$ is chosen, *i.e.* the reduced order model (4.22) is linear, with a nonlinear output map. In particular, $\Delta = 100$ is selected, which (approximately) preserves the real part of the slowest eigenvalue of the Jacobian linearisation of (4.21) about the origin.

8: The mathematical model represented with equation (4.21) corresponds to the averaged DC-to-DC Ćuk converter. The reader is referred to [225] for further detail.

Parameter	Value
L_1	10 [mH]
C_2	22 [μ F]
L_3	10 [mH]
C_4	22 [μ F]
E	20 [V]
R	0.04 [S]

Table 4.1: Parameters of the example case for nonlinear model reduction.

Figure 4.4 shows the output of the target system (4.21), and the output of the reduced order model (4.22), for a constant input of amplitude 0.7. It can be clearly appreciated that there is a perfect match between both the steady-state response of system (4.21), and the moment-matching-based reduced order system (4.22).

Remark 4.2.4 Note that the example case, provided and discussed above, heavily relies on the availability of an analytical expression for the mapping $h \circ \pi$. Clearly, this example is very specific, and the mapping can be deduced with a (relatively) mild algebraic effort. In the more general case, where both the mapping f and the signal generator (S, L) can be much more complex than those employed in this example (for instance, the wave energy case discussed throughout this manuscript), it is virtually impossible to compute an analytic expression for the moment $h \circ \pi$. In other words, without a proper approximation framework, the theory recalled in both Sections 4.1.2 and 4.2.2, is far from having any practical value. Note that, in light of this applicability limitation, different approximation techniques are proposed in this thesis, discussed in both Parts II and III of the manuscript.

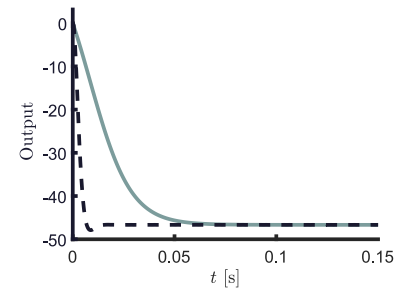


Figure 4.4: Output y of the non-linear system (4.21) (dashed), and the reduced order model by moment-matching (4.22) θ (solid), for a constant input $u = 0.7$.

Part II: Moment-based model reduction

Reduced models for linear SISO WECs

5

Contents of this chapter

5.1	Moment-based WEC formulation for model reduction	91
5.2	Reduced models achieving moment-matching	97
5.2.1	Input-output dynamics	97
5.2.2	Radiation dynamics	100
5.3	Case study: a toroidal geometry	101
5.3.1	Input-output model reduction	102
5.3.2	Radiation model reduction	105
5.4	On the properties of radiation models	107
5.4.1	Enforcing passivity	109
5.4.2	Enforcing zeros at $s = 0$	113
5.5	Conclusions	114

Recall, from Section 2.4, that the equation of motion for a WEC, under the assumptions of linear potential flow theory (see Section 2.3.1), can be expressed in terms of *Cummins'* equation (2.20). This equation is recalled below, for a 1-DoF WEC device, for convenience:

$$\Sigma : \begin{cases} \ddot{z} = \mathcal{M}(-k_r * \dot{z} - s_h z + f_e), \\ y = \dot{z}, \end{cases} \quad (5.1)$$

where $z : \mathbb{R}^+ \rightarrow \mathbb{R}$ is the displacement, $k_r : \mathbb{R}^+ \rightarrow \mathbb{R}$, $k_r \in L^2(\mathbb{R})$, the radiation impulse response function, $f_e : \mathbb{R}^+ \rightarrow \mathbb{R}$, the wave excitation, and $\mathcal{M} \in \mathbb{R}_{>0}$ is the inverse of the generalised mass matrix of the device (which is simply a scalar in this case).

As discussed in Section 2.4, the presence of the non-parametric convolution operation, related to radiation effects, represents both a representative and a computational drawback for a variety of applications (including WEC control and state-estimation). Model reduction techniques can be used to parameterise this non-parametric operator, commonly defined in terms of a state-space representation, which should ideally retain the underlying physical properties that characterise the WEC dynamical process.

Considering the ideal characteristics described above (and in Section 2.4), this chapter proposes an approximation framework based on model order reduction by moment-matching techniques, using a system-theoretic interpretation of *moments*, as introduced in Chapter 4. Recall that moment-based methods, for *linear* systems, interpolate a certain number of points on the complex plane, *i.e.* the so-called moments, which are directly related to the frequency response of the target dynamical system under analysis. In fact, the transfer

function of the approximating model obtained by this moment-based approach *exactly* matches the steady-state behavior of the target system at these specific interpolation points, which are user-selected. Furthermore, within this system-theoretic interpolation approach, essential physical properties of the device can be retained by the reduced order model, such as internal stability, passivity, and zero dynamics.

This moment-based approximation framework is presented in two different modalities: input-output (force-to-motion), and radiation effects model reduction. The former deals with producing (parametric) reduced order models from an input-output perspective, *i.e.* system Σ defined in equation (5.1), while the latter approximates the radiation subsystem Σ_r (defined in Section 2.4), to later 'embed' into Cummins' equations (see (2.22)).

The remainder of this chapter is organised as follows. Section 5.1 proposes a moment-based formulation for WECs, to explicitly compute the moment-domain equivalent associated with the non-parametric system (5.1). Using these theoretical results, Section 5.2 outlines the methodology behind the computation of moment-based reduced order models, both for the input-output system Σ , and the radiation dynamics, defined by Σ_r . Section 5.3 illustrates the framework proposed, by considering the model reduction problem for a specific WEC device. In the light of the discussion provided on the physical properties of radiation effects, Section 5.4 assesses the capabilities of this moment-based approach in retaining the underlying dynamics of Σ_r , proposing specific methods to *ensure*¹ passivity and zero dynamics properties. Finally, the main conclusions of this chapter are encompassed in Section 5.5.

5.1 Moment-based WEC formulation for model reduction

Note that moment-based theory, as recalled in Chapter 4, is inherently based on the knowledge of a state-space representation of the system to be reduced, which is clearly not the case for Cummins' formulation², recalled in equation (5.1). In other words, to consider the theoretical results discussed in Section 4.2 for this 1-DoF WEC case, the equation of motion characterised by Σ needs to be re-written in a more suitable structure. The following equivalent representation, for system Σ in equation (5.1), is proposed:

$$\Sigma : \begin{cases} \dot{w} = Aw + Bv, \\ y = Cw, \end{cases} \quad (5.2)$$

1: As discussed in Section 5.4, moment-based methods virtually always respect the inherent properties of radiation effects, without needing to 'impose' such characteristics. Nevertheless, if required by the application, this thesis also proposes methods to specifically *guarantee* each of the dynamical properties for radiation effects listed in Table 2.1.

2: This is, in fact, exactly the main objective of this chapter.

for $t \in \mathbb{R}^+$, where $w(t) = [z(t) \quad \dot{z}(t)]^\top \in \mathbb{R}^2$ contains displacement and velocity for the (single) DoF involved in the equation of motion, and the matrices $A \in \mathbb{R}^{2 \times 2}$, $B \in \mathbb{R}^2$ and $C^\top \in \mathbb{R}^2$ are defined as

$$A = \begin{bmatrix} 0 & 1 \\ -\mathcal{M}s_h & 0 \end{bmatrix}, \quad B = \begin{bmatrix} 0 \\ \mathcal{M} \end{bmatrix}, \quad C = \begin{bmatrix} 0 \\ 1 \end{bmatrix}^\top. \quad (5.3)$$

The ‘input’ function $v : \mathbb{R}^+ \rightarrow \mathbb{R}$, is defined as

$$v = f_e - k_r * \dot{z} = f_e - k_r * Cw, \quad (5.4)$$

where the radiation force, *i.e.* the system Σ_r defined in Section 2.4, is ‘decoupled’ as an output feedback term. This is schematically illustrated in Figure 5.1.

Remark 5.1.1 The radiation force convolution term is included as a feedback term in v , only as an algebraic manipulation to develop a ‘compatible’ representation of (5.1), with respect to the moment-based theory recalled in Chapter 4. Note that the meaningful external input is still the wave excitation force f_e .

Within the moment-based formulation of Chapter 4, the mapping corresponding with the external input f_e is written in terms of an autonomous single-output signal generator (analogously to the case of equation (4.3)), *i.e.* the set of differential equations

$$\begin{aligned} \dot{\xi} &= S\xi, \\ f_e &= L\xi, \end{aligned} \quad (5.5)$$

for $t \in \mathbb{R}^+$, with $\xi(t) \in \mathbb{R}^\nu$, $S \in \mathbb{R}^{\nu \times \nu}$ and $L^\top \in \mathbb{R}^\nu$. Recall that a set of standing assumptions on the nature of the signal generator (*i.e.* Assumptions 4.1.1 and 4.1.2), are required to have a well-posed system-theoretic definition of moments. These are discussed, for the WEC case, in the following paragraphs.

With respect to Assumption 4.1.2, which poses a set of characteristics³ for $\lambda(S)$, the following finite-set $\mathcal{F} = \{\omega_p\}_{p=1}^f \subset \mathbb{R}^+$ is considered, and the dynamic matrix S is written in a block-diagonal form as,

$$S = \bigoplus_{p=1}^f \begin{bmatrix} 0 & \omega_p \\ -\omega_p & 0 \end{bmatrix}, \quad (5.6)$$

where $\nu = 2f$, $f \in \mathbb{N}_{\geq 1}$, and hence $\lambda(S) = (j\mathcal{F}) \cup (-j\mathcal{F}) \subset \mathbb{C}^0$.

With respect to Assumption 4.1.1⁴, and without any loss of generality, the initial condition of the signal generator is chosen as $\xi(0) = \varepsilon_\nu$, so that it is straightforward to check that the minimality

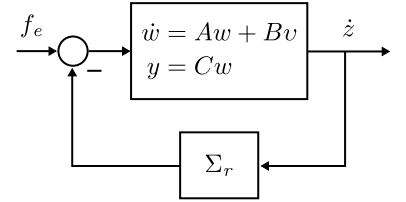


Figure 5.1: Radiation system Σ_r as a feedback term.

3: Assumption 4.1.2: The matrix S is such that $\lambda(S) \subset \mathbb{C}^0$ with simple eigenvalues.

4: Assumption 4.1.1: The triple $(L, S, \xi(0))$ is minimal.

condition on the triple (L, S, ε_ν) holds as long as the pair (S, L) is observable.

Remark 5.1.2 Note that each ω_p in (5.6) effectively represents a desired interpolation point for the model reduction process, *i.e.* a frequency where the frequency response of the reduced order model matches the frequency response of the target system. In other words, the objective now is to use the representation given by the signal generator (5.6) to interpolate the f frequencies defined in the (user-selected) set \mathcal{F} .

To accomplish the model reduction by a moment-matching objective, the key theoretical step is to compute the moments of system Σ (defined in equation (5.2)) driven by the signal generator (5.6), characterised by the pair (S, L) . In other words, the aim is to compute the *moment-domain equivalent of the velocity* of the device, *i.e.* $\dot{\underline{Z}}$. Under the representation presented in (5.2), these moments can be computed by solving a specific equation (analogously⁵ to Lemma 4.1.1). Such an equation can be specialised for the WEC case as

$$A\Pi + B(L - \underline{K}_r) = \Pi S, \quad (5.7)$$

where $\Pi \in \mathbb{R}^{2 \times \nu}$ and $\underline{K}_r \in \mathbb{R}^\nu$ is the moment-domain equivalent of the radiation force (*i.e.* the output of Σ_r).

Remark 5.1.3 The moment-domain equivalent of the velocity can be expressed in terms of the solution of (5.7) (provided it exists) straightforwardly as $\dot{\underline{Z}} = C\Pi$. This is schematically illustrated in Figure 5.2

The term \underline{K}_r clearly depends⁶ on Π , hence one cannot yet solve (5.7), until it is properly defined. In the following, the quantity \underline{K}_r is explicitly derived, to then provide sufficient conditions for existence and uniqueness of the solution of (5.7).

Proposition 5.1.1 *The moment-domain equivalent of the convolution integral in (5.1) can be computed as*

$$\underline{K}_r = \dot{\underline{Z}}\mathcal{R}, \quad (5.8)$$

where the operator $\mathcal{R} \in \mathbb{R}^{\nu \times \nu}$ is a block-diagonal matrix, defined as

$$\mathcal{R} = \bigoplus_{p=1}^f \begin{bmatrix} r_{\omega_p} & m_{\omega_p} \\ -m_{\omega_p} & r_{\omega_p} \end{bmatrix}, \quad (5.9)$$

with

$$r_{\omega_p} = B_r(\omega_p), \quad m_{\omega_p} = \omega_p [A_r(\omega_p) - m_\infty], \quad (5.10)$$

5: Note that direct application of Lemma 4.1.1 is not possible due to the non-parametric structure of Σ .

6: Note the convolution operator depends on the output of system Σ .

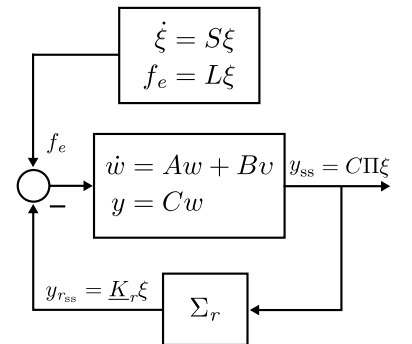


Figure 5.2: Moment-based analysis of the WEC system Σ .

where $A_r(\omega)$ is the radiation added-mass, and $B_r(\omega)$ is the radiation damping of the device (see Section 2.3.2.2), evaluated at each specific frequency induced by the eigenvalues of S .

Proof. The steady-state response of the velocity can be written in terms of its moment-domain equivalent (provided it exists), i.e. $\dot{z}_{ss} = \underline{\dot{Z}}\xi$. Direct replacement into the radiation convolution operation yields,

$$\int_{\mathbb{R}^+} k_r(\tau)\dot{z}_{ss}(t-\tau)d\tau = \underline{\dot{Z}} \int_{\mathbb{R}^+} k_r(\tau)\xi(t-\tau)d\tau. \quad (5.11)$$

Note now that that the vector $\xi(t) \in \mathbb{R}^\nu$ can be conveniently expanded as

$$\xi(t) = e^{St}\varepsilon_\nu = \sum_{p=1}^f e_p^f \otimes \begin{bmatrix} p\xi^+(t) \\ p\xi^-(t) \end{bmatrix}, \quad (5.12)$$

where, for this particular initial condition $\xi(0)$, the mappings ${}^p\xi : \mathbb{R}^+ \rightarrow \mathbb{R}$ are given by ${}^p\xi^+(t) = \cos(\omega_p t)$ and ${}^p\xi^-(t) = -\sin(\omega_p t)$, for all $p \in \mathbb{N}_f$.

Analysing equation (5.11) in 'blocks', i.e. for a particular frequency ω_p , with $p \in \mathbb{N}_f$, it is possible to directly recognise two different convolution operations: $k_r * {}^p\xi^+$ and $k_r * {}^p\xi^-$. Expanding the former expression, and considering well-known trigonometric identities, yields

$$\begin{aligned} (k_r * {}^p\xi^+)(t) &= \cos(\omega_p t) \int_{\mathbb{R}^+} k_r(t) \cos(\omega_p t) dt + \\ &\quad \sin(\omega_p t) \int_{\mathbb{R}^+} k_r(t) \sin(\omega_p t) dt. \end{aligned} \quad (5.13)$$

Using Oglivie's relationships, defined in Section 2.3.2.2, the integral operations involved in (5.13) can be evaluated explicitly, using the frequency-dependent parameters $B_r(\omega)$ and $A_r(\omega)$, i.e.

$$\begin{aligned} \int_{\mathbb{R}^+} k_r(t) \cos(\omega_p t) dt &= B_r(\omega_p) = r_{\omega_p}, \\ \int_{\mathbb{R}^+} k_r(t) \sin(\omega_p t) dt &= -\omega_p [A_r(\omega_p) - m_\infty] = -m_{\omega_p}. \end{aligned} \quad (5.14)$$

Performing similar operations on $k * {}^p\xi^-$, the expression

$$\begin{bmatrix} k_r * {}^p\xi^+ \\ k_r * {}^p\xi^- \end{bmatrix} = \begin{bmatrix} r_{\omega_p} & m_{\omega_p} \\ -m_{\omega_p} & r_{\omega_p} \end{bmatrix} \begin{bmatrix} {}^p\xi^+ \\ {}^p\xi^- \end{bmatrix}, \quad (5.15)$$

holds. Finally, the claim of this proposition, i.e. $\underline{K}_r = \underline{\dot{Z}}\mathcal{R}$, follows from simply repeating the same analysis for each $p \in \mathbb{N}_f$. \square

Remark 5.1.4 The statement of Proposition 5.1.1 can be proved straightforwardly for any initial condition $\xi(0)$, *i.e.* the definition of the moment-based representation of the radiation force is *independent* of the initial condition of the signal generator⁷. The objective behind the selection of $\xi(0) = \varepsilon_\nu$ is twofold: Firstly, to illustrate a suitable selection of the initial condition $\xi(0)$ such that the pair $(S, \xi(0))$ is excitable (given that the geometric definition of excitability is not ‘standard’ in the control literature); and secondly, to simplify the notation used throughout the proof of Proposition 5.1.1.

7: Clearly, this assertion is directly related to the underlying linearity property of the radiation force system Σ_r .

Using the analytical definition of the moment-domain equivalent of the radiation convolution term in (5.8), the following two propositions, that address the uniqueness of the solution of the Sylvester equation (5.7), and the explicit computation of the moment equivalent \dot{Z} , are now stated.

Proposition 5.1.2 *The solution of the Sylvester equation (5.7) is unique if and only if*

$$\lambda \left(\bigoplus_{p=1}^f \begin{bmatrix} T_p & 0 \\ 0 & \overline{T_p} \end{bmatrix} \right) \cap \lambda(S) = \emptyset, \quad (5.16)$$

where the matrix T_p is defined as

$$T_p = A - B(r_{\omega_p} + jm_{\omega_p})C. \quad (5.17)$$

Proof. A direct application of the vec operator to equation (5.7) (and considering Property 1.3.1 and the bilinearity and associativity property of the Kronecker product) yields the equivalent linear system of equations

$$\Phi \text{vec}\{\Pi\} = \text{vec}\{-BL\}, \quad (5.18)$$

where the matrix $\Phi \in \mathbb{R}^{2\nu \times 2\nu}$ is defined as

$$\Phi = (S \hat{\oplus} A) + \mathcal{R}^\top \otimes -BC. \quad (5.19)$$

It is straightforward to conclude from (5.18) that the solution of the Sylvester equation (5.7) is unique if and only if $0 \notin \lambda(\Phi)$. As a consequence of the block-structure of each of the matrices involved in (5.19), the matrix Φ can be always written in a block-diagonal structure, *i.e.* $\Phi = \bigoplus_{p=1}^f \Phi_p$. Therefore, the matrix Φ is invertible if and only if each block Φ_p is invertible.

After algebraic manipulation of (5.19), each block composing Φ can

be expressed as

$$\Phi_p = \begin{bmatrix} A - Br_{\omega_p}C & \omega_p \mathbb{I}_2 + Bm_{\omega_p}C \\ -\omega_p \mathbb{I}_2 - Bm_{\omega_p}C & A - Br_{\omega_p}C \end{bmatrix}. \quad (5.20)$$

Consider now the (invertible) matrix

$$W = \begin{bmatrix} \mathbb{I}_2 & j\mathbb{I}_2 \\ \mathbb{I}_2 & -j\mathbb{I}_2 \end{bmatrix}, \quad (5.21)$$

and the similarity transformation ${}^W\Phi_p = W\Phi_p W^{-1}$, which yields

$${}^W\Phi_p = - \begin{bmatrix} j\omega_p \mathbb{I}_2 - T_p & 0 \\ 0 & j\omega_p \mathbb{I}_2 - T_p \end{bmatrix}. \quad (5.22)$$

Since the spectrum of a matrix remains invariant under a coordinate transformation, one can conclude from (5.22) that Φ_p is invertible if and only if⁸

$$\lambda \left(\begin{bmatrix} T_p & 0 \\ 0 & T_p \end{bmatrix} \right) \cap \lambda(S) = \emptyset. \quad (5.23)$$

Finally, the claim follows repeating the same analysis for each block of Φ_p with $p \in \mathbb{N}_f$. \square

8: Note that, the following equality $\lambda(\alpha \mathbb{I} + A) = \alpha +_M \lambda(A)$, for any matrix $A \in \mathbb{C}^{n \times n}$, holds, where the notation $+_M$ is used for the Minkowski sum of two sets (see, for instance, [226]).

Proposition 5.1.3 *Suppose (5.16) holds. Then, the moment-domain equivalent of the output y of system (5.2) (the velocity of the device \dot{z}) can be uniquely determined as*

$$\underline{\dot{Z}} = L\Phi_{\mathcal{R}}^T, \quad (5.24)$$

where the matrix $\Phi_{\mathcal{R}} \in \mathbb{R}^{\nu \times \nu}$ is defined as

$$\begin{aligned} \Phi_{\mathcal{R}} &= (\mathbb{I}_{\nu} \otimes C)\Phi^{-1}(\mathbb{I}_{\nu} \otimes -B), \\ \Phi &= (S \hat{\oplus} A) + \mathcal{R}^T \otimes -BC, \end{aligned} \quad (5.25)$$

with $\Phi \in \mathbb{R}^{2\nu \times 2\nu}$.

Proof. Recall that $\underline{\dot{Z}} = C\Pi$. Then equation (5.24) follows directly from (5.18), noting that $\text{vec}\{\underline{\dot{Z}}\} = \underline{\dot{Z}}^T$ and $\text{vec}\{L\} = L^T$. \square

Remark 5.1.5 Equation (5.16) always holds for the WEC device case: it follows from the internal stability of (5.2) (see Section 2.4) that $\lambda(T_p) \subset \mathbb{C}_{<0}$ for all $p \in \mathbb{N}_f$, where the matrices T_p are as in Proposition 5.1.2.

With the results provided in Propositions 5.1.2 and 5.1.3, it is possible to define a suitable family of reduced order models achieving moment-

matching both for the input-output system Σ , and the radiation dynamics Σ_r . This is directly addressed in Section 5.2.

5.2 Reduced models achieving moment-matching

With the theoretical results proposed in Section 5.1, it is possible to compute reduced order models both for the input-output (force-to-motion) dynamics, *i.e.* a system $\tilde{\Sigma}$ approximating Σ in (5.2), and the radiation system, *i.e.* a system $\tilde{\Sigma}_r$ approximating Σ_r . Both approaches are discussed in the following subsections, starting from the input-output model reduction case, in Section 5.2.1, following with the radiation dynamics case, in Section 5.2.2.

5.2.1 Input-output dynamics

Propositions 5.1.2 and 5.1.3 explicitly show how to compute the (unique) moment-domain equivalent of the output of system (5.2), *i.e.* the moment-based representation of the velocity of the WEC. This, together with Definition 4.2.1 and Lemma 4.2.1, allow for the computation of a reduced order model of system (5.2), from an *input-output (force-to-motion)* perspective, *i.e.* $f_e \mapsto \dot{z}$, achieving moment-matching at (S, L) . Explicitly:

$$\Sigma \approx \tilde{\Sigma}_{\mathcal{F}} : \begin{cases} \dot{\Theta} = (S - \Delta L)\Theta + \Delta f_e, \\ \tilde{y} = \underline{\dot{Z}}\Theta, \end{cases} \quad (5.26)$$

is the family of reduced order models, for $t \in \mathbb{R}^+$, parameterised in $\Delta \in \mathbb{R}^{\nu}$, containing *all* the models of dimension ν achieving moment-matching at (S, L) , *i.e.* interpolating the moments of system (5.2) at the eigenvalues of the matrix S (which are fully characterised by the set of user-selected frequencies \mathcal{F}), and where $\underline{\dot{Z}} = L\Phi_{\mathcal{D}}^T$ (as in Proposition 5.1.3).

Remark 5.2.1 The reduced order model (5.26) has dimension (order) $\nu = 2f$, where f is the number of (user-selected) interpolation points (frequencies in this case). This is a consequence of the fact that, for each frequency ω_i , both $\pm j\omega_i$ are chosen as eigenvalues of the real-valued⁹ matrix S .

Remark 5.2.2 The notation $\tilde{\Sigma}_{\mathcal{F}}$ refers to an approximated time-domain model of the force-to-motion dynamics of the device under analysis, by matching the frequencies selected in $\lambda(S)$, fully characterised by the set \mathcal{F} .

9: One could select only $+\omega_p$ or $-\omega_p$, instead of $\pm\omega_p$. This, in turn, results in a reduced order model of dimension f rather than $2f$, but defined over the field \mathbb{C} . In other words, the matrix S has necessarily complex entries. Note that $\mathbb{C}^{f \times f}$ is effectively isomorphic to $\mathbb{R}^{2f \times 2f}$, so that no 'real' computational saving is achieved.

As highlighted previously in Remark 4.2.2, the additional degree of freedom provided by the matrix Δ can be exploited to assign the eigenvalues of the reduced order model (5.26): Given the observability condition of the pair (S, L) , the set $\lambda(S - \Delta L)$ can be arbitrarily assigned.

In this particular case, the set of desired eigenvalues is chosen within a particular optimisation-based formulation, which aims to minimise the Euclidean distance between the device frequency response $G(\omega)$ (see Section 3.1), constructed with data obtained with hydrodynamic codes, and the reduced order model (achieving moment-matching at the frequencies induced by the set \mathcal{F}) frequency response $\tilde{G}_{\mathcal{F}}(\omega)$. The complete procedure is summarised in the following steps, listed below.

Procedure 1: SISO model reduction procedure for WECs

- 1 Select a set of f interpolation points (frequencies) $\mathcal{F} = \{\omega_p\}_{p=1}^f \subset \mathbb{R}^+$ to achieve moment-matching.
- 2 Compute the matrix S following (5.6) and select any L such that the pair (S, L) is observable.
- 3 Calculate the moment-domain equivalent of the output of system (5.2), *i.e.* \dot{Z} , using the result of Proposition 5.1.3.
- 4 Consider the frequency response of (5.26) as a function of Δ *i.e.* the mapping $\tilde{G}_{\mathcal{F}} : \mathbb{R} \times \mathbb{R}^\nu \rightarrow \mathbb{C}$ given by

$$\tilde{G}_{\mathcal{F}}(\omega, \Delta) = \dot{Z} (j\omega \mathbb{I}_\nu - S + \Delta L)^{-1} \Delta. \quad (5.27)$$

- 5 Let $\Omega = \{\omega_i\}_{i=1}^M \subset W$ be the (finite) frequency set utilised to compute the hydrodynamic coefficients $B_r(\omega)$ and $A_r(\omega)$, in the frequency range¹⁰ $W = [\omega_l, \omega_u] \subset \mathbb{R}^+$. Then, compute the input matrix Δ^{opt} with the following optimisation-based procedure:

$$\Delta^{\text{opt}} = \arg \min_{\Delta \in \mathcal{D}} \sum_{i=1}^M \left| \tilde{G}_{\mathcal{F}}(\omega_i, \Delta) - G(\omega_i) \right|^2, \quad (5.28)$$

where \mathcal{D} is defined as $\mathcal{D} = \{\Delta \in \mathbb{R}^\nu \mid \lambda(S - \Delta L) \subset \mathbb{C}_{<0}\}$.

- 6 Compute a ν -dimensional input-output WEC time-domain model achieving moment-matching at (S, L) from (5.26) as

$$\Sigma \approx \tilde{\Sigma}_{\mathcal{F}} : \begin{cases} \dot{\Theta} = (S - \Delta^{\text{opt}} L)\Theta + \Delta^{\text{opt}} f_e, \\ \tilde{y} = \dot{Z}\Theta. \end{cases} \quad (5.29)$$

10: The selection of this frequency range is strongly linked both with the application for which the reduced model is computed for, and the SDF characterising the external input f_e .

Briefly summarising, the procedure proposed above is based on the idea of building the parametric model $\tilde{\Sigma}_{\mathcal{F}}$, matching the f (user-defined) frequencies of the set \mathcal{F} , exploiting the system structure

of (5.26), and solving for an optimisation problem on Δ . This optimisation process aims to compute the input matrix Δ^{opt} which minimises the difference between the target frequency response and that of (5.26) (in terms of the Euclidean norm) while guaranteeing internal stability of the parametric model.

Remark 5.2.3 The optimisation problem described in Step 5 above can be solved using a variety of techniques, including, for example, interior-point methods [209]. Numerical convergence towards a global minimiser can be performed using local optimisation routines (with multiple starting points), or global optimisation routines (see, for instance, [227]) directly¹¹.

11: Though the latter family of techniques can be computationally demanding, that does not constitute an issue for the model reduction case, which has to be run only *once* to compute the approximating model $\tilde{\Sigma}_{\mathcal{F}}$.

5.2.1.1 Force-to-displacement dynamics

Section 5.2.1 describes the theoretical framework to compute an input-output reduced model, *i.e.* a parametric form of Cummins' equation in (5.2), for the force-to-velocity dynamics, where the output of Σ is \dot{z} . As discussed throughout Chapters 3 and 4, the selection of the output as $y = \dot{z}$ is motivated by the specifics of the energy-maximising optimal control problem for WECs, which directly depends on the velocity of the device. Nevertheless, if a force-to-displacement parametric form is required, one could either change the vector C in (5.2) accordingly (to select \dot{z} as the output of system Σ), or consider the following procedure, which further exploits the properties of the moment-based formulation.

Proposition 5.2.1 Consider a dynamical system given, for $t \in \mathbb{R}^+$, by the differential equation

$$\dot{w} = u. \quad (5.30)$$

Suppose u is described by a signal generator characterised by the pair (S, L) , and that Assumptions 4.1.1 and 4.1.2 hold. Let \underline{W} be the moment-domain equivalent of w . Then, the moment-domain equivalent of \dot{w} is $\underline{W}S$. In an analogous form, the moment-domain equivalent of $\int w(\tau)d\tau$ is given by $\underline{W}S^{-1}$.

Proof. The proof of this proposition stems directly from [228, Corollary 1] and, hence, is omitted. \square

The result of Proposition 5.2.1 allows for the computation of a reduced model for the force-to-displacement dynamics, by using the exact same results computed for the force-to-velocity response. In

particular, one can compute the moment-domain equivalent of the displacement z directly from equation (5.24) as

$$\underline{Z} = \dot{Z}S^{-1} = L\Phi_{\mathcal{R}}^T S^{-1}. \quad (5.31)$$

Remark 5.2.4 The same procedure proposed to compute Δ^{opt} for the force-to-velocity case, *i.e.* Procedure 1, can be directly adapted to the force-to-displacement dynamics, by simply changing \dot{Z} by Z , and the force-to-velocity frequency response $G(\omega)$ by $P(\omega) = G(\omega)/j\omega$.

5.2.2 Radiation dynamics

As discussed previously, in Section 2.4, the radiation impulse response function k_r completely characterises a LTI dynamical system Σ_r , describing the mapping $\dot{z} \mapsto y_r = k_r * \dot{z}$.

A reduced order model can be obtained following an analogous procedure to that considered for the force-to-motion case. In particular, let the velocity \dot{z} be expressed as a signal generator, in the same fashion as equation (5.5), *i.e.*

$$\begin{aligned} \dot{\xi} &= S\xi, \\ \dot{z} &= L\xi, \end{aligned} \quad (5.32)$$

where the structure of S is as in equation (5.6), and any L such that the pair (S, L) is observable. Then, recalling the result posed in Proposition 5.1.1, the moment-domain equivalent of system Σ_r , *i.e.* y_r , can be directly computed as $\underline{Y}_r = L\mathcal{R}$. Analogously to equation (5.26), the family of reduced order models, parameterised by $\Delta \in \mathbb{R}^\nu$, containing *all* the models of dimension ν achieving moment-matching at (S, L) , *i.e.* interpolating the moments of system Σ_r at the eigenvalues of the matrix S , can be directly written as

$$\Sigma_r \approx \tilde{\Sigma}_{r\mathcal{F}} : \begin{cases} \dot{\Theta} = (S - \Delta L)\Theta + \Delta\dot{z}, \\ \tilde{y}_r = \underline{Y}_r\Theta. \end{cases} \quad (5.33)$$

Remark 5.2.5 Similarly to the force-to-velocity (or force-to-displacement) case, Procedure 1 (described in Section 5.2.1) can be directly adapted to a family of models for the radiation system (6.37), by simply replacing \dot{Z} by \underline{Y}_r , and the device frequency response $G(\omega)$ by that of the radiation force, *i.e.* $K_r(\omega)$ (defined in Section 2.3.2.2).

5.3 Case study: a toroidal geometry

The case study, selected to illustrate the moment-based reduction strategy proposed in this chapter, is based on a toroidal geometry¹² (floater), which constitutes one of the main components of devices such as, for instance, the Ocean Power Technologies (OPT) point absorber WEC [229], and Wavebob [230]. The specific geometry considered is depicted in Figure 5.3 (dimensions are in metres), and is assumed to be constrained to move in heave (translational motion), which is effectively the DoF from where energy is absorbed in [229].

12: The selection of this geometry is motivated by the underlying complexity of its associated (multi-modal) frequency response, aiming to fully illustrate the capabilities of the moment-based approach.

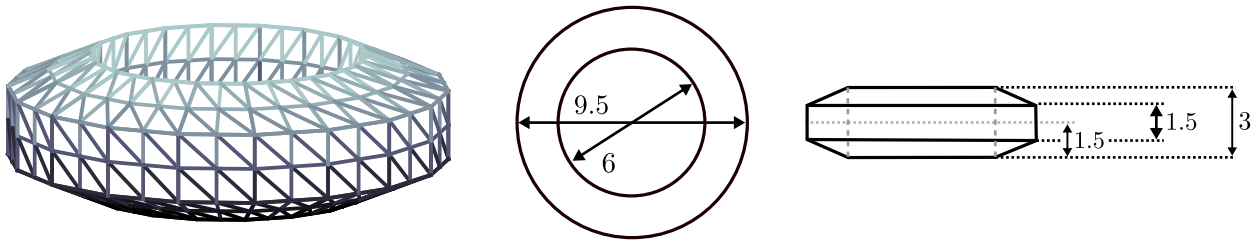


Figure 5.3: Schematic of the toroidal device analysed in this section. Dimensions are in metres.

Aiming to fully characterise this device, Figure 5.4 presents the hydrodynamic characteristics of this WEC, in terms of the following frequency-domain key quantities: **(a)** radiation damping and radiation added-mass, *i.e.* $B_r(\omega)$ and $A_r(\omega)$, respectively; **(b)** frequency response of the radiation dynamics Σ_r , *i.e.* $K_r(\omega)$; **(c)** and the input-output (force-to-velocity) frequency response of the device, *i.e.* $G(\omega)$.

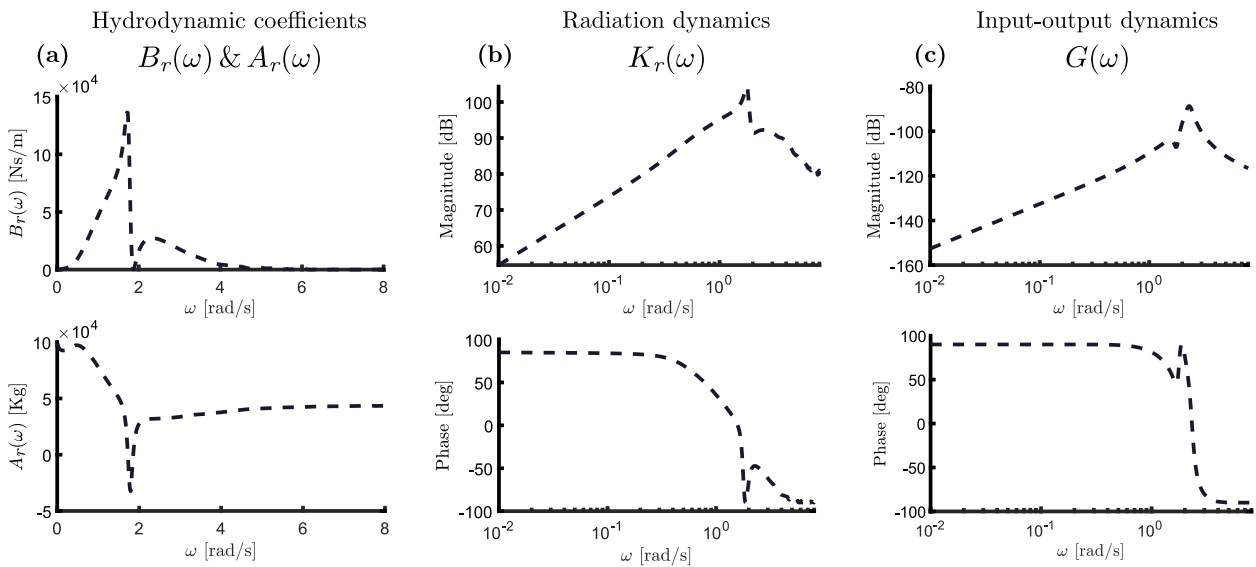


Figure 5.4: Frequency-domain characteristics of the toroidal device analysed in this section. In particular, **(a)** presents the hydrodynamic coefficients $B_r(\omega)$ and $A_r(\omega)$, while **(b)** and **(c)** illustrate the frequency response of the radiation system $K_r(\omega)$ and that of the input-output system $G(\omega)$, respectively.

Remark 5.3.1 Note that ocean wave peak periods typically lie between 3 [s] and 16 [s], which directly implies that the frequency range that characterises the significant dynamics for the wave excitation force is always approximately $[0.4, 2.1]$ [rad/s]. This phenomenon is consistent across different geographical locations, as discussed in [231].

In the light of Remark 5.3.1, a more conservative frequency range $W = [0.3, 3]$ [rad/s] is considered here, to solve for the model reduction problem, as described in Section 5.2. This effectively ensures that the reduced models, computed with the presented moment-based strategy, represent the target system in the frequency range characterising the wave input.

For the time-domain numerical simulation cases provided in this section, a JONSWAP spectrum (see Section 2.1.2) is considered, characterised by a significant wave height $\bar{H}_w = 2$ [m], a peak wave period $\bar{T}_w = 8$ [s], and a peak enhancement factor of $\gamma = 3.3$. The SDF S_w , corresponding with such a stochastic description of ocean waves, is illustrated in Figure 5.5. The total duration of each generated wave and, hence, each simulation, is set to 200 [s].

In order to obtain statistically meaningful and consistent results for the time-domain scenario, and since the waves are generated from sets of random amplitudes [36], it is found that the mean of 15 simulations is necessary to obtain a 95% confidence interval with a half-width of 0.2% of the mean, computed as in [90].

5.3.1 Input-output model reduction

This section discusses the performance of the moment-based reduced models, for the input-output dynamics (force-to-velocity) case, following the theoretical results developed in Section 5.1, and the methodology proposed in Section 5.2.1. Recall that a key feature of this moment-based strategy is that the user is allowed to select a set of frequencies \mathcal{F} to guarantee frequency-domain interpolation, *i.e.* a set where the approximating reduced model $\tilde{\Sigma}_{\mathcal{F}}$ exactly matches the steady-state response of Σ in (5.2).

A sensible selection of this set of interpolation points can be performed by analysing the gain of the target frequency response $G(\omega)$ in Figure 5.4 (c), and selecting points that characterise dynamically important features of the WEC. By way of example, a sensible selection normally includes the resonant frequency of the device under analysis (in the DoF) considered. Note that this is, effectively, the frequency where the maximum amplification occurs, *i.e.* the frequency characterising the \mathcal{H}_{∞} -norm of the WEC system. Based

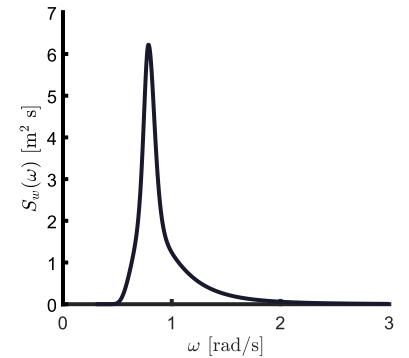


Figure 5.5: SDF S_w corresponding with the JONSWAP spectrum utilised to generate the wave input.

on the previous discussion, different sets of interpolation frequencies are chosen as follows:

- ▶ $\mathcal{F}_1 = \{2.3\}$,
- ▶ $\mathcal{F}_2 = \{1, 2.3\}$,
- ▶ $\mathcal{F}_3 = \{1, 1.8, 2.3\}$,
- ▶ $\mathcal{F}_4 = \{1, 1.6, 1.8, 2.3\}$.

Note that $\mathcal{F}_i \subset \mathcal{F}_j$ for $i < j$, with $\{i, j\} \subset \mathbb{N}_4$. As can be appreciated from Figure 5.4 (c), the set \mathcal{F}_1 includes a key interpolation point, which explicitly characterises the \mathcal{H}_∞ -norm of the WEC system, *i.e.* the resonant frequency associated with the DoF under analysis (heave for this case study).

Remark 5.3.2 The presented moment-based strategy is able to preserve the \mathcal{H}_∞ -norm of the target system by simply including the corresponding frequency, characterising such a norm, in the interpolation set.

The set \mathcal{F}_2 additionally includes a low-frequency component, while the sets \mathcal{F}_3 and \mathcal{F}_4 further expand \mathcal{F}_2 by including different mid-frequency components.

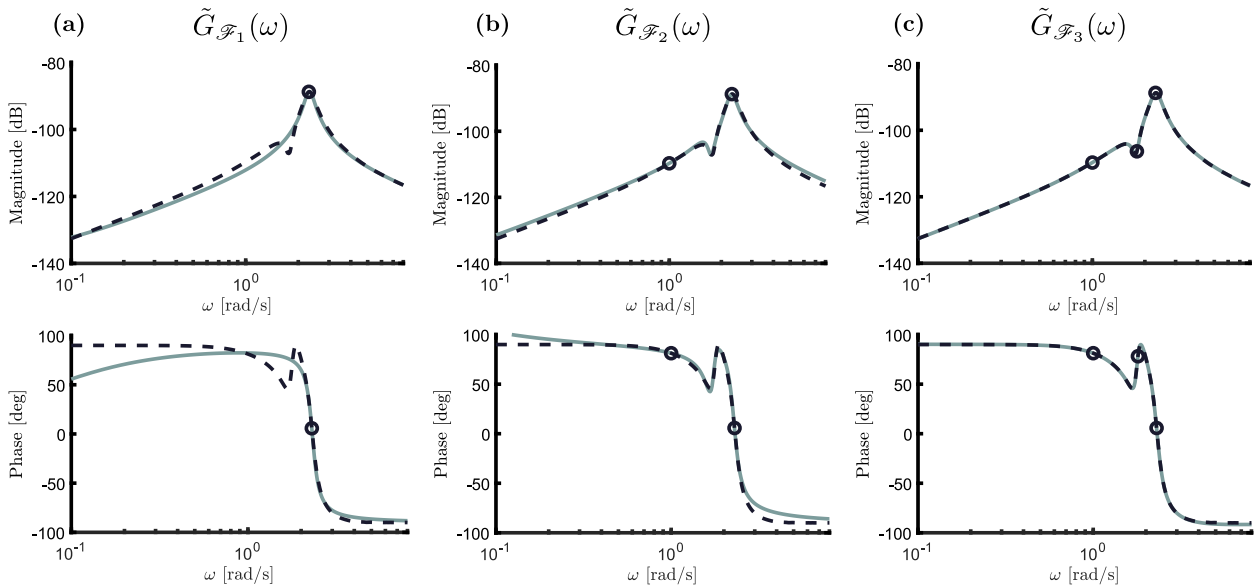


Figure 5.6: Frequency-domain performance of the moment-based reduced models for the toroidal device. In particular, (a), (b) and (c), show the frequency response of the moment-based systems (solid) $\tilde{\Sigma}_{\mathcal{F}_1}$, $\tilde{\Sigma}_{\mathcal{F}_2}$ and $\tilde{\Sigma}_{\mathcal{F}_3}$, *i.e.* $\tilde{G}_{\mathcal{F}_1}$, $\tilde{G}_{\mathcal{F}_2}$ and $\tilde{G}_{\mathcal{F}_3}$, respectively. The target frequency response $G(\omega)$ is depicted in all plots with a dashed line.

The performance of these moment-based reduced models is now discussed and illustrated for the first three interpolation sets, *i.e.* \mathcal{F}_1 , \mathcal{F}_2 and \mathcal{F}_3 . Figure 5.6 presents the Bode plot, for both the target frequency response $G(\omega)$ (dashed), and the approximating frequency response mappings¹³ (solid) $\tilde{G}_{\mathcal{F}_1}(\omega)$ in (a), $\tilde{G}_{\mathcal{F}_2}(\omega)$ in (b), and $\tilde{G}_{\mathcal{F}_3}(\omega)$ in (c). The interpolation points selected for the computation of each approximating parametric structure are denoted by an empty

13: Note that the notation $\tilde{G}_{\mathcal{F}}$ is used for the frequency response of the input-output reduced model by moment-matching $\tilde{\Sigma}_{\mathcal{F}}$, as in equation (5.27).

black circle. Note that, as expected by the theoretical foundations of this moment-based strategy, the approximating models have *exactly* the same frequency-domain behaviour as the target model $G(\omega)$ of the WEC system, for each element of the corresponding interpolation set \mathcal{F} . In addition, it can be readily appreciated that, by a sensible selection of the interpolation frequency set \mathcal{F}_1 , the model $\tilde{G}_{\mathcal{F}_1}$, *i.e.* a parametric description computed using a single interpolation point, already provides a reasonably accurate frequency-domain characterisation when compared with the target steady-state response of the toroidal WEC under study. Though considering \mathcal{F}_1 as an interpolation set provides quite accurate results, the decrease in the overall approximation error from system $\tilde{G}_{\mathcal{F}_1}$ towards $\tilde{G}_{\mathcal{F}_3}$ can be clearly appreciated (see also Table 5.1).

Aiming to provide a precise (and more detailed) measure of the performance of the moment-based reduced models for the toroidal WEC device considered in this case study, Table 5.1 offers a numerical comparison in terms of the following key performance indicators:

- Dim** Dimension (order) of the approximating parametric model.
- NRMSE_F** Normalised Root Mean Square Error (NRMSE) computed against the target WEC frequency response $G(\omega)$, with $\omega \in W$.
- NRMSE_T** NRMSE computed (in steady-state) against the target time-domain response of the WEC system obtained directly from Σ (*i.e.* explicitly solving the corresponding convolution integral associated with radiation effects). The wave excitation input is computed from the (JONSWAP) SDF S_w of Figure 5.5.

Model	Dim	NRMSE _F	NRMSE _T
$\tilde{\Sigma}_{\mathcal{F}_1}$	2	13.90%	26.76%
$\tilde{\Sigma}_{\mathcal{F}_2}$	4	9.09%	4.09%
$\tilde{\Sigma}_{\mathcal{F}_3}$	6	0.20%	0.19%
$\tilde{\Sigma}_{\mathcal{F}_4}$	8	0.15%	0.13%

Table 5.1: Performance of the input-output (force-to-velocity) moment-based reduced models for the toroidal device.

Note that, for this case study, little improvement can be observed when considering more than three frequencies in the moment-based interpolation framework, as can be directly appreciated from Table 5.1. The increase in approximation quality, when considering the different interpolation sets in time-domain simulations, is consistent with the previously discussed frequency-domain results, though it can be appreciated that the approximating model $\tilde{\Sigma}_{\mathcal{F}_1}$ presents quite different behavior in the time-domain compared to the frequency-domain. This is due to the fact that the waves generated as inputs for this simulation scenario correspond to a JONSWAP spectrum with $\bar{T}_w = 8[s]$, *i.e.* a peak SDF frequency of ≈ 0.84 [rad/s]. As can be appreciated from Figure 5.6 (a), the fit between the frequency response of $\tilde{\Sigma}_{\mathcal{F}_1}$ and the target response of the WEC is relatively poor in the neighborhood of 0.84 [rad/s], hence directly implying a loss of performance in this particular time-domain scenario. Finally, and to further illustrate the time-domain performance of the different moment-based models, Figure 5.7 presents steady-state motion

(velocity) time-traces for a particular sea-state realisation, both for $\tilde{\Sigma}_{\mathcal{F}_1}$ in **(a)**, and $\tilde{\Sigma}_{\mathcal{F}_3}$ in **(b)**. Note that, while differences can be effectively appreciated for the case of $\tilde{\Sigma}_{\mathcal{F}_1}$, *i.e.* a reduced model by moment-matching using a single interpolation frequency, the steady-state response of the moment-based system $\tilde{\Sigma}_{\mathcal{F}_3}$ is virtually identical to that of Σ in (5.2).

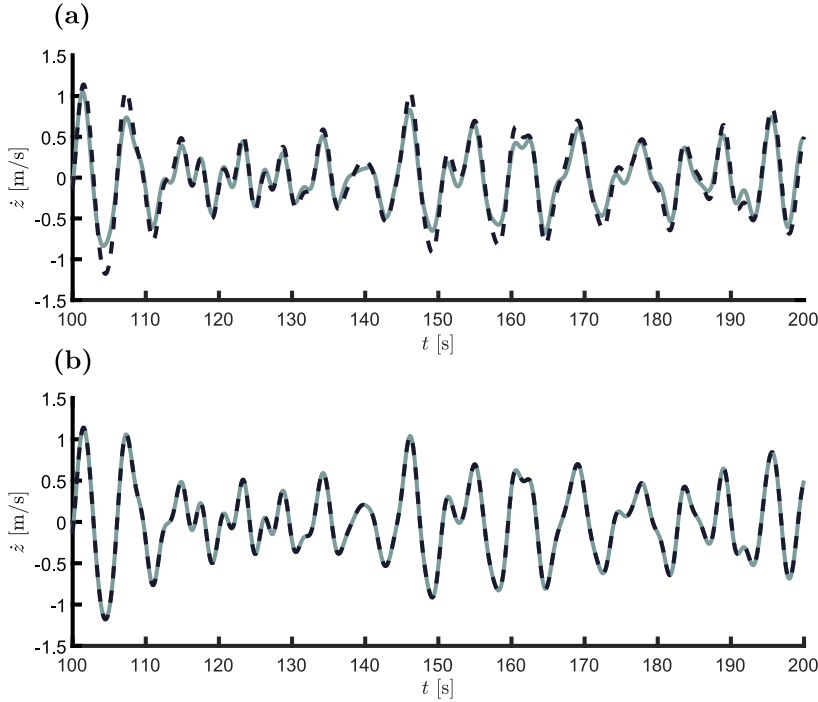


Figure 5.7: Time-domain performance (for a particular sea-state realisation) of the moment-based reduced models for the toroidal device. In particular, **(a)** and **(b)**, show the steady-state (velocity) response of the moment-based systems (solid) $\tilde{\Sigma}_{\mathcal{F}_1}$, and $\tilde{\Sigma}_{\mathcal{F}_3}$, respectively. The target response, *i.e.* the steady-state response of system Σ in (5.2), is depicted in all plots with a dashed line.

5.3.2 Radiation model reduction

Following Section 5.3.1, an equivalent procedure can be carried out to compute moment-based reduced order models for the radiation dynamics, using the theoretical results developed in Section 5.1, and the methodology proposed in Section 5.2.2.

In other words, selection of the interpolation points can be done analogously, where any sensible set \mathcal{F} would contain the frequency characterising the \mathcal{H}_∞ -norm of the radiation system Σ_r , which appears at ≈ 1.75 [rad/s], for the toroidal device considered in this case study (see Figure 5.4 **(b)**). In particular, the following interpolation sets are considered:

- ▶ $\mathcal{F}_1 = \{1.75\}$,
- ▶ $\mathcal{F}_2 = \{0.8, 1.75\}$,
- ▶ $\mathcal{F}_3 = \{0.8, 1.75, 2.6\}$,
- ▶ $\mathcal{F}_4 = \{0.5, 0.8, 1.75, 2.6\}$,

where, naturally, $\mathcal{F}_i \subset \mathcal{F}_j$ for $i < j$, with $\{i, j\} \subset \mathbb{N}_4$. Similarly to the input-output case presented in Section 5.3.1, the performance

of these moment-based reduced models, for the radiation system Σ_r , is now discussed and illustrated for the first three interpolation sets, *i.e.* \mathcal{F}_1 , \mathcal{F}_2 and \mathcal{F}_3 defined above. Figure 5.8 shows the Bode plot, for both the target frequency response $K_r(\omega)$ (dashed), and the approximating frequency response mappings¹⁴ (solid) $\tilde{K}_{r\mathcal{F}_1}(\omega)$ in (a), $\tilde{K}_{r\mathcal{F}_2}(\omega)$ in (b), and $\tilde{K}_{r\mathcal{F}_3}(\omega)$ in (c). The interpolation points selected for the computation of each approximating parametric structure are denoted by an empty black circle.

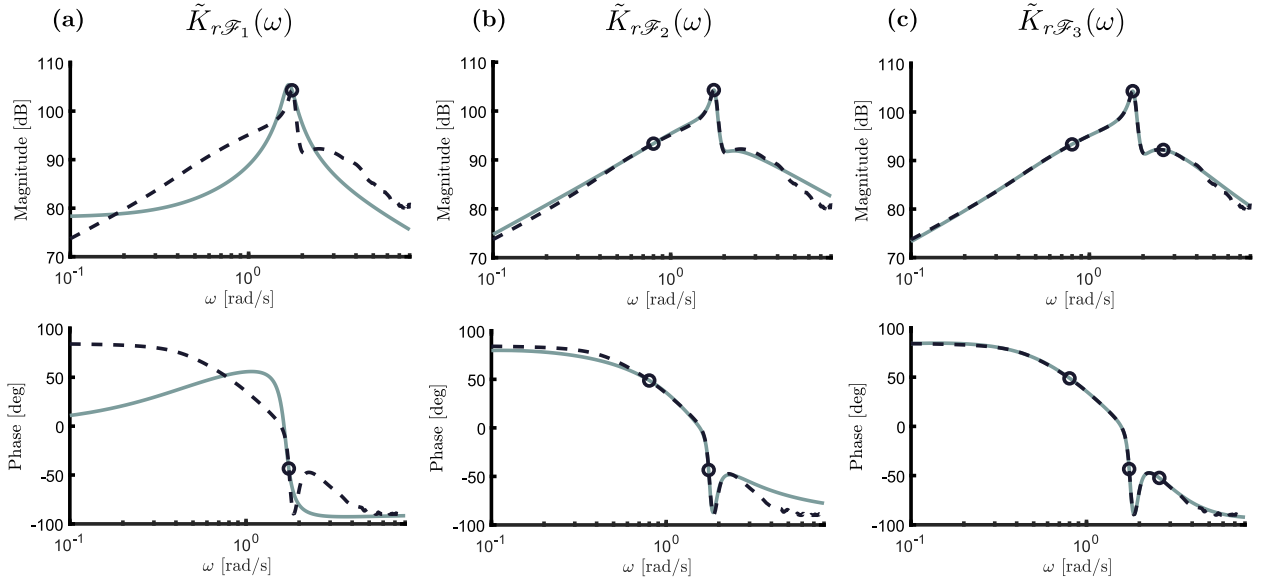


Figure 5.8: Frequency-domain performance of the moment-based reduced models for the radiation dynamics of the toroidal device. In particular, (a), (b) and (c), show the frequency response of the moment-based systems (solid) $\tilde{\Sigma}_{r\mathcal{F}_1}$, $\tilde{\Sigma}_{r\mathcal{F}_2}$ and $\tilde{\Sigma}_{r\mathcal{F}_3}$, *i.e.* $\tilde{K}_{r\mathcal{F}_1}$, $\tilde{K}_{r\mathcal{F}_2}$ and $\tilde{K}_{r\mathcal{F}_3}$, respectively. The target frequency response $K_r(\omega)$ is depicted in all plots with a dashed line.

In contrast to the input-output reduction case, the performance obtained with a single frequency component is not sufficiently accurate; as discussed previously in Section 2.6, the input-output model reduction approach virtually always provides a lower order description to that characterising the radiation dynamics, for equal fidelity of the overall model. This is easily solved by considering a higher number of interpolation points, as can be appreciated from Figure 5.8 (and Table 5.2).

Finally, and to provide a precise measure of the frequency-domain performance of the moment-based reduced models for the radiation dynamics of the toroidal WEC considered in this case study, Table 5.2 offers a numerical comparison in terms of the same key indicators utilised in Section 5.3.1, *i.e.*

Dim Dimension (order) of the approximating parametric model.
NRMSE_F NRMSE computed against the target WEC radiation frequency response $K_r(\omega)$, with $\omega \in W$.

Note that, similarly to the input-output dynamics case, little improve-

14: Analogously to the input-output case, the notation $\tilde{K}_{r\mathcal{F}}$ is used for the frequency response of the radiation reduced model by moment-matching $\tilde{\Sigma}_{r\mathcal{F}}$.

Model	Dim	NRMSE _F
$\tilde{\Sigma}_{r\mathcal{F}_1}$	2	68.73%
$\tilde{\Sigma}_{r\mathcal{F}_2}$	4	5.84%
$\tilde{\Sigma}_{r\mathcal{F}_3}$	6	1.41%
$\tilde{\Sigma}_{r\mathcal{F}_4}$	8	0.98%

Table 5.2: Performance of the radiation moment-based reduced models for the toroidal device.

ment can be observed when considering more than three frequencies in the interpolation scheme, as can be directly appreciated from Table 5.2.

5.4 On the properties of radiation models

Though Section 5.3.2 presents performance results for the radiation moment-based reduced models in terms of their accuracy in the frequency domain (with respect to the target response K_r), a discussion on the fundamental physical properties of radiation effects, introduced in Section 2.4, is presented in this section. These properties, for any approximating (reduced) model $\tilde{\Sigma}_r$, are briefly recalled below, for convenience¹⁵.

- ▶ **Property 1:** $\tilde{\Sigma}_r$ is BIBO stable.
- ▶ **Property 2:** The complex (transfer) function $\tilde{K}_r(s)$ is positive-real.
- ▶ **Property 3:** $\tilde{K}_r(s)$ has zeros at $s = 0$.
- ▶ **Property 4:** $\tilde{\Sigma}_r$ is strictly proper.

An assessment on the fundamental properties listed above is now provided, for the moment-based reduced models $\tilde{\Sigma}_{r\mathcal{F}_2}$, $\tilde{\Sigma}_{r\mathcal{F}_3}$ and $\tilde{\Sigma}_{r\mathcal{F}_4}$, computed in Section 5.3.2 for the toroidal device described in Figure 5.3.

Remark 5.4.1 $\tilde{\Sigma}_{r\mathcal{F}_1}$ (or, equivalently, $\tilde{K}_{r\mathcal{F}_1}$) does not provide a sufficiently representative response for the radiation dynamics Σ_r and, hence, it is excluded from the analysis performed in this section.

As discussed in the following paragraphs, Properties 1 and 4 are guaranteed by construction, *i.e.* they are always fulfilled by the family of models defined in equation (6.37).

Remark 5.4.2 As a matter of fact, for the case of Property 1, internal stability (in the Lyapunov sense) is guaranteed by the strategy, which is naturally a stronger result than BIBO stability.

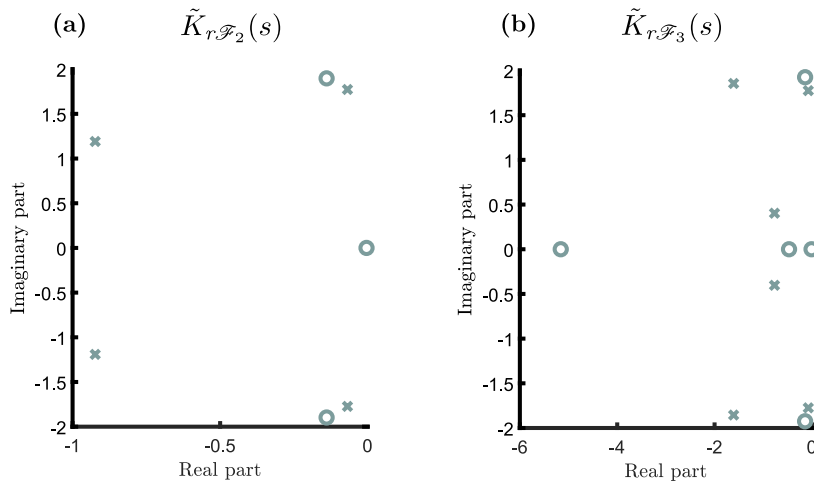
On the other hand, Properties 2 and 3 are not explicitly guaranteed, though they are, effectively, virtually always respected by the moment-based strategy: since the reduced order model matches the moments of the system, it is not just the result of a low-order reduction but it actually retains some key properties of the system under analysis [232]. Nevertheless, aiming to provide as complete a model reduction framework as possible, systematic methods to guarantee Properties 2 and 3 are given in Sections 5.4.1 and 5.4.2, respectively.

15: The reader is referred to Sections 2.3.2.2 and 2.4 for a comprehensive discussion on these properties.

Property 1

The process to compute the optimal input matrix Δ^{opt} guarantees internal stability of the family of reduced models by moment-matching defined in equation (6.37). In other words, internal stability can be retained by construction, given that $\lambda(S - \Delta L)$ can always be assigned such that $\lambda(S - \Delta L) \subset \mathbb{C}_{<0}$, as a consequence of the observability of the pair (S, L) . This can be clearly appreciated in the pole-zero maps¹⁶ presented in Figure 5.9.

Remark 5.4.3 Note that, unlike this moment-based approach, many of the available model reduction strategies utilised in the wave energy field (and other marine applications) cannot inherently preserve internal stability (see Section 2.6).



16: Following standard conventions in system dynamics, poles are denoted with \times , while zeros are depicted with \circ .

Figure 5.9: Pole-zero map for the moment-based reduced models $\tilde{K}_{r, \mathcal{F}_2}(s)$, in (a), and $\tilde{K}_{r, \mathcal{F}_3}(s)$, in (b).

Property 2

Positive-realness of \tilde{K}_r , for this linear case, is directly related to the property of passivity (see Section 2.4). If the target frequency-response data $K_r(\omega)$ effectively comes from a passive model¹⁷, the reduced models obtained with the proposed moment-based strategy are virtually always inherently passive. This can be appreciated in Figure 5.10, which depicts the Nyquist plot for both $\tilde{K}_{r, \mathcal{F}_2}(\omega)$ and $\tilde{K}_{r, \mathcal{F}_3}(\omega)$. It is clear that $\Re\{\tilde{K}_{r, \mathcal{F}}(\omega)\} > 0$, for all $\omega \in \mathbb{R}/0$ which, together with the internal stability shown in the pole zero map of Figure 5.9, directly imply that the models are passive.

17: This is clarified since errors can manifest in BEM codes, producing target hydrodynamic coefficients that corresponds with a non-passive system, even though (uncontrolled) WEC systems are, by definition, inherently passive.

Properties 3 & 4

Property 3 manifests itself explicitly in Figure 5.9, where there is clearly a zero at $s = 0$, both for the moment-based model $\tilde{K}_{r, \mathcal{F}_2}(s)$, and $\tilde{K}_{r, \mathcal{F}_3}(s)$.

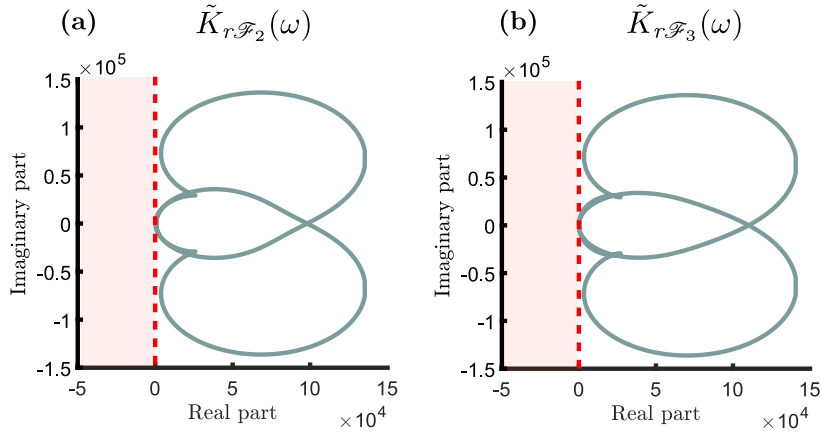


Figure 5.10: Nyquist plot for the moment-based reduced models $\tilde{K}_{r, \mathcal{F}_2}(\omega)$, in (a), and $\tilde{K}_{r, \mathcal{F}_3}(\omega)$, in (b).

With respect to Property 4, the family of models defined in equation (6.37) is strictly proper by construction: the feed-through matrix of $\tilde{\Sigma}_{r, \mathcal{F}}$ is always zero, independently on the selection of the interpolation set \mathcal{F} involved.

5.4.1 Enforcing passivity

Though, as discussed in Section 5.4, passivity is virtually always retained by the moment-based strategy (if the interpolation points are effectively selected in a sensible manner), some specific applications may require a *guarantee* of passivity for the reduced model of the radiation system. In this thesis, an optimisation-based approach is used to ensure passivity, together with the so-called *scattering representation* of a system. To begin this discussion, the following assumption is required.

Assumption 5.4.1 Consider the set $\mathcal{F} = \{\omega_p\}_{p=1}^f$, fully characterising the dynamics of the signal generator defined in equation (5.32). Then, the target interpolation frequency-domain data points (computed with any suitable hydrodynamic solver) are such that $\{\Re\{K_r(\omega_p)\}\}_{p=1}^f \subset \mathbb{R}_{\geq 0}$.

Remark 5.4.4 Assumption 5.4.1 guarantees that the target interpolation values $K_r(\omega_p)$ effectively correspond with a passive system, for all $p \in \mathbb{N}_f$. Note that this assumption is only required for any $\omega_p \in \mathcal{F}$. In other words, no hypothesis is required for the remainder of the frequency points selected in the discretisation set¹⁸ Ω .

Remark 5.4.5 Under Assumption 5.4.1, the family of models for the radiation system (6.37) parameterised in $\Delta \in \mathbb{R}^\nu$, which contains *all* models of dimension ν achieving moment-matching at (S, L) (see Section 4.2.1), naturally includes a passive model.

18: Recall that the set Ω contains the totality of the frequency points utilised to compute the hydrodynamic coefficients of the corresponding WEC.

The problem now boils down to the selection of a suitable Δ such that the reduced model (6.37) is, effectively, passive. To achieve such an objective, the so-called *scattering representation* of a system is considered herein, as defined below.

Definition 5.4.1 (Scattering representation [233]) *Let \mathcal{W} be a system defined, for $t \in \mathbb{R}^+$, by the set of differential equations*

$$\mathcal{W} : \begin{cases} \dot{x} = Ax + Bu, \\ y = Cx. \end{cases}$$

The scattering representation of system \mathcal{W} is defined as

$$\mathcal{W}^s : \begin{cases} \dot{x} = (A - BC)x + \sqrt{2}Bl, \\ o = \sqrt{2}Cx - l, \end{cases} \quad (5.34)$$

which is obtained by the following coordinate transformation¹⁹ :

$$\begin{aligned} l &= \frac{1}{\sqrt{2}}(u + y), \\ o &= \frac{1}{\sqrt{2}}(y - u). \end{aligned} \quad (5.35)$$

19: The variables l and o are usually referred to as the “incoming” and “outgoing” waves, respectively [233].

This particular coordinate transformation is now considered, since it provides a condition for the passivity of the original system \mathcal{W} in terms of the L_2 -gain of its scattering representation \mathcal{W}^s , as recalled in the following theorem.

Theorem 5.4.1 [224, 233] *The system \mathcal{W} is passive if and only if its scattering representation \mathcal{W}^s has L_2 -gain ≤ 1 .*

Theorem 5.4.2 [234] *Let $W : \mathbb{C} \rightarrow \mathbb{C}, s \mapsto W(s)$, be the transfer function associated with system \mathcal{W} . The L_2 -gain of \mathcal{W} is equal to its \mathcal{H}_∞ -norm, i.e. $\|\mathcal{W}\|_2 \equiv \|W(s)\|_\infty$.*

Remark 5.4.6 From Definition 5.4.1, one can easily derive that, in the frequency-domain, the input-output dynamics $l \mapsto o$ can be written in terms of $W(\omega)$ as

$$W^s(\omega) = \frac{W(\omega) - 1}{W(\omega) + 1}. \quad (5.36)$$

Based on the theory presented in this section, one can adapt the procedure to compute the optimal gain Δ^{opt} for the radiation dynamics, i.e. Procedure 1 described in Section 5.2, by simply changing Steps 4 and 5 as follows. Let $K_r^s : \mathbb{R} \rightarrow \mathbb{C}$ be the frequency-response mapping of the scattering representation associated with the radiation

dynamics K_r , *i.e.*

$$K_r^s(\omega) = \frac{K_r(\omega) - 1}{K_r(\omega) + 1}. \quad (5.37)$$

Then, Steps 4 and 5 of Procedure 1, can be modified as follows:

- 4 Consider the frequency response of the scattering representation (as in Definition 5.4.1) of system (6.37) as a function of Δ , *i.e.* the mapping $\tilde{K}_{r\mathcal{F}}^s : \mathbb{R} \times \mathbb{R}^\nu \rightarrow \mathbb{C}$ given by

$$\tilde{K}_{r\mathcal{F}}^s(\omega, \Delta) = 2\underline{Y}_r(j\omega\mathbb{I}_\nu - S + (L + \underline{Y}_r)\Delta)^{-1} \Delta - 1. \quad (5.38)$$

- 5 Let $\Omega = \{\omega_i\}_{i=1}^M \subset W$ be the (finite) frequency set utilised to compute the hydrodynamic coefficients $B_r(\omega)$ and $A_r(\omega)$, in the frequency range $W = [\omega_l, \omega_u] \subset \mathbb{R}^+$. Then, compute the input matrix Δ^{opt} with the following optimisation-based procedure:

$$\Delta^{\text{opt}} = \arg \min_{\Delta \in \mathbb{R}^\nu} \sum_{i=1}^M \left| \tilde{K}_{r\mathcal{F}}^s(\omega_i, \Delta) - K_r^s(\omega_i) \right|^2, \quad (5.39)$$

subject to:

$$\|\tilde{K}_{r\mathcal{F}}^s(\omega, \Delta)\|_\infty \leq 1,$$

where $K_r^s(\omega)$ is defined as in (5.37).

The objective of the optimisation-based procedure described above is to compute an optimal input matrix Δ^{opt} such that the reduced model $\tilde{\Sigma}_{r\mathcal{F}}$ minimises the Euclidean distance between $\tilde{K}_{r\mathcal{F}}$ and the target frequency response K_r , while ensuring passivity in the approximating structure. This is demonstrated below by the use of a particular case study, where the same toroidal device used in Section 5.3 is considered.

Let the frequency set used to compute a reduced model for the radiation system (as in Section 5.2.2) be $\mathcal{F} = \{1, 1.6, 1.8, 2.3, 2.8\}$, and the corresponding frequency range, utilised to minimise the corresponding Euclidean distance to the target data $K_r(\omega)$, be $W = [0.3, 3]$ [rad/s]. With this specific selection of points in \mathcal{F} , the specific frequency range defined in W , and the geometry associated with the toroidal device presented in Figure 5.3, the resulting moment-based reduced model, computed following Procedure 1 (see Section 5.2), is non-passive. In the light of this, the passivity enforcement method proposed in this section is applied to the toroidal device, considering the same interpolation set \mathcal{F} and frequency range W . The frequency-domain behaviour associated with the moment-based non-passive (solid) and passive (dotted) models, for the interpolation set \mathcal{F} , is illustrated in Figure 5.11 (a).

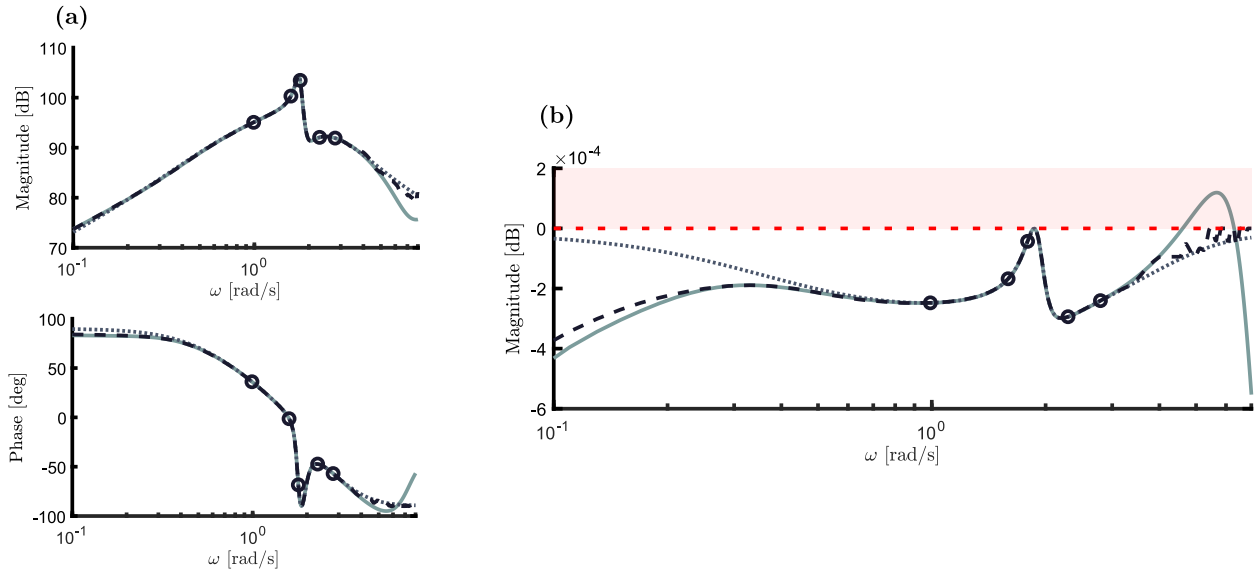


Figure 5.11: Frequency-domain characteristics of moment-based radiation models with preservation of passivity. In particular, (a) shows the Bode plot of a non-passive (solid) and passive (dotted) moment-based models, for the interpolation set $\mathcal{F} = \{1, 1.6, 1.8, 2.3, 2.8\}$ (denoted with black circles), while (b) illustrates the magnitude of their corresponding scattering representations. The target data $K_r(\omega)$, in (a), and $K_r^s(\omega)$, in (b), are depicted in dashed lines.

Figure 5.11 (b) shows the frequency response of the scattering representations associated with non-passive (solid), and passive (dotted), moment-based models, along with the target scattering (dashed-black) data $K_r^s(\omega)$. The corresponding passivity violation can be clearly appreciated, *i.e.* the frequency-response (magnitude) of the scattering representation associated with the non-passive model has values over the 0 [dB] line (depicted in dashed-red), while that of the model computed with the moment-based passivity preserving strategy, described in this section, effectively has a \mathcal{H}_∞ -norm less than 1 (see Theorem 5.4.1). This can be also appreciated in Figure 5.12, where the Nyquist plot of the non-passive (solid), and passive (dotted) moment-based models, are presented. Note that the real part of the frequency response associated with the passive model is *a/ways* defined over the positive real axis, for all $\omega \in \mathbb{R}$, directly agreeing with Property 2 listed in the first paragraph of Section 5.4.

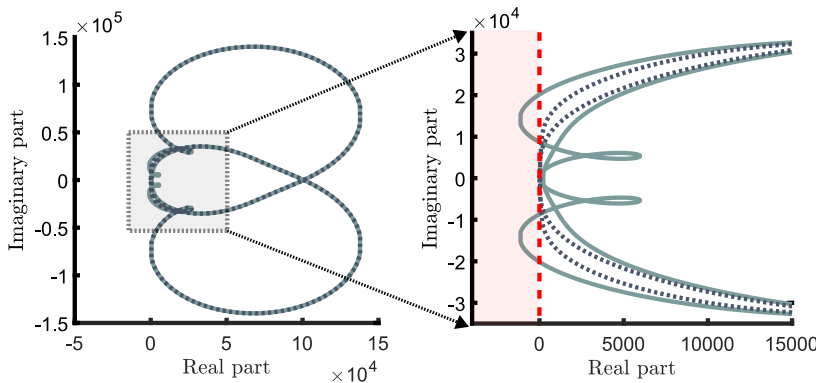


Figure 5.12: Nyquist plot for a non-passive (solid) and passive (dotted) moment-based radiation models, for the interpolation set $\mathcal{F} = \{1, 1.6, 1.8, 2.3, 2.8\}$.

5.4.2 Enforcing zeros at $s = 0$

The existence of zeros at $s = 0$ is directly related to the hydrodynamic nature of the radiation process. As discussed in Section 2.3.2.2, the impulse response function k_r , characterising the memory effects of the fluid, is such that

$$\lim_{\omega \rightarrow 0} K_r(\omega) = 0, \quad (5.40)$$

which automatically implies that $s = 0$ is a zero²⁰ of $K_r(s)$.

That said, if required, enforcing (5.40) for the reduced model $\tilde{\Sigma}_r$ can be carried out straightforwardly with the presented moment-based strategy, by simply matching the 0-order moment of Σ_r at $s = 0$. This can be done by proposing a suitable modification of the signal generator defined in equation (5.32). In particular, the dynamic matrix S in (5.6) can be modified to include $s = 0$ as an interpolation point, by using an appropriate direct sum, *i.e.*

$$S_0 = 0 \oplus \left(\bigoplus_{p=1}^f \begin{bmatrix} 0 & \omega_p \\ -\omega_p & 0 \end{bmatrix} \right) = 0 \oplus S, \quad (5.41)$$

where the matrix $S_0 \in \mathbb{R}^{\nu+1 \times \nu+1}$.

Remark 5.4.7 Note that the interpolation points defined in the matrix S_0 are now fully characterised by the set $\mathcal{F}_0 = 0 \cup \{\omega_p\}_{p=1}^f = 0 \cup \mathcal{F} \subset \mathbb{R}^+$.

Following the same steps of Proposition 5.1.1, it can be proved straightforwardly that the moment-domain equivalent for the radiation system, for a signal generator defined by the (observable) pair (S_0, L_0) , $L_0^T \in \mathbb{R}^{\nu+1}$, is given by,

$$\underline{Y}_{r_0} = L_0 (K_r(0) \oplus \mathcal{R}) = L_0 (0 \oplus \mathcal{R}), \quad (5.42)$$

where the matrix $\mathcal{R} \in \mathbb{R}^{\nu \times \nu}$ is as in Proposition 5.1.1, and the relation $K_r(0) = 0$ follows directly from equation (5.40). With this result, one can automatically write the family of models achieving moment-matching for the radiation system Σ_r at (S_0, L_0) , as

$$\Sigma_r \approx \tilde{\Sigma}_{r\mathcal{F}_0} : \begin{cases} \dot{\Theta} = (S_0 - \Delta_0 L_0) \Theta + \Delta_0 \dot{z}, \\ \tilde{y}_r = \underline{Y}_{r_0} \Theta, \end{cases} \quad (5.43)$$

where the input matrix $\Delta_0 \in \mathbb{R}^{\nu+1}$ can be computed following an analogous procedure to that described in Section 5.2.1, *i.e.* Procedure 1.

20: The algebraic multiplicity of this zero is, in principle, dependent on the geometry under analysis.

5.5 Conclusions

Motivated by the inherent necessity of suitable model reduction techniques to express Cummins' formulation in a state-space (parametric) form (see Section 2.4), this chapter presents a moment-matching model reduction framework, for linear SISO WEC devices (*i.e.* constrained to move in a single DoF). To fulfill such an objective, the moment of the non-parametric system Σ , defined in equation (5.1), is derived, to later define a suitable family of models achieving moment-matching. In particular, the proposed moment-based formulation allows the user to *exactly* match the steady-state behaviour of the device under analysis at a set of key frequencies, such as the resonant frequency (*i.e.* the frequency characterising the \mathcal{H}_∞ -norm of the specific DoF under analysis), retaining important physical properties of the studied WEC.

The methodology is proposed both to compute a reduced order model for the input-output (force-to-motion), and radiation dynamics. Unlike the strategies proposed in the literature of linear model reduction for WEC applications, reviewed in Section 2.6, specific methodologies are presented to preserve *all* the physical properties associated with radiation effects: *BIBO stability*, *passivity*, *zero dynamics*, and *strict properness*. Both the efficacy, and each of the underlying features of this moment-based model reduction framework, are presented and demonstrated with a case study, where a toroidal WEC is considered, constrained to move in heave.

Though not discussed in this chapter, the family of moment-based reduced models presented shares a strong connection with unknown-input estimation techniques applied in the wave energy field, which can be exploited to provide efficient parameterisations, tailored for wave excitation force estimation (see Section 3.2.1). This is discussed in detail in Chapter 6, where a linear MIMO moment-matching model reduction framework is proposed for WECs, extending the results of this chapter to either multi-DoFs or arrays of wave energy systems.

Reduced models for linear MIMO WECs

6

Contents of this chapter

6.1	Model reduction by moment-matching for linear MIMO systems	117
6.2	Moment-based WEC formulation for MIMO model reduction	120
6.3	Reduced models achieving moment-matching	124
6.3.1	Input-output dynamics	125
6.3.2	Radiation dynamics	127
6.4	Input-output case study: an array of CorPower-like devices	127
6.5	Synergy between moments and unknown-input estimation	134
6.6	Radiation case study: a multi-DoF CorPower-like device	140
6.6.1	On the properties of radiation models	142
6.7	Conclusions	144

Recall, from Section 2.4, that the equation of motion for a WEC, under the assumptions of linear potential flow theory (see Section 2.3.1), can be expressed in terms of *Cummins'* equation (2.20). This equation is recalled below, for a N -DoF WEC device, with $N \in \mathbb{N}$ for convenience:

$$\Sigma : \begin{cases} \ddot{z} = \mathcal{M}(-k_r * \dot{z} - s_h z + f_e), \\ y = \dot{z}, \end{cases} \quad (6.1)$$

where $z : \mathbb{R}^+ \rightarrow \mathbb{R}^N$ is the displacement vector, $k_r : \mathbb{R}^+ \rightarrow \mathbb{R}^{N \times N}$, $k_{r_{ij}} \in L^2(\mathbb{R})$, $\forall \{i, j\} \subset \mathbb{N}_N$, the radiation impulse response (matrix) function, $f_e : \mathbb{R}^+ \rightarrow \mathbb{R}^N$ the wave excitation, and \mathcal{M} is the inverse of the generalised mass matrix of the device.

Remark 6.0.1 As discussed in Section 2.4, note that the structure of equation (6.1) can be used to alternatively describe the motion of a N -DoF WEC device, or an array of N devices, with each WEC constrained to move in a single DoF¹. Only the specific entries of k_r , s_h and \mathcal{M} are different. The reader is referred to [49] for further detail on this topic.

Remark 6.0.2 Throughout the theoretical results of this chapter, the term N -th order WEC system (or device), is utilised to refer either to an N -DoF WEC device, or an array of N devices, each constrained to move in a single-DoF. Each 'order' represents either a DoF associated with a multi-DoF WEC, or a single device composing a WEC farm, respectively.

1: Naturally, one can also consider arrays of multi-DoF WECs within the same formulation, by 'extending' the dimensions (order) associated with the matrices in (6.1). Nevertheless, this is omitted in this chapter, aiming to alleviate the notation used throughout each corresponding section.

In contrast to the case of a single-DoF device, an N -th order WEC represents not only a wave absorber but also a wave generator [49], *i.e.* the motion of each 'order' of the WEC is directly affected by

the waves generated by other devices/DoF, due to radiation effects. This ‘feature’ often produces mathematical representations that are not tractable (either computationally or representatively) for key components facilitating the maximisation of energy absorption from ocean waves, such as real-time optimal controllers and wave excitation force estimators.

Similarly as in the SISO case presented in Chapter 5, the presence of the non-parametric convolution operation in equation (6.1), related to radiation effects, represents both a representative and a computational drawback for a variety of applications (including WEC control and state-estimation design). Model reduction techniques can be used to parameterise this non-parametric operator, in terms of a state-space representation, which should ideally retain the underlying physical properties that characterise the WEC dynamics.

This chapter proposes an extension of the moment-matching-based model reduction framework, developed in Chapter 5, for MIMO systems. To achieve such an objective, the first contribution of this chapter is the formal extension of the system-theoretic definition of *moments*², as provided in Chapter 4, for linear MIMO systems. This is achieved by proposing a suitable modification of the single-output signal generator introduced in Section 4.1.1, and by providing a formal definition of a MIMO reduced order model by moment-matching, for a generic linear system structure. With this definition, a family of reduced order models, achieving moment-matching, is proposed for the non-parametric equation (6.1), hence providing a moment-based model reduction approach for N -th order WEC systems. As per the SISO linear model reduction theory recalled in Chapter 4, these MIMO moment-based reduced structures are such that the transfer function, associated with such approximating models, *exactly* matches the steady-state behavior of the target system at a specific user-selected set of interpolation frequencies.

As in the single-DoF (SISO) WEC case, the moment-based approximation framework, proposed in this chapter, is presented in two different modalities: input-output (force-to-motion), and radiation effects model reduction. The former deals with producing (parametric) reduced order models from an input-output perspective, *i.e.* system Σ defined in equation (6.1), while the latter approximates the radiation subsystem Σ_r (defined in Section 2.4), to later ‘embed’ into Cummins’ formulation, as demonstrated in equation (2.22).

In addition, taking explicit advantage of the (frequency) interpolation feature of the proposed moment-based strategy, the existence of an intrinsic connection between the wave excitation force estimation problem, and the moment-based parameterisation method

2: Previous literature in moment-matching, for the MIMO case, utilises the so-called *tangential interpolation* framework [221]. This is not pursued herein, given that these models based on tangential interpolation do not exactly preserve steady-state response characteristics. This is discussed with more detail in Section 6.1.

proposed in this thesis, is explicitly shown, in terms of the unknown-input estimation strategy presented in [90]. Particularly, the strategy presented in [90] has been proven to outperform state-of-the-art unknown-input (observer) strategies applied in the wave energy field, both in terms of estimation accuracy and computational time [15]. This technique is based on optimal state-estimation theory, and presents a combination of Kalman filtering [235] and the internal model principle³ of control theory [236]. This mathematical correlation can be exploited to compute low-order models which provide a high degree of wave excitation force estimation accuracy, with a significant improvement in terms of computational requirements. This has strong practical implications, being particularly appealing for real-time (combined) estimation and optimal control of wave energy farms.

The remainder of this chapter is organised as follows. Section 6.1 generalises the notion of moments for MIMO linear systems, giving an explicit definition of a MIMO reduced order model by moment-matching. Using these results and definitions, Section 6.2 proposes a MIMO moment-based formulation for WECs, to explicitly compute the moment-domain equivalent associated with the non-parametric system (6.1). Section 6.3 outlines the proposed methodology behind the computation of moment-based reduced order models, both for the input-output system Σ , and the radiation dynamics, defined by Σ_r . Section 6.4 provides a case study for the input-output dynamics reduction case, utilising a particular WEC array composed of 1-DoF state-of-the-art devices. Using this same array layout, Section 6.5 discusses and illustrates the synergy between the unknown-input estimation problem in wave energy, and the moment-based MIMO framework developed in this chapter. For the radiation dynamics case, Section 6.6 provides a case study in terms of a multi-DoF WEC (instead of a WEC array as in the input-output case), to illustrate the performance of the presented strategy, making emphasis in the capabilities of retaining the physical properties associated with radiation effects (listed in Table 2.1). Finally, the main conclusions of this chapter are encompassed in Section 6.7.

3: Note that, as reported in [15], the combination of modern state-estimation strategies and the internal model principle has been exploited in several wave excitation force estimation studies, using a variety of state observers.

6.1 Model reduction by moment-matching for linear MIMO systems

Consider a finite-dimensional, MIMO, continuous-time system described, for $t \in \mathbb{R}^+$, by the state-space model

$$\begin{aligned} \dot{x} &= Ax + Bu, \\ y &= Cx, \end{aligned} \tag{6.2}$$

with⁴ $x(t) \in \mathbb{R}^n$, $u(t) \in \mathbb{R}^q$ and $y(t) \in \mathbb{R}^q$. The (constant) matrices composing (6.2) are such that $A \in \mathbb{R}^{n \times n}$, $\{B, C^\top\} \subset \mathbb{R}^{n \times q}$. Consider the associated transfer function $W : \mathbb{C} \rightarrow \mathbb{C}^{q \times q}$, $s \mapsto C(s\mathbb{I}_n - A)^{-1}B$, and assume that (6.2) is minimal.

Consider the following multiple-output signal generator described, for $t \in \mathbb{R}^+$, by the set of differential equations

$$\begin{aligned}\dot{\xi} &= (\mathbb{I}_q \otimes S)\xi, \\ u &= L\xi,\end{aligned}\tag{6.3}$$

with $\xi(t) \in \mathbb{R}^{qv}$, $L \in \mathbb{R}^{q \times qv}$, $\xi(0) \in \mathbb{R}^{qv}$, and the matrix $S \in \mathbb{R}^{\nu \times \nu}$ is exactly as in the single-output signal generator defined in equation (4.3). An analogous assumption, to that defined in Assumption 4.1.1, is now introduced.

Assumption 6.1.1 The triple of matrices $(L, \mathbb{I}_q \otimes S, \xi(0))$ is minimal.

A proposition is now presented, which provides an ‘adaptation’ of Lemma 4.1.1 for the MIMO case, exploiting an explicit connection with the signal generator defined for the SISO case (4.3), in terms of the operator S .

Proposition 6.1.1 Suppose Assumptions 4.1.2 and 6.1.1 hold, and that system (6.2) is asymptotically stable in the Lyapunov sense, i.e. $\lambda(A) \subset \mathbb{C}_{<0}$. Then, there is a unique matrix $\Pi \in \mathbb{R}^{n \times qv}$ which solves the Sylvester equation

$$\Pi(\mathbb{I}_q \otimes S) = A\Pi + BL,\tag{6.4}$$

and the steady-state response of the interconnected system (6.2)-(6.3) is $x_{ss}(t) = \Pi\xi(t)$, for any $x(0)$ and $\xi(0)$.

Moreover, under the same set of assumptions, there exists a one-to-one relation between the moments⁵ $\eta_0(s_1), \eta_0(s_2), \dots, \eta_0(s_\nu)$, with $s_i \in \lambda(S)$, $\forall i \in \mathbb{N}_\nu$, and the steady-state output response $y_{ss}(t) = C\Pi\xi(t)$. In fact, the moments are uniquely determined by the matrix $C\Pi$.

4: Without any loss of generality, the focus is put on square systems, aiming to simplify the notation.

5: Recall that the 0-order moment is $\eta_0(s^*) = C(s^*\mathbb{I}_n - A)^{-1}B \in \mathbb{C}^{q \times q}$, with $s^* \in \mathbb{C}/\lambda(A)$ (see Definition 4.1.1).

Proof. The proof of this proposition follows the same arguments as those for the SISO case considered in [20] and, hence, it is omitted. \square

Definition 6.1.1 Suppose the assumptions of Proposition 6.1.1 are fulfilled. The matrix $C\Pi$ is the moment of system (6.2) at (S, L) , i.e. at the signal generator (6.3).

Remark 6.1.1 Previous literature in moment-matching, for the MIMO case, utilises the so-called *tangential interpolation* framework [221], which does not ‘extend’ the matrix S as a function of the number of inputs, *i.e.* $q \in \mathbb{N}_{\geq 1}$. Here, and as in the SISO case discussed in Chapter 3, there is special interest in retaining the *exact* same steady-state response for the N -th order WEC system, in spite of the consequent increase in model order with respect to the tangential approach, which interpolates $W(s)$ at specific ‘directions’ in \mathbb{C}^q , rather than complex points. One of the main motivations behind this argument stems from the fact that retaining an *exact* steady-state response in the reduced model greatly increases the accuracy of unknown-input estimation procedures, as discussed and illustrated in Section 6.5. This exact steady-state response connection is also exploited for control purposes, in Chapter 9.

Remark 6.1.2 Analogously to the linear SISO case, presented in Section 4.1.1, the moment for system (6.2) is computed in terms of the unique solution of a Sylvester equation, *i.e.* equation (6.4). In addition, the matrix $C\Pi \equiv \underline{Y}$ is referred to as the *moment-domain equivalent* of y .

Based on this steady-state characterisation of moments, provided in Proposition 6.1.1, Definition 4.2.1 and Lemma 4.2.1 can be adapted for the MIMO case straightforwardly, as detailed in the following.

Definition 6.1.2 Consider the signal generator (6.3). The system described by the equations

$$\begin{aligned}\dot{\Theta} &= F\Theta + \Delta u, \\ \theta &= Q\Theta,\end{aligned}\tag{6.5}$$

with $\Theta(t) \in \mathbb{R}^{q\nu}$, $\theta(t) \in \mathbb{R}^q$, $F \in \mathbb{R}^{q\nu \times q\nu}$ and $\{\Delta, Q^\top\} \subset \mathbb{R}^{q\nu \times q}$, is a model of system (6.2) at (S, L) if system (6.5) has the same moments at (S, L) as system (6.2). In addition, system (6.5) is a reduced order model of system (6.2) at (S, L) if $q\nu < n$.

Lemma 6.1.2 [20, 21] Consider system (6.2) and the signal generator (6.3). Suppose Assumptions 4.1.2 and 6.1.1 hold, and that system (6.2) is asymptotically stable, *i.e.* $\lambda(A) \subset \mathbb{C}_{<0}$. Then, system (6.5) is a model of system (6.2) at S if⁶ $\lambda(F) \cap \lambda(S) = \emptyset$ and

$$C\Pi = QP,\tag{6.6}$$

where $C\Pi = \underline{Y}$ is the moment-domain equivalent of the output of system (6.2), computed from (6.4), and P is the unique solution

6: Note that $\lambda(\mathbb{I} \otimes M) = \lambda(M)$ for any matrix $M \in \mathbb{R}^{n \times n}$ [24].

of the Sylvester equation

$$P(\mathbb{I}_q \otimes S) = FP + \Delta L. \quad (6.7)$$

Remark 6.1.3 As in the linear SISO case of Section 4.2.1, the steady-state output of the reduced order model (6.5) *exactly* matches the steady-state output of the system resulting from the interconnection of system (6.2) and the signal generator (6.3), provided $\lambda(F) \subset \mathbb{C}_{<0}$.

6.2 Moment-based WEC formulation for MIMO model reduction

As in the SISO model reduction technique introduced in Chapter 5, and given that moments for MIMO systems, as defined herein in Section 6.1, are also inherently based on the knowledge of a state-space representation of the system to be reduced, the equation of motion characterising Σ , *i.e.* equation (6.1), needs to be re-written in a more suitable structure. The following equivalent representation, is proposed:

$$\Sigma : \begin{cases} \dot{w} = Aw + Bv, \\ y = Cw, \end{cases} \quad (6.8)$$

for $t \in \mathbb{R}^+$, where $w(t) = \sum_{i=1}^N e_i^N \otimes [z_i(t) \quad \dot{z}_i(t)]^T \in \mathbb{R}^{2N}$ contains displacement and velocities for each N -th device or DoF involved in the equation of motion, *i.e.* each ‘order’ of the WEC system⁷, and the (constant) matrices $A \in \mathbb{R}^{2N \times 2N}$, $B \in \mathbb{R}^{2N \times N}$ and $C \in \mathbb{R}^{N \times 2N}$ are defined as

$$\begin{aligned} A &= \sum_{i=1}^N \sum_{j=1}^N e_{ij}^N \otimes \begin{bmatrix} 0 & {}^i_j \delta \\ -\mathcal{M}_{ij} s_{h_i} & 0 \end{bmatrix}, \\ B &= \sum_{i=1}^N \sum_{j=1}^N e_{ij}^N \otimes \begin{bmatrix} 0 \\ \mathcal{M}_{ij} \end{bmatrix}, \\ C &= \mathbb{I}_N \otimes [0 \ 1], \end{aligned} \quad (6.9)$$

Analogously to equation (5.4), the ‘input’ function $v : \mathbb{R}^+ \rightarrow \mathbb{R}^N$, is defined as

$$v = f_e - k_r * \dot{z} = f_e - k_r * Cw. \quad (6.10)$$

Within the moment-based formulation introduced in Section 6.1, the mapping associated with the external input, f_e , is written in terms of an autonomous multiple-output signal generator (analogously to the

7: Notation directly inherited from Remark 6.0.2.

case of equation (6.3)), *i.e.* using the set of differential equations

$$\begin{aligned}\dot{\xi} &= (\mathbb{I}_N \otimes S)\xi, \\ f_e &= L\xi,\end{aligned}\tag{6.11}$$

for $t \in \mathbb{R}^+$, with $\xi(t) \in \mathbb{R}^{N\nu}$, $S \in \mathbb{R}^{\nu \times \nu}$ and $L \in \mathbb{R}^{N \times N\nu}$. Recall that Assumptions 6.1.1 and 4.1.2 are required to have a well-posed system-theoretic definition of moments. These are discussed, for the MIMO WEC case, in the following paragraphs.

With respect to Assumption 4.1.2, which poses a set of characteristics for $\lambda(S)$, a finite-set $\mathcal{F} = \{\omega_p\}_{p=1}^f \subset \mathbb{R}^+$ is considered (as for the SISO case of Section 5.1), and the dynamic matrix S is written in a block-diagonal form as,

$$S = \bigoplus_{p=1}^f \begin{bmatrix} 0 & \omega_p \\ -\omega_p & 0 \end{bmatrix},\tag{6.12}$$

with $\nu = 2f$, $f \in \mathbb{N}_{\geq 1}$, and $\lambda(S) = (j\mathcal{F}) \cup (-j\mathcal{F}) \subset \mathbb{C}^0$.

Remark 6.2.1 As per the theory proposed in Section 6.1, the dynamic matrix S for this MIMO case is shared with the SISO technique proposed in Chapter 5: Each ω_p defined in (6.12) represents a desired interpolation point for the MIMO model reduction process.

With respect to Assumption 6.1.1, and without any loss of generality, the initial condition of the signal generator is set to $\xi(0) = \varepsilon_{N\nu}$, so that the minimality condition on the triple $(L, \mathbb{I}_N \otimes S, \varepsilon_{N\nu})$ holds as long as the pair $(\mathbb{I}_N \otimes S, L)$ is observable.

Under this selection of matrices, the moments of system (6.8), driven by the signal generator (6.11), can be computed by solving a specific Sylvester equation (as in Proposition 6.1.1). Such a moment equation can be specialised for the MIMO WEC case as

$$A\Pi + B(L - \underline{K}_r) = \Pi(\mathbb{I}_N \otimes S),\tag{6.13}$$

where $\Pi \in \mathbb{R}^{2N \times N\nu}$ and $\underline{K}_r \in \mathbb{R}^{N \times N\nu}$ is the moment-domain equivalent of the radiation force, for the MIMO radiation system Σ_r . The moment-domain equivalent of the velocity, which is the key theoretical tool to develop reduced order models by moment-matching (as in Lemma 6.1.2), can be expressed in terms of the solution of (6.13) as $\underline{\dot{Z}} = C\Pi$.

As in the SISO case, the term \underline{K}_r clearly depends on the matrix Π . A formal definition for the moment-domain equivalent \underline{K}_r is given in the following.

Proposition 6.2.1 *The moment-domain equivalent of the convolution integral in (6.1) can be computed as*

$$\underline{K}_r = \sum_{i=1}^N \sum_{j=1}^N e_{ij}^N \dot{\underline{Z}} (\mathbb{I}_N \otimes \mathcal{R}_{ij}), \quad (6.14)$$

where each $\mathcal{R}_{ij} \in \mathbb{R}^{\nu \times \nu}$ is a block-diagonal matrix defined as

$$\mathcal{R}_{ij} = \bigoplus_{p=1}^f \begin{bmatrix} {}^i_j r_{\omega_p} & {}^i_j m_{\omega_p} \\ -{}^i_j m_{\omega_p} & {}^i_j r_{\omega_p} \end{bmatrix}, \quad (6.15)$$

with

$${}^i_j r_{\omega_p} = B_{ij}(\omega_p) \quad {}^i_j m_{\omega_p} = \omega_p [A_{ij}(\omega_p) - m_{\infty ij}], \quad (6.16)$$

where $A_{ij}(\omega)$ and $B_{ij}(\omega)$ are the ij -th entries of the added-mass and radiation damping matrix of the MIMO WEC, respectively, at each specific frequency induced by the eigenvalues of S , and $m_{\infty ij}$ is the ij -th entry of the matrix m_{∞} .

Proof. The proof of this statement follows the same arguments presented for the SISO case (see Proposition 5.1.1), and, hence, is omitted. \square

Finally, the following two propositions, that address the uniqueness of the solution of the Sylvester equation (6.13), for the MIMO WEC case, and the explicit computation of the moment equivalent $\dot{\underline{Z}}$, are now stated.

Proposition 6.2.2 *The solution of the Sylvester equation (6.13) is unique if and only if*

$$\lambda \left(\bigoplus_{p=1}^f \begin{bmatrix} T_p & 0 \\ 0 & T_p \end{bmatrix} \right) \cap \lambda(S) = \emptyset, \quad (6.17)$$

where each matrix T_p is defined as

$$T_p = A - B(\mathcal{T}_{r_{\omega_p}} + j\mathcal{T}_{m_{\omega_p}})C, \quad (6.18)$$

with

$$\mathcal{T}_{r_{\omega_p}} = \sum_{i=1}^N \sum_{j=1}^N {}^i_j r_{\omega_p} \otimes e_{ij}^N, \quad \mathcal{T}_{m_{\omega_p}} = \sum_{i=1}^N \sum_{j=1}^N {}^i_j m_{\omega_p} \otimes e_{ij}^N. \quad (6.19)$$

Proof. A direct application of the vec operator to equation (6.13) (and considering Property 1.3.1 and the bilinearity and associativity

property of the Kronecker product) yields the equivalent linear system of equations

$$(\mathbb{I}_N \otimes \Phi) \text{vec}\{\Pi\} = \text{vec}\{-BL\}, \quad (6.20)$$

where the matrix $\Phi \in \mathbb{R}^{2N\nu \times 2N\nu}$ is defined as

$$\Phi = (S \hat{\oplus} A) + \sum_{i=1}^N \sum_{j=1}^N \mathcal{R}_{ij}^T \otimes -Be_{ij}^N C. \quad (6.21)$$

From (6.20), one can automatically conclude that the solution of the Sylvester equation (6.13) is unique if and only if $0 \notin \lambda(\Phi)$. As a consequence of the block-structure of each of the matrices involved in (5.19), the matrix Φ can be always written in a block-diagonal structure, *i.e.* $\Phi = \bigoplus_{p=1}^f \Phi_p$. Therefore, the matrix Φ is invertible if and only if⁸ each block Φ_p is invertible.

⁸: Note that, for any matrix $M \in \mathbb{C}^{n \times n}$, $\lambda(\mathbb{I} \otimes M) = \lambda(M)$ [24].

After algebraic manipulation of (6.21), each block composing Φ can be expressed as

$$\Phi_p = \begin{bmatrix} A - B\mathcal{T}_{r\omega_p} C & \omega_p \mathbb{I}_{2N} + B\mathcal{T}_{m\omega_p} C \\ -\omega_p \mathbb{I}_{2N} - B\mathcal{T}_{m\omega_p} C & A - B\mathcal{T}_{r\omega_p} C \end{bmatrix}, \quad (6.22)$$

where $\mathcal{T}_{r\omega_p}$ and $\mathcal{T}_{m\omega_p}$ are defined in (6.19). Consider now the (invertible) matrix

$$W = \begin{bmatrix} \mathbb{I}_{2N} & j\mathbb{I}_{2N} \\ \mathbb{I}_{2N} & -j\mathbb{I}_{2N} \end{bmatrix}, \quad (6.23)$$

and the similarity transformation ${}^W\Phi_p = W\Phi_p W^{-1}$, which yields

$${}^W\Phi_p = - \begin{bmatrix} j\omega_p \mathbb{I}_{2N} - T_p & 0 \\ 0 & j\omega_p \mathbb{I}_{2N} - T_p \end{bmatrix}, \quad (6.24)$$

where one can straightforwardly conclude that Φ_p is invertible if and only if

$$\lambda \left(\begin{bmatrix} T_p & 0 \\ 0 & \overline{T_p} \end{bmatrix} \right) \cap \lambda(S) = \emptyset \quad (6.25)$$

Finally, the claim follows repeating the same analysis for each block of Φ_p with $p \in \mathbb{N}_f$. \square

Proposition 6.2.3 *Suppose (6.17) holds. Then, the moment-domain equivalent of the output y of the MIMO WEC system (6.8) can be uniquely determined as*

$$\text{vec}\{\dot{Z}\} = (\mathbb{I}_N \otimes \Phi_{\mathcal{R}}) \text{vec}\{L\}, \quad (6.26)$$

where

$$\begin{aligned}\Phi_{\mathcal{F}} &= (\mathbb{I}_{N\nu} \otimes C)\Phi^{-1}(\mathbb{I}_{N\nu} \otimes -B), \\ \Phi &= (S \hat{\oplus} A) + \sum_{i=1}^N \sum_{j=1}^N \mathcal{R}_{ij}^T \otimes -Be_{ij}^N C,\end{aligned}\quad (6.27)$$

with $\Phi \in \mathbb{R}^{2N\nu \times 2N\nu}$ and $\Phi_{\mathcal{F}} \in \mathbb{R}^{N\nu \times N\nu}$.

Proof. Recall that $\dot{\underline{Z}} = C\Pi$. Then, if equation (6.17) holds, equation (6.26) follows directly from (6.20). \square

Remark 6.2.2 Similarly to the SISO WEC case of Chapter 5, equation (6.17) always holds for the MIMO WEC case, since it follows from the internal stability of (6.8) (see Section 2.4) that $\lambda(T_p) \subset \mathbb{C}_{<0}$ for all $p \in \mathbb{N}_f$.

6.3 Reduced models achieving moment-matching

With the theoretical results proposed in Section 6.2, it is possible to compute reduced order models both for the input-output (force-to-motion) dynamics, *i.e.* a system $\tilde{\Sigma}$ approximating Σ in (6.8), and the radiation system, *i.e.* a system $\tilde{\Sigma}_r$ approximating Σ_r . In contrast to the SISO case discussed in Chapter 5, this section considers the theoretical structure behind the family of systems (6.5) achieving moment-matching at the user-selected set of frequencies \mathcal{F} , in synergy with some of the main notions behind frequency-domain subspace-based identification methods, as proposed in [237], and briefly recalled in the subsequent sections.

Remark 6.3.1 Consider the input-output dynamics Σ . One could follow an analogous procedure to that of Chapter 5: Let P in equation (6.7) be such that $P = \mathbb{I}_{N\nu}$. Then,

$$\Sigma \approx \tilde{\Sigma}_{\mathcal{F}} : \begin{cases} \dot{\Theta} = (\mathbb{I}_N \otimes S - \Delta L)\Theta + \Delta f_e, \\ \tilde{y} = \underline{\dot{Z}}\Theta, \end{cases}\quad (6.28)$$

is the family of reduced order models, for $t \in \mathbb{R}^+$, parameterised in $\Delta \in \mathbb{R}^{N\nu \times N}$, containing *all* the models of dimension $N\nu$ achieving moment-matching at (S, L) , *i.e.* interpolating the moments of system (6.8) at the eigenvalues of the matrix S , and where $\underline{\dot{Z}}$ is as in Proposition 6.2.3. Note that, observability of the pair $(\mathbb{I}_N \otimes S, L)$ guarantees that the eigenvalues of (6.28) can be assigned arbitrarily. Nevertheless, for this MIMO case, there is

an infinite set of (constant) gains Δ for each particular desired set of eigenvalues [75]. In other words, if one attempts to follow an analogous procedure to that described in Section 5.2, *i.e.* Procedure 1, the search space of the related optimisation problem becomes substantially more complex.

6.3.1 Input-output dynamics

The rationality behind Remark 6.3.1 motivates the following procedure, where an optimal input matrix Δ^{opt} is computed, based on the concepts discussed below.

Following well-established theory on subspace-based methods, reported in, for instance, [237], both the dynamic and output matrix from system (6.8) can be approximated in terms of the singular value decomposition of the Hankel matrix \hat{H} , constructed⁹ from the input-output frequency-domain data of the MIMO WEC, computed (with BEM solvers) at the finite set of uniformly spaced frequencies Ω . The α -dimensional approximated matrices ${}^d\hat{A}_\alpha \in \mathbb{R}^{\alpha \times \alpha}$, $\hat{C}_\alpha \in \mathbb{R}^{N \times \alpha}$ (where ${}^d\hat{A}_\alpha$ corresponds to a discrete-time model) can be computed [237] as

$${}^d\hat{A}_\alpha = (J_1 \hat{U}_\alpha)^\dagger J_2 \hat{U}_\alpha, \quad \hat{C}_\alpha = J_3 \hat{U}_\alpha, \quad (6.29)$$

where the singular value decomposition of the Hankel matrix is written as

$$\hat{H} = \begin{bmatrix} \hat{U}_\alpha & \hat{U}_o \end{bmatrix} \begin{bmatrix} \hat{\Sigma}_\alpha & 0 \\ 0 & \hat{\Sigma}_o \end{bmatrix} \begin{bmatrix} \hat{V}_\alpha^\top \\ \hat{V}_o^\top \end{bmatrix}, \quad (6.30)$$

and the matrices $\{J_1, J_2\} \subset \mathbb{R}^{(N-1)N \times N^2}$, $J_3 \in \mathbb{R}^{N \times N^2}$ are

$$J_1 = \begin{bmatrix} \mathbb{I}_{(N-1)N} \\ 0 \end{bmatrix}^\top, \quad J_2 = \begin{bmatrix} 0 \\ \mathbb{I}_{(N-1)N} \end{bmatrix}^\top, \quad J_3 = \begin{bmatrix} \mathbb{I}_N \\ 0 \end{bmatrix}^\top. \quad (6.31)$$

Remark 6.3.2 Note that, with knowledge of the frequency sampling value associated with the set Ω , the continuous-time equivalent matrix \hat{A}_α can be computed directly from ${}^d\hat{A}_\alpha$ using, for instance, the bilinear (Tustin) mapping, as discussed in [237].

Remark 6.3.3 If ${}^d\hat{A}_\alpha$, computed as in (6.29), has unstable eigenvalues, one can always project such a set into the complex unit circle, following the procedure described in [237]. This guarantees the computation of a Jury matrix ${}^d\hat{A}_\alpha$, if required.

With the theory recalled above, an algorithm to compute a moment-matching-based reduced model of the input-output WEC dynamics, is proposed, explicitly exploiting the result of Proposition 6.2.3 and

9: The reader is referred to [237] for further details on the computation of the Hankel matrix \hat{H} associated with a given dynamical system Σ .

the system-theoretic structure of the family of systems (6.5). The complete procedure is summarised in the following steps, listed below.

Procedure 2: MIMO model reduction procedure for WECs

- 1 Select a set of f interpolation points (frequencies) $\mathcal{F} = \{\omega_p\}_{p=1}^f \subset \mathbb{R}^+$ to achieve moment-matching.
- 2 Compute the matrix $\mathbb{I}_N \otimes S$ following (6.12) and select any L such that the pair $(\mathbb{I}_N \otimes S, L)$ is observable.
- 3 Calculate the moment-domain equivalent of the output of system (6.8), i.e. \dot{Z} , using the result of Proposition 6.2.3.
- 4 Compute the matrices $\hat{A}_{N\nu}$ and $\hat{C}_{N\nu}$ using the frequency-domain data points associated with the input-output response of the WEC $G(\omega)$, as described in equation (6.29).
- 5 Consider the family of systems (6.5) and set $F = \hat{A}_{N\nu}$ and $Q = \hat{C}_{N\nu}$.
- 6 Consider the frequency response of (6.5) as a function of Δ i.e. the mapping $\tilde{G}_{\mathcal{F}} : \mathbb{R} \times \mathbb{R}^{N\nu \times N} \rightarrow \mathbb{C}^{N \times N}$ given¹⁰ by

$$\tilde{G}_{\mathcal{F}}(\omega, \Delta) = Q(j\omega\mathbb{I}_{N\nu} - F)^{-1} \Delta. \quad (6.32)$$

10: Note that the mapping $\tilde{G}_{\mathcal{F}}$ is linear in the argument Δ .

- 7 Let $\Omega = \{\omega_i\}_{i=1}^M \subset W$ be the (finite) frequency set utilised to compute the hydrodynamic coefficients $B_r(\omega)$ and $A_r(\omega)$, in the frequency range $W = [\omega_l, \omega_u] \subset \mathbb{R}^+$. Then, compute the input matrix Δ^{opt} with the following optimisation-based procedure:

$$\Delta^{\text{opt}} = \arg \min_{\Delta \in \mathbb{R}^{N\nu \times N}} \sum_{i=1}^M \left\| \tilde{G}_{\mathcal{F}}(\omega_i, \Delta) - G(\omega_i) \right\|_F^2, \quad (6.33)$$

subject to:

$$FP + \Delta L = P(\mathbb{I}_N \otimes S),$$

$$QP = \dot{Z}.$$

- 8 Compute an $N\nu$ -dimensional input-output WEC time-domain model achieving moment-matching at (S, L) from (6.5) as

$$\Sigma \approx \tilde{\Sigma}_{\mathcal{F}} : \begin{cases} \dot{\Theta} = F\Theta + \Delta^{\text{opt}} f_e, \\ \tilde{y} = Q\Theta. \end{cases} \quad (6.34)$$

Procedure 2 is based on the idea of building the reduced order model $\tilde{\Sigma}_{\mathcal{F}}$, matching the f (user-defined) frequencies of the set \mathcal{F} , exploiting the system structure of (6.5), and solving an equality-constrained optimisation problem. Summarising, this optimisation process computes the input matrix Δ^{opt} that minimises the difference between the target frequency response and that of (6.5) (in terms of the matrix Euclidean norm) while guaranteeing the moment-

matching conditions in the obtained reduced model. The optimisation problem of Procedure 2 is a constrained least-squares problem and can be solved using state-of-the-art solvers, such as those detailed in, for instance, [207].

Remark 6.3.4 The model computed with Procedure 2 has dimension $N\nu$ with $\nu = 2f$, where N is either the number of devices in the WEC array, or the number of DoF considered for a single device, and f is the number of interpolation points (frequencies) selected in the set \mathcal{F} .

6.3.2 Radiation dynamics

A reduced order model for the radiation system Σ_r can be obtained following an analogous procedure to that considered for the input-output (force-to-motion) case. In particular, let the velocity vector \dot{z} be expressed as a multiple-output signal generator, in the same fashion as equation (6.11), *i.e.*

$$\begin{aligned}\dot{\xi} &= (\mathbb{I}_N \otimes S)\xi, \\ \dot{z} &= L\xi,\end{aligned}\tag{6.35}$$

where the structure of S is as in equation (5.6), and any L such that the pair $(\mathbb{I}_N \otimes S, L)$ is observable. Then, recalling the result posed in Proposition 6.2.1, the moment-domain equivalent of system Σ_r , *i.e.* y_r , can be directly obtained as

$$\underline{Y}_r = \sum_{i=1}^N \sum_{j=1}^N e_{ij}^N L (\mathbb{I}_N \otimes \mathcal{R}_{ij}),\tag{6.36}$$

and a reduced order model can be computed as

$$\Sigma_r \approx \tilde{\Sigma}_{r\mathcal{F}} : \begin{cases} \dot{\Theta} = F\Theta + \Delta^{\text{opt}}\dot{z}, \\ \tilde{y}_r = Q\Theta,\end{cases}\tag{6.37}$$

where the set of matrices $\{F, Q, \Delta^{\text{opt}}\}$ can be analogously computed using Procedure 2 (described in Section 6.3.1), by simply replacing $\underline{\dot{Z}}$ by \underline{Y}_r , and the device frequency response $G(\omega)$ by that of the radiation force, *i.e.* $K_r(\omega)$ (defined in Section 2.3.2.2).

6.4 Input-output case study: an array of CorPower-like devices

This section presents an application case to illustrate and analyse the proposed strategy for the input-output model reduction by

moment-matching case, based on the square WEC array layout studied in [90], and depicted in Figure 6.1. This particular layout is composed of $N = 4$ energy converters, where the geometry of each of the four devices composing the WEC farm corresponds with a state-of-the-art full-scale CorPower¹¹-like device oscillating in heave (translational motion). Such a device is illustrated in Figure 6.2, along with its corresponding physical dimensions specified in metres. These dimensions are based on the experimental study performed in [239], which have also been considered in [240].

11: See [238] for up-to-date detail on this device.

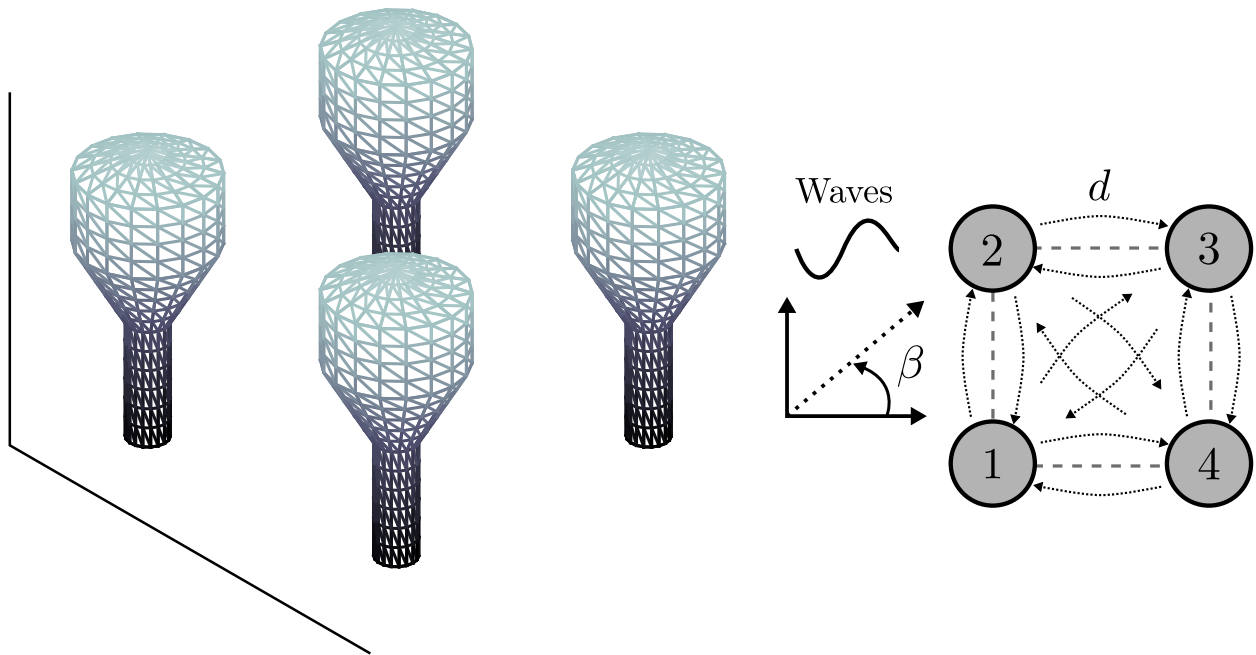


Figure 6.1: Regular-polytope-type WEC array layout considered for the application case. The distance d between devices is set to twice the diameter of the upper part of the float, *i.e.* $d \approx 17$ [m]. The dotted arrows represent the hydrodynamic interaction between WECs in the array, while β denotes the incident wave direction.

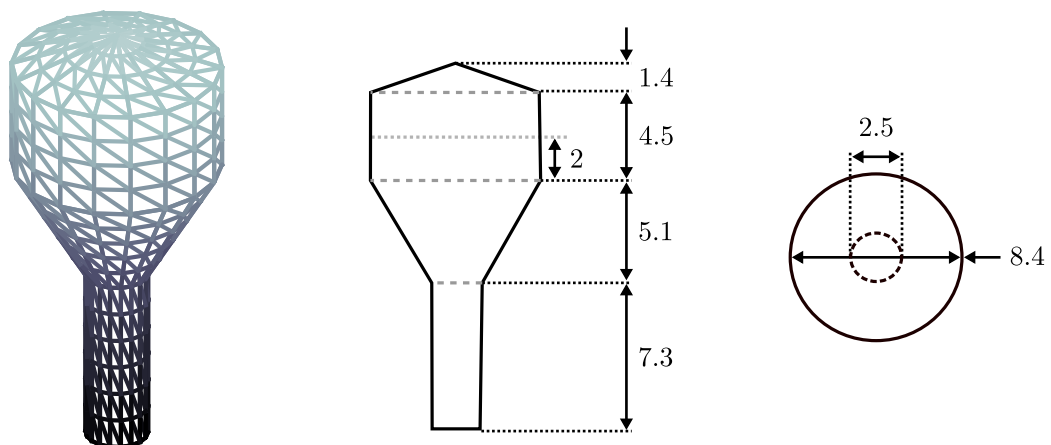
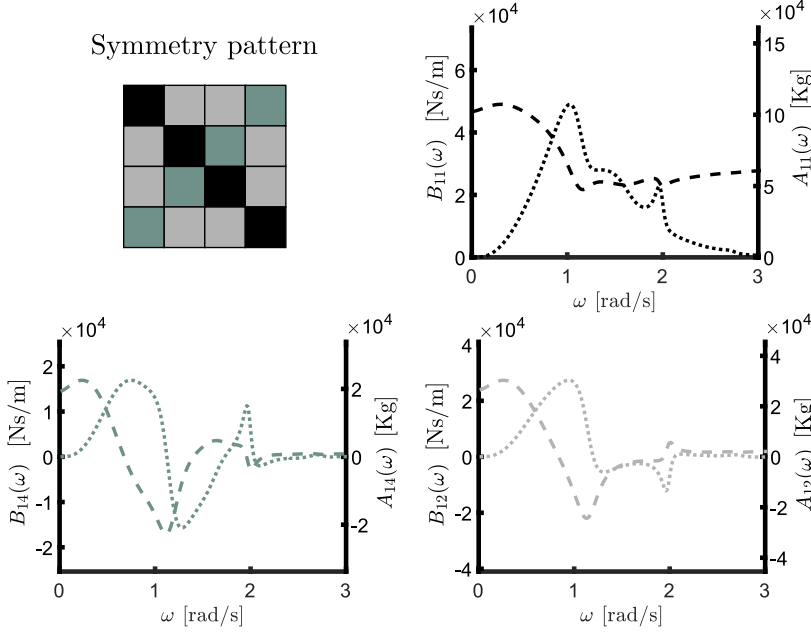


Figure 6.2: Schematic and dimensions of the CorPower-like device as studied in [239, 240]. Dimensions are in metres.

To fully characterise this farm, Figure 6.3 presents the hydrodynamic characteristics of the WEC array considered in this application case, in terms of its corresponding radiation damping and radiation added-

mass matrices, *i.e.* $B_r(\omega)$ and $A_r(\omega)$, respectively. Note that, since the devices composing the WEC farm are identical (*i.e.* CorPower-like devices), the corresponding hydrodynamic characteristics (including interactions arising due to radiation effects) present symmetrical behavior, in accordance with the layout depicted in Figure 6.1. That said, only three elements of the matrices $\{B_r(\omega), A_r(\omega)\} \subset \mathbb{R}^{4 \times 4}$ are required to completely characterise the hydrodynamic parameters of the complete array. These are plotted in Figure 6.3, along with the corresponding symmetry pattern¹² for $B_r(\omega)$ and $A_r(\omega)$.



12: The reader is referred to [49] for an extensive discussion on the hydrodynamic coefficients of WEC arrays and the principles behind this symmetrical behaviour.

Figure 6.3: Hydrodynamic characteristics of the CorPower-like WEC farm, in terms of the matrices $B_r(\omega)$ (dotted, left axis) and $A_r(\omega)$ (dashed, right axis). Note that there is a one-to-one relation between the colors of the lines and the corresponding symmetry pattern depicted in the figure.

Irregular waves are considered as inputs, corresponding with a JONSWAP SDF S_w (see Section 2.1.2) with a peak period $\bar{T}_w = 7.5$ [s], significant wave height \bar{H}_w in the set $\{1.5, 2, 3\}$ [m] and peak enhancement factor $\gamma = 3.3$ (shown in Figure 6.4). The total duration of each generated wave and, hence, each simulation, is set to 200 [s]. Analogously to the SISO case discussed in Section 5.3, the frequency set W , used explicitly to compute the reduced order models by moment-matching considered in this section, is set to $W = [0.3, 3]$ [rad/s]. Finally, without any loss of generality, the incident wave direction β is set to $\beta = 0$ (see Figure 6.1).

Similarly to the SISO case presented in Chapter 5, and aiming to obtain statistically meaningful and consistent results for the time-domain scenarios, it is found that the mean of 15 simulations is necessary to obtain a 95% confidence interval with a half-width of 0.2% of the mean, also computed as in [90].

Remark 6.4.1 From now on, the notation $G_{ij}(\omega)$ is used for the ij -th element of the matrix $G(\omega)$. More precisely, $G_{ij} : \mathbb{R} \rightarrow \mathbb{C}$

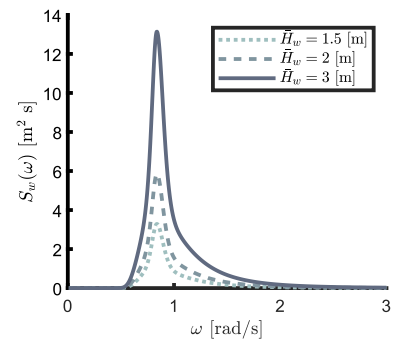


Figure 6.4: JONSWAP spectra utilised to generate the wave inputs, with $\bar{T}_w = 7.5$ [s], $\bar{H}_w \in \{1.5, 2, 3\}$ [m] and $\gamma = 3.3$.

is the frequency response mapping between the wave excitation force acting on the i -th device f_{e_i} , and the output velocity of the j -th device \dot{z}_j .

Following the theoretical results developed in Section 6.3, and the method proposed in Procedure 2, an explicit computation of a moment-based reduced model $\tilde{\Sigma}_{\mathcal{F}}$ is considered, aiming to approximate the force-to-velocity dynamics Σ described in Equation (6.8). To fulfill this objective, the target frequency response operator $G(\omega)$, computed using BEM codes, is explicitly used (as per Procedure 2 in Section 6.3). Recall that a key feature of this moment-based strategy is that the user is allowed to select a set of frequencies \mathcal{F} to interpolate, *i.e.* a set of frequency points where the approximating model $\tilde{\Sigma}_{\mathcal{F}}$ *exactly* matches the steady-state response of (6.8).

As discussed in Section 5.3 for the SISO case (*i.e.* equivalent to a single device in the array), a sensible selection of the interpolation set can be achieved by analysing the gain of the target frequency response, and selecting points that characterise dynamically important features of the WEC system. In the SISO WEC case, a sensible selection always includes the resonant frequency of the device under analysis, *i.e.* the frequency characterising the \mathcal{H}_∞ -norm of the WEC system. For this MIMO case, it is well-known that the system gain depends intrinsically on the so-called *input directions* (see, for instance, [234]), hence the selection of these dynamically relevant points cannot be done by simply inspecting each mapping $G_{ij}(\omega)$ individually. As a matter of fact, the 'gain' of a MIMO system is defined in terms of the *singular values* of $G(\omega)$, plotted, for the CorPower-array case, in Figure 6.5.

Based on the previous discussion, and to test the proposed strategy in the motion (velocity) simulation case, different frequency interpolation points sets \mathcal{F} are considered, as follows:

- ◇ $\mathcal{F}_1^{\text{sim}} = \{1.17\}$,
- ◇ $\mathcal{F}_2^{\text{sim}} = \{1.17, 1.11\}$,
- ◇ $\mathcal{F}_3^{\text{sim}} = \{1.17, 1.11, 1.8\}$,
- ◇ $\mathcal{F}_4^{\text{sim}} = \{1.17, 1.11, 1.8, 0.6\}$.

Note that $\mathcal{F}_i^{\text{sim}} \subset \mathcal{F}_j^{\text{sim}}$ for $i < j$, with $\{i, j\} \subset \mathbb{N}_4$. As can be appreciated from Figure 6.6, the set $\mathcal{F}_1^{\text{sim}}$ includes a key interpolation point, which explicitly characterises the \mathcal{H}_∞ -norm of the WEC array. To be precise, and analogous to the SISO case of Chapter 5, the presented MIMO moment-based strategy is able to preserve the \mathcal{H}_∞ -norm of the target system by simply including the corresponding frequency in the interpolation set. The set $\mathcal{F}_2^{\text{sim}}$ additionally includes the frequency point where the second maximum amplification peak

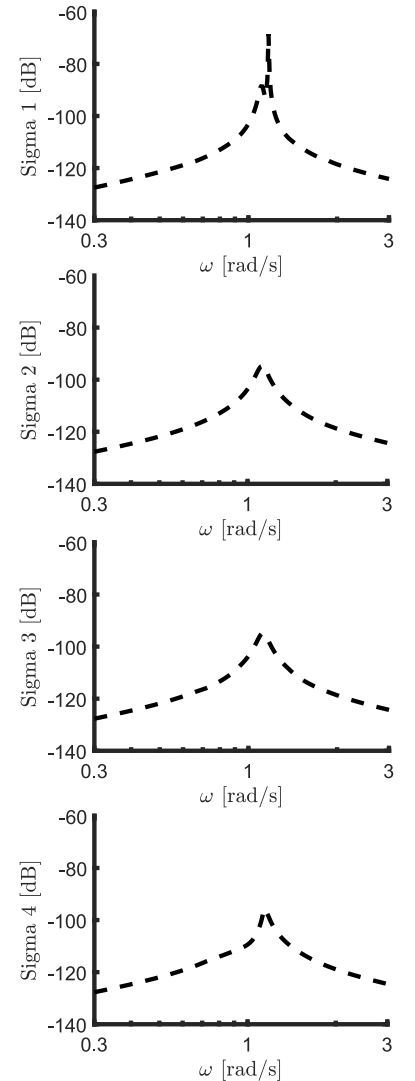


Figure 6.5: Singular values plot (also known as *sigma* plot) for the target response of the WEC array $G(\omega)$.

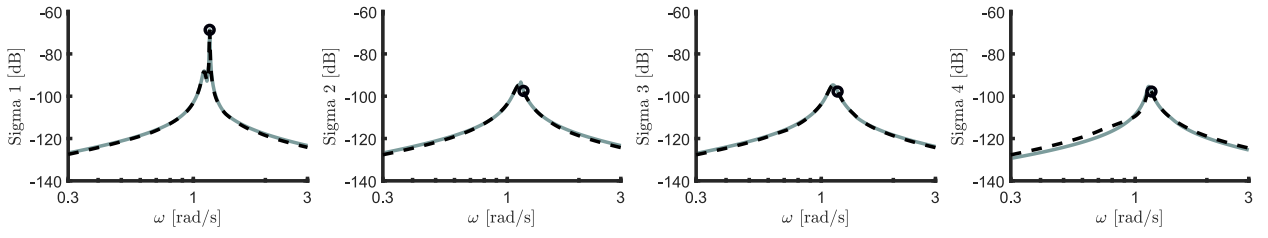
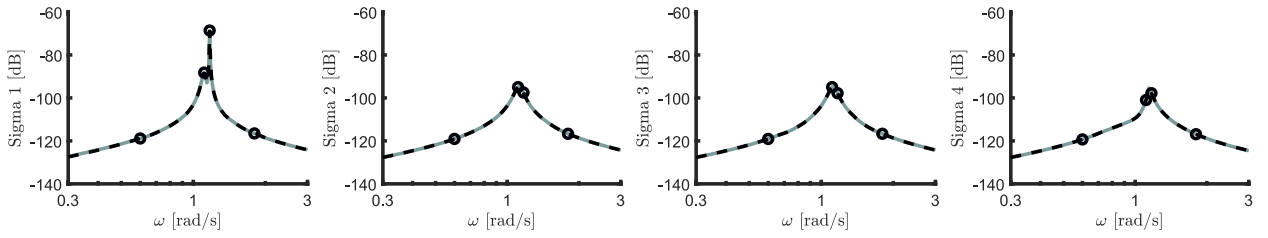
Interpolation set $\mathcal{F}_1^{\text{sim}}$ Interpolation set $\mathcal{F}_4^{\text{sim}}$ 

Figure 6.6: Singular values plot (also known as *sigma* plot) (inputs 1 to 4) for both the target response $G(\omega)$ (dashed), and the approximating sigma mappings (solid) corresponding with $\tilde{\Sigma}_{\mathcal{F}_1^{\text{sim}}}$ (top) and $\tilde{\Sigma}_{\mathcal{F}_4^{\text{sim}}}$ (bottom). The interpolation points are denoted by an empty black circle.

occurs. Finally, the sets $\mathcal{F}_3^{\text{sim}}$ and $\mathcal{F}_4^{\text{sim}}$ expand $\mathcal{F}_2^{\text{sim}}$ by including a low-, and a low- and high- frequency component, respectively.

One can begin the assessment of the moment-based model reduction approach in terms of WEC array motion simulation, by illustrating the performance of the reduced models $\tilde{\Sigma}_{\mathcal{F}_1^{\text{sim}}}$ and $\tilde{\Sigma}_{\mathcal{F}_4^{\text{sim}}}$. Figure 6.6 presents the singular values plot (also known as *sigma* plot), for both the target response $G(\omega)$ (dashed), and the approximating frequency response mappings (solid) corresponding with the models $\tilde{\Sigma}_{\mathcal{F}_1^{\text{sim}}}$ (top) and $\tilde{\Sigma}_{\mathcal{F}_4^{\text{sim}}}$ (bottom). The interpolation points selected for the computation of each approximating parametric structure are denoted by an empty black circle. Note that, as imposed by the theoretical foundations of this moment-based strategy, the approximating models have *exactly* the same gain as the target model $G(\omega)$ of the WEC array, for each element of the corresponding interpolation set \mathcal{F}^{sim} . In addition, it can be readily appreciated that, by a sensible selection of the interpolation frequency set $\mathcal{F}_1^{\text{sim}}$, the model $\tilde{\Sigma}_{\mathcal{F}_1^{\text{sim}}}$, *i.e.* a reduced order model by moment-matching computed using a single interpolation point, already provides a relatively accurate frequency-domain description when compared with the target steady-state response of the WEC array under study. Though considering $\mathcal{F}_1^{\text{sim}}$ as an interpolation set provides quite accurate results, the decrease in the overall approximation error from system $\tilde{\Sigma}_{\mathcal{F}_1^{\text{sim}}}$ to $\tilde{\Sigma}_{\mathcal{F}_4^{\text{sim}}}$ can be clearly appreciated (discussed in Table 6.1).

As a conclusive graphical illustration of the frequency-domain performance for the models computed via this moment-based strategy, Figure 6.7 presents the Bode diagrams for the mappings $G_{11}(\omega)$,

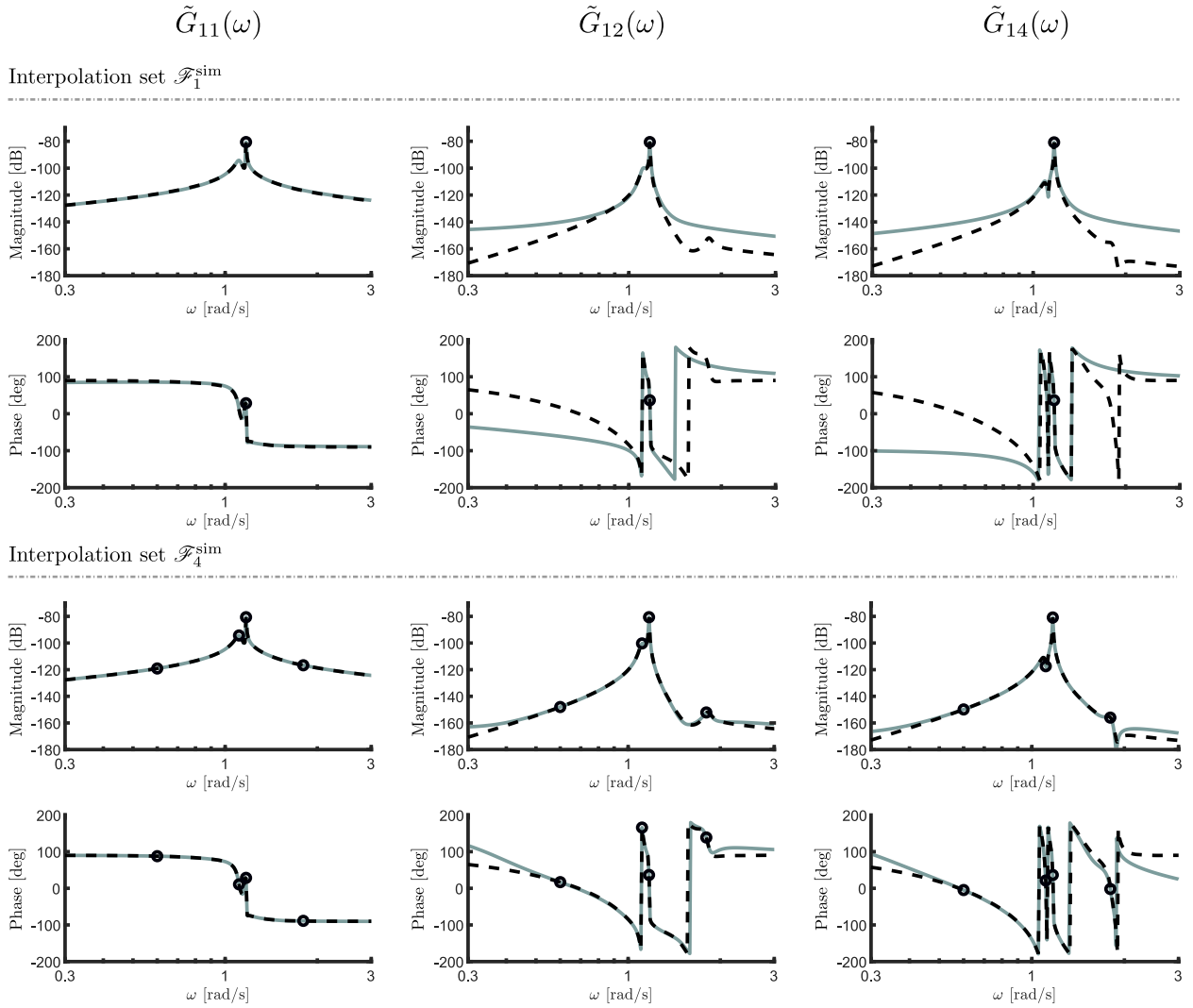


Figure 6.7: Bode plots for the elements $\{1, 1\}$, $\{1, 2\}$ and $\{1, 4\}$, for both the target response $G(\omega)$ (dashed), and the approximating frequency response mappings (solid) $\tilde{G}_{\mathcal{F}_1^{\text{sim}}}$ (top) and $\tilde{G}_{\mathcal{F}_4^{\text{sim}}}$ (bottom). The interpolation points are denoted by an empty black circle.

$G_{12}(\omega)$ and $G_{14}(\omega)$. Note that, due to the underlying symmetry of the WEC array illustrated in Figure 6.3, these mappings are sufficient to completely characterise the frequency response function $G(\omega)$. Analogously to what is presented in Figure 6.6, Figure 6.7 uses the same line convention to characterise the target response, and the approximating frequency responses $\tilde{G}_{\mathcal{F}_1^{\text{sim}}}$ (top) and $\tilde{G}_{\mathcal{F}_4^{\text{sim}}}$ (bottom). Once again, it can be appreciated that, by a sensible selection of the set \mathcal{F}_1 , the moment-based approximating model, computed using a single interpolation point, already presents reasonably accurate results, though this performance is significantly improved by the set \mathcal{F}_4 . Note that both parametric models have *exactly* the same response (both in magnitude and phase) as the target WEC array $G(\omega)$, for each element contained in the corresponding interpolation sets \mathcal{F}^{sim} .

To provide a precise measure of the performance of the moment-

based reduced order models computed for the WEC array considered in this case study, Table 6.1 offers a numerical comparison in terms of the following key indicators:

- Dim** Dimension (order) of the approximating reduced model.
- NRMSE_F** NRMSE computed against the target WEC array frequency response $G(\omega)$, with $\omega \in W$.
- NRMSE_T** NRMSE computed (in steady-state) against the target time-domain response of the WEC array computed directly from Σ (*i.e.* explicitly solving each corresponding convolution integral associated with radiation effects). The corresponding wave excitation force inputs are computed from the (JONSWAP) SDFs of Figure 6.4.

Model	Dim	NRMSE _F	NRMSE _T
$\tilde{\Sigma}_{\mathcal{F}_1^{\text{sim}}}$	8	4.82%	13.77%
$\tilde{\Sigma}_{\mathcal{F}_2^{\text{sim}}}$	16	0.44%	1.78%
$\tilde{\Sigma}_{\mathcal{F}_3^{\text{sim}}}$	24	0.16%	0.65%
$\tilde{\Sigma}_{\mathcal{F}_4^{\text{sim}}}$	32	0.09%	0.34%

Table 6.1: Simulation results comparison table.

It is straightforward to acknowledge, from Table 6.1, that the frequency-domain performance of the moment-matching-based models is always more than 95% accurate, being able to successfully represent the target WEC array even in the case where a single interpolation frequency is (sensibly) chosen. This performance is progressively improved by using the interpolation sets $\mathcal{F}_2^{\text{sim}}$, $\mathcal{F}_3^{\text{sim}}$ and $\mathcal{F}_4^{\text{sim}}$.

The increase of approximation quality, when considering the different interpolation sets in time-domain simulations, is consistent with the previous frequency-domain results, though it can be appreciated that the reduced order model $\tilde{\Sigma}_{\mathcal{F}_1^{\text{sim}}}$ presents quite different behavior in time-domain, compared to the frequency-domain. This is due to the fact that the waves generated as inputs for this simulation scenario correspond to a JONSWAP SDF with $\bar{T}_w = 7.5$ [s], *i.e.* a peak frequency of ≈ 0.84 [rad/s]. As can be appreciated from Figure 6.7, the fit between the frequency response of $\tilde{\Sigma}_{\mathcal{F}_1^{\text{sim}}}$ and the target response of the WEC array is relatively poor in the neighborhood of 0.84 [rad/s], hence directly implying a loss of performance in this particular time-domain scenario.

Finally, and to briefly illustrate the transient response of the reduced models computed with the presented strategy, Figure 6.8 presents three different velocity curves for a particular realisation with $\bar{H}_w = 2$ [m]: Target steady-state response (dashed), target transient response (dotted), and transient response of the moment-matching-based model $\tilde{\Sigma}_{\mathcal{F}_4^{\text{sim}}}$ (solid), for each of the devices composing the WEC array under analysis. The target transient response is computed by explicitly solving the convolution operation in equation (6.8). It can be readily noted that the velocity computed with the target and approximating model perfectly overlap throughout both the transient period (approximate time-length of 20 [s]), and the steady-state regime.

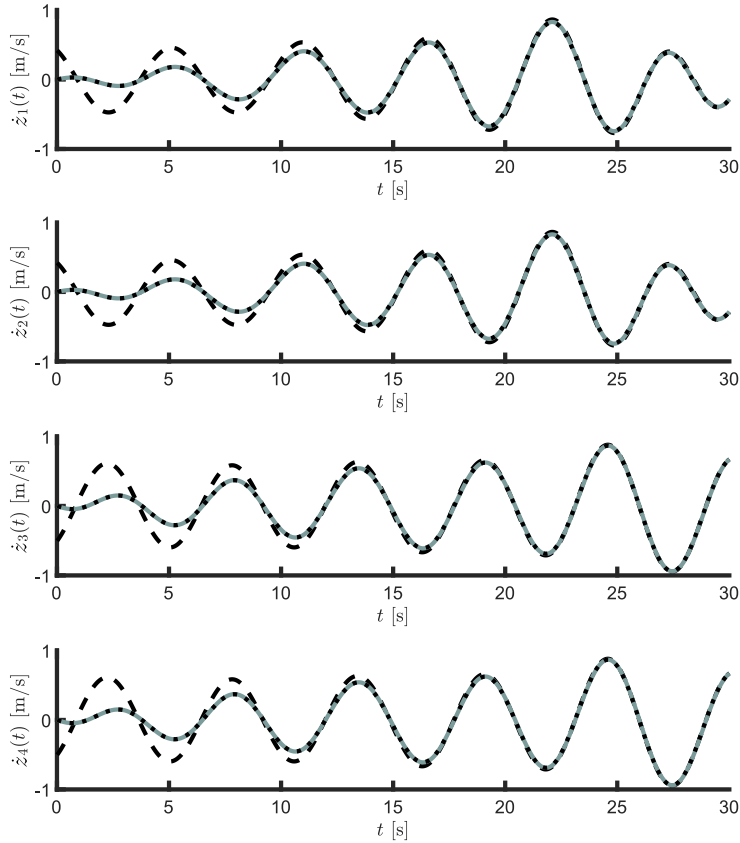


Figure 6.8: Target steady-state response (dashed), target transient response (dotted), and transient response of the moment-matching-based model $\tilde{\Sigma}_{\mathcal{F}_4^{\text{sim}}}$ (solid), for each of the devices composing the WEC array under analysis.

6.5 Synergy between moments and unknown-input estimation

The unknown-input estimation strategy considered in this section is that utilised in [90], where the estimation of wave excitation force for a WEC array is discussed. This strategy belongs to the class of unknown-input observers, where the system's input (wave excitation force f_e acting on the device) is estimated using only velocity measurements of the WEC array (*i.e.* the vector \dot{z}) based on a direct application of the internal model principle [236]. To this end, a Kalman Filter¹³ (KF) [235] is used, in conjunction with a harmonic oscillator model, to (approximately) describe the dynamics of the excitation force. In fact, note that the dynamical model used to describe the wave excitation effect is *exactly* defined by the multiple-output signal generator proposed in (6.11). In other words, there is a natural synergy between the moment-matching-based parameterisation strategy proposed in this thesis, and the unknown-input estimation problem inherently present in wave energy systems. This intrinsic connection, together with a summary of the unknown-input estimation strategy presented in [90] (for the sake of completeness), are discussed in the subsequent paragraph.

13: Note that [90] uses a discrete-time KF. Herein the continuous-time counterpart, *i.e.* a Kalman-Bucy filter, is considered. The reader is referred to, for instance, [241], for further detail on Kalman-Bucy filtering.

Remark 6.5.1 Note that, as reported in [15], the harmonic description of excitation forces (in spirit of the internal model principle) has been exploited in several studies, using a variety of state observers. In other words, the discussion and results provided in this section are not specific to the strategy reported in [90], and can also be automatically extended to a larger class of unknown-input strategies for WECs.

With regard to the unknown-input observer design, the so-called *augmented* system (see [236]) can be defined in terms of the following finite-dimensional continuous-time system, described, for $t \in \mathbb{R}^+$, in state-space form, as

$$\begin{aligned}\dot{\Upsilon} &= F_a \Upsilon + \epsilon, \\ v &= Q_a \Upsilon + \zeta,\end{aligned}\quad (6.38)$$

where ϵ and ζ represent the process and measurement (white) noises, with associated covariance matrices Ω_ϵ and \mathfrak{R}_ζ , respectively. The extended matrices, and state-vector, involved in (6.38), are defined as

$$F_a = \begin{bmatrix} F & \Delta^{\text{opt}} L \\ 0 & \mathbb{I}_N \otimes S \end{bmatrix}, \quad Q_a = \begin{bmatrix} Q & 0 \end{bmatrix}, \quad \Upsilon = \begin{bmatrix} \Theta \\ \xi \end{bmatrix}, \quad (6.39)$$

where $\Upsilon(t) \in \mathbb{R}^{2N\nu}$ contains the system and signal generator state-vectors, *i.e.* Θ and ξ , respectively. Following [90], an optimal continuous-time KF observer, can be defined as

$$\dot{\tilde{\Upsilon}} = F_a \tilde{\Upsilon} + \mathfrak{K}(y - Q_a \tilde{\Upsilon}), \quad (6.40)$$

where y represents the output of the WEC array system Σ , and the optimal gain $\mathfrak{K} : \mathbb{R}^+ \rightarrow \mathbb{R}^{N \times N}$, $t \mapsto \mathfrak{K}(t)$, can be computed [241] as,

$$\begin{aligned}\dot{D} &= F_a D + D F_a^\top - D Q_a^\top \mathfrak{R}_\zeta^{-1} Q_a D + \Omega_\epsilon, \\ \mathfrak{K} &= D Q_a^\top \mathfrak{R}^{-1}.\end{aligned}\quad (6.41)$$

Finally, the estimated wave excitation force can be directly computed in terms of the estimated state-vector as

$$\tilde{f}_e = L [0 \ \mathbb{I}_{N\nu}] \tilde{\Upsilon}. \quad (6.42)$$

As can be directly appreciated from Equation (6.39), F_a explicitly includes the dynamic matrix of the signal generator (6.11), which is utilised in the moment-based model reduction method discussed in Section 6.3. This mathematical connection can be exploited to improve the performance of the unknown-input observer substantially,

by a wise selection of the set of interpolation points contained in the set \mathcal{F} . To be precise, one can compute a reduced model by moment-matching for the input-output dynamics of the WEC array, *i.e.* an approximating model $\tilde{\Sigma}_{\mathcal{F}}$, interpolating the same set of frequencies used to describe the internal model of the wave excitation force in the observer defined in (6.40) (*i.e.* the set $\lambda(S)$). Such a practice guarantees that the moment-matching-based model, computed with the strategy presented in Section 6.3, has the *exact* same steady-state response as the target non-parametric model of the WEC array Σ , at the key frequencies utilised to describe the excitation input. This improvement in performance is now discussed both in terms of estimation quality, and computational effort required by the observer, as demonstrated in the remainder of this section.

To illustrate the advantages of using the moment-based model reduction method proposed in this chapter, within the unknown-input estimation problem, a KF observer is designed for the array of CorPower-like devices presented in Figure 6.1, where the spectrum of the matrix S is completely characterised by the sets,

$$\begin{aligned}\mathcal{F}_1^{\text{est}} &= \{0.84\}, \\ \mathcal{F}_2^{\text{est}} &= \{0.84, 1.17\}.\end{aligned}\tag{6.43}$$

Note that $\mathcal{F}_1^{\text{est}} \subset \mathcal{F}_2^{\text{est}}$. The definition of the set $\mathcal{F}_1^{\text{est}}$ is made using explicit knowledge of the stochastic description of the wave excitation input: a key frequency to take into account in the internal model description is the characteristic ‘peak’ (maximum) of the JONSWAP SDF presented in Figure 6.4, *i.e.* $2\pi/7.5 \approx 0.84$ [rad/s]. The second set includes the frequency point 1.17 [rad/s] which, as discussed previously in Section 6.4, characterises the \mathcal{H}_∞ -norm of the WEC array¹⁴. Using the frequency sets defined in equation (6.43), one can compute the moment-based state-space models $\tilde{\Sigma}_{\mathcal{F}_1^{\text{est}}}$ and $\tilde{\Sigma}_{\mathcal{F}_2^{\text{est}}}$ following Procedure 2 (see Section 6.3.1).

Considering these two moment-based models, specifically designed to correlate with the optimal observer of equation (6.40), and the moment-matching models $\tilde{\Sigma}_{\mathcal{F}_1^{\text{sim}}}$ and $\tilde{\Sigma}_{\mathcal{F}_2^{\text{sim}}}$, computed for the WEC array motion simulation case of Section 6.4, a KF is designed, using each of these reduced models. The performance of these different unknown-input observers is assessed in Table 6.2, in terms of the indicators listed in the following.

Remark 6.5.2 The so-called ‘multi-SISO’ approach is also included in Table 6.2, which essentially constitutes a reduced order model of the WEC array Σ described in (6.8), obtained by approximating each individual convolution operator associated with the radiation impulse response mapping k_r (arising due to hy-

14: The reader is referred to [15, 90] for further discussion on the selection of the frequency points to represent stochastic wave excitation forces in spirit of the internal model principle.

hydrodynamic interaction between devices) with a SISO system, *i.e.* in a ‘decoupled’ fashion. This is, indeed, the predominant approach utilised in the wave energy literature, and hence is included in Table 6.2 for the sake of comparison. The strategy used to compute an approximation of each of these convolution terms separately, follows the most-widely used method available in the WEC literature, *i.e.* the frequency-domain parameterisation approach presented in [71, 242] (see also Section 2.6.1.2). The dimension of each approximating model is set to 4, which results in a full state-space description of the input-output dynamics of the WEC array of dimension (order) 72.

- Dim** Dimension (order) of the reduced model describing the WEC array dynamics.
- Dim^e** Dimension (order) of the wave excitation force estimator.
- NRMSE_F** NRMSE of the reduced model approximating the WEC array dynamics computed against the target WEC array frequency response $G(\omega)$, with $\omega \in W$.
- NRMSE_T^e** NRMSE computed (in steady-state) against the target wave excitation force signal, computed from a JONSWAP SDF with $\bar{H}_w \in \{1.5, 2, 3\}$ [m], $\bar{T}_w = 7.5$ [s] and $\gamma = 3.3$ (see Figure 6.4).
- T-Gain** % improvement in *normalised run-time*¹⁵ (*i.e.* the ratio between the time required to compute the estimated wave excitation force, and the length of the simulation itself) with respect to the slowest model (normalised run-time indicated in table between parenthesis).

15: The computations are performed using Matlab®, running on a PC composed of an Intel Xeon CPU E5-1620 processor with 16 GB of RAM. The time is measured using the embedded functions Tic and Toc.

Model	Dim	Dim ^e	NRMSE _F	NRMSE _T ^e	T-Gain
Multi-SISO	72	88	0.76%	4.37%	(1.96×10^{-2})
$\tilde{\Sigma}_{\mathcal{F}_1^{\text{sim}}}$	8	16	4.82%	23.59%	80.16%
$\tilde{\Sigma}_{\mathcal{F}_1^{\text{est}}}$	8	16	31.12%	9.82%	80.16%
$\tilde{\Sigma}_{\mathcal{F}_2^{\text{sim}}}$	16	24	0.44%	4.28%	68.92%
$\tilde{\Sigma}_{\mathcal{F}_2^{\text{est}}}$	16	24	5.02%	2.04%	68.92%

Table 6.2: Estimation results comparison table.

The analysis of Table 6.2 is begun by making an explicit performance comparison between the moment-matching-based models $\tilde{\Sigma}_{\mathcal{F}_1^{\text{sim}}}$ and $\tilde{\Sigma}_{\mathcal{F}_1^{\text{est}}}$, for the unknown-input estimation problem. Note that the dimension (order) of both models is exactly the same, *i.e.* the same number of interpolation points are used to compute both reduced (parametric) representations. Despite sharing the same model complexity, the performance results are significantly different, as discussed in the following.

While $\tilde{\Sigma}_{\mathcal{F}_1^{\text{sim}}}$ provides a much better overall approximation in the frequency-domain (with almost 96% of accuracy) than $\tilde{\Sigma}_{\mathcal{F}_1^{\text{est}}}$, the

performance of the estimator designed using $\tilde{\Sigma}_{\mathcal{F}_1^{\text{sim}}}$ is quite poor, with a NRMSE_T^e of $\approx 24\%$. In contrast, having a frequency-domain NRMSE_F of almost 32%, the KF designed using $\tilde{\Sigma}_{\mathcal{F}_1^{\text{est}}}$ performs substantially better in terms of wave excitation force estimate quality, with less than 10% of estimation error. This can be attributed to the fact that $\tilde{\Sigma}_{\mathcal{F}_1^{\text{est}}}$ has the *exact* same steady-state response as the WEC array, at the frequency points selected to represent the internal model of the wave excitation force embedded in the optimal observer (6.40), where the majority of the spectral content of the input signal is contained (see Figure 6.4).

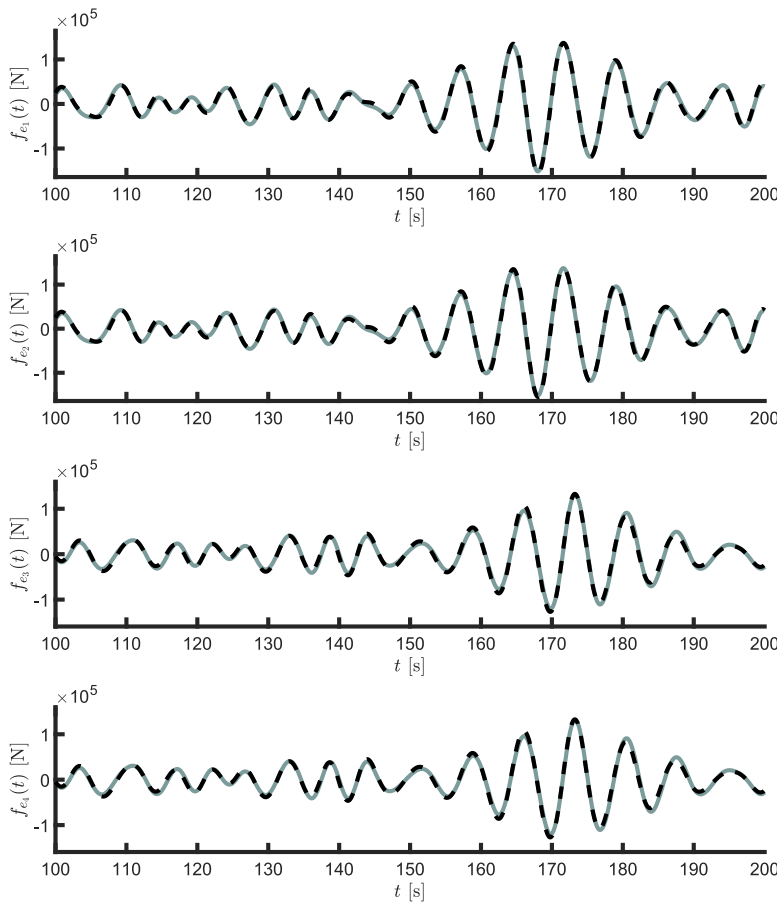


Figure 6.9: Target (dashed) and estimated (solid) wave excitation forces for each device in the WEC array, using a KF designed with the moment-based parametric model $\tilde{\Sigma}_{\mathcal{F}_1^{\text{est}}}$.

Figure 6.9 graphically illustrates the performance of the KF designed using $\tilde{\Sigma}_{\mathcal{F}_1^{\text{est}}}$ for a time-window of 100 [s], where it can be appreciated that both time traces, *i.e.* target (dashed) and estimated (solid) wave excitation force, for each of the four devices composing the analysed WEC array, are qualitatively identical.

Figure 6.10 shows a Bode diagram analogous to that of Figure 6.7, where the frequency-domain description and performance of the parametric models $\tilde{\Sigma}_{\mathcal{F}_1^{\text{sim}}}$ and $\tilde{\Sigma}_{\mathcal{F}_1^{\text{est}}}$ can be explicitly appreciated. Note that, consistent with the results of Table 6.2, the overall frequency-domain fit of $\tilde{\Sigma}_{\mathcal{F}_1^{\text{sim}}}$, for the selected frequency range W , is clearly better than $\tilde{\Sigma}_{\mathcal{F}_1^{\text{est}}}$, though $\tilde{\Sigma}_{\mathcal{F}_1^{\text{est}}}$ interpolates in a key

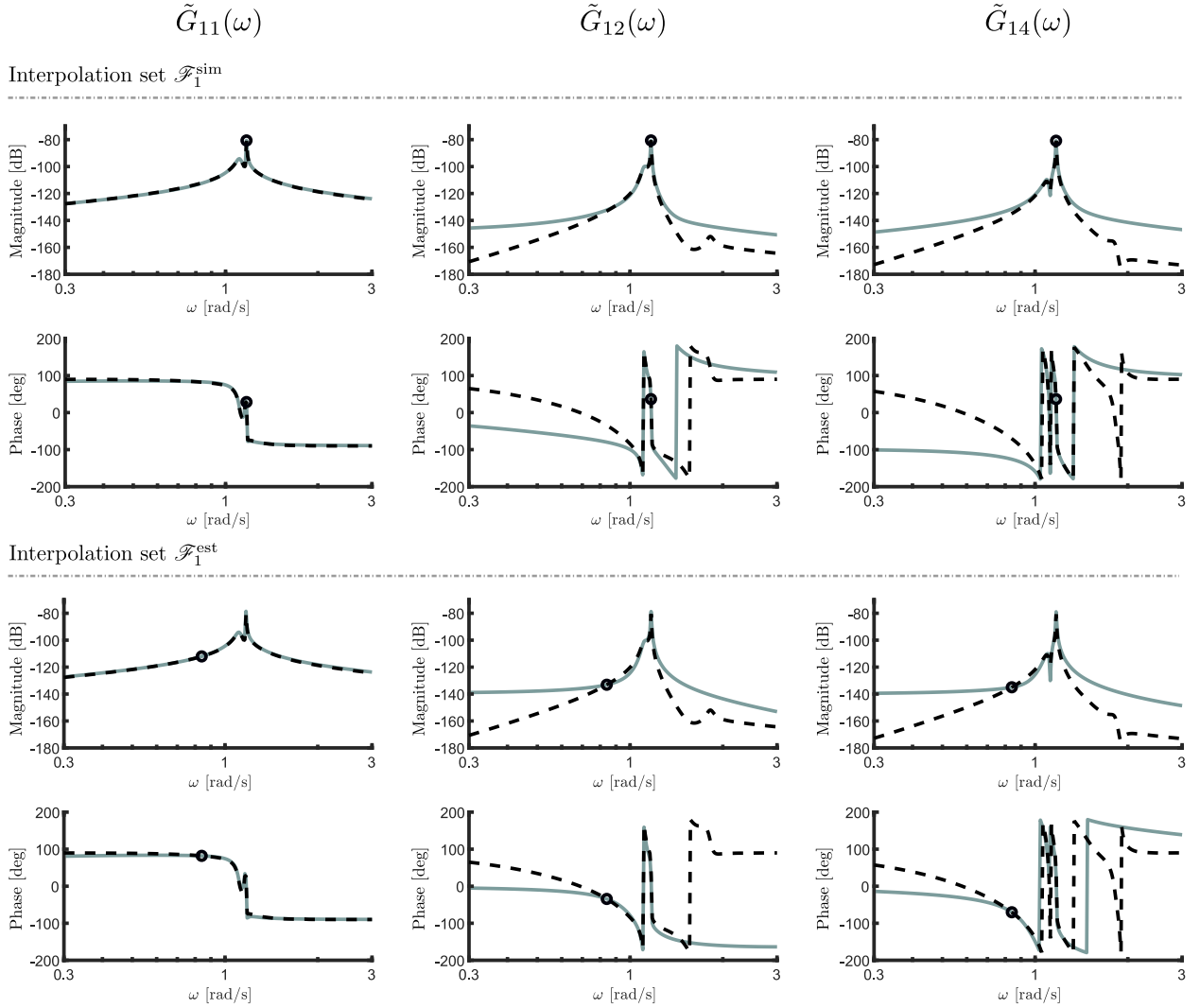


Figure 6.10: Bode plots for the elements $\{1, 1\}$, $\{1, 2\}$ and $\{1, 4\}$, for both the target response $G(\omega)$ (dashed), and the approximating frequency response mappings (solid) $\tilde{G}_{\mathcal{F}_1^{\text{sim}}}$ (top) and $\tilde{G}_{\mathcal{F}_1^{\text{est}}}$ (bottom). The interpolation points are denoted by an empty black circle.

frequency point for the unknown-input estimation problem, thus significantly improving the performance of the corresponding KF.

It is noteworthy to highlight that exploiting this inherent relationship between model reduction by moment-matching and the internal model principle, considered for the estimation of the wave excitation force, using a single interpolation point $\mathcal{F}_1^{\text{est}}$, provides similar estimation accuracy results to the case where the ‘multi-SISO’ approach is considered, but with $\approx 81\%$ improvement in computational requirements¹⁶. In other words, the estimator using the moment-based model $\tilde{\Sigma}_{\mathcal{F}_1^{\text{est}}}$ computes 8 times faster, for the same degree of wave excitation force estimation accuracy, and is therefore especially suited for real-time applications.

Finally, Table 6.2 also provides results for the KF observers designed using the moment-based models $\tilde{\Sigma}_{\mathcal{F}_2^{\text{sim}}}$ and $\tilde{\Sigma}_{\mathcal{F}_2^{\text{est}}}$, where the

16: As defined in Table 6.2.

performance (frequency-domain fitting and wave excitation force estimation quality) is subsequently improved, for both cases. Note that the situation described in the previous paragraph is repeated, *i.e.* the KF designed using $\tilde{\Sigma}_{\mathcal{F}_2}^{\text{est}}$ provides better estimation performance due to the particular selection of the interpolation points (which are those carefully selected to describe the internal model associated with the wave excitation input in (6.40)).

6.6 Radiation case study: a multi-DoF CorPower-like device

To illustrate the performance of the MIMO moment-based model reduction approach for the radiation dynamics, proposed in Section 6.3.2, a single CorPower-like device (as in Figure 6.2) is considered, but in a multi-DoF configuration. In particular, *surge*, *heave*, and *pitch* are considered in the following, referred to as modes 1, 2 and 3, respectively. The corresponding hydrodynamic parameters $B_r(\omega)$ and $A_r(\omega)$ can be appreciated in Figure 6.11. Note that the elements $\{1, 2\}$, $\{2, 1\}$, $\{2, 3\}$, $\{3, 2\}$ of the matrices $B_r(\omega)$ and $A_r(\omega)$ are not shown in Figure 6.11, given that there is no interaction due to radiation forces between these particular modes of motions, *i.e.* they are exactly zero for all $\omega \in \mathbb{R}^+$.

From now on, the notation $K_{r_{ij}}(\omega)$ is used for the ij -element of the matrix $K_r(\omega)$, characterising the radiation system Σ_r associated with the CorPower-like device considered in this section. More precisely, $K_{r_{ij}} : \mathbb{R} \rightarrow \mathbb{C}$ is the frequency response mapping between the output i (radiation force exerted on the i -th mode) and the input j (velocity of the j -th mode).

The computation of a moment-based approximation $\tilde{\Sigma}_{r, \mathcal{F}}$ for the radiation subsystem Σ_r , is now specifically addressed, based on knowledge of the target frequency response $K_r(\omega)$, and using the procedure described in Section 6.3.2.

Analogously to the input-output dynamics case of Section 6.4, and by analysing the singular values plot associated with the radiation frequency-domain response $K_r(\omega)$, in Figure 6.12, the following interpolation sets \mathcal{F} are considered:

- ▶ $\mathcal{F}_1 = \{0, 1.7\}$,
- ▶ $\mathcal{F}_2 = \{0, 0.8, 1.7\}$,

where, naturally, $\mathcal{F}_1 \subset \mathcal{F}_2$. Note that $\omega \approx 1.7$ [rad/s] corresponds with the frequency characterising the \mathcal{H}_∞ -norm of the system. The set \mathcal{F}_2 extends \mathcal{F}_1 by adding a low-frequency component in the interpolation scheme. The frequency range W , selected to perform

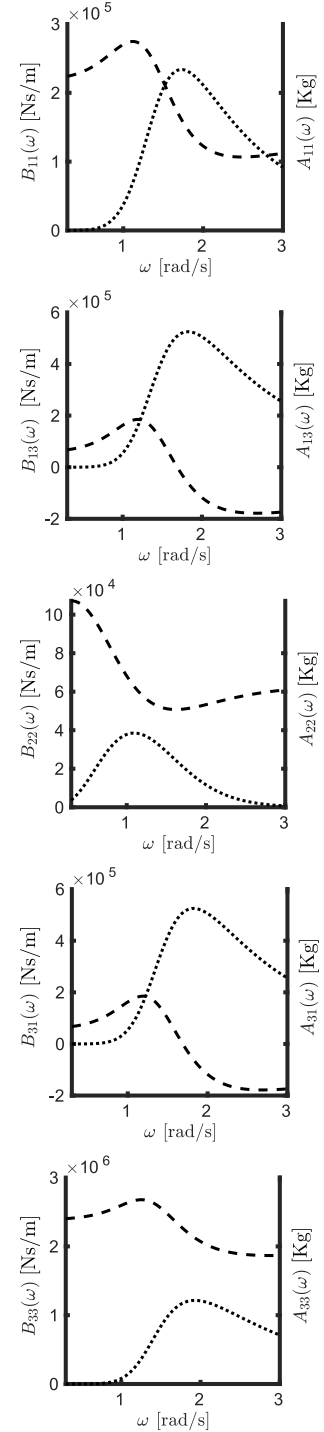


Figure 6.11: Hydrodynamic parameters $B_r(\omega)$ (dotted) and $A_r(\omega)$ (dashed) for the multi-DoF CorPower-like device considered herein.

the model reduction process described in Procedure 2, is chosen as in the input-output dynamics case, *i.e.* $W = [0.3, 3]$ [rad/s].

Given that heave (mode 2) is the main DoF of this WEC (in which the PTO is active), Figure 6.13 presents the Bode diagram for the target response $K_{r22}(\omega)$ (dashed), and the corresponding frequency-response associated with the moment-based radiation reduced models (solid) $\tilde{\Sigma}_{r\mathcal{F}_1}$ (a) and $\tilde{\Sigma}_{r\mathcal{F}_2}$ (b). The interpolation points for each model are denoted by an empty black circle. As expected, the approximating reduced systems have the *exact* same frequency response as the target model for each corresponding element of the sets \mathcal{F}_1 and \mathcal{F}_2 , respectively. Though using the set \mathcal{F}_1 as interpolation set provides quite accurate results, the decrease in the approximation error from system $\tilde{\Sigma}_{r\mathcal{F}_1}$ to $\tilde{\Sigma}_{r\mathcal{F}_2}$ is also evident.

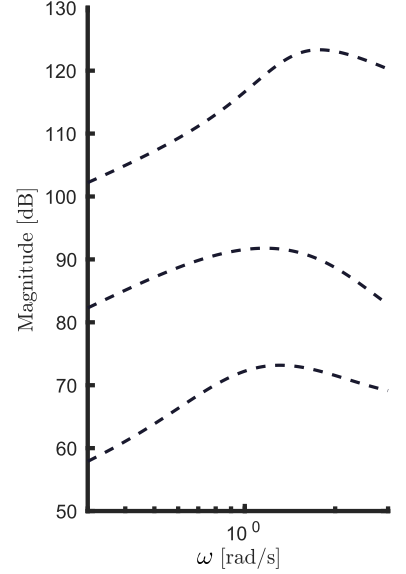
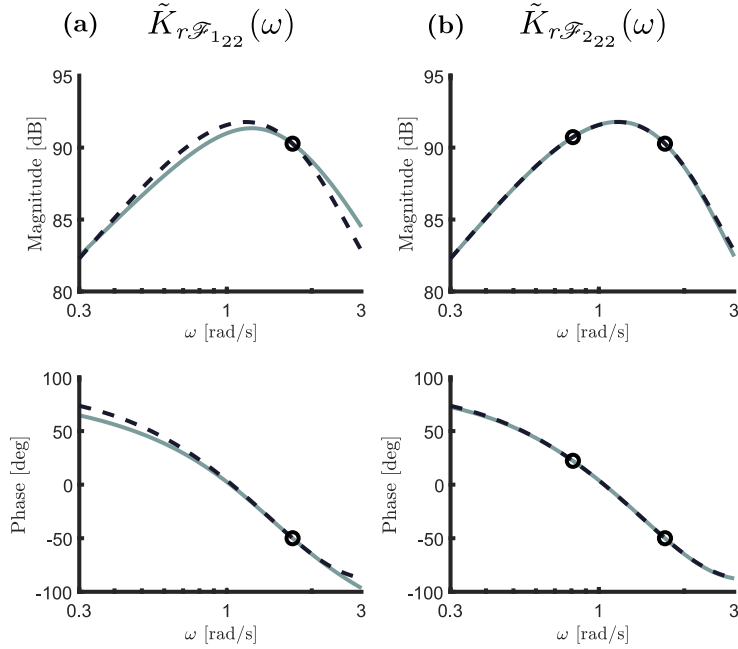


Figure 6.12: Singular values plot for the radiation system $K_r(\omega)$.

Figure 6.13: Bode diagram for $K_{r22}(\omega)$ (dashed), and $\tilde{K}_{r\mathcal{F}_1}(\omega)$ (solid), for both reduced models $\tilde{\Sigma}_{r\mathcal{F}_1}$ (a) and $\tilde{\Sigma}_{r\mathcal{F}_2}$ (b). The interpolation points are denoted by an empty black circle

As a conclusive graphical illustration of the frequency-domain performance for the models computed via the proposed moment-based strategy, Figure 6.14 presents the singular value plot for the target response $K_r(\omega)$, and the approximated mapping $\tilde{K}_{r\mathcal{F}}(\omega)$, both for $\tilde{\Sigma}_{r\mathcal{F}_1}$ (a) and $\tilde{\Sigma}_{r\mathcal{F}_2}$ (b). It can be readily appreciated that both models can effectively approximate the target singular values in every principal direction, *i.e.* the target MIMO gain, with a natural increase in accuracy when using the interpolation set \mathcal{F}_2 instead of \mathcal{F}_1 .

Similarly to the input-output dynamics case of Section 6.4, and aiming to further assess the performance of the proposed moment-based strategy for the radiation system, Table 6.3 offers a numerical appraisal of each of the moment-matching-based reduced models in terms of the following parameters:

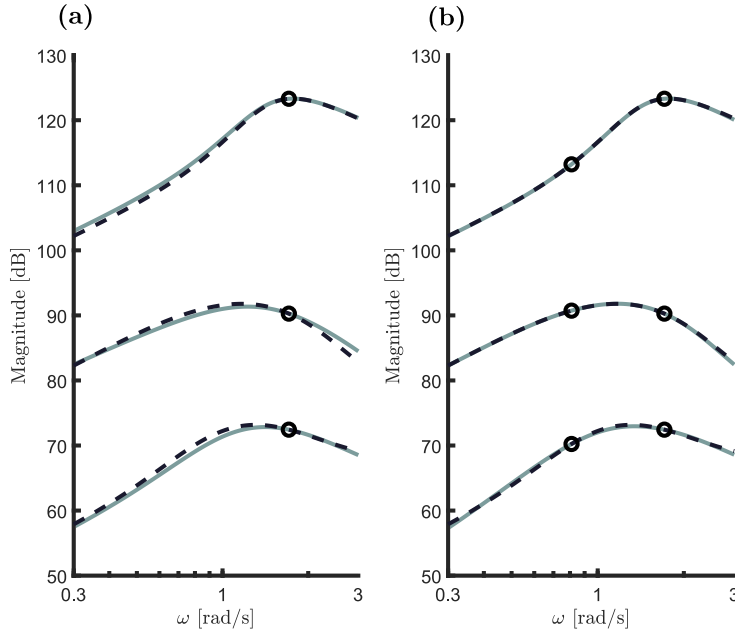


Figure 6.14: Singular value plot for $K_r(\omega)$ (dashed) and $\tilde{K}_r(\omega)$ (solid) for $\tilde{K}_{r\mathcal{F}_1}(\omega)$ (a) and $\tilde{K}_{r\mathcal{F}_2}(\omega)$ (b). The interpolation points are denoted by an empty black circle.

Dim Dimension (order) of the parametric model.

NRMSE_F NRMSE computed against the target radiation frequency response $\forall \omega \in W$.

NRMSE_T NRMSE computed (in steady-state) against the target steady-state radiation system response using inputs generated with frequency content inside the set W .

Model	Dim	NRMSE _F	NRMSE _T
$\tilde{\Sigma}_{r\mathcal{F}_1}$	6	6.06%	8.04%
$\tilde{\Sigma}_{r\mathcal{F}_2}$	12	1.09%	1.06%

Table 6.3: Numerical comparison table for the radiation dynamics case.

It is worth highlighting that, as can be appreciated in Table 6.3, the approach proposed here provides accurate results even with a single interpolation point, with only $\approx 4\%$ of error in both the frequency- and time-domain, and with an intrinsic decrease in computational complexity, given the low dimension (order) of the resulting model.

6.6.1 On the properties of radiation models

Analogously to the SISO case presented in Chapter 5, a discussion on the fundamental physical properties of radiation effects, introduced in Section 2.4, is presented in this section, for the MIMO case. These properties, for any approximating (reduced) model $\tilde{\Sigma}_r$, are briefly recalled below, for convenience¹⁷.

- ▶ **Property 1:** $\tilde{\Sigma}_r$ is BIBO stable.
- ▶ **Property 2:** The complex (transfer) function $\tilde{K}_r(s)$ is positive-real.
- ▶ **Property 3:** $\tilde{K}_r(s)$ has *transmission zeros*¹⁸ at $s = 0$.
- ▶ **Property 4:** $\tilde{\Sigma}_r$ is strictly proper.

An assessment on these properties, for the moment-based computed models $\tilde{\Sigma}_{r\mathcal{F}_1}$ and $\tilde{\Sigma}_{r\mathcal{F}_2}$, is now given in the following.

17: The reader is referred to Sections 2.3.2.2 and 2.4 for a comprehensive discussion on these properties.

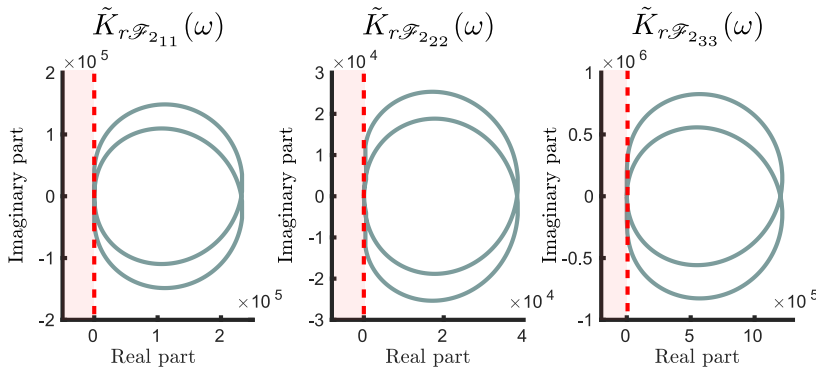
18: The name *transmission zero* is originated within the electronic engineering community, referring to a complex number at which the transfer function of an electrical network has zero transmission [86]. In the control community, this set of zeros are often called *invariant zeros*, i.e. they define a particular invariant set associated with a (minimal) state-space system. The reader is referred to, for instance, [75], for further discussion on this topic.

Property 1

The process proposed to compute the optimal input matrix Δ^{opt} , *i.e.* Procedure 2 in Section 6.3, always guarantees internal stability of the family of reduced models by moment-matching (see Remark 6.3.3). By way of example, Figure 6.15 shows the pole-zero map for system $\tilde{\Sigma}_{r\mathcal{F}_1}$ computed, in Section 6.6, for the multi-DoF CorPower-like device. It can be appreciated that all the poles are contained in the open left-half of the complex plane, *i.e.* $\tilde{\Sigma}_{r\mathcal{F}_1}$ is BIBO stable.

Property 2

Positive-realness of \tilde{K}_r , for this linear case, is directly related to the property of passivity (see Section 2.4). Similarly as in the SISO case of Chapter 5, if the target frequency-response data $K_r(\omega)$ effectively corresponds with a passive model, the reduced models obtained with the proposed moment-based strategy are virtually always inherently passive. By way of example, Figure 6.16 depicts the Nyquist plot for the diagonal elements of $\tilde{K}_{r\mathcal{F}}(\omega)$ for $\tilde{\Sigma}_{r\mathcal{F}_2}$, where it can be appreciated that $\Re\{\tilde{K}_{r\mathcal{F}ii}(\omega)\} > 0$, for all $\omega \in \mathbb{R}/0$ and $i \in \mathbb{N}_3$ and, hence, $\tilde{\Sigma}_{r\mathcal{F}_2}$ is passive.



Properties 3 & 4

Property 3 manifests itself explicitly in the example case of Figure 6.15, where there is clearly a zero at $s = 0$.

With respect to Property 4, the family of models defined by Procedure 2 (see Section 6.3.2) is strictly proper by construction: the feed-through matrix of $\tilde{\Sigma}_{r\mathcal{F}}$ is always zero, independently on the selection of the interpolation set \mathcal{F} involved.

Remark 6.6.1 (On the enforcement of passivity and zero dynamics for the MIMO radiation case) If required by the application, passivity and zero dynamics can be enforced by using an anal-

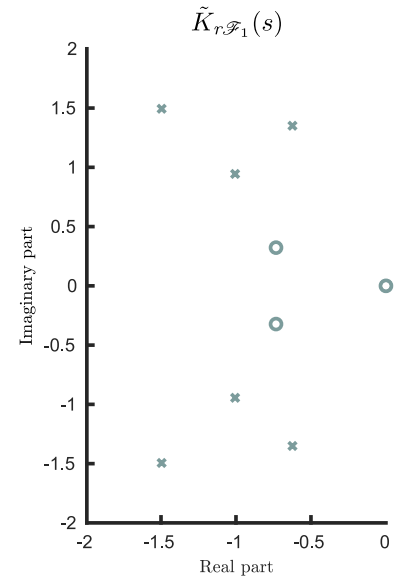


Figure 6.15: Pole-zero map for the approximating model $\tilde{\Sigma}_{r\mathcal{F}_1}$.

Figure 6.16: Nyquist plot (diagonal elements) of $\tilde{K}_{r\mathcal{F}}(\omega)$ for $\tilde{\Sigma}_{r\mathcal{F}_2}$.

ogous procedure to that described in Sections 5.4.1 and 5.4.2, for the SISO case, respectively. In particular, note that for the zero dynamics case, one can re-define the dynamic matrix S in equation (6.12) to include $s = 0$ as an interpolation point, as follows:

$$S_0 = 0 \oplus S, \quad (6.44)$$

where the matrix $S_0 \in \mathbb{R}^{\nu+1 \times \nu+1}$. The moment-domain equivalent for the radiation system, for a signal generator defined by the (observable) pair $(\mathbb{I}_N \otimes S_0, L_0)$, with $L_0 \in \mathbb{R}^{N \times N(\nu+1)}$, is then straightforwardly given by,

$$\underline{Y}_{r_0} = \sum_{i=1}^N \sum_{j=1}^N e_{ij}^N L_0 \left(\mathbb{I}_N \otimes \mathcal{R}_{0ij} \right), \quad (6.45)$$

where each matrix $\mathcal{R}_{0ij} \in \mathbb{R}^{\nu+1 \times \nu+1}$ follows the expression,

$$\mathcal{R}_{0ij} = K_{r_{ij}}(0) \oplus \mathcal{R}_{ij} = 0 \oplus \mathcal{R}_{ij}, \quad (6.46)$$

with $K_{r_{ij}} : \mathbb{R} \rightarrow \mathbb{C}$, and \mathcal{R}_{ij} as in Proposition 6.2.1, for all $\{i, j\} \subset \mathbb{N}_N$. Note that the relation $K_r(0) = 0$ follows directly from Section 2.3.2.2. Then, Procedure 2, described in Section 6.3.2, can be carried out in an analogous form, by simply replacing \underline{Y}_r by \underline{Y}_{r_0} , and adjusting the dimensions (order) for the computation of the triple of matrices $(F, Q, \Delta^{\text{opt}})$ accordingly.

6.7 Conclusions

This chapter presents a MIMO moment-based model reduction framework for wave energy applications. In particular, non-parametric models associated with both multi-DoF WECs, and arrays of wave energy devices (referred to as N -th order WEC systems/devices), are considered within this model reduction formulation.

Analogously to the SISO case of Chapter 5, this MIMO moment-based framework allows for the computation of state-space representations characterising either the input-output, or the radiation force dynamics, for a generic type of N -th order WEC system. These moment-based reduced models *exactly* match the target steady-state behavior at a set of user-selected frequencies and allow for the preservation of the relevant dynamic characteristics of the device.

Moreover, for the particular case of the radiation dynamics, this chapter shows that this moment-based model reduction framework is effectively able to retain important physical properties, such as input-output stability, passivity, and zero dynamics, agreeing with the underlying physics that characterise such a system.

In addition, an intrinsic mathematical relationship between the unknown-input wave excitation force estimation problem, and the moment-based strategy presented in both Chapters 5 and 6, is shown and exploited by a sensible selection of the set of interpolation points, in synergy with the internal model principle utilised to estimate f_e .

For the input-output dynamics case, both simulation and wave excitation force estimation performance are assessed, in terms of a case study, involving an array of state-of-the-art CorPower-like devices, constrained to oscillate in heave (translational motion). For the radiation dynamics case, a multi-DoF CorPower-like device is considered, assumed to oscillate in three different modes of motion, *i.e.* surge, heave and pitch. In both model reduction scenarios, *i.e.* input-output and radiation force dynamics, the performance of the strategy is demonstrated and analysed from both a time- and a frequency-domain perspective. In the particular case of wave excitation force estimation, the synergy between moments and the unknown-input observer design allows for the computation of models tailored for a particular sea state, with relatively mild computational requirements, hence providing parametric representations that are especially suited to the design of real-time energy-maximisation strategies.

Reduced models for nonlinear WECs

7

Contents of this chapter

7.1	Nonlinear moment-based WEC formulation for model reduction	148
7.2	On the approximation of π	152
7.2.1	A Galerkin-like approach	155
7.3	Practical aspects and considerations	156
7.3.1	Projection of the residual mapping	156
7.3.2	Extension to multiple trajectories	157
7.3.3	Modifications to the mapping Ω^k	158
7.3.4	On the eigenvalues of the reduced model	159
7.4	Extension to MIMO WEC systems	160
7.5	WEC systems under regular wave excitation	162
7.5.1	Deterministic regular excitation	164
7.5.2	Stochastic regular excitation	166
7.6	WEC systems under irregular wave excitation	168
7.6.1	On the definition of the signal generator	168
7.6.2	On the definition of the set of training trajectories	169
7.6.3	Numerical study	170
7.7	Conclusions	175

Following the hydrodynamic modelling basics presented in Chapter 2, recall, from Section 2.4, that the equation of motion for a WEC, under the assumptions of potential flow theory (see Section 2.3.1), can be expressed in terms of the so-called *extended Cummins'* equation. This equation is recalled below, for the SISO case, for convenience:

$$\Sigma : \begin{cases} \ddot{z} = \mathcal{M}(-k_r * \dot{z} - s_h z + f_e + f_{nl}), \\ y = \dot{z}, \end{cases} \quad (7.1)$$

where $z : \mathbb{R}^+ \rightarrow \mathbb{R}$ is the displacement, $k_r : \mathbb{R}^+ \rightarrow \mathbb{R}$, $k_r \in L^2(\mathbb{R})$, the radiation force impulse response function, $f_e : \mathbb{R}^+ \rightarrow \mathbb{R}$, the wave excitation force, and $\mathcal{M} \in \mathbb{R}_{>0}$ is the inverse of the generalised mass matrix of the device. In contrast to the cases discussed in Chapters 5 and 6, equation (7.1) incorporates nonlinear behaviour: the mapping $f_{nl} : \mathbb{R}^+ \rightarrow \mathbb{R}$, $t \mapsto f_{nl}(t)$ represents potential nonlinear effects, which give rise to the so-called nonlinear extensions of Cummins' equation, described in Section 2.5.

Remark 7.0.1 A SISO WEC system is considered at the beginning of this chapter, aiming to simplify the notation utilised, particularly throughout the theoretical propositions posed in both Sections 7.1 and 7.2. Nevertheless, note that a specific section is dedicated to the extension of the proposed model reduction framework for

nonlinear MIMO WECs, *i.e.* Section 7.4.

The equation of motion describing system Σ is not only non-parametric, but can also present complex nonlinear effects via the mapping f_{nl} , which can potentially render control and/or state-estimation strategies unsuitable for realistic applications: There is a limit for both the analytical complexity for which an energy-maximising controller can effectively guarantee existence of solutions, and the underlying computational complexity that can be handled in real-time. The latter is especially true for the case of WEC arrays, where the ‘number’ of nonlinear effects, involved in the definition of the equation of motion, naturally increases when considering several devices.

Remark 7.0.2 If nonlinear effects are considered in control/state-estimation for WEC applications, only the issue, regarding the non-parametric nature of Σ in (7.1), is commonly tackled in the literature by computing an approximating model for the *linear* radiation dynamics¹, and simply accommodating the nonlinear effects in the corresponding augmented system (see equation (2.22)). In other words, there is no nonlinear model reduction process taking place, but only the linear system, fully characterised by the radiation impulse response k_r , is approximated with a parametric form, hence avoiding the computational complexity and representational drawback of the associated convolution operator.

1: Assuming that the non-parametric nature of Σ is only due to linear radiation dynamics. This is not always necessarily the case, since f_{nl} can be potentially non-parametric.

As discussed in² Chapter 2, and to the best of the author’s knowledge, there is currently no literature on systematic nonlinear model reduction methods proposed (or even applied) within the scope of WEC technology, even though this would represent a valuable tool for a variety of applications, including, but not limited to, state-estimation and energy-maximising optimal control of WECs.

2: See, in particular, the state-of-the-art of model reduction techniques, detailed in Section 2.6.

Though the nonlinear moment-based framework for model reduction, recalled in Section 4.2, can present a valuable tool for the nonlinear WEC case (given the inherent preservation of steady-state response characteristics), the computation of a reduced model by moment-matching relies on the availability of a closed-form solution of the nonlinear partial differential equation (4.8), which fully characterises the corresponding *moment*. Although one can explicitly provide conditions for existence and uniqueness of such a solution, an analytic closed-form (if it exists) is virtually impossible to compute. In other words, without a suitable approximation framework, the theory recalled in Section 4.2 for nonlinear systems is far from having any practical value for this WEC case.

In the light of this, this chapter presents a moment-matching model reduction framework for the nonlinear and non-parametric WEC

equation (7.1), tackling each of the following aspects. Firstly, and similar to the linear cases discussed in Chapters 5 and 6, a moment-based formulation for the WEC is provided in Section 7.1, where the existence and uniqueness of the associated moment is discussed and ensured for the case of wave energy systems. Secondly, an approximation framework for the computation of the nonlinear moment is proposed in Section 7.2, based on the family of mean weighted residual methods³. Practical aspects and considerations behind this approximation framework are discussed in Section 7.3, while the extension of the nonlinear model reduction by moment-matching technique to MIMO WEC systems is posed in Section 7.4. Sections 7.5 and 7.6 discuss the case of model reduction for WEC systems under regular, and irregular, wave excitation inputs, respectively. Finally, the main conclusions of this chapter are encompassed in Section 7.7.

3: Note that the underlying characteristics of these methods is discussed, in this thesis, in Section 3.4.1.2.

7.1 Nonlinear moment-based WEC formulation for model reduction

Similarly to both Chapters 5 and 6, the nonlinear moment-based theory, recalled and discussed in Chapter 4, directly depends on the availability of a state-space representation of the system to be reduced, which is not the case for the non-parametric equation described by system Σ in (7.1). In the light of this, the following equivalent representation is proposed:

$$\Sigma : \begin{cases} \dot{w} = f_{\Sigma}(w, f_e) = Aw + B(f_e - k_r * Cw) + f(w), \\ y = h_{\Sigma}(w) = Cw, \end{cases} \quad (7.2)$$

for $t \in \mathbb{R}^+$, where $w(t) = [z(t) \quad \dot{z}(t)]^T \in \mathbb{R}^2$ contains the displacement and velocity corresponding with system Σ , and the (constant) matrices $A \in \mathbb{R}^{2 \times 2}$, $B \in \mathbb{R}^2$ and $C^T \in \mathbb{R}^2$ are defined as

$$A = \begin{bmatrix} 0 & 1 \\ -\mathcal{M}s_h & 0 \end{bmatrix}, \quad B = \begin{bmatrix} 0 \\ \mathcal{M} \end{bmatrix}, \quad C = \begin{bmatrix} 0 \\ 1 \end{bmatrix}^T. \quad (7.3)$$

The nonlinear mapping $f : \mathbb{R}^2 \rightarrow \mathbb{R}^2$ is given by

$$f(w) = \begin{bmatrix} 0 \\ \mathcal{M}f_{nl}(w) \end{bmatrix} = Bf_{nl}(w). \quad (7.4)$$

Remark 7.1.1 In line with the nonlinear hydrodynamic effects described in Section 2.5 (which are indeed the most utilised nonlinear effects in WEC control/estimation applications), it is assumed

that the mapping f_{nl} depends only on w , *i.e.* the displacement and velocity of the WEC system involved. Nevertheless note that, if required by a particular application, a more general class of nonlinear effects can be considered, such as, for instance, non-ideal PTO dynamics⁴.

Within the moment-based formulation of Chapter 4, the mapping corresponding with the external input f_e is written in terms of an autonomous single-output signal generator (analogously⁵ to the case of equation (4.3)), *i.e.* the set of equations

$$\begin{aligned}\dot{\xi} &= S\xi, \\ f_e &= L\xi,\end{aligned}\tag{7.5}$$

for $t \in \mathbb{R}^+$, with $\xi(t) \in \mathbb{R}^\nu$, $S \in \mathbb{R}^{\nu \times \nu}$ and $L^\top \in \mathbb{R}^\nu$. The set of standing Assumptions, 4.1.1 and 4.1.2, are ensured as follows.

In contrast to the linear model reduction cases discussed in Chapters 5 and 6, Assumption 4.1.2, which concerns the definition of the spectrum of the matrix S , is addressed by recalling⁶ that ocean waves are commonly generated as a finite sum of harmonics of a so-called *fundamental frequency* ω_0 . To be precise, let $\mathcal{F} = \{h_p \omega_0\}_{p=1}^f \subset \mathbb{R}^+$, where $\mathcal{H} = \{h_p\}_{p=1}^f \subset \mathbb{N}_{\geq 1}$, with $h_1 < \dots < h_f$, be a set composed of a finite number of harmonics of the fundamental frequency ω_0 . In particular, the matrix S is defined in a block-diagonal form as

$$S = \bigoplus_{p=1}^f \begin{bmatrix} 0 & h_p \omega_0 \\ -h_p \omega_0 & 0 \end{bmatrix},\tag{7.6}$$

where $\nu = 2f$, $f \in \mathbb{N}_{\geq 1}$, and the spectrum of S is given by $\lambda(S) = (j\mathcal{F}) \cup (-j\mathcal{F}) \subset \mathbb{C}^0$, so that Assumption 4.1.2 clearly holds.

Unlike the linear moment-based formulation presented in Chapters 5 and 6, the definition of a nonlinear moment, presented in Section 4.2.2, inherently depends on the initial condition $\xi(0)$ of the signal generator⁷ defined in (7.6). In the light of this, Assumption 4.1.1 is ensured as follows: From now, the output vector L is given by a Hadamard identity on the space $\mathbb{R}^{1 \times \nu}$, *i.e.*, $L^\top = \mathbf{1}_\nu$, so that the minimality of the triple $(\mathbf{1}_\nu^\top, S, \xi(0))$ holds as long as the pair $(S, \xi(0))$ is excitable.

Remark 7.1.2 (On the definition of $\xi(0)$) Let $\xi(0) = \sum_{p=1}^f e_p^f \otimes [\alpha_p \ \beta_p]^\top$, where the set of coefficients $\{\alpha_p, \beta_p\}_{p=1}^f \subset \mathbb{R}$. Then,

4: The reader is referred to Section 3.4.2.1 for further detail on nonlinear mappings considered within the WEC control literature, including non-ideal PTO dynamics.

5: See also Section 5.1.

6: See Section 2.1.2 and, in particular, Remark 2.1.3.

7: As a matter of fact, note that the computation of the corresponding nonlinear moment is locally defined in a neighborhood Ξ of $\xi = 0$.

the vector ξ can be conveniently expanded as

$$\xi(t) = e^{St}\xi(0) = \sum_{p=1}^f e_p^f \otimes \begin{bmatrix} p\xi^+(t) \\ p\xi^-(t) \end{bmatrix}, \quad (7.7)$$

where the mappings $p\xi$ are defined as

$$\begin{aligned} p\xi^+ : \mathbb{R}^+ &\rightarrow \mathbb{R}, & t &\mapsto \alpha_p \cos(h_p \omega_0 t) + \beta_p \sin(h_p \omega_0 t), \\ p\xi^- : \mathbb{R}^+ &\rightarrow \mathbb{R}, & t &\mapsto \beta_p \cos(h_p \omega_0 t) - \alpha_p \sin(h_p \omega_0 t). \end{aligned} \quad (7.8)$$

Remark 7.1.3 Note that the excitability condition on the pair $(S, \xi(0))$ holds as long as α_p and β_p are not simultaneously zero, for all $p \in \mathbb{N}_f$.

Remark 7.1.4 Consider the sets of functions $\mathcal{X}_\xi^f = \{p\xi^+, p\xi^-\}_{p=1}^f$ and $\mathcal{X}_0^f = \{\cos(h_p \omega_0 t), \sin(h_p \omega_0 t)\}_{p=1}^f$. Note that, given the excitability condition on the pair $(S, \xi(0))$, it is straightforward to check that $\text{span}\{\mathcal{X}_\xi^f\} = \text{span}\{\mathcal{X}_0^f\}$. As a consequence, the input f_e is always T -periodic, where $T = 2\pi/\omega_0 \in \mathbb{R}^+$ is the *fundamental period* of f_e .

Without any loss of generality, the following standard assumption on the nonlinear mapping f is posed to later prove existence and uniqueness of the nonlinear moment of system (7.2) at the signal generator (S, L) .

Assumption 7.1.1 The mapping $f : \mathbb{R}^2 \rightarrow \mathbb{R}^2$ is such that

$$f(0) = 0, \quad \left. \frac{\partial f(w)}{\partial w} \right|_{w=0} = 0. \quad (7.9)$$

Note that this assumption is without loss of generality, since the matrices in (7.2), and the mapping f , can always be redefined to satisfy it⁸.

Finally, an assumption on the stability in the first approximation of system (7.2), is introduced.

Assumption 7.1.2 The zero equilibrium of system

$$\dot{w} = Aw - B(k_r * Cw), \quad (7.10)$$

is asymptotically stable.

As discussed in Section 2.4, including also several studies, such as [53, 123], the linear equation of motion (7.10) is asymptotically stable for any meaningful values of the involved parameters (and

8: This claim, which directly relates to Jacobian analysis, is considered standard in nonlinear dynamics. Further detail can be found in, for instance, [22, Chapter 8].

impulse response function k_r). Thus, this assumption is, in practice, also without loss of generality.

Proposition 7.1.1 *Suppose the triple $(L, S, \xi(0))$ is minimal, and Assumption 7.1.1 and 7.1.2 hold. Then, there exists a unique mapping π , locally defined in a neighborhood Ξ of $\xi = 0$, which solves the partial differential equation*

$$\frac{\partial \pi(\xi)}{\partial \xi} S \xi = f_{\Sigma}(\pi(\xi), L \xi), \quad (7.11)$$

and the moment of system (7.2) at the signal generator (S, L) , i.e. the mapping⁹ $h_{\Sigma} \circ \pi$, computed along a particular trajectory $\xi(t)$, coincides with the well-defined steady-state output response of such an interconnected system, i.e. $y_{ss}(t) = h_{\Sigma}(\pi(\xi(t)))$.

9: See Definition 4.1.3 for further detail.

Proof. Let $L^T = \mathbf{1}_{\nu}$ and let the initial condition $\xi(0)$ be as defined in Remark 7.1.3. Then, it is straightforward to check that minimality of the triple $(L, S, \xi(0))$ holds. Moreover, note that the signal generator defined in equation (7.5) is always such that $\lambda(S) \subset \mathbb{C}^0$ with simple eigenvalues, in line with Assumption 4.1.2. Therefore, Proposition 7.1.1 automatically holds as long as the zero equilibrium of system $\dot{w} = f_{\Sigma}(w, 0)$ is locally exponentially stable (see Lemma 4.1.2). Since this is the case by Assumption 7.1.2, the proof is concluded. \square

Remark 7.1.5 Under the assumptions of Proposition 7.1.1, the moment of system Σ , defined in (7.2), at the signal generator (S, L) , defined in (7.5), can be computed as $h_{\Sigma} \circ \pi$, with π the solution of equation (7.11).

In slightly different words, Proposition 7.1.1, via Remark 7.1.5, guarantees that the steady-state response of system (7.2), driven by (7.5), can be effectively computed using the corresponding moment at (S, L) . In particular, and following the result of Lemma 4.2.2, a family of reduced models achieving moment-matching at (S, L) of order (dimension) $\nu = 2f$, for the WEC system defined in equation (7.1) (alternatively (7.2)), can be written in terms of the mapping $h_{\Sigma} \circ \pi$, with π the solution of (7.11), as

$$\begin{aligned} \dot{\Theta} &= (S - \Delta L)\Theta + \Delta f_e, \\ \tilde{y} &= h_{\Sigma}(\pi(\Theta)) = C\pi(\Theta), \end{aligned} \quad (7.12)$$

with $\Delta \in \mathbb{R}^{\nu}$ a free (design) parameter.

Remark 7.1.6 If the mapping π is effectively known, the family of models (7.12) *exactly* matches the steady-state response of the target nonlinear WEC system Σ at the signal generator (S, L) .

Remark 7.1.7 The family of models defined in (7.12) is input-to-state *linear*, and any nonlinear effects are (statically) present in the output mapping $h_\Sigma \circ \pi$ (i.e. it is described by a Wiener model¹⁰). Note that, similarly to the linear case presented in Chapters 5 and 6, the set $\lambda(S - \Delta L)$ can be assigned arbitrarily, as a consequence of the observability of the pair (S, L) .

Remark 7.1.8 Unlike the nonlinear system Σ (7.1), which is effectively non-parametric, the family of systems achieving moment-matching at (S, L) is in state-space form. In other words, this model reduction process not only reduces complexity, but inherently computes a parametric form for the WEC system, in a single ‘step’.

10: Further detail on Wiener models, including origin and applications in nonlinear system identification, can be found in [243].

Though the family of models (7.12) provides a strong result to tackle the nonlinear model reduction problem for WECs, there is clearly an intrinsic downside to its definition: Even if the existence and uniqueness of π (solution of (7.11)) are guaranteed by the result of Proposition 7.1.1, it is virtually impossible to compute its analytic expression, given the nonlinearity of the mapping f_Σ . In other words, the family of models defined in (7.12) lacks any practical value, unless one can appropriately approximate the mapping π . This is explicitly addressed in Section 7.2.

7.2 On the approximation of π

The very nature of the mapping π intrinsically depends on both the characteristics of the signal generator (7.5), and the system dynamics defined by the mapping f_Σ . The following proposition is introduced, aiming to formally characterise π .

Proposition 7.2.1 *Suppose the triple $(L, S, \xi(0))$ is minimal, and that Assumptions 7.1.1 and 7.1.2 hold. Then, for a given trajectory $\xi(t)$, each element of the mapping π , which solves equation (7.11), i.e. π_i , with $i \in \mathbb{N}_2$, belongs to the Hilbert space $L^2(\mathcal{T})$ with $\mathcal{T} = [0, T] \subset \mathbb{R}^+$, where $T = 2\pi/\omega_0$.*

Proof. Given the nature of the signal generator defined in equation (7.5), the function f_e is T -periodic, with $T = 2\pi/\omega_0$ (see Remark 7.1.4). Moreover, under the above assumptions, the zero equilibrium of $\dot{w} = f_\Sigma(w, 0)$ is locally exponentially stable and its (well-defined) steady-state solution is also T -periodic [244, Section VI], i.e. $w_{ss}(t) = w_{ss}(t - T)$. Given that, under the minimality of the triple $(L, S, \xi(0))$ and Assumptions 7.1.1 and 7.1.2, $w_{ss}(t) = \pi(\xi(t))$

(see Proposition 7.1.1), it is straightforward to conclude that each element of the mapping π belongs to $L^2(\mathcal{T})$. \square

Following the characterisation offered in the result of Proposition 7.2.1, and aiming to propose a method to approximate π , let the family of complex-valued mappings $\Omega_q^{\mathbb{C}} : \mathbb{R}^\nu \rightarrow \mathbb{C}$, $\xi \mapsto \Omega_q^{\mathbb{C}}(\xi)$, with $q \in \mathbb{N}_{\geq 1}$, be defined such as

$$\Omega_q^{\mathbb{C}}(\xi) = \sum_{p=1}^f (\gamma_p \xi)^{q/h_p}, \quad (7.13)$$

where $\gamma_p^{\top} \in \mathbb{C}^\nu$ is such that $\gamma_p^{\top} = e_{2p-1}^\nu + j e_{2p}^\nu$, for all $p \in \mathbb{N}_f$.

This mapping can be effectively used to span $L^2(\mathcal{T})$, as explicitly demonstrated in the following proposition.

Proposition 7.2.2 *Let $\mathcal{X}_0^k = \{\cos(q\omega_0 t), \sin(q\omega_0 t)\}_{q=1}^k$ be a canonical set in $L^2(\mathcal{T})$, with $\mathcal{T} = [0 T] \subset \mathbb{R}^+$, $T = 2\pi/\omega_0$, and consider the family of real-valued functions*

$$\begin{aligned} \Omega_q^+ : \mathbb{R}^\nu &\rightarrow \mathbb{R}, & \xi &\mapsto \Re \left\{ \Omega_q^{\mathbb{C}}(\xi) \right\}, \\ \Omega_q^- : \mathbb{R}^\nu &\rightarrow \mathbb{R}, & \xi &\mapsto \Im \left\{ \Omega_q^{\mathbb{C}}(\xi) \right\}. \end{aligned} \quad (7.14)$$

Let the set $\mathcal{X}_\Omega^k = \{\Omega_q^+(\xi), \Omega_q^-(\xi)\}_{q=1}^k$. Then,

$$\text{span}\{\mathcal{X}_\Omega^k\} = \text{span}\{\mathcal{X}_0^k\}. \quad (7.15)$$

Proof. Note that the key term, composing the family of complex-valued mappings in (7.13), can be alternatively written as

$$\gamma_p \xi = {}^p\xi^+ + j {}^p\xi^- \in \mathbb{C}, \quad (7.16)$$

for all $p \in \mathbb{N}_f$, and where each of the mappings ${}^p\xi^+$ and ${}^p\xi^-$ are defined as in equation (7.8) (see also Remark 7.1.2). Moreover, note that these functions can be equivalently written as,

$$\begin{aligned} {}^p\xi^+(t) &= \Re \left\{ (\alpha_p + j\beta_p) e^{j h_p \omega_0 t} \right\}, \\ {}^p\xi^-(t) &= \Im \left\{ (\alpha_p + j\beta_p) e^{j h_p \omega_0 t} \right\}, \end{aligned} \quad (7.17)$$

so that, clearly, the following expression

$$(\gamma_p \xi)^{q/h_p} = \left({}^p\xi^+ + j {}^p\xi^- \right)^{q/h_p} = (\alpha_p + j\beta_p)^{q/h_p} e^{j q \omega_0 t}, \quad (7.18)$$

for all $p \in \mathbb{N}_f$ and $q \in \mathbb{N}_{\geq 1}$, holds. In other words, only the q -th harmonic of the fundamental frequency, *i.e.* $q\omega_0$, is present in the output of the complex-valued mapping $\Omega_q^{\mathbb{C}}$.

Given the excitability condition on the pair $(S, \xi(0))$, α_p and β_p cannot be simultaneously zero, for all $p \in \mathbb{N}_f$ (see Remark 7.1.3), so that $\text{span}\{\Omega_q^+(\xi), \Omega_q^-(\xi)\} = \text{span}\{\cos(q\omega_0 t), \sin(q\omega_0 t)\}$, and the proof follows. \square

Remark 7.2.1 Naturally, the set \mathcal{X}_Ω^k forms an orthogonal basis of $L^2(\mathcal{T})$, under the standard inner-product operator of such a space, as $k \rightarrow \infty$.

The result of Proposition 7.2.2, together with Remark 7.2.1, allows each element of the mapping π , i.e. π_i , with $i \in \mathbb{N}_2$, to be uniquely expressed in terms of the set \mathcal{X}_Ω^k as a linear combination of its elements, i.e.

$$\pi_i(\xi) = \sum_{q=1}^k \begin{bmatrix} c_q^+ & c_q^- \end{bmatrix} \begin{bmatrix} \Omega_q^+(\xi) \\ \Omega_q^-(\xi) \end{bmatrix} + \epsilon_i(\xi) = \tilde{\Pi}_i \Omega^k(\xi) + \epsilon_i(\xi), \quad (7.19)$$

with $\Omega^k(\xi(t)) \in \mathbb{R}^{2k}$ such that $\Omega^k(\xi) = \sum_{q=1}^k e_q^k \otimes \begin{bmatrix} \Omega_q^+(\xi) & \Omega_q^-(\xi) \end{bmatrix}^\top$, and where the mapping $\epsilon_i : \mathbb{R}^\nu \rightarrow \mathbb{R}$ is given by,

$$\epsilon_i(\xi) = \sum_{q=k+1}^{+\infty} \begin{bmatrix} c_q^+ & c_q^- \end{bmatrix} \begin{bmatrix} \Omega_q^+(\xi) \\ \Omega_q^-(\xi) \end{bmatrix}. \quad (7.20)$$

Remark 7.2.2 Note that, following equation (7.19), π can be compactly expressed as

$$\pi(\xi) = \begin{bmatrix} \tilde{\Pi}_1 \\ \tilde{\Pi}_2 \end{bmatrix} \Omega^k(\xi) + \begin{bmatrix} \epsilon_1(\xi) \\ \epsilon_2(\xi) \end{bmatrix} = \tilde{\Pi} \Omega^k(\xi) + E(\xi), \quad (7.21)$$

where the operator $E : \mathbb{R}^\nu \rightarrow \mathbb{R}^2$ is the *truncation error*.

If the truncation error E is 'ignored', the mapping π can be effectively approximated as $\pi \approx \tilde{\pi}(\xi) = \tilde{\Pi} \Omega^k(\xi)$, i.e. by its expansion on the $2k$ -dimensional set \mathcal{X}_Ω^k . This motivates the following key definition.

Definition 7.2.1 The mapping $h_\Sigma \circ \tilde{\pi}$, where $\tilde{\pi}(\xi) = \tilde{\Pi} \Omega^k(\xi)$, is the approximated moment of system (7.2) at the signal generator (S, L) .

With this definition, and following equation (7.12), a family of reduced models of order (dimension) $\nu = 2f$, for the WEC system defined in equation (7.1), can be written in terms of the approximated moment (see Definition 7.2.1) as

$$\Sigma \approx \tilde{\Sigma}_{nl} : \begin{cases} \dot{\Theta} = (S - \Delta L)\Theta + \Delta f_e, \\ \tilde{y} = C\tilde{\Pi}\Omega^k(\Theta), \end{cases} \quad (7.22)$$

parameterised by the design matrix $\Delta \in \mathbb{R}^{\nu}$.

Remark 7.2.3 Note that not only the family of systems (7.22) is input-to-state linear, but the user also has full control over the complexity of the output mapping, *i.e.* one can define how ‘complex’ is Ω^k by simply adjusting the number k of harmonics utilised to approximate π with $\tilde{\pi}$.

Within the proposed framework, the computation of a reduced system by moment-matching, as defined in equation (7.22), now boils down to the computation of the matrix $\tilde{\Pi}$, for a given selection of order k in Ω^k , *i.e.* a given number of harmonic functions associated with the fundamental frequency ω_0 (dictated by the nature of the input f_e). This is specifically addressed in Section 7.2.1.

7.2.1 A Galerkin-like approach

Aiming to propose a method to compute $\tilde{\Pi}$, and inspired by the family of mean weighted residual methods [150, 154] (see also Section 3.4.1.2), the following *residual* mapping $r : \mathbb{R}^2 \rightarrow \mathbb{R}^2$ can be defined as

$$r(\tilde{\Pi}\Omega^k(\xi)) := \tilde{\Pi} \frac{\partial \Omega^k(\xi)}{\partial \xi} S\xi - f_{\Sigma}(\tilde{\Pi}\Omega^k(\xi), L\xi), \quad (7.23)$$

which directly arises from ‘replacing’ the mapping π by the approximating function $\tilde{\pi}$ in equation (7.11).

Remark 7.2.4 Similarly to the linear moment-based model reduction framework described in Chapters 5 and 6, the non-parametric terms associated with the mapping f_{Σ} , *i.e.* radiation effects, can be written in terms of a matrix product. In particular, note that the residual function, defined in (7.23), can be conveniently expanded in terms of $\tilde{\Pi}$ as

$$r(\tilde{\Pi}\Omega^k(\xi)) = \tilde{\Pi} \frac{\partial \Omega^k(\xi)}{\partial \xi} S\xi - (A\tilde{\Pi} - BC\tilde{\Pi}\mathcal{R})\Omega^k(\xi) - BL\xi - f(\tilde{\Pi}\Omega^k(\xi)), \quad (7.24)$$

where the matrix $\mathcal{R} \in \mathbb{R}^{2k \times 2k}$ arises from the convolution operator, involved in system (7.1), associated with the radiation effects. In particular, and analogously to Proposition 5.1.1, the matrix \mathcal{R} is given in block diagonal form as,

$$\mathcal{R} = \bigoplus_{q=1}^k \begin{bmatrix} r_{q\omega_0} & m_{q\omega_0} \\ -m_{q\omega_0} & r_{q\omega_0} \end{bmatrix}, \quad (7.25)$$

where the set of parameters $\{r_{q\omega_0}, m_{q\omega_0}\} \subset \mathbb{R}$ are defined in equation (5.10), for all $q \in \mathbb{N}_k$.

Following the so-called Galerkin (or spectral) approach (see, for instance, [245]), which effectively belongs to the family of mean weighted residual methods discussed in Section 3.4.1.2, the constant matrix $\tilde{\Pi}$ can be computed by projecting the residual mapping onto the space spanned by the set of k harmonics of the fundamental frequency defined by \mathcal{X}_Ω^k , i.e. the entries of $\Omega_\Omega^k(\xi)$. In contrast to the 'traditional' Galerkin formulation, a *Galerkin-like* method is proposed, as detailed in the following.

Let $\Omega_0^k(t) = \sum_{q=1}^k e_q^k \otimes [\cos(q\omega_0 t) \quad -\sin(q\omega_0 t)]^\top \in \mathbb{R}^{2k}$ be a vector containing the $2k$ canonical harmonic functions on $L^2(\mathcal{T})$. Then, given a fixed trajectory $\xi(t)$, the constant matrix $\tilde{\Pi} \in \mathbb{R}^{2 \times 2k}$ can be computed by zeroing the projection of the residual mapping onto the set spanned by the elements (entries) of the vector Ω_0^k , i.e. as the solution of the following algebraic system of $4k$ equations:

$$\langle r(\tilde{\Pi}\Omega^k(\xi)), \Omega_0^{k\top} \rangle = 0, \quad (7.26)$$

where $\langle \cdot \rangle$ denotes the inner-product operator in $L^2(\mathcal{T})$, as defined in Section 1.3.

Remark 7.2.5 In the proposed Galerkin-like approach, the canonical vector Ω_0^k is utilised when projecting the residual mapping, instead of the entries of Ω^k (which would be the case in a 'traditional' Galerkin method¹¹). This substantially simplifies the computation of the projections involved in (7.26), which are effectively inner-product operations in $L^2(\mathcal{T})$. This simplification is specifically discussed in Section 7.3.1.

11: See, for instance, [154].

Remark 7.2.6 The existence of solutions of equation (7.26), under the hypothesis of Proposition 7.2.1, is always guaranteed for all sufficiently large k [245].

Remark 7.2.7 The system of algebraic equations (7.26) on the $4k$ entries of $\tilde{\Pi}$, can be computed using state-of-the-art root finding algorithms, such as those described in, for instance, [246].

7.3 Practical aspects and considerations

7.3.1 Projection of the residual mapping

This section begins by noting that the selection of the vector Ω_0^k , involved in the projection of the residual mapping within the Galerkin-like approach proposed in Section 7.2.1, has a very specific purpose,

which is detailed in the following. Recall that the Fourier transform of a T -periodic function, *i.e.* a function $x \in L^2(\mathcal{T})$, is always well-defined, and can be computed with the expression

$$\begin{aligned} X(\omega) &= \int_{\mathcal{T}} x(t) e^{-j\omega t} dt, \\ &= \int_{\mathcal{T}} x(t) \cos(\omega t) dt - i \int_{\mathcal{T}} x(t) \sin(\omega t) dt. \end{aligned} \quad (7.27)$$

Note that, due to the specific selection of the entries of Ω_0^k , each of the inner-product operations involved in the Galerkin-like method proposed in (7.26) are, effectively, either the real or the imaginary parts of the Fourier transform of the residual mapping r , evaluated at each of the k harmonics of the fundamental frequency ω_0 , *i.e.* at the set $\{q\omega_0\}_{q=1}^k$. In other words, the system of equations (7.26) characterising $\tilde{\Pi}$ can be equivalently written as

$$\left[\Re\{R(\omega_0)\} \Im\{R(\omega_0)\} \dots \Re\{R(k\omega_0)\} \Im\{R(k\omega_0)\} \right] = 0, \quad (7.28)$$

where $R : \mathbb{R} \rightarrow \mathbb{C}^2$ denotes the Fourier transform of the residual mapping r .

Remark 7.3.1 The evaluation of the Fourier transform at each frequency $q\omega_0$, can be done both efficiently and robustly using well-established fast Fourier transform (FFT) algorithms (see, for instance, [247]).

7.3.2 Extension to multiple trajectories

Until this point, a single trajectory $\xi(t)$ has been considered, *i.e.* a single initial condition $\xi(0)$ for the signal generator (S, L) . In other words, a single input $f_e(t) = Le^{St}\xi(0)$ has been taken into account for the computation of the approximating $\tilde{\pi}$. Though this might be appropriate for some cases, such as, for instance, the case of WECs under (deterministic) regular wave excitation (further discussed in Section 7.5.1), constraining the approximation method to a single initial condition can be limiting for the case of WEC systems subject to irregular wave excitation. This issue is addressed, for the Galerkin-like approach of Section 7.2.1, as follows¹².

Let $\xi(0) \in \Xi$, where $\Xi = \{\zeta_i\}_{i=1}^l \subset \mathbb{R}^\nu$ represents a set with l initial conditions, defined in a neighbourhood of $\xi = 0$. Suppose the pairs of matrices (S, ζ_i) are excitable for all $i \in \mathbb{N}_l$. Let the vector ξ , generated as a function of the initial condition ζ_i , be denoted as $\xi_{\zeta_i} = e^{St}\zeta_i$. Then, the Galerkin-like procedure, proposed in Section 7.2.1, can be adapted for the case of multiple trajectories, where the constant matrix $\tilde{\Pi}$, which completely characterises the

12: The extension to multiple trajectories presented in this section is proposed in the spirit of the so-called \mathcal{U}/\mathcal{X} variation [232].

approximating mapping $\tilde{\pi}(\xi) = \tilde{\Pi}\Omega^k(\xi)$, is computed in terms of a minimisation procedure:

$$\min_{\tilde{\Pi} \in \mathbb{R}^{2 \times 2k}} \left\| \begin{bmatrix} \langle r(\tilde{\Pi}\Omega^k(\xi_{\zeta_1})), \Omega_0^k(\xi_{\zeta_1}) \rangle \\ \vdots \\ \langle r(\tilde{\Pi}\Omega^k(\xi_{\zeta_l})), \Omega_0^k(\xi_{\zeta_l}) \rangle \end{bmatrix} \right\|_{\mathbb{F}}^2, \quad (7.29)$$

where the inner product operations, for each initial condition ζ_i , with $i \in \mathbb{N}_l$, can be computed using FFT operations, as detailed in Section 7.3.1.

The minimisation procedure described in equation (7.29) is effectively utilised both for the case of nonlinear model reduction by moment-matching for WECs under regular, and irregular wave excitation, further discussed and illustrated in Sections 7.5 and 7.6, respectively.

7.3.3 Modifications to the mapping Ω^k

This section introduces a modification for the vector valued function Ω^k , utilised to approximate the nonlinear moment of system (7.1) at the signal generator (7.5), aiming to ‘simplify’ the description of the output mapping involved in (7.12). In particular, one can modify the entries of $\Omega^k(\xi)$ such that only integer exponents of ξ are required, and a fixed maximum number of harmonics associated with a given multiple $h_p\omega_0$, involved in the definition of the matrix S in equation (7.6), is considered, for each $p \in \mathbb{N}_f$. This is explicitly addressed in the following.

Let k_p^{\max} denote the maximum number of harmonics of a given multiple of the fundamental frequency $h_p\omega_0$, with $p \in \mathbb{N}_f$. Then, the complex-valued mapping $\Omega_q^{\mathbb{C}}$ defined in equation (7.13), which fully characterises the entries of Ω^k , can be modified as follows:

$$\Omega_q^{\mathbb{C}}(\xi) = \sum_{p=1}^f a_{qp} (\gamma_p \xi)^{q/h_p}, \quad (7.30)$$

where the coefficients a_{qp} are defined as

$$a_{qp} = \begin{cases} 1 & \text{if } \text{mod}(q, h_p) = 0 \quad \wedge \quad \frac{q}{h_p} \leq k_p^{\max}, \\ 0 & \text{if } \text{mod}(q, h_p) \neq 0 \quad \vee \quad \frac{q}{h_p} > k_p^{\max}, \end{cases} \quad (7.31)$$

and $\text{mod} : \mathbb{N} \times \mathbb{N}_{\geq 1} \rightarrow \mathbb{N}$ denotes the modulo operator.

Remark 7.3.2 With the introduction of this set of coefficients a_{qp} , the mapping Ω^k *only depends* on natural powers involving

the entries of ξ , *i.e.* it becomes *polynomial*. In other words, the output of the reduced model \tilde{y} (7.22) is always smooth.

To clarify the use and ‘evolution’ of the set of coefficients a_{qp} , for a given signal generator, an illustrative example is considered in the following. Let the fundamental frequency be $\omega_0 = 1$ and consider a signal generator with a dynamic matrix S given by

$$S = \begin{bmatrix} 0 & 1 & 0 & 0 & 0 & 0 \\ -1 & 0 & 0 & 0 & 0 & 0 \\ 0 & 0 & 0 & 3 & 0 & 0 \\ 0 & 0 & -3 & 0 & 0 & 0 \\ 0 & 0 & 0 & 0 & 0 & 4 \\ 0 & 0 & 0 & 0 & -4 & 0 \end{bmatrix}, \quad (7.32)$$

where, clearly, the set of coefficients $\mathcal{H} = \{h_p\}_{p=1}^3$ is given by $h_1 = 1$, $h_2 = 3$ and $h_3 = 4$. Suppose the maximum number of harmonics associated with each h_p , to compute the vector Ω^k , are set to $k_1^{\max} = 10$, $k_2^{\max} = 3$ and $k_3^{\max} = 2$. The coefficients a_{qp} are illustrated, for this example case, in Figure 7.1, with $q \in \mathbb{N}_{10}$. Non-zero values of a_{qp} are indicated with a black dot.

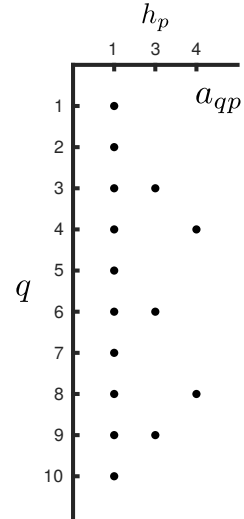


Figure 7.1: Coefficients a_{qp} for the mapping Ω^k , for $h_1 = 1$, $h_2 = 3$ and $h_3 = 4$, where $q \in \mathbb{N}_{10}$. Non-zero values of a_{qp} are indicated with a black dot.

7.3.4 On the eigenvalues of the reduced model

As discussed in Remark 7.1.7, the family of reduced models by moment-matching defined in equation (7.22) is input-to-state linear. Furthermore, the eigenvalues characterising such a system, *i.e.* the set $\lambda(S - \Delta L)$, can be assigned arbitrarily, as a consequence of the observability of the pair (S, L) .

It is proposed to assign such a set of eigenvalues using information from the Jacobian linearisation of system (7.1) about the origin, *i.e.* the non-parametric *linear* Cummins’ equation (7.10). In particular, and similarly to the linear model reduction case presented in Chapter 6, one can estimate a set $\Lambda \subset \mathbb{C}$ of ν eigenvalues for system (7.10) in terms of the singular value decomposition of the Hankel matrix \hat{H} , constructed from the input-output frequency-domain data of the WEC, computed with BEM solvers (see Section 6.3.1 for a detailed discussion on this procedure).

Once this set Λ is obtained, the matrix Δ can always be computed such that $\lambda(S - \Delta L) = \Lambda$, due to the observability of (S, L) , using standard algorithms.

7.4 Extension to MIMO WEC systems

Although, until this point, a SISO nonlinear WEC has been considered, the methodology to produce reduced models by moment-matching proposed in Sections 7.1 and 7.2, can be extended to the MIMO nonlinear case, with some minor considerations. These are explicitly addressed in the following.

Recall, from Section 2.4, that the equation of motion for a N -th order WEC system¹³, with $N \in \mathbb{N}_{\geq 1}$, can be expressed as:

$$\Sigma : \begin{cases} \ddot{z} = \mathcal{M}(-k_r * \dot{z} - s_h z + f_e + f_{nl}), \\ y = \dot{z}, \end{cases} \quad (7.33)$$

where $z : \mathbb{R}^+ \rightarrow \mathbb{R}^N$ is the displacement vector, $k_r : \mathbb{R}^+ \rightarrow \mathbb{R}^{N \times N}$, $k_{r_{ij}} \in L^2(\mathbb{R})$, $\forall \{i, j\} \subset \mathbb{N}_N$, the radiation force impulse response (matrix) function, $f_e : \mathbb{R}^+ \rightarrow \mathbb{R}^N$ the wave excitation force, and \mathcal{M} is the inverse of the generalised mass matrix of the device. Similar to the SISO case of equation (7.1), the mapping $f_{nl} : \mathbb{R}^+ \rightarrow \mathbb{R}^N$, $t \mapsto f_{nl}(t)$, represents potential nonlinear effects. The same procedure described in Sections 7.1 and 7.2 can be straightforwardly applied to a N -th order WEC system (*i.e.* MIMO WEC case), with the following modifications.

Analogously to Section 7.1, the following equivalent representation for the N -th order (MIMO) WEC system can be proposed:

$$\Sigma : \begin{cases} \dot{w} = f_\Sigma(w, f_e) = Aw + B(f_e - k_r * Cw) + f(w), \\ y = h_\Sigma(w) = Cw, \end{cases} \quad (7.34)$$

for $t \in \mathbb{R}^+$, where $w(t) = \sum_{i=1}^N e_i^N \otimes [z_i(t) \quad \dot{z}_i(t)]^T \in \mathbb{R}^{2N}$ contains displacement and velocity corresponding with system Σ in (7.33), and the (constant) matrices $A \in \mathbb{R}^{2N \times 2N}$, $B \in \mathbb{R}^{2N \times N}$ and $C \in \mathbb{R}^{N \times 2N}$ are defined as

$$\begin{aligned} A &= \sum_{i=1}^N \sum_{j=1}^N e_{ij}^N \otimes \begin{bmatrix} 0 & i_j \delta \\ -\mathcal{M}_{ij} s_{h_i} & 0 \end{bmatrix}, \\ B &= \sum_{i=1}^N \sum_{j=1}^N e_{ij}^N \otimes \begin{bmatrix} 0 \\ \mathcal{M}_{ij} \end{bmatrix}, \\ C &= \mathbb{I}_N \otimes \begin{bmatrix} 0 & 1 \end{bmatrix}. \end{aligned} \quad (7.35)$$

The nonlinear mapping $f : \mathbb{R}^{2N} \rightarrow \mathbb{R}^{2N}$ is given by

$$f(w) = B f_{nl}(w). \quad (7.36)$$

Following the MIMO formulation presented in Chapter 6, the signal

13: As previously described in Remark 6.0.2, the term N -th order WEC system (or device), is utilised to refer either to a N -DoF WEC device, or an array of N devices, constrained to move in a single DoF.

generator defined in equation (7.5) is modified accordingly, *i.e.* it is written in terms of an autonomous multiple-output signal generator, using the set of differential equations

$$\begin{aligned}\dot{\xi} &= (\mathbb{I}_N \otimes S)\xi, \\ f_e &= L\xi,\end{aligned}\tag{7.37}$$

for $t \in \mathbb{R}^+$, and where the triple $(L, \mathbb{I}_N \otimes S, \xi(0))$ is such that $L = \mathbb{I}_N \otimes \mathbf{1}_J^+$ and $(\mathbb{I}_N \otimes S, \xi(0))$ is excitable (as detailed in Remark 7.1.3). The matrix S , involved in the definition of the multiple-output signal generator (7.37), is exactly the same as in the SISO case, *i.e.* as defined in equation (7.6).

Posing an analogous assumption for the mapping f , to that defined in Assumption 7.1.1 for the SISO case, the existence and uniqueness of the nonlinear moment of system Σ (7.33) at the signal generator (7.37) can be automatically guaranteed, following the same arguments of Proposition 7.1.1. In other words, the definition of the nonlinear moment of the MIMO system Σ at the signal generator (S, L) is always well-posed.

An approximation of the mapping $\pi : \mathbb{R}^{N\nu} \rightarrow \mathbb{R}^{2N}$, $\xi \mapsto \pi(\xi)$, for this MIMO case, can be computed exactly as in the Galerkin-like procedure proposed in Section 7.2.1 for the nonlinear SISO case. To be precise, an approximating mapping $\tilde{\pi}$ can be computed as

$$\pi \approx \tilde{\pi}(\xi) = C\tilde{\Pi}(\mathbf{1}_N \otimes \Omega^k(\xi)).\tag{7.38}$$

Remark 7.4.1 The matrix $\tilde{\Pi} \in \mathbb{R}^{N \times N\nu}$, which completely characterises the approximating mapping $\pi \approx \tilde{\pi}(\xi) = C\tilde{\Pi}(\mathbf{1}_N \otimes \Omega^k(\xi))$, can be computed in an exact same manner than that proposed in Section 7.2, with appropriate changes to the residual equation defined in (7.24). Summarising, one has to replace the quantities in (7.24) as follows:

$$\begin{aligned}S &\text{ by } \mathbb{I}_N \otimes S, \\ \Omega^k(\xi) &\text{ by } \mathbf{1}_N \otimes \Omega^k(\xi), \\ \Omega_0^k(\xi) &\text{ by } \mathbf{1}_N \otimes \Omega_0^k(\xi), \\ C\tilde{\Pi}\mathcal{R} &\text{ by } \sum_{i=1}^N \sum_{j=1}^N e_{ij}^N \otimes C\tilde{\Pi}(\mathbb{I}_N \otimes \mathcal{R}_{ij}),\end{aligned}\tag{7.39}$$

where each \mathcal{R}_{ij} directly stems from Proposition 6.2.1, *i.e.* it can

be written as a block-diagonal matrix defined as

$$\mathcal{R}_{ij} = \bigoplus_{q=1}^k \begin{bmatrix} {}^i_j r_{q\omega_0} & {}^i_j m_{q\omega_0} \\ -{}^i_j m_{q\omega_0} & {}^i_j r_{q\omega_0} \end{bmatrix}, \quad (7.40)$$

for $\{i, j\} \subset \mathbb{N}_N$, and where the set $\{{}^i_j r_{q\omega_0}, {}^i_j m_{q\omega_0}\} \subset \mathbb{R}$ is as defined in equation (6.16), for all $q \in \mathbb{N}_k$.

Finally, a family of reduced models of order (dimension) $2Nf$ for the WEC system defined in equation (7.33), can be written in terms of the approximating moment $h_\Sigma \circ \tilde{\pi}$, for this MIMO case, as

$$\Sigma \approx \tilde{\Sigma}_{nl} : \begin{cases} \dot{\Theta} = (\mathbb{I}_N \otimes S - \Delta L)\Theta + \Delta f_e, \\ \tilde{y} = C\tilde{\Pi}(\mathbf{1}_N \otimes \Omega^k(\Theta)), \end{cases} \quad (7.41)$$

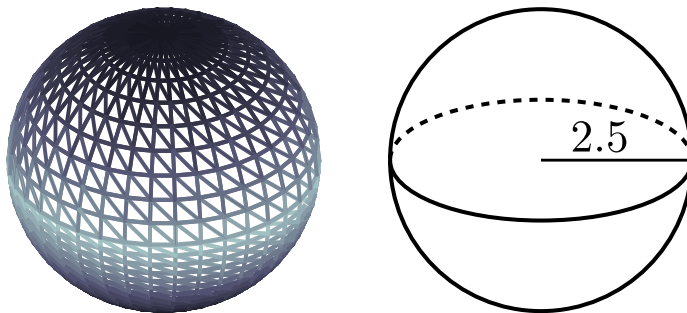
parameterised in $\Delta \in \mathbb{R}^{N\nu \times N}$.

Remark 7.4.2 Note that, similarly to the case presented in equation (7.12), the set $\lambda(\mathbb{I}_N \otimes S - \Delta L)$ can be assigned arbitrarily, as a consequence of the observability of the pair $(\mathbb{I}_N \otimes S, L)$.

7.5 WEC systems under regular wave excitation

To illustrate the performance of the model reduction by moment-matching technique presented in this chapter, a clear distinction has to be made, in terms of the nature of the wave excitation input, *i.e.* regular or irregular. In particular, this section analyses a WEC system under regular wave excitation, assuming two different cases concerning the wave height: Deterministic and stochastic¹⁴.

For the remainder of this section, a spherical heaving point absorber WEC is considered, with a radius of 2.5 [m]. Such a geometry is schematically illustrated in Figure 7.2. The hydrodynamic coefficients $B_r(\omega)$ and $A_r(\omega)$, for this spherical-type device, are those shown in Figure 2.8.



14: Note that the analysis provided in this section motivates the methodology proposed for the more complex irregular wave input case, described in Section 7.6.

Figure 7.2: Spherical heaving point absorber WEC considered for the case of nonlinear model reduction under regular wave excitation.

The nonlinear mapping f_{nl} , characterising the nonlinear effects present in the non-parametric WEC equation (7.1), is assumed to be given, for this spherical heaving point absorber case, by:

$$\begin{aligned} f_{nl}(z, \dot{z}) &= f_{re}^{nl}(z) + f_v(\dot{z}), \\ f_{re}^{nl}(z) &= \frac{1}{3}\rho g \pi z^3, \\ f_v(\dot{z}) &= -2\rho\pi(2.5)^2 C_d \dot{z}|\dot{z}|, \end{aligned} \quad (7.42)$$

where ρ is the water density, g the gravitational constant, and f_v and f_{re}^{nl} represent nonlinear viscous and hydrostatic restoring effects (see Section 2.5), respectively¹⁵. The value for the viscous drag coefficient is set to $C_d = 1$, following the study on consistency of viscous drag identification for WECs, performed in [18].

To illustrate the proposed nonlinear model reduction by moment-matching technique for devices under regular excitation, it is assumed that the WEC is subject to regular waves with a given frequency ω^* and height H_w . As a matter of fact, note that ω^* is indeed the fundamental frequency defined in Section 7.1, *i.e.* $\omega_0 = \omega^*$. Under these conditions, the wave excitation input f_e can be written¹⁶ as,

$$f_e(t) = A^* \cos(\omega^* t), \quad (7.43)$$

where $A^* = |K_e(\omega^*)| \frac{H_w}{2} \in \mathbb{R}^+$, with $K_e : \mathbb{R} \rightarrow \mathbb{C}$ the Fourier transform of the excitation impulse response function (see Section 2.3.2.1). This input can be clearly generated following Section 7.1, *i.e.* as the output of a signal generator, analogously to equation (7.5), characterised by the one-dimensional set $\mathcal{F} = \{\omega^*\}$:

$$\begin{aligned} \dot{\xi} &= S\xi = \begin{bmatrix} 0 & \omega^* \\ -\omega^* & 0 \end{bmatrix} \xi, \\ f_e &= L\xi = \begin{bmatrix} 1 & 1 \end{bmatrix} \xi, \\ \xi(0) &= \begin{bmatrix} \alpha & \beta \end{bmatrix}^\top = \begin{bmatrix} \frac{A^*}{2} & \frac{A^*}{2} \end{bmatrix}^\top. \end{aligned} \quad (7.44)$$

A clear distinction is now made, with respect to the nature of the wave height H_w and, hence, the amplitude A^* of the excitation signal f_e . In particular, if the wave height is assumed to be fixed and known, then a single initial condition $\xi(0)$ (as in equation (7.44)) is required to fully characterise the approximating moment and, hence, the corresponding reduced order model by moment-matching. This case is referred to as *deterministic regular excitation*, and is illustrated and discussed in Section 7.5.1. In contrast, if the wave height is only known to lie in a given set, then a set of multiple initial conditions is required to characterise the corresponding reduced order model, by following Section 7.3. This case is referred to as *stochastic regular*

15: The mapping f_{re}^{nl} is geometry dependent and, for the spherical heaving point absorber case, can be found in, for instance, [125].

16: Note that, without any loss of generality, the phase shift is assumed to be zero.

excitation, and is illustrated and discussed in Section 7.5.2.

7.5.1 Deterministic regular excitation

Recall that, for this regular excitation case, the so-called fundamental frequency ω_0 is indeed ω^* . As discussed previously in Section 7.5, if the wave height is fixed and known, then a single initial condition $\xi(0)$ is required to fully characterise the reduced order model by moment-matching, defined in equation (7.22). To be precise, the computation of the matrix $\tilde{\Pi}$, fully characterising the approximating moment (as in Definition 7.2.1), can be computed using the Galerkin-like approach proposed in Section 7.2.1, without any further modifications. This case is explicitly discussed in the following.

Let $\omega^* = 0.8$ [rad/s], which corresponds with a wave period of approximately $T_w = 8$ [s], and suppose the wave height, which characterises the amplitude A^* of the wave excitation force, is fixed to $H_w = 2$ [m]. A nonlinear model, reduced by moment-matching, for the heaving sphere considered in this section, can be computed directly from (7.22) as

$$\Sigma \approx \tilde{\Sigma}_{nl} : \begin{cases} \dot{\Theta} = \left(\begin{bmatrix} 0 & 0.8^* \\ -0.8^* & 0 \end{bmatrix} - \Delta \begin{bmatrix} 1 & 1 \end{bmatrix} \right) \Theta + \Delta f_e, \\ \tilde{y} = C\tilde{\Pi}\Omega^k(\Theta), \end{cases} \quad (7.45)$$

where the mapping Ω^k is characterised by equation (7.14), for a given number of harmonics k of the fundamental frequency ω^* , and where the matrix $\tilde{\Pi}$ is computed following Section 7.2.1. Note that the initial condition $\xi(0)$, involved in the computation of $\tilde{\Pi}$, is exactly as described in equation (7.44). The matrix Δ , assigning the eigenvalues of the reduced model (7.45), is computed following Section 7.3.4.

Remark 7.5.1 Given that only the fundamental frequency is explicitly present in the definition of the signal generator (7.44) and, hence, in the model reduced by moment-matching defined in equation (7.45), the mapping Ω^k is, effectively, polynomial (*i.e.* no fractional exponents of ξ are required for the regular wave input case).

To begin with the assessment of this case study, Figure 7.3 illustrates the performance of a nonlinear moment-based reduced model as in equation (7.45), computed with $k = 3$ (*i.e.* with Ω^k including three harmonics of the fundamental frequency ω^*). In particular, Figure 7.3 shows both the output of the target (dashed) nonlinear model of the WEC system (7.1), computed with a Runge-Kutta method (time step of 10^{-4} [s]), where the non-parametric convolution operator

is explicitly solved, and the output of the moment-based reduced order model (7.45) (solid), with $k = 3$.

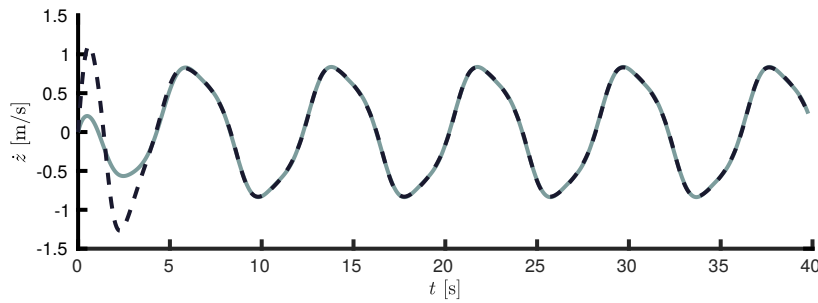


Figure 7.3: Output of both the target nonlinear model (dashed) and the moment-based reduced order model (solid), with $k = 3$.

It can be readily appreciated that, after the corresponding transient period, the steady-state response of both target and approximating models are effectively indistinguishable, as a virtue of the inherent moment-matching feature of the reduced model. To illustrate the improvement in (steady-state) accuracy for higher values of k , Figure 7.4 shows (in logarithmic scale) the absolute value of the difference between target and approximating output for $k \in \{3, 5, 7\}$, as a function of time. In addition, the error corresponding with the output of the system arising from Jacobian linearisation, *i.e.* the linear Cummins' equation in (7.10), corresponding with the spherical heaving point absorber considered in this section, is also shown. Although, as can be concluded from both Figures 7.3 and 7.4, selecting $k = 3$ provides accurate results, these can be improved by increasing k accordingly.

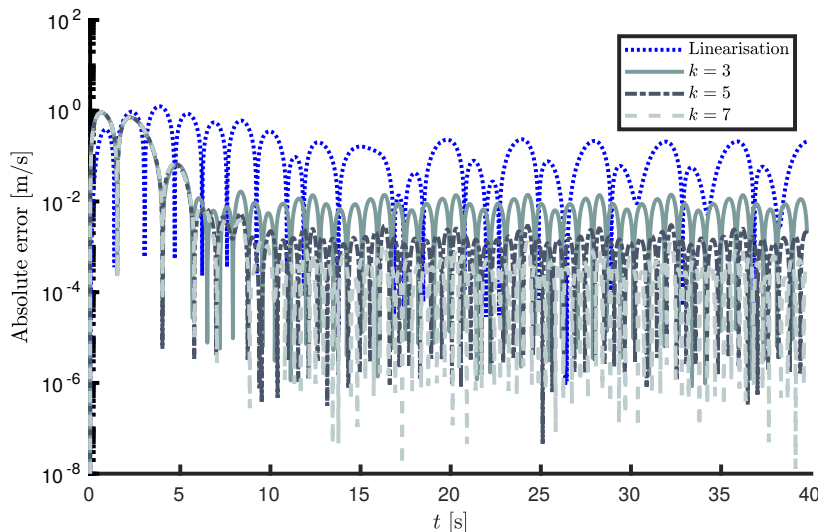


Figure 7.4: Absolute value of the difference between target and approximating output for $k \in \{3, 5, 7\}$, as a function of time. In addition, the error corresponding with the output of the Jacobian linearisation is also shown.

Aiming to provide a conclusive performance indicator for this regular deterministic wave input case and given that, unlike the linear case presented in Chapters 5 and 6, only a time-domain comparison can be performed for this nonlinear WEC case, the normalised mean

absolute percentage error NMAPE is considered, defined as

$$\text{NMAPE}(\tilde{y}_{ss}) = \frac{100}{N_s} \sum_{i=1}^{N_s} \frac{|\tilde{y}_{ss}(t_i) - y_{ss}(t_i)|}{\max\{|y_{ss}(t_i)|\}}, \quad (7.46)$$

where $N_s \in \mathbb{N}_{\geq 1}$ denotes the number of (time-domain) samples available for the time-traces of the steady-state target, and approximating output signals y_{ss} and \tilde{y}_{ss} , respectively. Table 7.1 shows the NMAPE for the nonlinear moment-based models computed from equation (7.45), with $k \in \{3, 5, 7\}$, and that corresponding with the Jacobian linearisation about the origin, *i.e.* equation (7.10). Clearly, a result consistent with that shown in Figure 7.4 can be straightforwardly concluded.

# of harmonics	NMAPE
(Jacobian linearisation)	10.12 %
$k = 3$	0.76 %
$k = 5$	0.14 %
$k = 7$	0.04 %

Table 7.1: NMAPE for the moment-based reduction strategy, for WECs under regular excitation.

7.5.2 Stochastic regular excitation

Section 7.5.1 discusses a case study where the amplitude associated with the regular wave excitation input f_e is exactly known. In other words, a single trajectory $\xi(t)$ of the signal generator (7.44), obtained from a unique initial condition $\xi(0)$, is required to fully characterise the approximating moment $h_{\Sigma} \circ \tilde{\pi}$, in terms of the Galerkin-like approach presented in Section 7.2.1. If the wave height, characterising the wave excitation amplitude, is only known to lie on a certain set, *i.e.* $H_w \in \mathcal{H}$, with $\mathcal{H} = [H_w^{\min}, H_w^{\max}] \subset \mathbb{R}^+$, then the approximation of the corresponding nonlinear moment depends on an *infinite* number of initial conditions (each for every possible wave height in the set \mathcal{H}).

Though an adaptation of the Galerkin-like approach, proposed in Section 7.2.1, is given in Section 7.3.2 for the multiple trajectory case, the number of initial conditions is assumed to be finite. Motivated by this, a *worst-case approach* is considered in the following: Only the set of initial conditions $\Xi_t = \{\zeta^{\min}, \zeta^{\max}\} \subset \mathbb{R}^2$ are taken into account for the computation of the matrix $\tilde{\Pi}$, where ζ^{\min} and ζ^{\max} correspond with the inputs with height H_w^{\min} and H_w^{\max} , respectively.

Remark 7.5.2 From now on, the elements of the set of initial conditions Ξ_t , associated with the worst-case approach described in this section, are referred to as *training initial conditions*. Analogously, the trajectories generated as a function of the set Ξ_t , *i.e.* $\{\xi_{\zeta^{\min}}, \xi_{\zeta^{\max}}\}$, are referred to as *training trajectories*.

Note that the set of training initial conditions can be computed analogously to equation (7.43), *i.e.*

$$\begin{aligned} \zeta^{\min} &= \begin{bmatrix} \frac{A_1^*}{2} & \frac{A_1^*}{2} \end{bmatrix}^\top, & A_1^* &= |K_\epsilon(\omega^*)| \frac{H_w^{\min}}{2}, \\ \zeta^{\max} &= \begin{bmatrix} \frac{A_2^*}{2} & \frac{A_2^*}{2} \end{bmatrix}^\top, & A_2^* &= |K_\epsilon(\omega^*)| \frac{H_w^{\max}}{2}. \end{aligned} \quad (7.47)$$

For this case study, it is assumed that $H_w^{\min} = 1.6$ [m] and $H_w^{\max} = 2.4$ [m], *i.e.* the actual value of the wave height can vary $\pm 20\%$ of the nominal value $H_w = 2$ [m], adopted in Section 7.5.1. The approximating moment is then computed as detailed in Section 7.3.2, for the set of training trajectories Ξ_t , and where, in light of the results computed for the deterministic case of Section 7.5.1, the number of harmonics involved in the definition of Ω^k is set to $k = 5$. Figure 7.5 illustrates the output of the nonlinear moment-based reduced order model (in steady-state, solid), for the inputs corresponding with the training trajectories $\xi_{\zeta^{\min}}$ and $\xi_{\zeta^{\max}}$. The target outputs, computed from system Σ in (7.1) using a Runge-Kutta method with a time-step of 10^{-4} [s] (as in Section 7.5.1), are denoted with a dashed line.

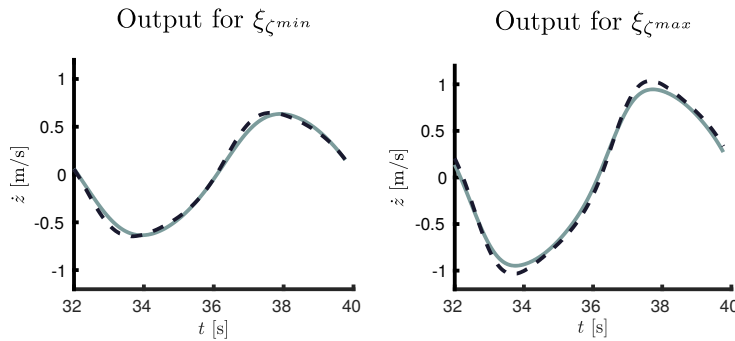


Figure 7.5: Output of the nonlinear moment-based reduced order model (in steady-state, solid), for the inputs corresponding with the training trajectories $\xi_{\zeta^{\min}}$ and $\xi_{\zeta^{\max}}$. The target outputs are denoted with a dashed line.

Remark 7.5.3 Note that, as expected from the method proposed in Section 7.3.1, the performance of the approximating outputs for the training trajectories $\xi_{\zeta^{\min}}$ and $\xi_{\zeta^{\max}}$, is not as accurate as in the deterministic case presented in Section 7.5.1. In particular, the latter is fully characterised by a single trajectory ξ , and the approximating moment can be computed with the Galerkin-like approach proposed in this chapter, with an arbitrary degree of precision (facilitated by an appropriate selection of k in the mapping Ω^k). When multiple trajectories for the signal generator (S, L) are considered, a minimisation approach is utilised, where a single matrix $\tilde{\Pi}$ is computed to characterise the approximating moment $h_\Sigma \circ \tilde{\pi}$ for *all* the training trajectories involved, hence providing a more versatile reduced order model (*i.e.* valid for a larger class of inputs) but, naturally, with a corresponding loss in performance.

To illustrate the performance of the moment-based reduced model computed in this section, a set of 1000 randomly generated realisations of regular wave inputs with wave heights in the set $[1.6, 2.4]$ [m], is considered. In particular, Figure 7.6 shows the NMAPE (computed as in equation (7.46)) for each wave realisation involved. Note that the average NMAPE value is $\overline{\text{NMAPE}} \approx 3\%$, and the maximum error registered is of $\approx 4\%$. In other words, using the methodology proposed in this section for the selection of an appropriate set of training trajectories to compute the approximating moment, the reduced order model by moment-matching (7.45) is able to successfully approximate the behaviour of the target non-parametric WEC system Σ , for regular wave excitation inputs with varying (stochastic) wave height.

7.6 WEC systems under irregular wave excitation

The case of model order reduction by moment-matching for irregular sea states has a number of distinctive features with respect to the regular wave excitation cases discussed in Section 7.5, which, unless addressed appropriately, can substantially compromise the synthesis of such a nonlinear reduced structure. To begin with, both the wave height and wave period are not fixed, and only knowledge of the significant wave height \bar{H}_w and peak period \bar{T}_w are commonly available, for a given stochastic sea-state characterisation in terms of a particular SDF (see Section 2.1.2). This clearly has several implications, both on the definition of the signal generator characterising the wave excitation effect (as in equation (7.6)), and the methodology involved in the computation of the approximating moment. These implications are addressed and discussed in the following subsections.

7.6.1 On the definition of the signal generator

The signal generator (7.6) is composed of f harmonics of a fundamental frequency ω_0 , i.e. the set $\mathcal{F} = \{h_p \omega_0\}_{p=1}^f$, with $\mathcal{H} = \{h_p\}_{p=1}^f \subset \mathbb{N}_{\geq 1}$, and where $h_1 < \dots < h_f$. Though this assumption is, in principle, not restrictive (see Section 2.1.2), an accurate representation of wave excitation effects potentially requires both a *sufficiently small* fundamental frequency ω_0 , and a *sufficiently large* number of harmonics f . This, in turn, has the following consequences:

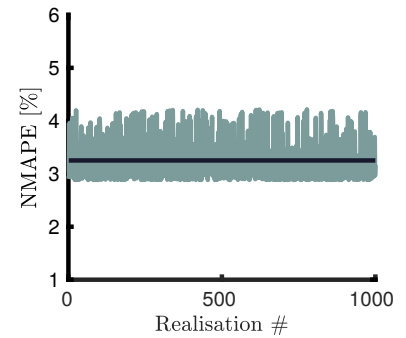


Figure 7.6: NMAPE for 1000 realisations of regular wave inputs with $H_w \in [1.6, 2.4]$ [m]. The average value $\overline{\text{NMAPE}} \approx 3\%$ is denoted with a horizontal black line.

- 1) A small fundamental frequency implies that the projection, involved in the Galerkin-like procedure proposed to compute the approximating moment, has to be performed on a larger time interval $\mathcal{T} = [0, 2\pi/\omega_0]$. Though this can be still performed efficiently using FFTs (see Section 7.3), it can also increase the computational complexity involved in the solution of the projected residual equation (7.26).
- 2) A large number of harmonics f in the definition of the signal generator (7.6) directly affects the complexity of the resulting reduced model by moment-matching: the order (dimension) ν of the family of reduced order models achieving moment-matching (7.22) depends linearly on f .

The issue discussed in item 1) above, can be easily overcome by a sensible selection of the fundamental frequency, which should take into account the particular sea state under analysis (further discussed in the case study provided in this section). Item 2) above can be overcome in the spirit of the linear moment-based technique proposed in Chapters 5 and 6: Only a set of *dynamically relevant* frequencies should be selected to represent the wave excitation effects and, hence, to characterise the corresponding reduced order model by moment-matching. As demonstrated in Chapters 5 and 6, this set, for the WEC case, includes the resonant frequency associated with the linearised behaviour of the WEC system (*i.e.* the frequency characterising the \mathcal{H}_∞ -norm of the linearised system), and the peak frequency characterising the input SDF, *i.e.* $\bar{\omega}_w = 2\pi/\bar{T}_w$.

7.6.2 On the definition of the set of training trajectories

Given the stochastic nature of the wave process, and once the set of frequencies \mathcal{F} involved in the definition of the corresponding signal generator is selected (following Section 7.6.1), a method to choose a set of training trajectories is required, similarly to the case discussed in Section 7.5.2.

Inspired by the worst-case approach defined for the case of regular wave excitation with stochastic height, the following procedure is proposed. Recall that every initial condition $\xi(0)$ can be written as in Remark 7.1.2, *i.e.* in terms of a set of coefficients $\{\alpha_p, \beta_p\}_{i=1}^f \subset \mathbb{R}$, associated to each harmonic $h_p\omega_0$ involved in the definition of the signal generator. Let $A_p = \sqrt{\alpha_p^2 + \beta_p^2} \in \mathbb{R}^+$, with $p \in \mathbb{N}_f$, be a set of positive real-valued ‘amplitudes’ associated with¹⁷ each harmonic h_p . Then:

17: The use of the term ‘amplitude’ for A_p is justified in Remark 7.6.1.

- ▶ Generate a random set of $N_t \in \mathbb{N}_{\geq 1}$ initial conditions $\Xi = \{\zeta_i\}_{i=1}^{N_t}$ (i.e. wave inputs), according to the SDF S_w characterising the sea state under analysis.
- ▶ Compute the set $\mathcal{A}_p = \{A_p^i\}_{i=1}^{N_t}$, with $p \in \mathbb{N}_f$, for each randomly generated initial condition ζ_i , where A_p^i denotes the amplitude associated with the harmonic $h_p\omega_0$.
- ▶ Select the set of initial conditions Ξ_t that maximise and minimise each \mathcal{A}_p , denoted as ζ_p^{\min} and ζ_p^{\max} , for every $p \in \mathbb{N}_f$. Note that this automatically implies that $2f$ initial conditions are selected (one amplitude maximiser and one minimiser for each harmonic h_p involved in the definition of the signal generator).
- ▶ Compute the set of *training trajectories* using Ξ_t , directly from the definition of the signal generator (7.5), i.e. the set $\{\xi_{\zeta_p^{\min}}, \xi_{\zeta_p^{\max}}\}_{p=1}^f$.

Remark 7.6.1 The method proposed in this section is indeed analogous to the worst-case approach proposed in Section 7.5.2: Note that the value $A_p = \sqrt{\alpha_p^2 + \beta_p^2}$ corresponds to the absolute value of the complex number $(\alpha_p + j\beta_p)e^{h_p\omega_0 t}$, which characterises the entries of the trajectory $\xi(t)$ associated with the harmonic $h_p\omega_0$ (see Remark 7.1.2). In other words, the method outlined in this section retains as training trajectories only those trajectories associated with the maximum and minimum input amplitudes, for each harmonic $h_p\omega_0$, with $p \in \mathbb{N}_f$.

7.6.3 Numerical study

For the remainder of this numerical study of nonlinear model reduction by moment-matching, under irregular wave excitation, an array of two identical spherical heaving point absorber WECs is considered, each device with a radius of 2.5 [m] (as in Section 7.5), in the layout configuration presented in Figure 7.7. The distance between devices is set to one diameter, i.e. $d = 5$ [m].

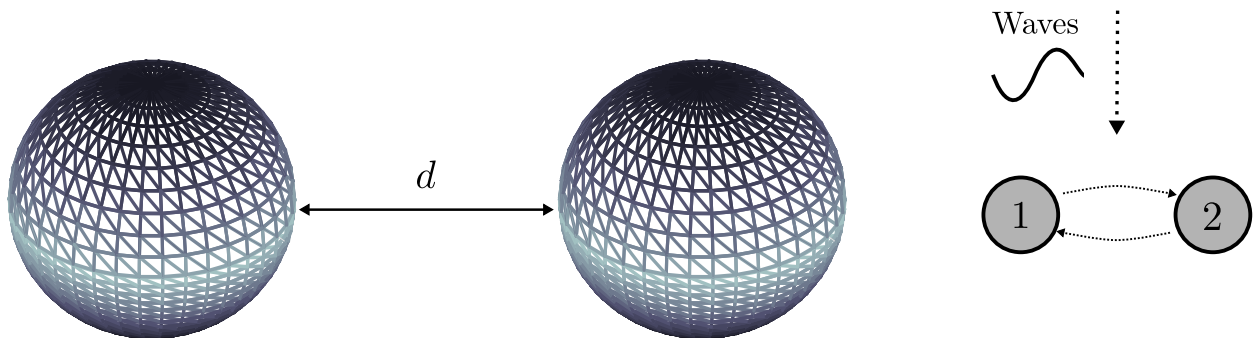


Figure 7.7: Spherical heaving point absorber WEC layout considered for the case of nonlinear model reduction under irregular wave excitation.

The nonlinear mapping f_{nl} , characterising the nonlinear effects for this WEC system, is given by:

$$f_{nl}(z, \dot{z}) = \begin{bmatrix} f_{re}^{nl}(z_1) + f_v(\dot{z}_1) \\ f_{re}^{nl}(z_2) + f_v(\dot{z}_2) \end{bmatrix}, \quad (7.48)$$

where the mappings f_{re}^{nl} and f_v are defined as in equation (10.34), and where $z_1 : \mathbb{R}^+ \rightarrow \mathbb{R}$ and $z_2 : \mathbb{R}^+ \rightarrow \mathbb{R}$ denote the displacement of device 1 and 2, respectively.

Remark 7.6.2 Note that the WEC system, presented in the layout of Figure 7.7, can be regarded as a single-input system: Given the direction of the incident waves, and the underlying symmetry of the layout, the wave excitation force experienced by both devices is indeed the same. In other words, the single-output signal generator defined in equation (7.5) can be utilised to describe f_e . In addition, from now on, the velocity of device 1, *i.e.* \dot{z}_1 , is selected as target output¹⁸.

The numerical generation of the irregular input waves, for this case study, is fully characterised by a JONSWAP spectrum with $\bar{H}_w = 2$ [m] and $\bar{T}_w = 8$ [s]. The peak enhancement factor is set to $\gamma = 3.3$. The corresponding SDF S_w is that illustrated in Figure 7.8.

Following Section 7.6.1, and given the specific SDF selected for the generation of numerical waves, the fundamental frequency is set to a value of $\omega_0 = 0.1$ [rad/s], which facilitates a sufficiently accurate representation of the wave process for the synthesis of the corresponding reduced order model, as demonstrated in the remainder of this section. In addition, the signal generator involved in the definition of the reduced model by moment-matching, *i.e.* equation (7.5), is characterised with the set of frequencies $\mathcal{F} = \{0.8, 2\}$, where, given the selection of $\omega_0 = 0.1$ [rad/s], the set $\mathcal{H} = \{h_1, h_2\} = \{8, 20\}$.

Remark 7.6.3 Note that, as discussed in Section 7.6.1, the selection of the set \mathcal{F} is not arbitrary: 0.8 [rad/s] represents the frequency corresponding with the peak characterising the input SDF (see Figure 7.8), while 2 [rad/s] is the frequency characterising the \mathcal{H}_∞ -norm of the Jacobian linearisation of the WEC system, *i.e.* the resonant frequency corresponding to heave motion.

Remark 7.6.4 With the selection of frequencies in the set \mathcal{F} , the order (dimension) of the reduced model by moment-matching (as in equation (7.22)) is $\nu = 2f = 4$.

18: This is considered to simplify the case study, and focus on the performance of the nonlinear reduction technique. If the wave direction is different, then one can simply apply the extension to MIMO systems presented in Section 7.4.

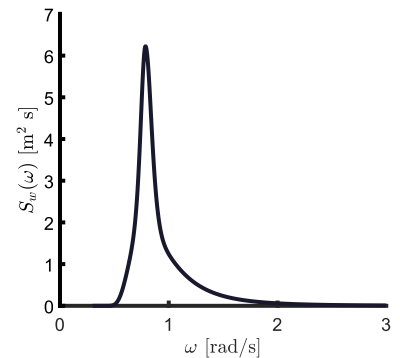


Figure 7.8: SDF corresponding with a JONSWAP spectrum utilised to generate the wave input.

Remark 7.6.5 The generation of waves for the assessment of the proposed strategy, *i.e.* in the simulation stage, is naturally performed using both a smaller value of ω_0 , and a higher number of harmonics, than those specified in the signal generator used to synthesise the moment-based reduced model. This is specified and detailed in the following paragraphs.

Once the set \mathcal{F} is defined, the set of training trajectories, utilised to compute an approximation of the moment of the WEC system at the signal generator (S, L) , is obtained following Section 7.6.2. In particular, a set of $N_t = 50$ random initial conditions is considered¹⁹ to compute the sets $\mathcal{A}_1 = \{A_1^i\}_{i=1}^{50}$ and $\mathcal{A}_2 = \{A_2^i\}_{i=1}^{50}$, associated with the harmonics corresponding with $h_1 = 8$ (0.8 [rad/s]) and $h_2 = 20$ (2 [rad/s]), respectively. These sets are illustrated in Figure 7.9, where the maximum and minimum values for each set \mathcal{A} are denoted using the black color.

19: Computed randomly according to the SDF of Figure 7.8.

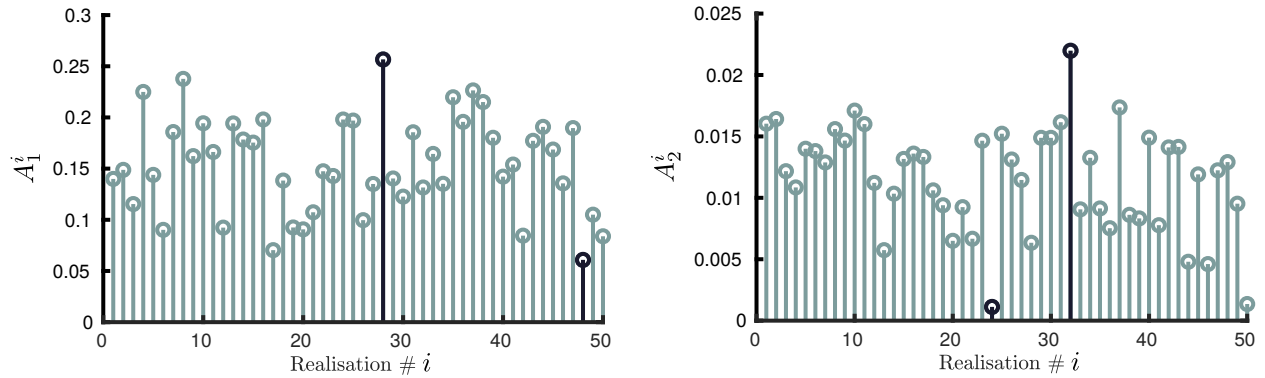


Figure 7.9: Sets of amplitudes $\mathcal{A}_1 = \{A_1^i\}_{i=1}^{50}$ and $\mathcal{A}_2 = \{A_2^i\}_{i=1}^{50}$, associated with the harmonics corresponding with $h_1 = 8$ and $h_2 = 20$, respectively.

With the result presented in Figure 7.9, one can completely characterise the set of training trajectories, *i.e.* the set of trajectories $\{\xi_{\zeta_1^{\min}}, \xi_{\zeta_1^{\max}}, \xi_{\zeta_2^{\min}}, \xi_{\zeta_2^{\max}}\} \subset \mathbb{R}^4$. Finally, aiming to keep the output mapping, characterising the reduced model by moment-matching, to a polynomial form (analogously to the case of regular input waves discussed in Section 7.5), the mapping Ω^k , utilised to compute the approximating moment $h_{\Sigma} \circ \tilde{\pi}$, is chosen as described in Section 7.3.2. In particular, the maximum number of harmonics associated with each frequency in the set \mathcal{F} is set to $k_1^{\max} = 5$ and $k_2^{\max} = 3$, *i.e.* 5 and 3 harmonics associated with the frequencies 0.8 [rad/s] and 2 [rad/s], respectively. Analogously to the regular input case with stochastic height of Figure 7.5, the steady-state output of the nonlinear moment-based reduced order model computed in this section, for the inputs corresponding with each training trajectory, is shown in Figure 7.10 (solid). The target outputs, for each corresponding training trajectory, are computed from the non-parametric WEC system Σ (as in equation (7.1), with a Runge-Kutta method

(time-step of 10^{-4} [s]), and can be appreciated in Figure 7.10 with dashed lines.

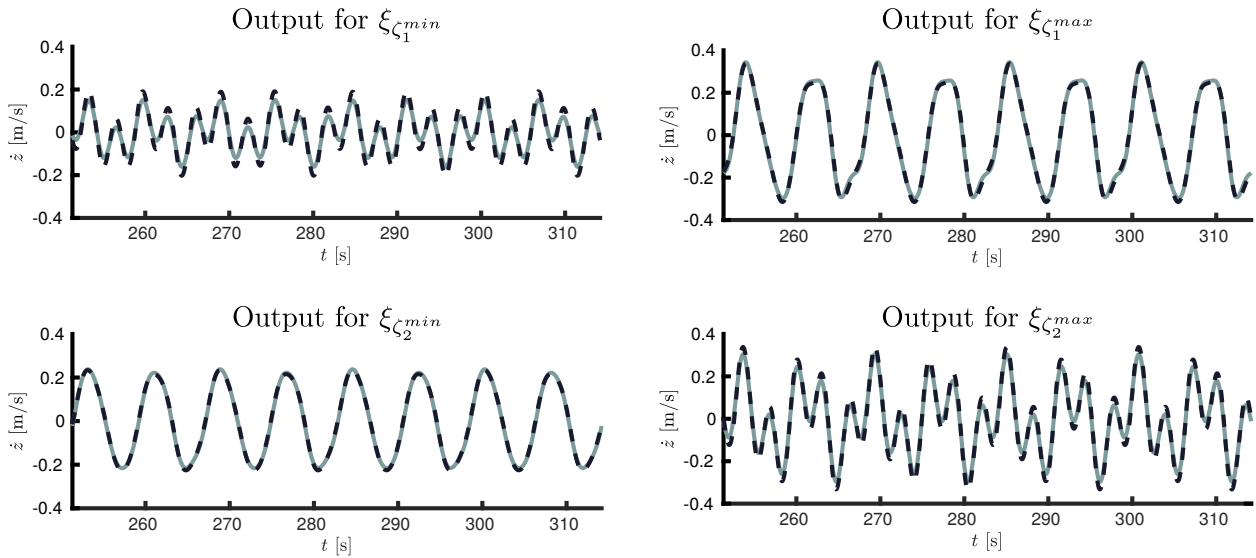


Figure 7.10: Output of the nonlinear moment-based reduced order model under irregular wave excitation (in steady-state, solid), for the inputs corresponding with each training trajectory. The target outputs are denoted with a dashed line.

To begin with the assessment of the resulting reduced order model by moment-matching, Figure 7.11 presents results for a particular (randomly generated) sea state realisation, where the input waves, considered for this simulation stage, are computed as in Remark 2.1.3, using a fundamental frequency $\omega_0 = 0.01$ [rad/s] and 400 harmonics (*i.e.* with a cut-off frequency of 4 [rad/s]). As can be directly appreciated from Figure 7.11, the output of the reduced order model by moment-matching (solid) is effectively able to approximate the target output (dashed), even during the transient period. Note that the output corresponding with the Jacobian linearisation about the origin, *i.e.* linear Cummins' equation (7.10) for the analysed WEC system, is also shown, using a dotted line. A significant overprediction of velocity can be appreciated by the linear model, potentially leading to an overprediction of power production. The NMAPE, computed as in equation (7.46) for 100 [s] of simulation time (as shown in Figure 7.11), is $\approx 4.6\%$ for the nonlinear reduced model computed in this section, and $\approx 40\%$ for the case of the Jacobian linearisation.

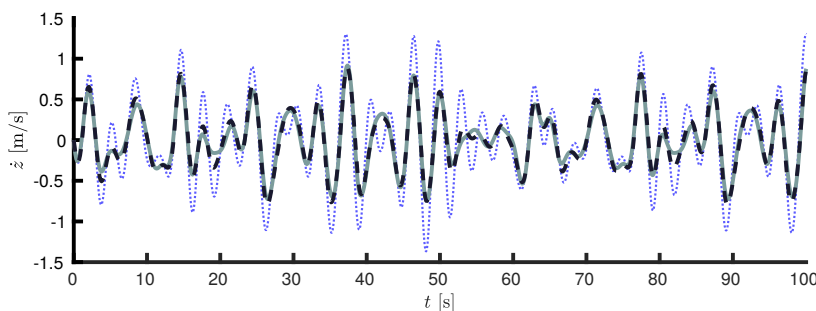


Figure 7.11: Output of the reduced order model by moment-matching (solid) and target motion (dashed), for a randomly generated sea-state realisation, with SDF as in Figure 7.8. The output corresponding with the Jacobian linearisation about the origin is also shown, using a dotted blue line.

A more detailed characterisation of the approximation error can be appreciated in Figure 7.12, where the absolute value of the difference between target and approximating output is shown, for both the reduced model by moment-matching, and the output arising from Jacobian linearisation.

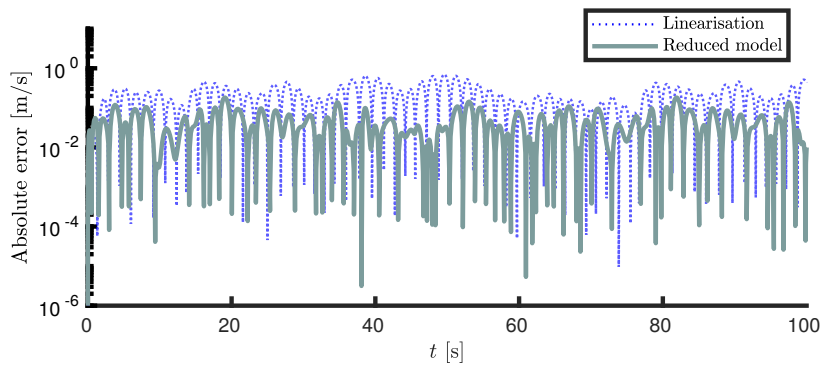


Figure 7.12: Absolute value of the difference between target and approximating output, for the case of irregular wave excitation. The error corresponding with the output of the Jacobian linearisation is also shown.

To provide a conclusive illustration of the capabilities and performance of the moment-based model, the NMAPE for a set of 100 random realisations of wave inputs, according to the JONSWAP spectrum considered (see Figure 7.8), is explicitly shown in Figure 7.13. Note that the mean NMAPE is $\overline{\text{NMAPE}} \approx 4.5\%$, with any individual errors always below 6%, effectively showing the capabilities of the moment-based strategy, presented in this chapter, to approximate the behaviour of a nonlinear WEC system under stochastic irregular wave excitation.

Finally, and aiming to assess the computational features of the nonlinear moment-based reduced model computed in this section, Figure 7.14 shows:

- A) Normalised run-time²⁰ for a parametric nonlinear model of the WEC system, where the convolution operation associated with radiation forces is replaced with a reduced order model (in state-space) of order 8, following the *linear* moment-based strategy presented in Chapter 5 using the same frequency interpolation set considered in this section, *i.e.* $\mathcal{F} = \{0.8, 2\}$.
- B) Normalised run-time for the nonlinear reduced model by moment-matching computed as detailed in this section.

Remark 7.6.6 Note that for case A), detailed above, no ‘nonlinear model reduction’ takes place, but only the *linear* convolution term is replaced with a state-space form to alleviate the computational requirements of the convolution itself (see Remark 7.0.2).

It can be readily appreciated that the reduced nonlinear model, presented in this chapter, computes in an order of magnitude faster than the original parametric model, which can be attributed to

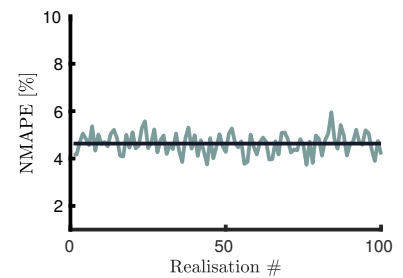


Figure 7.13: NMAPE for 100 realisations of irregular wave inputs according to the SDF presented in Figure 7.8. The average value $\overline{\text{NMAPE}} \approx 4.5\%$ is denoted with a horizontal black line.

²⁰ Ratio between the time required to compute the output of each corresponding model, and the length of the simulation itself. The computations are performed using Matlab®, running on a PC composed of an Intel Core i7-5550U processor with 8GB of RAM.

two main features. Firstly, a smaller order (dimension) is required to represent the behaviour of the WEC system, which effectively leads to faster computations. Secondly, and more importantly, the input-to-state dynamics are *linear*, and only the output mapping presents nonlinear behaviour (which is *static*). In other words, the main computational cost behind the moment-based reduced model is simply solving a set of first order *linear* ordinary differential equations. This feature is indeed appealing from a control/state-estimation perspective, where both efficient and precise models are required.

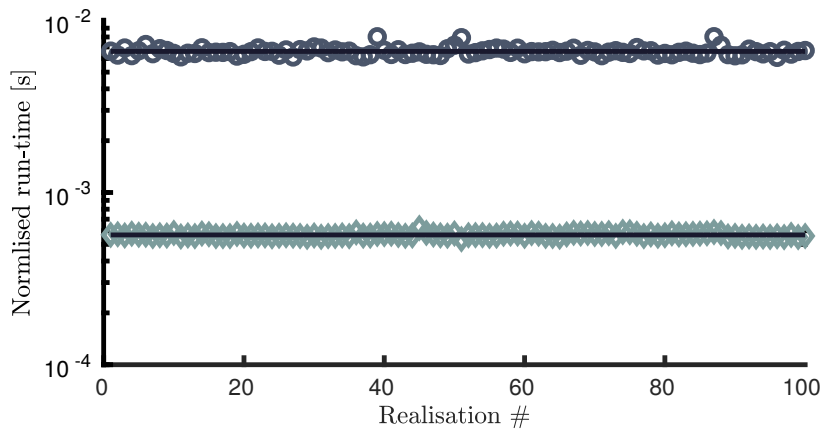


Figure 7.14: Normalised run-time for a parametric nonlinear model of the WEC system (circles, upper trace), where the convolution operation is replaced with a reduced order model (in state-space), and for the nonlinear reduced model by moment-matching computed as detailed in this section (diamonds, lower trace). Mean values are indicated with black horizontal lines.

7.7 Conclusions

This chapter presents a nonlinear model reduction framework for wave energy applications, based on moment-matching techniques, which inherently preserve steady-state response characteristics. This is, to the best of the author's knowledge, the first systematic nonlinear model reduction technique proposed in the wave energy field. The first contribution of this chapter concerns the proof of existence and uniqueness of the corresponding nonlinear moment for the non-parametric WEC system Σ . Secondly, and given the intrinsic necessity of an analytic expression for the corresponding nonlinear moment, a consistent approximation method is presented, by a suitably defined family of functions, in terms of a Galerkin-like methodology. Practical aspects behind this approximation framework are given and discussed, including the connection (and use) of well-established algorithms, to efficiently compute such an approximating moment.

The family of nonlinear models reduced by moment-matching proposed in this chapter is inherently parametric (given specifically in state-space form), and input-to-state *linear*, with any nonlinear behaviour confined to the output mapping only. Moreover, given the nature of the Galerkin-like method proposed to approximate

the corresponding moment, the user can manipulate the degree of complexity of this nonlinear output mapping, hence having full control of the underlying characteristics of the reduced structure.

Two different model reduction cases are clearly defined, in terms of the nature of the input: model reduction of nonlinear WEC systems under regular, and irregular, wave excitation. For WECs under regular wave excitation, both deterministic and stochastic wave height cases are considered. In the deterministic case, the wave height is assumed to be known, and the approximating moment can be characterised in terms of a single trajectory associated with the corresponding signal generator. For the stochastic case, the wave height is only assumed to lie on a certain (given) set, which directly implies that, in principle, an infinite number of inputs needs to be considered within the approximation process. In the light of this, a worst-case approach is proposed to select a finite set of so-called training trajectories, representing the 'limit' cases associated with the set of heights. Case studies are presented for both deterministic and stochastic cases, in terms of a spherical heaving point absorber WEC, including both nonlinear viscous, and hydrostatic restoring effects. It is shown that the nonlinear models reduced by moment-matching, can successfully approximate the nonlinear target WEC system Σ , with a NMAPE always below 4%, clearly showing the capabilities of the strategy.

For the case of irregular waves, given the (fully) stochastic nature of the wave input, methods are provided to select the characteristics describing the wave excitation effects, both in terms of the fundamental frequency, and the harmonics required in the definition of the signal generator. In addition, and analogously to the stochastic regular input case, a methodology to select a set of training trajectories is provided, also based on a worst-case approach. A numerical case study is provided, considering a WEC system composed of two heaving point absorber devices, presenting nonlinear behaviour (nonlinear viscous and hydrostatic restoring effects). The average NMAPE for this case study is $\approx 4.5\%$, effectively showing the capabilities of the proposed moment-based strategy to approximate the behaviour of a nonlinear WEC system under stochastic irregular wave excitation. Finally, a study on the normalised run-time is provided, showing that the presented strategy computes in an order of magnitude less than when solving the nonlinear Cummins' equation (7.1) with a state-space description approximating the non-parametric (convolution) terms.

Part III: Moment-based optimal control

Energy-maximising control for linear SISO WECs

8

Contents of this chapter

8.1	Optimal control problem	180
8.2	Moment-based WEC formulation for optimal control	182
8.3	Energy-maximising moment-based control formulation	185
8.3.1	Handling of state and input constraints	189
8.4	Case study: a CorPower-like device	191
8.5	Receding-horizon optimal control problem	194
8.6	Receding-horizon energy-maximising moment-based control formulation	196
8.6.1	Input representation	196
8.6.2	Receding-horizon controller	199
8.7	Case study revisited: inclusion of estimation and forecasting	200
8.7.1	Sensitivity analysis: Estimation	202
8.7.2	Sensitivity analysis: Forecasting	205
8.8	Conclusions	206

Recall, from Section 2.4, that the equation of motion for a *controlled* WEC, under the assumptions of linear potential flow theory (see Section 2.3.1), can be expressed in terms of *Cummins'* equation (2.20). This equation is recalled below, for a 1-DoF WEC device, for convenience:

$$\Sigma : \begin{cases} \ddot{z} = \mathcal{M}(-k_r * \dot{z} - s_h z + f_e - u), \\ y = \dot{z}, \end{cases} \quad (8.1)$$

where $z : \mathbb{R}^+ \rightarrow \mathbb{R}$ is the displacement, $k_r : \mathbb{R}^+ \rightarrow \mathbb{R}$, $k_r \in L^2(\mathbb{R})$, the radiation impulse response function, $f_e : \mathbb{R}^+ \rightarrow \mathbb{R}$, the wave excitation, and $\mathcal{M} \in \mathbb{R}_{>0}$ is the inverse of the generalised mass matrix of the device (which is simply a scalar in this case). The control input $u : \mathbb{R}^+ \rightarrow \mathbb{R}$, supplied by means of the so-called power take-off system, plays a key role in the optimisation of the operation of wave energy devices, as discussed in Section 3.

In particular, *energy-maximising* control of wave energy converters has been shown to be one of the fundamental contributions towards efficient energy extraction from ocean waves: Optimal control strategies significantly improve maximum time-averaged power extraction from waves, potentially reducing the LCoE, and hence contributing to the roadmap towards successful commercialisation of WECs.

Any energy-maximising control strategy for WECs *must* take into account the inherent physical limitations of both the device itself, and the PTO (actuator) dynamics, such that energy extraction is maximised, while systematically minimising the risk of component damage¹. The above control specifications form the basis for a

1: See section 3.2 for further detail on the definition of these device limitations.

range of studies, which are mostly formulated in terms of an *optimal control problem* subject to both state and input constraints (see Section 3.4).

This chapter presents a solution for the energy-maximising optimal control problem for linear SISO WECs, explicitly using moment-based theory. In particular, this chapter shows that, besides being a powerful model reduction tool (as demonstrated in the strategies proposed in Part II of this thesis), the parameterisation of the steady-state response of a system in terms of moments (*i.e.* in terms of the solution of a specific invariant equation, see Chapter 4), can be explicitly used to transcribe the (infinite-dimensional) energy-maximising control problem to a finite-dimensional optimisation program. To be specific, within the moment-based optimal control framework proposed in this chapter, the energy-maximising OCP can be mapped into a *strictly concave* quadratic program (QP), systematically guaranteeing a unique solution for the energy-maximising control objective, subject to both state and input constraints. This clearly has a strong impact on the practical viability of the proposed moment-based approach, facilitating the utilisation of state-of-the-art QP solvers (such as those described in [207]), providing a computationally efficient energy-maximising control framework. In addition, unlike most of the model-based energy-maximising control strategies reported² for WECs, this moment-based strategy does not require *a-priori* parametric approximation (*i.e.* model reduction) of the radiation force (convolution) term, but actually provides an analytical description of the convolution in the moment-domain³, further reducing the computational burden when solving the target energy-maximising OCP.

In particular, Section 8.1 formalises the definition of the OCP for linear SISO WEC systems, while Section 8.2 presents the fundamental results required to guarantee existence and uniqueness of a moment-based representation of the WEC system. Section 8.3 proposes a moment-based control framework for WECs, in which the target OCP is mapped to a finite-dimensional QP, deriving explicit conditions for the existence of a unique globally optimal control law. The main features and capabilities of the strategy are discussed in Section 8.4, which presents a case study, using the CorPower-like device considered in Chapter 6 (see also Figure 6.2).

Up until this point, the wave excitation force f_e , numerically generated as in Section 2.1.2 (*i.e.* in terms of the so-called fundamental frequency $\omega_0 = 2\pi/T$), is assumed to be *known* for a sufficiently large time period T .

2: See Section 3.4 for a review on the state-of-the-art of optimal control techniques for WECs.

3: This is, indeed, the moment-domain equivalent of the radiation force subsystem Σ_r , defined in Section 5.1.

Remark 8.0.1 Despite the fact that having full (*i.e. instantaneous and future*) knowledge of the excitation input (for a sufficiently large period T) is, in general, not viable in practice, such an assumption does not pose any loss of generality with respect to the theoretical results developed in Sections 8.2 and 8.3: Uniqueness and existence of a moment-based representation and, consequently, a moment-based parameterisation of the OCP can be ensured *independently* of the available knowledge of f_e .

Aiming to drop the assumptions described in Remark 8.0.1 (which may not be applicable in practice), the moment-based framework, proposed in Section 8.3, is appropriately modified to incorporate estimation and forecasting algorithms accordingly⁴, in terms of a *real-time* moment-based *receding-horizon* optimal control framework for WEC systems. To fulfill such an objective, an explicit definition for the receding-horizon energy-maximising OCP for WECs is formalised in Section 8.5. The representation of the wave excitation force input in the moment-domain (as posed in Section 8.2) is adequately adapted to incorporate estimated and forecasted values of f_e in Section 8.6, dropping the requirements stated in Remark 8.0.1, *without affecting* the theoretical results derived in Sections 8.2 and 8.3. In other words, this (subtle) modification maintains the intrinsic computational efficiency and uniqueness of the corresponding solution, facilitated through the convenient parameterisation of the corresponding OCP in the moment-domain.

Using the unknown-input estimation strategy presented in [90] (recalled and explicitly considered in Section 6.5), and the autoregressive (AR) model of [16], the performance of the moment-based receding-horizon strategy is assessed, in Section 8.7, revisiting the case study of Section 8.4 (*i.e.* where a CorPower-like device is considered, and full knowledge of the wave excitation input is available). Furthermore, Section 8.7 provides a sensitivity analysis, addressing the impact of estimation and forecasting errors in the computation of the moment-based optimal control input and, hence, on total energy absorption. Finally, the main conclusions of this chapter are encompassed in Section 8.8.

8.1 Optimal control problem

Recall, from Section 3.2, that WEC optimal control design entails an *energy-maximisation* criterion, where the objective is to maximise the absorbed energy from ocean waves over a finite time interval⁵ $\mathcal{T} = [0, T] \subset \mathbb{R}^+$. To be precise, the useful energy absorbed from incoming waves is converted in the PTO system, and can be directly

4: Unknown-input state-estimation strategies are required to provide *instantaneous* values of f_e , while forecasting techniques are employed to predict *future* wave excitation force within a certain time interval. The reader is referred to Section 3.2.1 for further detail on this topic.

5: Note that there is no loss of generality in considering 0 as initial time.

computed as the time integral of converted (instantaneous) power, *i.e.* this energy-maximising control procedure can be cast as an optimal control problem, with *objective function* $\mathcal{J} : \mathbb{R} \rightarrow \mathbb{R}$, $u \mapsto J(u)$, $u(t) \in \mathbb{R}$, defined as

$$\mathcal{J}(u) = \frac{1}{T} \int_{\mathcal{T}} u(\tau) \dot{z}(\tau) d\tau, \quad (8.2)$$

where $u : \mathcal{T} \rightarrow \mathbb{R}$ denotes the control (PTO) force. As discussed in Section 3.2, the computation of the control law which optimises (8.2) is non-trivial, mainly due to the irregularity of the input (the wave excitation f_e) to the system (see equation (8.1)).

As is well known in the wave energy literature, and is specifically discussed throughout Chapter 3, the unconstrained energy-maximising optimal control law, *i.e.* maximiser of \mathcal{J} in (8.2), often implies unrealistic device motion and excessively high PTO (control) forces, which consign this optimal unconstrained solution to the academic realm, far from being practically viable. Aiming to derive an implementable solution, constraints on both the displacement and velocity of the WEC, z and \dot{z} , and the exerted control force u , need to be considered appropriately. This guarantees that the physical limits associated with device and actuator dynamics (PTO) are consistently respected, while effectively maximising, at the same time, absorbed energy from incoming waves. This set of constraints can be compactly written⁶ as

$$\mathcal{C} : \begin{cases} |z(t)| \leq Z_{\max}, \\ |\dot{z}(t)| \leq \dot{Z}_{\max}, \\ |u(t)| \leq U_{\max}, \end{cases} \quad (8.3)$$

with $t \in \mathcal{T}$, and where $\{Z_{\max}, \dot{Z}_{\max}, U_{\max}\} \subset \mathbb{R}^+$.

Given the control objective function defined in (8.2), the governing dynamics of the WEC in (8.1), and the set of state and input constraints defined in (8.3), the constrained energy-maximising OCP can be posed as

$$\begin{aligned} u^{\text{opt}} &= \arg \max_u \mathcal{J}(u), \\ &\text{subject to:} \\ &\begin{cases} \text{WEC dynamics } \Sigma \text{ (8.1),} \\ \text{state and input constraints } \mathcal{C} \text{ (8.3).} \end{cases} \end{aligned} \quad (8.4)$$

⁶: See also Section 3.2.

8.2 Moment-based WEC formulation for optimal control

As discussed in the case of linear model reduction by moment-matching for WECs, presented in Chapters 5 and 6, moment-based theory is inherently based on the knowledge of a state-space representation of the system under analysis, which is clearly not the case for Cummins' formulation. Analogously to Section 5.1, and aiming to consider the theoretical results discussed in Section 4.1.1 for this 1-DoF WEC case, the equation of motion characterising the WEC system Σ is written using the following equivalent representation:

$$\Sigma : \begin{cases} \dot{w} = Aw + Bv, \\ y = Cw, \end{cases} \quad (8.5)$$

for $t \in \mathbb{R}^+$, where $w(t) = [z(t) \quad \dot{z}(t)]^\top \in \mathbb{R}^2$ contains displacement and velocity for the (single) DoF involved in the equation of motion, and the (constant) matrices $A \in \mathbb{R}^{2 \times 2}$, $B \in \mathbb{R}^2$ and $C^\top \in \mathbb{R}^2$ are defined as

$$A = \begin{bmatrix} 0 & 1 \\ -\mathcal{M}s_h & 0 \end{bmatrix}, \quad B = \begin{bmatrix} 0 \\ \mathcal{M} \end{bmatrix}, \quad C = \begin{bmatrix} 0 \\ 1 \end{bmatrix}^\top. \quad (8.6)$$

The 'input' function $v : \mathbb{R}^+ \rightarrow \mathbb{R}$, is defined as

$$v = f_e - k_r * Cw - u. \quad (8.7)$$

Remark 8.2.1 In contrast to the model reduction by moment-matching case, the input v now includes the external PTO (control) force to be optimally designed, using the system-theoretic definition of moments.

Within the moment-based formulation, recalled in Chapter 4, the mappings corresponding to both external inputs, *i.e.* the wave excitation f_e , and control force u , are written in terms of an autonomous single-output signal generator (analogously to the case of equation (4.3)), *i.e.* the set of differential equations

$$\begin{aligned} \dot{\xi} &= S\xi, \\ f_e &= L_e\xi, \\ u &= L_u\xi, \end{aligned} \quad (8.8)$$

for $t \in \mathbb{R}^+$, with $\xi(t) \in \mathbb{R}^\nu$, $S \in \mathbb{R}^{\nu \times \nu}$ and $L^\top \in \mathbb{R}^\nu$. Recall that a set of standing assumptions on the nature of the signal generator (*i.e.* Assumptions 4.1.1 and 4.1.2), are required to have a well-posed

system-theoretic definition of moments. These are discussed, for the WEC control case, in the following paragraphs.

Assumption 4.1.2 is ensured by recalling, from Section 2.1.2, that ocean waves are commonly generated as a finite sum of harmonics of a (sufficiently small) fundamental frequency ω_0 . To be precise, let the finite-set $\mathcal{F} = \{p\omega_0\}_{p=1}^f \subset \mathbb{R}^+$, with $f \in \mathbb{N}_{\geq 1}$. The dynamic matrix S in equation (8.8) is defined in block-diagonal form as

$$S = \bigoplus_{p=1}^f \begin{bmatrix} 0 & p\omega_0 \\ -p\omega_0 & 0 \end{bmatrix}, \quad (8.9)$$

where $\nu = 2f$, and hence $\lambda(S) = (j\mathcal{F}) \cup (-j\mathcal{F}) \subset \mathbb{C}^0$.

Remark 8.2.2 For this moment-based WEC formulation for optimal control, the definition of the matrix S , associated with the signal generator (8.8), explicitly considers an (increasing) number of harmonics of the fundamental frequency ω_0 . This contrasts with the model reduction by moment-matching cases presented in Chapters 5 and 6, where the signal generator includes a set of interpolation frequencies, which does not necessarily correspond with any (pre-defined) fundamental frequency.

Remark 8.2.3 From now on, and aiming to simplify the notation used throughout the theoretical results posed in the upcoming sections, it is assumed that the moment-domain equivalent L_e , characterising the wave excitation f_e as in equation (8.8) is known, *i.e.* full knowledge of f_e is available, in the spirit of the separation principle [75]. Note that this assumption is dropped later on, in Section 8.6, where both estimated and forecasted values of the wave excitation effects are explicitly considered in the control formulation. In addition, it is important to document the maximum achievable control performance in the absence of estimation/forecasting errors.

With respect to Assumption 4.1.1, and without any loss of generality, the initial condition on the signal generator is chosen as $\xi(0) = \varepsilon_\nu \in \mathbb{R}^\nu$. Given that, in contrast to the model reduction case of Chapter 5, the input to the WEC system is now composed of a (linear) combination of both the wave excitation force f_e and the control law u , the following assumption is required to have a well-posed system-theoretic definition of moments.

Assumption 8.2.1 The pair of matrices $(S, L_e - L_u)$ is observable.

The objective is now to compute a moment-based description for one of the key variables in the optimal control problem defined in equation (8.4): the velocity \dot{z} of the WEC device to be controlled.

Adopting similar theoretical arguments to those in Section 5.1, the moment of system Σ at the signal generator $(S, L_e - L_u)$ can be computed by solving a specific Sylvester equation, which can be written, for the controlled WEC case, as

$$A\Pi + B(L_e - L_u - \underline{K}_r) = \Pi S, \quad (8.10)$$

where $\Pi \in \mathbb{R}^{2 \times \nu}$ and $\underline{K}_r^\top \in \mathbb{R}^\nu$ is the moment-domain equivalent of the radiation convolution term (see Proposition 5.1.1).

Remark 8.2.4 If Assumption 8.2.1 holds, the definition of the moment-domain equivalent of the velocity is well-posed, and its computation can be directly expressed in terms of the solution of (8.10) as $\underline{\dot{z}} = C\Pi$.

The Sylvester equation posed in (8.10) can be solved analogously to equation (5.7). In particular, using the results of Propositions⁷ 5.1.2 and 5.1.3, the following proposition, guaranteeing existence and uniqueness of $\underline{\dot{z}}$ for the WEC under control conditions, can be straightforwardly stated.

7: Note that the result of Proposition 5.1.2 holds independently of the definition of the output vectors of the signal generator, i.e. it can be directly applied for the WEC under controlled conditions.

Proposition 8.2.1 *Suppose Assumption 8.2.1 and condition (5.16) hold. Then, the moment-domain equivalent of the output y of system (8.5) (the velocity of the device \dot{z}) can be uniquely determined as*

$$\underline{\dot{z}} = (L_e - L_u)\Phi_{\mathcal{R}}^\top, \quad (8.11)$$

where the matrix $\Phi_{\mathcal{R}} \in \mathbb{R}^{\nu \times \nu}$ is defined as

$$\begin{aligned} \Phi_{\mathcal{R}} &= (\mathbb{I}_\nu \otimes C)\Phi^{-1}(\mathbb{I}_\nu \otimes -B), \\ \Phi &= (S \hat{\oplus} A) + \mathcal{R}^\top \otimes -BC, \end{aligned} \quad (8.12)$$

with $\Phi \in \mathbb{R}^{2\nu \times 2\nu}$, and the block-diagonal operator $\mathcal{R} \in \mathbb{R}^{\nu \times \nu}$, characterising the radiation effects in the moment-domain, is given by

$$\mathcal{R} = \bigoplus_{p=1}^f \begin{bmatrix} r_{p\omega_0} & m_{p\omega_0} \\ -m_{p\omega_0} & r_{p\omega_0} \end{bmatrix}, \quad (8.13)$$

where the set of parameters $\{r_{p\omega_0}, m_{p\omega_0}\}_{p=1}^f \subset \mathbb{R}$ is defined as in equation (5.10).

Proof. Recall that, under Assumption 8.2.1, the moment of system Σ at the signal generator $(S, L_e - L_u)$ is $\underline{\dot{z}} = C\Pi$. Then, given that condition (5.16) holds by hypothesis, the result posed in equation (8.11) follows directly from Proposition 5.1.3, with an appropriate change of the moment-domain equivalent associated with radiation

effects, *i.e.* the matrix \mathcal{R} described in (8.13). \square

Remark 8.2.5 As previously discussed in Section 5.1, the condition stated in (5.16) (which guarantees existence and uniqueness of the moment-domain equivalent $\dot{\underline{Z}}$) always holds for the WEC device case, as a result of the internal stability of (8.5) (see Section 2.4).

Remark 8.2.6 The computation of the moment of system Σ at $(S, L_e - L_u)$, which directly provides a parameterisation of the state-variables in terms of moments, can be done without the necessity of an a-priori state-space representation of the radiation system Σ_r , described by the impulse response function k_r . In other words, and in contrast to MPC algorithms, the parameterisation of the state-variables can be performed using the (non-parametric) integro-differential equation (8.1) directly, without the necessity of ‘augmenting’ system Σ^8 .

8: See Section 2.4 for further detail.

Using the result posed in Proposition 8.2.1 as stepping stone, the energy-maximising OCP, posed in equation (8.4), can be solved using a moment-based representation, by taking explicit advantage of the steady-state response parameterisation provided by the corresponding system-theoretic definition of moments. This is explicitly addressed in Section 8.3.

8.3 Energy-maximising moment-based control formulation

Recall that the objective function, involved in the definition of the energy-maximising OCP (8.4), explicitly depends on the velocity \dot{z} of the WEC system. The following proposition makes use of the moment-domain equivalent of such a quantity, showing that the target optimal control problem (8.4) (which is originally defined on an infinite-dimensional space), can be parameterised in terms of moments.

Proposition 8.3.1 *Suppose Assumption 8.2.1 and condition (5.16) hold. Then the objective function \mathcal{J} defined in (8.2), *i.e.* absorbed energy from ocean waves over the time period $\mathcal{T} = [0, T] \subset \mathbb{R}^+$, where $T = 2\pi/\omega_0$, can be computed in the moment-domain as*

$$\mathcal{J} \mapsto \frac{1}{2} \dot{\underline{Z}} L_u^T, \quad (8.14)$$

where $\dot{\underline{Z}}$ denotes the moment-domain equivalent of the velocity of the device, as in Proposition 8.2.1.

Proof. Under Assumption 8.2.1 and condition (5.16), the objective function \mathcal{J} , which is defined over the time period $\mathcal{T} = [0, T]$, can be expressed in terms of $\dot{\underline{Z}}$ and L_u as

$$\begin{aligned}\mathcal{J} &\mapsto \frac{1}{T} \int_{\mathcal{T}} \left(\dot{\underline{Z}} \xi(\tau) \right) \left(L_u \xi(\tau) \right) d\tau \\ &= \frac{1}{T} \dot{\underline{Z}} \left[\int_{\mathcal{T}} \xi(\tau) \xi^\top(\tau) d\tau \right] L_u^\top, \\ &= \frac{1}{T} \dot{\underline{Z}} \mathcal{I} L_u^\top.\end{aligned}\quad (8.15)$$

Note now that, similarly to equation (5.12), the vector $\xi(t) \in \mathbb{R}^\nu$ can be conveniently expanded as

$$\xi(t) = e^{St} \varepsilon_\nu = \sum_{p=1}^f e_p^f \otimes \begin{bmatrix} p\xi^+(t) \\ p\xi^-(t) \end{bmatrix}, \quad (8.16)$$

where the mappings ${}^p\xi$ are defined as

$$\begin{aligned}{}^p\xi^+ : \mathbb{R}^+ &\rightarrow \mathbb{R}, & t &\mapsto \cos(p\omega_0 t), \\ {}^p\xi^- : \mathbb{R}^+ &\rightarrow \mathbb{R}, & t &\mapsto -\sin(p\omega_0 t).\end{aligned}\quad (8.17)$$

The matrix $\mathcal{I} \in \mathbb{R}^{\nu \times \nu}$ is symmetric, *i.e.* $\mathcal{I} = \mathcal{I}^\top$, and is entirely composed of inner-product operations defined on the space $L^2(\mathcal{T})$. In particular, the following operations can be found in the main diagonal of \mathcal{I} :

$$\begin{aligned}\langle {}^p\xi^+, {}^p\xi^+ \rangle &= \int_{\mathcal{T}} \cos^2(p\omega_0 \tau) d\tau = \frac{T}{2}, \\ \langle {}^p\xi^-, {}^p\xi^- \rangle &= \int_{\mathcal{T}} \sin^2(p\omega_0 \tau) d\tau = \frac{T}{2},\end{aligned}\quad (8.18)$$

for all $p \in \mathbb{N}_f$, while, outside the main diagonal, the entries of the matrix \mathcal{I} are given by

$$\begin{aligned}\langle {}^p\xi^+, {}^q\xi^+ \rangle &= \int_{\mathcal{T}} \cos(p\omega_0 \tau) \cos(q\omega_0 \tau) d\tau = 0, \\ \langle {}^p\xi^+, {}^q\xi^- \rangle &= - \int_{\mathcal{T}} \cos(p\omega_0 \tau) \sin(q\omega_0 \tau) d\tau = 0, \\ \langle {}^p\xi^-, {}^q\xi^+ \rangle &= - \int_{\mathcal{T}} \sin(p\omega_0 \tau) \cos(q\omega_0 \tau) d\tau = 0, \\ \langle {}^p\xi^-, {}^q\xi^- \rangle &= \int_{\mathcal{T}} \sin(p\omega_0 \tau) \sin(q\omega_0 \tau) d\tau = 0,\end{aligned}\quad (8.19)$$

for all $p \neq q$, $\{p, q\} \subset \mathbb{N}_f$. Clearly, from both equations (8.18) and (8.19), the matrix \mathcal{I} , directly involved in the definition of \mathcal{J} in the moment-domain (*i.e.* equation (8.15)), is such that $\mathcal{I} = (T/2)\mathbb{I}_\nu$, which automatically proves the claim. \square

Using the result of Proposition (8.3.1), the optimal control problem

of (8.4) can be fully written using moments. In particular, the following result considers the unconstrained version of (8.4), *i.e.* without considering state and input constraints.

Proposition 8.3.2 Consider the unconstrained⁹ OCP (8.4) and suppose Assumption 8.2.1 and condition (5.16) hold. Then, the optimal control law u^{opt} that maximises the objective function \mathcal{J} over the time period \mathcal{T} , can be computed in the moment-domain as the solution of the QP problem

$$\begin{aligned} u^{opt} &= L_u^{opt} \xi, \\ L_u^{opt} &= \arg \max_{L_u^T \in \mathbb{R}^\nu} -\frac{1}{2} L_u \Phi_{\mathcal{R}}^T L_u^T + \frac{1}{2} L_e \Phi_{\mathcal{R}}^T L_u^T. \end{aligned} \quad (8.20)$$

9: The term unconstrained here refers to optimal control problem (8.4) without consideration of the set of state and input constraints \mathcal{C} .

Proof. Consider the result of Proposition 8.3.1 (*i.e.* equation (8.14)). Then, given that Assumption 8.2.1 and condition (5.16) hold by hypothesis, the claim follows by simply replacing $\dot{\underline{z}}$ according to equation (8.11). \square

The result of Proposition 8.3.2 explicitly shows that the computation of an energy-maximising control law, using the proposed moment-based framework, boils down to solving a QP problem. This QP formulation can be solved efficiently *if and only if* equation (8.20) has a unique global maximiser, *i.e.* the problem is *strictly concave*. Existence and uniqueness of a global maximiser, for this moment-based approach, is explicitly guaranteed, as detailed in Proposition 8.3.3 and Corollary 8.3.4, in the following paragraphs.

Proposition 8.3.3 Let $T_p = A - B(r_{p\omega_0} + jm_{p\omega_0})C$, for all $p \in \mathbb{N}_f$. The QP optimisation problem defined in (8.20) has a unique global solution if and only if

$$\lambda(\Re\{C(jp\omega_0\mathbb{I}_2 - T_p)^{-1}B\}) \subset \mathbb{R}^+, \quad (8.21)$$

for all $p \in \mathbb{N}_f$.

Proof. This proof can be started by noting that (8.20) has a unique global solution if and only if the symmetric part of $\Phi_{\mathcal{R}}$ is positive-definite¹⁰, *i.e.* $\lambda(\mathcal{H}\{\Phi_{\mathcal{R}}\}) \subset \mathbb{R}^+$. Following the proofs of Propositions 5.1.2 and 8.2.1, note that one can always write the matrix $\Phi_{\mathcal{R}}$ in a block-diagonal form, *i.e.* $\Phi_{\mathcal{R}} = \bigoplus_{p=1}^f \Phi_{\mathcal{R}_p}$ with each p -block defined as

$$\Phi_{\mathcal{R}_p} = -CW^{-1} \left({}^W\Phi_p \right)^{-1} WB, \quad (8.22)$$

10: The reader is referred to, for instance, [207]

where the matrices W and ${}^W\Phi_p$ are defined as in Proposition 5.1.2. A direct algebraic manipulation of (8.22) yields

$$\Phi_{\mathcal{R}_p} = \begin{bmatrix} \Re\{\psi_p\} & \Im\{\psi_p\} \\ -\Im\{\psi_p\} & \Re\{\psi_p\} \end{bmatrix}, \quad (8.23)$$

where $\psi_p \in \mathbb{C}^{2 \times 2}$ is defined as

$$\psi_p = C(jp\omega_0\mathbb{I}_2 - T_p)^{-1}B. \quad (8.24)$$

It follows from the particular structure of the matrix $\Phi_{\mathcal{R}_p}$ that $\lambda(\mathcal{H}\{\Phi_{\mathcal{R}_p}\}) = \lambda(\Re\{\psi_p\})$ for all $p \in \mathbb{N}_f$, which proves the claim. \square

Proposition 8.3.3 gives explicit conditions for the well-posedness of the QP optimisation problem of (8.20). Nevertheless, note that the specific role of each parameter (or quantity) characterising the equation of motion (8.1), in the existence of a unique global solution, is not immediately clear from condition (8.21). This is explicitly addressed in the following corollary, where a simple relation is given in terms of the radiation damping characteristics associated with the WEC device under analysis.

Corollary 8.3.4 *Condition (8.21) holds if and only if $r_{p\omega_0} > 0$, for all $p \in \mathbb{N}_f$.*

Proof. Note that, using well-known matrix identities¹¹, the inverse of the matrix $(jp\omega_0\mathbb{I}_2 - T_p) \in \mathbb{C}^{2 \times 2}$ in (8.21) can be computed as

$$(jp\omega_0\mathbb{I}_2 - T_p)^{-1} = \frac{-\det(T_p)T_p^{-1} + jp\omega_0\mathbb{I}_2}{\det(T_p) - p^2\omega_0^2 - jp\omega_0\text{tr}(T_p)}. \quad (8.25)$$

Given the structure of the matrices involved, one can directly verify that $\det(T_p) \in \mathbb{R}$, $CT_p^{-1}B = 0$ and

$$\text{tr}(T_p) = -r_{p\omega_0}\mathcal{M} + jm_{p\omega_0}\mathcal{M}, \quad (8.26)$$

for all $p \in \mathbb{N}_f$. Then, each of the matrices $\Re\{\psi_p\}$, with ψ_p defined as in equation (8.24), become

$$\begin{aligned} \Re\{\psi_p\} &= -\frac{p^2\omega_0^2 CB \Re\{\text{tr}(T_p)\}}{\alpha_p^2 + \beta_p^2} \mathbb{I}_2, \\ \text{with } \alpha_p &= \det(T_p) - p^2\omega_0^2 + \Im\{\text{tr}(T_p)\}, \\ \beta_p &= p\omega_0 \Re\{\text{tr}(T_p)\}, \end{aligned} \quad (8.27)$$

noting that $CB = \mathcal{M}$. It is then clear that $\lambda(\Re\{\psi_p\}) \subset \mathbb{R}^+$ if and only if

$$\mathcal{M}^2 p^2 \omega_0^2 r_{p\omega_0} > 0 \quad (8.28)$$

11: See, for instance, [226].

which holds if and only if $r_{p\omega_0} > 0$, for all $p \in \mathbb{N}_f$, proving the claim. \square

Corollary 8.3.4 states that the existence of a unique globally optimal energy-maximising solution for the moment-based QP problem (8.20) is completely determined by one particular quantity: the radiation damping of the device evaluated at the frequencies induced by the eigenvalues of the matrix S , *i.e.* at the set $\mathcal{F} = \{p\omega_0\}_{p=1}^f$, characterising the signal generator (8.8).

Remark 8.3.1 $r_{p\omega_0} = B(p\omega_0) > 0$, for all $p \in \mathbb{N}_f$, as a consequence of the passivity property associated with radiation effects (see Section 2.4). In other words, the moment-based QP problem, defined in Proposition 8.3.2 *always has a unique global maximiser* for the WEC case.

Remark 8.3.2 The existence and uniqueness of an energy-maximising global solution allows the utilisation of well-known and efficient quadratic programming solvers (see for instance, [207]). This, naturally, facilitates the computation of an optimal control input in a computationally efficient manner, *i.e.* achieving *real-time* performance. This is further discussed in Sections 8.4 and 8.6.

8.3.1 Handling of state and input constraints

Using the moment-based representations developed throughout Section 8.3, the set of state and input constraints (8.3) can be mapped using their respective moment-domain equivalents¹², as

$$\mathcal{C} : \begin{cases} |z(t)| \leq Z_{\max}, \\ |\dot{z}(t)| \leq \dot{Z}_{\max}, \\ |u(t)| \leq U_{\max}, \end{cases} \mapsto \begin{cases} |\dot{Z}S^{-1}\xi(t)| \leq Z_{\max}, \\ |\dot{Z}\xi(t)| \leq \dot{Z}_{\max}, \\ |L_u\xi(t)| \leq U_{\max}. \end{cases} \quad (8.29)$$

Let $\mathcal{T}_c = \{t_i\}_{i=1}^{N_c} \subset \mathcal{T} \subset \mathbb{R}^+$, be a finite set of (specified) uniformly-spaced time instants, with $N_c \in \mathbb{N}_{\geq 1}$. The constraints defined in (8.29) can be enforced at the set \mathcal{T}_c , *i.e.* using a collocation approach, through the definition of the following matrices. Let $\Lambda \in \mathbb{R}^{\nu \times N_c}$ and $\Upsilon \in \mathbb{R}^{\nu \times 2N_c}$ be defined as

$$\Lambda = \begin{bmatrix} \xi(t_1) & \dots & \xi(t_{N_c}) \end{bmatrix}, \quad \Upsilon = \begin{bmatrix} \Lambda & -\Lambda \end{bmatrix}. \quad (8.30)$$

Finally, one can formulate a moment-based energy-maximising constrained optimal control solution for WECs in terms of an inequality-constrained concave QP problem, as follows.

12: Note that the moment-domain equivalent of the displacement z can be expressed as $\dot{Z}S^{-1}$, following the result of Proposition 5.2.1.

Proposition 8.3.5 Consider the state and input constrained OCP (8.4) and suppose Assumption 8.2.1 and condition (5.16) hold. Then, the optimal control law u^{opt} , that maximises the objective function \mathcal{J} over the time period \mathcal{T} , can be computed in the moment-domain as the solution of the inequality-constrained concave QP problem

$$\begin{aligned} u^{opt} &= L_u^{opt} \xi, \\ L_u^{opt} &= \arg \max_{L_u^T \in \mathbb{R}^\nu} -\frac{1}{2} L_u \Phi_{\mathcal{R}}^T L_u^T + \frac{1}{2} L_e \Phi_{\mathcal{R}}^T L_u^T, \\ &\text{subject to:} \\ &L_u \mathcal{A}_z \leq \mathcal{B}_z, \\ &L_u \mathcal{A}_{\dot{z}} \leq \mathcal{B}_{\dot{z}}, \\ &L_u \mathcal{A}_u \leq \mathcal{B}_u, \end{aligned} \quad (8.31)$$

where the matrices $\{\mathcal{A}_z, \mathcal{A}_{\dot{z}}, \mathcal{A}_u\} \subset \mathbb{R}^{\nu \times 2N_c}$ and $\{\mathcal{B}_z, \mathcal{B}_{\dot{z}}, \mathcal{B}_u\} \subset \mathbb{R}^{1 \times 2N_c}$ are defined as

$$\begin{aligned} \mathcal{A}_z &= -\Phi_{\mathcal{R}}^T S^{-1} \Upsilon \\ \mathcal{B}_z &= Z_{max} \mathbf{1}_{1 \times 2N_c} + L_e \mathcal{A}_z, \\ \mathcal{A}_{\dot{z}} &= -\Phi_{\mathcal{R}}^T \Upsilon, \\ \mathcal{B}_{\dot{z}} &= \dot{Z}_{max} \mathbf{1}_{1 \times 2N_c} + L_e \mathcal{A}_{\dot{z}}, \\ \mathcal{A}_u &= \Upsilon, \\ \mathcal{B}_u &= U_{max} \mathbf{1}_{1 \times 2N_c}. \end{aligned} \quad (8.32)$$

Proof. Note that, under the set of assumptions considered in this proposition, equation (8.31) follows directly from Proposition 8.3.2. With respect to the incorporation of the set of state and input constraints, defined in (8.29), consider first the constraint associated with the control input and note that

$$|L_u \xi(t)| \leq U_{max} \Rightarrow -U_{max} \leq L_u \xi(t) \leq U_{max}. \quad (8.33)$$

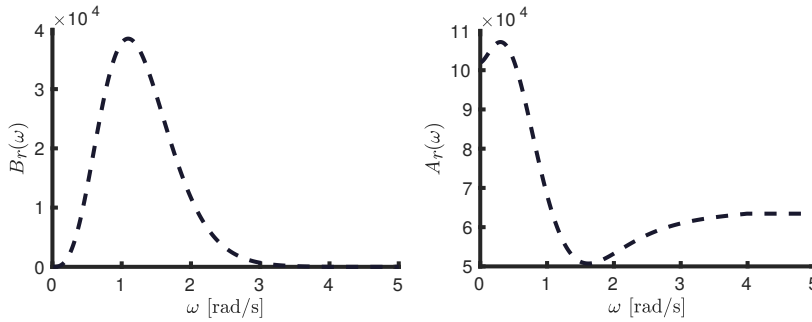
Equation (8.33), enforced at the set of collocation instants \mathcal{T}_c , can be straightforwardly written in terms of the matrix Υ defined in (8.30), i.e.

$$L_u \Upsilon \leq U_{max} \mathbf{1}_{1 \times 2N_c}. \quad (8.34)$$

from where both matrices \mathcal{A}_u and \mathcal{B}_u follow directly. Finally, the claim of this proposition follows by writing the set of constraints associated with displacement and velocity, defined in (8.29), as in equation (8.34), i.e. in terms of the matrix Υ . \square

8.4 Case study: a CorPower-like device

To demonstrate the performance of the moment-based energy-maximising control proposed in Section 8.3, the CorPower-like wave energy device, presented in Figure 6.2, is considered, and constrained to oscillate in heave¹³ (translational motion). The corresponding hydrodynamic characteristics, in terms of $B_r(\omega)$ and $A_r(\omega)$, are presented below, in Figure 8.1.



13: Note that this is, effectively, the DoF from where mechanical energy is converted.

Figure 8.1: Hydrodynamic coefficients $B_r(\omega)$ and $A_r(\omega)$ for the CorPower-like device, constrained to oscillate in heave.

In the remainder of this case study, two types of input waves are considered: regular (numerically generated as in Section 2.1.1), and irregular (numerically generated as in Section 2.1.2) inputs. Though the former case does not represent a realistic sea-state, it is useful to evaluate the control strategy in terms of well-known analytical results, which are directly connected to the underlying theory of impedance-matching-based control (see Section 3.1).

From now on, to fully expose the capabilities of the moment-based strategy to optimise energy absorption in constrained scenarios, the set of state and input limitations $\{Z_{\max}, \dot{Z}_{\max}, U_{\max}\} \subset \mathbb{R}^+$ is defined such that,

$$Z_{\max} = 2 \text{ [m]}, \quad \dot{Z}_{\max} = 2 \text{ [m/s]}, \quad U_{\max} = 1 \times 10^6 \text{ [N]}. \quad (8.35)$$

Following the arguments previously stated in the current section, the performance assessment of the presented moment-based strategy initially considers the case of regular waves, taking into consideration both state and input constraints. The reader is reminded that, as discussed in Section 3.2, the necessity of considering motion limitations stems from the fact that the unconstrained energy-maximising optimal solution often requires unrealistic values for the physical variables of the analysed WEC system, *i.e.* displacement, velocity, and applied control force.

Figure 8.2 illustrates the (steady-state) WEC motion **(a)** under optimally controlled conditions, along with the corresponding moment-based energy-maximising control law **(b)**. The input wave is fully

characterised by height $H_w = 2$ [m] and period $T_w = 8$ [s]. The state and input constraints are set as in equation (8.35).

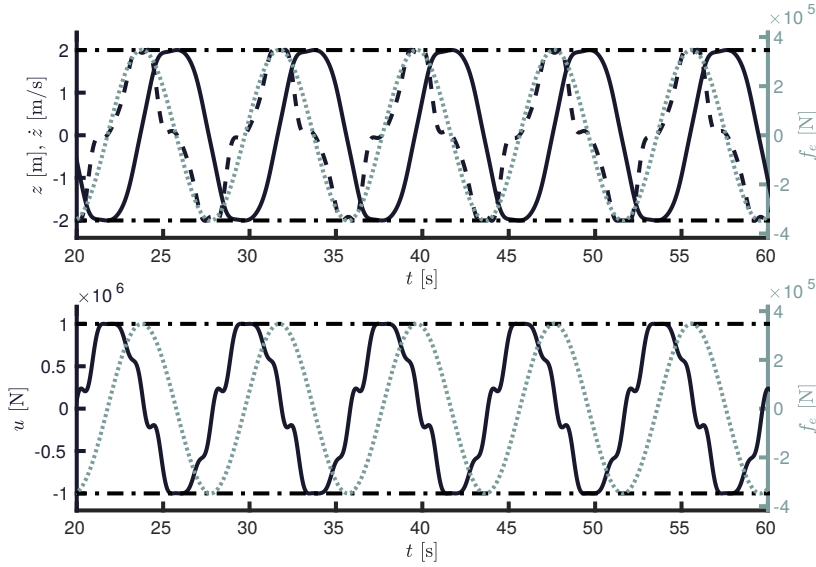


Figure 8.2: Motion and control results for regular wave excitation. **(a)** shows displacement (left axis, solid), velocity (left axis, dashed) and wave excitation force input (right axis, dotted), for the WEC system. **(b)** presents the corresponding moment-based control input (left axis, solid), used to elicit the corresponding motion results, along with the wave excitation force input (right axis, dotted). The horizontal dash-dotted lines represent constraint values.

Some key aspects can be immediately appreciated from the results presented in Figure 8.2. To begin with, it is straightforward to check that both state and input constraints are being consistently respected, illustrating the capability of the moment-based strategy to maximise energy absorption while simultaneously respecting the inherent physical limitations of the WEC system. From Figure 8.2 **(a)**, a particular aspect, noteworthy of special attention, is that (even in this fully constrained case) the velocity of the device under optimal control conditions remains ‘in-phase’¹⁴ with the wave excitation input, agreeing with well-known results for unconstrained energy absorption, presented in Section 3.1. Figure 8.2 **(b)** presents the control force computed with the presented moment-based strategy, used to elicit the corresponding motion results, along with the (regular) wave excitation input. Note that the control force is ‘shifted’ by $\approx \pi/2$ [rad] with respect to f_e , also agreeing with the theoretical (unconstrained maximum) energy absorption conditions, presented in Section 3.1.

Remark 8.4.1 Note that, though the regular wave excitation input f_e is composed of a single frequency component, *i.e.* the fundamental frequency $\omega_0 = 2\pi/T_w$, the control input u (for this constrained control case) is allowed to be composed of $f > 1$ (f integer) harmonics of ω_0 , as detailed in the signal generator of equation (8.8). The output vector L_e , fully characterising the regular input f_e , is simply completed with zeros accordingly¹⁵.

Remark 8.4.2 The selection of f in (8.8) determines the so-called *cut-off frequency*, *i.e.* the highest harmonic $f\omega_0$ present

14: Let $f(t) \in \mathbb{R}$ and $g(t) \in \mathbb{R}$ be time-traces. From now on, the term ‘in-phase’ is used to denote that $f(t)$ and $g(t)$ are synchronised in terms of *instantaneous* phase.

15: Note that this is indeed an inclusion map [226]. Though not further discussed throughout this chapter, this inclusion mapping is a stepping stone for the nonlinear moment-based technique presented in this thesis, and is formalised accordingly in Chapter 11.

in the definition of the signal generator (largest element of the set $\mathcal{F} = \{p\omega_0\}_{p=1}^f$). For this regular wave input case, it is found (using numerical simulation) that no significant improvement in terms of energy absorption can be achieved beyond a cut-off frequency of 6 [rad/s] (which corresponds with $f = 8$ in (8.8)).

In the remainder of this section, irregular waves, generated stochastically from a JONSWAP spectrum (see Section 2.1.2), are considered. The corresponding SDF S_w is fully characterised by a significant wave height \bar{H}_w of 2 [m], varying peak period $\bar{T}_w \in [5, 12]$ [s], and peak shape parameter $\gamma = 3.3$. The total time-length (fundamental period) of each wave record is set to of $T = 120$ [s]. The corresponding spectral density functions are illustrated, for reference, in Figure 8.3. Since the waves are generated from sets of random amplitudes (see Remark 2.1.3), it is found that a mean of ≈ 40 simulations (per sea state) is necessary to obtain statistically consistent performance results for the moment-based controller presented in this chapter. Following the same argument as for the regular input case (see Remark 8.4.2), the cut-off frequency is also selected as 6 [rad/s].

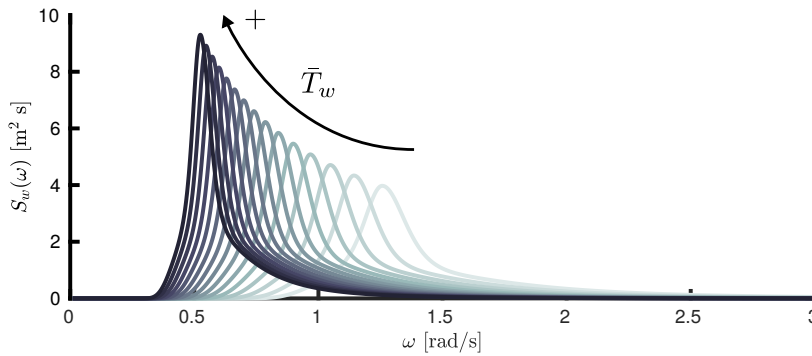


Figure 8.3: Spectral density functions for different JONSWAP spectra with fixed wave height of $\bar{H}_w = 2$ [m] and varying peak period $\bar{T}_w \in [5, 12]$. The peak shape parameter is fixed to $\gamma = 3.3$.

Figure 8.4 presents performance results for the proposed moment-based energy-maximising controller, in terms of energy absorption, under both displacement and velocity constraints (simultaneously). To be precise, Figure 8.4 explicitly shows the value of the objective function \mathcal{J} (black circles), for sea states with $\bar{H}_w = 2$ [m] and $\bar{T}_w \in [5, 12]$ [s] (*i.e.* corresponding with the set of SDFs presented in Figure 8.3), where the displacement and velocity of the CorPower-like device are constrained to $Z_{\max} = 2$ [m] and $\dot{Z}_{\max} = 2$ [m/s], respectively.

Finally, Figure 8.5 presents both motion, and energy-maximising control input results for a particular sea state, characterised by a JONSWAP spectrum with $\bar{H}_w = 2$ [m] and $\bar{T}_w = 8$ [s] (see Figure 8.3). Both the state and input constraints are also set to the exact same values as those for the regular excitation case of Figure 8.2, *i.e.* $Z_{\max} = 2$ [m], $\dot{Z}_{\max} = 2$ [m/s] and $U_{\max} = 1 \times 10^6$ [N] (see also Equation (8.36)). Note that this figure is analogous to Figure 8.2, and the same indexing to variables is used.

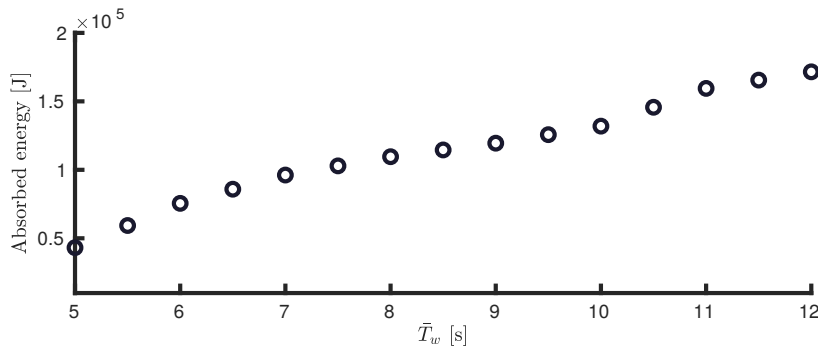


Figure 8.4: Constrained (displacement and velocity) energy absorption for the moment-based energy maximising controller proposed in this chapter.

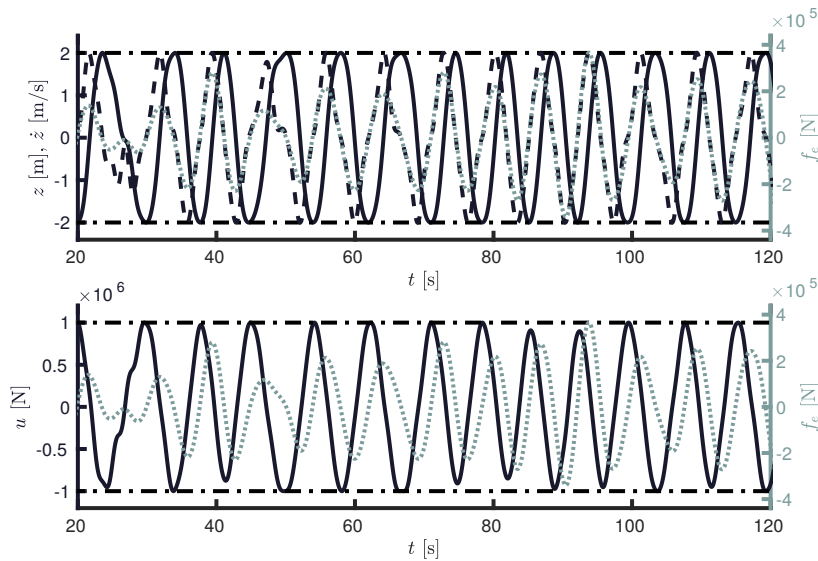


Figure 8.5: Motion results for irregular wave excitation. **(a)** shows displacement (left axis, solid), velocity (left axis, dashed) and wave excitation force input (right axis, dotted), for the WEC system. **(b)** presents the corresponding moment-based control input (left axis, solid), used to elicit the corresponding motion results, along with the wave excitation force input (right axis, dotted). The horizontal dash-dotted lines represent constraint values.

In particular, note that, as can be appreciated from Figure 8.5, the moment-based strategy is able to maximise energy absorption while systematically respecting both state and input constraints for this irregular wave input case, according to the control design objective, and hence providing energy-maximising performance in a realistic sea description. A noteworthy feature, which can be directly appreciated from Figure 8.5 **(a)**, is that the velocity and wave excitation force (external input) present the same ‘in-phase’ optimal energy absorption condition, inherently present for the case of regular unconstrained motion.

8.5 Receding-horizon optimal control problem

As discussed in the introduction to this chapter¹⁶, motivated by both the real-time requirements, and the intrinsic estimation and forecasting needs associated with the WEC energy-maximising control problem, the optimal formulation described in equation (8.4) can be re-written in a *receding-horizon* approach. In particular, note that the energy-maximising OCP posed in equation (8.4) can be

¹⁶: Further discussed in Section 3.2.

generally defined within a receding-horizon framework, simply as

$$u_N^{\text{opt}} = \arg \max_{u_N} \frac{1}{T_h} \int_{\Xi_N} u_N(\tau) \dot{z}(\tau) d\tau,$$

subject to:

$$\begin{cases} \text{WEC dynamics } \Sigma \text{ (8.1),} \\ \text{state and input constraints } \mathcal{C} \text{ (8.3),} \\ z(t_N^m) = z^m(t_N^m), \\ \dot{z}(t_N^m) = \dot{z}^m(t_N^m), \end{cases} \quad (8.36)$$

with $T_h \in \mathcal{T} \subset \mathbb{R}^+$, $T_h < T$, the *time-horizon*, where one effectively optimises energy-capture within the *time-window* $\Xi_N = [N\Delta_h, N\Delta_h + T_h] \subset \mathbb{R}^+$, $N \in \mathbb{N}$, by means of an optimal control input $u_N^{\text{opt}} : \Xi_N \rightarrow \mathbb{R}$, and where Δ_h is denoted as the *receding time-step*.

Remark 8.5.1 The variable T in (8.4), which fully describes the (total) time interval \mathcal{T} , is now replaced by the time-horizon $T_h < T$. In other words, the optimal control input is computed such that the energy absorbed from ocean waves is optimised throughout the time-window Ξ_N .

Remark 8.5.2 Note that the definition of the time-window Ξ_N is strongly linked to the estimation and forecasting requirements of the wave excitation effects, and the representation of f_e in the moment-domain, according to its corresponding signal generator. This last statement is further discussed throughout Section 8.6.

Following Remark 8.5.2, the set Ξ_N is formally written as

$$\begin{aligned} \Xi_N &= [N\Delta_h, t_N^m] \cup t_N^m \cup (t_N^m, N\Delta_h + T_h], \\ &= \Xi_N^e \cup t_N^m \cup \Xi_N^f, \end{aligned} \quad (8.37)$$

where Ξ_N^e and Ξ_N^f correspond with *past* (estimated) and *future* (forecasted) values of f_e , respectively. The variable $t_N^m \in \Xi_N$ corresponds to the *current* time instant, which (without any loss of generality) is located in the centre of the time-window Ξ_N , i.e. $t_N^m = T_h/2 + N\Delta_h$.

The distribution of the sets and time constants described above is illustrated in Figure 8.6. The additional set of (two) equality constraints in (8.36), which is standard in any receding-horizon control formulation¹⁷, is used to guarantee continuity of the WEC variables z and \dot{z} , under the optimal control input u_N^{opt} , where z^m and \dot{z}^m denote the *measured* values of displacement and velocity, respectively.

17: The reader is referred to, for instance, [148], for further information on this topic.

The receding-horizon optimal control procedure described in equation (8.36) can be summarised in three basic steps:

- 1) $u_N^{\text{opt}} \leftarrow$ Solve (8.36) for the time-window Ξ_N .
- 2) Apply u_N^{opt} in the interval $\Xi_N^u = [N\Delta_h, (N+1)\Delta_h]$.
- 3) Replace Ξ_N by Ξ_{N+1} accordingly and go back to 1).

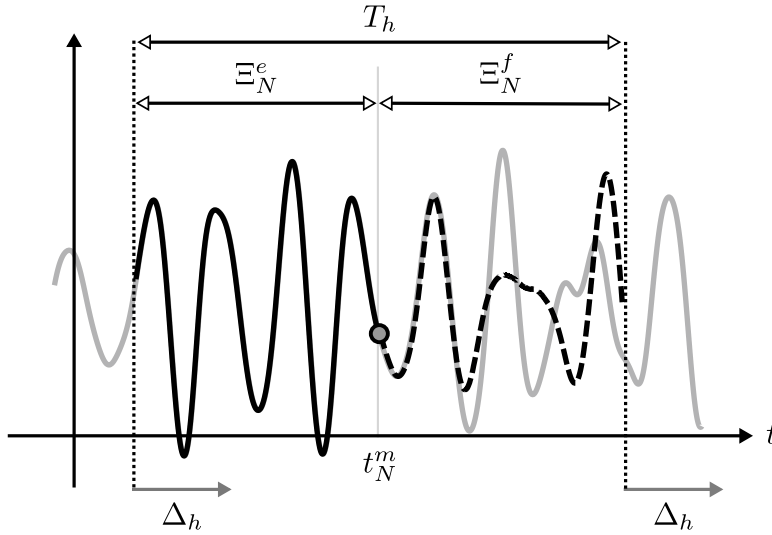


Figure 8.6: Sets and time constants involved in the receding-horizon OCP defined in (8.36). The solid- and dashed-black lines represent *estimated* and *forecasted* values of \tilde{f}_e (i.e., the approximated wave excitation input), respectively, while the solid grey line is the target excitation input f_e . The solid-grey circle represents the *current* time instant.

8.6 Receding-horizon energy-maximising moment-based control formulation

Based on the receding-horizon OCP posed in (8.36), and the theoretical framework developed in Sections 8.2 and 8.3, a moment-based receding-horizon controller is now proposed. In particular, Section 8.6.1 discusses the representation of the input f_e in the moment-domain, for this receding-horizon approach, while Section 8.6.2 effectively proposes a moment-based energy-maximising real-time controller for WECs, based on the proposed representation of f_e .

8.6.1 Input representation

Though highly computationally efficient, a standing assumption for the moment-based control strategy, presented in Sections 8.2 and 8.3, is that the wave excitation input f_e can be characterised by a T -periodic mapping, with a fundamental period $T = 2\pi/\omega_0$, where ω_0 is the so-called fundamental frequency (see Section 2.1.2). If the wave excitation estimation and forecasting requirements are effectively introduced to the optimal control formulation, then this assumption can be limiting in practice, as further discussed throughout this section. The framework presented in the following aims to alleviate the effect (and limitations) behind this assumption, by the

introducing a simple modification to the representation of the wave excitation signal.

Remark 8.6.1 Note that, if T is considered to be sufficiently large (*i.e.* the fundamental frequency is sufficiently small) then the signal f_e can be effectively considered T -periodic, for any practical purposes¹⁸.

18: See also the discussion provided in Section 2.1.2.

Remark 8.6.1 itself poses a contradiction: While the moment-based controller developed in Section 8.3 would require a sufficiently large time T (equivalent to a sufficiently large time-horizon in equation (8.36)), state-of-the-art forecasting algorithms are not usually able to provide an accurate prediction of f_e for more than a couple of seconds [90], *i.e.* precise information is only available throughout a shorter time-horizon T_h .

Motivated by this limitation in terms of implementation, this section introduces a modification of the representation of f_e in the moment-domain, suitable for receding-horizon control, as follows. Suppose $\tilde{f}_{e_N} : \Xi_N \rightarrow \mathbb{R}$ denotes the approximated wave excitation input for the time-window Ξ_N , composed of *both* estimated and forecasted values (see Figure 8.6). Using the underlying philosophy of the *short-term Fourier transform* (see [192]), the so-called *apodised* wave excitation input can be written as

$$[\tilde{f}_{e_N}]_{\vartheta} = \vartheta \tilde{f}_{e_N}, \quad (8.38)$$

where the *apodisation*¹⁹ mapping $\vartheta : \Xi_N \times \mathbb{R}^+ \rightarrow [0, 1]$ is used to smoothly bring the wave excitation signal, defined for a time-horizon T_h , down to zero at the edges of the set Ξ_N . This effectively reduces the spectral leakage produced by the discontinuities arising from truncating the signal \tilde{f}_e on the (potentially) short time-horizon T_h (see also [57]). In other words, the apodised signal $[\tilde{f}_{e_N}]_{\vartheta}$ is smoothly brought to zero at the boundaries so that the derivative of its periodic extension is sufficiently smooth. The family of apodisation functions considered here are the so-called *Planck-taper* mappings [248]. This set of functions, which optimally preserves the power spectrum of the signal, was first suggested within the theory of gravitational waves, and stem from the functional form of the Planck distribution, *i.e.*

19: Often also called *windowing* (see [192]).

$$\vartheta(t, \gamma) = \begin{cases} \frac{1}{e^{\mathcal{E}_+(t, \gamma)} + 1}, & t_N^i \leq t < \gamma t_N^f, \\ 1, & \gamma t_N^f \leq t < (1 - \gamma) t_N^f, \\ \frac{1}{e^{\mathcal{E}_-(t, \gamma)} + 1}, & (1 - \gamma) t_N^f \leq t \leq t_N^f, \\ 0, & t < t_N^i \vee t > t_N^f, \end{cases} \quad (8.39)$$

where $\{t_N^i, t_N^f\} \subset \Xi_N$ are defined as $t_N^i = N\Delta_h$ and $t_N^f = N\Delta_h + T_h$, and the mapping \mathcal{Z} is such that

$$\mathcal{Z}_{\pm}(t, \gamma) = \frac{2\gamma}{1 \pm \left(\frac{2\gamma}{t_N^f} - 1\right)} + \frac{2\gamma}{1 - 2\gamma \pm \left(\frac{2\gamma}{t_N^f} - 1\right)}. \quad (8.40)$$

An example, showing both \tilde{f}_e and $\lfloor \tilde{f}_{e_N} \rfloor_{\vartheta}$ for a time-window Ξ_N and parameter $\gamma = 0.5$, is shown in Figure 8.7.

Let $\omega_{h_0} \in \mathbb{R}^+$ be the fundamental frequency associated with the time-horizon T_h , *i.e.* $\omega_{h_0} = 2\pi/T_h$. Following the theoretical framework proposed in Section 8.2, both the apodised wave excitation input $\lfloor \tilde{f}_{e_N} \rfloor_{\vartheta}$ and the control input u_N are expressed analogously to (8.8), *i.e.* in terms of the signal generator

$$\begin{aligned} \dot{\xi} &= S_h \xi, \\ \lfloor \tilde{f}_{e_N} \rfloor_{\vartheta} &= L_{e_N} \xi, \\ u_N &= L_{u_N} \xi, \end{aligned} \quad (8.41)$$

for $t \in \Xi_N$, where $\xi(t) \in \mathbb{R}^{\nu_h}$, $\{L_{u_N}^T, L_{e_N}^T\} \subset \mathbb{R}^{\nu_h}$, and the dynamic matrix $S_h \in \mathbb{R}^{\nu_h \times \nu_h}$ is defined analogously to (8.9), *i.e.* in block-diagonal form as

$$S_h = \bigoplus_{p=1}^{f_h} \begin{bmatrix} 0 & p\omega_{h_0} \\ -p\omega_{h_0} & 0 \end{bmatrix}, \quad (8.42)$$

with $\nu_h = 2f_h$, $f_h \in \mathbb{N}_{\geq 1}$. The initial condition is set exactly as in the case discussed in Section 8.2, *i.e.* $\xi(0) = \varepsilon_{\nu_h}$, and the pair $(S_h, L_{e_N} - L_{u_N})$ is assumed observable (analogously to Assumption 8.2.1).

Within this framework, the excitation input vector L_{e_N} , for a particular time-window Ξ_N , can be straightforwardly defined using a least-squares approach: Let $\mathcal{T}_{\xi} = \{t_i\}_{i=1}^P \subset \Xi_N$ be a finite set of $P \in \mathbb{N}_{\geq \nu_h}$ uniformly-spaced time instants, and let $\Lambda_{\mathcal{T}_{\xi}} \in \mathbb{R}^{\nu_h \times P}$ and $\Lambda_{\lfloor \tilde{f}_{e_N} \rfloor_{\vartheta}}^T \in \mathbb{R}^P$ be defined as

$$\begin{aligned} \Lambda_{\mathcal{T}_{\xi}} &= \begin{bmatrix} \xi(t_1) & \dots & \xi(t_P) \end{bmatrix}, \\ \Lambda_{\lfloor \tilde{f}_{e_N} \rfloor_{\vartheta}} &= \begin{bmatrix} \lfloor \tilde{f}_{e_N} \rfloor_{\vartheta}(t_1) & \dots & \lfloor \tilde{f}_{e_N} \rfloor_{\vartheta}(t_P) \end{bmatrix}. \end{aligned} \quad (8.43)$$

Then, the vector L_{e_N} can be readily defined in terms of the following expression:

$$L_{e_N} := \Lambda_{\lfloor \tilde{f}_{e_N} \rfloor_{\vartheta}} \Lambda_{\mathcal{T}_{\xi}}^T (\Lambda_{\mathcal{T}_{\xi}} \Lambda_{\mathcal{T}_{\xi}}^T)^{-1}, \quad (8.44)$$

where the invertibility of the matrix $\Lambda_{\mathcal{T}_{\xi}} \Lambda_{\mathcal{T}_{\xi}}^T$ is guaranteed by the excitability of the pair $(S_h, \varepsilon_{\nu_h})$, see [223].

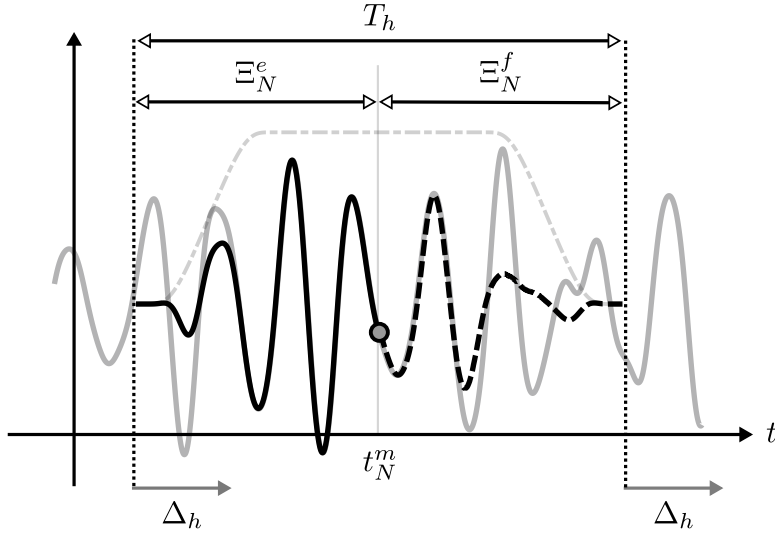


Figure 8.7: Target excitation input f_{e_N} (solid grey), and the (apodised) approximated wave excitation input $[f_{e_N}]_{\vartheta} = L_{e_N} \xi$ (black), with L_{e_N} as in (8.44), for the time-window Ξ_N . The apodisation mapping ϑ is plotted with a dash-dotted grey line, while the solid-grey circle represents the *current* time.

Remark 8.6.2 Though real-time performance is already available with (8.44) (see Section 8.7), note that, if required, extra computational speed could be achieved using a *recursive* least-squares implementation²⁰ instead of (8.44).

20: Plenty of literature on recursive least-squares strategies is available, such as, for instance, [44, 232].

8.6.2 Receding-horizon controller

Based on the moment-domain representation of the (apodised) wave excitation input, discussed in Section 8.6.1, and the equation of motion (8.5), a receding-horizon moment-based energy-maximising controller subject to state and input constraints, is proposed in this section, following an analogous procedure to that presented in Section 8.3.

In particular, let $\mathcal{T}_{c_N} = \{t_i\}_{i=1}^{N_c} \subset \Xi_N$ be a set of uniformly-distributed time-instants, *i.e.* collocation points, and define $\Lambda_N \in \mathbb{R}^{\nu_h \times N_c}$ and $\Upsilon_N \in \mathbb{R}^{\nu_h \times 2N_c}$ as

$$\Lambda_N = [\xi(t_1) \ \dots \ \xi(t_{N_c})], \quad \Upsilon_N = [\Lambda_N \quad -\Lambda_N]. \quad (8.45)$$

With the definition of Λ_N and Υ_N in (8.45), one can write the moment-based control input u_N^{opt} , for a given time window Ξ_N , in

terms of the unique global solution of the concave QP problem, as

$$\begin{aligned}
u_N^{\text{opt}} &= L_{u_N}^{\text{opt}} \xi, \\
L_{u_N}^{\text{opt}} &= \arg \max_{L_{u_N}^{\text{T}} \in \mathbb{R}^{\nu_h}} -\frac{1}{2} L_{u_N} \Phi_{\mathcal{R}}^{\text{T}} L_{u_N}^{\text{T}} + \frac{1}{2} L_{e_N} \Phi_{\mathcal{R}}^{\text{T}} L_{u_N}^{\text{T}}, \\
&\text{subject to:} \\
L_{u_N} \mathcal{A}_z &\leq \mathcal{B}_z, \\
L_{u_N} \mathcal{A}_{\dot{z}} &\leq \mathcal{B}_{\dot{z}}, \\
L_{u_N} \mathcal{A}_u &\leq \mathcal{B}_u, \\
L_{u_N} \mathcal{A}_z^{\text{eq}} &= \mathcal{B}_z^{\text{eq}}, \\
L_{u_N} \mathcal{A}_{\dot{z}}^{\text{eq}} &= \mathcal{B}_{\dot{z}}^{\text{eq}},
\end{aligned} \tag{8.46}$$

where the pairs of matrices $(\mathcal{A}_z, \mathcal{B}_z)$, $(\mathcal{A}_{\dot{z}}, \mathcal{B}_{\dot{z}})$ and $(\mathcal{A}_u, \mathcal{B}_u)$, associated with the state and input inequality constraints in (8.3) on displacement, velocity and control (PTO) input, respectively, are defined analogously as in Proposition 8.3.5. Note that, in contrast to Proposition 8.3.5, the pairs of matrices $(\mathcal{A}_z^{\text{eq}}, \mathcal{B}_z^{\text{eq}})$ and $(\mathcal{A}_{\dot{z}}^{\text{eq}}, \mathcal{B}_{\dot{z}}^{\text{eq}})$ are now included, aiming to fulfill the equality constraints in (8.36) at each current time instant, *i.e.* at $t = t_N^m \in \Xi_N$. In particular, these matrices are defined²¹ as

$$\begin{aligned}
\mathcal{A}_z^{\text{eq}} &= -\Phi_{\mathcal{R}}^{\text{T}} S_h^{-1} \xi(t_N^m), \\
\mathcal{B}_z^{\text{eq}} &= z^m(t_N^m) + L_{e_N} \mathcal{A}_z^{\text{eq}}, \\
\mathcal{A}_{\dot{z}}^{\text{eq}} &= -\Phi_{\mathcal{R}}^{\text{T}} \xi(t_N^m), \\
\mathcal{B}_{\dot{z}}^{\text{eq}} &= \dot{z}^m(t_N^m) + L_{e_N} \mathcal{A}_{\dot{z}}^{\text{eq}}.
\end{aligned} \tag{8.47}$$

21: The explicit derivation of the set of matrices $(\mathcal{A}_z^{\text{eq}}, \mathcal{B}_z^{\text{eq}})$ and $(\mathcal{A}_{\dot{z}}^{\text{eq}}, \mathcal{B}_{\dot{z}}^{\text{eq}})$ can be obtained directly from Proposition 8.3.5.

Remark 8.6.3 Following the receding-horizon approach to WEC control discussed in Section 8.5, the moment-based OCP, proposed in (8.46), is solved for a particular time window Ξ_N , and then applied to the system for the time interval $\Xi_N^u = [N\Delta_h, (N+1)\Delta_h]$, *i.e.* for a single receding time-step Δ_h . The time window is then subsequently shifted, *i.e.* $\Xi_N \mapsto \Xi_{N+1}$, and the process is repeated.

8.7 Case study revisited: inclusion of estimation and forecasting

To demonstrate the performance of the receding-horizon moment-based controller proposed in Section 8.6, this section considers the same device analysed in Section 8.4, *i.e.* a CorPower-like device, subject to irregular wave excitation, corresponding with the set of SDFs presented in Figure 8.3.

From now on, the time-horizon is selected as $T_h = 60$ [s], *i.e.* 30 [s] of both estimated and forecasted values of f_e are considered. This corresponds with a fundamental frequency $\omega_{h_0} = 2\pi/60$ [rad/s], which provides accurate results with respect to the least-square procedure described in (8.44), with mild computational requirements. The receding time-step is fixed as $\Delta_h = 0.1$ [s], while the dimension (order) of the signal generator (8.41) is chosen as $\nu = 60$ (following an analogous procedure to that described in Remark 8.4.2). With respect to state constraints, the maximum allowed displacement and velocity values are set to $Z_{\max} = 2$ [m] and $\dot{Z}_{\max} = 2$ [m/s], respectively (*i.e.* same values as in the case study of Section 8.4).

Remark 8.7.1 Note that the moment-based controller run-time, *i.e.* the time required to compute the energy-maximising optimal control input for the duration of the receding-step Δ_h , is of the order of $t^2 \sim 1$ [ms] $\ll \Delta_h$ for the totality of the preceding simulations (implemented in Matlab®), hence *always achieving real-time performance*. Naturally, the speed at which computations are performed can be further improved (if required) by simply implementing this algorithm in a compiled language, such as C or C++.

22: Measured with the Matlab® native function `tic-toc`.

As discussed in the introduction to this chapter, the unknown-input estimation strategy, selected to compute the estimation section of \tilde{f}_{e_N} , for each time-window Ξ_N^e , is based on a combination of Kalman filtering and the internal model principle of control theory, as presented (and tuned) in the study [90]. The forecasting algorithm considered, over the set Ξ_N^f , is the AR model proposed in [16], where the order \mathcal{O} is set to 200 (see also Section 8.7.2).

Remark 8.7.2 As a matter of fact, the wave excitation estimation algorithm presented in [90] has been explicitly described in this thesis, in Section 6.5. The parametric form, required to facilitate a state-space representation for the WEC system, is obtained with the input-output moment-matching-based model reduction strategy presented in Chapter 5, where the set of interpolation frequencies is selected as $\mathcal{F} = \{0.8, 2\}$. These frequencies correspond with the resonant frequency of the device (constrained to move in heave) ≈ 2 [rad/s], and a low frequency component.

Initial controller performance assessment focuses on energy absorption under both displacement and velocity constraints. Figure 8.8 shows absorbed energy for the sea states characterised in Figure 8.3, where the displacement and velocity of the CorPower-like device are constrained to Z_{\max} and \dot{Z}_{\max} , respectively. Circles represent the *ideal* (performance) scenario, where the wave excitation input

is assumed to be *perfectly* known over the entire simulation time (*i.e.* the case studied in Section 8.4), while diamonds denote the *actual* performance of the receding-horizon moment-based controller, where the *approximated* (estimated and forecasted) excitation force \tilde{F}_{e_N} is utilised. Clearly, the *actual* performance of the proposed receding-horizon moment-based approach is almost indistinguishable from its *ideal* counterpart, being able to perform optimally, with differences of less than 5% in terms of energy absorption.

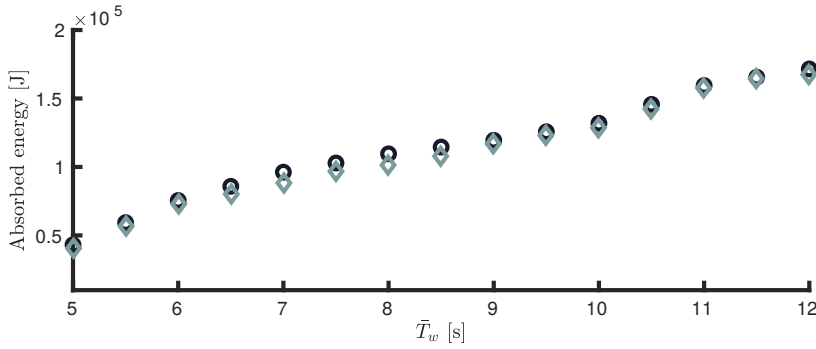


Figure 8.8: Constrained (displacement and velocity) energy absorption for the receding-horizon moment-based energy-maximising controller proposed in this section. Black circles and grey diamonds represent the *ideal* and *actual* performance results, respectively.

8.7.1 Sensitivity analysis: Estimation

A sensitivity analysis for the proposed receding-horizon moment-based controller is now presented, concerning errors in the *estimated* wave excitation force, over the time-interval Ξ_N^e . From now on, aiming to simplify the presentation of results, the wave peak period is fixed to $\bar{T}_w = 8$ [s], given that almost identical conclusions can be drawn using different values for $\bar{T}_w \in [5, 12]$ [s].

As discussed in the comparison study [15], there are two main sources of errors affecting \tilde{f}_{e_N} , arising from improper tuning of any unknown-input estimator: Constant errors in instantaneous amplitude (*i.e.* constant deviations in envelope), and instantaneous phase (*i.e.* time-delays). These imperfections are represented, within the estimation stage, using the criterion specified in what follows.

Remark 8.7.3 Another possible error source is the presence of measurement noise, *i.e.* the estimator is tuned in such a way that high frequency noise (affecting motion sensors) is *not* filtered. This effect is not analysed here. However, note that the moment-based representation for the input (discussed in Section 8.6.1) can intrinsically filter high frequency components, via a suitable selection of ν in equation (8.42) (*i.e.* by a sensible selection of the so-called cut-off frequency²³).

Let $\{F_\alpha, F_\phi\} \subset \Omega_F$, with $\Omega_F = [0.75, 1.25]$, be (error) factors associated with²⁴ the amplitude (**A**) and phase (**P**) of \tilde{f}_{e_N} . The

23: See Remark 8.4.2.

24: From now on, *instantaneous amplitude* and *instantaneous phase* are referred to simply as *amplitude* and *phase*, respectively.

following error sources, for $t \in \Xi_N^e$, are analysed:

$$\mathbf{A}: \tilde{f}_{e_N}(t) \mapsto F_\alpha \tilde{f}_{e_N}(t),$$

$$\mathbf{P}: \tilde{f}_{e_N}(t) \mapsto \tilde{f}_{e_N}(t + (F_\phi - 1)\bar{T}_w).$$

$$\mathbf{A+P}: \tilde{f}_{e_N}(t) \mapsto F_\alpha \tilde{f}_{e_N}(t + (F_\phi - 1)\bar{T}_w).$$

Case **A** assumes that the amplitude of the estimated signal is not estimated correctly, *i.e.* \tilde{f}_e is multiplied by a factor F_α , while case **P** effectively considers the existence of a time (phase) delay (positive or negative) between estimated and true excitation force, proportional to the peak period \bar{T}_w . Lastly, case **A+P** combines both amplitude and phase sources of error, for all possible combinations of $\{F_\alpha, F_\phi\}$ in $[0.75, 1.25]$.

Remark 8.7.4 Due to the underlying linearity of the AR model considered in this case study, if \tilde{f}_{e_N} is modified either by scaling, shifting in time, or superposing both cases, for $t \in \Xi_N^e$, this modification propagates within the forecasted time-window Ξ_N^e in the exact same manner. In other words, the sources of estimation error described in cases **A**, **P** and **A+P** affect the forecasted signal in the exact same proportions.

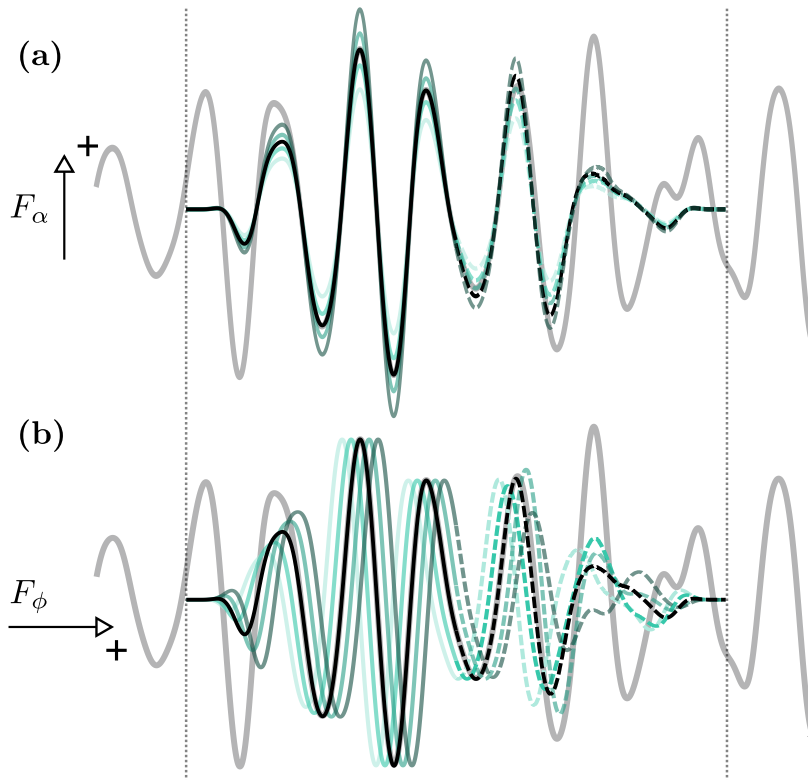


Figure 8.9: Illustrative example of cases **A** ((a), green) and **P** ((b), green), for a particular estimated (apodised) excitation force signal $[\tilde{f}_{e_N}]_\vartheta$ (solid-black). The target excitation force f_e is depicted with a solid-grey line.

Figure 8.9 presents an illustrative example of a wave excitation force signal affected by cases **A** and **P**, for a time-window Ξ_N . In particular, the estimated and forecasted excitation force with $F_\alpha = F_\phi = 1$, *i.e.* error-free (solid-black), are shown, for various values of F_α ((a), green) and F_ϕ ((b), green).

Define the following performance indicator $R_{\mathcal{J}}^e$ as $R_{\mathcal{J}}^e(F_\alpha, F_\phi) = \mathcal{J}(F_\alpha, F_\phi) / \mathcal{J}(1, 1)$, where the image of the mapping $\mathcal{J} : \Omega_F \times \Omega_F \rightarrow \mathbb{R}$ is the absorbed energy throughout the complete simulation time, for any pair of values (F_α, F_ϕ) , under controlled conditions, *i.e.* $R_{\mathcal{J}}^e$ is the ratio between the absorbed energy under the moment-based control strategy, *with* and *without* the presence of estimation errors.

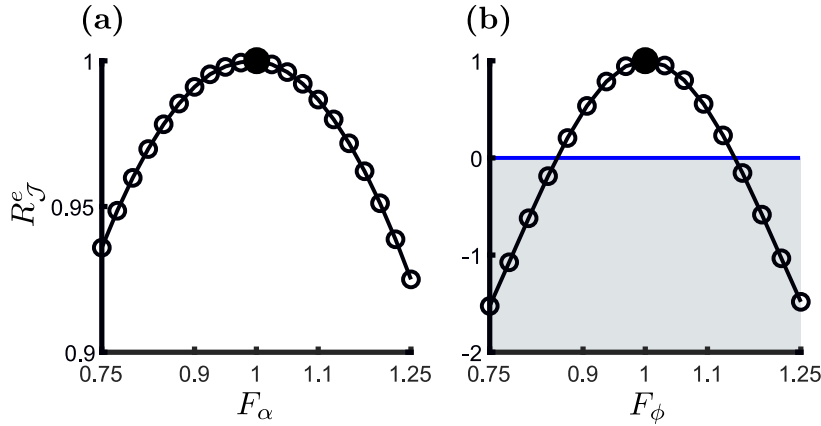


Figure 8.10: $R_{\mathcal{J}}^e$ for cases **A** (a) and **P** (b). A value of $R_{\mathcal{J}}^e$ below zero (solid-blue line) indicates negative energy absorption. The filled black circle indicates absorption with $F_\alpha = F_\phi = 1$.

Figure 8.10 shows performance results for cases **A** (a) and **P** (b), in terms of $R_{\mathcal{J}}^e(F_\alpha, 1)$ and $R_{\mathcal{J}}^e(1, F_\phi)$, respectively. For case **A**, it can be appreciated that, even under an amplitude deviation of $\pm 25\%$ from its true value, the absorbed energy always remains above 90% of its optimal achievable performance (computed without any amplitude or phase estimation errors). In other words, deviations in amplitude, for the estimated wave excitation force, generate only small deviations in absorbed energy, under controlled conditions. This is clearly not the case for phase deviations, *i.e.* case **P**, where a delay (positive or negative) of $\approx 10\%$ of the peak period (around 0.8 [s], for this case study), not only dramatically affects optimal energy absorption, but actually generates negative power (the device starts to drain energy from the electric grid).

Remark 8.7.5 A key point stems directly from the sensitivity analysis presented in this section: maximal effort should be put into tuning the estimator to guarantee *phase* synchronisation with the target wave excitation signal, hence achieving optimal energy-maximisation, under controlled conditions.

Finally, Figure 8.11 shows results for case **A+P**, where both errors in amplitude and phase are analysed simultaneously. Similarly to case **P**, it is clear that the presence of a time-delay (positive or negative) has a much greater impact on energy absorption than any existing differences in estimated amplitude. Interestingly, while positive or negative delays have an almost symmetric effect, underprediction of the wave excitation force amplitude has a lesser impact on perfor-

mance than overprediction. Note that this behaviour is consistent with that of Figure 8.10 (a).

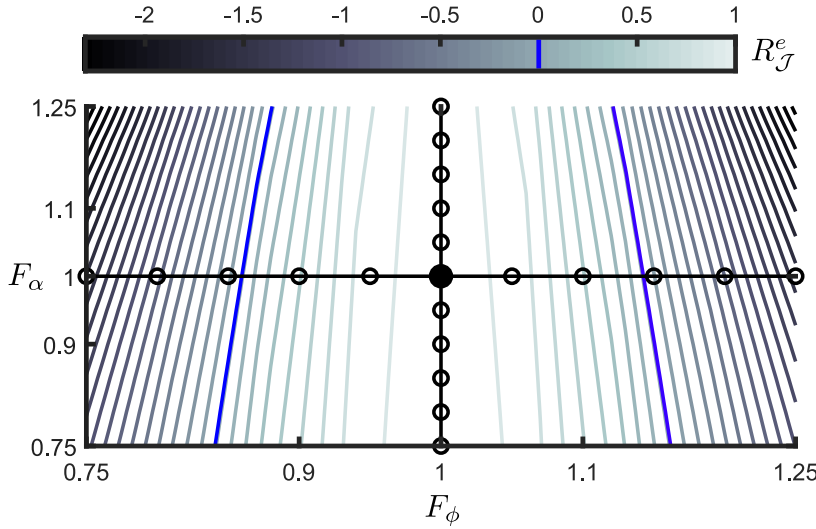


Figure 8.11: $R_{\mathcal{J}}^e$ for case **A + P**. A value of $R_{\mathcal{J}}^e$ below zero (solid-blue line) indicates negative energy absorption. Cases **A** and **B** are depicted with solid-black (empty circle) lines. The filled black circle indicates absorption with $F_{\alpha} = F_{\phi} = 1$.

8.7.2 Sensitivity analysis: Forecasting

Errors arising purely from the forecasting procedure are now considered, *i.e.* assuming that the unknown-input estimator is well-tuned (achieving convergence towards the target excitation force), and that any potential mismatch is only present within the forecasted window Ξ_N^f .

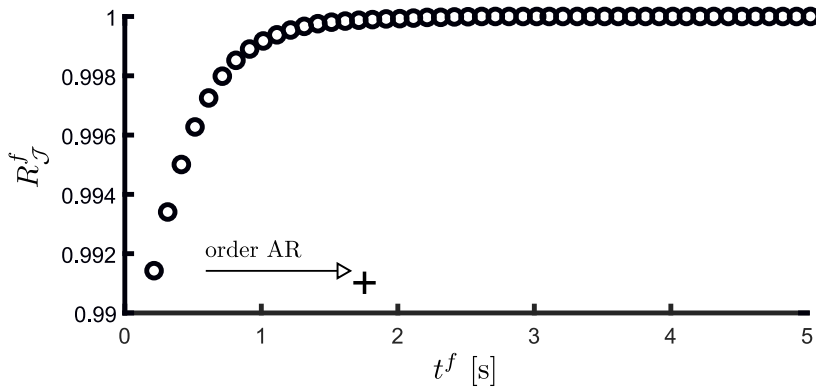


Figure 8.12: Sensitivity analysis with respect to forecasting errors in terms of the performance indicator $R_{\mathcal{J}}^f$.

Figure 8.12 presents performance results in terms of the indicator $R_{\mathcal{J}}^f(t^f) = \mathcal{J}(t^f)/\mathcal{J}(5)$, where the image of the operator $\mathcal{J} : \mathbb{R}^+ \rightarrow \mathbb{R}$ is the energy absorbed, assuming $t^f < 5$ seconds of forecast within 99% and 100% of accuracy. In other words, $R_{\mathcal{J}}^f$ is the ratio of absorbed energy, under controlled conditions, between energy extraction assuming quasi-perfect knowledge of the forecasted signal for a section of Ξ_N^f , and the maximum time-length with a forecast accuracy of better than 99%, *i.e.* ≈ 5 [s], obtained for a sufficiently large AR model order \mathcal{O} (here chosen as $\mathcal{O} = 200$). Figure 8.13

presents an illustrative example of a forecasted excitation force signal with $t^f = 5$ [s] (dashed-black), and for $t^f < 5$ (dashed-green).

Unlike the *estimation* case discussed in Section 8.7.1, where deviations from the target excitation force can effectively generate negative power absorption, the impact of *forecasting* errors, for the moment-based controller presented in this chapter, is almost negligible. Even with $t^f \approx 1$ [s], the controller is able to perform within 99% of its optimal performance, *i.e.* the performance obtained with an AR model with a sufficiently large order.

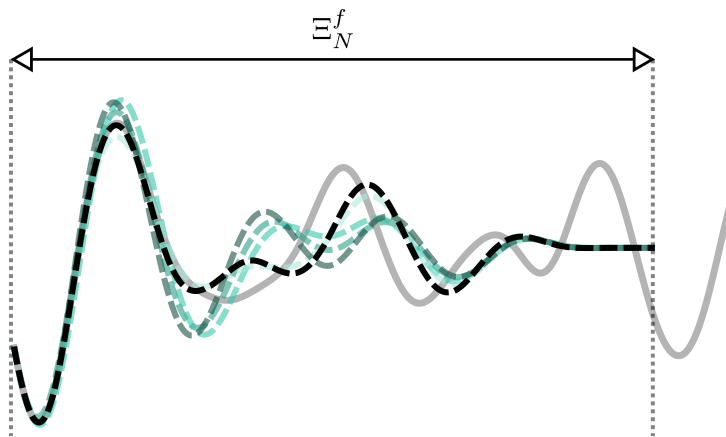


Figure 8.13: Illustrative example of a forecasted (apodised) excitation force signal with $t^f = 5$ [s] (dashed-black), and for $t^f < 5$ [s] (dashed-green). The target excitation force f_e is depicted with a solid-grey line.

8.8 Conclusions

This chapter presents a moment-based energy-maximising framework for linear SISO WECs. In particular, the moment-based parameterisation of the steady-state response of the WEC system is shown to provide a significant simplification of the target OCP, transcribing such an infinite-dimensional problem to a finite-dimensional quadratic program. Existence and uniqueness results for such a moment-based parameterisation are explicitly formalised. In addition, the resulting QP problem is shown to be *strictly convex* for the WEC case, systematically guaranteeing a unique globally optimal solution for the energy-maximising OCP in the moment-domain, subject to both state and input constraints. This allows for the utilisation of state-of-the-art QP solvers, which, in turn, provide a computationally efficient framework for optimal control of WECs. This chapter considers, to the best of the author's knowledge, the first application of moment-based theory to solve a constrained optimal control problem.

A case study is presented, in terms of a CorPower-like device, constrained to move in heave (translational motion). The capabilities of the proposed moment-based strategy are explicitly highlighted, showing that the framework is effectively able to maximise energy

absorption, while simultaneously considering state and input constraints.

In addition, and to give practical value to the presented strategy, a real-time moment-based *receding-horizon* OCP is also presented, which incorporates both wave excitation force estimation and forecasting algorithms. The optimal control objective is stated accordingly, using a receding-horizon approach, while retaining the intrinsic computational efficiency and uniqueness of the energy-maximising solution provided by the moment-based framework. This receding-horizon formulation is able to perform to virtually ideal levels, where full knowledge of f_e is available over the time-horizon, with differences of less than 5% in terms of power absorption for the range of analysed sea-states.

Finally, a sensitivity analysis, addressing the impact of estimation and forecasting errors on total energy absorption under controlled conditions, is presented. Two main conclusions can be directly extracted from this analysis: Forecasting mismatches have a negligible impact on the overall performance of the strategy, while differences arising from unknown-input estimators can effectively generate negative power absorption. In particular, phase errors (positive or negative) in the estimated excitation force have a substantial impact on the energy-maximising performance of the controller, suggesting that maximal design effort should be put in tuning the observer such that (instantaneous) phase synchronisation is achieved with the target excitation force.

Energy-maximising control for linear MIMO WECs

9

Contents of this chapter

9.1	Optimal control problem	210
9.2	Moment-based WEC array formulation for optimal control	211
9.3	Energy-maximising moment-based WEC array control formulation	214
9.3.1	Handling of state and input constraints	216
9.4	Case study: an array of CorPower-like devices	218
9.5	Conclusions	223

Recall, from Section 2.4, that the equation of motion for a WEC, under the assumptions of linear potential flow theory (see Section 2.3.1), can be expressed in terms of *Cummins'* equation (2.20). This equation is recalled below, for a N -DoF WEC device, with $N \in \mathbb{N}$ for convenience:

$$\Sigma : \begin{cases} \ddot{z} = \mathcal{M}(-k_r * \dot{z} - s_h z + f_e - u), \\ y = \dot{z}, \end{cases} \quad (9.1)$$

where $z : \mathbb{R}^+ \rightarrow \mathbb{R}^N$ is the displacement vector, $k_r : \mathbb{R}^+ \rightarrow \mathbb{R}^{N \times N}$, $k_{r_{ij}} \in L^2(\mathbb{R})$, $\forall \{i, j\} \subset \mathbb{N}_N$, the radiation impulse response (matrix-valued) function, $f_e : \mathbb{R}^+ \rightarrow \mathbb{R}^N$ the wave excitation, and \mathcal{M} is the inverse of the generalised mass matrix of the device.

Remark 9.0.1 From now on, it is considered that the equation of motion (6.1) represents an array of N devices, constrained to move in a single DoF. Such a choice is motivated in the following paragraphs. Note that a similar analysis, to that presented in this chapter, can be carried out for energy-maximisation of a multi-DoF device, with slight changes in the control objective¹.

¹: In particular, in the objective function characterising the OCP.

The control input $u : \mathbb{R}^+ \rightarrow \mathbb{R}^N$, supplied by means of the so-called power take-off system, plays a key role in the optimisation of the operation of the wave energy array, and has to be designed such that the *total energy absorbed by the array* is maximised.

Aiming to put things in perspective, recall, from Section 3.4, that despite the fact that energy from ocean waves has one of the highest power densities available among renewable energy resources, the current high installation, operation, maintenance, and decommissioning costs hinder wave energy extraction technologies in reaching economic viability. As a direct consequence of this, the roadmap to successful commercialisation of WECs naturally embodies the development of so-called WEC arrays (or *farms*), which effectively

incorporates several devices in a common sea area, potentially reducing the levelised cost of energy (LCoE) through an economy of scale. In other words, any realistic effort to commercialise a novel WEC technology requires both a single WEC, and a WEC farm development process.

To further reduce the levelised cost of energy, it is well-known that wave energy systems require optimal operational behaviour ensuring maximum time-averaged power extraction from ocean waves. In the case of an array of WECs, the devices composing a WEC farm are commonly installed in close proximity, mainly motivated by the underlying practical considerations, such as space limits, sharing of electrical and mooring infrastructure, and general maintenance [14]. Given that each WEC represents not only a wave absorber but also a wave generator [49], the motion of each WEC is directly affected by the waves generated by adjacent devices (*i.e.* radiation effects). This feature complicates optimal control design, when compared to the case of a single device, sometimes rendering the energy-maximising control task unsuitable for real-time applications if all these interactions are considered within the design dynamical model.

Following the array roadmap for successful WEC commercialisation, and given the desirable properties of the SISO moment-based strategy presented in Chapter 8, this chapter presents a MIMO moment-based energy-maximising optimal control framework, incorporating WEC farms into this moment-based control methodology. Within this framework, the hydrodynamic interactions between bodies (or devices) are fully exploited to compute the optimal control law, therefore optimally maximising the energy extraction of a WEC array from a given wave field, subject to both state and input constraints. The desirable properties of the moment-based strategy proposed in Chapter 8 are retained in this WEC device farm case. In particular, unlike most of the model based energy-maximising control strategies reported for both single WECs and WEC farms, this moment-based strategy does not require an a-priori parametric approximation of the radiation force (convolution) term, but rather provides an analytical description of the convolution operation in the moment-domain. This characteristic, together with the *strictly concave* QP formulation presented in the upcoming sections, renders this moment-based strategy highly efficient in computational terms, and hence appealing for real-time applications, especially in a high-dimensional setting, such as WEC arrays.

Remark 9.0.2 Throughout this chapter, aiming both to simplify the notation, and to solely focus the upcoming sections on the formulation of a MIMO moment-based controller, the excitation

force is assumed to be *known* over the complete time interval $\mathcal{T} \subset \mathbb{R}^+$, where energy absorption from incoming waves is maximised. This is done without any loss of generality, since a receding-horizon formulation can be achieved *directly*, by simply following the theory² presented in Section 8.6, without further modifications.

The remainder of this chapter is organised as follows. Section 9.1 formally introduces the energy-maximising problem for WEC farms, while Section 9.2 details the moment-based analysis of the WEC array, and guarantees existence and uniqueness of such a moment-domain representation. Section 9.3 details the moment-based energy-maximising constrained optimal control formulation. Finally, Section 9.4 discusses a case study, considering an array of CorPower-like devices (see Figure 6.2), while Section 9.5 encompasses the main conclusions of this study.

2: In particular, by following the adaptation of the moment-based representation of the wave excitation input, to alleviate the effects of considering a (potentially) short time-horizon for the computation of the control law (see Section 8.6.1).

9.1 Optimal control problem

The control problem for a wave energy farm composed of N WEC devices can be informally posed as follows: compute the optimal control input (PTO force) acting on each body $u_i : \mathbb{R}^+ \rightarrow \mathbb{R}$ such that the time-averaged energy absorbed by the (complete) wave energy array is maximised over a time interval $\mathcal{T} = [0, T] \subset \mathbb{R}^+$. To state this energy-maximising criterion in terms of an objective function $\mathcal{J} : \mathbb{R}^N \rightarrow \mathbb{R}$, $u \mapsto \mathcal{J}(u)$, note that the total useful energy converted by the PTO of each WEC in the array can be computed as

$$\mathcal{J}(u) = \sum_{i=1}^N \frac{1}{T} \int_{\mathcal{T}} u_i(\tau) \dot{z}_i(\tau) d\tau = \frac{1}{T} \int_{\mathcal{T}} P(\tau) d\tau, \quad (9.2)$$

where $\dot{z}_i : \mathbb{R}^+ \rightarrow \mathbb{R}$ and $P : \mathbb{R}^+ \rightarrow \mathbb{R}$ denote the velocity of the i -th device and the total instantaneous power of the WEC array, respectively.

As discussed throughout Chapter 3, any optimal control approach for WECs should consider both state (displacement and velocity) and input (PTO force) constraints, since the unconstrained optimal solution that maximises energy absorption is often unrealistic in terms of body motion and PTO force requirements.

In particular, constraints on the displacement and velocity of each WEC composing the array, z_i and \dot{z}_i , respectively, simultaneously with constraints on each device PTO force u_i , are considered. This

set of constraints can be compactly written, for all $i \in \mathbb{N}_N$, as³

$$\mathcal{C} : \begin{cases} |z_i(t)| \leq Z_{\max}, \\ |\dot{z}_i(t)| \leq \dot{Z}_{\max}, \\ |u_i(t)| \leq U_{\max}, \end{cases} \quad (9.3)$$

with $t \in \mathcal{T}$, and where $\{Z_{\max}, \dot{Z}_{\max}, U_{\max}\} \subset \mathbb{R}^+$.

Given the objective function defined in (9.2), the governing dynamics of the WEC array in (9.1), and the set of state and input constraints defined in (9.3), the energy-maximising optimal control problem can be stated as

$$\begin{aligned} u^{\text{opt}} &= \arg \max_u \mathcal{J}(u), \\ \text{subject to:} & \\ & \begin{cases} \text{WEC array dynamics } \Sigma \text{ (9.1),} \\ \text{state and input constraints } \mathcal{C} \text{ (9.3).} \end{cases} \end{aligned} \quad (9.4)$$

9.2 Moment-based WEC array formulation for optimal control

Analogously to Section 6.2, let the equation of motion be re-written (without any loss of generality) using the following equivalent representation,

$$\Sigma : \begin{cases} \dot{w} = Aw + Bv, \\ y = Cw, \end{cases} \quad (9.5)$$

for $t \in \mathbb{R}^+$, where $w(t) = \sum_{i=1}^N e_i^N \otimes [z_i(t) \quad \dot{z}_i(t)]^T \in \mathbb{R}^{2N}$ contains displacement and velocities for device involved in the WEC array, and the (constant) matrices $A \in \mathbb{R}^{2N \times 2N}$, $B \in \mathbb{R}^{2N \times N}$ and $C \in \mathbb{R}^{N \times 2N}$ are defined as

$$\begin{aligned} A &= \sum_{i=1}^N \sum_{j=1}^N e_{ij}^N \otimes \begin{bmatrix} 0 & {}^i_j \delta \\ -\mathcal{M}_{ij} s_{h_i} & 0 \end{bmatrix}, \\ B &= \sum_{i=1}^N \sum_{j=1}^N e_{ij}^N \otimes \begin{bmatrix} 0 \\ \mathcal{M}_{ij} \end{bmatrix}, \end{aligned} \quad (9.6)$$

$$C = \mathbb{I}_N \otimes [0 \ 1],$$

The 'input' function $v : \mathbb{R}^+ \rightarrow \mathbb{R}^N$, is defined as

$$v = f_e - k_r * Cw - u, \quad (9.7)$$

where the convolution mapping is incorporated as a feedback term, as before.

3: Note that there is no loss of generality in assuming that the maximum allowed values are the same for the N devices composing the array. This is considered to simplify the notation. In addition, there is also a likelihood that WEC arrays will be composed of a homogeneous collection of devices, for reasons of economy of production, installation and management (see, for instance, [14]).

The stepping stone towards a moment-based WEC array representation, for control purposes, relies on the MIMO moment-based theory proposed in Section 6.1, with appropriate modifications. In particular, each i -th entry of the vectors f_e and u are expressed as the output of the single-output signal generators

$$\begin{aligned}\dot{\xi}_i &= S\xi_i, \\ f_{e_i} &= L_{e_i}\xi_i, \\ u_i &= L_{u_i}\xi_i,\end{aligned}\tag{9.8}$$

for $t \in \mathbb{R}^+$, with $\xi(t) \in \mathbb{R}^\nu$, $S \in \mathbb{R}^{\nu \times \nu}$ and $\{L_{e_i}^\top, L_{u_i}^\top\}_{i=1}^N \subset \mathbb{R}^\nu$. Analogously to the moment-based representation discussed in the SISO control case (see Section 8.2), and following the requirement of Assumption 4.1.2 to have a well-posed system-theoretic definition of moments, a finite-set $\mathcal{F} = \{p\omega_0\}_{p=1}^f \subset \mathbb{R}^+$, with $f \in \mathbb{N}_{\geq 1}$, is considered. This set contains a finite number of harmonics of a (sufficiently small) fundamental frequency ω_0 , fully characterising the numerical generation of ocean waves⁴. Using the set \mathcal{F} , the dynamic matrix S in (9.8) is written in block-diagonal form as,

$$S = \bigoplus_{p=1}^f \begin{bmatrix} 0 & p\omega_0 \\ -p\omega_0 & 0 \end{bmatrix},\tag{9.9}$$

where $\nu = 2f$. Finally, both the wave excitation force f_e and control force u are expressed as the solution of the autonomous multiple-output signal generator as

$$\begin{aligned}\dot{\xi} &= (\mathbb{I}_N \otimes S)\xi, \\ f_e &= \left(\sum_{i=1}^N e_{ii}^N \otimes L_{e_i} \right) \xi = L_e \xi, \\ u &= \left(\sum_{i=1}^N e_{ii}^N \otimes L_{u_i} \right) \xi = L_u \xi.\end{aligned}\tag{9.10}$$

Remark 9.2.1 From now on, it is assumed that the moment-domain equivalent L_e , fully characterising the wave excitation force vector f_e , is known. Note that this is done without any loss of generality, as discussed in Remark 9.0.2.

Finally, with respect to Assumption 4.1.1, the following is considered. Firstly, and without loss of generality, the initial condition of the multiple-output signal generator (9.10) is set to $\xi(0) = \varepsilon_{N\nu} \in \mathbb{R}^{N\nu}$. Secondly, and analogously to the SISO control case discussed in Section 8.2, the input to the WEC system (described in terms of the signal generator (9.10)), is now composed of both the wave excitation force f_e , and control input u . This motivates the following

4: See Section 2.1.2 for further detail.

standing assumption.

Assumption 9.2.1 Let $\mathcal{L} = \{(S, L_{e_i} - L_{u_i})\}_{i=1}^N \subset (\mathbb{R}^{1 \times \nu} \times \mathbb{R}^{\nu \times \nu})$. Then, each element of the set \mathcal{L} is observable.

The objective is now to compute a parameterisation of the velocity \dot{z} in terms of moments. In particular, the computation of the moment of system Σ at the signal generator $(S, L_e - L_u)$, can be computed by solving a specific Sylvester equation (as in Proposition 6.1.1). Such a moment equation can be specialised for the WEC array case as

$$A\Pi + B(L_e - L_u - \underline{K}_r) = \Pi(\mathbb{I}_N \otimes S), \quad (9.11)$$

where $\Pi \in \mathbb{R}^{2N \times N\nu}$ and $\underline{K}_r \in \mathbb{R}^{N \times N\nu}$ is the moment-domain equivalent of the radiation convolution mapping.

Remark 9.2.2 If the observability condition posed in Assumption 9.2.1 holds, the definition of the moment-domain equivalent of the velocity is well-posed, and can be directly expressed in terms of the solution of (9.11), *i.e.* $\dot{\underline{Z}} = C\Pi$.

The Sylvester equation posed in (9.11) can be solved using the results of Propositions⁵ 6.2.2 and 6.2.3. In particular, $\dot{\underline{Z}}$, for the controlled WEC array case, can be computed in terms of the following proposition. This result is explicitly used to parameterise the optimal control problem for WEC arrays, in Section 9.3.

Proposition 9.2.1 Suppose Assumption 9.2.1 and condition (6.17) hold. Then, the moment-domain equivalent of the output y of system (9.5) (the velocity vector of the WEC array \dot{z}) can be uniquely determined as

$$\text{vec}\{\dot{\underline{Z}}\} = (\mathbb{I}_N \otimes \Phi_{\mathcal{R}}) \text{vec}\{L_e - L_u\}, \quad (9.12)$$

where the matrix $\Phi_{\mathcal{R}} \in \mathbb{R}^{N\nu \times N\nu}$ is defined as

$$\begin{aligned} \Phi_{\mathcal{R}} &= (\mathbb{I}_\nu \otimes C)\Phi^{-1}(\mathbb{I}_\nu \otimes -B), \\ \Phi &= (S \hat{\oplus} A) + \sum_{i=1}^N \sum_{j=1}^N \mathcal{R}_{ij}^T \otimes -Be_{ij}^N C, \end{aligned} \quad (9.13)$$

with $\Phi \in \mathbb{R}^{2N\nu \times 2N\nu}$, and where each $\mathcal{R}_{ij} \in \mathbb{R}^{\nu \times \nu}$, characterising the radiation effects in moment-domain, is given by

$$\mathcal{R}_{ij} = \bigoplus_{p=1}^f \begin{bmatrix} {}^i_j r_{p\omega_0} & {}^i_j m_{p\omega_0} \\ -{}^i_j m_{p\omega_0} & {}^i_j r_{p\omega_0} \end{bmatrix}, \quad (9.14)$$

where the set of parameters $\{{}^i_j r_{p\omega_0}, {}^i_j m_{p\omega_0}\}_{p=1}^f \subset \mathbb{R}$ is defined as in equation (6.16), for all $\{i, j\} \subset \mathbb{N}_f$.

5: Note that the result of Proposition 6.2.2 holds independently of the definition of the output vectors of the signal generator, *i.e.* it can be directly applied for this WEC control case.

Proof. Recall that, under Assumption 9.2.1, the moment of system Σ at the signal generator $(S, L_e - L_u)$ is $\dot{\underline{Z}} = C\Pi$. Then, given that condition (6.17) holds by hypothesis, the result posed in equation (9.12) follows directly from Proposition 6.2.3, with an appropriate change of the moment-domain equivalent associated with radiation effects, *i.e.* the set of matrices \mathcal{B}_{ij} , with $\{i, j\} \subset \mathbb{N}_f$ described in (9.14). \square

Remark 9.2.3 Note that, as previously discussed in Section 6.2, condition (6.17) is guaranteed for the WEC array case. In other words, the existence and uniqueness of the moment-domain equivalent $\dot{\underline{Z}}$ always holds, as a result of the internal stability of (9.5) (see Section 2.4).

Remark 9.2.4 Given the structure of the matrices L_u and L_e in (9.10), the moment-domain equivalent $\dot{\underline{Z}}$ can always be expressed as $\dot{\underline{Z}} = \sum_{i=1}^N e_{ii}^N \otimes \dot{\underline{Z}}_i$, where $\dot{\underline{Z}}_i^T \in \mathbb{R}^\nu$ denotes the moment-domain equivalent of the velocity of the i -th device.

9.3 Energy-maximising moment-based WEC array control formulation

The target energy-maximising OCP for arrays, formalised in Section 9.1, is now recalled. This OCP explicitly depends on the velocity of each device composing the farm, *i.e.* $\dot{z}_i, \forall i \in \mathbb{N}_N$. The following proposition makes use of the moment of system Σ (defined in equation (9.1)) at the signal generator $(S, L_e - L_u)$ (defined in equation (9.10)), to write the energy-maximising objective function \mathcal{J} in terms of moments.

Proposition 9.3.1 *Suppose Assumption 9.2.1 and condition (6.17) hold. Then the objective function \mathcal{J} defined in (9.2), *i.e.* total absorbed energy from ocean waves over the time period $\mathcal{T} = [0, T] \subset \mathbb{R}^+$, where $T = 2\pi/\omega_0$, can be computed in the moment-domain as*

$$\mathcal{J} \mapsto \frac{1}{2} \sum_{i=1}^N \dot{\underline{Z}}_i^T L_{u_i}^T, \quad (9.15)$$

where $\dot{\underline{Z}}_i$ denotes the moment-domain equivalent of the velocity of the i -th device⁶.

6: See Remark 9.2.4.

Proof. The proof of this statement follows the same steps of the proof of Proposition 8.3.1 and, hence, is omitted for brevity. \square

Proposition 9.3.1 shows that, under the proposed moment-based strategy, the objective function of (9.2) can be mapped (and computed) as the sum of N inner-product operations in $\mathbb{R}^{1 \times N\nu}$. Furthermore, as explicitly shown in the following, under the presented moment-based strategy, the unconstrained⁷ OCP (9.2) can be computed as the solution of a *strictly concave* QP problem.

Proposition 9.3.2 *Consider the unconstrained energy-maximising OCP for WEC arrays (9.2) and suppose Assumption 9.2.1 and condition (6.17) hold. Then, the optimal control law u^{opt} , that maximises the objective function \mathcal{J} over the time period \mathcal{T} , can be computed in the moment-domain as the solution of the QP problem*

$$\begin{aligned} u^{\text{opt}} &= L_u^{\text{opt}} \xi, \\ L_u^{\text{opt}} &= \arg \max_{L_u \in \mathbb{R}^{N \times N\nu}} -\frac{1}{2} \text{vec}\{L_u\}^\top (\mathbb{I}_N \otimes \Phi_{\mathcal{R}}^\top) \text{vec}\{L_u\} + \\ &\quad \frac{1}{2} \text{vec}\{L_e\}^\top (\mathbb{I}_N \otimes \Phi_{\mathcal{R}}^\top) \text{vec}\{L_u\}. \end{aligned} \quad (9.16)$$

7: This refers to the objective function (9.2) under the assumption that the state and input constraints defined in (9.3) are not considered in the formulation.

Proof. Note that, since $\dot{Z}_i^\top = \text{vec}\{\dot{Z}_i\}$ and $L_{u_i}^\top = \text{vec}\{L_{u_i}\}$, the expression of the moment-domain time-averaged power (9.15) can be written as

$$L_u^{\text{opt}} = \arg \max_{L_u} \frac{1}{2} \sum_{i=1}^N \text{vec}\{\dot{Z}_i\}^\top \text{vec}\{L_{u_i}\}. \quad (9.17)$$

Furthermore, the relations

$$\begin{aligned} \text{vec}\{\dot{Z}_i\} &= (\mathbb{I}_{N\nu} \otimes e_{ii}^N) \text{vec}\{\dot{Z}\}, \\ \text{vec}\{L_{u_i}\} &= (\mathbb{I}_{N\nu} \otimes e_{ii}^N) \text{vec}\{L_u\}, \end{aligned} \quad (9.18)$$

for $i \in \mathbb{N}_N$, hold. Replacing (9.12) in the objective function of (9.17), and noting that $e_{ii}^N = (e_{ii}^N)^\top$, yields

$$\begin{aligned} L_u^{\text{opt}} &= \arg \max_{L_u} \frac{1}{2} \text{vec}\{L_e - L_u\}^\top M \text{vec}\{L_u\}, \\ M &= \sum_{i=1}^N (\mathbb{I}_N \otimes \Phi_{\mathcal{R}}^\top) (\mathbb{I}_{N\nu} \otimes e_{ii}^N), \end{aligned} \quad (9.19)$$

where, considering the bilinearity and associativity properties of the Kronecker product, the matrix M can be equivalently written as

$$M = \mathbb{I}_N \otimes \Phi_{\mathcal{R}}^\top \left(\sum_{i=1}^N \mathbb{I}_{N\nu} \otimes e_{ii}^N \right) = \mathbb{I}_N \otimes \Phi_{\mathcal{R}}^\top, \quad (9.20)$$

from which the claim follows. \square

Proposition 9.3.3 *The QP formulation in (9.16) is strictly concave for any physically meaningful values of the parameters of (9.5).*

Proof. Note that the QP defined in (9.16) is strictly concave if and only if $\mathcal{H}\{\mathbb{I}_N \otimes \Phi_{\mathcal{D}}^T\} = \mathbb{I}_N \otimes \mathcal{H}\{\Phi_{\mathcal{D}}^T\}$ is positive-definite.

Let $\mathcal{D}(t) = f_e(t) - u(t) = [d_1(t), \dots, d_N(t)]$. Recall that, since system (9.5) is strictly passive, the relation [224]

$$\int_{t_1}^{t_2} \mathcal{D}(\tau)^T \dot{z}(\tau) d\tau = \sum_{i=1}^N \int_{t_2}^{t_1} d_i(\tau) \dot{z}_i(\tau) d\tau > 0, \quad (9.21)$$

for any time interval $[t_1, t_2] \in \mathbb{R}$, holds. Assume, without any loss of generality, that the time interval is set to $\mathcal{T} = [0, T]$. Then, it follows from the representation of the input $\mathcal{D}(t)$ as in (9.10), i.e. $\mathcal{D} = L_d \Xi$, Proposition 9.3.1, and the condition in equation (9.21), that the relation

$$\sum_{i=1}^N \int_{\mathcal{T}} d_i(\tau) \dot{z}_i(\tau) d\tau = \frac{1}{2} \sum_{i=1}^N \dot{Z}_i L_{d_i}^T > 0, \quad (9.22)$$

holds. Performing the same analysis as in Proposition 9.3.2, the proof of the claim follows noting that

$$\sum_{i=1}^N \dot{Z}_i L_{d_i}^T = \text{vec}\{L_d\}^T (\mathbb{I}_N \otimes \Phi_{\mathcal{D}}^T) \text{vec}\{L_d\} > 0, \quad (9.23)$$

which holds if and only if $\mathcal{H}\{\Phi_{\mathcal{D}}^T\}$ is positive-definite, proving the claim. \square

Remark 9.3.1 Propositions 9.3.2 and 9.3.3 have a strong impact on the practicality of the moment-based solution proposed in this chapter: the target optimal control formulation of (9.2), for WEC arrays, can be transformed into a QP program, which always has a unique (global) maximum due to the fact that strict concavity is always guaranteed. Hence, well-known and highly efficient state-of-the-art quadratic programming solvers can be used (see, for instance, [207]).

9.3.1 Handling of state and input constraints

Following the SISO control case presented in Chapter 8, the state and input constraints, defined in equation (9.3) for the array case,

are mapped to their respective moment-domain equivalents⁸, *i.e.*

$$\begin{cases} |z_i(t)| \leq Z_{\max}, \\ |\dot{z}_i(t)| \leq \dot{Z}_{\max}, \\ |u_i(t)| \leq U_{\max}, \end{cases} \mapsto \begin{cases} |\underline{\dot{Z}}_i(\mathbb{I}_N \otimes S^{-1})\xi(t)| \leq Z_{\max}, \\ |\underline{\dot{Z}}_i\xi(t)| \leq \dot{Z}_{\max}, \\ |L_{u_i}\xi(t)| \leq U_{\max}. \end{cases} \quad (9.24)$$

Let $\mathcal{T}_c = \{t_i\}_{i=1}^{N_c} \subset \mathcal{T} \subset \mathbb{R}^+$, be a finite set of (specified) uniformly-spaced time instants, with $N_c \in \mathbb{N}_{\geq 1}$. The constraints defined in (9.24) can be enforced at the set of time instants \mathcal{T}_c , *i.e.* using a collocation approach. Let the matrices $\Lambda \in \mathbb{R}^{NN_c \times N^2\nu}$ and $\Upsilon \in \mathbb{R}^{2NN_c \times N^2\nu}$ be defined as

$$\Lambda = [\xi(t_1) \otimes \mathbb{I}_N \dots \xi(t_{N_c}) \otimes \mathbb{I}_N]^\top, \quad \Upsilon = [\Lambda^\top \quad -\Lambda^\top]^\top. \quad (9.25)$$

With the definition of Υ in (9.25), one can formulate a moment-based energy-maximising constrained optimal control solution for WEC arrays in terms of an inequality-constrained concave QP problem, as follows.

Proposition 9.3.4 *Consider the state and input constrained OCP for WEC arrays (9.2), and suppose Assumption 9.2.1 and condition (6.17) hold. Then, the optimal control law u^{opt} , that maximises the objective function \mathcal{J} over the time period \mathcal{T} , can be computed in the moment-domain as the solution of the inequality-constrained concave QP problem*

$$\begin{aligned} u^{\text{opt}} &= L_u^{\text{opt}}\xi, \\ L_u^{\text{opt}} &= \arg \max_{L_u \in \mathbb{R}^{N \times N\nu}} -\frac{1}{2} \text{vec}\{L_u\}^\top (\mathbb{I}_N \otimes \Phi_{\mathcal{R}}^\top) \text{vec}\{L_u\} + \\ &\quad \frac{1}{2} \text{vec}\{L_e\}^\top (\mathbb{I}_N \otimes \Phi_{\mathcal{R}}^\top) \text{vec}\{L_u\}. \end{aligned}$$

subject to:

$$\mathcal{A}_z \text{vec}\{L_u\} \leq \mathcal{B}_z,$$

$$\mathcal{A}_{\dot{z}} \text{vec}\{L_u\} \leq \mathcal{B}_{\dot{z}},$$

$$\mathcal{A}_u \text{vec}\{L_u\} \leq \mathcal{B}_u,$$

(9.26)

8: Recall, from Proposition 5.2.1, that the moment-domain equivalent of the displacement z_i can be directly expressed as $\underline{\dot{Z}}_i(\mathbb{I}_N \otimes S^{-1})$.

where the matrices $\{\mathcal{A}_z, \mathcal{A}_{\dot{z}}, \mathcal{A}_u\}$ and $\{\mathcal{B}_z, \mathcal{B}_{\dot{z}}, \mathcal{B}_u\}$ are defined as

$$\begin{aligned}
 \mathcal{A}_z &= -\Upsilon \left(\mathbb{I}_N \otimes (S^{-1} \otimes \mathbb{I}_N)^\top \Phi_{\mathcal{R}} \right), \\
 \mathcal{B}_z &= Z_{\max} \mathbf{1}_{2NN_c} - \mathcal{A}_z \text{vec}\{L_e\}, \\
 \mathcal{A}_{\dot{z}} &= -\Upsilon (\mathbb{I}_N \otimes \Phi_{\mathcal{R}}), \\
 \mathcal{B}_{\dot{z}} &= \dot{Z}_{\max} \mathbf{1}_{2NN_c} - \mathcal{A}_{\dot{z}} \text{vec}\{L_e\}, \\
 \mathcal{A}_u &= \Upsilon, \\
 \mathcal{B}_u &= U_{\max} \mathbf{1}_{2NN_c}.
 \end{aligned} \tag{9.27}$$

Proof. Note that under the set of assumptions considered in this proposition, equation (9.26) follows directly from Proposition 9.3.2. The derivation of the set of inequality constraints in L_u , defined in (9.26), follows the same arguments as those of Proposition 8.3.5 and, hence, is omitted for brevity. \square

9.4 Case study: an array of CorPower-like devices

This section presents a case study to illustrate the proposed strategy, based on the regular-polytope-type WEC array layout depicted in Figure 9.1, composed of $N = 5$ converters. Each of the five devices composing this WEC farm is a full-scale CorPower-like device (see Figure 6.2) oscillating in heave (translational motion). To fully characterise this wave farm, Figure 9.2 presents the hydrodynamic characteristics of the WEC array considered in this application case, in terms of its corresponding radiation damping and radiation added-mass matrices, *i.e.* $B_r(\omega)$ and $A_r(\omega)$, respectively. Note that, due to the fact that the devices composing the WEC farm are identical (*i.e.* CorPower-like devices), the corresponding hydrodynamic characteristics (including interactions due to radiation effects) present symmetrical behaviour, in accordance with the layout depicted in Figure 9.1. That said, only three elements of the matrices⁹ $\{B_r(\omega), A_r(\omega)\} \subset \mathbb{R}^{5 \times 5}$ are required to completely characterise the hydrodynamic parameters of the farm. These are plotted in Figure 9.2, along with the corresponding symmetry pattern for both matrices $B_r(\omega)$ and $A_r(\omega)$.

The performance assessment of the presented moment-based strategy initially considers the case of regular input waves (see Section 2.1.1), taking into consideration both state and input constraints. Recall that, as discussed in Section 3.2, the necessity of considering motion constraints stems from the fact that the unconstrained energy-maximising optimal solution often requires unrealistic values for the physical variables of the analysed WEC system. Naturally,

9: The reader is referred to [49, Chapter 8] for an extensive discussion on the hydrodynamic coefficients of WEC arrays and the principles behind this symmetrical behaviour.

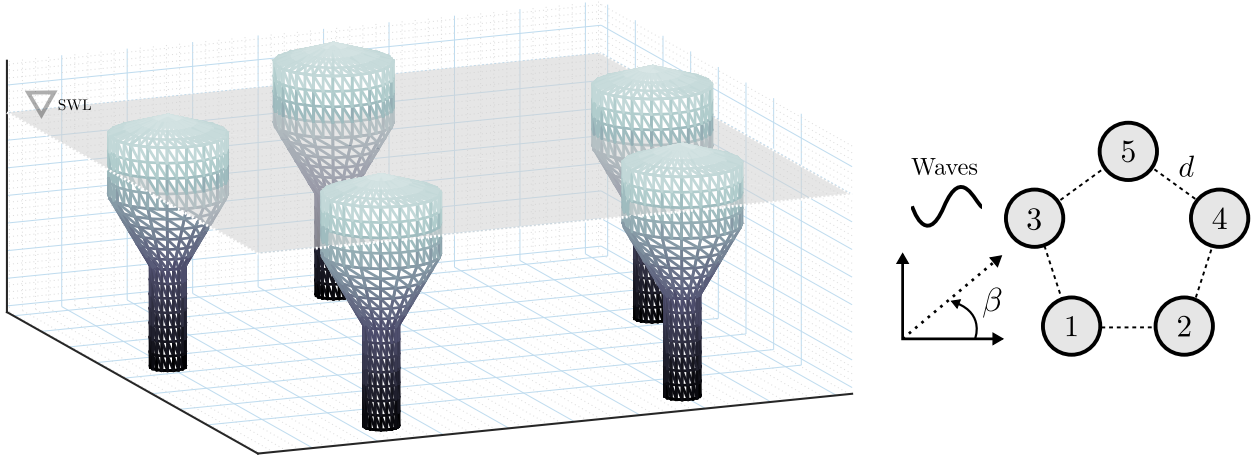


Figure 9.1: Regular-polytope-type WEC array layout considered for the application case. The distance d between devices is set to twice the diameter of the upper part of the float, *i.e.* $d \approx 17$ [m].

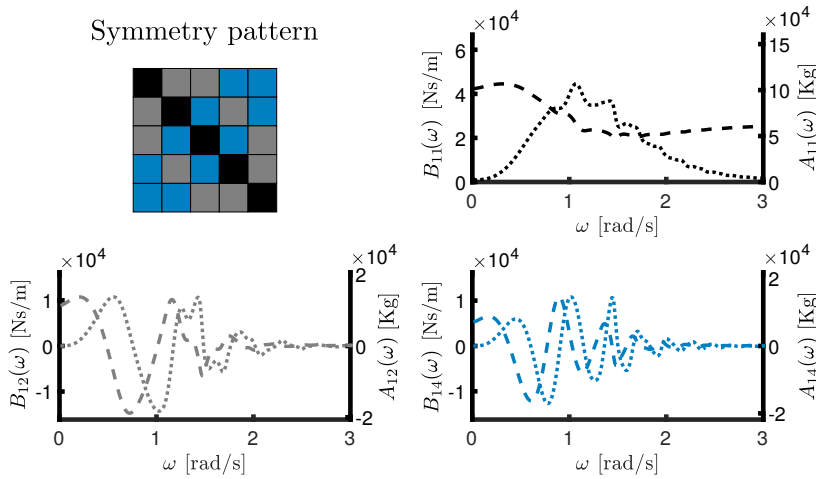


Figure 9.2: Hydrodynamic coefficients $B_r(\omega)$ (solid, left axis) and $A_r(\omega)$ (dashed, right axis) for the CorPower-like WEC array. Note that there is a one-to-one relation between the colors of the lines and the corresponding symmetry pattern depicted in the figure.

constraining the motion of the device leads to a decrease in the total absorbed power. This provides motivation to explicitly analyse how the state and input constraints affect the total power absorbed by the WEC farm of Figure 9.1, when using the moment-based strategy proposed in this chapter. To fulfill this objective, the definition of a power absorption ratio is proposed, as a function of the constrained variable (*i.e.* motion variable or control input). To be precise, let $z_{\text{unc}}^{\text{opt}}$ and $u_{\text{unc}}^{\text{opt}}$ be the displacement and control force for the WEC array under unconstrained optimal conditions, for a particular wave excitation force f_e .

Then, the following power absorption ratio is proposed, as a performance indicator:

$$R_P = \frac{\mathcal{J}_T^{\text{con}, R_{A|C}}}{\mathcal{J}_T^{\text{unc}}}, \quad (9.28)$$

where $\mathcal{J}_T^{\text{con}, R_{A|C}}$ is the total power absorption for a regular wave of period T_w with either displacement ($\mathcal{J}^{\text{con}, R_A}$) or control force

$(\mathcal{J}^{\text{con}, R_C})$ constrained to

$$Z_{\max} = R_A \max |z_T^{\text{unc}}|, \quad R_A \in [0, 1], \quad (9.29)$$

$$U_{\max} = R_C \max |u_T^{\text{unc}}|, \quad R_C \in [0, 1]. \quad (9.30)$$

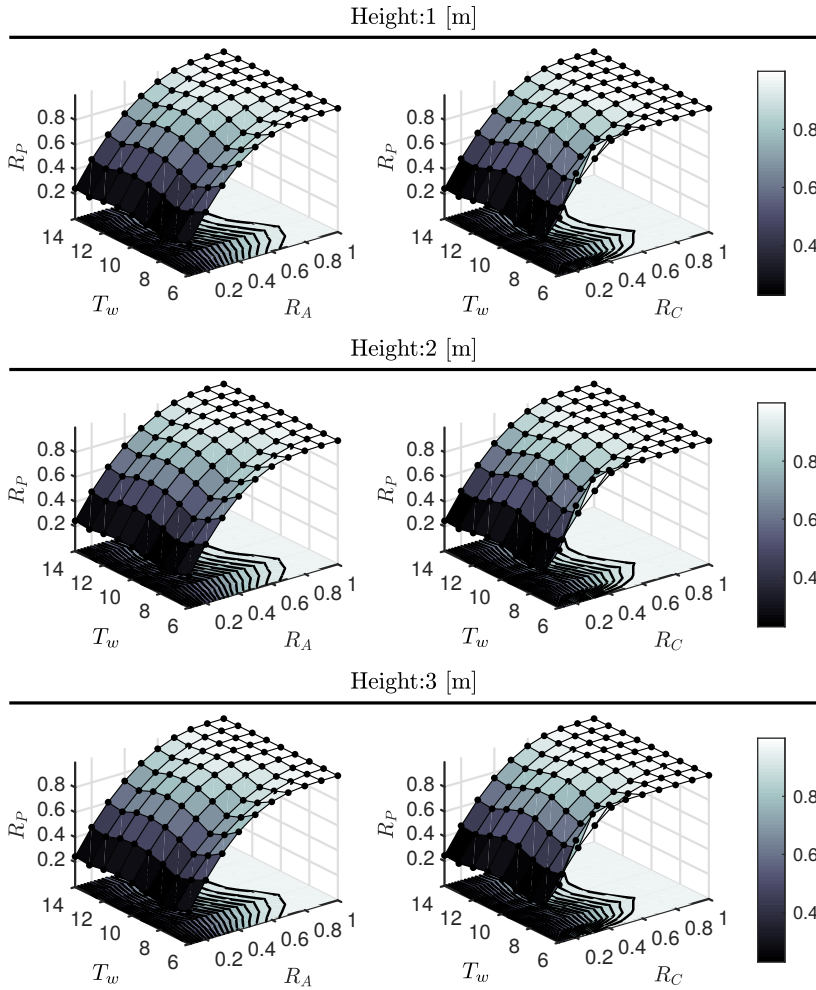


Figure 9.3: Power absorption ratio R_p for different wave period T_w , where the displacement of the device (left column) and control input are constrained following equations (9.29) and (9.30), respectively. Each row of the figure represents a different wave height H_w .

Figure 9.3 illustrates the results obtained for R_p with varying wave period T_w , considering both displacement and control force constraint factors R_A (left column) and R_C (right column), respectively. Furthermore, the results presented here are for three different wave heights, *i.e.* $H_w \in \mathbb{N}_3$ [m]. A key element to highlight from Figure 9.3 is that the proposed moment-based strategy is able to maintain consistent performance with respect to variations in H_w , giving almost identical power absorption ratio results for the full set of analysed wave heights. Focusing on the left column of Figure 9.3, where the displacement of the device is constrained following equation (9.29), it is noteworthy that with a constraint of 40% of the optimal unconstrained motion, the energy-maximising moment-based strategy is capable of extracting $\approx 80\%$ of the unconstrained optimal result for the totality of the analysed periods, with almost 90% for

some values of T_w . Similar behaviour can be appreciated in the right column of Figure 9.3, where now the maximum PTO force is constrained within the optimal energy-maximising control computation, as in equation (9.30). Note that the deterioration in power performance becomes higher in the case where the PTO force (control input) is constrained, while a milder effect can be appreciated in the case of displacement constraints. This is indeed consistent with previous results, such as those reported in [249] (simplified theoretical analysis) and [176, 219] (numerical assessment).

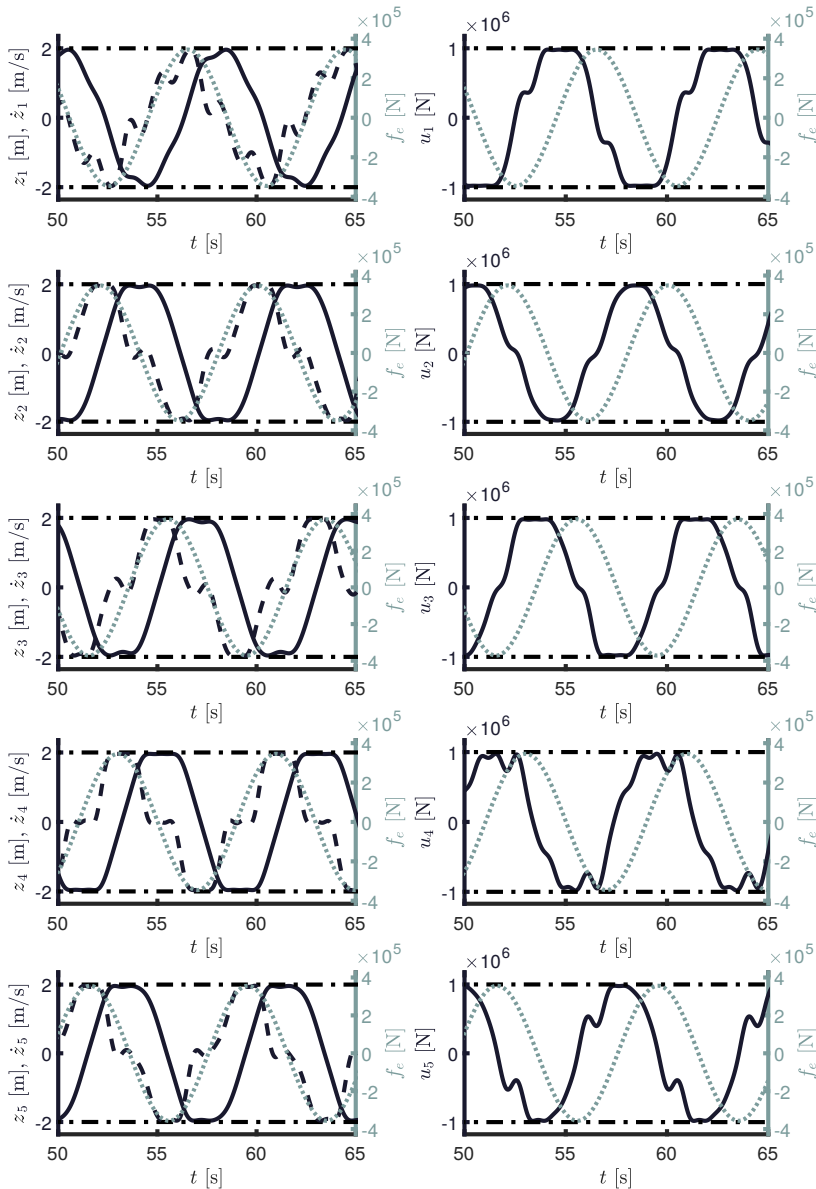


Figure 9.4: Results for regular input wave excitation. The left column of Figure 9.4 shows displacement (solid black), velocity (dashed black) and wave excitation force input (dotted grey), for each device composing the array, for devices 1 (top) to 5 (bottom). The right column of Figure 9.4 presents (in the same order) the corresponding control inputs for each device computed with the moment-based strategy (solid black), along with the wave excitation force (dotted gray) experienced by each device. The horizontal dash-dotted lines represent constraint values.

Completing the results for regular wave excitation, Figure 9.4 illustrates the WEC array motions under moment-based optimal control conditions (left column), along with each corresponding moment-based energy-maximising control laws (right column). The input wave is considered to have a wave height $H_w = 2$ [m] and a period $T_w = 8$ [s]. The state and input constraints, for each device

composing the array, are set as follows:

$$Z_{\max} = 2 \text{ [m]}, \quad \dot{Z}_{\max} = 2 \text{ [m/s]}, \quad U_{\max} = 1 \times 10^6 \text{ [N]}. \quad (9.31)$$

More precisely, the left column of Figure 9.4 shows displacement (solid black), velocity (dashed black) and wave excitation force input (dotted grey), for each device composing the array, in ‘increasing’ order of appearance (*i.e.* from device 1 to device 5). The constraint limits for displacement and velocity are denoted with a horizontal dash-dotted line.

Some key features can be directly appreciated in the left column of Figure 9.4, which are detailed in the following. To begin with, it is straightforward to notice that the state constraints are being consistently respected for all the devices composing the WEC array, illustrating the capability of the moment-based strategy to maximise energy-absorption while respecting the physical limitations of each device. Moreover, note that even in this fully constrained case, the velocity of the device under optimal control conditions remains ‘in-phase’ with the wave excitation force, agreeing with the well-known theoretical results for unconstrained energy-maximisation of (single) WECs (see Section 3.1). The right column of Figure 9.4 presents the control inputs for each device computed with the moment-based strategy (solid black), along with the wave excitation force (dotted gray) experienced by each device. Once again, it can be appreciated that the PTO force constraints (dash-dotted) are being respected consistently, showing the ability of the strategy to handle both state and input constraints simultaneously. Finally, note that the moment-based optimal control force is shifted by $\approx \pi/2$ [rad] with respect to the wave excitation force input, also agreeing with the theoretical (unconstrained maximum) power absorption conditions for an isolated WEC device (see Section 3.1).

Results under irregular wave excitation, randomly generated using a JONSWAP SDF (see Section 2.1.2), are now presented. In particular, a JONSWAP spectrum, analogous to the regular excitation case presented in Figure 9.4, is considered, *i.e.* with peak period $\bar{T}_w = 8$ [s] and significant wave height $\bar{H}_w = 2$ [m]. The peak enhancement factor is set to $\gamma = 3.3$. Both the state and input constraints for each device are also set to the same values as those for the regular excitation case of Figure 9.4, *i.e.* equation (9.31).

Figure 9.5 presents motion (left column) and energy-maximising control input (right column) results for this irregular wave input case. Note that this figure uses the same indexing to variables and devices as Figure 9.4. As can be appreciated from Figure 9.5, the MIMO moment-based strategy presented in this chapter, is able to maximise energy-absorption, while systematically respecting both

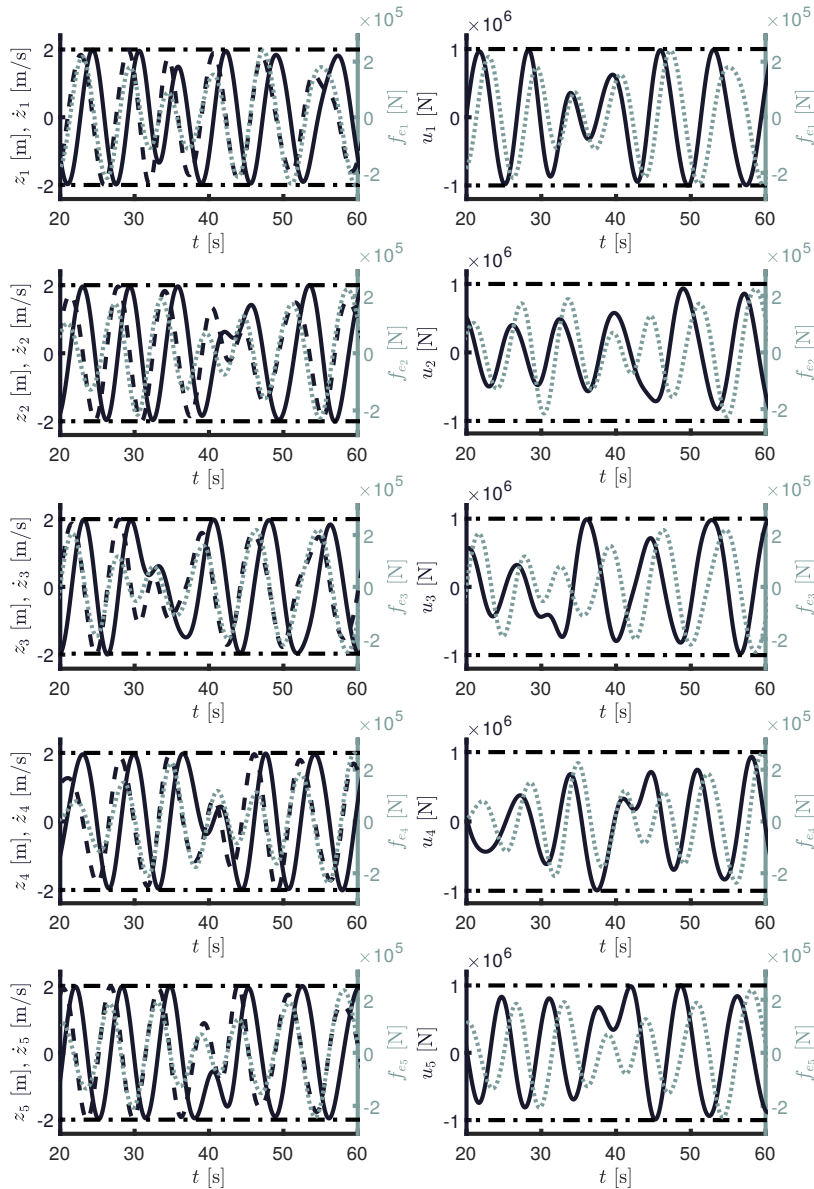


Figure 9.5: Results for irregular input wave excitation. The left column of Figure 9.5 shows displacement (solid black), velocity (dashed black) and wave excitation force input (dotted grey), for each device composing the array, for devices 1 (top) to 5 (bottom). The right column of Figure 9.5 presents (in the same order) the corresponding control inputs for each device computed with the moment-based strategy (solid black), along with the wave excitation force (dotted gray) experienced by each device. The horizontal dash-dotted lines represent constraint values.

state and input constraints for the case of this irregular wave input, according to the control design objective, and hence providing a strong practical result in a realistic sea description. In addition, note that the velocity and excitation force of each device presents the ‘in-phase’ optimal energy absorption condition for regular unconstrained motion. In fact, this behaviour is consistent with what has been reported previously in the energy-maximising moment-based strategy presented in Chapter 8, for the isolated (single) WEC case.

9.5 Conclusions

This chapter formally introduces an extension of the moment-based energy-maximising technique for a single WEC (SISO system) developed throughout Chapter 8 to a WEC farm (MIMO system),

providing a mathematical framework for array optimal control design with strong practical value, thus helping in the roadmap towards successful commercialisation of WEC technologies. This chapter demonstrates that the desirable properties of the moment-based strategy presented for the single WEC case, such as the mapping of the original objective function to a concave QP problem (which can be efficiently solved using state-of-the-art-solvers), are also retained in this WEC array optimal control framework. The chapter also details how to systematically handle both state and input constraints simultaneously, by making explicit use of the advantages inherently present in the moment-domain formulation. The combination between energy-maximisation, successful simultaneous state and input constraint handling, and computational efficiency (due to the nature of the objective function in moment-domain) has strong practical advantages, providing an optimal control framework that can maximise energy absorption from incoming sea waves, respect intrinsic physical limitations, and compute efficiently. Finally, this chapter demonstrates the usage of the proposed method by means of a full-scale WEC array composed of five CorPower-like devices, explicitly assessing the performance of the moment-based strategy for both regular and irregular wave excitation.

Contents of this chapter

10.1	Moment-based control under <i>system</i> uncertainty	228
10.1.1	Robust formulation under system uncertainty	232
10.1.2	Handling of state and input constraints	234
10.2	Moment-based control under <i>input</i> uncertainty	236
10.2.1	Robust formulation under input uncertainty	239
10.2.2	Handling of state and input constraints	241
10.3	A note on considering system and input uncertainty simultaneously	242
10.4	Case study: WEC under system uncertainty	243
10.4.1	On the definition of the uncertainty polytope \mathcal{P}	243
10.4.2	Performance assessment under regular waves	245
10.4.3	Performance assessment under irregular waves	248
10.4.4	Data-driven characterisation of system uncertainty	251
10.5	Case study: WEC under input uncertainty	254
10.5.1	On the definition of the uncertainty polytope \mathcal{P}	255
10.5.2	Performance assessment	256
10.6	Conclusions	258

Recall, from Section 2.4 and Chapter 8, that the equation of motion for a *controlled* WEC, under the assumptions of linear potential flow theory (see Section 2.3.1), can be expressed in terms of *Cummins'* equation (2.20). This equation is recalled below, for a 1-DoF WEC device, for convenience:

$$\Sigma^0 : \begin{cases} \ddot{z} = \mathcal{M}(-k_r * \dot{z} - s_h z + f_e - u), \\ y^0 = \dot{z}, \end{cases} \quad (10.1)$$

where $z : \mathbb{R}^+ \rightarrow \mathbb{R}$ is the displacement, $k_r : \mathbb{R}^+ \rightarrow \mathbb{R}$, $k_r \in L^2(\mathbb{R})$, the radiation impulse response function, $f_e : \mathbb{R}^+ \rightarrow \mathbb{R}$, the wave excitation force, and $\mathcal{M} \in \mathbb{R}_{>0}$ is the inverse of the generalised mass matrix of the device. Finally, $u : \mathbb{R}^+ \rightarrow \mathbb{R}$ represents the control input, supplied by means of the PTO system, and computed in terms of the energy-maximising optimal control problem defined in (8.4).

Remark 10.0.1 A SISO WEC system is considered in this section, aiming to simplify the notation. Nonetheless, note that MIMO WEC systems can be considered analogously, by simply following the theoretical framework presented in Chapter 9.

As discussed and detailed throughout Chapter 3, despite the fact that the number of control techniques, proposed in the literature, has increased considerably during recent years, only a few studies address the robustness of energy-maximising controllers; the optimal

control input is mostly computed based only on a *nominal* model, without considering possible dynamical deviations, *i.e.* *system uncertainty*, which are ubiquitous in hydrodynamic modelling. By way of example, some parameters of the WEC hydrodynamic model can vary significantly due to the change in the relative motion of the device (see, for instance, [18]), or simply due to unmodelled dynamics, not captured by the nominal WEC model. The scarcity of robust strategies among WEC control methods can be attributed to the fact that the design of energy-maximising controllers does not directly fit into a 'traditional' form, unlike the well-known reference tracking problem. This, in turn, intrinsically complicates the application of well-developed robust control strategies.

System uncertainty is not the only source of error inherently present in the WEC energy-maximising optimal control problem: Given that the wave excitation force, which is a key variable in the OCP (8.4), is virtually always approximated by means of unknown-input estimation (instantaneous values) and forecasting (future values) techniques, *input uncertainty* is also ubiquitous. Moreover, and to the best of the author's knowledge¹, robustness with respect to errors in the estimation and forecasting of the excitation effect, *i.e.* input uncertainty, has not been yet addressed in the current WEC control synthesis literature².

Motivated by the discussion provided above, this chapter details an energy-maximising moment-based framework which explicitly considers *system* and *input* uncertainty in the computation of the optimal control law, while systematically respecting motion and PTO (state and input) constraints. In particular, this is achieved by a suitable moment-based characterisation for the uncertainty, taking into consideration an appropriate uncertainty set, written in terms of a convex polytope defined over a real vector space. To this end, the concept of moments is combined with the robust optimisation principles considered in [182, 184], by proposing a *worst-case performance* (WCP) approach. Necessary and sufficient conditions on the definition of the uncertainty polytope are explicitly derived, so that this novel moment-based robust optimal control framework *always has a unique global energy-maximising solution*, preserving all the appealing characteristics of the (nominal) strategy developed in Chapter 8, hence leading to a computationally efficient robust control solution for WECs. The performance of the proposed controller is illustrated and analysed by means of a case study, considering a heaving point absorber WEC, subject to system and input uncertainty.

The remainder of this chapter is organised as follows. Section 10.1 describes and formalises the moment-based description of the energy-

1: See Section 3.4.2.1 for further detail on robust solutions for WECs available in the literature.

2: An assessment on the robustness of certain families of WEC control systems can be found in, for instance, [19, 88].

maximising optimal control problem under system uncertainty, and poses the so-called robust moment-based optimal control problem for uncertain WEC systems. Analogously, Section 10.2 formalises the robust moment-based optimal control problem for WEC systems under input uncertainty, *i.e.* considering that the wave excitation force measurement/estimate is affected by an external source of error. Section 10.3 briefly discusses the technicalities behind considering system and input uncertainty *simultaneously*. The use and performance of the robust moment-based control framework, proposed in this chapter, is illustrated using two case studies, presented in Sections 10.4 and 10.5, based on a spherical heaving point absorber WEC, under system and input uncertainty, respectively. Both sections include insight in the definition and computation of the corresponding uncertainty sets, which, ultimately, play a fundamental role in setting up the trade-off between performance and conservativeness of the control law. Finally, the main conclusions of this chapter are presented in Section 10.6.

Remark 10.0.2 Section 10.4 also offers a *data-driven* method to identify and define the (system) uncertainty set. In other words, (output) time-traces, obtained from nonlinear WEC models (including high-fidelity solvers such as those based in CFD), can be directly incorporated in this framework by means of a suitable approximation technique (specifically proposed in Section 10.4.4), which ‘maps’ each nonlinear output onto a suitably defined uncertainty set.

Remark 10.0.3 Throughout this chapter, aiming both to simplify the notation, and to solely focus the upcoming sections on the formulation of a robust moment-based approach under system and input uncertainty, the excitation force is assumed to be *available* over the complete time interval $\mathcal{T} \subset \mathbb{R}^+$, where energy absorption from incoming waves is maximised. This is done without any loss of generality, since a receding-horizon formulation can be achieved *directly*, by simply following the theory³ presented in Section 8.6, without further modifications. Naturally, *availability* of the excitation force *does not imply* perfect knowledge, but rather that a wave excitation measurement/estimate, potentially subject to uncertainty, is available throughout the time interval \mathcal{T} , in which the energy-maximising control law is computed.

3: In particular, by following the adaptation of the moment-based representation of the wave excitation input, to alleviate the effects of considering a (potentially) short time-horizon for the computation of the control law (see Section 8.6.1).

10.1 Moment-based control under *system uncertainty*

Consider the *nominal* WEC model Σ^0 , defined in equation (10.1), and suppose the mappings corresponding to both external inputs, *i.e.* the wave excitation force f_e , and control force u , are written in terms of the autonomous single-output signal generator $(S, L_e - L_u)$ (see equation (8.8)), with dynamic matrix S as in (8.9). In addition, suppose Assumption 8.2.1 and condition (5.16) hold. Then, the result of Proposition 8.2.1 follows, and the moment-domain equivalent of the output $y = \dot{z}$ of the nominal system Σ^0 is given by

$$\underline{\dot{z}}^0 = (L_e - L_u)\Phi_{\mathcal{D}}^T. \quad (10.2)$$

Remark 10.1.1 From now on, the matrix $\underline{\dot{z}}^0$ is referred to as the moment-domain equivalent of the velocity of the *nominal* WEC system Σ^0 .

In a more realistic scenario, the model describing the WEC dynamics is affected by modelling errors, which can be written in terms of a suitably defined *uncertainty*. This statement, together with a suitable definition for the uncertainty, is formalised in the following paragraphs.

Suppose Σ^Δ is a *stable* (in the Lyapunov sense) linear time invariant system describing the dynamics of the WEC under the presence of modelling errors, with output $y^\Delta = \dot{z}^\Delta$. As discussed in the introduction to this chapter, these errors can arise as a function of, for instance, the presence of parametric uncertainty in the definition of the WEC model, or simply as a consequence of unmodelled dynamics. Independent of the specific definition of the dynamics of Σ^Δ , the moment-domain equivalent of its output can always be *uniquely*⁴ computed analogously to equation (10.2), *i.e.* $\underline{\dot{z}}^\Delta$ can be computed as

$$\underline{\dot{z}}^\Delta = (L_e - L_u)\Phi_\Delta^T, \quad (10.3)$$

where the matrix $\Phi_\Delta^T \in \mathbb{R}^{\nu \times \nu}$ depends on the specification of Σ^Δ , and can be simply defined analogously to (8.12). To be precise, in terms of the formal definition of the (system) uncertainty allowed throughout this chapter, the definition of *uncertain WEC system* Σ^Δ , adopted for the remainder of this analysis, is provided below.

4: Uniqueness of the moment-domain equivalent $\underline{\dot{z}}^\Delta$ is a direct consequence of the internal stability of Σ^Δ (see the discussion provided in Section 5.1).

Definition 10.1.1 (Uncertain WEC system) *Suppose Assumption 8.2.1 and condition (5.16) hold. A system describing the dynamics of a WEC is termed an uncertain WEC system if it's defined by a stable linear time invariant system Σ^Δ , and the moment of Σ^Δ at the signal generator $(S, L_e - L_u)$ is given by,*

$$\underline{\dot{Z}}^\Delta = \underline{\dot{Z}}^0 + \underline{\dot{Z}}^0 \Delta, \quad (10.4)$$

where $\underline{\dot{Z}}^0$ is as in equation (10.2), and the matrix $\Delta \in \mathbb{R}^{\nu \times \nu}$ is given by

$$\Delta = (\Phi_{\mathcal{R}}^\top)^{-1} \Phi_\Delta^\top - \mathbb{I}_\nu. \quad (10.5)$$

Definition 10.1.1 can be easily interpreted from a 'traditional' robust control theory viewpoint. In particular, it stems directly from considering that the nominal WEC system Σ^0 is *perturbed* by a *multiplicative output uncertainty* [234]. This output uncertainty is characterised by a stable linear time-invariant system H^Δ , with input y^0 (i.e. nominal velocity of the WEC), and where the moment-domain equivalent of its output d^Δ is given by,

$$\underline{D}^\Delta = \underline{\dot{Z}}^0 \Delta. \quad (10.6)$$

The discussion provided above is schematically illustrated in Figure 10.1, also including the description of each steady-state output in terms of the corresponding moments.

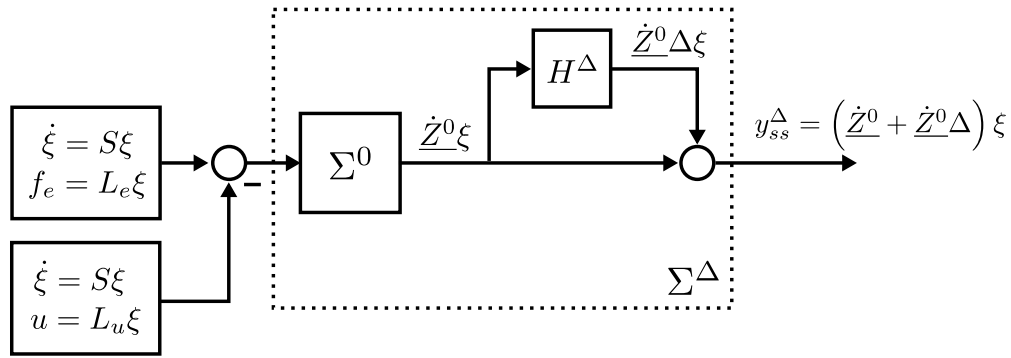


Figure 10.1: Schematic illustration of nominal WEC system Σ^0 subject to multiplicative output uncertainty, including each corresponding moment-based representation.

Remark 10.1.2 From now on, the matrix $\underline{\dot{Z}}^\Delta$ is referred to as the moment-domain equivalent of the velocity of the *uncertain* WEC system Σ^Δ .

Remark 10.1.3 Note that the definition of the matrix Δ follows immediately from equations (10.3) and (10.4), i.e.

$$\underline{\dot{Z}}^\Delta = (L_e - L_u) \Phi_\Delta^\top = (L_e - L_u) \Phi_{\mathcal{R}}^\top (\mathbb{I}_\nu + \Delta), \quad (10.7)$$

which, taking into account that the matrix $\Phi_{\mathcal{R}}^{\top}$ is always invertible, as a consequence of the uniqueness of the moment-domain equivalent of the nominal system \dot{Z}^0 (under Assumption 8.2.1 and condition (5.16)), automatically implies (10.5).

Remark 10.1.4 Given the specific structure of the matrices involved in equation (10.5), it is straightforward to note that the matrix Δ can always be written as,

$$\Delta = \bigoplus_{p=1}^f \begin{bmatrix} p\delta^+ & p\delta^- \\ -p\delta^- & p\delta^+ \end{bmatrix}, \quad (10.8)$$

where $\{p\delta^+, p\delta^-\}_{p=1}^f \subset \mathbb{R}$.

Not only is Δ always structured as (10.8), but it can also be fully characterised in terms of a vector $\delta \in \mathbb{R}^{\nu}$, which is especially useful for the upcoming definitions and computations. The nature of this vector is formalised in the following. Let $\delta \in \mathbb{R}^{\nu}$ be the *uncertainty vector*, defined as

$$\delta = \sum_{p=1}^f e_p^f \otimes \begin{bmatrix} p\delta^+ \\ p\delta^- \end{bmatrix}. \quad (10.9)$$

Following Remark 10.1.4, it is clear that the matrix Δ can always be written in terms of the uncertainty vector δ , provided a suitable mapping $\delta \mapsto \Delta$ is defined. In particular, the following mapping $\Gamma : \mathbb{R}^{\nu} \rightarrow \mathbb{R}^{\nu \times \nu}$, $\delta \mapsto \Gamma(\delta)$, is proposed, defined as below:

$$\begin{aligned} \Gamma(\delta) &= \sum_{p=1}^f \left(\delta^{\top} e_{2p-1}^f \right) \begin{bmatrix} 1 & 0 \\ 0 & 1 \end{bmatrix} + \left(\delta^{\top} e_{2p}^f \right) \begin{bmatrix} 0 & 1 \\ -1 & 0 \end{bmatrix}, \\ &= \bigoplus_{p=1}^f \begin{bmatrix} p\delta^+ & p\delta^- \\ -p\delta^- & p\delta^+ \end{bmatrix} = \Delta. \end{aligned} \quad (10.10)$$

Remark 10.1.5 Note that, as per equation (10.10), the mapping Γ is *linear* in the argument δ . As discussed in Section 10.1.1, the linearity of the mapping Γ plays a fundamental role in the existence, uniqueness, and tractability of the robust moment-based energy-maximising procedure, proposed in this chapter.

Recall that the objective function, involved in the definition of the energy-maximising OCP (8.4), explicitly depends on the velocity of the WEC system. Suppose now that, instead of considering the nominal system Σ^0 (as in the energy-maximising control framework of Chapter 8), the WEC system is now affected by the presence of modelling errors, *i.e.* the uncertain WEC system Σ^{Δ} is considered

(see Definition 10.1.1). The following proposition is analogous to Proposition 8.3.2, and makes use of the moment-domain equivalent of the output of the uncertain WEC system, *i.e.* $\underline{\dot{Z}}^\Delta$, to show that the target optimal control problem (8.4) (which is originally defined over an infinite-dimensional space), can be parameterised in terms of moments.

Proposition 10.1.1 Consider the unconstrained⁵ OCP (8.4) and suppose Assumption 8.2.1 and condition (5.16) hold. Then, given a fixed uncertainty vector $\delta \in \mathbb{R}^\nu$, the optimal control law u^{opt} which maximises the objective function \mathcal{J} over the time period \mathcal{T} , for the uncertain system Σ^Δ , can be computed in the moment-domain as the solution of the QP problem

$$\begin{aligned} u^{opt} &= L_u^{opt} \xi, \\ L_u^{opt} &= \arg \max_{L_u^\top \in \mathbb{R}^\nu} -\frac{1}{2} L_u \Phi_{\mathcal{R}}^\top (\mathbb{I}_\nu + \Gamma(\delta)) L_u^\top + \\ &\quad \frac{1}{2} L_e \Phi_{\mathcal{R}}^\top (\mathbb{I}_\nu + \Gamma(\delta)) L_u^\top. \end{aligned} \quad (10.11)$$

5: The term unconstrained here refers to the optimal control problem (8.4) without consideration of the set of state and input constraints \mathcal{C} .

Proof. Consider the result of Proposition 8.3.1 (*i.e.* equation (8.14)). Then, given that Assumption 8.2.1 and condition (5.16) hold by hypothesis, the moment-domain equivalent of the output of the uncertain system is always well-defined, and the claim follows by simply replacing $\underline{\dot{Z}}^\Delta$ according to equation (10.7). \square

The result of Proposition 10.1.1 explicitly shows that the computation of a moment-based energy-maximising control law, in the presence of modelling uncertainty, boils down to solving a QP problem. As in the nominal case discussed in Chapter 8, this QP formulation can be solved efficiently *if and only if* equation (10.11) has a unique global maximiser, *i.e.* the problem is *strictly concave*.

Remark 10.1.6 In contrast to the moment-based optimal control framework for the nominal WEC model Σ^0 , presented in Chapter 8, the existence and uniqueness of a global maximiser for the QP (10.11) explicitly depend upon the definition of the uncertainty vector δ . In the light of this, necessary and sufficient conditions for strict concavity of this QP are explicitly given in Proposition 10.1.2.

Proposition 10.1.2 The QP problem defined in (10.11) has a unique global energy-maximising solution if and only if

$$\Re\{\psi_p\} + \begin{bmatrix} \Re\{\psi_p\} & -\Im\{\psi_p\} \end{bmatrix} \begin{bmatrix} p\delta^+ \\ p\delta^- \end{bmatrix} > 0, \quad (10.12)$$

for all $p \in \mathbb{N}_f$, and where each $\psi_p \in \mathbb{C}^{2 \times 2}$ is defined as in (8.24).

Proof. This proof can be started by noting that (10.11) has a unique global solution if and only if the symmetric part of $\Phi_\Delta^\top = \Phi_\Delta^\top(\mathbb{I}_\nu + \Gamma(\delta))$ is positive-definite. Following the proof of Proposition 8.3.3, note that one can always write the matrix Φ_Δ in a block-diagonal form, i.e. $\Phi_\Delta = \bigoplus_{p=1}^f \Phi_{\Delta_p}$, with each p -block defined as

$$\Phi_{\Delta_p}^\top = \begin{bmatrix} \Re\{\psi_p\} & \Im\{\psi_p\} \\ -\Im\{\psi_p\} & \Re\{\psi_p\} \end{bmatrix} \left(\mathbb{I}_2 + \begin{bmatrix} p\delta^+ & p\delta^- \\ -p\delta^- & p\delta^+ \end{bmatrix} \right), \quad (10.13)$$

for all $p \in \mathbb{N}_f$, and where each matrix ψ_p is defined as in (8.23). Hence, the symmetric-part of Φ_Δ can be written as,

$$\mathcal{H}\{\Phi_\Delta^\top\} = \bigoplus_{i=1}^f \begin{bmatrix} \psi_p^\Delta & 0 \\ 0 & \psi_p^\Delta \end{bmatrix}, \quad (10.14)$$

with each $\psi_p^\Delta \in \mathbb{R}$ defined as

$$\Re\{\psi_p\} + \Re\{\psi_p\}^p \delta^+ - \Im\{\psi_p\}^p \delta^-, \quad (10.15)$$

for all $p \in \mathbb{N}_f$. Clearly, $\mathcal{H}\{\Phi_\Delta^\top\}$ is positive-definite if and only if $\psi_p^\Delta > 0$, for all $p \in \mathbb{N}_f$, which proves the claim. \square

Remark 10.1.7 Note that, if $\|\delta\|_2 < \epsilon$, with ϵ sufficiently small, then the condition expressed in (10.12) always holds, as a consequence that $\Re\{\psi_p\} > 0$, for all $p \in \mathbb{N}_f$ (see Remark 8.3.1).

10.1.1 Robust formulation under system uncertainty

In this section, and following the approach proposed in [182], the moment-domain optimisation problem (10.11) is re-formulated based on the underlying principles of robust optimisation theory, developed in key studies such as [184]. The underpinning concept behind this approach originates in the field of decision theory, and is known as *Wald's Minimax (Maximin) paradigm* [250], also commonly referred to as the *Worst-Case Performance (WCP)* method. Before going further with the formal definition of a robust moment-based energy-maximising QP formulation, the following standing assumption is introduced.

Assumption 10.1.1 The uncertainty vector δ is such that $\delta \in \mathcal{P}$, where $\mathcal{P} \subset \mathbb{R}^\nu$ is a convex \mathcal{V} -polytope⁶, defined as the convex hull of a finite set of N_V points (vertices) in space $V_\delta = \{\delta_1^V, \dots, \delta_{N_V}^V\}$, i.e. $\mathcal{P} = \text{conv}\{V_\delta\}$.

6: The reader is referred to [234] for further detail in convex polytopes and their use in robust control applications.

Finally, in the spirit of the WCP method, and using the result of (10.11), the robust moment-based energy-maximising QP formulation, for uncertain WEC systems, is defined as follows.

Problem 10.1.1 (Robust energy-maximising OCP under system uncertainty) Suppose condition 10.1.2 holds for every uncertainty vector $\delta \in \mathcal{P}$, and Assumption 10.1.1 holds. Then, the robust formulation of the (unconstrained) energy-maximising QP problem (10.11) under system uncertainty can be written as

$$\begin{aligned} u^{\text{RC}} &= L_u^{\text{RC}} \xi, \\ L_u^{\text{RC}} &= \arg \max_{L_u^{\text{T}} \in \mathbb{R}^{\nu}} \arg \min_{\delta \in \mathcal{P}} -\frac{1}{2} L_u \Phi_{\mathcal{R}}^{\text{T}} (\mathbb{I}_{\nu} + \Gamma(\delta)) L_u^{\text{T}} + \quad (10.16) \\ &\quad \frac{1}{2} L_e \Phi_{\mathcal{R}}^{\text{T}} (\mathbb{I}_{\nu} + \Gamma(\delta)) L_u^{\text{T}}, \end{aligned}$$

where u^{RC} denotes the worst-case performance moment-based energy-maximising optimal control law.

Problem 10.1.1 computes the *worst-case scenario* for the energy-maximising problem (10.11), with respect to *every possible uncertainty vector* δ , lying inside the polytope \mathcal{P} .

Remark 10.1.8 Assumption 10.1.1 plays a fundamental role in the definition of Problem 10.1.1, as detailed in the following. Note that, as a direct consequence of the linearity of the mapping Γ (see Remark 10.1.5), the minimisation problem in (10.16) is *affine* in δ . Then, taking into account that δ is such that condition 10.1.2 holds, *i.e.* the QP problem in L_u is always *strictly concave*, the solution of the moment-based robust formulation (10.16) is reached precisely on the convex hull of the uncertainty set \mathcal{P} [207]. Moreover, given that \mathcal{P} is convex by Assumption 10.1.1, the solution of (10.16) lies precisely at one of the vertices of \mathcal{P} , *i.e.* it is *sufficient to solve equation (10.16) only for the N_V elements of the finite set V_{δ}* (see, for instance, [207, 251]).

Two main conclusions can be directly extracted from Remark 10.1.8. Firstly, the robust energy-maximising framework, defined in Problem 10.1.1, *always has a unique globally optimal* solution. Secondly, the optimisation problem to be solved is *tractable*⁷, *i.e.* it is sufficient to solve (10.16) for a small number of ‘points’, characterising the vertices of the uncertainty polytope. This, in turn, directly implies that (10.16) can be effectively solved using computationally efficient minimax optimisation routines [207, 253, 254].

Remark 10.1.9 The definition of the uncertainty set \mathcal{P} plays a key role on the actual performance of the proposed robust approach:

7: The reader is referred to [252] for a formal definition of a tractable optimisation problem.

a 'larger' polytope \mathcal{P} , naturally covers a 'wider' uncertainty set, at the expense of computing a more conservative WCP energy-maximising solution. In other words, the definition of the set \mathcal{P} has to be done *sensibly*, ideally using *a-priori* information of the potential modelling errors present in the analysed WEC system. Insight on how to achieve a suitable definition for such a polytope, for the case of system uncertainty, can be explicitly found in Section 10.4, including an explicit procedure to compute \mathcal{P} .

10.1.2 Handling of state and input constraints

In principle, the handling of state and input constraints can be done somewhat 'analogously' to the nominal moment-based controller developed throughout Chapter 8, with some additional considerations, given the inherent presence of uncertainty in this robust moment-based control case. That said, the set of state and input constraints (8.3) can be mapped using their respective (uncertain) moment-domain equivalents, as

$$\mathcal{C} : \begin{cases} |z(t)| \leq Z_{\max}, \\ |\dot{z}(t)| \leq \dot{Z}_{\max}, \\ |u(t)| \leq U_{\max}, \end{cases} \mapsto \begin{cases} |\dot{Z}^{\Delta} S^{-1} \xi(t)| \leq Z_{\max}, \\ |\dot{Z}^{\Delta} \xi(t)| \leq \dot{Z}_{\max}, \\ |L_u \xi(t)| \leq U_{\max}. \end{cases} \quad (10.17)$$

Following the collocation approach presented in Section 8.3.1, let $\mathcal{T}_c = \{t_i\}_{i=1}^{N_c} \subset \mathcal{T} \subset \mathbb{R}^+$, be a finite set of (specified) uniformly-spaced time instants, with $N_c \in \mathbb{N}_{\geq 1}$. Let $\Upsilon \in \mathbb{R}^{\nu \times 2N_c}$ be defined as in (8.30).

Remark 10.1.10 Given that it is sufficient to solve the robust formulation defined in Problem 10.1.1 *only* at the finite-set of vertices of the convex polytope \mathcal{P} (see Remark 10.1.8), a sensible approach to incorporate state constraints into Problem 10.1.1 is to guarantee that such constraints are satisfied at every point of the set of vertices V_{δ} . This effectively ensures that the state constraints in (10.17) are consistently fulfilled *for every* $\delta \in \mathcal{P}$ [207, 251].

Finally, one can formulate a robust moment-based energy-maximising *constrained* optimal control law for WECs, explicitly considering the presence of uncertainty in the WEC model, in terms of an inequality-constrained minimax QP problem, which always has a *unique* globally optimal solution. This is addressed in the following proposition.

Proposition 10.1.3 Consider Problem 10.1.1 and the uncertain WEC system Σ^Δ . Suppose condition 10.1.2 holds for every uncertainty vector $\delta \in \mathcal{P}$, and Assumption 10.1.1 holds. Then, the state and (control) input constrained robust moment-based energy-maximising control law u^{RC} can be computed in terms of the following minimax QP problem,

$$\begin{aligned} u^{RC} &= L_u^{RC} \xi, \\ L_u^{RC} &= \arg \max_{L_u^T \in \mathbb{R}^\nu} \arg \min_{\delta \in V_\delta \subset \mathcal{P}} -\frac{1}{2} L_u \Phi_{\mathcal{R}}^T (\mathbb{I}_\nu + \Gamma(\delta)) L_u^T + \\ &\quad \frac{1}{2} L_e \Phi_{\mathcal{R}}^T (\mathbb{I}_\nu + \Gamma(\delta)) L_e^T, \end{aligned} \quad (10.18)$$

subject to:

$$L_u \mathcal{A}_z^{RC} \leq \mathcal{B}_z^{RC},$$

$$L_u \mathcal{A}_{\dot{z}}^{RC} \leq \mathcal{B}_{\dot{z}}^{RC},$$

$$L_u \mathcal{A}_u \leq \mathcal{B}_u,$$

where the pair of matrices $(\mathcal{A}_u, \mathcal{B}_u)$ is defined as in (8.31), and where

$$\begin{aligned} \mathcal{A}_z^{RC} &= [\mathcal{A}_z^{\delta_1^V} \quad \dots \quad \mathcal{A}_z^{\delta_N^V}], \quad \mathcal{B}_z^{RC} = [\mathcal{B}_z^{\delta_1^V} \quad \dots \quad \mathcal{B}_z^{\delta_N^V}], \\ \mathcal{A}_{\dot{z}}^{RC} &= [\mathcal{A}_{\dot{z}}^{\delta_1^V} \quad \dots \quad \mathcal{A}_{\dot{z}}^{\delta_N^V}], \quad \mathcal{B}_{\dot{z}}^{RC} = [\mathcal{B}_{\dot{z}}^{\delta_1^V} \quad \dots \quad \mathcal{B}_{\dot{z}}^{\delta_N^V}], \end{aligned} \quad (10.19)$$

with each element of the sets $\{\mathcal{A}_z^{\delta_i^V}, \mathcal{A}_{\dot{z}}^{\delta_i^V}\}$ and $\{\mathcal{B}_z^{\delta_i^V}, \mathcal{B}_{\dot{z}}^{\delta_i^V}\}$ defined as,

$$\begin{aligned} \mathcal{A}_z^{\delta_i^V} &= -\Phi_{\mathcal{R}}^T S^{-1} \Upsilon - \Phi_{\mathcal{R}}^T \Gamma(\delta_i^V) S^{-1} \Upsilon = \mathcal{A}_z + \tilde{\mathcal{A}}_z(\delta_i^V), \\ \mathcal{B}_z^{\delta_i^V} &= Z_{\max} \mathbf{1}_{1 \times 2N_c} + L_e \mathcal{A}_z^{\delta_i^V} = \mathcal{B}_z + \tilde{\mathcal{B}}_z(\delta_i^V), \\ \mathcal{A}_{\dot{z}}^{\delta_i^V} &= -\Phi_{\mathcal{R}}^T \Upsilon - \Phi_{\mathcal{R}}^T \Gamma(\delta_i^V) \Upsilon = \mathcal{A}_{\dot{z}} + \tilde{\mathcal{A}}_{\dot{z}}(\delta_i^V), \\ \mathcal{B}_{\dot{z}}^{\delta_i^V} &= \dot{Z}_{\max} \mathbf{1}_{1 \times 2N_c} + L_e \mathcal{A}_{\dot{z}}^{\delta_i^V} = \mathcal{B}_{\dot{z}} + \tilde{\mathcal{B}}_{\dot{z}}(\delta_i^V), \end{aligned} \quad (10.20)$$

for all $\delta_i^V \in V_\delta$.

Proof. The proof of this proposition follows the same steps as those employed in Proposition 8.3.5, taking into account that the set of constraints (10.17) are enforced, in Problem 10.1.1, at each element of the set of vertices V_δ (defining the uncertainty polytope \mathcal{P}) and, hence, is omitted for brevity. \square

Remark 10.1.11 The computation of the matrices \mathcal{A}_u and \mathcal{B}_u can be performed exactly as in the nominal case presented in Chapter 8: the definition of the PTO force constraint *does not* depend upon the definition of the uncertainty set \mathcal{P} . Although this is not

the case with the pairs of matrices $(\mathcal{A}_z^{\text{RC}}, \mathcal{B}_z^{\text{RC}})$ and $(\mathcal{A}_{\dot{z}}^{\text{RC}}, \mathcal{B}_{\dot{z}}^{\text{RC}})$, which explicitly depend on the nature of the uncertainty polytope \mathcal{P} (*i.e.* the set of vertices V_δ), it is sufficient to compute these matrices *only once*, which can be readily done offline⁸, following the definition of the set \mathcal{P} .

Remark 10.1.12 It is noteworthy that the matrices $\{\mathcal{A}_z^{\delta_i^V}, \mathcal{A}_{\dot{z}}^{\delta_i^V}\}$ and $\{\mathcal{B}_z^{\delta_i^V}, \mathcal{B}_{\dot{z}}^{\delta_i^V}\}$ can be computed, for all $\delta_i^V \in V_\delta$, as the sum of the nominal constraint matrices $\{\mathcal{A}_z, \mathcal{A}_{\dot{z}}\}$ and $\{\mathcal{B}_z, \mathcal{B}_{\dot{z}}\}$, defined in Proposition 8.3.5, and a linear ‘perturbation’ term, accounting for the effect of the uncertainty vector δ .

8: In other words, the computation of the set of constraints does not influence the computational complexity of the proposed solution.

10.2 Moment-based control under *input* uncertainty

As previously discussed in the introduction to this chapter, the wave excitation force f_e inherently arises from a combination of unknown-input estimation, and forecasting techniques. In other words, the excitation force signal, utilised by the energy-maximising controller, is prone to be affected by uncertainty, arising directly from errors in both the estimation and forecasting processes. Moreover, as detailed in Section 8.7, the computation of the moment-based energy-maximising strategy is especially sensitive to estimation errors, particularly those manifested as a ‘delay’ in the excitation force estimate (*i.e.* errors in instantaneous phase). Motivated by the discussion provided above, this section details a moment-based energy-maximising control framework which is robust with respect to *input* uncertainty. From now on, and borrowing the notation from Chapter 8, the *approximated* wave excitation force signal⁹, arising from both estimation and forecasting processes, is denoted as \tilde{f}_e .

To be precise, suppose now that the WEC system Σ is assumed to be that defined as the nominal system, *i.e.* $\Sigma = \Sigma^0$ (see equation (10.1)), and that the uncertainty is assumed to be ‘located’ in the input mapping \tilde{f}_e only. Analogously to Section 10.1, this section begins by providing a suitable definition of a *nominal* signal generator \mathcal{G}^0 , *i.e.*

$$\mathcal{G}^0 : \begin{cases} \dot{\xi} = S\xi, \\ \tilde{f}_e^0 = L_e^0 \xi, \\ u = L_u \xi, \end{cases} \quad (10.21)$$

where S and L_u are defined as in (8.8), and $L_e^0 \in \mathbb{R}^{1 \times \nu}$ characterises the *nominal wave excitation force* \tilde{f}_e^0 .

9: Often referred to, throughout this section, as either *wave excitation force estimate*, or simply *wave excitation force* (when clear from the context).

Remark 10.2.1 From now on, the matrix L_e^0 is referred to as the *nominal output vector* for the wave excitation force, associated with the nominal signal generator (10.21).

Based on the definition of the nominal excitation force \tilde{f}_e^0 , the aim is now to consider the presence of uncertainty in the definition of the wave excitation force input \tilde{f}_e . Suppose the excitation force affected by uncertainty, denoted as \tilde{f}_e^Δ , is defined in terms of ξ as,

$$\tilde{f}_e^\Delta = L_e^\Delta \xi, \quad (10.22)$$

with $L_e^\Delta \in \mathbb{R}^{1 \times \nu}$. Similarly to the case of Section 10.1, and to be precise in terms of the formal definition of the (input) uncertainty specified throughout this section, the definition of the so-called *uncertain signal generator* \mathcal{G}^Δ is now provided, inspired by Definition 10.1.1.

Remark 10.2.2 Note that the same notation considered in Section 10.1 is used for the definition of the variables related to input uncertainty in this section, for the sake of simplicity. That said, note that both the use, and specific meaning of each of these variables, is *always* clear from the context.

Definition 10.2.1 (Uncertain signal generator) *Let S and L_u be as in (8.8). The exogenous system \mathcal{G}^Δ is termed an uncertain signal generator if it is described by the set of equations,*

$$\mathcal{G}^\Delta : \begin{cases} \dot{\xi} = S\xi, \\ \tilde{f}_e^\Delta = (L_e^0 + L_e^0 \Delta)\xi, \\ u = L_u \xi, \end{cases} \quad (10.23)$$

where L_e^0 is as in equation (10.21), and the matrix $\Delta \in \mathbb{R}^{\nu \times \nu}$ is such that,

$$L_e^0 \Delta = L_e^\Delta - L_e^0. \quad (10.24)$$

Similarly to the uncertain WEC system in Definition 10.1.1, the uncertain signal generator, in Definition 10.2.1, can also be interpreted from a robust control theory viewpoint. In particular, Definition 10.2.1 stems directly from considering that the nominal signal generator \mathcal{G}^0 is affected by a *multiplicative output uncertainty* in a *single output channel*, i.e. the output associated with the wave excitation force f_e . This uncertainty is characterised by a *stable* linear time-invariant system H^Δ , with input \tilde{f}_e^0 (i.e. the nominal excitation force), and where the moment-domain equivalent of its output d^Δ is given by,

$$\underline{D}^\Delta = L_e^0 \Delta. \quad (10.25)$$

Analogously to the case presented in Figure 10.1, the viewpoint

provided in the discussion above, is schematically illustrated in Figure 10.2.

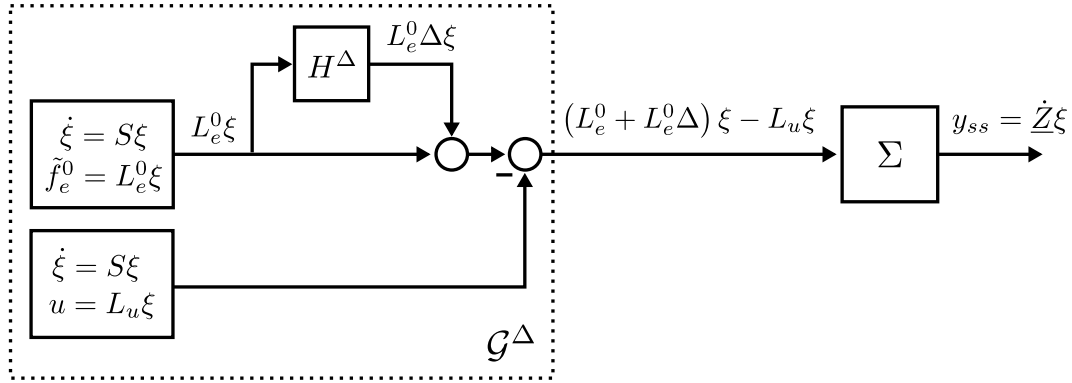


Figure 10.2: Schematic illustration of the nominal signal generator \mathcal{G}^0 , subject to multiplicative output uncertainty, including each corresponding moment-based representation.

Remark 10.2.3 From now on, the matrix L_e^Δ is referred to as the *uncertain output vector* for the wave excitation force, associated with the uncertain signal generator (10.23).

Remark 10.2.4 The matrix Δ is also structured as in Remark 10.1.4 and, hence, can be fully characterised in terms of an *uncertainty vector* $\delta \in \mathbb{R}^\nu$, by means of the linear mapping Γ defined in (10.10).

Aiming to pose a robust moment-based energy-maximising formulation for WECs under input uncertainty, the first fundamental step is to provide an expression for the moment-domain equivalent of the device velocity \dot{Z} , considering the uncertain wave excitation force \tilde{f}_e^Δ . This is, indeed, straightforward to compute from the result of Proposition 8.2.1, by introducing the following standing assumption.

Assumption 10.2.1 The pair of matrices $(S, L_e^0 + L_e^0 \Delta - L_u)$ is observable.

Remark 10.2.5 Assumption 10.2.1 is analogous to Assumption 8.2.1 (considered for the nominal moment-based WEC controller developed throughout Chapter 8), and guarantees that the definition of moments, for the WEC device under input uncertainty, is always well-posed.

That said, suppose Assumption 10.2.1 and condition (5.16) hold. Then, the moment-domain equivalent of the WEC velocity under the effect of input uncertainty can be computed as,

$$\dot{Z} = (L_e^0 + L_e^0 \Delta - L_u) \Phi_{\mathcal{R}}^T, \quad (10.26)$$

where the matrix $\Phi_{\mathcal{R}}^T \in \mathbb{R}^{\nu \times \nu}$ is defined as in (8.12).

With the definition of $\dot{\underline{z}}$ in equation (10.26), the energy-maximising OCP (8.4), considering the uncertain wave excitation force \tilde{f}_e^Δ , can be mapped to a finite-dimensional *strictly concave* QP problem, using the associated moment-based representations. This is addressed in the following proposition¹⁰.

Proposition 10.2.1 *Consider the unconstrained OCP (8.4) and suppose Assumption 10.2.1 and condition (5.16) hold. Then, given a fixed uncertainty vector δ , the optimal control law u^{opt} , which maximises the objective function \mathcal{J} over the time period \mathcal{T} , for the uncertain signal generator \mathcal{G}^Δ , can be computed in the moment-domain as the solution of the QP problem*

$$\begin{aligned} u^{opt} &= L_u^{opt} \xi, \\ L_u^{opt} &= \arg \max_{L_u^T \in \mathbb{R}^\nu} -\frac{1}{2} L_u \Phi_{\mathcal{R}}^T L_u^T + \frac{1}{2} L_e^0 (\mathbb{I}_\nu + \Gamma(\delta)) \Phi_{\mathcal{R}}^T L_u^T. \end{aligned} \quad (10.27)$$

Proof. This proof follows the same arguments as those considered in the proof of Proposition 10.1.1, taking into account the expression for the moment-domain equivalent of the device velocity $\dot{\underline{z}}$ under the presence of input uncertainty, *i.e.* equation (10.26) and, hence, is omitted for brevity. \square

Remark 10.2.6 There is a fundamental difference between the result of Proposition 10.1.1, *i.e.* energy-maximisation under *system* uncertainty, and Proposition 10.2.1, *i.e.* energy-maximisation under *input* uncertainty, as discussed in the following. Unlike the case of Proposition 10.1.1, the QP formulation presented in (10.27) is *always strictly concave independent of the definition of δ* . Concavity, for this case, is simply a direct result of Corollary 8.3.4, in the light of Remark 8.3.1. In other words, given *any* fixed uncertainty vector δ , there exists a *unique global energy-maximising solution* for the moment-based WEC optimal control problem under input uncertainty.

10.2.1 Robust formulation under input uncertainty

Based on the results and definitions posed in Section 10.2, an analogous robust moment-based procedure (to that outlined in Section 10.1.1 for uncertain WEC systems), can be carried out for the input uncertainty case. In particular, in the spirit of the WCP

10: Note that Proposition 10.2.1 is analogous to Proposition 10.1.1, considering input, rather than system, uncertainty.

method, the following robust energy-maximising QP formulation is defined, for the case of an uncertain signal generator \mathcal{G}^Δ .

Problem 10.2.1 (Robust energy-maximising OCP under input uncertainty) Suppose Assumption 10.1.1 holds. Then, the robust formulation of the (unconstrained) energy-maximising QP problem (10.11) under input uncertainty can be written as,

$$\begin{aligned} u^{\text{RC}} &= L_u^{\text{RC}} \xi, \\ L_u^{\text{RC}} &= \arg \max_{L_u^{\text{T}} \in \mathbb{R}^{\nu}} \arg \min_{\delta \in \mathcal{P}} -\frac{1}{2} L_u \Phi_{\mathcal{R}}^{\text{T}} L_u^{\text{T}} + \\ &\quad \frac{1}{2} L_e^0 (\mathbb{I}_{\nu} + \Gamma(\delta)) \Phi_{\mathcal{R}}^{\text{T}} L_u^{\text{T}}, \end{aligned} \quad (10.28)$$

where u^{RC} denotes the worst-case performance moment-based energy-maximising optimal control law.

Analogously to Problem 10.1.1, Problem 10.2.1 computes the worst-case scenario for the energy-maximising problem (10.27), taking into account *every possible uncertainty vector* δ , lying inside the polytope \mathcal{P} (*i.e.* the uncertainty set).

Remark 10.2.7 Note that, as in the case of Section 10.1.1 for uncertain WEC systems, the polytope \mathcal{P} , defining the uncertainty affecting the wave excitation force estimate, is such that Assumption 10.1.1 holds, *i.e.* \mathcal{P} is a \mathcal{V} -convex polytope, defined by finite set of vertices V_δ .

Remark 10.2.8 Assumption 10.1.1 plays the same role as in the robust formulation under system uncertainty. In particular, as a direct consequence of the linearity of the mapping Γ , (10.28) is *affine* in δ . Taking into account that the QP problem in L_u is always strictly concave for any δ (see Remark 10.2.6), the solution of the moment-based robust formulation under input uncertainty (10.28) is reached on the convex hull of the uncertainty set \mathcal{P} . Since \mathcal{P} is convex by Assumption 10.1.1, the solution of (10.28) lies precisely at one of the vertices of \mathcal{P} , and it is sufficient to solve (10.28) only for the finite-set of N_V vertices V_δ (see [207, 251]).

Remark 10.2.9 Once again, the definition of the uncertainty set \mathcal{P} determines the performance of the proposed robust approach, following the discussion provided in Remark 10.1.9. A methodology to compute this uncertainty polytope is specifically discussed, for the input uncertainty case, in Section 10.5.

10.2.2 Handling of state and input constraints

Following the same approach as in Section 10.1.2, *i.e.* using a collocation approach, the incorporation of state and input constraints in Problem 10.2.1 can be performed by making explicit use of the set \mathcal{T}_c , and the matrix Υ defined in equation (8.30).

In the light of Remark 10.1.10, the constraints are formulated such that they are satisfied at each point contained in the set of vertices V_δ , ensuring that the state constraints are consistently fulfilled at every $\delta \in \mathcal{P}$. This is formalised in the following proposition, which presents a robust moment-based energy-maximising constrained optimal control law for WECs, in terms of an inequality-constrained minimax QP problem which has a *unique* solution, explicitly considering the presence of uncertainty in the wave excitation estimate.

Proposition 10.2.2 *Consider Problem 10.2.1 and the uncertain signal generator \mathcal{G}^Δ . Suppose Assumption 10.1.1 holds. Then, the state and (control) input constrained robust moment-based energy-maximising control law u^{RC} , can be computed in terms of the following minimax QP problem,*

$$\begin{aligned} u^{RC} &= L_u^{RC} \xi, \\ L_u^{RC} &= \arg \max_{L_u^T \in \mathbb{R}^\nu} \arg \min_{\delta \in V_\delta \subset \mathcal{P}} -\frac{1}{2} L_u \Phi_{\mathcal{R}}^T L_u^T + \\ &\quad \frac{1}{2} L_e^0 (\mathbb{I}_\nu + \Gamma(\delta)) \Phi_{\mathcal{R}}^T L_u^T, \end{aligned} \quad (10.29)$$

subject to:

$$\begin{aligned} L_u \mathcal{A}_{\dot{z}}^{RC} &\leq \mathcal{B}_z^{RC}, \\ L_u \mathcal{A}_{\dot{z}}^{RC} &\leq \mathcal{B}_{\dot{z}}^{RC}, \\ L_u \mathcal{A}_u &\leq \mathcal{B}_u, \end{aligned}$$

where the pair of matrices $(\mathcal{A}_u, \mathcal{B}_u)$ is defined as in (8.31), and where

$$\begin{aligned} \mathcal{A}_z^{RC} &= \mathcal{A}_z \otimes \mathbf{1}_{1 \times N_V}, \quad \mathcal{B}_z^{RC} = \begin{bmatrix} \mathcal{B}_z^{\delta_1^V} & \dots & \mathcal{B}_z^{\delta_N^V} \end{bmatrix}, \\ \mathcal{A}_{\dot{z}}^{RC} &= \mathcal{A}_{\dot{z}} \otimes \mathbf{1}_{1 \times N_V}, \quad \mathcal{B}_{\dot{z}}^{RC} = \begin{bmatrix} \mathcal{B}_{\dot{z}}^{\delta_1^V} & \dots & \mathcal{B}_{\dot{z}}^{\delta_N^V} \end{bmatrix}, \end{aligned} \quad (10.30)$$

with $\{\mathcal{A}_z, \mathcal{A}_{\dot{z}}\}$ as in (8.31), and each element of the set $\{\mathcal{B}_z^{\delta_i^V}, \mathcal{B}_{\dot{z}}^{\delta_i^V}\}$ defined as,

$$\begin{aligned} \mathcal{B}_z^{\delta_i^V} &= Z_{\max} \mathbf{1}_{1 \times 2N_c} + L_e^0 (\mathbb{I}_\nu + \Gamma(\delta_i^V)) \mathcal{A}_z = \mathcal{B}_z + \tilde{\mathcal{B}}_z(\delta_i^V), \\ \mathcal{B}_{\dot{z}}^{\delta_i^V} &= \dot{Z}_{\max} \mathbf{1}_{1 \times 2N_c} + L_e^0 (\mathbb{I}_\nu + \Gamma(\delta_i^V)) \mathcal{A}_{\dot{z}} = \mathcal{B}_{\dot{z}} + \tilde{\mathcal{B}}_{\dot{z}}(\delta_i^V), \end{aligned} \quad (10.31)$$

for all $\delta_i^V \in V_\delta$.

Proof. The proof of this proposition follows the same steps as those employed in Proposition 8.3.5 and Proposition 10.1.3, taking into account that the set of state and input constraints for the WEC system are enforced, in Problem 10.2.1, at each element of the set of vertices $V_\delta \subset \mathcal{P}$ and, hence, is omitted for brevity. \square

Remark 10.2.10 In contrast to the moment-based robust formulation for the uncertain WEC system, when the uncertainty is ‘located’ in the approximated wave excitation input, not only is the computation of the matrices \mathcal{A}_u and \mathcal{B}_u exactly as in the nominal case presented in Chapter 8, but also $\mathcal{A}_z^{\text{RC}}$ and $\mathcal{B}_z^{\text{RC}}$ can be directly computed as per the nominal moment-based control formulation. This is related to the fact that these matrices are only *system* dependent, and system uncertainty is not considered within this section. Clearly, this is not the case for the set of matrices $\{\mathcal{B}_z^{\text{RC}}, \mathcal{B}_z^{\text{RC}}\}$, which explicitly depend upon the nature of the uncertainty polytope \mathcal{P} (*i.e.* the set of vertices V_δ). Nevertheless, note that it is sufficient to compute this set of matrices *only once*, which can be performed offline, immediately after the definition of the set \mathcal{P} .

10.3 A note on considering system and input uncertainty simultaneously

One might be tempted to consider a ‘combination’ of input and system uncertainty, by defining different uncertainty vectors $\delta_{\text{in}} \in \mathcal{P}_{\text{in}}$ and $\delta_{\text{sys}} \in \mathcal{P}_{\text{sys}}$, respectively, and where $\{\mathcal{P}_{\text{in}}, \mathcal{P}_{\text{sys}}\} \subset \mathbb{R}^\nu$ are convex polytopes describing each corresponding uncertainty set. Although considering system and input uncertainty simultaneously can be effectively achieved by ‘merging’ the robust formulations, proposed in Sections 10.1 and 10.2, into a single minimax optimisation problem, there is, in general, no guarantee of uniqueness of a global energy-maximising solution: It is relatively straightforward to show that the resulting problem is *bilinear* in the uncertainty, *i.e.* it contains terms of the form $\delta_{\text{in}}^T Q \delta_{\text{sys}}$, with $Q \in \mathbb{R}^{\nu \times \nu}$, and, hence, is inherently *non-convex* (see, for instance, [255]).

In other words, the solution to this ‘combined’ problem inherently requires global optimization routines, whose complexity is directly affected by the ‘size’ of the search space defined by the polytopes $\{\mathcal{P}_{\text{in}}, \mathcal{P}_{\text{sys}}\} \subset \mathbb{R}^\nu$, given that the solution is no longer guaranteed to be attained at the convex hull of the uncertainty set. This, in turn, requires both complex optimisation routines, and an inherent discretisation of the uncertainty set, which can increase the computational complexity required to solve the corresponding robust

moment-based energy-maximising solution, directly compromising its real-time capabilities. For the reasons listed above, the combination of system and input uncertainty is not considered within the scope of this thesis¹¹.

10.4 Case study: WEC under system uncertainty

This section analyses and illustrates the performance of the robust moment-based energy-maximising control framework, presented in this chapter, for the case of WECs under *system* uncertainty. To be precise, a spherical heaving point absorber WEC is considered, with a radius of 2.5 [m], *i.e.* the same device considered in Chapter 7, to illustrate the proposed nonlinear moment-based model reduction technique. The geometry of such a device is schematically illustrated in Figure 7.2. The hydrodynamic coefficients, $B_r(\omega)$ and $A_r(\omega)$, for this spherical-type device, are those presented in Figure 2.8.

Aiming to (intuitively) illustrate the performance of the moment-based strategy, presented throughout Section 10.1.1, it is assumed that the parameters of the WEC system, defined in equation (10.1), are imprecisely known, *i.e.* the uncertainty is considered to be of a *parametric* nature. In particular, the hydrostatic stiffness s_h of the spherical heaving point absorber WEC is considered uncertain.

Remark 10.4.1 A single parameter is assumed to be uncertain, aiming to simplify the presentation of results throughout the following paragraphs. Nevertheless, note that this is done without any loss of generality, since multiple parameters can be considered to be imprecisely known within the presented robust moment-based framework, by means of a suitable uncertainty polytope \mathcal{P} .

Remark 10.4.2 Parametric uncertainty is considered mainly to give a relatively ‘intuitive’ example on how to compute the corresponding uncertainty set \mathcal{P} . Nonetheless, note that *any* source of uncertainty that can be written in terms of a (stable) *linear* system H^Δ (as in Figure 10.1), can be straightforwardly considered within this robust framework.

10.4.1 On the definition of the uncertainty polytope \mathcal{P}

This section outlines a method to compute the uncertainty set \mathcal{P} , generated in terms of uncertain parameters in the WEC model.

11: Though not considered here, the reader interested in performing such an uncertainty combination is encouraged to contact the author if any further assistance is required.

Nonetheless, as detailed in Remark 10.4.2, any source of uncertainty, represented in terms of a stable linear system H^Δ , can be straightforwardly included (see Remark 10.4.2).

Let s_h^0 denote the *nominal* hydrostatic stiffness, and suppose its *actual* value is such that $s_h \in \mathcal{S}_h$, with $\mathcal{S}_h = [-1.3s_h^0, 1.3s_h^0] \subset \mathbb{R}$, *i.e.* it can vary within $\pm 30\%$ of its nominal value s_h^0 . This parametric uncertainty, defined by means of the set \mathcal{S}_h , needs to be written in terms of the so-called uncertainty vector δ (see equation (10.9)), such that $\delta \in \mathcal{P}$. Once the dynamics of the signal generator are chosen, *i.e.* the corresponding dynamic matrix S in equation (8.9) is selected, the following procedure can be directly considered to construct the corresponding uncertainty set \mathcal{P} .

Procedure 1: Polytope definition under parametric uncertainty

- 1] Discretise the set \mathcal{S}_h , *i.e.* construct the finite-set $\mathcal{S}_h^\Delta = \{s_{h_i}^\Delta\}_{i=1}^{N^\Delta} \subset \mathcal{S}_h$, containing $N^\Delta \in \mathbb{N}_{\geq 1}$ possible values for the hydrostatic stiffness.
- 2] Consider the WEC system defined in equation (10.1). Construct¹² the set of systems $\{\Sigma^{\Delta_i}\}_{i=1}^{N^\Delta}$, corresponding with *each* possible value for the hydrostatic stiffness $s_{h_i}^\Delta$ in the set \mathcal{S}_h^Δ .
- 3] Compute the set of matrices $\{\Phi_{\Delta_i}^\top\}_{i=1}^{N^\Delta} \subset \mathbb{R}^{\nu \times \nu}$, characterising the moment-domain equivalent of the output of each uncertain WEC system in the set $\{\Sigma^{\Delta_i}\}_{i=1}^{N^\Delta}$ (see equation (10.3)), which can be done straightforwardly, making explicit use of the result posed in equation (8.12).
- 4] Compute the set of matrices $\{\Delta_i\}_{i=1}^{N^\Delta} \subset \mathbb{R}^{\nu \times \nu}$, corresponding with each matrix in the set $\{\Phi_{\Delta_i}^\top\}_{i=1}^{N^\Delta}$, using the relation posed in equation (10.5).
- 5] Construct the set of *uncertainty vectors* $\{\delta_i\}_{i=1}^{N^\Delta} \subset \mathbb{R}^\nu$, corresponding with each matrix in the set $\{\Delta_i\}_{i=1}^{N^\Delta}$, which can be done straightforwardly following the structure of Δ in (10.8).
- 6] Finally, compute the polytope \mathcal{P} as the *convex hull* of the set $\{\delta_i\}_{i=1}^{N^\Delta}$. In addition, extract the set of vertices of the resulting \mathcal{P} , *i.e.* construct the set V_δ .

12: Note that this can be done by simply ‘substituting’ s_h in (10.1) by each element of the set \mathcal{S}_h^Δ .

Remark 10.4.3 Steps 1 to 5 above can be compactly summarised in terms of the following sequence of operations:

$$\begin{array}{ccccccccc}
 s_{h_i}^\Delta & \rightarrow & \Sigma^{\Delta_i} & \rightarrow & \Phi_{\Delta_i}^\top & \rightarrow & \Delta_i & \rightarrow & \delta_i \\
 \text{Uncertain} & & \text{Uncertain} & & \text{Moment} & & \text{Uncertainty} & & \text{Uncertainty} \\
 \text{parameter} & & \text{system} & & & & \text{matrix} & & \text{vector}
 \end{array}$$

for every $i \in \mathbb{N}_{N^\Delta}$. Once the set $\{\delta_i\}_{i=1}^{N^\Delta}$ is computed, Step 6 can be performed using well-known higher-dimensional convex hull algorithms. A particularly well-established algorithm, is that presented in [256], implemented in Matlab® by means of the

native function `convhulln`¹³.

Once the uncertainty polytope \mathcal{P} is defined, the robust moment-based control solution (under system uncertainty) can be readily computed, using the framework proposed in Section 10.1.1.

10.4.2 Performance assessment under regular waves

This section evaluates the performance of the robust moment-based framework proposed throughout Section 10.1, explicitly using Procedure 1, to characterise the corresponding uncertainty set \mathcal{P} under regular wave excitation.

Remark 10.4.4 The case of regular wave excitation is first considered here mainly to (graphically) illustrate the result of Procedure 1: a regular wave input directly implies that the matrix S (see equation (8.9)), characterising the corresponding signal generator, is composed of a single frequency component ω_0 , and, hence, the dimension of S is $\nu = 2$. Using different words, the polytope \mathcal{P} , arising from Procedure 1, can be visualised in a 2D-plot, along with its corresponding set of vertices V_δ .

Consider that the regular wave input is such that $T_w = 9$ [s], which corresponds with a fundamental frequency $\omega_0 = 2\pi/9 \approx 0.7$ [rad/s]. Figure 10.3 illustrates the polytope \mathcal{P} obtained using Procedure 1 (grey filling), plotted in terms of its set of vertices, *i.e.* $\delta_i^V = [\delta^+, \delta^-]^T \in V_\delta \subset \mathbb{R}^2$. These vertices are represented with black (empty-filled) circles. Note that, the nominal value for the hydrostatic stiffness ($s_h^0 = 196.87 \times 10^3$ [kg/s²]), is represented in Figure 10.3 with a black-filled circle, *i.e.* by the point in \mathbb{R}^2 corresponding with the zero uncertainty vector $\delta = [0, 0]^T$.

Note that Procedure 1, described in Section 10.4.1, relies on having a-priori knowledge of the parametric uncertainty set S_h , *i.e.* the ‘range’ of variation for the uncertain parameter under analysis. If this set is not known (or only partially known), one can potentially define a more ‘conservative’ uncertainty set, by simply covering a ‘larger’ set for the uncertainty vector δ . To illustrate this, Figure 10.3 shows the set \mathcal{P}_\square (green-filled), which has the shape of a parallelogram, fully defined by four vertices, denoted with black (empty-filled) squares.

Remark 10.4.5 The ‘larger’ set \mathcal{P}_\square , illustrated in Figure 10.3, simply constitutes an *example* shape. Note that *any polytope* can be considered, as long as it is *convex* (in line with Assumption 10.1.1), and condition (10.12) holds.

13: Note that this Matlab® function is based on the open-source software *Qhull*, which can be downloaded for free from [257].

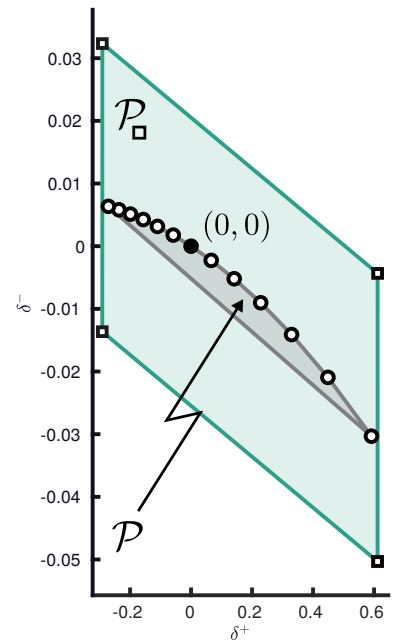


Figure 10.3: Polytope $\mathcal{P} \subset \mathbb{R}^2$ for $T_w = 9$ [s], obtained using Procedure 1 (grey filling), and its corresponding set of vertices V_δ , denoted with black (empty-filled) circles. In addition, a more conservative uncertainty set \mathcal{P}_\square is also illustrated (green filling), fully defined by four vertices, denoted with black (empty-filled) squares.

Remark 10.4.6 The definition of the polytopes presented in Figure 10.3 is particular to the case of a (regular) wave with $T_w = 9$ [s]. Nonetheless, note that the *exact same procedure* can be applied for any $T_w \in \mathbb{R}^+$, obtaining analogous results.

Though, naturally, both polytopes \mathcal{P} and \mathcal{P}_\square can be considered for the computation of a robust moment-based energy-maximising solution, the performance obtained with the latter is consequently adversely affected by its more conservative nature. This is explicitly discussed and illustrated in the upcoming paragraphs. From now on, the following convention is adopted, to define three different assessment (performance) scenarios:

- ▶ *Ideal performance*¹⁴ : the optimal control input is computed using the *nominal* approach presented in Chapter 8, *i.e.* only using knowledge of the *nominal* model Σ^0 without considering any possible source of uncertainty, and applied to the same *nominal* system Σ^0 .
- ▶ *Nominal performance*¹⁵ : the optimal control input is computed using the *nominal* approach presented in Chapter 8, *i.e.* only using knowledge of the *nominal* model Σ^0 without considering any possible source of uncertainty, but applied to the *actual* system Σ^Δ , characterised by the uncertainty δ .
- ▶ *Robust performance*¹⁶ : the optimal control input is computed using the *robust* approach proposed in this chapter, *i.e.* the control law explicitly considers the knowledge of the uncertainty polytope, and applied to the *actual* system Σ^Δ , characterised by the uncertainty δ .

14: *i.e.* nominal control - nominal system.

15: *i.e.* nominal control - uncertain system.

16: *i.e.* robust control - uncertain system.

Figure 10.4 shows (state and input unconstrained) *nominal* and *robust* performance results, in terms of energy absorption for different ‘levels’ of uncertainty in the parameter s_h (given in % of deviation from its nominal value s_h^0), for a regular input wave with height $H_w = 2$ [m], and period $T_w = 9$ [s]. The case of nominal performance is denoted with black circles. Two different robust performance cases are considered in Figure 10.4: robust performance arising from computing a moment-based control solution considering the polytope \mathcal{P} (denoted with grey diamonds), and a more conservative case (denoted with green squares), arising from the (parallelogram) boundary \mathcal{P}_\square (as shown in Figure 10.3). The WCP, for the three cases, occurs when the parameter s_h has a deviation of -30% from its nominal value. Note that, as discussed previously in this same section, the optimal WCP is obtained with the robust energy-maximising strategy computed with the polytope arising from Procedure 1, which explicitly uses a-priori knowledge of the ‘range’ of variation of the uncertain parameter, while a clear drop in performance (in terms of WCP), can be directly observed for the case

where the more conservative polytope \mathcal{P}_\square is considered.

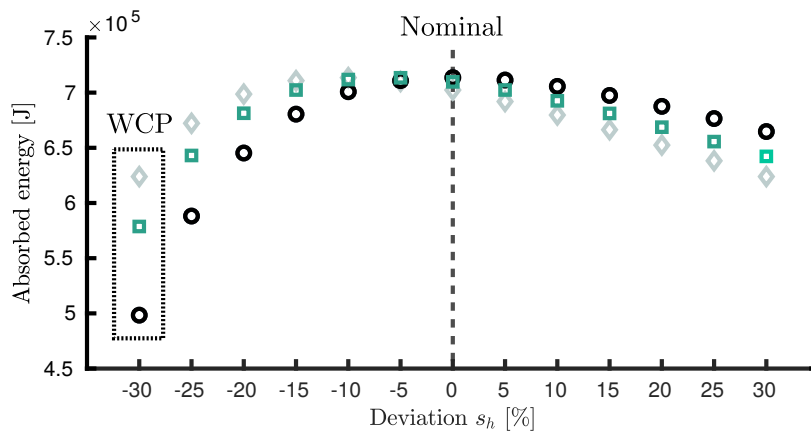


Figure 10.4: Nominal performance (black circles), and robust performance for the polytope \mathcal{P} (grey diamonds) and the more conservative boundary set \mathcal{P}_\square (green squares), as a function of the parametric uncertainty (% of deviation from its nominal value), for an input wave with $T_w = 9$ [s]. The performance for the nominal system is denoted with a vertical dashed line.

Note that Figure 10.4 clearly shows an ‘inflexion’ point in terms of performance results, which, for this case, happens exactly when there is no deviation in the hydrostatic stiffness (*i.e.* s_h coincides with its nominal value s_h^0). In other words, for negative deviations in the parameter s_h^0 , the robust moment-based approach outperforms the nominal moment-based controller, with this difference being larger at the point where the WCP is located (which is exactly the optimisation criterion used in the robust energy-maximising framework proposed). For positive deviations, the exact opposite happens, and the controller based on the nominal model outperforms the robust approach presented in this chapter.

Remark 10.4.7 Following the discussion provided immediately above, note that the robust performance case is conservative *by definition*, given that it optimises for the worst-case scenario, in terms of the (defined) system uncertainty. If an accurate nominal WEC model is available, then the nominal moment-based solution is more appropriate, since it delivers optimal results for Σ^0 , and can be computed independent of the definition of the uncertainty set. On the other hand, if the presence of uncertainty is known to be significant, then the robust approach is preferred, given that it ‘alleviates’ the potential drop in performance arising from not having an accurate WEC model, by optimising for the worst-case (uncertainty) scenario.

Figure 10.5 extends the results of Figure 10.4 to different wave periods, specifically contained in the set $T_w \in [6, 10]$ [s]. Note that, for the remainder of this section (including the results presented in Figure 10.5), the robust performance (denoted with diamonds) *only* corresponds with the robust moment-based controller computed with the uncertainty polytope \mathcal{P} , arising directly from Procedure 1, considering a signal generator according to each wave period T_w analysed. Similar results, to those previously presented in Figure

10.4, can be observed in Figure 10.5, where it is clear that the WCP occurs when the parameter s_h has a deviation of -30% from its nominal value, for the totality of the analysed wave periods in the set $[6, 10]$ [s].

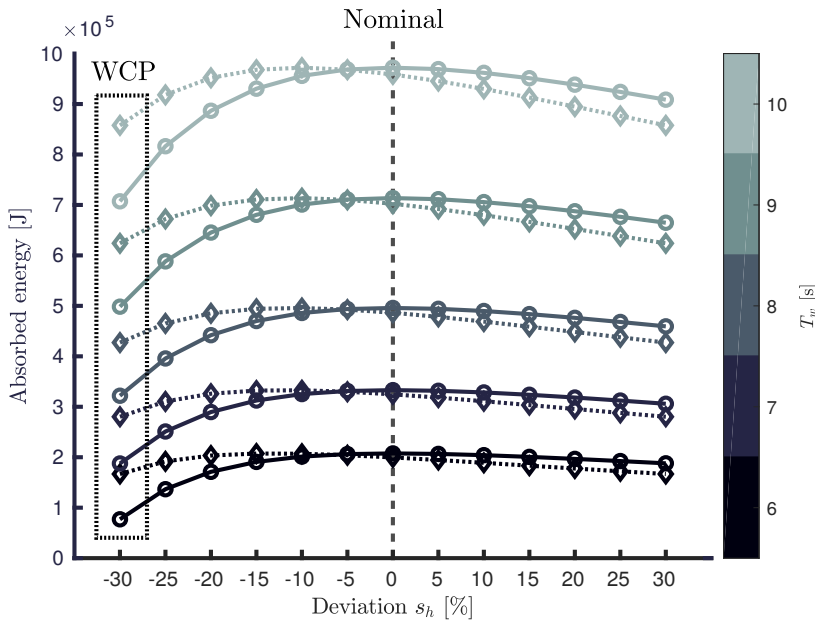


Figure 10.5: Nominal performance (circles), and robust performance (diamonds), as a function of the parametric uncertainty (% of deviation from its nominal value), for input waves with $T_w \in [6, 10]$ [s]. The performance for the nominal system is indicated with a vertical dashed line.

To complete the results of this section, and aiming to fully illustrate the optimality of the robust moment-based solution with respect to the WCP (in terms of the defined system uncertainty), Figure 10.6 shows the so-called *normalised WCP*, both for nominal (circles), and robust (diamonds) performance scenarios. In the case of the former, the normalised WCP is defined as the ratio between energy absorbed for the worst-case scenario (in terms of uncertainty) when the nominal moment-based control law is applied, and the *ideal* performance, corresponding with each wave period T_w . The latter is defined analogously, but in terms of the energy absorbed with the robust moment-based control framework presented in this chapter. It is noteworthy that the robust moment-based controller is able to perform, in the worst-case scenario, at over $\%80$ of the ideal performance (denoted in Figure 10.6 with a horizontal dashed-line), for the totality of the analysed wave periods. This is clearly not the case for the controller computed using only the nominal WEC system Σ^0 , whose WCP drops significantly, absorbing between $\approx \%40$ and $\%65$ of the energy obtained in the ideal scenario.

10.4.3 Performance assessment under irregular waves

This section analyses the performance of the robust moment-based strategy when irregular wave excitation is considered, and where the WEC system is subject to parametric uncertainty (characterised

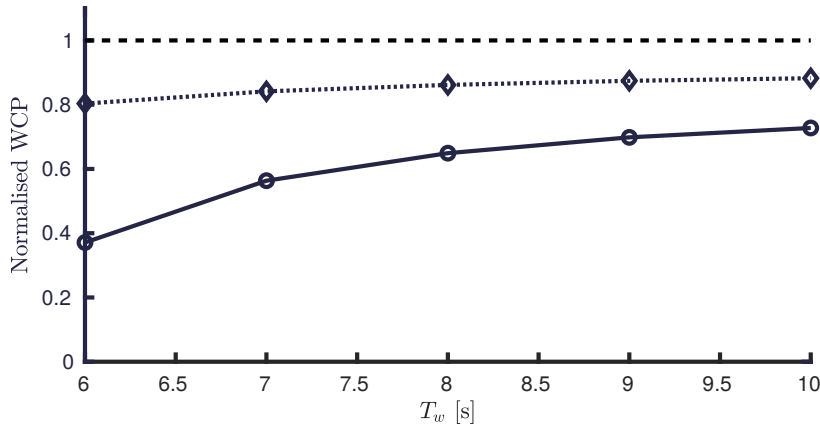


Figure 10.6: Normalised WCP for nominal (circles) and robust (diamonds) performance scenarios. The ideal performance scenario is denoted with a horizontal dashed line.

as previously described in Section 10.4). In particular, this section analyses the performance of the strategy subject to *state* constraints, *i.e.* the performance of the control solution outlined in Proposition 10.1.3.

Remark 10.4.8 If irregular input waves are considered, the computation of the corresponding uncertainty polytope \mathcal{P} can be done following the procedure described in Section 10.4.1, *i.e.* Procedure 1. Naturally, given the intrinsic (high) dimension of the associated matrix S (which for irregular input waves is composed of $f \gg 1$ harmonics of a fundamental frequency ω_0), such an uncertainty polytope cannot be (graphically) illustrated.

Remark 10.4.9 *State* constraints are explicitly selected to illustrate the performance of the robust moment-based controller, since their formulation explicitly depends upon the definition of the uncertainty polytope \mathcal{P} . Note that this is not the case for the *control* constraint, which can always be written *independent* of the nature of the uncertainty (see Remark 10.1.11).

The results presented in this section are computed considering irregular input waves, generated from a JONSWAP SDF S_w (see Section 2.1.2) with significant wave height $\bar{H}_w = 2$ [m], peak period $\bar{T}_w = 9$ [s], and peak enhancement factor $\gamma = 3.3$. Figure 10.7 illustrates motion results (displacement and velocity) for both nominal (dotted), and robust (solid) performance scenarios, for a particular wave input, randomly generated according to S_w . The WEC system, considered to elicit such a response, is such that its hydrostatic stiffness is defined as $s_h = -1.2s_h^0$, *i.e.* with a deviation of -20% from its nominal value. The state constraints are defined such that the limitations in displacement and velocity are set to $Z_{\max} = 2$ [m] and $\dot{Z}_{\max} = 2$ [m/s], respectively.

It can be immediately highlighted that the motion arising from the moment-based control law, computed using only the nominal

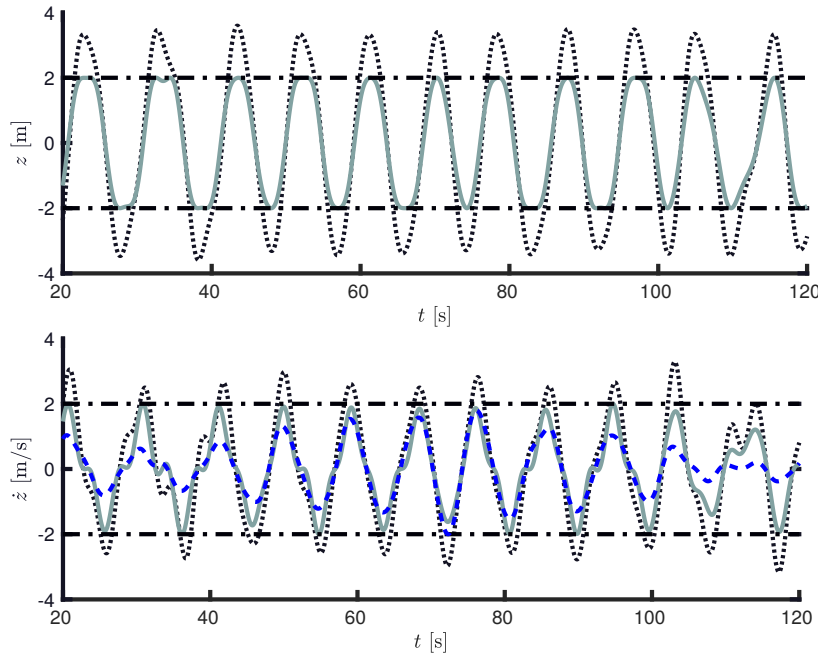


Figure 10.7: Motion results (displacement and velocity) for both nominal (dotted), and robust (solid) performance scenarios, for a particular wave input, randomly generated according to S_w . The WEC system, considered to elicit such a response, is such that its hydrostatic stiffness is defined as $s_h = -1.2s_h^0$. The (scaled) wave excitation force is plotted using a dashed-blue line. The constraint values are indicated with horizontal dash-dotted lines.

WEC model, presents constraint violations, consistently occurring throughout the entire simulation time. This is not the case for the robust moment-based framework, presented in this chapter, which is always within the specified limits, as a consequence of the incorporation of the uncertainty-dependent set of state constraints (as per the result of Proposition 10.1.3). Note that the velocity of the device, arising both from applying the moment-based nominal, and robust control signals, is always ‘in-phase’ (*instantaneous* phase) with the wave excitation force input, plotted¹⁷ (dashed-blue) in Figure 10.7, along with the velocity time-traces.

Finally, and aiming to show that the robust moment-based controller can respect constraints *for any* uncertainty vector inside the polytope \mathcal{P} , Figure 10.8 shows time-snippets of displacement, for both nominal (dotted), and robust (solid) moment-based control strategies, for different WEC systems, all of which have been computed by a random generation of uncertainty vectors δ in the defined polytope \mathcal{P} . To be precise, each of these systems corresponds with a different value of hydrostatic stiffness s_h^{Δ} , lying in the set \mathcal{S}_h . The wave input is the *exact same* input used to elicit the motion results of Figure 10.7. Note that, unlike the motion results arising from the nominal moment-based controller, the robust framework, presented in this chapter, is able to consistently respect the defined state constraint, for each of the WEC systems considered. Once again, this is merely a consequence of the definition of the state constraints in Proposition 10.1.3, which explicitly depend upon the uncertainty set \mathcal{P} .

17: Note that, aiming to show the synchronisation in terms of instantaneous phase, the wave excitation input is scaled in Figure 10.7.

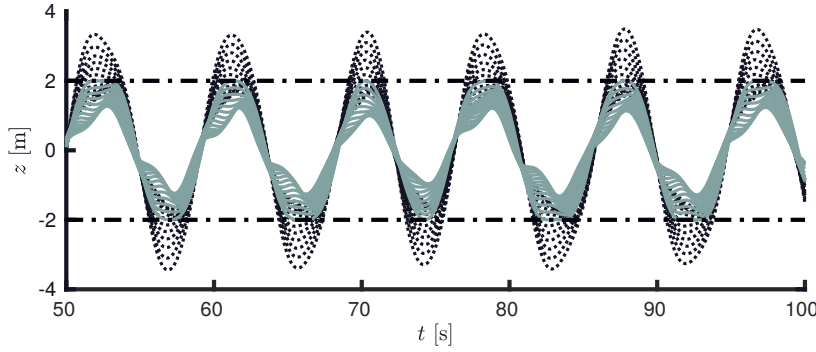


Figure 10.8: Displacement results for nominal (dotted) and robust (solid) moment-based control techniques, for different WEC systems, all of which have been computed by a random generation of parametric uncertainty. The state constraints are indicated with dash-dotted horizontal lines.

10.4.4 Data-driven characterisation of system uncertainty

Within the robust framework, presented in Section 10.2.1, a standing assumption is that the uncertainty can be written in terms of a matrix Δ , which directly arises from the moment-domain representation of the output of a linear stable system H^Δ , characterising the corresponding multiplicative output uncertainty. If, for instance, the uncertainty considered (10.1) is 'located' in the parameters of the WEC, then this perturbation can always be written in terms of a matrix Δ , hence the framework applies straightforwardly, as illustrated previously in Section 10.4.

This subsection considers the case where the user *does not know* if the uncertainty, characterising the WEC device, can be effectively written in terms of a *linear* system. This is the case when, for instance, one considers that the WEC system is affected by errors arising from *nonlinear* unmodelled dynamics. As a matter of fact, this is exactly what motivates the following *data-driven approach* to characterise the uncertainty polytope \mathcal{P} .

Suppose a (potentially) nonlinear WEC system Σ_{nl} (with some stability properties¹⁸) is available, whose output is the velocity of the device, denoted, from now on, as y_{nl} .

Remark 10.4.10 System Σ_{nl} *does not have to be known analytically*. As a matter of fact, Σ_{nl} can represent, for instance, CFD based numerical models, or even an actual WEC in an experimental environment.

That said, Procedure 1, presented in Section 10.4.1, can be 'adapted' so that the uncertainty polytope is constructed and characterised in terms of the (potentially) nonlinear system Σ_{nl} . This can be achieved by changing Steps 1 to 4 in Procedure 1, for the following three steps:

- 1 Define a set of N^Δ wave excitation inputs $\{f_e^i\}_{i=1}^{N^\Delta}$ according to a specific SDF S_w , with $N^\Delta \in \mathbb{N}_{\geq 1}$, *i.e.* in terms of a signal

18: It is assumed that, given a bounded input, the nonlinear WEC model produces bounded outputs.

generator¹⁹ with dynamic matrix S , and a set of output vectors $\{L_e^i\}_{i=1}^{N_\Delta}$.

- 2 Using the nonlinear WEC system Σ_{nl} , compute the set of outputs (velocities) $\{y_{\text{nl}}^i\}_{i=1}^{N_\Delta}$, corresponding with each wave excitation input signal generated with the set of output vectors $\{L_e^i\}_{i=1}^{N_\Delta}$.
- 3 Select a set of time-instants $\mathcal{T}_\Delta = \{t_j\}_{j=1}^{N_\Delta} \subset \mathcal{T}$, where \mathcal{T} represents the time-interval in which energy absorption is maximised. For each input-output pair (f_e^i, y_{nl}^i) , compute the corresponding matrix $\Delta_i = \Gamma(\delta_i)$, $\Delta_i \in \mathbb{R}^{\nu \times \nu}$, such that

$$\min_{\delta_i \in \mathbb{R}^\nu} \sum_{j=1}^{N_\Delta} \left(y_{\text{nl}}^i(t_j) - L_e^i \Phi_{\mathcal{R}}^T (1 + \Gamma(\delta_i)) \xi(t_j) \right)^2, \quad (10.32)$$

for all $i \in \mathbb{N}_{N_\Delta}$.

Aiming to clarify the nature and rationality of the steps proposed above, the following remarks are offered below.

Remark 10.4.11 Step 1 is a fundamental stepping stone for the definition of the uncertainty polytope \mathcal{P} , in terms of the output of the nonlinear system Σ_{nl} . Unlike the case presented in Section 10.4.1, where the uncertainty is linear, and can be characterised *independently* of the wave input (*i.e.* the computation of the matrices Δ_i can be done independently of the wave excitation force vector L_e), multiple inputs are required to characterise the uncertainty in terms of Σ_{nl} . Naturally, this directly stems from the fact that the superposition principle does not hold anymore (*i.e.* the WEC system is nonlinear). Once this set of multiple inputs is defined, Step 2 follows immediately.

Remark 10.4.12 Given an excitation force input $f_e = L_e \xi$, Step 3 is based on finding the ‘closest’ matrix Δ (equivalently the closest uncertainty vector δ), in a Euclidean norm sense, such that it minimises the difference between the output of the nonlinear system y_{nl} , and the steady-state output response of the *linear* ‘perturbed’ WEC system, *i.e.* $y_{\text{ss}}^\Delta = L_e \Phi_{\mathcal{R}}^T (1 + \Gamma(\delta_i)) \xi$ (see equation (10.4)). Note that, due to the linearity of the mapping Γ (see Remark 10.1.5), the minimisation operation proposed in Step 3 is a linear least squares procedure, and always has a unique solution δ , for each input-output pair (f_e, y_{nl}) .

Once the uncertainty polytope \mathcal{P} is obtained (following the modification to Procedure 1 proposed in this section), the robust moment-based control input can be directly computed following the framework developed throughout Section 10.2. To explicitly illustrate the data-driven characterisation of uncertainty, proposed in this section, the

19: Recall that the initial condition $\xi(0)$ is fixed to $\xi(0) = \varepsilon_\nu$, so it is sufficient to change the output vector L_e to generate the different wave inputs.

following nonlinear WEC model is considered:

$$\Sigma_{nl} : \begin{cases} \ddot{z} = \mathcal{M}(-k_r * \dot{z} - s_h z + f_e + f_{nl}), \\ y = \dot{z}, \end{cases} \quad (10.33)$$

where Σ_{nl} is defined *exactly* as the linear WEC system (10.1), but with the addition of the nonlinear mapping $f_{nl} : \mathbb{R}^+ \rightarrow \mathbb{R}$. This nonlinear map is (partially) borrowed from Chapter 7, where the same heaving point absorber WEC is considered. In particular, f_{nl} is defined such that it represents nonlinear viscous effects²⁰, *i.e.*

$$f_{nl} = 2\rho\pi(2.5)^2 C_d \dot{z} |\dot{z}|, \quad (10.34)$$

where ρ is the water density, and C_d is the so-called viscous drag coefficient (see Section 2.5). For this case study, C_d is fixed as $C_d = 2$. To generate the set of multiple excitation inputs, required in Step 1 above, a JONSWAP SDF is considered, with significant wave height $\bar{H}_w = 2$ [m], peak wave period $\bar{T}_w = 8$ [s], and peak enhancement factor $\gamma = 3.3$. A set of $N^\Delta = 20$ waves is considered, which generates a polytope \mathcal{P} characterised by 12 vertices in \mathbb{R}^ν . To compute the robust moment-based energy-maximising input, the result of Proposition 10.1.1 is considered, with a displacement constraint set to a value of $Z_{\max} = 2$ [m].

20: The definition of these effects can be found, in this thesis, in Section 2.5.

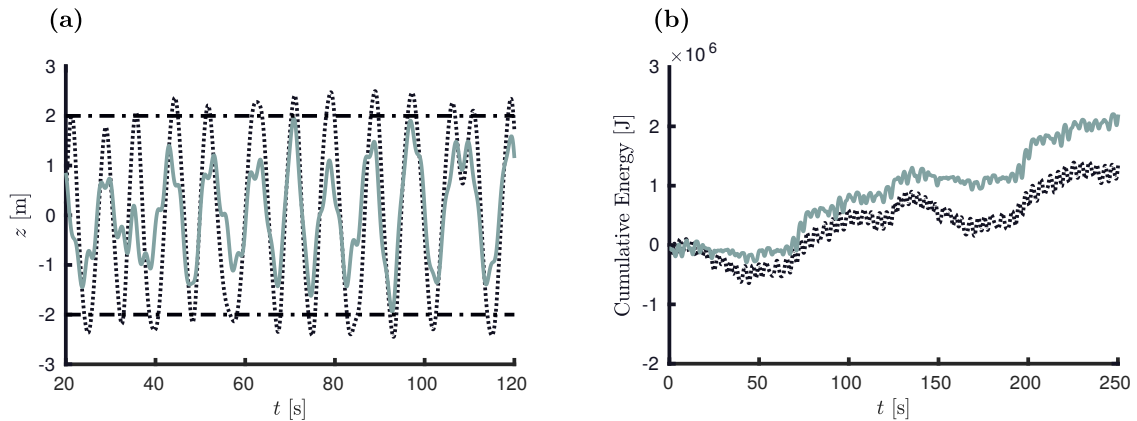


Figure 10.9: (a) shows displacement results for the nonlinear WEC system Σ_{nl} , both for the nominal moment-based control case (dotted), and the robust moment-based control case (solid). The constraint limitation is denoted with a horizontal dash-dotted line. (b) shows cumulative energy absorption for both cases, using the same line code.

Figure 10.9 (a) shows displacement results for a particular realisation of wave excitation input, both for the nominal moment-based control case (dotted), *i.e.* computed using the *linear* nominal model Σ^0 (defined in equation (10.1)), and the robust moment-based control case (solid), *i.e.* computed using the uncertainty polytope \mathcal{P} , characterised with the aid of the nonlinear WEC model Σ_{nl} , as described in this same section. It is straightforward to note that, for this wave input realisation, the robust controller is effectively respecting the displacement limitation, as a consequence of a suitable definition

of the set \mathcal{P} . In contrast, the nominal controller, which *does not* have any information on the nonlinear viscous effects present in the WEC model, has constraint violations throughout the simulation time. Finally, using the knowledge of the polytope not only helps in guaranteeing constraint satisfaction, but, as can be directly appreciated from Figure 10.9 (b), the robust controller effectively outperforms the nominal controller (for this wave input case), in terms of (cumulative) energy absorption²¹.

Remark 10.4.13 Note that, for the case study described above, the nonlinear WEC model (10.33) is assumed to be *known analytically*. If this is the case, instead of using such a model to characterise a given uncertainty set, the author recommends to consider the nonlinear moment-based control framework proposed in Chapter 11.

21: Similar conclusions can be drawn for different input waves, generated randomly according to the corresponding SDF S_w

10.5 Case study: WEC under input uncertainty

As recalled in the introduction to this chapter, input uncertainty is also ubiquitous in the WEC control problem, given the intrinsic necessity of both unknown-input estimation, and forecasting, strategies, to provide information on the force exerted by waves, *i.e.* the wave excitation. This section illustrates the robust moment-based technique presented in Section 10.2, where uncertainty in the definition of the wave excitation force input is explicitly incorporated in the energy-maximising control problem. To that end, the same heaving point absorber WEC, as that utilised in Section 10.4, is considered throughout this section.

Motivated by the sensitivity analysis performed in Section 8.7, the existence of errors in the instantaneous phase (*i.e.* time-delays) of the wave excitation force is considered, to characterise the (input) uncertainty polytope \mathcal{P} . In particular, as demonstrated in Section 8.7, this error source can cause significant losses in terms of energy-maximising performance, if the time delay is sufficiently large.

Remark 10.5.1 Constant deviations in instantaneous amplitude are not considered in the upcoming analysis, motivated by the results offered in Section 8.7, which explicitly show that the performance of the (nominal) moment-based control solution remains almost unaffected with respect to amplitude errors in the wave excitation force estimate²².

22: Nonetheless, these can be incorporated in the computation of the uncertainty polytope \mathcal{P} straightforwardly, if required by the particular application under analysis.

10.5.1 On the definition of the uncertainty polytope \mathcal{P}

Analogously to Section 10.4.1, this section outlines a methodology to compute the polytope characterising input uncertainty, arising from the presence of errors in the instantaneous phase of the wave excitation force.

In particular, suppose the dynamic matrix $S \in \mathbb{R}^{\nu \times \nu}$ is given, and let \tilde{f}_e^0 be the *nominal* wave excitation force, generated in terms of the nominal signal generator \mathcal{G}^0 (see equation (10.21)). Let the ‘perturbed’ excitation be defined as $\tilde{f}_e^\Delta = \tilde{f}_e^0(t - \tau)$, *i.e.* as a ‘delayed’ version of the nominal wave excitation mapping \tilde{f}_e^0 . Suppose $\tau \in \mathcal{F} \subset \mathbb{R}$, where, for this case study, $\mathcal{F} = [-1.25, 1.25]$ [s] (which corresponds with a shift in time τ between -1.25 and 1.25 seconds). To consider the robust moment-based control framework, presented in Section 10.5, the input uncertainty generated by the set \mathcal{F} needs to be written in terms of an uncertain polytope \mathcal{P} . Before proposing a method to compute such a set \mathcal{P} , note that the following relation,

$$\tilde{f}_e^0(t - \tau) = L_e^0 e^{S(t-\tau)} \xi(0) = L_e^0 e^{-S\tau} \xi(t), \quad (10.35)$$

holds, so that, for a given $\tau \in \mathcal{F}$, the matrix $\Delta \in \mathbb{R}^{\nu \times \nu}$, characterising the so-called uncertain signal generator \mathcal{G}^Δ (see Definition 10.2.1 and equation (10.24)), can be directly obtained as $\Delta = e^{-S\tau}$. Based on the discussion provided above, the following procedure, which computes the uncertainty set \mathcal{P} , is proposed.

Procedure 2: Polytope definition under input uncertainty

- 1] Discretise the set \mathcal{F} , *i.e.* construct the finite-set $\mathcal{F}^\Delta = \{\tau_i\}_{i=1}^{N^\Delta} \subset \mathcal{F}$, containing $N^\Delta \in \mathbb{N}_{\geq 1}$ possible values for the wave excitation input delay.
- 2] Compute the set of matrices $\{\Delta_i\}_{i=1}^{N^\Delta} \subset \mathbb{R}^{\nu \times \nu}$, corresponding with each delay τ_i in the set \mathcal{F}^Δ , using the relation posed in equation (10.35).
- 3] Construct the set of *uncertainty vectors* $\{\delta_i\}_{i=1}^{N^\Delta} \subset \mathbb{R}^\nu$, corresponding with each matrix in the set $\{\Delta_i\}_{i=1}^{N^\Delta}$, which can be done straightforwardly following the structure of Δ in (10.8).
- 4] Finally, compute the polytope \mathcal{P} as the *convex hull* of the set $\{\delta_i\}_{i=1}^{N^\Delta}$. In addition, extract the set of vertices of the resulting \mathcal{P} , *i.e.* construct the set V_δ .

Remark 10.5.2 Once the set $\{\delta_i\}_{i=1}^{N^\Delta}$ is computed, Step 4 above can be performed analogously to Step 6 of Procedure 1, *i.e.* using well-known and readily available higher-dimensional convex hull algorithms (see, for instance, [256]).

10.5.2 Performance assessment

This section evaluates the performance of the robust moment-based framework proposed throughout Section 10.2, explicitly using Procedure 2, to characterise the corresponding uncertainty set \mathcal{P} under regular wave excitation.

Remark 10.5.3 Similarly to Section 10.4.2, regular waves are considered to explicitly illustrate the resulting uncertainty set \mathcal{P} (see Remark 10.4.4). In addition, for this uncertain input case, almost identical conclusions can be drawn for irregular waves, in terms of controller performance.

Consider first that the regular wave input is such that $T_w = 9$ [s], which corresponds with a wave frequency $\omega_0 = 2\pi/9 \approx 0.7$ [rad/s]. Figure 10.10 illustrates the polytope \mathcal{P} obtained using Procedure 2 (grey filling), plotted in terms of its set of vertices, *i.e.* $\delta_i = [\delta^+, \delta^-]^\top \in V_\delta \subset \mathbb{R}^2$. These vertices are represented with black (empty-filled) circles. Note that the ‘nominal’ value for the time delay ($\tau = 0$ [s]), is represented in Figure 10.10 with a black-filled circle, *i.e.* by the point in \mathbb{R}^2 corresponding with the *zero* uncertainty vector $\delta = [0, 0]^\top$.

Remark 10.5.4 Though not explicitly considered in this section, a more conservative polytope can potentially be selected, following an procedure analogous to that presented in Section 10.4.2. The only condition is that such a polytope *must* be *convex*, in line with Assumption 10.1.1.

Similarly to the case of WECs under *system* uncertainty, the following convention is adopted, to define three different assessment (performance) scenarios, under *input* uncertainty:

- ▶ *Ideal performance*²³: the optimal control input is computed using the *nominal* wave excitation force input, and the WEC system is effectively driven by the *nominal* signal generator \mathcal{G}^0 .
- ▶ *Nominal performance*²⁴: the optimal control input is computed using the *nominal* wave excitation force input, and the WEC system is driven by the uncertain signal generator \mathcal{G}^Δ , characterised by the uncertainty vector δ .
- ▶ *Robust performance*²⁵: the optimal control input is computed using the *robust* approach proposed in this chapter, *i.e.* the control law explicitly considers the knowledge of the (input) uncertainty polytope \mathcal{P} , and the WEC system is driven by the uncertain signal generator \mathcal{G}^Δ , characterised by the uncertainty vector δ .

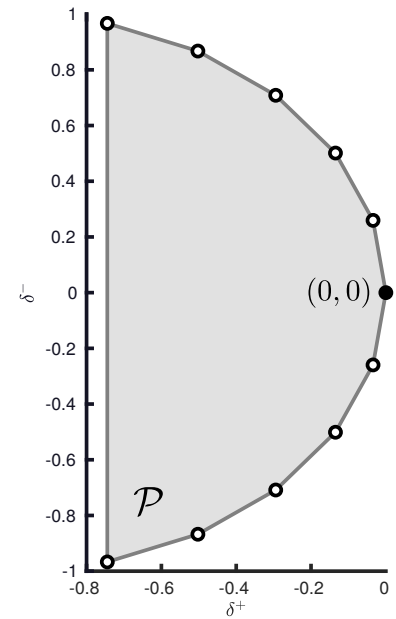


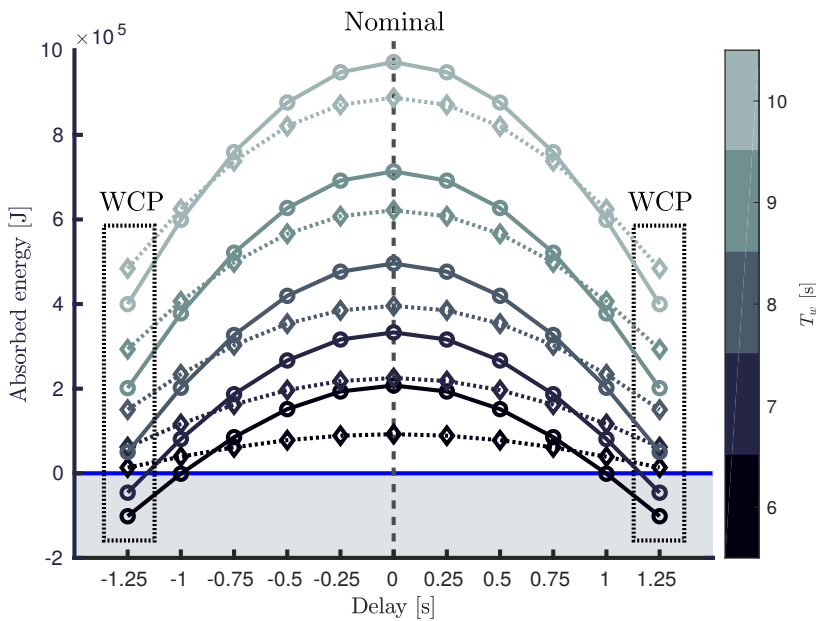
Figure 10.10: Polytope $\mathcal{P} \subset \mathbb{R}^2$ for $T_w = 9$ [s], obtained using Procedure 2 (grey filling), and its corresponding set of vertices V_δ , denoted with black (empty-filled) circles.

23: *i.e.* nominal control - nominal input.

24: *i.e.* nominal control - uncertain input.

25: *i.e.* robust control - uncertain input.

Figure 10.11 shows (state and input unconstrained²⁶) *nominal* and *robust* performance results, in terms of energy absorption for different ‘levels’ of uncertainty in the delay parameter τ (in seconds), where the input waves are regular, with height $H_w = 2$ [m], and different wave periods $T_w \in [6, 10]$ [s]. The case of nominal performance is denoted with black circles. The robust performance (denoted with diamonds), corresponds with the robust moment-based controller computed with the uncertainty polytope \mathcal{P} , arising directly from Procedure 2, considering a signal generator according to each wave period T_w analysed. Note that the WCP, for both scenarios, occurs when the delay takes the boundary values -1.25 [s] and 1.25 [s], in a symmetric fashion.



26: Identical conclusions can be drawn for the constrained case.

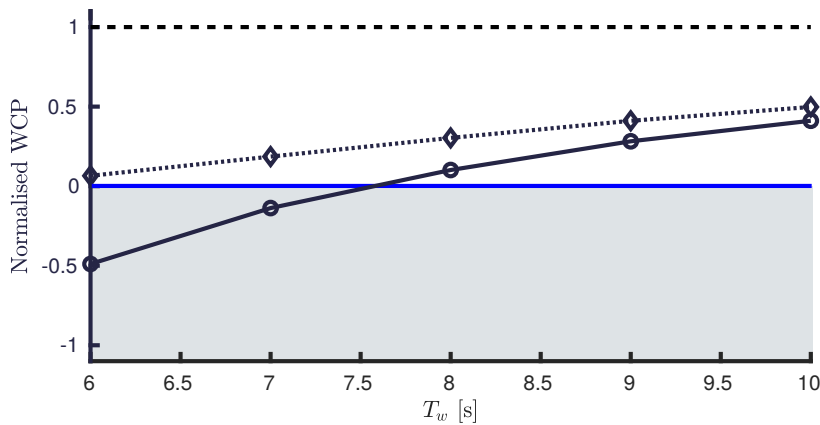
Figure 10.11: Nominal performance (circles), and robust performance (diamonds), as a function of the input delay τ (in seconds), for input waves with $T_w \in [6, 10]$ [s]. The performance for the nominal wave input (*i.e.* with zero delay) is indicated with a horizontal dashed line. A value below zero (solid-blue line) indicates negative energy absorption.

Remark 10.5.5 Note that, for $|\tau| \geq 1$, the nominal performance drops below zero, *i.e.* the controlled device ‘drains’ energy from the grid, which is effectively consistent with the sensitivity results presented in Section 8.7. In contrast, the robust performance case *always* delivers positive energy absorption, as a consequence of the worst-case robust control objective.

Remark 10.5.6 Once again, note that the robust performance case is conservative by definition, given that it optimises for the worst-case scenario in terms of the possible delays defined for the wave excitation input. That said, if the time delay is known to lie approximately in the region $[-0.75, 0.75]$ [s], then the nominal controller is indeed preferred for this case study, since it outperforms the robust approach in terms of energy absorption.

To complete the results for this section, and aiming to fully illustrate the optimality of the robust moment-based solution with respect to the WCP (under the presence of input uncertainty), Figure 10.12

shows the *normalised* WCP²⁷. While the nominal controller presents negative WCP results (*i.e.* negative energy absorption) for certain wave periods, the robust moment-based controller is *always* able to deliver positive energy absorption even in a worst-case scenario, for each of the wave periods analysed. This is effectively a fundamental feature of the proposed robust moment-based framework, which always guarantees positive results in terms of absorbed energy, as an intrinsic consequence of the worst-case optimisation approach employed.



27: Defined analogously to Figure 10.6, but considering input, rather than system, uncertainty.

Figure 10.12: Normalised WCP for nominal (circles) and robust (diamonds) performance scenarios, under the presence of input uncertainty. The ideal performance scenario is denoted with a vertical dashed line. A value below zero (solid-blue line) indicates negative energy absorption.

10.6 Conclusions

Motivated by the ubiquitous presence of input and system uncertainty in the WEC energy-maximising optimal control problem, this chapter introduces an extension of the moment-based energy-maximising technique developed throughout Chapter 8, allowing the user to explicitly consider both system, and input, uncertainty, in the computation of the energy-maximising optimal control input. This constitutes, to the best of the author's knowledge, the first energy-maximising framework, within the WEC control literature, which is robust with respect to uncertainty in the wave excitation force input.

In particular, this robust approach effectively incorporates system and input uncertainty in the WEC moment-based energy-maximising optimisation problem, by a suitable definition of an uncertainty (convex) polytope \mathcal{P} , and exploiting the underpinning concept of the worst-case performance method. The proposed control law is computed in terms of an optimisation procedure, formulated as a *minimax* problem, which has to be solved *only* at the set of vertices of the polytope, as a result of the nature of the objective function, arising from mapping the state variables, and both the external and control inputs, into their respective moment-domain

representations. This minimax optimisation problem is shown to have a *unique globally optimal* control solution, and hence can be solved using computationally efficiently state-of-the-art numerical routines. As a result, this robust moment-based framework provides a computationally efficient robust optimal control method, which, unlike its nominal counterpart, is able to consistently respect state and input constraint limitations under the presence of uncertainty. As a matter of fact, note that consistent constraint violations are likely to have a significant effect on LCoE, further highlighting the benefits of this robust moment-based approach.

In addition, and given the importance of a suitable definition for the uncertainty polytope \mathcal{P} , this chapter offers different procedures to obtain such a set, both for the case of input, and system uncertainty. For the latter, a *data-driven* method, to characterise the uncertainty in terms of unmodelled nonlinear effects, is also presented, which is only based on the knowledge of the output of the 'target' nonlinear WEC model. This, in turn, gives the user the possibility of using high-fidelity numerical solvers (such as those based on CFD), to characterise the polytope \mathcal{P} in terms of a large class of unmodelled dynamic effects, with mild assumptions.

A case study is presented, based on a spherical heaving point absorber WEC. The performance of the robust strategy is explicitly illustrated, and compared against its nominal counterpart, both when input and system uncertainty are present. This includes both regular, and irregular wave excitation inputs, as well as (state and input) unconstrained, and constrained control scenarios. For the case of system uncertainty, it is first assumed that the hydrostatic stiffness of the WEC is imprecisely known. In addition, and to illustrate the capabilities of the data-driven method proposed (to compute the uncertainty set), nonlinear viscous effects are also considered, showing the potential of this robust technique to 'accommodate' nonlinear effects in terms of the set \mathcal{P} . For the case of input uncertainty, it is assumed that the wave excitation input can potentially have a time-delay, arising from an improper tuning of the estimator/forecaster, employed for its computation. A key feature can be highlighted for this type of input uncertainty: while the WCP for the nominal moment-based controller can reach negative energy absorption results (for certain values of delay), the robust strategy *always* delivers positive performance, as an intrinsic consequence of the worst-case optimisation approach employed.

Contents of this chapter

11.1 Optimal control problem	262
11.2 Nonlinear moment-based WEC formulation for optimal control	263
11.2.1 On the approximation of π for optimal control	266
11.3 Nonlinear moment-based energy-maximising OCP	271
11.3.1 Handling of state and input constraints	275
11.4 Case study: A CorPower-like device	277
11.4.1 Characterisation of nonlinear hydrodynamic effects	277
11.4.2 Results and discussion	279
11.5 Conclusions	282

Following the hydrodynamic modelling basics presented in Chapter 2, recall, from Section 2.4, that the equation of motion for a WEC, under the assumptions of potential flow theory (see Section 2.3.1), can be expressed in terms of the so-called *extended Cummins'* equation (2.20). This equation is recalled below, for the SISO case, for convenience:

$$\Sigma : \begin{cases} \ddot{z} = \mathcal{M}(-k_r * \dot{z} - s_h z + f_e + f_{nl} - u), \\ y = \dot{z}, \end{cases} \quad (11.1)$$

where $z : \mathbb{R}^+ \rightarrow \mathbb{R}$ is the displacement, $k_r : \mathbb{R}^+ \rightarrow \mathbb{R}$, $k_r \in L^2(\mathbb{R})$, the radiation force impulse response function, $f_e : \mathbb{R}^+ \rightarrow \mathbb{R}$, the wave excitation force, $u : \mathbb{R}^+ \rightarrow \mathbb{R}$, the control input, and $\mathcal{M} \in \mathbb{R}_{>0}$ is the inverse of the generalised mass matrix of the device. In contrast to the moment-based WEC control cases discussed in Chapters 8, 9 and 10, equation (11.1) incorporates *nonlinear* behaviour: the mapping $f_{nl} : \mathbb{R}^+ \rightarrow \mathbb{R}$, $t \mapsto f_{nl}(t)$ represents potential nonlinear effects, which is precisely what gives origin to the so-called nonlinear extensions of Cummins' equation, described in Section 2.5.

Remark 11.0.1 A SISO WEC system is considered in this section, aiming to simplify the notation. Nonetheless, note that MIMO WEC systems can be considered analogously, by simply following the theoretical moment-based framework presented in Chapter 9.

As discussed throughout Chapter 3, *linear* dynamics are virtually always considered when designing optimal controllers for WECs, motivated by both their simplicity (in terms of formulation and solution of the corresponding OCP), and their associated computational convenience. In other words, these model-based control strategies must be computed in real-time, therefore limiting the computational complexity of the hydrodynamic models employed. Moreover,

there is also a limit to the complexity of mathematical models for which an optimal control solution can be effectively found, either algebraically or numerically. Another strongly contributing factor to the use of linear dynamics is that linear hydrodynamic theory is a well-established field where considerable effort and refinement has been expended in the calculation of *linear* hydrodynamic parameters. There is, therefore, little appetite to extend these models to include nonlinear effects.

Nonetheless, despite the list of motives described above, the linearity assumption has been recently an object of debate: WECs are, by their nature, prone to show significant and diverse *nonlinear* effects, since their principal aim, pursued by the optimal controller, is to enhance the amplitude of motion to maximise power extraction¹.

Though a small number of the WEC control studies reviewed² do consider nonlinear dynamics, *none* of them give formal and explicit conditions for existence and uniqueness of globally optimal energy-maximising control solutions (see Remark 3.4.9). As a matter of fact, even if a control solution is found, it is not clear under which conditions this energy-maximising control law is effectively a globally optimal solution. This naturally generates a great deal of uncertainty, specifically concerning which class of nonlinear models can be *actually* used within the available nonlinear formulations, and even if the reported performance corresponds with a global solution at all. This provides significant motivation for optimal control strategies that can effectively handle a large class of nonlinear effects, both in terms of the well-posedness of the OCP (*i.e.* existence of global energy-maximising solutions), and real-time capabilities.

Exploiting the concept of nonlinear moment, introduced in Chapter 4, this chapter presents an energy-maximising control strategy for WECs subject to *nonlinear* dynamics. In particular, a method to map the objective function (and system variables) to a finite-dimensional tractable nonlinear program (NP), is proposed, which can be efficiently solved using state-of-the-art nonlinear programming solvers (see, for instance, [258]). In addition, by showing that the objective function arising from the proposed moment-based strategy belongs to a family of approximately convex/concave mappings (particularly to the so-called outer Γ -convex/concave [259] functions), the existence of a global energy-maximising solution is guaranteed, under *mild* assumptions. Similarly to the case of convex/concave functions, where each local solution is also global, explicit conditions to determine whether a local energy-maximising solution is, effectively, a global maximiser for the proposed moment-based OCP, are given, having strong practical value when numerically solving the associated NP. Finally, a case study, based on the energy-maximisation problem for

1: The reader is referred to Chapter 3 for further discussion on this topic.

2: See the state-of-the-art review provided in Section 3.4.

a state-of-the-art CorPower-like WEC, is presented, where the WEC model is subject to different sources of hydrodynamic nonlinearity.

Remark 11.0.2 Throughout this chapter, aiming both to simplify the notation, and to solely focus the upcoming sections on the formulation of a *nonlinear* moment-based controller, the excitation force is assumed to be *known* over the complete time interval $\mathcal{T} \subset \mathbb{R}^+$, where energy absorption from incoming waves is maximised. This is done without any loss of generality, since a receding-horizon formulation can be achieved *directly*, by simply following the theory³ presented in Section 8.6, without further modifications.

The remainder of this chapter is organised as follows. Section 11.1 describes and formalises the energy-maximising problem for WECs subject to nonlinear dynamics, while Section 11.2 details the nonlinear moment-based representation for WECs, including a suitable approximation technique for the corresponding nonlinear moment. Section 11.3 effectively describes and formalises the nonlinear moment-based optimal control strategy, including state and input constraints. Finally, Section 11.3 discusses the application of this approach to a CorPower-like WEC constrained to move in heave (translational motion), while Section 11.5 encompasses the main conclusions of this chapter.

3: In particular, by following the adaptation of the moment-based representation of the wave excitation input, to alleviate the effects of considering a (potentially) short time-horizon for the computation of the control law (see Section 8.6.1).

11.1 Optimal control problem

The energy-maximising control problem for nonlinear WECs can be defined analogously to the linear case presented in Section 8.1, with one key (major) difference: the dynamic equality constraint in the OCP (8.4) is now fully *nonlinear*, *i.e.* the WEC is described by the nonlinear system Σ in equation (11.1).

To be specific in the definition of the corresponding OCP, let the objective function $\mathcal{J} : \mathbb{R} \rightarrow \mathbb{R}$, $u \mapsto \mathcal{J}(u)$, be defined as in (8.2), *i.e.* reflecting an energy-maximising control objective. In addition, let the set of state and input constraints \mathcal{C} be defined as in equation (8.3). Then, the energy-maximising OCP for *nonlinear* WECs can be posed as

$$\begin{aligned}
 u^{\text{opt}} &= \arg \max_u \mathcal{J}(u), \\
 &\text{subject to:} \\
 &\left\{ \begin{array}{l} \text{Nonlinear WEC dynamics } \Sigma \text{ (11.1),} \\ \text{state and input constraints } \mathcal{C} \text{ (8.3).} \end{array} \right.
 \end{aligned} \tag{11.2}$$

11.2 Nonlinear moment-based WEC formulation for optimal control

Recall, from Chapter 4, that nonlinear moment-based theory directly depends on the knowledge of a state-space representation of the system to be reduced, which is not the case for the non-parametric equation described by system Σ in (11.1). In the light of this, the following equivalent representation is proposed:

$$\Sigma : \begin{cases} \dot{w} = f_{\Sigma}(w, f_e) = Aw + B(v - k_r * Cw) + f(w), \\ y = h_{\Sigma}(w) = Cw, \end{cases} \quad (11.3)$$

for $t \in \mathbb{R}^+$, where $w(t) = [z(t) \ \dot{z}(t)]^T \in \mathbb{R}^2$ contains displacement and velocity corresponding with system Σ , and the (constant) matrices $A \in \mathbb{R}^{2 \times 2}$, $B \in \mathbb{R}^2$ and $C^T \in \mathbb{R}^2$ are defined as

$$A = \begin{bmatrix} 0 & 1 \\ -Ms_h & 0 \end{bmatrix}, \quad B = \begin{bmatrix} 0 \\ \mathcal{M} \end{bmatrix}, \quad C = \begin{bmatrix} 0 \\ 1 \end{bmatrix}^T. \quad (11.4)$$

The 'input' function $v : \mathbb{R}^+ \rightarrow \mathbb{R}$, is defined as

$$v = f_e - u, \quad (11.5)$$

i.e. a linear combination of the external inputs f_e and u , and the nonlinear mapping $f : \mathbb{R}^2 \rightarrow \mathbb{R}^2$ is given by

$$f(w) = \begin{bmatrix} 0 \\ \mathcal{M}f_{nl}(w) \end{bmatrix} = Bf_{nl}(w), \quad (11.6)$$

with $f_{nl} : \mathbb{R}^+ \rightarrow \mathbb{R}$ as in equation (11.1).

Remark 11.2.1 Following the nonlinear hydrodynamic effects described in Section 2.5 (which constitute the set of the most utilised nonlinear effects within WEC control/estimation applications), it is assumed that the mapping f_{nl} depends only on w , i.e. displacement and velocity of the WEC system involved. Nonetheless, note that, if required by a particular application, a more general class of nonlinear effects can be considered, such as non-ideal PTO dynamics⁴.

Recall, from Section 2.1.2, that the standard assumption for the mathematical representation of wave excitation forces is that f_e can be written as a finite sum of harmonics of a so-called *fundamental frequency* $\omega_0 \in \mathbb{R}^+$. Following the moment-based theory presented in Chapter 4, the wave excitation force input can be written as a

4: The reader is referred to Section 3.4.2.1 for further detail on nonlinear mappings considered within the WEC control literature, including non-ideal PTO dynamics.

signal generator described, for $t \in \mathbb{R}^+$, by the set of equations

$$\begin{aligned}\dot{\xi} &= S\xi, \\ f_e &= L_e\xi,\end{aligned}\tag{11.7}$$

where $\xi(t) \in \mathbb{R}^\nu$, $L_e^\top \in \mathbb{R}^\nu$ and the dynamic matrix $S \in \mathbb{R}^{\nu \times \nu}$ can be written in terms of the set $\mathcal{F} = \{p\omega_0\}_{p=1}^f \subset \mathbb{R}^+$, with $f \in \mathbb{N}_{\geq 1}$, in block-diagonal form, as

$$S = \bigoplus_{p=1}^f \begin{bmatrix} 0 & p\omega_0 \\ -p\omega_0 & 0 \end{bmatrix},\tag{11.8}$$

with $\nu = 2f$, and where, clearly, $\lambda(S) = (j\mathcal{F}) \cup (-j\mathcal{F}) \subset \mathbb{C}^0$, so that Assumption 4.1.2 automatically holds.

Even though the wave excitation force is composed of f harmonic multiples of the (angular) fundamental frequency ω_0 , it is convenient (for the subsequent theoretical results) to assume that the control input u can be composed of a higher number $f+d$ of harmonics, with $d \in \mathbb{N}_{\geq 1}$ integer. For this purpose, the following auxiliary ‘extended’ signal generator, is defined as follows. Let $\bar{S} \in \mathbb{R}^{(\nu+\iota) \times (\nu+\iota)}$ be such that

$$\bar{S} = S \oplus \left(\bigoplus_{p=1}^d \begin{bmatrix} 0 & (p+f)\omega_0 \\ -(p+f)\omega_0 & 0 \end{bmatrix} \right),\tag{11.9}$$

with $\iota = 2d$. One can now directly express the wave excitation force f_e , and the control input u , as a function of this extended signal generator, *i.e.*

$$\begin{aligned}\dot{\bar{\xi}} &= \bar{S}\bar{\xi}, \\ f_e &= [L_e \ 0]\bar{\xi} = \bar{L}_e\bar{\xi}, \\ u &= \bar{L}_u\bar{\xi},\end{aligned}\tag{11.10}$$

where $\bar{\xi}(t) \in \mathbb{R}^{\nu+\iota}$, and $\bar{\xi}(0) = [\xi(0)^\top, \xi^*(0)^\top]^\top$, $\xi^*(0) \in \mathbb{R}^\iota$. Note that the input defined in (11.5) can be expressed accordingly as $v = (\bar{L}_e - \bar{L}_u)\bar{\xi}$.

Remark 11.2.2 The signal generator (11.10) is an extension of the one defined in (11.7) in the sense that it inherently incorporates the matrix S , while adding d harmonics of the fundamental frequency ω_0 . With the selected initial condition $\bar{\xi}(0)$, the wave excitation force f_e can be written as a function of $\bar{\xi}$ by simply using an appropriate inclusion mapping, *i.e.* completing L_e with zeros accordingly⁵.

In preparation for the upcoming results, and without loss of generality,

5: The reader is referred to, for instance, [226], for further detail on the formal definition of an inclusion map.

three further assumptions are presented. The first concerns the signal generator defined in equation (11.10).

Assumption 11.2.1 The triple of matrices $(\bar{L}_e - \bar{L}_u, \bar{S}, \bar{\xi}(0))$ is minimal, *i.e.* observable and excitable.

Assumption 11.2.1 is required to have a well-posed definition of moment (see Section 4.1.2). Note that the previous assumption is without loss of generality, since the signal generator is user-defined and so it can always be constructed such that the assumption holds.

Remark 11.2.3 Let $\bar{\xi}_i$ be the i -th entry of $\bar{\xi}$, with $i \in \mathbb{N}_{\nu+\iota}$, and define the set $\mathcal{X} = \{\bar{\xi}_i\}_{i=1}^{\nu+\iota}$. Note that, if Assumption 11.2.1 holds, then the pair $(\bar{S}, \bar{\xi}(0))$ is excitable and it is straightforward to check that $\text{span}\{\mathcal{X}\} = \text{span}\{\{\cos(p\omega_0 t), -\sin(p\omega_0 t)\}_{p=1}^{f+d}\}$. As a consequence, the input v is always T -periodic, where $T = 2\pi/\omega_0 \in \mathbb{R}^+$ is the *fundamental period* of v .

The second standing assumption, required to prove existence and uniqueness of the moment of system (11.3) at the signal generator $(\bar{S}, \bar{L}_e - \bar{L}_u)$, is Assumption 7.1.1, *i.e.* the mapping $f: \mathbb{R}^2 \rightarrow \mathbb{R}^2$ is such that,

$$f(0) = 0, \quad \left. \frac{\partial f(w)}{\partial w} \right|_{w=0} = 0. \quad (11.11)$$

Note that this assumption is without loss of generality, since the matrices in (11.3), and the mapping f , can always be redefined to satisfy it⁶.

Finally, the third standing assumption concerns the stability in the first approximation of system (11.3), *i.e.* Assumption 7.1.2. To be precise, the zero equilibrium of system

$$\dot{w} = Aw - B(k_r * Cw), \quad (11.12)$$

is asymptotically stable. As discussed in Section 2.4, and in several studies (such as [53, 123]), the linear equation of motion (11.12) is asymptotically stable for any meaningful values of the involved parameters (and impulse response function k_r). Thus, this assumption is, in practice, also without loss of generality.

Proposition 11.2.1 Suppose Assumptions 11.2.1, 7.1.1 and 7.1.2 hold. Then, there exists a unique mapping π , locally defined in a neighborhood Ξ of $\xi = 0$, which solves the partial differential equation

$$\frac{\partial \pi(\bar{\xi})}{\partial \bar{\xi}} \bar{S} \bar{\xi} = f_{\Sigma}(\pi(\bar{\xi}), (\bar{L}_e - \bar{L}_u) \bar{\xi}). \quad (11.13)$$

6: This claim, which directly relates to Jacobian analysis, is considered standard in nonlinear dynamics. Further detail can be found in, for instance, [22, Chapter 8].

Moreover, the moment of system (11.3) at the extended signal generator $(\bar{S}, \bar{L}_e - \bar{L}_u)$ computed along a particular trajectory $\bar{\xi}(t)$ coincides with the well-defined steady-state output response of the interconnected system (11.3)-(11.4)-(11.10), i.e. $y_{ss}(t) = h_{\Sigma}(\pi(\bar{\xi}(t)))$.

Proof. Note that, under Assumption 11.2.1, the triple of matrices $(\bar{L}_e - \bar{L}_u, \bar{S}, \bar{\xi}(0))$ is minimal. Moreover, the extended signal generator defined in (11.10) is such that $\lambda(S) \subset \mathbb{C}^0$ with simple eigenvalues, in line with Assumption 4.1.2. Therefore, Proposition 11.2.1 automatically holds as long as the zero equilibrium of system $\dot{w} = f_{\Sigma}(w, 0)$ is locally exponentially stable (see Lemma 4.1.2). Since this is the case by Assumption 7.1.2, the proof is concluded. \square

In slightly different words, Proposition 11.2.1 guarantees that the steady-state response of system (11.3), driven by the extended signal generator (11.10), can be effectively computed using the corresponding moment at $(\bar{S}, \bar{L}_e - \bar{L}_u)$. Nevertheless, even if the existence of π (solution of (11.13)) is guaranteed, it is virtually impossible to compute its analytic expression when the mapping f in (11.3) is nonlinear.

Remark 11.2.4 Similarly to the nonlinear model reduction by moment-matching case, introduced in Chapter 7, a suitable approximation method is required for the computation of the mapping π , *tailored* for the optimal control design case⁷. This is specifically addressed in Section 11.2.1.

11.2.1 On the approximation of π for optimal control

The very nature of the mapping π in (11.13) intrinsically depends on both the characteristics of the extended signal generator (11.10) and the system dynamics defined by the nonlinear mapping f_{Σ} . Aiming to formally characterise π , the following key remarks are introduced, which drive the next main result.

Remark 11.2.5 Let \mathcal{T} be defined as $\mathcal{T} = [0, T] \subset \mathbb{R}^+$. Note that the set $\bar{\mathcal{X}}$, defined in Remark 11.2.3, belongs to the Hilbert space $L^2(\mathcal{T})$ and is orthogonal under the standard inner-product operator. Moreover, if Assumption 11.2.1 holds, one can always complete $\bar{\mathcal{X}}$ to an orthogonal basis \mathcal{X} of $L^2(\mathcal{T})$, i.e. define⁸

$$\mathcal{X} = \bar{\mathcal{X}} \cup \check{\mathcal{X}},$$

$$\check{\mathcal{X}} = \{\cos(p\omega_0 t), -\sin(p\omega_0 t)\}_{p=f+d+1}^{\infty} = \{\check{\mathcal{X}}_i\}_{i=\nu+\iota+1}^{\infty}.$$

7: Though the approximation method for nonlinear moments proposed in Chapter 7, can be considered within this optimal control procedure, its definition, which is tailored for the *model reduction* case (where the initial condition of the signal generator is not known), complicates the transcription of the energy-maximising OCP when using moments.

8: See [260, Chapter 8].

Remark 11.2.6 If Assumption 11.2.1 holds, one can always find a set of mappings $\mathcal{I}_i : \mathbb{R}^{\nu+\iota} \rightarrow \mathbb{R}$ such that $\check{\mathcal{X}}_i = \mathcal{I}_i(\bar{\xi})$, for every $i > \nu + \iota$ integer. This (standard) result states that one can always generate the elements of the set $\check{\mathcal{X}}$ (i.e. higher order harmonics of the fundamental frequency ω_0) by solely operating on the $\nu + \iota$ trigonometric polynomials defined by the entries of $\bar{\xi}$ (see, for example, [261]).

Proposition 11.2.2 Suppose Assumptions 11.2.1, 7.1.1 and 7.1.2 hold. Then, for a given trajectory $\bar{\xi}(t)$, each element of the mapping π , as the solution to (11.13), i.e. π_k , $k \in \mathbb{N}_2$, belongs to the Hilbert space $L^2(\mathcal{T})$ with $\mathcal{T} = [0, T] \subset \mathbb{R}^+$, where $T = 2\pi/\omega_0$, i.e. it can be uniquely expressed as

$$\pi_k(\bar{\xi}) = \sum_{i=1}^{\nu+\iota} \alpha_{k_i} \bar{\xi}_i + \epsilon_k(\bar{\xi}) = \bar{\Pi}_k \bar{\xi} + \epsilon_k(\bar{\xi}), \quad (11.14)$$

where $\epsilon_k(\bar{\xi}) = \sum_{i=\nu+\iota+1}^{\infty} \alpha_{k_i} \mathcal{I}_i(\bar{\xi})$, $\alpha_{k_i} \in \mathbb{R} \forall i$, with \mathcal{I}_i as defined in Remark 11.2.6, and the matrix $\bar{\Pi}_k \in \mathbb{R}^{\nu+\iota}$ is given by $\bar{\Pi}_k = [\alpha_{k_1}, \dots, \alpha_{k_{\nu+\iota}}]$.

Proof. Given the nature of the signal generator defined in equation (11.10), the function v is T -periodic, with $T = 2\pi/\omega_0$ (see Remark 11.2.3). Moreover, under the above assumptions, the zero equilibrium of $\dot{w} = f_{\Sigma}(w, 0)$ is locally exponentially stable and its (well-defined) steady-state solution is also T -periodic [244, Section VI], i.e. $w_{ss}(t) = w_{ss}(t - T)$. Since under Assumptions 11.2.1, 7.1.1 and 7.1.2, $w_{ss}(t) = \pi(\bar{\xi}(t))$ (see Proposition 11.2.1), it is straightforward to conclude that each element of the mapping π belongs to $L^2(\mathcal{T})$, i.e. it can be expressed as a unique linear combination of the orthogonal basis $\check{\mathcal{X}}$ (as defined in Remark 11.2.5), which concludes the proof. \square

Remark 11.2.7 The result of Proposition 11.2.2 allows π to be compactly expressed as

$$\pi(\bar{\xi}) = \begin{bmatrix} \bar{\Pi}_1 \\ \bar{\Pi}_2 \end{bmatrix} \bar{\xi} + \begin{bmatrix} \epsilon_1(\bar{\xi}) \\ \epsilon_2(\bar{\xi}) \end{bmatrix} = \bar{\Pi} \bar{\xi} + E(\bar{\xi}), \quad (11.15)$$

where the term $E : \mathbb{R}^{\nu+\iota} \rightarrow \mathbb{R}^2$ is called the *truncation error*.

Note that, if the truncation error E is 'ignored', the mapping π can be effectively approximated as $\bar{\pi}(\bar{\xi}) = \bar{\Pi} \bar{\xi}$, i.e. by its expansion on the $(\nu + \iota)$ -dimensional set $\check{\mathcal{X}}$. This motivates the following key definition.

Definition 11.2.1 The function $C\bar{\pi}$, where $\bar{\pi}(\bar{\xi}) = \bar{\Pi}\bar{\xi}$, is called the approximated moment⁹ of system (11.3) at the signal generator $(\bar{S}, \bar{L}_e - \bar{L}_u)$. In addition, the matrix $\bar{Y} = C\bar{\Pi}$ is referred to as the approximated moment-domain equivalent¹⁰ of y .

9: This notion is analogous to the one given in [232].

Remark 11.2.8 Under the same set of assumptions as Proposition 11.2.2, the approximated moment-domain equivalent of y can be effectively used to approximate the steady-state output of system (11.3) driven by $(\bar{S}, \bar{L}_e - \bar{L}_u)$, i.e. $y_{ss}(t) \approx C\bar{\Pi}\bar{\xi}(t) = \bar{Y}\bar{\xi}(t)$.

10: This definition is analogous to that used in the linear moment-based WEC control framework proposed in Chapters 8, 9 and 10. In addition, note that, since $y = \dot{z}$ in the WEC case, one could also use the notation \bar{Z} , following that used in Chapters 8, 9 and 10. Nonetheless, the symbol \bar{Y} is preferred over \bar{Z} throughout this chapter, for convenience of notation.

Aiming to propose a method to compute \bar{Y} , and inspired by the family of mean weighted residual methods [150, 154], the following residual mapping $\mathcal{R} : \mathbb{R}^2 \rightarrow \mathbb{R}^2$ is defined, as

$$\mathcal{R}(\bar{\Pi}\bar{\xi}) := \bar{\Pi}\bar{S}\bar{\xi} - f_{\Sigma}(\bar{\Pi}\bar{\xi}, (\bar{L}_e - \bar{L}_u)\bar{\xi}), \quad (11.16)$$

which directly arises from ‘replacing’ π with $\bar{\pi}$ in equation (11.13). Using this residual equation, a *collocation* approach [154, Chapter 4] is considered, to compute the approximated moment-domain equivalent $\bar{Y} = C\bar{\Pi}$. In other words, equation (11.16) is forced to be exactly zero at a finite set of *collocation* points. This approximation method is made explicit in the following proposition.

Proposition 11.2.3 Consider the nonlinear system (11.3) and the signal generator defined by equation (11.10). Suppose Assumptions 11.2.1, 7.1.1 and 7.1.2 hold. Then, the approximated moment-domain equivalent of y can be computed as $C\bar{\Pi}$, where $\bar{\Pi}$ is the solution of the algebraic system of equations

$$(\bar{\Pi}\bar{S} - A\bar{\Pi} + BC\bar{\Pi}\mathcal{R} - B(\bar{L}_e - \bar{L}_u))\langle\bar{\xi}, \delta_{t_j}\rangle - \langle f(\bar{\Pi}\bar{\xi}), \delta_{t_j}\rangle = 0, \quad (11.17)$$

with $\mathcal{T}_{\delta} = \{t_i\}_{i=1}^{\nu+\iota} \subset \mathcal{T}$, a set of uniformly-distributed time instants, and where the matrix $\mathcal{R} \in \mathbb{R}^{(\nu+\iota) \times (\nu+\iota)}$, characterising the radiation effects in moment-domain, is defined as

$$\mathcal{R} = \bigoplus_{p=1}^{f+d} \begin{bmatrix} r_{p\omega_0} & m_{p\omega_0} \\ -m_{p\omega_0} & r_{p\omega_0} \end{bmatrix}, \quad (11.18)$$

where the set of parameters $\{r_{p\omega_0}, m_{p\omega_0}\}_{p=1}^{f+d} \subset \mathbb{R}$ is defined as in equation (5.10).

Proof. Note that, using (11.3), the residual equation (11.16) can be equivalently written as

$$(\bar{\Pi}\bar{S} - A\bar{\Pi} - B(\bar{L}_e - \bar{L}_u))\bar{\xi} + B(k_r * C\bar{\Pi}\bar{\xi}) - f(\bar{\Pi}\bar{\xi}), \quad (11.19)$$

where the convolution operation involved, associated with the effect

of radiation forces acting on the device, can be shown to be such that (see Proposition 5.1.1)

$$k_r * C\bar{\Pi}\bar{\xi} = C\bar{\Pi}\mathcal{R}\bar{\xi}, \quad (11.20)$$

with \mathcal{R} as in equation (11.18). Then, following the well-known collocation approach¹¹, the residual function is forced to be orthogonal (under the standard inner-product of $L^2(\mathcal{T})$) to the set of translated Dirac- δ functions $\{\delta_{t_i}\}_{i=1}^{\nu+\iota}$. Equation (11.17) follows after considering the superposition property of the inner-product operator. \square

11: See [154, Chapter 4].

Corollary 11.2.4 *The system of algebraic equations (11.17) can be equivalently written in matrix form as*

$$(\bar{\Pi}\bar{S} - A\bar{\Pi} + BC\bar{\Pi}\mathcal{R} - B(\bar{L}_e - \bar{L}_u)) - F_{\text{nl}}(\bar{\Pi})\Omega^{-1} = 0, \quad (11.21)$$

where the matrices $F_{\text{nl}}(\bar{\Pi}) \in \mathbb{R}^{2 \times (\nu+\iota)}$ and $\Omega \in \mathbb{R}^{(\nu+\iota) \times (\nu+\iota)}$ are defined as

$$\begin{aligned} \Omega &= \begin{bmatrix} \bar{\xi}(t_1) & \dots & \bar{\xi}(t_{\nu+\iota}) \end{bmatrix}, \\ F_{\text{nl}}(\bar{\Pi}) &= \begin{bmatrix} f(\bar{\Pi}\bar{\xi}(t_1)) & \dots & f(\bar{\Pi}\bar{\xi}(t_{\nu+\iota})) \end{bmatrix}. \end{aligned} \quad (11.22)$$

Proof. Note that if the set $\{t_j\} \subset \mathcal{T}$, then $\langle l, \delta_{t_j} \rangle = l(t_j)$, for any continuous function $l : \mathcal{T} \rightarrow \mathbb{R}$. Then, the result follows as a consequence of the excitability of the pair $(\bar{S}, \bar{\xi}(0))$, which implies that the matrix Ω is always full rank [223]. \square

Remark 11.2.9 If the set of uniformly-distributed time instants $\mathcal{T}_\delta \subset \mathcal{T}$ is chosen such that $t_k = -T/2 + Tk/(\nu + \iota)$, $t_k \in \mathcal{T}_\delta$ for all $k \in \mathbb{N}_{\nu+\iota}$, then the collocation approach utilised in Proposition 11.2.3 is *identical* to the Galerkin method [154, Chapter 4]. The main advantage of Proposition 11.2.3 (collocation) lies in its simplicity of implementation, *i.e.* one simply uses function evaluation (see Corollary 11.2.4).

Remark 11.2.10 In the light of Remark 11.2.9, standard results for Galerkin methods (see [245]) apply to this WEC case. In particular, the existence of solutions to system (11.17) (equivalently equation (11.21)), under the hypothesis of Proposition 11.2.3, is always guaranteed for all sufficiently large ι . Moreover, the approximated moment $\bar{\pi}(\bar{\xi}) = \bar{\Pi}\bar{\xi}$ converges uniformly towards the exact solution (11.15) as $\iota \rightarrow \infty$ (see also [245]).

A corollary is now presented, which illustrates the result of Proposition 11.2.3 (through Corollary 11.2.4) in a more convenient form for

the upcoming nonlinear moment-based energy-maximising control formulation. In particular, this result shows that equation (11.21) can be fully expressed in terms of the approximated moment-domain equivalent $\bar{Y} = C\bar{\Pi}$, effectively reducing the number of variables involved in such an equation.

Corollary 11.2.5 *The system of algebraic equations (11.21) can be fully written as a function of the approximated moment-domain equivalent $\bar{Y} = C\bar{\Pi}$ as*

$$\bar{Y} - (\bar{L}_e - \bar{L}_u)\bar{\Phi}_{\mathcal{R}}^T + \text{vec}\{F_{nl}(g(\bar{Y}))\}^T\Phi_{\Omega}^T = 0, \quad (11.23)$$

where $\bar{\Phi}_{\mathcal{R}} \in \mathbb{R}^{(\nu+\iota) \times (\nu+\iota)}$ and $\Phi_{\Omega} \in \mathbb{R}^{(\nu+\iota) \times 2(\nu+\iota)}$ are given by the expressions

$$\begin{aligned} \bar{\Phi}_{\mathcal{R}} &= (\mathbb{I}_{\nu+\iota} \otimes C)\Phi^{-1}(\mathbb{I}_{\nu+\iota} \otimes -B), \\ \Phi_{\Omega} &= (\mathbb{I}_{\nu+\iota} \otimes C)\Phi^{-1}(\Omega^{-1T} \otimes \mathbb{I}_2), \\ \Phi &= \bar{S}\hat{\otimes}A + \mathcal{R}^T \otimes -BC, \end{aligned} \quad (11.24)$$

and the mapping $g : \mathbb{R}^{1 \times (\nu+\iota)} \rightarrow \mathbb{R}^{2 \times (\nu+\iota)}$ is defined as

$$g(\bar{Y}) = (\mathbb{I}_2 \otimes \bar{Y}) \begin{bmatrix} \bar{S}^{-1} \\ \mathbb{I}_{\nu+\iota} \end{bmatrix}. \quad (11.25)$$

Proof. A direct application of the vec operator¹² to equation (11.21), yields

$$\begin{aligned} \text{vec}\{\bar{\Pi}\} + \Phi^{-1}(\mathbb{I}_{\nu+\iota} \otimes B)\text{vec}\{\bar{L}_e - \bar{L}_u\} + \\ \Phi^{-1}(\Omega^{-1T} \otimes \mathbb{I}_2)\text{vec}\{F_{nl}(\bar{\Pi})\} = 0, \end{aligned} \quad (11.26)$$

in which explicit use of the skew-symmetry of \bar{S} is made, *i.e.* $-\bar{S}^T = \bar{S}$, to obtain Φ as in (11.24). Equation (11.23) follows after multiplying both sides of (11.26) by $(\mathbb{I}_{\nu+\iota} \otimes C)$, noting that $\text{vec}\{C\bar{\Pi}\} = \text{vec}\{\bar{Y}\} = \bar{Y}^T$ and $\text{vec}\{\bar{L}_e - \bar{L}_u\} = (\bar{L}_e - \bar{L}_u)^T$. Finally, the mapping g arises as a result of Proposition 5.2.1: given that $\dot{w}_1 = w_2 = y$ in (11.3), $\bar{\Pi}$ can be written in terms of \bar{Y} simply as

$$\bar{\Pi} = \begin{bmatrix} \bar{Y}\bar{S}^{-1} \\ \bar{Y} \end{bmatrix} = (\mathbb{I}_2 \otimes \bar{Y}) \begin{bmatrix} \bar{S}^{-1} \\ \mathbb{I}_{\nu+\iota} \end{bmatrix} = g(\bar{Y}), \quad (11.27)$$

which concludes the proof. \square

Remark 11.2.11 If $F_{nl}(g(\bar{Y})) = 0$, *i.e.* system (11.3) is *linear*, the approach of Proposition 11.2.3 (through Corollary 11.2.5) recovers (without approximation) the linear moment-domain equivalent $\bar{Y} = (\bar{L}_e - \bar{L}_u)\bar{\Phi}_{\mathcal{R}}^T$, presented in Section 8.3. In other words,

12: See also Property 1.3.1.

equation (11.23) can be regarded as the linear moment-domain equivalent of y plus a *nonlinear* ‘perturbation’ term.

11.3 Nonlinear moment-based energy-maximising OCP

The results presented in Section 11.2.1 can be effectively used to approximate the energy-maximising optimal control problem presented in Section 11.1, making explicit use of the connection between moments and the steady-state behaviour of system (11.3). In the following, a definition of the so-called *approximated energy-maximising OCP* is explicitly provided¹³, using the approximated moment-domain equivalent \bar{Y} , presented in Definition 11.2.1.

Problem 11.3.1 (Approximated energy-maximising OCP) Suppose Assumptions 11.2.1, 7.1.1 and 7.1.2 hold. Find the optimal control input $\bar{u}^{\text{opt}} = \bar{L}_u^{\text{opt}} \bar{\xi}$ such that

$$\begin{aligned} \bar{L}_u^{\text{opt}} &= \arg \max_{\bar{L}_u \in \mathbb{R}^{\nu+\iota}} \frac{1}{T} \int_{\mathcal{T}} \bar{L}_u \bar{\xi}(\tau) \bar{Y} \bar{\xi}(\tau) d\tau, \\ &\text{subject to:} \\ \bar{Y} - (\bar{L}_e - \bar{L}_u) \bar{\Phi}_{\mathcal{D}}^T + \text{vec}\{F_{nl}(g(\bar{Y}))\}^T \Phi_{\Omega}^T &= 0, \end{aligned} \quad (11.28)$$

where \bar{Y} is the approximated moment-domain equivalent of the output of system (11.3) (see Definition 11.2.1), and $\bar{\xi}$ is the solution of (11.10).

Remark 11.3.1 The main idea behind Problem 11.3.1 relies on substituting the integro-differential (equality) constraint, corresponding with the nonlinear WEC dynamics (11.3), by the *algebraic* equation (11.23). Note that the latter characterises the approximated moment-domain equivalent of the velocity of the device $\dot{z} = y$ (which is the key state variable involved in the energy-maximising objective function (3.11)). In other words, the approximated OCP posed in Problem 11.3.1 explicitly utilises an approximation of the steady-state (output) behaviour of system (11.3), parameterised in terms of \bar{Y} , *i.e.* $\dot{z}_{\text{ss}}(t) = y_{\text{ss}}(t) \approx \bar{Y} \bar{\xi}(t)$ (see Remark 11.2.8), to solve for the corresponding optimal control input \bar{u}^{opt} , in terms of the signal generator (11.10).

Remark 11.3.2 Following Remark 11.2.10, if $\iota \rightarrow \infty$, then the steady-state output response of system (11.3) is exactly given by $y_{\text{ss}}(t) = \bar{Y} \bar{\xi}(t)$, and the algebraic equality constraint in the OCP of Problem 11.3.1 corresponds to the exact steady-state motion of the device, without approximation.

13: Note that the set of state and input constraints defined in (3.12) are not yet included. These are explicitly incorporated in Section 11.3.1.

Based on Problem 11.3.1, a solution to the motion unconstrained energy-maximising optimal control problem, *i.e.* (11.2) without considering input and state constraints (see Problem 11.3.1), can be now proposed, in terms of a specific tractable finite-dimensional nonlinear program (NP). This claim is formalised in the following proposition.

Proposition 11.3.1 (Nonlinear moment-based unconstrained NP)

Suppose Assumptions 11.2.1, 7.1.1 and 7.1.2 hold, and let $\bar{\xi}(0) = \varepsilon_{\nu+\iota}$. Then, for ι sufficiently large, the solution of the (motion unconstrained) approximated energy-maximising OCP, posed in Problem 11.3.1, can be computed as $\bar{u}^{\text{opt}} = \bar{L}_u^{\text{opt}} \bar{\xi}$, where

$$\bar{L}_u^{\text{opt}} = - \left(\bar{Y}^{\text{opt}} + \text{vec}\{F_{\text{nl}}(g(\bar{Y}^{\text{opt}}))\}^\top \Phi_\Omega^\top - \bar{L}_e \right) \bar{\Phi}_{\mathcal{R}}^{-1\top}, \quad (11.29)$$

and the matrix \bar{Y}^{opt} is the solution of the finite-dimensional nonlinear program

$$\bar{Y}^{\text{opt}} = \arg \max_{\bar{Y}^\top \in \mathbb{R}^{\nu+\iota}} \bar{\mathcal{J}}_{\text{QP}}(\bar{Y}) + \bar{\mathcal{J}}_{\text{nl}}(\bar{Y}), \quad (11.30)$$

with $\bar{\mathcal{J}}_{\text{QP}} : \mathbb{R}^{\nu+\iota} \rightarrow \mathbb{R}$, $\bar{\mathcal{J}}_{\text{nl}} : \mathbb{R}^{\nu+\iota} \rightarrow \mathbb{R}$ defined as

$$\begin{aligned} \bar{\mathcal{J}}_{\text{QP}}(\bar{Y}) &= -\frac{1}{2} \bar{Y} \bar{\Phi}_{\mathcal{R}}^{-1} \bar{Y}^\top + \frac{1}{2} \bar{Y} \bar{L}_e^\top, \\ \bar{\mathcal{J}}_{\text{nl}}(\bar{Y}) &= -\frac{1}{2} \bar{Y} \bar{\Phi}_{\mathcal{R}}^{-1} \Phi_\Omega \text{vec}\{F_{\text{nl}}(g(\bar{Y}))\}. \end{aligned} \quad (11.31)$$

Proof. The fundamental step towards this proof lies in Proposition 8.3.1. In particular, due to the (harmonic) nature of the signal generator defined in equation (11.10), the objective function corresponding with the approximated OCP, *i.e.* equation (11.28), can be equivalently written as

$$\bar{\mathcal{J}} = \frac{1}{T} \int_{\mathcal{T}} \bar{Y} \bar{\xi}(\tau) \bar{L}_u \bar{\xi}(\tau) d\tau = \frac{1}{2} \bar{Y} \bar{L}_u^\top, \quad (11.32)$$

for $\bar{\xi}(0) = \varepsilon_{\nu+\iota}$. Substituting \bar{L}_u in (11.32), using the result of Corollary 11.2.5, $\bar{\mathcal{J}}$ can be written exclusively as a function of \bar{Y} , *i.e.*

$$\begin{aligned} \bar{\mathcal{J}} &= -\frac{1}{2} \bar{Y} \bar{\Phi}_{\mathcal{R}}^{-1} \bar{Y}^\top + \frac{1}{2} \bar{Y} \bar{L}_e^\top - \frac{1}{2} \bar{Y} \bar{\Phi}_{\mathcal{R}}^{-1} \Phi_\Omega \text{vec}\{F_{\text{nl}}(g(\bar{Y}))\}, \\ \bar{\mathcal{J}} &= \bar{\mathcal{J}}_{\text{QP}}(\bar{Y}) + \bar{\mathcal{J}}_{\text{nl}}(\bar{Y}), \end{aligned} \quad (11.33)$$

where the optimal control input $\bar{u}^{\text{opt}} = \bar{L}_u^{\text{opt}} \bar{\xi}$ can be straightforwardly recovered using equality (11.23), yielding equation (11.29), which concludes the proof. \square

Proposition 11.3.1 explicitly uses the approximated moment-domain equivalent $\bar{\underline{Y}}$ to propose a finite-dimensional tractable optimisation problem, allowing for the computation of an energy-maximising control solution for the approximated OCP posed in Problem 11.3.1, when the WEC is subject to *nonlinear* dynamics. Note that there is (almost) no restriction on the nature of the nonlinear mapping f , so that a general class of nonlinear effects can be considered, including complex hydrodynamic nonlinearities, such as those discussed in Chapter 2.

Remark 11.3.3 The moment-based NP stated in Proposition 11.3.1 has to be solved over the approximated moment-domain equivalent $\bar{\underline{Y}}^\top \in \mathbb{R}^{\nu+\iota}$ *only*, and can be solved using efficient state-of-the-art numerical routines, such as¹⁴ interior-point methods (IPMs) [208].

Remark 11.3.4 There is an intrinsic trade-off between the degree of accuracy incorporated in the approximated OCP, controlled by the parameter ι (see Remark 11.3.2), and the underlying computational complexity of equation (11.30). In other words, a higher ι results in improved energy absorption, but also intrinsically increases the computational requirements of the strategy.

Remark 11.3.5 If $\bar{\mathcal{J}}_{nl}(\bar{\underline{Y}}) = 0$, Proposition 11.3.1 recovers the optimal moment-based control input proposed in Chapter 8 for the *linear* WEC case. To be precise, if there are no nonlinearities involved in (11.3), equation (11.30) is of a concave quadratic type, *i.e.* a quadratic program (QP), written as

$$\bar{\underline{Y}}_l^{\text{opt}} = \arg \max_{\bar{\underline{Y}}^\top \in \mathbb{R}^{\nu+\iota}} -\frac{1}{2} \bar{\underline{Y}} \bar{\Phi}^{-1} \bar{\underline{Y}}^\top + \frac{1}{2} \bar{\underline{Y}} \bar{L} \bar{\underline{I}}_e, \quad (11.34)$$

where the function $\bar{\mathcal{J}}_{QP}$ is strictly concave for any physically meaningful parameters involved in the WEC equation (11.3).

Following Remark 11.3.5, it is straightforward to note that the NP stated in Proposition 11.3.1 can be seen as a QP problem characterised by the objective function $\bar{\mathcal{J}}_{QP}$, and ‘perturbed’ by the action of the nonlinear mapping $\bar{\mathcal{J}}_{nl}$. Nevertheless, unlike the linear moment-based energy-maximising OCP of Chapter 8 (recalled herein in Remark 11.3.5), there is no guarantee that the nonlinear OCP of Proposition 11.3.1 admits a global maximiser. Aiming to secure the existence of a global solution to problem (11.30), the following standing assumption is introduced, to later formalise an appropriate proposition guaranteeing the existence of a global energy-maximising solution to (11.30).

14: Another suitable optimisation approach is that based on sequential quadratic programming, *i.e.* so-called SQP methods. The reader is referred to, for instance, [210], for an in-depth treatment of SQP.

Assumption 11.3.1 The mapping $\bar{\mathcal{J}}_{nl} : \mathbb{R}^{1 \times (\nu + \iota)} \rightarrow \mathbb{R}$ is bounded by a parameter $\alpha_{nl} \in \mathbb{R}^+$, i.e.

$$\sup_{\bar{\mathbf{Y}}^T \in \mathbb{R}^{\nu + \iota}} |\bar{\mathcal{J}}_{nl}(\bar{\mathbf{Y}})| \leq \alpha_{nl} < +\infty. \quad (11.35)$$

Proposition 11.3.2 Suppose Assumption 11.3.1 holds. Then, the NP with objective function $\bar{\mathcal{J}}$ defined in Proposition 11.3.1 always admits a global maximum $\bar{\mathbf{Y}}^{\text{opt}}$.

Proof. The key concept behind this proposition lies in the decomposition of $\bar{\mathcal{J}}$ as in equation (11.31), i.e. as the sum of a concave problem $\bar{\mathcal{J}}_{\text{QP}}$ and, under Assumption 11.3.1, a bounded perturbation $\bar{\mathcal{J}}_{nl}$. To be precise, if $\bar{\mathcal{J}}_{nl}$ is bounded, then the function $-\bar{\mathcal{J}}$ is strictly outer Γ -convex [259], for $\Gamma \subset \mathbb{R}^{1 \times (\nu + \iota)}$, where the set Γ is given by

$$\Gamma = \mathcal{B}(0, r), \quad r = \sqrt{\frac{2\alpha_{nl}}{\min \lambda(\mathcal{H}\{\bar{\Phi}_{\mathcal{R}}^{-1}\})}}. \quad (11.36)$$

Finally, given that the mapping $\bar{\mathcal{J}}_{\text{QP}}$ has a unique global maximiser¹⁵ $\bar{\mathbf{Y}}_l^{\text{opt}}$, and the set $\Gamma \cap \mathbb{R}^{1 \times (\nu + \iota)}$ is closed, the NP defined by the objective function $\bar{\mathcal{J}}$ always admits a global optimal solution $\bar{\mathbf{Y}}^{\text{opt}}$ [262, Lemma 4.3]. \square

15: See Remark 11.3.5.

Proposition 11.3.2 makes explicit use of the strictly outer Γ -convexity of the function $-\bar{\mathcal{J}}$ to ensure existence of a global solution to the moment-based energy-maximising OCP proposed in this chapter. Moreover, recalling key theoretical results from [262], one can use the following property of strictly outer convex functions, which establishes a direct relationship between local and global maximisers for $\bar{\mathcal{J}}$, having strong practical implications.

Property 11.3.1 [262] Let $\bar{\mathbf{Y}}^{\text{opt}}$ be a Γ -maximiser of $\bar{\mathcal{J}}$, i.e.

$$\bar{\mathcal{J}}(\bar{\mathbf{Y}}^{\text{opt}}) = \max_{\bar{\mathbf{Y}} \in \mathcal{B}(\bar{\mathbf{Y}}^{\text{opt}}, r)} \bar{\mathcal{J}}(\bar{\mathbf{Y}}), \quad (11.37)$$

with r as in (11.36). Then, $\bar{\mathbf{Y}}^{\text{opt}}$ is a global maximiser of $\bar{\mathcal{J}}$.

Property 11.3.1 acts as the analogue of the global optimality property of concave functions (i.e. every local solution is a global solution). In other words, if $\bar{\mathbf{Y}}^{\text{opt}}$ is a maximiser for $\mathcal{B}(\bar{\mathbf{Y}}^{\text{opt}}, r)$, a subset of $\mathbb{R}^{1 \times (\nu + \iota)}$, then it is automatically a global maximiser of $\bar{\mathcal{J}}$. This not only gives explicit conditions for global energy-maximisation within the proposed nonlinear moment-based approach, but also considerably reduces the ‘search’ space when numerically solving (11.30), enhancing the efficiency behind the proposed moment-based strategy.

11.3.1 Handling of state and input constraints

As discussed throughout Chapter 3, any energy-maximising optimal control strategy *must* take into account physical limitations, arising from both the device itself, and the actuator (PTO system) dynamics. Following the moment-based NP defined in Proposition 11.3.1, a framework to incorporate the set of state and input constraints \mathcal{C} , defined in Section 11.1, into the energy-maximising unconstrained solution of Proposition 11.3.1, is now proposed.

To be precise, and in line with the linear moment-based control framework proposed in Chapter 8, the set of constraints \mathcal{C} is mapped onto each respective moment-domain equivalent as

$$\begin{cases} |z(t)| \leq Z_{\max}, \\ |\dot{z}(t)| \leq \dot{Z}_{\max}, \\ |u(t)| \leq U_{\max}, \end{cases} \mapsto \begin{cases} |\bar{Y}S^{-1}\bar{\xi}(t)| \leq Z_{\max}, \\ |\bar{Y}\bar{\xi}(t)| \leq \dot{Z}_{\max}, \\ |\bar{L}_u\bar{\xi}(t)| \leq U_{\max}, \end{cases} \quad (11.38)$$

The set of mapped constraints (11.38) is enforced only at a finite set of N_c uniformly-spaced time instants $\mathcal{T}_c = \{t_i\}_{i=1}^{N_c} \subset \mathcal{T}$, i.e. using a collocation approach. To that end, the matrices $\bar{\Lambda} \in \mathbb{R}^{(\nu+\iota) \times N_c}$ and $\bar{\Upsilon} \in \mathbb{R}^{(\nu+\iota) \times 2N_c}$ are defined as

$$\bar{\Lambda} = [\bar{\xi}(t_1) \quad \dots \quad \bar{\xi}(t_{N_c})], \quad \bar{\Upsilon} = [\bar{\Lambda} \quad -\bar{\Lambda}]. \quad (11.39)$$

Finally, a moment-based energy-maximising constrained optimal control solution for WECs, subject to nonlinear dynamics, can be proposed as follows.

Proposition 11.3.3 (Nonlinear moment-based constrained NP)

Suppose Assumptions 11.2.1, 7.1.1 and 7.1.2 hold, and let $\bar{\xi}(0) = \varepsilon_{\nu+\iota}$. Then, for ι sufficiently large, the solution of the approximated energy-maximising OCP, posed in Problem 11.3.1, subject to the set of state and input constraints (11.38), can be computed as $\bar{u}^{\text{opt}} = \bar{L}_u^{\text{opt}}\bar{\xi}$, where

$$\bar{L}_u^{\text{opt}} = - \left(\bar{Y}^{\text{opt}} + \text{vec}\{F_{\text{nl}}(g(\bar{Y}^{\text{opt}}))\}^{\top} \Phi_{\Omega}^{\top} - \bar{L}_e \right) \bar{\Phi}_{\mathcal{R}}^{-1\top}, \quad (11.40)$$

and the matrix \bar{Y}^{opt} is the solution of the inequality-constrained

finite-dimensional nonlinear program

$$\begin{aligned} \bar{\underline{Y}}^{\text{opt}} &= \arg \max_{\bar{\underline{Y}}^{\text{T}} \in \mathbb{R}^{\nu+\iota}} \bar{\mathcal{J}}_{QP}(\bar{\underline{Y}}) + \bar{\mathcal{J}}_{nl}(\bar{\underline{Y}}), \\ &\text{subject to:} \\ &\begin{cases} \bar{\underline{Y}} \mathcal{A}_z \leq \mathcal{B}_z, \\ \bar{\underline{Y}} \mathcal{A}_z \leq \mathcal{B}_z, \\ \bar{\underline{Y}} \mathcal{A}_u + \mathcal{N}_u(\bar{\underline{Y}}) \leq \mathcal{B}_u, \end{cases} \end{aligned} \quad (11.41)$$

where

$$\begin{aligned} \mathcal{A}_z &= \bar{S}^{-1} \bar{\Upsilon}, & \mathcal{B}_z &= Z_{\max} \mathbf{1}_{1 \times 2N_c}, \\ \mathcal{A}_z &= \bar{\Upsilon}, & \mathcal{B}_z &= \dot{Z}_{\max} \mathbf{1}_{1 \times 2N_c}, \\ \mathcal{A}_u &= -\bar{\Phi}_{\mathcal{R}}^{-1\text{T}} \bar{\Upsilon}, & \mathcal{B}_u &= U_{\max} \mathbf{1}_{1 \times 2N_c} + \bar{L}_e \mathcal{A}_u, \\ \mathcal{N}_u(\bar{\underline{Y}}) &= -\text{vec}\{F_{nl}(g(\bar{\underline{Y}}))\}^{\text{T}} \Phi_{\Omega}^{\text{T}} \mathcal{A}_u. \end{aligned} \quad (11.42)$$

Proof. Note that under the set of assumptions considered in this proposition, equations (11.40) and (11.41) follow directly from Proposition 11.3.1. With respect to the incorporation of the set of state and input constraints defined in (11.38), consider first the constraint associated with the control input, and note that

$$|\bar{L}_u S^{-1} \bar{\xi}(t)| \leq U_{\max} \Rightarrow -U_{\max} \leq \bar{L}_u \bar{\xi}(t) \leq U_{\max}. \quad (11.43)$$

Equation (11.43), enforced at the set of collocation instants \mathcal{T}_c , can be straightforwardly written in terms of the matrix $\bar{\Upsilon}$ defined in (11.39), *i.e.*

$$\bar{L}_u \bar{\Upsilon} \leq U_{\max} \mathbf{1}_{1 \times 2N_c}. \quad (11.44)$$

The left hand side of equation (11.44) can be expanded using the result of Corollary 11.2.5 as

$$\bar{L}_u \bar{\Upsilon} = \bar{\underline{Y}} \mathcal{A}_u - \bar{L}_e \mathcal{A}_u + \text{vec}\{F_{nl}(g(\bar{\underline{Y}}))\}^{\text{T}} \Phi_{\Omega}^{\text{T}} \mathcal{A}_u, \quad (11.45)$$

from where both the matrix \mathcal{B}_u and the nonlinear mapping \mathcal{N}_u follow directly. Finally, the claim of this proposition follows by writing the set of constraints associated with displacement and velocity, defined in (11.38), as in equation (11.44), *i.e.* in terms of the matrix $\bar{\Upsilon}$. \square

Remark 11.3.6 Note that, the set of inequality constraints associated with displacement and velocity are *linear* in $\bar{\underline{Y}}$. This is not the case for the control input-related constraint, which can be decomposed as the sum of a linear and a nonlinear mapping $\mathcal{N}_u : \mathbb{R}^{1 \times (\nu+\iota)} \rightarrow \mathbb{R}^{1 \times 2N_c}$.

11.4 Case study: A CorPower-like device

To demonstrate the performance of the nonlinear moment-based controller proposed throughout this chapter, the CorPower-like wave energy device, presented in Figure 6.2, is considered, constrained to oscillate in heave¹⁶ (translational motion). The corresponding hydrodynamic characteristics, in terms of $B_r(\omega)$ and $A_r(\omega)$, are those presented in Figure 8.1.

In the remainder of this section, irregular waves generated stochastically from a JONSWAP spectrum (see Section 2.1.2), are considered. The corresponding SDF S_w is fully characterised by a significant wave height \bar{H}_w of 2 [m], varying peak period $\bar{T}_w \in [5, 12]$ [s], and peak shape parameter $\gamma = 3.3$. The total time-length (fundamental period) of each wave is set to $T = 120$ [s]. The corresponding spectral density functions are illustrated, for reference, in Figure 8.3. Since the waves are generated from sets of random amplitudes (see Remark 2.1.3), it is found that a mean of ≈ 40 simulations (per sea state) is necessary to obtain statistically consistent performance results for the nonlinear moment-based controller presented in this chapter.

11.4.1 Characterisation of nonlinear hydrodynamic effects

In this section, the nonlinear effects considered for the CorPower-like device of this case study are characterised in terms of the mapping f_{nl} in (11.1). In particular, two main hydrodynamic forces are considered: viscous effects f_v , and the presence of a nonlinear restoring force f_{re}^{nl} , so that $f_{nl} = f_v + f_{re}^{nl}$.

Viscous effects, arising from vortex shedding and turbulence, are particularly present in heaving point absorber devices [263], such as the CorPower-like WEC considered. These are included via a Morison-like equation¹⁷, *i.e.*

$$f_v(\dot{z}) = -\beta_v |\dot{z}| \dot{z}, \quad (11.46)$$

where $\beta_v = \frac{1}{2} \rho C_d D$, $C_d \in \mathbb{R}^+$ is the so-called drag coefficient, and D is the characteristic area of the device. The drag coefficient is set to $C_d = 0.35$, based on the analysis performed in [179] for the device of Figure 6.2. Figure 11.1 (right axis, dashed line) illustrates the output of the mapping f_v .

The mapping f_{re}^{nl} , characterising nonlinear restoring effects, due to a non-uniform device cross-sectional area, is computed based on the experimental results presented in [239] for this CorPower-like device.

16: Note that this is, effectively, the DoF from where mechanical energy is converted.

17: See Section 2.5.2 for further detail.

In particular, inspired by the results presented in [239], the following definition is provided

$$f_{re}^{nl}(z) = \beta_{r_1} z^2 + \beta_{r_2} z^3, \quad (11.47)$$

where the coefficients $\{\beta_{r_1}, \beta_{r_2}\} \subset \mathbb{R}$ are determined based on a least-squares fit, using the experimental results of [239] as a target set, giving a final result of $\beta_{r_1} = -1.55 \times 10^4$ [kg/ms²] and $\beta_{r_2} = 0.82 \times 10^4$ [kg/m²s²]. The output of the nonlinear restoring force mapping f_{re}^{nl} is presented in Figure 11.1 (left axis, solid line).

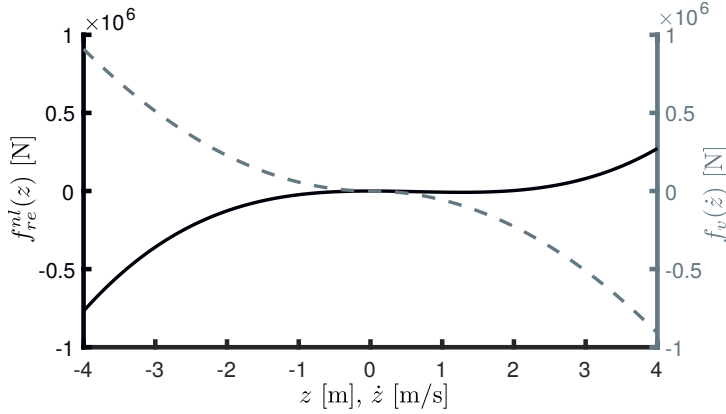


Figure 11.1: Nonlinear hydrodynamic effects considered in this chapter: hydrostatic force (displacement-dependent, left axis), and viscous force (velocity-dependent, right axis).

Note that both nonlinear effects, as described in equations (11.46) and (11.47), fulfill Assumption 7.1.1. To show that Assumption 11.3.1 holds, recall that the energy-maximising optimal control law is such that the state-variables $w_1 = z$ and $w_2 = \dot{z}$ have maximum allowed values Z_{\max} and \dot{Z}_{\max} , respectively (see equation (11.38)). Then, the following inequality, involving the nonlinear mapping $f_{nl} = f_v + f_{re}^{nl}$,

$$\begin{aligned} |f_{nl}(w)| &= \beta_v |w_2|^2 + \beta_{r_1} |w_1|^2 + \beta_{r_2} |w_1|^3 \\ &\leq \beta_v \dot{Z}_{\max} + (\beta_{r_1} + \beta_{r_2} Z_{\max}) Z_{\max}^2 = \tilde{\alpha}_{nl}, \end{aligned} \quad (11.48)$$

holds for all $t \in \mathcal{T}$. Using equation (11.48), and considering well-known (Euclidean) norm properties, it is straightforward to show that

$$\|\text{vec}\{F_{nl}(g(\bar{Y}))\}\|_2 \leq (\nu + \iota) \tilde{\alpha}_{nl}^2. \quad (11.49)$$

Recalling, from the set of moment-domain constraints (11.38), that $|\bar{Y}\bar{\xi}(t)| \leq \dot{Z}_{\max}$ for all $t \in \mathcal{T}$, and, if $\bar{\xi}(0) = \varepsilon_{\nu+\iota}$, then $\|\bar{\xi}\|_2^2 = \sum_{i=1}^{\nu+\iota} \langle \bar{\xi}_i, \bar{\xi}_i \rangle = T(\nu + \iota)/2$, one can directly obtain the following estimate for α_{nl} in equation (11.35):

$$|\bar{\mathcal{J}}_{nl}(\bar{Y})| \leq \frac{1}{2T} \left(\dot{Z}_{\max} \left\| \bar{\Phi}_{\mathcal{R}}^{-1} \Phi_{\Omega} \right\|_{\mathbb{F}} \tilde{\alpha}_{nl} \right)^2 = \alpha_{nl} < +\infty, \quad (11.50)$$

and, hence, the moment-based energy-maximising OCP always admits a global maximiser under the effect of the nonlinear dynamics defined in f_{nl} (see Proposition 11.3.2).

11.4.2 Results and discussion

Based on the CorPower-like device of Figure 6.2, subject to the nonlinear effects described in Section 11.4.1, results from applying the nonlinear moment-based energy-maximising control strategy developed throughout Section 11.3 are now presented and discussed, under the effect of irregular wave excitation.

Let the maximum allowed displacement and velocity values be chosen as $Z_{\max} = 2$ [m] and $\dot{Z}_{\max} = 2$ [m/s]. For this case study, the wave excitation force f_e is computed using $\nu = 60$ components in (11.8), while the order of the extended signal generator (11.10) is set to $\nu + \iota = 100$. The constrained moment-based optimal control problem, stated in Proposition 11.3.3, can be solved using a variety of state-of-the-art numerical routines, belonging to the families of both local and global optimisation methods.

In this chapter, a local IPM is chosen, where explicit advantage of the strict outer convexity of the energy-related objective function, when mapped to the moment-domain, is used: Property 11.3.1 can be used to numerically ensure that the (potentially local) solution computed with interior-point methods is, effectively, a global energy-maximiser. In particular, the following simple algorithm is proposed, written in pseudo-code.

```

1: init algorithm
2: Set initial guess  $\bar{Y}_0^{\text{opt}} = \bar{Y}_l^{\text{opt}}$ ;
3: global = 0;
4: while global  $\neq$  1 do
5:    $\bar{Y}^{\text{opt}} \leftarrow$  Solve the OCP (11.41) using IPM with  $\bar{Y}_0^{\text{opt}}$ ;
6:   Generate a random set  $\mathcal{P} = \{\bar{Y}_i\}_{i=1}^P$  with  $P \in \mathbb{N}_{\geq 1}$  elements,
   such that  $\mathcal{P} \subset \mathcal{B}(\bar{Y}^{\text{opt}}, r)$  and where  $\bar{Y}_i$  is such that the set
   of constraints defined in (11.41) hold for all  $i \in \mathbb{N}_P$ ;
7:   if  $\bar{J}(\bar{Y}^{\text{opt}}) \leq \bar{J}(\bar{Y}_i)$  for all  $\bar{Y}_i \in \mathcal{P}$  then
8:     global = 1;
9:   else if  $\exists \bar{Y}_i \in \mathcal{P}$  such that  $\bar{J}(\bar{Y}_i) \leq \bar{J}(\bar{Y}^{\text{opt}})$  then
10:     $\bar{Y}_0^{\text{opt}} = \bar{Y}_i$ ;
11:   end if
12: end while
13:  $\bar{L}_u^{\text{opt}} = - \left( \bar{Y}^{\text{opt}} + \text{vec}\{F_{nl}(g(\bar{Y}^{\text{opt}}))\}^\top \Phi_\Omega^\top - \bar{L}_e \right) \bar{\Phi}_{\mathcal{D}}^{-1\top}$ ;
14:  $\bar{u}^{\text{opt}} = \bar{L}_u^{\text{opt}} \bar{\xi}$ ;
15: end algorithm.

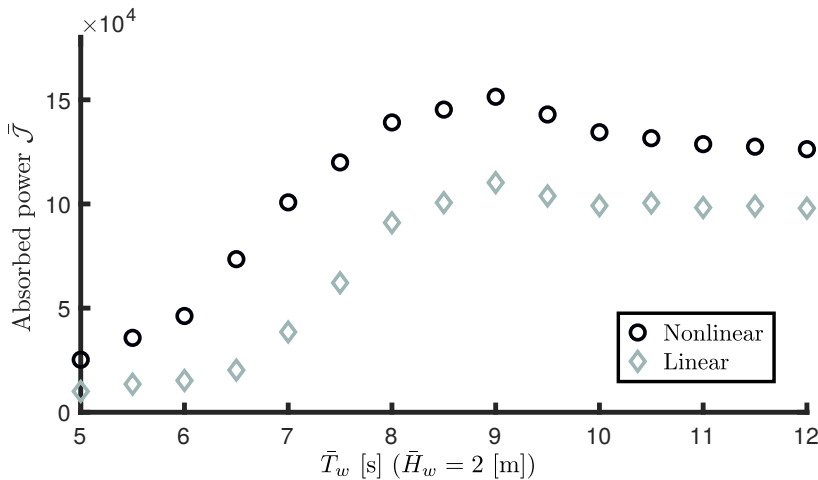
```

Starting from the linear solution \bar{Y}_l^{opt} of the concave QP problem of Corollary 11.3.3, *i.e.* with $F_{nl}(g(\bar{Y})) = 0$, this heuristic attempts to compute a local solution using IPMs, and simply uses function evaluation at a finite set of P random points, contained in the

set $\mathcal{B}(\bar{\mathbf{Y}}^{\text{opt}}, r)$, to (approximately) determine whether the solution corresponds to a global maximiser, using the result expressed by Property 11.3.1. If one can find an element $\bar{\mathbf{Y}}_i$, contained in the set \mathcal{P} , such that $\bar{\mathcal{J}}(\bar{\mathbf{Y}}_i) \leq \bar{\mathcal{J}}(\bar{\mathbf{Y}}^{\text{opt}})$, then the algorithm is re-started, but now updating the initial guess for the IPM to $\bar{\mathbf{Y}}_i$.

Remark 11.4.1 For the nonlinear mapping associated with the CorPower-like device defined in Section 11.4.1, the heuristic discussed above provides a global solution virtually always after a single iteration¹⁸. The interior-point method utilised to solve (11.41) is based on [209].

Remark 11.4.2 The moment-based controller normalised runtime, *i.e.* the ratio between the time required to compute the energy-maximising optimal control input for the duration of the simulation, and the length of the simulation itself, is always less than one for the totality of the preceding simulations, being consistent with the typical sampling time of a full-scale WEC (≈ 1 [s]), hence achieving real-time performance¹⁹.



Performance results, for the proposed nonlinear moment-based controller, are now presented, in terms of energy absorption, under both displacement and velocity constraints. Figure 11.2 explicitly shows the value of $\bar{\mathcal{J}}$ (black circles), for sea states with $\bar{H}_w = 2$ [m] and $\bar{T}_w \in [5, 12]$, where the displacement and velocity of device are constrained to $Z_{\text{max}} = 2$ [m] and $\dot{Z}_{\text{max}} = 2$ [m/s], respectively. In addition, Figure 11.2 demonstrates the performance of the *linear* moment-based controller (grey diamonds), *i.e.* solving the OCP in Proposition 11.3.3 assuming that $\bar{\mathcal{J}}_{\text{nl}}$ is zero²⁰, applied to the nonlinear system described by (11.3). It can be readily appreciated that the performance of the proposed nonlinear approach significantly outperforms its linear counterpart, for the totality of the sea-states analysed in this study, with differences of up to $\approx 45\%$ in total power absorption. In addition, note that, though not penalised in

18: Comparisons have been carried out against global optimisation routines based on genetic algorithms (GA), to determine whether the solution obtained with the proposed heuristic effectively coincides with that computed by GA.

19: Implemented in Matlab®. Further computational savings can be easily achieved by implementing this controller in, for instance, C or C++.

Figure 11.2: Constrained (displacement and velocity) power absorption for the nonlinear moment-based energy maximising controller proposed in this chapter (black circles), and its linear counterpart (grey diamonds).

20: Also equivalent to the moment-based OCP defined in Chapter 8.

the results of Figure 11.2 (to offer a best-case scenario for the linear controller), the solution based on linear assumptions can often violate the physical limitations imposed as state constraints, as a direct consequence of ignoring nonlinear effects in the computation of such an energy-maximising control law. This is illustrated and discussed in the following paragraph, where the capabilities of the nonlinear moment-based control strategy, presented in this chapter, are fully exposed.

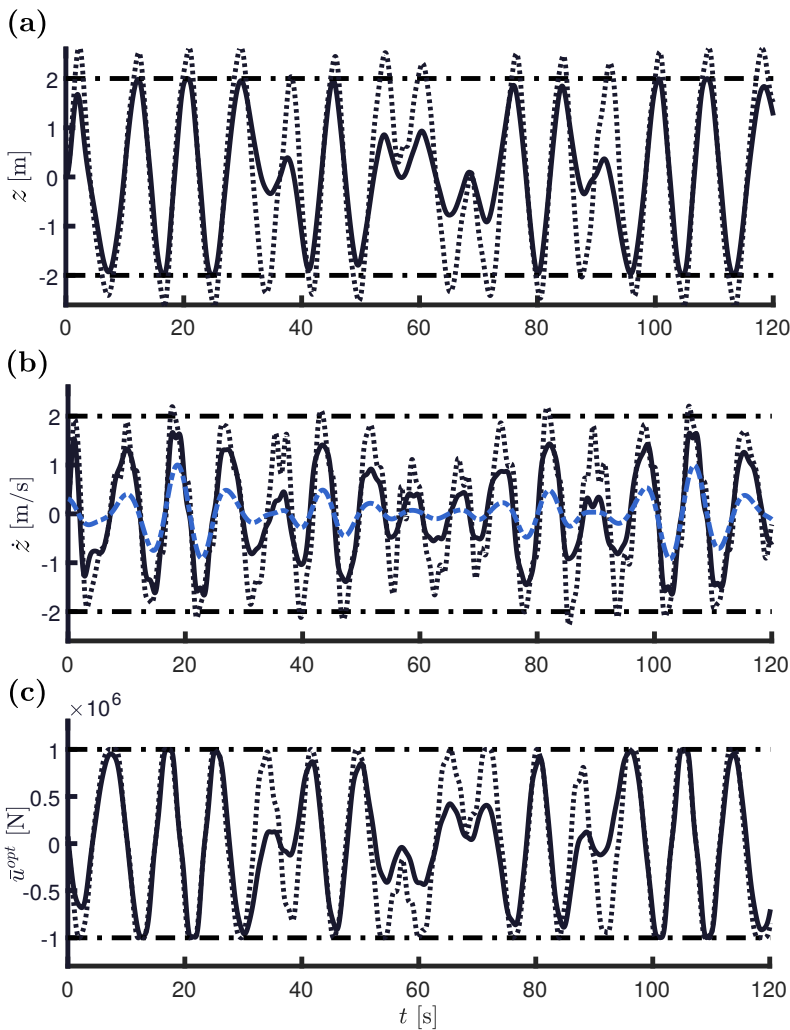


Figure 11.3: Motion and control results for irregular wave excitation with $\bar{H}_w = 2$ [m] and $\bar{T}_w = 10$ [s], for both linear (dotted black) and nonlinear (solid black) moment-based controllers. (a) shows displacement, (b) velocity and (scaled) wave excitation force input (dash-dotted blue), whilst (c) presents the corresponding control inputs, used to elicit the motion results. The dash-dotted horizontal lines represent constraint values.

Figure 11.3 presents time histories of displacement (a), velocity (b) and control input (c), for a specific example of sea-state realisation with $\bar{T}_w = 10$ [s], and where a maximum control (PTO) force constraint $U_{\max} = 1 \times 10^6$ [N] is also included. Some key features associated with the presented moment-based strategy can be directly appreciated from Figure 11.3, as discussed in the following. To begin with, the state and input limits, under the action of the nonlinear moment-based control strategy (solid black), are being consistently respected throughout the complete simulation, hence illustrating the capability of the approach to maximise energy absorption for WECs subject to nonlinear hydrodynamic effects, whilst respecting

the physical limitations of both device and actuator (PTO). This is clearly not the case for the solution based on linear assumptions (dotted black), where a consistent violation can be appreciated, for both displacement and velocity (state constraints). Though not significant (in magnitude) for this particular sea state, this violation happens consistently in time and can potentially damage device components.

Finally, note that, as can be appreciated in Figure 11.3 (b), the velocity of the device under optimal control conditions, for both linear and nonlinear moment-based controllers, remains 'in-phase'²¹ with the (scaled) wave excitation force (dash-dotted blue), agreeing with well-known theoretical results for unconstrained energy-maximisation of WECs (presented in Chapter 3).

21: The term 'in-phase' is used here to denote synchronisation of two signals in terms of instantaneous phase.

11.5 Conclusions

This chapter introduces a *nonlinear* moment-based energy-maximising control framework for wave energy converters, subject to both state and input constraints. The use of nonlinear moments, in conjunction with an appropriate approximation method (based on the family of weighted residual methods), allows the objective function, associated with the energy-maximising OCP, to be mapped to a finite-dimensional nonlinear program, which can be solved efficiently by state-of-the-art numerical solvers.

Unlike the current state-of-the-art in WEC control, the existence of a *globally optimal* solution within the presented framework is guaranteed, under mild assumptions. In addition, explicit conditions, which relate local and global optima, are given. These are effectively exploited in the numerical implementation, further enhancing the computational efficiency behind this nonlinear moment-based control solution. The performance of this method is illustrated by means of a case study, where a CorPower-like device is considered, subject to nonlinear hydrostatic restoring force and viscous forces. Physical limitations are shown to be consistently respected within this nonlinear moment-based framework, maximising absorbed energy while effectively minimising the risk of component damage. Comparisons are presented with its linear counterpart, consistently showing improved performance for the totality of the sea states analysed, with up to $\approx 45\%$ of increase in energy absorption.

Part IV: Conclusions and future work

Contents of this chapter

12.1 Main conclusions	284
12.2 Future directions	287
12.2.1 Model reduction	287
12.2.2 Optimal control	288

A fundamental stepping stone towards the commercialisation of wave energy technology is the availability of appropriate control technology: *regardless of the type of WEC considered, energy conversion must be performed as economically as possible, aiming to minimise the delivered energy cost, while also maintaining the structural integrity of the device, minimising wear on WEC components, and operating across a wide range of sea conditions.* Energy-maximising control design for WECs, based on an optimal control approach, inherently requires both control-oriented dynamical models, and appropriate approximation methods, to solve for the energy-maximising control law efficiently, while guaranteeing globally optimal performance.

This thesis proposes a comprehensive framework for model reduction and energy-maximising optimal control for WECs, based on the concept of *moments*. Moments are intrinsically connected to the input-output characteristics of the dynamical system describing the motion of the WEC, and provide a very specific parameterisation of the steady-state output response of such a system. This thesis demonstrates that moment-based theory perfectly *fits* with the wave energy control application, and can be exploited both to produce control-oriented models, via model reduction by moment-matching, and to efficiently transcribe the energy-maximising OCP for WECs, subject to state and input constraints.

The main conclusions¹ that stem from this thesis are encompassed in Section 12.1, while future directions, both for model reduction, and optimal control cases, are discussed in Section 12.2.

1: Note that specific conclusions are also offered at the end of each chapter, offering both qualitative and quantitative details.

12.1 Main conclusions

Following a critical analysis of the state-of-the-art of model reduction techniques considered (and utilised) in the wave energy research field, this thesis presents a model reduction by moment-matching framework *tailored* for the WEC application. The proposed framework,

which inherits steady-state response characteristics, includes both *linear*, and *nonlinear* WEC systems, in SISO and MIMO formulations. For the case of *linear* systems (where parameterisation of Cummins' equation is fundamental for control/estimation applications)², this moment-based formulation allows the user to *exactly* match the steady-state behaviour of the device under analysis at a set of key frequencies, including, for instance, the resonant frequency³, retaining important physical properties of the studied WEC. As a matter of fact, and unlike the state-of-the-art model reduction strategies reviewed, specific methodologies are presented to preserve *all* the physical properties associated with radiation effects.

Additionally, given the intrinsic connection between moments, and the steady-state response characteristics of the WEC, a specific relationship between the unknown-input wave excitation force estimation problem, and the moment-based model reduction framework presented in this thesis, is shown and exploited by a sensible selection of the set of interpolation points, in synergy with the internal model principle, commonly utilised to estimate the wave excitation effect. Such a relationship allows for the computation of control-oriented models tailored for a particular sea state, with relatively mild computational requirements, hence providing parametric representations that are especially suited to the design of real-time energy-maximisation strategies.

Recognising the necessity of control/estimation-oriented *nonlinear* models in the WEC application, this thesis presents a nonlinear model reduction framework for wave energy applications, based on moment-matching techniques, which inherently preserve steady-state response characteristics, with substantial computational savings. This is, to the best of the author's knowledge, the first systematic nonlinear model reduction technique proposed in the wave energy field. The proposed framework is based on mild assumptions, which virtually always hold in practice. This, in turn, allows for the computation of control-oriented models from a large class of nonlinear WEC structures, potentially featuring complex nonlinear hydrodynamic effects, and non-ideal PTO dynamics. The degree of complexity of the computed control-oriented models can be fully manipulated by the user, hence having full control on the underlying characteristics of the reduced structure. Practical aspects behind this approximation framework are given and discussed, illustrating the use of the proposed technique in various wave conditions.

In addition to the moment-based model reduction framework (discussed in the previous paragraphs), and following the critical review on the state-of-the-art WEC optimal control strategies, this thesis introduces an energy-maximising optimal control framework based

2: The methodology is proposed both to compute a reduced order model for the input-output (force-to-motion), and radiation dynamics.

3: Note that for MIMO systems this concept translates to the frequency characterising the \mathcal{H}_∞ -norm of the WEC.

on moments, *tailored* for the WEC application. In particular, the moment-based parameterisation of the steady-state response of the WEC system is shown to provide a significant simplification of the target OCP, transcribing such an infinite-dimensional problem to a finite-dimensional nonlinear program. This thesis proposes, to the best of the author's knowledge, the first application of moment-based theory to solve a constrained optimal control problem.

The proposed optimal control framework includes both *linear*, and *nonlinear* WEC systems, featuring SISO and MIMO formulations. In the *linear* case, the corresponding OCP is transcribed to a finite-dimensional quadratic program, which is always strictly concave: unlike most of the linear WEC control strategies reviewed, the proposed moment-based parameterisation systematically guarantees a unique globally optimal solution for the energy-maximising OCP, subject to both state and input constraints. This allows for the utilisation of state-of-the-art QP solvers, which, in turn, provide a computationally efficient framework to solve the WEC OCP in *real-time*.

Furthermore, motivated by the ubiquitous presence of *input* and *system* uncertainty in the WEC energy-maximising optimal control problem, a *robust* moment-based energy-maximising technique is proposed, allowing the user to explicitly consider both system, and input uncertainty, in the computation of the energy-maximising optimal control input. This constitutes, to the best of the author's knowledge, the first energy-maximising optimisation-based framework, within the WEC control literature, which is robust with respect to uncertainty in the wave excitation force input. This robust approach incorporates a suitable defined uncertainty set⁴, and exploits the underpinning concept of the worst-case performance method. The proposed control law is computed in terms of an optimisation procedure, formulated as a minimax problem, which has to be solved only at a small number of points in the uncertainty set⁵, as a result of the nature of the objective function in moment-domain. This minimax optimisation problem is shown to have a unique globally optimal control solution which, in turn, provides a computationally efficient robust optimal control framework, able to consistently respect state and input constraint limitations under the presence of uncertainty. In addition, and further adding practical value to the proposed robust strategy, different procedures are proposed to compute the uncertainty set, both for the case of input, and system uncertainty. For the latter, a data-driven method, to characterise the uncertainty in terms of unmodelled nonlinear effects, is also presented, which is only based on the knowledge of the output of the 'target' nonlinear WEC model. This, in turn, gives the user the possibility of using high-fidelity numerical solvers (such as those

4: In particular, this set is assumed to be a polytope defined over \mathbb{R} .

5: *i.e.* the vertices of the uncertainty polytope.

based on CFD), to characterise the uncertainty in terms of a large class of unmodelled dynamic effects, with mild assumptions.

Finally, given that WECs are, by their nature, prone to show significant and diverse nonlinear effects, this thesis introduces a *nonlinear* moment-based energy-maximising control framework, subject to both state and input constraints. The use of nonlinear moments, in conjunction with the proposition of an appropriate approximation method, allows the objective function, associated with the energy-maximising OCP, to be mapped to a finite-dimensional nonlinear program. Unlike the current state-of-the-art in WEC control, the existence of a globally optimal solution within the presented framework is guaranteed for a large class of nonlinear effects, under mild assumptions. In addition, explicit conditions, which relate local and global optima, are given. These are effectively exploited in the numerical implementation, enhancing the computational efficiency behind this nonlinear moment-based control solution.

12.2 Future directions

This section outlines future work and potential research directions, for both model reduction, and optimal control procedures, based on moments.

12.2.1 Model reduction

- A potential direction is to move from a real- to a complex-valued convention. To be precise, suppose the input is characterised by a single frequency component $\omega \in \mathbb{R}^+$. Then, the following representations are equivalent:

$$(1): \quad \dot{\xi} = \begin{bmatrix} 0 & \omega \\ -\omega & 0 \end{bmatrix} \xi, \quad (2): \quad \dot{\xi} = j\omega\xi.$$

Both **(1)** and **(2)** generate the same class of inputs, but they are defined over different (isomorphic) spaces, *i.e.* \mathbb{R}^2 and \mathbb{C} , respectively. The latter provides a compact representation, which can be potentially useful in simplifying analytical manipulations⁶. Nonetheless, with this convention, the approximating model is represented by complex-valued matrices, hence potentially losing any ‘physical’ meaning.

- Finally, a further direction is that related to *data-driven nonlinear model reduction*: the model reduction procedure, described in Chapter 7, depends upon the availability of an analytical

⁶: An additional advantage of this complex-valued convention is highlighted in Section 12.2.2.

expression of the system to be reduced, which can be limiting in certain cases. To circumvent this issue, a data-driven method can be proposed, using the very same approximating mapping Ω_k , and slightly changing the Galerkin-like approach proposed. This, in turn, would allow the consideration of input-output data directly, generated either experimentally, or via high-fidelity hydrodynamic solvers, such as those based in CFD.

12.2.2 Optimal control

- ▶ Recall the real- and complex-valued conventions **(1)** and **(2)**, presented in Section 12.2.1. Let f be the number of frequencies used to represent the wave excitation input: if **(1)** is considered, the corresponding energy-maximising OCP is parameterised in \mathbb{R}^{2f} while, if **(2)** is adopted, then the OCP is parameterised in \mathbb{C}^f . Though, clearly, \mathbb{R}^{2f} is isomorphic to \mathbb{C}^f , recent research suggest that further computational savings could be achieved by solving the optimisation problem directly using a complex convention (see, for instance, [264]).
- ▶ The optimal control solutions presented in Part III of this thesis lies on what one could call ‘the solution space’, presenting results for a general class of systems (devices), and where the mathematical assumptions adopted along the way are consistent with the physical ‘reality’, being always driven by the practical WEC control problem. That said, even though some features of this moment-based approach have been assessed in a high-fidelity (CFD) environment (see [265]), ‘real-world’ validation of these strategies clearly constitutes a future research direction.

Bibliography

Here are the references in citation order.

- [1] G. Captur. 'Memento for René Favalaro'. In: *Texas Heart Institute Journal* 31.1 (2004), p. 47 (cited on page vii).
- [2] M. Decker and L. Vasakova. 'Energy Roadmap 2050: Impact assessment and scenario analysis'. In: *European Commission, Energy, Unit A1 – Energy policy and analysis* (2011) (cited on page 1).
- [3] M. Grubb et al. *The Kyoto Protocol: a guide and assessment*. Vol. 10. Royal Institute of International Affairs London, 1999 (cited on page 1).
- [4] H. Ritchie and M. Roser. 'Energy'. In: *Our World in Data* (2020). <https://ourworldindata.org/energy> (cited on page 1).
- [5] G. Mork et al. 'Assessing the global wave energy potential'. In: *ASME 2010 29th International Conference on Ocean, Offshore and Arctic Engineering*. American Society of Mechanical Engineers. 2010, pp. 447–454 (cited on page 2).
- [6] O. Edenhofer et al. *Renewable energy sources and climate change mitigation: Special report of the intergovernmental panel on climate change*. Cambridge University Press, 2011 (cited on page 2).
- [7] M. E. McCormick. *Ocean wave energy conversion*. Courier Corporation, 2013 (cited on page 2).
- [8] B. Drew, A. R. Plummer, and M. N. Sahinkaya. *A review of wave energy converter technology*. 2009 (cited on page 2).
- [9] A. Pecher and J. P. Kofoed. *Handbook of ocean wave energy*. Springer London, 2017 (cited on page 2).
- [10] J. Cruz. *Ocean wave energy: current status and future perspectives*. Springer Science & Business Media, 2008 (cited on page 2).
- [11] J. Hals. 'Modelling and phase control of wave-energy converters'. PhD thesis. NTNU, 2010 (cited on page 2).
- [12] J. V. Ringwood, G. Bacelli, and F. Fusco. 'Energy-maximizing control of wave-energy converters: The development of control system technology to optimize their operation'. In: *IEEE Control Systems* 34.5 (2014), pp. 30–55 (cited on pages 2, 20, 46, 56, 57, 64).
- [13] U. A. Korde and J. V. Ringwood. *Hydrodynamic control of wave energy devices*. Cambridge University Press, 2016 (cited on pages 2, 57, 64).
- [14] K. Ruehl and D. Bull. 'Wave Energy Development Roadmap: Design to commercialization'. In: *OCEANS 2012 MTS/IEEE: Harnessing the Power of the Ocean* (2012) (cited on pages 2, 66, 209, 211).
- [15] Y. Peña-Sanchez et al. 'A Critical Comparison of Excitation Force Estimators for Wave-Energy Devices'. In: *IEEE Transactions on Control Systems Technology* (2019) (cited on pages 3, 53, 117, 135, 136, 202).

- [16] Y. Peña-Sanchez, A. Mérigaud, and J. V. Ringwood. 'Short-term forecasting of sea surface elevation for wave energy applications: The autoregressive model revisited'. In: *IEEE Journal of Oceanic Engineering* (2018) (cited on pages 3, 53, 180, 201).
- [17] H. Noura et al. *Fault-tolerant control systems: Design and practical applications*. Springer Science & Business Media, 2009 (cited on pages 4, 53).
- [18] G. Giorgi and J. V. Ringwood. 'Consistency of viscous drag identification tests for wave energy applications'. In: *Proceedings of the 12th European Wave and Tidal Energy Conference (EWTEC)*. Cork. 2017 (cited on pages 7, 40, 67, 163, 226).
- [19] F. Fusco and J. V. Ringwood. 'A study of the prediction requirements in real-time control of wave energy converters'. In: *IEEE Transactions on Sustainable Energy* 3.1 (2012), pp. 176–184 (cited on pages 7, 68, 226).
- [20] A. Astolfi. 'Model reduction by moment matching for linear and nonlinear systems'. In: *IEEE Transactions on Automatic Control* 55.10 (2010), pp. 2321–2336 (cited on pages 7, 78–82, 84, 86, 87, 118, 119).
- [21] G. Scarciotti and A. Astolfi. 'Nonlinear Model Reduction by Moment Matching'. In: *Foundations and Trends in Systems and Control* 4.3-4 (2017), pp. 224–409 (cited on pages 7, 78–82, 84, 86, 119).
- [22] A. Isidori. *Nonlinear control systems*. Springer Science & Business Media, 2013 (cited on pages 8, 80, 83, 150, 265).
- [23] J. Cunningham, N. Faedo, and J. V. Ringwood. 'Excitation force estimation for wave energy systems using a moment-domain representation'. In: *European Wave and Tidal Energy Conference (EWTEC), Naples*. 2019, pp. 1449-1 –1449-10 (cited on page 13).
- [24] J. Brewer. 'Kronecker products and matrix calculus in system theory'. In: *IEEE Transactions on circuits and systems* 25.9 (1978), pp. 772–781 (cited on pages 18, 119, 123).
- [25] W. Cummins. *The impulse response function and ship motions*. Tech. rep. DTIC Document, 1962 (cited on pages 20, 27, 34).
- [26] F. M. White. *Fluid Mechanics*. McGraw-Hill series in mechanical engineering. McGraw Hill, 2011 (cited on pages 21, 27).
- [27] M. K. Ochi. *Ocean waves: the stochastic approach*. Vol. 6. Cambridge University Press, 2005 (cited on pages 21, 23).
- [28] L. Birk. *Fundamentals of Ship Hydrodynamics: Fluid Mechanics, Ship Resistance and Propulsion*. John Wiley & Sons, 2019 (cited on pages 21, 27, 28).
- [29] K. J. Rawson and E. C. Tupper. *Basic ship theory*. Vol. 1. Butterworth-Heinemann, 2001 (cited on page 21).
- [30] R. T. Hudspeth. *Waves and wave forces on coastal and ocean structures*. World Scientific, 2006 (cited on pages 21, 22).
- [31] D. C. Wright. 'The Published Works of Sir George Biddell Airy'. In: *Journal of the British Astronomical Association* 98 (1988), pp. 355–361 (cited on page 21).
- [32] A. Constantin. 'Nonlinear water waves: introduction and overview'. In: *Philosophical transactions. Series A, Mathematical, physical, and engineering sciences* 376.2111 (2017), pp. 1–6 (cited on page 22).

- [33] K. Hasselmann. 'Measurements of wind wave growth and swell decay during the Joint North Sea Wave Project (JONSWAP)'. In: *Dtsch. Hydrogr. Z.* 8 (1973), p. 95 (cited on pages 23, 24).
- [34] C. L. Bretschneider. *Wave variability and wave spectra for wind-generated gravity waves*. Tech. rep. 118. Beach Erosion Board, US Army, Corps of Engineers, 1959 (cited on page 23).
- [35] W. J. Pierson Jr and L. Moskowitz. 'A proposed spectral form for fully developed wind seas based on the similarity theory of SA Kitaigorodskii'. In: *Journal of geophysical research* 69.24 (1964), pp. 5181–5190 (cited on page 23).
- [36] A. Mérigaud and J. V. Ringwood. 'Free-surface time-series generation for wave energy applications'. In: *IEEE Journal of Oceanic Engineering* 43.1 (2018), pp. 19–35 (cited on pages 24, 102).
- [37] C. L. Fefferman. 'Existence and smoothness of the Navier-Stokes equation'. In: *The millennium prize problems -Clay Mathematics Institute* 57 (2006), p. 67 (cited on pages 25, 26).
- [38] Clay Mathematics Institute. *Millennium problems: Navier-Stokes equation*. Feb. 2020 (cited on page 26).
- [39] C. Windt, J. Davidson, and J. Ringwood. 'High-fidelity numerical modelling of ocean wave energy systems: A review of CFD-based numerical wave tanks'. In: *Renewable and Sustainable Energy Reviews* 93 (2018), pp. 610–630 (cited on page 26).
- [40] J. H. Ferziger, M. Perić, and R. L. Street. *Computational methods for fluid dynamics*. Vol. 3. Springer, 2002 (cited on page 26).
- [41] S. Giorgi. 'Linear and nonlinear parametric hydrodynamic models for wave energy converters identified from recorded data'. PhD thesis. Department of Electronic Engineering, Maynooth University, 2017 (cited on pages 27, 31).
- [42] G. Giorgi. 'Nonlinear hydrodynamic modelling of wave energy converters under controlled conditions'. PhD thesis. Department of Electronic Engineering, Maynooth University, 2018 (cited on pages 27, 31, 32, 38, 40).
- [43] A. Edo. 'Optimal control and robust estimation for ocean wave energy converters'. PhD thesis. Department of Aeronautics, Imperial College London, 2013 (cited on page 27).
- [44] L. Ljung. *System Identification: Theory for the User*. Prentice Hall, 1999 (cited on pages 27, 36, 199).
- [45] M. Bonnet. *Boundary integral equation methods for solids and fluids*. John Wiley, 1995 (cited on page 29).
- [46] M. Penalba, T. Kelly, and J. V. Ringwood. 'Using NEMOH for Modelling Wave Energy Converters: A Comparative Study with WAMIT'. In: *12th European Wave and Tidal Energy Conference (EWTEC), Cork*. 2017 (cited on page 29).
- [47] ANSYS. *AQWA: Reference manual*. Feb. 2020 (cited on page 29).
- [48] A. Babarit and G. Delhommeau. 'Theoretical and numerical aspects of the open source BEM solver NEMOH'. In: *11th European Wave and Tidal Energy Conference, Nantes*. 2015 (cited on page 29).
- [49] M. Folley and D. Forehand. 'Chapter 8 - Conventional Multiple Degree-of-Freedom Array Models'. In: *Numerical Modelling of Wave Energy Converters*. Ed. by M. Folley. Academic Press, 2016, pp. 151–164 (cited on pages 30, 115, 129, 209, 218).

- [50] Z. Yu and J. Falnes. 'State-space modelling of a vertical cylinder in heave'. In: *Applied Ocean Research* 17.5 (1995), pp. 265–275 (cited on pages 32, 41).
- [51] T. F. Ogilvie. 'Recent progress toward the understanding and prediction of ship motions'. In: *5th Symposium on naval hydrodynamics*. Vol. 1. 2. Bergen, Norway. 1964, pp. 2–5 (cited on page 33).
- [52] A.-M. Wazwaz. 'Volterra Integro-Differential Equations'. In: *Linear and Nonlinear Integral Equations*. Springer, 2011, pp. 175–212 (cited on page 34).
- [53] J. Falnes. *Ocean waves and oscillating systems: linear interactions including wave-energy extraction*. Cambridge university press, 2002 (cited on pages 35, 47, 150, 265).
- [54] K. Pavel and S. David. 'Algorithms for Efficient Computation of Convolution'. In: *Design and Architectures for Digital Signal Processing*. IntechOpen, 2013. Chap. 8 (cited on page 36).
- [55] M. Penalba Retes, G. Giorgi, and J. V. Ringwood. 'A review of non-linear approaches for wave energy converter modelling'. In: *Proceedings of the 11th European Wave and Tidal Energy Conference*. European Wave and Tidal Energy Conference 2015. 2015 (cited on page 38).
- [56] G. Li. 'Nonlinear model predictive control of a wave energy converter based on differential flatness parameterisation'. In: *International Journal of Control* (2015), pp. 1–10 (cited on pages 39, 65, 66, 70, 77).
- [57] C. Auger, A. Merigaud, and J. V. Ringwood. 'Receding-horizon pseudo-spectral control of wave energy converters using periodic basis functions'. In: *IEEE Transactions on Sustainable Energy* (2018) (cited on pages 39, 40, 66, 70, 73, 77, 197).
- [58] J. Morison, J. Johnson, S. Schaaf, et al. 'The force exerted by surface waves on piles'. In: *Journal of Petroleum Technology* 2.05 (1950), pp. 149–154 (cited on page 39).
- [59] G. Bacelli, R. Genest, and J. V. Ringwood. 'Nonlinear control of flap-type wave energy converter with a non-ideal power take-off system'. In: *Annual Reviews in Control* 40 (2015), pp. 116–126 (cited on pages 40, 66, 77).
- [60] G. Scarciotti. 'Approximation, analysis and control of large-scale systems'. PhD thesis. Control and Power Research Group, Imperial College London, 2016 (cited on page 40).
- [61] R. Taghipour, T. Perez, and T. Moan. 'Hybrid frequency–time domain models for dynamic response analysis of marine structures'. In: *Ocean Engineering* 35.7 (2008), pp. 685–705 (cited on page 41).
- [62] K. Unneland. 'Identification and order reduction of radiation force models of marine structures'. PhD thesis. NTNU, 2007 (cited on page 41).
- [63] A. Roessling and J. V. Ringwood. 'Finite order approximations to radiation forces for wave energy applications'. In: *Renewable Energies Offshore* (2015), p. 359 (cited on page 41).
- [64] H. Hatecke. 'The impulse response fitting and ship motions'. In: *Ship Technology Research* 62.2 (2015), pp. 97–106 (cited on pages 41–43).
- [65] E. Kristiansen, Å. Hjulstad, and O. Egeland. 'State-space representation of radiation forces in time-domain vessel models'. In: *Ocean Engineering* 32.17 (2005), pp. 2195–2216 (cited on pages 41, 42).
- [66] S. Kung. 'A new identification and model reduction algorithm via singular value decomposition'. In: *12th Asilomar Conf. on Circuits, Systems and Computers, Pacific Grove*. 1978 (cited on page 42).

- [67] B. Ho and R. E. Kálmán. 'Effective construction of linear state-variable models from input/output functions'. In: *Automatisierungstechnik* 14.1-12 (1966), pp. 545–548 (cited on page 42).
- [68] U. M. Al-Saggaf and G. F. Franklin. 'Model reduction via balanced realizations: an extension and frequency weighting techniques'. In: *IEEE Transactions on Automatic Control* 33.7 (1988), pp. 687–692 (cited on page 42).
- [69] S. Sutulo and C. G. Soares. 'An implementation of the method of auxiliary state variables for solving seakeeping problems'. In: *International shipbuilding progress* 52.4 (2005), pp. 357–384 (cited on pages 42, 43).
- [70] J. Xia, Z. Wang, and J. J. Jensen. 'Non-linear wave loads and ship responses by a time-domain strip theory'. In: *Marine structures* 11.3 (1998), pp. 101–123 (cited on pages 42, 43).
- [71] T. Pérez and T. I. Fossen. 'Time-vs. frequency-domain identification of parametric radiation force models for marine structures at zero speed'. In: *Modeling, Identification and Control* 29.1 (2008), pp. 1–19 (cited on pages 42–44, 137).
- [72] M. A. Jordán and R. Beltrán-Aguedo. 'Optimal identification of potential-radiation hydrodynamics for moored floating structures—a new general approach in state space'. In: *Ocean engineering* 31.14 (2004), pp. 1859–1914 (cited on pages 42, 43).
- [73] Ø. Y. Rogne, T. Moan, and S. Ersdal. 'Identification of passive state-space models of strongly frequency dependent wave radiation forces'. In: *Ocean Engineering* 92 (2014), pp. 114–128 (cited on pages 42, 43).
- [74] T. Perez and O. Lande. 'Time-domain models of marine surface vessels for simulation and control design based on seakeeping computations'. In: *IFAC Conference on Manoeuvring and Control of Marine Craft MCMC, Lisbon*. IFAC. 2006 (cited on page 43).
- [75] C.-T. Chen. *Linear system theory and design*. Oxford University Press, Inc., 1998 (cited on pages 43, 125, 142, 183).
- [76] R. Suchithra, K. Ezhilsabareesh, and A. Samad. 'Development of a reduced order wave to wire model of an OWC wave energy converter for control system analysis'. In: *Ocean Engineering* 172 (2019), pp. 614–628 (cited on page 44).
- [77] M. Penalba. 'Design, validation and application of wave-to-wire models for heaving point absorber wave energy converters'. PhD thesis. Department of Electronic Engineering, Maynooth University, 2018 (cited on page 44).
- [78] M. Penalba and J. V. Ringwood. 'Linearisation-based nonlinearity measures for wave-to-wire models in wave energy'. In: *Ocean Engineering* 171 (2019), pp. 496–504 (cited on page 44).
- [79] K. Budal and J. Falnes. 'A resonant point absorber of ocean-wave power'. In: *Nature* 256.5517 (1975), pp. 478–479 (cited on pages 47, 56).
- [80] K. Budal and J. Falnes. 'Optimum operation of improved wave-power converter'. In: *Mar. Sci. Commun.:(United States)* 3.2 (1977) (cited on page 47).
- [81] K. Budal and J. Falnes. 'Interacting point absorbers with controlled motion'. In: *Power from sea waves* (1980), pp. 381–399 (cited on page 47).
- [82] D. Evans. 'A theory for wave-power absorption by oscillating bodies'. In: *Journal of Fluid Mechanics* 77.1 (1976), pp. 1–25 (cited on page 47).

- [83] D. Evans. 'Some theoretical aspects of three-dimensional wave-energy absorbers'. In: *Proceedings of the first symposium on wave energy utilization, Chalmers University of Technology, Gothenburg, Sweden*. 1979, pp. 77–106 (cited on page 47).
- [84] S. H. Salter. 'Apparatus for use in the extraction of energy from waves on water'. US-patent 4134023. June 9, 1979 (cited on page 47).
- [85] D. Liberzon. *Calculus of variations and optimal control theory: a concise introduction*. Princeton University Press, 2011 (cited on pages 47, 57).
- [86] T. L. Floyd and E. Pownell. *Principles of electric circuits*. Prentice Hall, 2000 (cited on pages 48, 142).
- [87] E. T. Bell. *Men of mathematics*. Simon and Schuster, 2014 (cited on page 48).
- [88] J. V. Ringwood et al. 'An Analytical and Numerical Sensitivity and Robustness Analysis of Wave Energy Control Systems'. In: *IEEE Transactions on Control Systems Technology* (2019) (cited on pages 50, 226).
- [89] G. Bacelli and J. V. Ringwood. 'A geometrical interpretation of force and position constraints in the optimal control of wave energy devices'. In: *Proceedings of the 9th European Wave and Tidal Energy Conference (EWTEC)*. School of Civil Engineering and the Environment, University of Southampton. 2011 (cited on page 52).
- [90] Y. Peña-Sanchez et al. 'Estimation and Forecasting of Excitation Force for Arrays of Wave Energy Devices'. In: *IEEE Transactions on Sustainable Energy* 9.4 (2018), pp. 1672–1680 (cited on pages 53, 102, 117, 128, 129, 134–136, 180, 197, 201).
- [91] A. Chakrabarty et al. 'Unknown input estimation for nonlinear systems using sliding mode observers and smooth window functions'. In: *SIAM Journal on Control and Optimization* 56.5 (2018), pp. 3619–3641 (cited on page 53).
- [92] S. Salter. 'Power conversion systems for ducks'. In: *International Conference on Future Energy Concepts*. 1979, pp. 100–108 (cited on page 54).
- [93] P. Nebel. 'Maximizing the efficiency of wave-energy plant using complex-conjugate control'. In: *Proceedings of the Institution of Mechanical Engineers, Part I: Journal of Systems and Control Engineering* 206.4 (1992), pp. 225–236 (cited on page 54).
- [94] D. Evans. 'Maximum wave-power absorption under motion constraints'. In: *Applied Ocean Research* 3.4 (1981), pp. 200–203 (cited on page 54).
- [95] A. Clement and C. Maisondieu. 'Comparison of Time domain Control Law for a Piston wave Absorber'. In: *1993 European Wave Energy Symposium. 21-24 July 1993, Scotland, UK*. 1993 (cited on page 54).
- [96] H. Eidsmoen. 'Optimum control of a floating wave-energy converter with restricted amplitude'. In: *Journal of Offshore Mechanics and Arctic Engineering. Transactions of the ASME* 118.2 (1996), pp. 96–101 (cited on page 54).
- [97] H. Eidsmoen. 'Simulation of a Tight-Moored amplitude limited Heaving-Buoy Wave-Energy converter with phase control'. In: *Division of Physics, Norwegian University of Science and Technology* (1996) (cited on page 54).
- [98] H. Eidsmoen. 'Simulation of a slack-moored heaving-buoy wave-energy converter with phase control'. In: *Division of Physics, Norwegian University of Science and Technology NTNU, Trondheim, Norway, Technical report* (1996) (cited on page 54).

- [99] H. Eidsmoen. 'Tight-moored amplitude-limited heaving-buoy wave-energy converter with phase control'. In: *Applied Ocean Research* 20.3 (1998), pp. 157–161 (cited on page 54).
- [100] J. K. Shek et al. 'Reaction force control of a linear electrical generator for direct drive wave energy conversion'. In: *IET renewable power generation* 1.1 (2007), pp. 17–24 (cited on page 54).
- [101] U. A. Korde. 'Systems of reactively loaded coupled oscillating bodies in wave energy conversion'. In: *Applied ocean research* 25.2 (2003), pp. 79–91 (cited on page 54).
- [102] C. Liang and L. Zuo. 'On the dynamics and design of a two-body wave energy converter'. In: *Renewable Energy* 101 (2017), pp. 265–274 (cited on page 54).
- [103] F. Fusco and J. V. Ringwood. 'A simple and effective real-time controller for wave energy converters'. In: *IEEE Transactions on sustainable energy* 4.1 (2012), pp. 21–30 (cited on pages 54–56).
- [104] V. Kucera. *Discrete linear control: the polynomial equation approach*. John Wiley & Sons, Inc., 1980 (cited on page 54).
- [105] P. B. Garcia-Rosa et al. 'Real-time passive control of wave energy converters using the Hilbert-Huang transform'. In: *IFAC-PapersOnLine* 50.1 (2017), pp. 14705–14710 (cited on page 55).
- [106] N. E. Huang et al. 'The empirical mode decomposition and the Hilbert spectrum for nonlinear and non-stationary time series analysis'. In: *Proceedings of the Royal Society of London. Series A: mathematical, physical and engineering sciences* 454.1971 (1998), pp. 903–995 (cited on page 55).
- [107] D. García-Violini et al. 'An energy-maximising linear time invariant controller (LiTe-Con) for wave energy devices'. In: *IEEE Transactions on Sustainable Energy (early access available)* (2020) (cited on pages 55, 56).
- [108] G. Bacelli and J. V. Ringwood. 'Numerical optimal control of wave energy converters'. In: *IEEE Transactions on Sustainable Energy* 6.2 (2015), pp. 294–302 (cited on pages 56, 65, 73, 77).
- [109] D. A. Guenther, D. Jones, and D. G. Brown. 'An investigative study of a wave-energy device'. In: *Energy* 4.2 (1979), pp. 299–306 (cited on page 56).
- [110] M. French. 'A generalized view of resonant energy transfer'. In: *Journal of Mechanical Engineering Science* 21.4 (1979), pp. 299–300 (cited on page 56).
- [111] J. V. Ringwood and S. Butler. 'Optimisation of a wave energy converter'. In: *IFAC Proceedings Volumes* 37.10 (2004), pp. 155–160 (cited on page 56).
- [112] E. B. Lee and L. Markus. *Foundations of optimal control theory*. Tech. rep. DTIC Document, 1967 (cited on page 57).
- [113] S. Naito and S. Nakamura. 'Wave energy absorption in irregular waves by feedforward control system'. In: *Hydrodynamics of ocean wave-energy utilization*. Springer, 1986, pp. 269–280 (cited on page 57).
- [114] A. Babarit, G. Duclos, and A. H. Clément. 'Comparison of latching control strategies for a heaving wave energy device in random sea'. In: *Applied Ocean Research* 26.5 (2004), pp. 227–238 (cited on page 57).

- [115] A. Babarit and A. H. Clément. 'Optimal latching control of a wave energy device in regular and irregular waves'. In: *Applied Ocean Research* 28.2 (2006), pp. 77–91 (cited on page 57).
- [116] A. Babarit, M. Guglielmi, and A. H. Clément. 'Declutching control of a wave energy converter'. In: *Ocean Engineering* 36.12 (2009), pp. 1015–1024 (cited on page 57).
- [117] A. Babarit et al. 'Simulation of the SEAREV wave energy converter with a by-pass control of its hydraulic power take off'. In: *Proc. World Renewable Energy Congress, Glasgow, UK*. 2008, pp. 1004–1009 (cited on page 57).
- [118] Z. Feng and E. C. Kerrigan. 'Latching control of wave energy converters using derivative-free optimization'. In: *52nd Conference on Decision and Control, Florence*. IEEE. 2013, pp. 7474–7479 (cited on page 57).
- [119] Z. Feng and E. C. Kerrigan. 'Declutching control of wave energy converters using derivative-free optimization'. In: *IFAC Proceedings Volumes* 47.3 (2014), pp. 7647–7652 (cited on page 57).
- [120] Z. Feng and E. C. Kerrigan. 'Latching-declutching control of wave energy converters using derivative-free optimization'. In: *IEEE Transactions on Sustainable Energy* 6.3 (2015), pp. 773–780 (cited on page 57).
- [121] B. Teillant, J.-C. Gilloteaux, and J. V. Ringwood. 'Optimal damping profile for a heaving buoy wave energy converter'. In: *IFAC Proceedings Volumes* 43.20 (2010), pp. 360–365 (cited on page 57).
- [122] J. Scruggs. 'Multi-objective optimal causal control of an ocean wave energy converter in random waves'. In: *OCEANS 2011*. IEEE. 2011, pp. 1–6 (cited on page 57).
- [123] J. Scruggs et al. 'Optimal causal control of a wave energy converter in a random sea'. In: *Applied Ocean Research* 42 (2013), pp. 1–15 (cited on pages 57, 150, 265).
- [124] R. Nie et al. 'Optimal causal control of wave energy converters in stochastic waves—Accommodating nonlinear dynamic and loss models'. In: *International Journal of Marine Energy* 15 (2016), pp. 41–55 (cited on pages 57, 59).
- [125] S. R. Nielsen et al. 'Optimal control of nonlinear wave energy point converters'. In: *Ocean engineering* 72 (2013), pp. 176–187 (cited on pages 57, 163).
- [126] F. Ferri et al. 'Balancing power output and structural fatigue of wave energy converters by means of control strategies'. In: *Energies* 7.4 (2014), pp. 2246–2273 (cited on page 58).
- [127] A. Garcia-Teruel and D. Forehand. 'Optimal wave energy converter geometry for different modes of motion'. In: *Advances in Renewable Energies Offshore* (2018), pp. 299–307 (cited on page 58).
- [128] N. Sergiienko et al. 'Considerations on the control design for a three-tether wave energy converter'. In: *Ocean Engineering* 183 (2019), pp. 469–477 (cited on page 58).
- [129] A. J. Hillis et al. 'Power capture gains for the WaveSub submerged WEC using active control'. In: *13th European Wave and Tidal Energy Conference, Naples*. 2019 (cited on page 58).
- [130] A. J. Hillis et al. 'Simulation of a power electronic conversion system with short-term energy storage for actively controlled wave energy converters'. In: *2019 Offshore Energy and Storage Summit (OSES)*. IEEE. 2019, pp. 1–7 (cited on page 58).
- [131] M. Zanon et al. 'Direct optimal control and model predictive control'. In: *Optimal Control: Novel Directions and Applications*. Springer, 2017, pp. 263–382 (cited on pages 59, 65, 72).

- [132] A. K. Aziz. *Numerical solutions of boundary value problems for ordinary differential equations*. Academic Press, 2014 (cited on page 60).
- [133] I. V. Girsanov. *Lectures on mathematical theory of extremum problems*. Vol. 67. Springer Science & Business Media, 2012 (cited on page 60).
- [134] R. F. Hartl, S. P. Sethi, and R. G. Vickson. 'A survey of the maximum principles for optimal control problems with state constraints'. In: *SIAM review* 37.2 (1995), pp. 181–218 (cited on page 60).
- [135] H. J. Pesch and R. Bulirsch. 'The maximum principle, Bellman's equation, and Carathéodory's work'. In: *Journal of optimization theory and applications* 80.2 (1994), pp. 199–225 (cited on page 60).
- [136] P. Deufhard, H.-J. Pesch, and P. Rentrop. 'A modified continuation method for the numerical solution of nonlinear two-point boundary value problems by shooting techniques'. In: *Numerische Mathematik* 26.3 (1976), pp. 327–343 (cited on page 60).
- [137] S. Subchan and R. Zbikowski. *Computational optimal control: Tools and practice*. John Wiley & Sons, 2009 (cited on page 60).
- [138] G. Li et al. 'Wave energy converter control by wave prediction and dynamic programming'. In: *Renewable Energy* 48 (2012), pp. 392–403 (cited on pages 60, 64, 65, 77).
- [139] E. Abraham and E. C. Kerrigan. 'Optimal active control and optimization of a wave energy converter'. In: *IEEE Transactions on Sustainable Energy* 4.2 (2013), pp. 324–332 (cited on page 60).
- [140] T. Kovaltchouk et al. 'Model predictive control of a direct wave energy converter constrained by the electrical chain using an energetic approach'. In: *European Wave and Tidal Energy Conference 2015*. 2015 (cited on pages 60, 65).
- [141] J. T. Betts. *Practical methods for optimal control and estimation using nonlinear programming*. Vol. 19. Siam, 2010 (cited on page 60).
- [142] J. Richalet et al. 'Algorithmic control of industrial processes'. In: *Proceedings of the 4th IFAC symposium on identification and system parameter estimation*. 1976, pp. 1119–1167 (cited on page 60).
- [143] J. Richalet et al. 'Model predictive heuristic control: Applications to industrial processes'. In: *Automatica* 14.5 (1978), pp. 413–428 (cited on page 60).
- [144] C. R. Cutler and B. L. Ramaker. 'Dynamic matrix control: a computer control algorithm'. In: *Joint automatic control conference*. 17. 1980, p. 72 (cited on page 60).
- [145] D. Clarke, C. Mohtadi, and P. Tuffs. 'Generalized predictive control—Part I. The basic algorithm'. In: *Automatica* 23.2 (1987), pp. 137–148 (cited on page 61).
- [146] S. Li, K. Y. Lim, and D. G. Fisher. 'A state space formulation for model predictive control'. In: *AIChE Journal* 35.2 (1989), pp. 241–249 (cited on page 61).
- [147] C. E. Garcia, D. M. Prett, and M. Morari. 'Model predictive control: theory and practice—a survey'. In: *Automatica* 25.3 (1989), pp. 335–348 (cited on page 61).
- [148] E. F. Camacho and C. B. Alba. *Model predictive control*. Springer Science & Business Media, 2013 (cited on pages 61, 69, 71, 195).
- [149] J. M. Maciejowski. *Predictive control: with constraints*. Pearson education, 2002 (cited on page 61).

- [150] B. Finlayson and L. Scriven. 'The method of weighted residuals—a review'. In: *Appl. Mech. Rev* 19.9 (1966), pp. 735–748 (cited on pages 62, 155, 268).
- [151] I. M. Ross and M. Karpenko. 'A review of pseudospectral optimal control: From theory to flight'. In: *Annual Reviews in Control* 36.2 (2012), pp. 182–197 (cited on pages 62, 70).
- [152] F. Fahroo and I. M. Ross. 'Pseudospectral methods for infinite-horizon nonlinear optimal control problems'. In: *Journal of Guidance, Control, and Dynamics* 31.4 (2008), pp. 927–936 (cited on pages 62, 63).
- [153] W. Kang, I. M. Ross, and Q. Gong. 'Pseudospectral optimal control and its convergence theorems'. In: *Analysis and design of nonlinear control systems*. Springer, 2008, pp. 109–124 (cited on page 62).
- [154] J. P. Boyd. *Chebyshev and Fourier spectral methods*. Courier Corporation, 2001 (cited on pages 62, 155, 156, 268, 269).
- [155] B. Shizgal. 'Introduction to Spectral/Pseudospectral Methods'. In: *Spectral Methods in Chemistry and Physics*. Springer, 2015, pp. 1–27 (cited on page 62).
- [156] G. Grubb. *Distributions and operators*. Vol. 252. Springer Science & Business Media, 2008 (cited on page 63).
- [157] M. Richter et al. 'Nonlinear model predictive control of a point absorber wave energy converter'. In: *IEEE Transactions on Sustainable Energy* 4.1 (2013), pp. 118–126 (cited on pages 64–66, 69, 73, 77).
- [158] J. Wolfram. 'On alternative approaches to linearization and Morison's equation for wave forces'. In: *Proceedings of the Royal Society of London A: Mathematical, Physical and Engineering Sciences*. Vol. 455. 1988. The Royal Society. 1999, pp. 2957–2974 (cited on page 65).
- [159] N. Thin, N. Anh, and D. Cuong. 'An equivalent linearization for the drag force in the Morison's equation using Hermite polynomial error sample function'. In: *Vietnam Journal of Mechanics* 20.2 (1998), pp. 55–64 (cited on page 65).
- [160] M. Richter et al. 'Power optimisation of a point absorber wave energy converter by means of linear model predictive control'. In: *IET Renewable Power Generation* 8.2 (2014), pp. 203–215 (cited on pages 65, 66, 71, 77).
- [161] N. Tom and R. W. Yeung. 'Nonlinear model predictive control applied to a generic ocean-wave energy extractor'. In: *Journal of Offshore Mechanics and Arctic Engineering* 136.4 (2014), p. 041901 (cited on pages 65, 69, 77).
- [162] A. Van Der Schaft. 'Port-Hamiltonian systems: an introductory survey'. In: *Proceedings of the international congress of mathematicians*. Vol. 3. Citeseer. 2006, pp. 1339–1365 (cited on page 65).
- [163] G. Li and M. R. Belmont. 'Model predictive control of sea wave energy converters—Part I: A convex approach for the case of a single device'. In: *Renewable Energy* 69 (2014), pp. 453–463 (cited on pages 65, 71, 77).
- [164] D. R. Herber and J. T. Allison. 'Wave energy extraction maximization in irregular ocean waves using pseudospectral methods'. In: *ASME 2013 International Design Engineering Technical Conferences and Computers and Information in Engineering Conference*. American Society of Mechanical Engineers. 2013, V03AT03A018–V03AT03A018 (cited on pages 65, 70, 72, 77).

- [165] G. Li and M. R. Belmont. 'Model predictive control of sea wave energy converters—Part II: The case of an array of devices'. In: *Renewable Energy* 68 (2014), pp. 540–549 (cited on pages 65–67, 71, 77).
- [166] K. U. Amann, M. E. Magaña, and O. Sawodny. 'Model predictive control of a nonlinear 2-body point absorber wave energy converter with estimated state feedback'. In: *IEEE Transactions on Sustainable Energy* 6.2 (2015), pp. 336–345 (cited on pages 65, 66, 69, 71, 73, 77).
- [167] O. Abdelkhalik et al. 'On the control design of wave energy converters with wave prediction'. In: *Journal of Ocean Engineering and Marine Energy* 2.4 (2016), pp. 473–483 (cited on pages 66, 77).
- [168] A. Mérigaud and J. V. Ringwood. 'Towards realistic non-linear receding-horizon spectral control of wave energy converters'. In: *Control Engineering Practice* 81 (2018), pp. 145–161 (cited on pages 66, 73, 77).
- [169] A. C. M. O'Sullivan, W. Sheng, and G. Lightbody. 'An analysis of the potential benefits of centralised predictive control for optimal electrical power generation from wave energy arrays'. In: *IEEE Transactions on Sustainable Energy* 9.4 (2018), pp. 1761–1771 (cited on pages 66, 69, 71, 77).
- [170] A. Karthikeyan et al. 'Non-linear Model Predictive Control of Wave Energy Converters with Realistic Power Take-off Configurations and Loss Model'. In: *2019 IEEE Conference on Control Technology and Applications (CCTA)*. IEEE. 2019, pp. 270–277 (cited on pages 66, 71, 77).
- [171] Y.-H. Yu and Y. Li. *Preliminary results of a RANS simulation for a floating point absorber wave energy system under extreme wave conditions*. National Renewable Energy Laboratory, 2011 (cited on page 66).
- [172] G. Bacelli and J. V. Ringwood. 'Nonlinear optimal wave energy converter control with application to a flap-type device'. In: *IFAC Proceedings Volumes* 47.3 (2014), pp. 7696–7701 (cited on pages 66, 77).
- [173] D. Oetinger, M. E. Magaña, and O. Sawodny. 'Decentralized model predictive control for wave energy converter arrays'. In: *IEEE Transactions on Sustainable Energy* 5.4 (2014), pp. 1099–1107 (cited on pages 66, 67, 71, 77).
- [174] Q. Zhong and R. W. Yeung. 'Model-Predictive Control Strategy for an Array of Wave-Energy Converters'. In: *Journal of Marine Science and Application* 18.1 (2019), pp. 26–37 (cited on pages 66, 77).
- [175] J. Westphalen et al. 'Control strategies for arrays of wave energy devices'. In: *Proceedings of the 9th European Wave and Tidal Energy Conference (EWTEC)*. School of Civil Engineering and the Environment, University of Southampton. 2011 (cited on pages 66, 73, 77).
- [176] G. Bacelli, P. Balitsky, and J. V. Ringwood. 'Coordinated control of arrays of wave energy devices—Benefits over independent control'. In: *IEEE Transactions on Sustainable Energy* 4.4 (2013), pp. 1091–1099 (cited on pages 66, 67, 73, 77, 221).
- [177] P. B. Garcia-Rosa, G. Bacelli, and J. V. Ringwood. 'Control-informed optimal array layout for wave farms'. In: *IEEE Transactions on Sustainable Energy* 6.2 (2015), pp. 575–582 (cited on pages 66, 73, 77).
- [178] M. Penalba, G. Giorgi, and J. V. Ringwood. 'Mathematical modelling of wave energy converters: a review of nonlinear approaches'. In: *Renewable and Sustainable Energy Reviews* 78 (2017), pp. 1188–1207 (cited on page 67).

- [179] G. Giorgi and J. V. Ringwood. 'A Compact 6-DoF Nonlinear Wave Energy Device Model for Power Assessment and Control Investigations'. In: *IEEE Transactions on Sustainable Energy* 10.1 (2018), pp. 119–126 (cited on pages 67, 277).
- [180] M. Jama, A. Wahyudie, and H. Noura. 'Robust predictive control for heaving wave energy converters'. In: *Control Engineering Practice* 77 (2018), pp. 138–149 (cited on pages 68, 77).
- [181] J. Na et al. 'Robust optimal control of wave energy converters based on adaptive dynamic programming'. In: *IEEE Transactions on Sustainable Energy* (2018) (cited on page 68).
- [182] D. García-Violini and J. V. Ringwood. 'Energy maximising robust control for spectral and pseudospectral methods with application to wave energy systems'. In: *International Journal of Control* (2019), pp. 1–12 (cited on pages 68, 77, 226, 232).
- [183] D. García-Violini and J. V. Ringwood. 'Robust Control of Wave Energy Converters Using Spectral and Pseudospectral Methods: A Case Study'. In: *2019 American Control Conference (ACC)*. IEEE. 2019, pp. 4779–4784 (cited on pages 68, 77).
- [184] A. Ben-Tal and A. Nemirovski. 'Robust convex optimization'. In: *Mathematics of operations research* 23.4 (1998), pp. 769–805 (cited on pages 68, 226, 232).
- [185] G. F. Franklin, J. D. Powell, and M. L. Workman. *Digital control of dynamic systems*. Vol. 3. Addison-wesley Menlo Park, 1998 (cited on page 69).
- [186] J. A. Cretel et al. 'Maximisation of energy capture by a wave-energy point absorber using model predictive control'. In: *IFAC Proceedings Volumes* 44.1 (2011), pp. 3714–3721 (cited on pages 69, 71, 77).
- [187] A. C. O'Sullivan and G. Lightbody. 'Co-design of a wave energy converter using constrained predictive control'. In: *Renewable Energy* 102 (2017), pp. 142–156 (cited on pages 69, 71, 77).
- [188] A. de la Villa Jaén and A. G. Santana. 'Considering linear generator copper losses on model predictive control for a point absorber wave energy converter'. In: *Energy Conversion and Management* 78 (2014), pp. 173–183 (cited on pages 69, 71, 77).
- [189] P. Tona et al. 'An efficiency-aware model predictive control strategy for a heaving buoy wave energy converter'. In: *11th European Wave and Tidal Energy Conference (EWTEC), Nantes*. 2015 (cited on pages 69, 72, 73, 77).
- [190] H.-N. Nguyen et al. 'Experimental Validation of a Nonlinear MPC Strategy for a Wave Energy Converter Prototype'. In: *ASME 2016 35th International Conference on Ocean, Offshore and Arctic Engineering*. American Society of Mechanical Engineers. 2016, V006T09A019–V006T09A019 (cited on pages 69, 72, 77).
- [191] A. F. Beardon. *The geometry of discrete groups*. Vol. 91. Springer Science & Business Media, 2012 (cited on page 69).
- [192] K. M. Prabhu. *Window functions and their applications in signal processing*. CRC press, 2013 (cited on pages 70, 197).
- [193] J. Allen. 'Short term spectral analysis, synthesis, and modification by discrete Fourier transform'. In: *IEEE Transactions on Acoustics, Speech, and Signal Processing* 25.3 (1977), pp. 235–238 (cited on page 70).
- [194] G. Szeg. *Orthogonal polynomials*. Vol. 23. American Mathematical Soc., 1939 (cited on page 70).

- [195] R. Genest and J. V. Ringwood. 'Receding horizon pseudospectral control for energy maximization with application to wave energy devices'. In: *IEEE Transactions on Control Systems Technology* 25.1 (2017), pp. 29–38 (cited on pages 70, 77).
- [196] R. Genest and J. V. Ringwood. 'Receding horizon pseudospectral optimal control for wave energy conversion'. In: *Control (CONTROL), 2016 UKACC 11th International Conference on*. IEEE. 2016, pp. 1–6 (cited on pages 70, 77).
- [197] R. Genest and J. V. Ringwood. 'A critical comparison of model-predictive and pseudospectral control for wave energy devices'. In: *Journal of Ocean Engineering and Marine Energy* 2.4 (2016), pp. 485–499 (cited on pages 70, 77).
- [198] F. Paparella and J. V. Ringwood. 'Receding Horizon Pseudo-Spectral Control for energy maximization of a 1/25th Scale Hinge-Barge Wave Energy Converter'. In: *Submitted to proceedings of the 12th European wave and tidal energy conference, Cork*. European Wave and Tidal Energy Conference 2017. 2017 (cited on pages 70, 72, 73, 77).
- [199] D. Huybrechs. 'On the Fourier extension of nonperiodic functions'. In: *SIAM Journal on Numerical Analysis* 47.6 (2010), pp. 4326–4355 (cited on page 70).
- [200] B. Orel and A. Perne. 'Computations with half-range Chebyshev polynomials'. In: *Journal of Computational and Applied Mathematics* 236.7 (2012), pp. 1753–1765 (cited on page 70).
- [201] S. Olaya, J.-M. Bourgeot, and M. Benbouzid. 'Optimal control for a self-reacting point absorber: A one-body equivalent model approach'. In: *Power Electronics and Application Conference and Exposition (PEAC), 2014 International*. IEEE. 2014, pp. 332–337 (cited on pages 71, 77).
- [202] P. Andersen et al. 'Model predictive control of a wave energy converter'. In: *Control Applications (CCA), 2015 IEEE Conference on*. IEEE. 2015, pp. 1540–1545 (cited on pages 71, 77).
- [203] S. Zhan et al. 'Adaptive model predictive control of wave energy converters'. In: *IEEE Transactions on Sustainable Energy* 11.1 (2018), pp. 229–238 (cited on pages 71, 77).
- [204] A. Kody, N. Tom, and J. Scruggs. 'Model Predictive Control of a Wave Energy Converter Using Duality Techniques'. In: *2019 American Control Conference (ACC)*. IEEE. 2019, pp. 5444–5451 (cited on pages 71, 77).
- [205] G. Bracco, M. Canale, and V. Cerone. 'Optimizing energy production of an Inertial Sea Wave Energy Converter via Model Predictive Control'. In: *Control Engineering Practice* 96 (2020), p. 104299 (cited on pages 71, 77).
- [206] J. Cretel et al. 'An application of model predictive control to a wave energy point absorber'. In: *IFAC Proceedings Volumes* 43.1 (2010), pp. 267–272 (cited on pages 71, 77).
- [207] S. Boyd and L. Vandenberghe. *Convex optimization*. Cambridge university press, 2004 (cited on pages 72, 127, 179, 187, 189, 216, 233, 234, 240).
- [208] A. Forsgren, P. E. Gill, and M. H. Wright. 'Interior methods for nonlinear optimization'. In: *SIAM review* 44.4 (2002), pp. 525–597 (cited on pages 73, 273).
- [209] R. A. Waltz et al. 'An interior algorithm for nonlinear optimization that combines line search and trust region steps'. In: *Mathematical programming* 107.3 (2006), pp. 391–408 (cited on pages 73, 99, 280).
- [210] J. Nocedal and S. J. Wright. *Sequential quadratic programming*. Springer, 2006 (cited on pages 73, 273).

- [211] S. Olaya, J.-M. Bourgeot, and M. Benbouzid. 'On the Generator Constraint Design of a Wave Energy Converter at a Pre-Sizing Stage'. In: *11th European Wave and Tidal Energy Conference (EWTEC), Nantes*. 2015, 10B3 (cited on page 77).
- [212] M. Jama et al. 'Function-Based Model Predictive Control Approach for Maximum Power Capture of Heaving Wave Energy Converters'. In: *ICREGA'14-Renewable Energy: Generation and Applications*. Springer, 2014, pp. 299–313 (cited on page 77).
- [213] J. Hals, J. Falnes, and T. Moan. 'Constrained optimal control of a heaving buoy wave-energy converter'. In: *Journal of Offshore Mechanics and Arctic Engineering* 133.1 (2011), p. 011401 (cited on page 77).
- [214] D. Cavaglieri, T. R. Bewley, and M. Previsic. 'Model Predictive Control leveraging Ensemble Kalman forecasting for optimal power take-off in wave energy conversion systems'. In: *American Control Conference (ACC), 2015*. IEEE. 2015, pp. 5224–5230 (cited on page 77).
- [215] M. N. Soltani, M. T. Sichani, and M. Mirzaei. 'Model predictive control of buoy type wave energy converter'. In: *IFAC Proceedings Volumes* 47.3 (2014), pp. 11159–11164 (cited on page 77).
- [216] A. H. Hansen, M. F. Asmussen, and M. M. Bech. 'Hardware-in-the-Loop Validation of Model Predictive Control of a Discrete Fluid Power Power Take-Off System for Wave Energy Converters'. In: *Energies* 12.19 (2019), p. 3668 (cited on page 77).
- [217] B. A. Ling, B. Bosma, and T. Brekken. 'Experimental Validation of Model Predictive Control Applied to the Azura Wave Energy Converter'. In: *IEEE Transactions on Sustainable Energy* (2019) (cited on page 77).
- [218] G. Bacelli, J. V. Ringwood, and J.-C. Gilloteaux. 'A control system for a self-reacting point absorber wave energy converter subject to constraints'. In: *IFAC Proceedings Volumes* 44.1 (2011), pp. 11387–11392 (cited on page 77).
- [219] G. Bacelli and J. V. Ringwood. 'Constrained control of arrays of wave energy devices.' In: *International Journal of Marine Energy* 3 (2013), pp. 53–69 (cited on pages 77, 221).
- [220] F. Paparella and J. V. Ringwood. 'Optimal Control of a Three-Body Hinge-Barge Wave Energy Device Using Pseudospectral Methods'. In: *IEEE Transactions on Sustainable Energy* 8.1 (2017), pp. 200–207 (cited on page 77).
- [221] G. Scarciotti. 'Low computational complexity model reduction of power systems with preservation of physical characteristics'. In: *IEEE Transactions on Power Systems* 32.1 (2017), pp. 743–752 (cited on pages 78, 116, 119).
- [222] A. C. Antoulas. *Approximation of large-scale dynamical systems*. SIAM, 2005 (cited on page 79).
- [223] A. Padoan, G. Scarciotti, and A. Astolfi. 'A Geometric Characterization of the Persistence of Excitation Condition for the Solutions of Autonomous Systems'. In: *IEEE Transactions on Automatic Control* 62.11 (2017), pp. 5666–5677 (cited on pages 80, 198, 269).
- [224] H. K. Khalil. *Nonlinear Systems*. Prentice-Hall, New Jersey, 1996 (cited on pages 85, 110, 216).
- [225] H. Rodriguez, R. Ortega, and A. Astolfi. 'Adaptive partial state feedback control of the DC-to-DC Cuk converter'. In: *Proceedings of the 2005, American Control Conference, 2005*. IEEE. 2005, pp. 5121–5126 (cited on page 87).

- [226] F. Zhang. *Matrix theory: basic results and techniques*. Springer Science & Business Media, 2011 (cited on pages 96, 188, 192, 264).
- [227] R. Horst and H. Tuy. *Global optimization: Deterministic approaches*. Springer Science & Business Media, 2013 (cited on page 99).
- [228] G. Scarciotti and A. Astolfi. 'Moment-Based Discontinuous Phasor Transform and its Application to the Steady-State Analysis of Inverters and Wireless Power Transfer Systems'. In: *IEEE Transactions on Power Electronics* 31.12 (2016), pp. 8448–8460 (cited on page 99).
- [229] M. Mekhiche and K. A. Edwards. 'Ocean Power Technologies Powebuoy: System-level design, development and validation methodology'. In: *Proceedings of the 2nd Marine Energy Technology Symposium (METS), Seattle*. 2014, pp. 1–9 (cited on page 101).
- [230] J. Weber et al. 'Wavebob—research & development network and tools in the context of systems engineering'. In: *Proc. Eighth European Wave and Tidal Energy Conference, Uppsala, Sweden*. 2009, pp. 416–420 (cited on page 101).
- [231] M. Penalba et al. 'A numerical study on the hydrodynamic impact of device slenderness and array size in wave energy farms in realistic wave climates'. In: *Ocean Engineering* 142 (2017), pp. 224–232 (cited on page 102).
- [232] G. Scarciotti and A. Astolfi. 'Data-driven model reduction by moment matching for linear and nonlinear systems'. In: *Automatica* 79 (2017), pp. 340–351 (cited on pages 107, 157, 199, 268).
- [233] C. A. Desoer and M. Vidyasagar. *Feedback systems: input-output properties*. Vol. 55. SIAM, 1975 (cited on page 110).
- [234] K. Zhou and J. C. Doyle. *Essentials of robust control*. Vol. 104. Prentice hall Upper Saddle River, NJ, 1998 (cited on pages 110, 130, 229, 232).
- [235] D. Simon. *Optimal state estimation: Kalman, H infinity, and nonlinear approaches*. John Wiley & Sons, 2006 (cited on pages 117, 134).
- [236] B. A. Francis and W. M. Wonham. 'The internal model principle of control theory'. In: *Automatica* 12.5 (1976), pp. 457–465 (cited on pages 117, 134, 135).
- [237] T. McKelvey, H. Akçay, and L. Ljung. 'Subspace-based multivariable system identification from frequency response data'. In: *IEEE Transactions on Automatic Control* 41.7 (1996), pp. 960–979 (cited on pages 124, 125).
- [238] CorPower Ocean. <http://www.corpowerocean.com/>. Accessed: 31-10-2019 (cited on page 128).
- [239] J. Hals et al. 'Tank testing of an inherently phase-controlled wave energy converter'. In: *International Journal of Marine Energy* 15 (2016), pp. 68–84 (cited on pages 128, 277, 278).
- [240] G. Giorgi and J. V. Ringwood. 'Analytical representation of nonlinear Froude-Krylov forces for 3-DoF point absorbing wave energy devices'. In: *Ocean Engineering* 164 (2018), pp. 749–759 (cited on page 128).
- [241] P. A. Ruymgaart and T. T. Soong. *Mathematics of Kalman-Bucy Filtering*. Vol. 14. Springer Science & Business Media, 2013 (cited on pages 134, 135).
- [242] T. Perez and T. I. Fossen. 'A matlab toolbox for parametric identification of radiation-force models of ships and offshore structures'. In: *Modeling, Identification and Control* 30.1 (2009), p. 1 (cited on page 137).

- [243] T. Ogunfunmi. *Adaptive nonlinear system identification: The Volterra and Wiener model approaches*. Springer Science & Business Media, 2007 (cited on page 152).
- [244] A. Isidori and A. Astolfi. 'Disturbance attenuation and H_∞ -control via measurement feedback in nonlinear systems'. In: *IEEE transactions on automatic control* 37.9 (1992), pp. 1283–1293 (cited on pages 152, 267).
- [245] M. Urabe. 'Galerkin's procedure for nonlinear periodic systems'. In: *Archive for Rational Mechanics and Analysis* 20.2 (1965), pp. 120–152 (cited on pages 156, 269).
- [246] T. F. Coleman and Y. Li. 'An interior trust region approach for nonlinear minimization subject to bounds'. In: *SIAM Journal on optimization* 6.2 (1996), pp. 418–445 (cited on page 156).
- [247] K. R. Rao, D. N. Kim, and J. J. Hwang. *Fast Fourier transform-algorithms and applications*. Springer Science & Business Media, 2011 (cited on page 157).
- [248] D. McKechnan, C. Robinson, and B. S. Sathyaprakash. 'A tapering window for time-domain templates and simulated signals in the detection of gravitational waves from coalescing compact binaries'. In: *Classical and Quantum Gravity* 27.8 (2010), p. 084020 (cited on page 197).
- [249] G. Thomas and D. Evans. 'Arrays of three-dimensional wave-energy absorbers'. In: *Journal of Fluid Mechanics* 108 (1981), pp. 67–88 (cited on page 221).
- [250] M. Sniedovich. 'A classical decision theoretic perspective on worst-case analysis'. In: *Applications of Mathematics* 56.5 (2011), p. 499 (cited on page 232).
- [251] C. A. Floudas and V. Visweswaran. 'Quadratic optimization'. In: *Handbook of global optimization*. Springer, 1995, pp. 217–269 (cited on pages 233, 234, 240).
- [252] S. Arora and B. Barak. *Computational complexity: a modern approach*. Cambridge University Press, 2009 (cited on page 233).
- [253] R. Brayton et al. 'A new algorithm for statistical circuit design based on quasi-newton methods and function splitting'. In: *IEEE Transactions on Circuits and Systems* 26.9 (1979), pp. 784–794 (cited on page 233).
- [254] E. Polak, D. Q. Mayne, and J. E. Higgins. 'Superlinearly convergent algorithm for min-max problems'. In: *Journal of Optimization Theory and Applications* 69.3 (1991), pp. 407–439 (cited on page 233).
- [255] G. Gallo and A. Ülkücü. 'Bilinear programming: an exact algorithm'. In: *Mathematical Programming* 12.1 (1977), pp. 173–194 (cited on page 242).
- [256] C. B. Barber, D. P. Dobkin, and H. Huhdanpaa. 'The quickhull algorithm for convex hulls'. In: *ACM Transactions on Mathematical Software (TOMS)* 22.4 (1996), pp. 469–483 (cited on pages 244, 255).
- [257] The Geometry Center - University of Minnesota. *Qhull*. Apr. 2020 (cited on page 245).
- [258] D. P. Bertsekas. 'Nonlinear programming'. In: *Journal of the Operational Research Society* 48.3 (1997), pp. 334–334 (cited on page 261).
- [259] H. X. Phu. 'Outer Γ -convexity in vector spaces'. In: *Numerical Functional Analysis and Optimization* 29.7-8 (2008), pp. 835–854 (cited on pages 261, 274).
- [260] J.-P. Aubin. *Applied functional analysis*. Vol. 47. John Wiley & Sons, 2011 (cited on page 266).
- [261] J. J. Benedetto. *Harmonic analysis and applications*. Vol. 23. CRC Press, 1996 (cited on page 267).

- [262] H. Phu and V. Pho. 'Some properties of boundedly perturbed strictly convex quadratic functions'. In: *Optimization* 61.1 (2012), pp. 67–88 (cited on page 274).
- [263] G. Giorgi and J. V. Ringwood. 'Nonlinear Froude-Krylov and viscous drag representations for wave energy converters in the computation/fidelity continuum'. In: *Ocean Engineering* 141 (2017), pp. 164–175 (cited on page 277).
- [264] S. Zhang and Y. Xia. 'Solving nonlinear optimization problems of real functions in complex variables by complex-valued iterative methods'. In: *IEEE transactions on cybernetics* 48.1 (2016), pp. 277–287 (cited on page 288).
- [265] C. Windt et al. 'Assessment of the evaluation framework for energy maximising control systems for the Wavestar wave energy converter'. In: *American Control Conference (ACC), Philadelphia*. 2019, pp. 4791–4796 (cited on page 288).